6. SITE 647[1]

Shipboard Scientific Party[2]

HOLE 647A

Date occupied: 15 October 1985, 0715 UTC

Date departed: 24 October 1985, 0300 UTC

Time on hole: 8 days, 19 hr, 45 min

Position: 53°19.876′N, 45°15.717′W

Water depth (sea level; corrected m, echo-sounding): 3861.8

Water depth (rig floor; corrected m, echo-sounding): 3872.3

Bottom felt (rig floor, m, drill-pipe measurement): 3869.0

Distance between rig floor and sea level (m): 10.5

Total depth (rig floor, m): 4605.0

Penetration (m): 736.0

Number of cores (including cores with no recovery): 75

Total length of cored section (m): 716.6

Total core recovered (m): 445.19

Core recovery (%): 62

Oldest sediment cored:
Depth sub-bottom (m): 699
Nature: claystone
Age: early Eocene
Measured velocity (km/s): 2.0

Basement:
Depth sub-bottom (m): 699–736
Nature: basalt
Measured velocity range (km/s): 3.460–5.700

HOLE 647B

Date occupied: 24 October 1985, 0930 UTC

Date departed: 25 October 1985, 1215 UTC

Time on hole: 1 day, 2 hr, 45 min

Position: 53°19.876′N, 45°15.717′W

Water depth (sea level; corrected m, echo-sounding): 3861.8

Water depth (rig floor; corrected m, echo-sounding): 3872.3

Bottom felt (rig floor, m; drill-pipe measurement): 3870.7

Distance between rig floor and sea level (m): 10.5

Total depth (rig floor; m): 3974.0

Penetration (m): 103.3

Number of cores (including cores with no recovery): 11

Total length of cored section (m): 103.3

Total core recovered (m): 93.18

Core recovery (%): 90

Oldest sediment cored:
Depth sub-bottom (m): 103.3
Nature: silty clay, clayey muds, and clayey silts
Age: late Pliocene
Measured velocity (km/s): 1.7

Principal results: Holes 647A and 647B, Site 647, were drilled in a water depth of 3858.5 m, at 53°19.876′N, 45°15.717′W, in the southern Labrador Sea. The total depth of penetration was 736 mbsf; average recovery during rotary drilling at Hole 647A was 62% and during APC coring at Hole 647B, 90%. Four major sedimentary units were encountered between the seafloor and 699 mbsf, and basalt was recovered from 699 to 736 mbsf. The lithologic units are as follows:

Lithologic Unit I (Cores 105-647A-1R to 105-647A-12R; 105-647B-1H to 105-647B-11H) 0–116 mbsf. Age: late Pliocene to Holocene. Description: consists of interbedded gray to light brownish gray silty clays, clayey muds, and clayey silts containing highly variable amounts of biogenic carbonate (foraminifers, nannofossils) to a maximum of 40%–50%. Lithologies are interbedded on a scale of from 10 cm to 3 m, having both sharp and gradational contacts. Silty clays, clayey muds, and clayey silts are structureless to color mottled. Foraminifer-nannofossil silty clays or clayey silts are homogeneous, but pockets within or at the tops of beds are enriched in foraminifers; the tops of such thin beds have sharp contacts with overlying beds. Detrital (nonbiogenic) carbonate occurs as disseminated silt-sized grains (as much as 50%) and as concentrations of as much as 75% in thinly laminated silty clay to clayey silt layers. Some of these layers have sharp bases and exhibit grading. All facies except the laminated detricarbonate silty clay layers contain variable amounts of sand- and gravel-sized material to cobble size. The upper

---

[1] Srivastava, S. P., Arthur, M., Clement, B., et al., 1987. *Proc., Init. Repts. (Pt. A), ODP*, 105.

[2] Ali Aksu, Earth Sciences Department, Memorial University of Newfoundland, St. John's, Newfoundland A1B 3X5, Canada; Michael Arthur (Co-Chief Scientist), Graduate School of Oceanography, University of Rhode Island, Narragansett, RI 02882; Jack Baldauf, Ocean Drilling Program, 1000 Discovery Drive, College Station, TX 77840; Gerhard Bohrmann, Geologisch-Palaeontologisches Institut und Museum der CAU, Olshausenstr. 40, 2300 Kiel, Federal Republic of Germany; William Busch, Department of Geology and Geophysics, University of New Orleans, New Orleans, LA 70148; Tommy Cederberg, University of Copenhagen, Geological Institute, Oester Voldgade 10, DK-1350, Copenhagen, Denmark; Bradford Clement (Co-Chief Scientist), Ocean Drilling Program, 1000 Discovery Drive, College Station, TX 77840; Michel Cremer, Departement de Géologie et Océanographie, UA 197, Université de Bordeaux I, Avenue des Facultés, 33405 Talence Cedex, France; Kathleen Dadey, Graduate School of Oceanography, University of Rhode Island, Narragansett, RI 02882; Anne De Vernal, GEOTOP, Sciences de la Terre, Université du Quebec à Montreal, L.P. 8888, Succ "A", Montreal, Quebec H3C 3P8, Canada; John Firth, Department of Geology, Florida State University, Tallahassee, FL 32306; Frank Hall, Graduate School of Oceanography, University of Rhode Island, Narragansett, RI 02882; Martin Head, Department of Geology, University of Toronto, Toronto M5A 1A1, Canada; Richard Hiscott, Earth Sciences Department, Memorial University, St. John's, Newfoundland A1B 3X5, Canada; Rich Jarrard, Lamont-Doherty Geological Observatory, Palisades, NY 10964; Michael Kaminski, WHOI/MIT Joint Program in Oceanography, Woods Hole Oceanographic Institution, Clark 1, Woods Hole, MA 02543; David Lazarus, Woods Hole Oceanographic Institution, Department of Geology and Geophysics, Woods Hole, MA 02543; Anne-Lise Monjanel, Université de Bretagne Occidentale, G.I.S. Océanologie et Géodynamique, 6, Av. Victor le Gorgeu, 29283 Brest Cedex, France; Ole Bjorslev Nielsen, Department of Geology, Aarhus University, DK-8000 Aarhus C, Denmark; Surat P. Srivastava (Co-Chief Scientist), Atlantic Geoscience Centre, Geological Survey of Canada, P.O. Box 1006, Dartmouth, Nova Scotia B2Y A42, Canada; Ruediger Stein, Institute of Petroleum and Organic Geochemistry, KFA Julich, P.O. Box 1913, 5170 Julich, Federal Republic of Germany (current address: Institut fuer Geowissenschaften und Lithosphaeren forschung, Universitaet Giessen, Senckenbergstr. 3, 6300 Giessen, Federal Republic of Germany); Francois Thiebault, Lab. Dynamique Sédimentaire et Structurale, UA 713 UER, Sciences de le Terre, Université de Lille I, 59655 Villeneuve D'Ascq Cedex, France; James Zachos, Graduate School of Oceanography, University of Rhode Island, Narragansett, RI 02882; Herman Zimmerman, Department of Geology, Union College, Schenectady, NY 12308 (current address: Division of Polar Programs, National Science Foundation, Washington, D.C. 20550).

50 m of Unit I are coarser grained than the lower part, but no systematic trend to the biogenic content exists. However, intervals containing gravel and those relatively rich in biogenic constituents alternate in a cyclical but irregular pattern.

Lithologic Unit II (Cores 105-647A-13R to 105-647A-14R) 116.0–135.4 mbsf. Age: early Miocene to late Miocene. Description: primarily mottled olive-yellow to yellowish brown silty mud, clay, and nannofossil clay (Subunit IIA, 116–119 mbsf) and olive-yellow to grayish green silica-bearing (as much as 25%) clays lacking calcareous nannofossils (Subunit IIB, 119–135.4 mbsf). Subunit IIA contains quartz silt (as much as 25%) and scattered iron/manganese micronodules that increase in abundance toward the base; the sediment is bioturbated to homogeneous. Subunit IIB is marked by diatom- and spicule-bearing silty clay; biogenic silica (as much as 15%) contents increase toward the base. Dark-gray bands of iron/manganese micronodules occur in the upper part, and larger iron/manganese nodules appear near the base of the subunit. Subunit IIB is bioturbated and mottled.

Lithologic Unit III (Cores 105-647A-15R to 105-647A-55R) 135.4–530.3 mbsf. Age: early Oligocene to middle Eocene. Description: mainly moderately to strongly bioturbated greenish gray to light greenish gray biogenic clay (claystone) or clayey ooze (chalk or diatomite), lithified below 165 mbsf. Subunit IIIA (Cores 105-647A-15R to 105-647A-22R; 135.4–212.3 mbsf) contains both nannofossils and diatoms at a ratio of about 2:1. Subunit IIIB (Cores 105-647A-23R to 105-647A-25R; 212.3–241.1 mbsf) consists of biogenic claystones containing 25%–50% diatoms and sponge spicules without significant amounts of calcareous nannofossils. Subunit IIIC (Cores 105-647A-26R to 105-647A-55R; 241.1–530.3 mbsf) contains relatively little biogenic silica but is rich in calcareous nannofossils throughout and foraminifers in parts. Glauconite, pyrite, and carbonate concretions occur commonly throughout most of the unit. Darker colored subhorizontal burrows typically indicate bedding. Contorted burrows and intraformational breccias suggest possible downslope movement, but below 350 mbsf bedding locally dips as much as 40° in association with healed faults and fractures.

Lithologic Unit IV (Cores 105-647A-56R to 105-647A-71R) 530.3–699.0 mbsf. Age: middle Eocene to early Eocene. Description: predominantly greenish gray claystone and foraminifer-nannofossil-bearing claystone with some intervals of interbedded dusky red, light red, and violet claystone. Claystones are bioturbated, and burrows are highly compacted. Carbonate concretions, pyrite, and glauconite occur but are relatively minor constituents. Clay minerals are the only terrigenous component. The lowermost part of Unit IV contains fractures having calcite and/or quartz linings or partial replacement of surrounding sediment; the alteration is similar to that associated with the basalt/sediment contact at the base of the unit.

Basement (Cores 105-647A-71R to 105-647A-75R) 699.0–730.0 mbsf. Description: generally massive, aphyric to moderately pyroxene-phyric, fine- to medium-crystalline basalt, composing probable thick flow units. The contact with sediment above is sharp but characterized by large calcite- and chlorite-filled vesicles, and the overlying flow-top breccia and sediments contain hydrothermal precipitates. Veins in the basalt contain calcite and chlorite and, at deeper levels, massive serpentine. Otherwise the basalt appears fresh.

Summary

Rotary and APC cores provide a nearly complete sequence over the last 2.5 m.y. of deposition (late Pliocene–Pleistocene). Recognizable alternations of relatively nannofossil-rich silty clay and more gravel-rich, silty intervals appear to represent depositional cycles related to glacial-interglacial climatic changes. Sedimentation rates average about 46 m/m.y. (4.6 cm/k.y.). Sediment deposited over the last 1.2 m.y. contains more silt, sand, and detrital carbonate than the older part of Lithologic Unit I. Both bottom-current-winnowed beds enriched in biogenic components and detrital calcite-rich turbidites derived from spillover from the North Atlantic Mid-Ocean Canyon are present in the Pliocene–Pleistocene sequence. A suite of ice-rafted pebbles could have been derived from a broad region, including carbonate terrains in the northern Baffin Bay area. As at Site 646, the onset of glacial ice rafting occurred at about 2.5 Ma. Strata of this age, dominated by terrigenous input, directly overlie a hiatus at 116 mbsf, which encompasses the interval between at least 5.6 and 2.5 Ma. The hiatus forms a prominent reflector (R2) that can be traced regionally.

A condensed sedimentary sequence represents the early to late Miocene deposition (Lithologic Unit II) and contains at least one hiatus between the upper Miocene (8.2 Ma) and the lower Miocene (17.5 Ma). Iron/manganese and phosphate nodules, streaks, and bands characterize much of the interval. The hiatuses and slow sedimentation rate probably indicate scour by strong bottom currents and/or nondeposition in conjunction with low sediment supply during much of the early to late Miocene. This episode approximately coincides with the beginning of major drift sedimentation in the North Atlantic. An additional hiatus may be present between the lower Miocene and upper Oligocene.

A particularly important feature of the recovery at Site 647 is the continuous, high sedimentation rate revealed in the upper middle Eocene through lower Oligocene sequence. The biogenic claystones and clayey oozes were deposited at average rates of about 36 m/m.y. in the late middle Eocene to early Oligocene and are predominantly nannofossil rich, but biogenic opal occurs in the upper Eocene through lower Oligocene strata. Lower Oligocene strata between 212.3 and 241.1 mbsf are particularly biogenic opal rich. A prominent regional seismic reflector identified as R4 corresponds to the change from siliceous to calcareous biogenic claystones in the lower Oligocene at about 240 mbsf, corresponding to the previous identification of R4 at DSDP Site 112 nearby. The reflector appears to bear no direct relationship to changes in bottom-water circulation. A major but somewhat gradual change in the benthic foraminiferal fauna, from agglutinated- to calcareous-dominated, occurred during the late Eocene through earliest Oligocene (essentially complete by the time of the Eocene/Oligocene boundary at 290 mbsf), which is below the level of R4. The benthic faunal transition may indicate a change in bottom-water characteristics and, coupled with high rates of deposition and supply of terrigenous clay, may signify increased rates of deep circulation. However, the sediment textures and structures provide no indication of strong abyssal currents at the site during this time.

The seafloor at the site apparently subsided below the carbonate compensation depth (CCD) during the early to early middle Eocene, when Lithologic Unit IV was deposited. An extremely condensed section spanning about 8 m.y. (45.5–53.5 Ma) occurs within this unit at approximately 608–643 mbsf; poor core recovery causes difficulty in assigning an exact depth to the hiatus. The CCD apparently descended during the middle to late Eocene and into the early Oligocene, as indicated by predominance of biogenic carbonate-rich facies and fair to good preservation of calcareous microfossils. Carbonate productivity may also have increased over that time. A climatic optimum characterized by highest diversity of calcareous plankton occurred in the late middle Eocene (about 41 Ma). The early Oligocene episode of biosiliceous sediment deposition probably represents increased opal and decreased carbonate production in surface waters, a trend that began in the late Eocene, accompanied by cooling of surface waters. Opal-accumulation rates increased in that interval, while the carbonate-accumulation rate decreased. Organic-carbon-accumulation rates were at a maximum in the middle Eocene, in conjunction with high abundance of agglutinated benthic foraminifers.

The age of the uppermost basaltic basement is 55–56 Ma, on the basis of the immediately overlying oldest sediment. This age agrees with the age assigned by magnetic-anomaly correlations (anomaly 24), thus supporting geophysical data and validating our tectonic model for the evolution of the Labrador Sea. Evidence of some late hydrothermal activity and associated faults and fractures occurs in strata of Eocene age overlying the basement.

BACKGROUND AND OBJECTIVES

The Labrador Sea, along with Baffin Bay, forms an important connection for water-mass exchange between the Arctic and the North Atlantic, perhaps since the Late Cretaceous. To establish the history of such exchange of water mass, a north–south transect consisting of three sites, one in Baffin Bay and two in the Labrador Sea, was drilled during ODP Leg 105. Oceanic circulation in the Labrador Sea has been influenced not only by the exchange of water masses between the Arctic and the North Atlantic but also by the inflow of cold water masses from the Norwegian Sea since the middle Miocene. Thus, to study the

relative influence of these three different bodies of water in the Labrador Sea, we selected sites in regions where their effects are best recorded in the underlying sediments.

One of these sites (Site 646) is located in the southeastern part of the Labrador Sea, where bottom water derived from the Norwegian Sea has produced a large sediment-drift deposit, the Eirik Ridge, since middle Miocene time. The earlier history of deep-water circulation is recorded in sediments that lie buried beyond the reach of drilling in most places in the Labrador Sea except south of another large drift deposit, the Gloria Drift (Figs. 1 and 2).

Although some drilling was originally done in this region during Leg 12 of the Deep Sea Drilling Project (DSDP), the incomplete recovery of the sedimentary section as well as the lack of drilling constraints on basement age did not provide the answers to some critical tectonic and paleoceanographic problems. For this reason, another site, Site 647, was selected for drilling during Leg 105, about 100 km south of the Gloria Drift deposit in the southern Labrador Sea (Fig. 2). We chose Site 647 for several reasons: (1) It lies far enough from the Gloria Drift deposit to avoid a thick Neogene section, thereby allowing us to drill to basement and recover the overlying Paleogene sedimentary section; (2) the magnetic anomalies are well developed in this region; determining the age of basement will help resolve the tectonic history of the Labrador Sea; and (3) the region lies in a position that is sensitive to incursions of warmer North Atlantic waters and that should allow us to examine the nature of paleoclimatic and paleoceanographic north–south, east–west gradients. ODP Site 647 and DSDP Sites 403, 552, 553, and 554, west of Rockall Plateau, lie over crust formed contemporaneously north and south of the triple junction resulting from simultaneous seafloor spreading in the Labrador and Norwegian Seas. A comparative study of the drilling results from these sites will help us to understand better the paleoclimatic and paleoceanographic conditions that prevailed there during the Paleogene.

Background

Regional Setting

The evolutional history of crust in the Site 647 region has been extensively studied (Mayhew, 1969; Laughton, 1972; Vogt and Avery, 1974; Egloff and Johnson, 1975; Kristoffersen and Talwani, 1977; Srivastava, 1978). That the crust here was formed

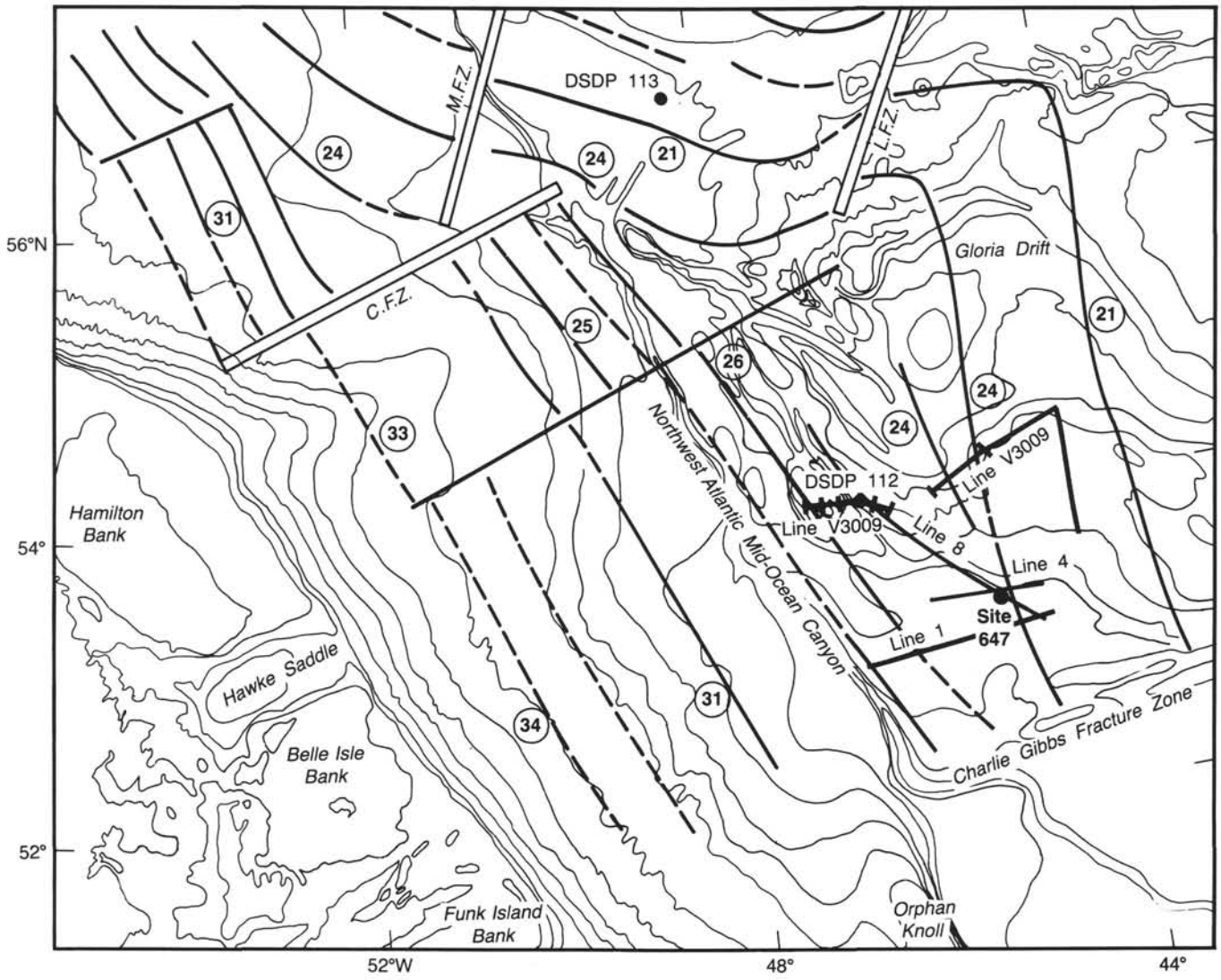

Figure 1. Bathymetry map of the Labrador Sea, showing locations of ODP Site 647 and DSDP Sites 112 and 113. Numbers of anomalies are circled.

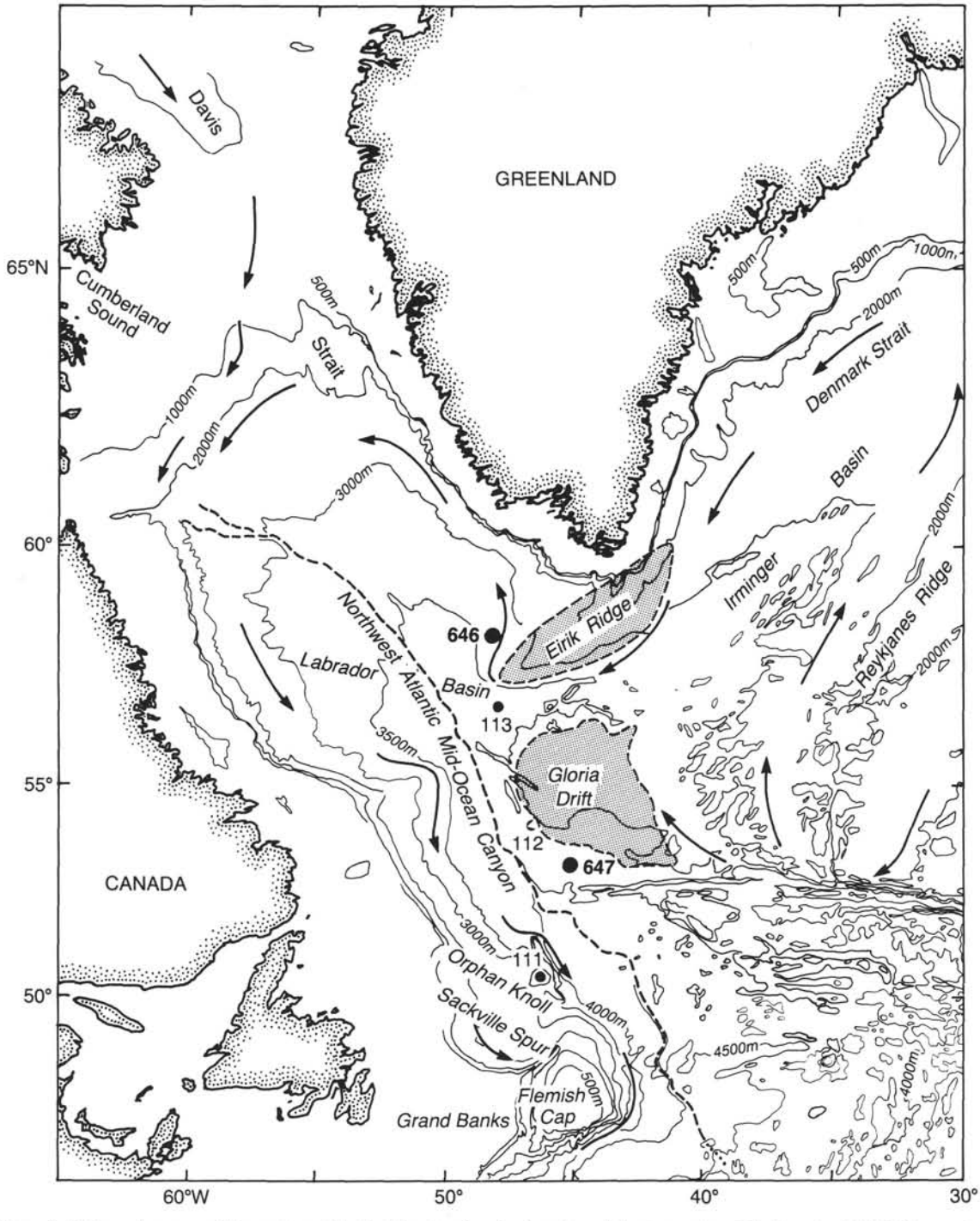

Figure 2. Bathymetry map of the northern North Atlantic, showing location of the two major drift deposits (Eirik Ridge and Gloria Drift) and ODP Sites 646 and 647 and DSDP Sites 111, 112, and 113. Arrows indicate deep-water circulation.

by seafloor spreading between the British Isles and North America during the early Tertiary is now well accepted. The main evidence of this is the magnetic anomalies in this region (Fig. 1, "Introduction" chapter, this volume), which resemble typical seafloor-spreading-generated anomalies. Site 647 lies just west of anomaly 24 crust. West of the site, another group of magnetic anomalies lies at a large angle to anomaly 24 and younger anomalies. Srivastava (1978) interpreted this as indicating a drastic change in the direction of spreading after Chron C24 when active seafloor spreading began in the Norwegian–Greenland Seas. As a result, spreading occurred simultaneously in the Labrador Sea, the Norwegian Sea, and the North Atlantic, and a triple junction formed north of the site and south of Greenland (Fig. 4, "Introduction" chapter, this volume). A number of basement highs, observed in the seismic profiles from this region, arise owing to the presence of fracture zones and to a jump on the ridge axis after Chron C25. The basement ridges forming since Chron C25 have greatly affected the bottom-water circulation, producing some large sediment-drift deposits like the Gloria Drift.

Much existing geophysical and geological data from this region (Fig. 3) were compiled in the form of maps showing depth

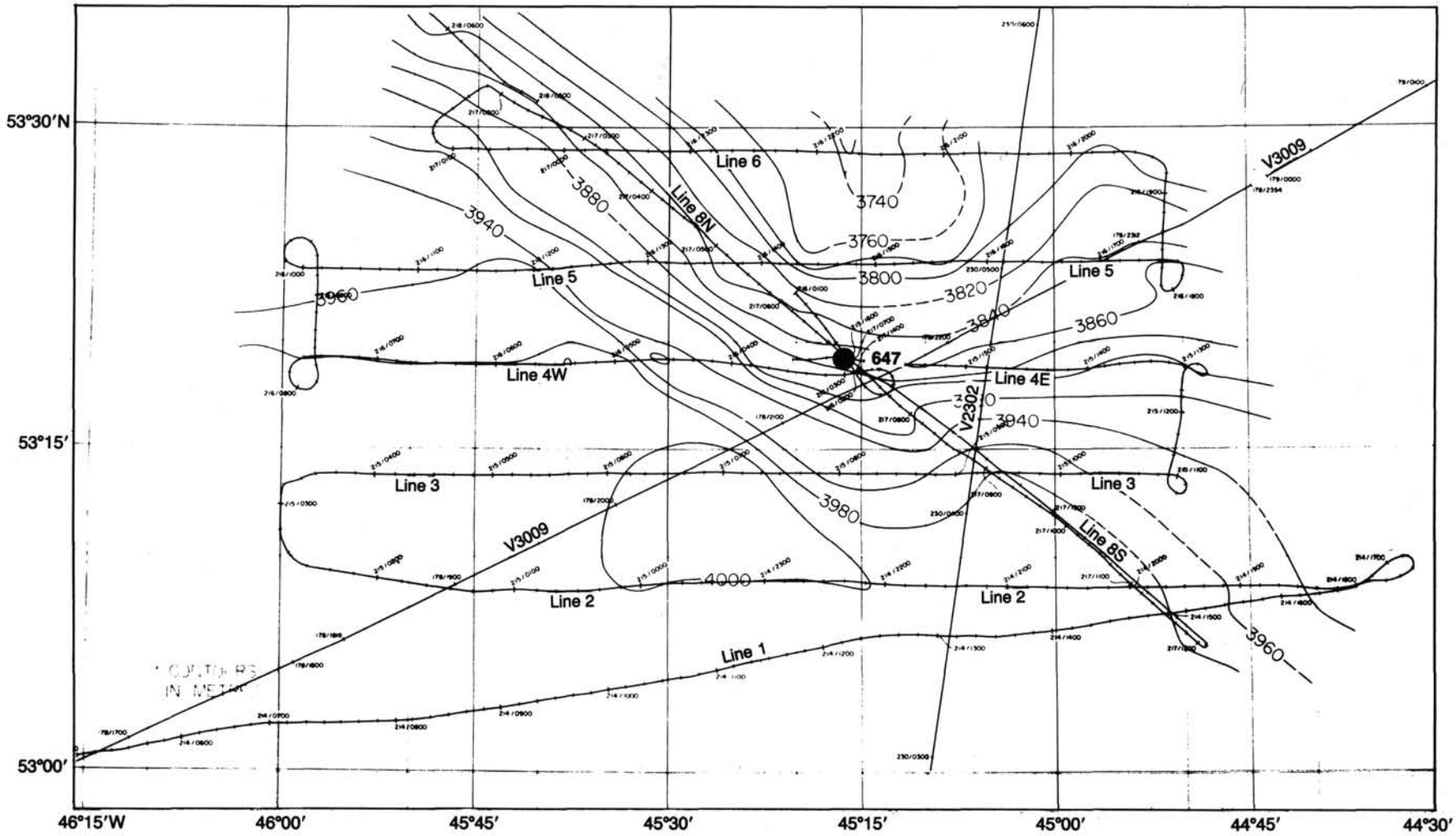

Figure 3. Map showing location of ship track (HD 84-30) along which gravity, magnetic, bathymetry, and seismic data were collected during a site-survey cruise. Bathymetry contours in meters.

to acoustic basement (Fig. 4), sediment thickness (Fig. 5), and depth to some of the seismic reflectors (Fig. 6) near the site. Seismic-reflection data near the site allow definition of several seismic units, which are described here briefly.

Seismic Unit 1, the uppermost unit, is about 0.12 s (102 m) thick at Site 647 and comprises a series of moderate- to high-amplitude reflectors that are parallel to subparallel to the seafloor (Figs. 7 and 8). The unit varies in thickness over the nearby region and has a maximum of about 0.3 s. It is thickest west of Site 647, presumably because of the inflow of turbidites from the North Atlantic Mid-Ocean Canyon (NAMOC). Near NAMOC, this unit is about 0.6 s thick. It is thinnest above basement highs. Reflectors within the unit are generally parallel to subparallel to each other except in regions where the unit thickens. In these regions, the lower reflectors onlap the top of seismic unit 2 (Fig. 7). The base of seismic unit 1 is characterized by a strong, continuous to discontinuous reflector, which may represent an unconformity, as indicated by the onlap of seismic unit 1 strata. The base of seismic unit 1 may characterize a change in the depositional environment.

Seismic Unit 2 occurs between 0.12 and 0.32 s bsf (102 and 273 mbsf) at Site 647, but it varies in thickness between 0.15 and 0.25 s in this region. Except for one reflector near the base of seismic unit 2, this unit is devoid of other recognizable reflectors; over many of the seismic-reflection records it appears transparent. Near Site 647 (Figs. 7 and 8), the top of the unit contains reflectors that are discontinuous. A weak discontinuous reflector also occurs about 0.04 s above the base of the unit. A high-amplitude, continuous to discontinuous reflector marks the base of the unit. This is the most prominent reflector and can be easily traced throughout the region. An equivalent reflector, drilled at DSDP Site 112 (Fig. 9) about 100 km northwest of Site 647, was called the mid-sediment reflector (Laughton, Berggren, et al., 1972). From the initial drilling results, it was thought to be late Eocene to early Oligocene in age. Subsequently, however, it has been termed the R3/R4 reflector, and its age was modified to mid-early Oligocene by Miller et al. (1982) and Miller and Tucholke (1983).

Seismic Unit 3, the deepest unit defined in the records crossing Site 647 (Figs. 7 and 8), lies below 0.32 s. It extends to the top of the fairly prominent basement reflector that marks the top of the oceanic crust at roughly 0.77-s depth near the site. Except for a few reflectors near the bottom of the unit, which lie conformably with the inferred basement surface, the unit is more or less transparent but has higher reflectivity than does seismic unit 2. The bottommost reflector abuts against the basement highs, which indicates that the sediments at or below that reflector were deposited in the basement valleys.

The seismic character of the basement rocks in the region varies somewhat from place to place. In some places, typical hyperbolic character is seen as the top of the oceanic layer 2, whereas in other places a very high-amplitude, flat reflector occurs under which no other reflectors are seen. Such a character can be seen in the line along which Site 647 is located (Fig. 7) at 0900/217 and at 0700/217. This may result from the presence of some sediments interbedded with basalt flows in these regions and forming a high-impedance layer on top of the basaltic layer. Normal faults are also visible in seismic records near Site 647. Our main objectives were to recover the sediment and date the major seismic reflector and their enclosed sediment packages for the reasons outlined in the following discussion.

Sedimentary and Paleoceanographic Setting

Gloria Drift (Egloff and Johnson, 1975), one of several sedimentary drift deposits in the northern North Atlantic (Fig. 2), formed by a combination of sediment erosion, redeposition, and

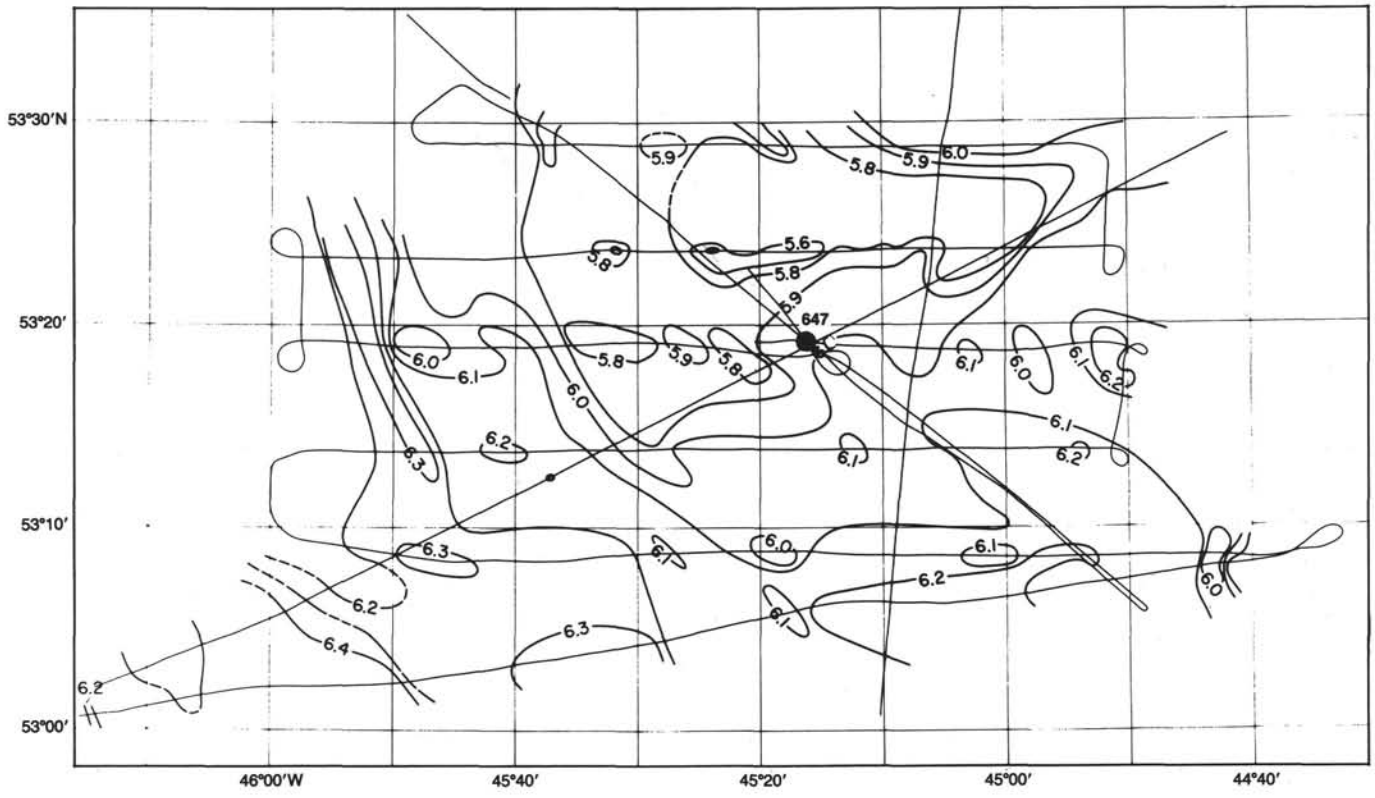

Figure 4. Map of depth to basement (from the sea surface) near Site 647. Contours in two-way traveltime (s).

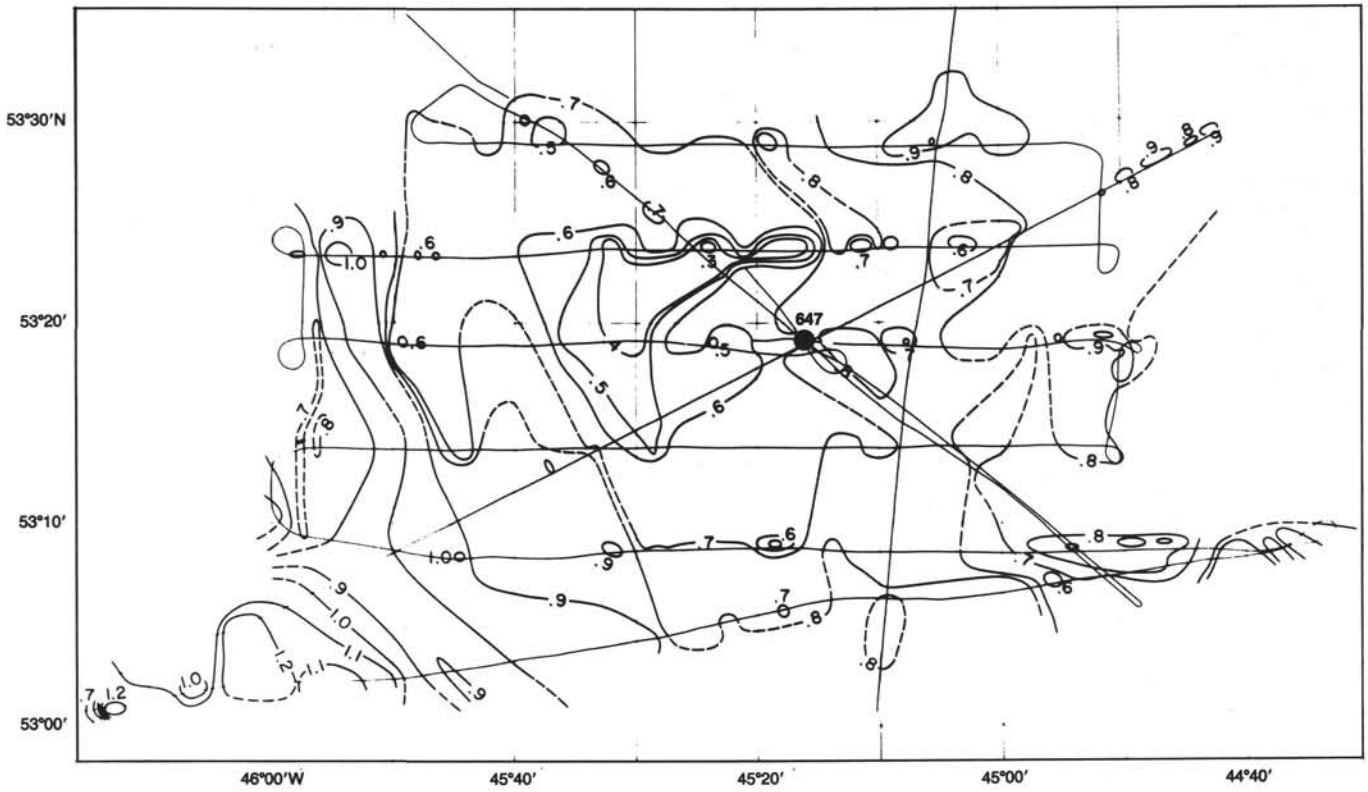

Figure 5. Total thickness of sediment map near Site 647. Contours in two-way traveltime (s).

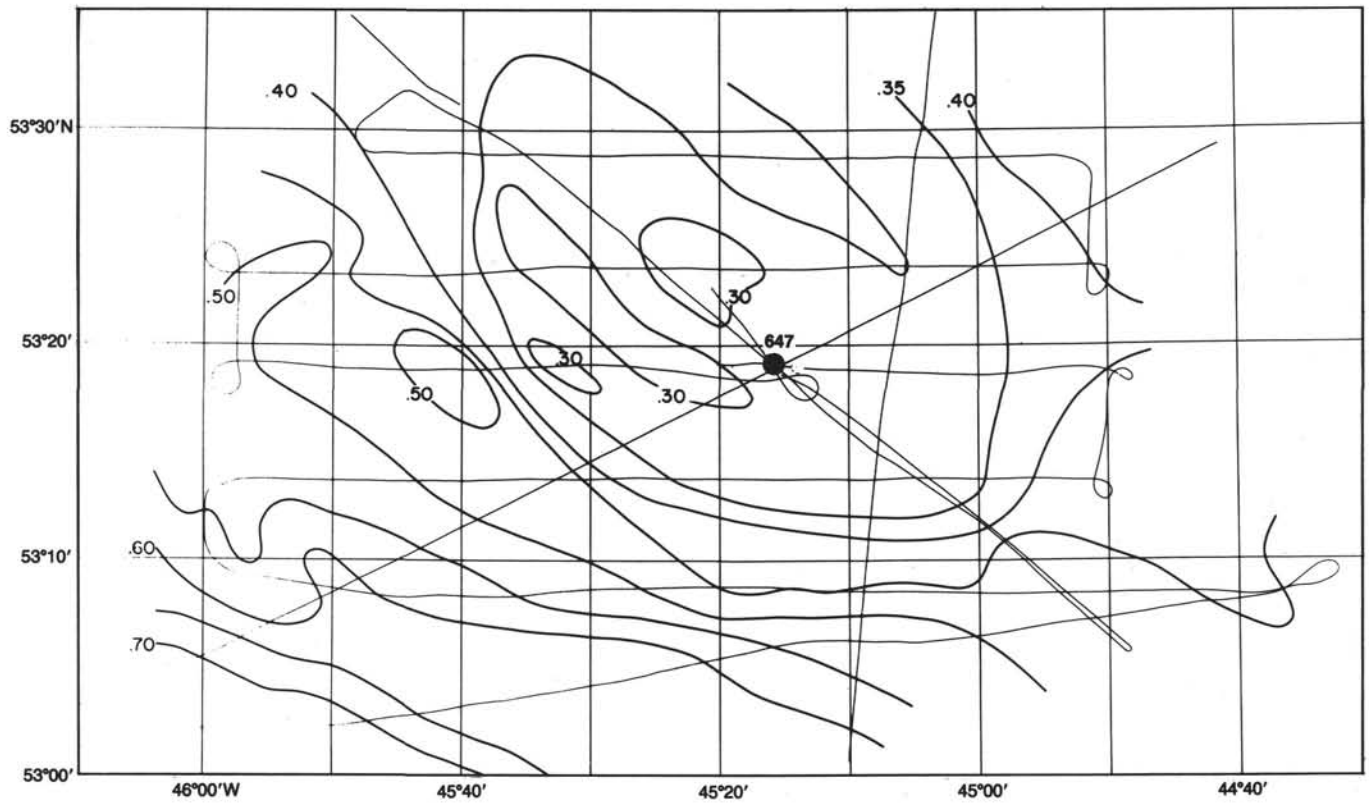

Figure 6. Map of depth to R3/R4 reflector below seafloor. Contours in two-way traveltime (s).

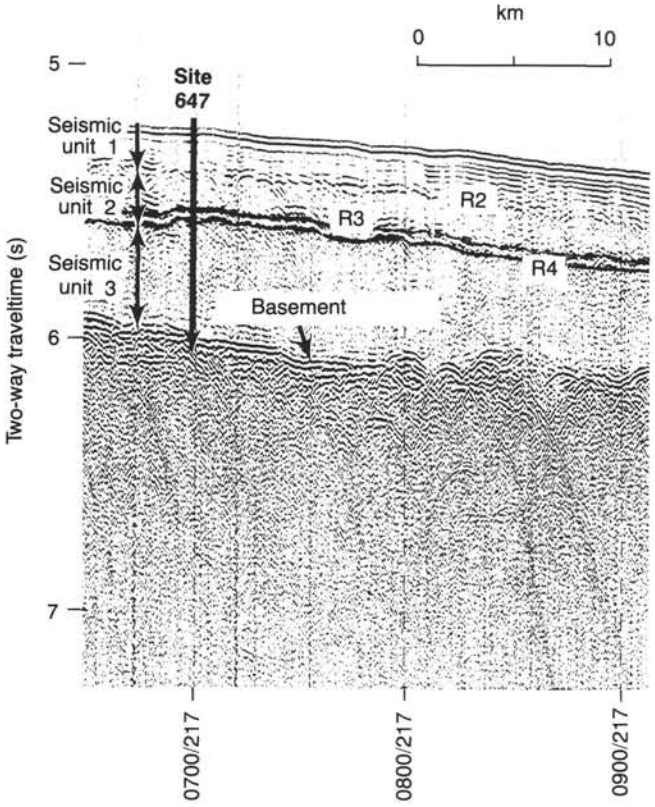

Figure 7. Part of seismic profile (HD 84-30, line 8) across Site 647. For location, see Figure 3.

smoothing of the seabed by strong contour currents (Johnson and Schneider, 1969; Jones et al., 1970). These deep currents originate by cooling and sinking of Norwegian Sea Overflow Water (NSOW) (Worthington and Volkmann, 1965; Worthington and Wright, 1970), which spills over the Greenland–Scotland Ridge through major channels at the Denmark Strait and the Faeroe–Shetland Channel. The NSOW from the Faeroe–Shetland Channel source follows the base of slope as it flows south around the Reykjanes Ridge and turns north and circulates counterclockwise, influenced by the Coriolis acceleration, around the Irminger Basin. Along its path, the main body of NSOW is joined by other portions of the overflow that follow the Charlie Gibbs Fracture Zone and pour through the Denmark Strait (Fig. 2). This flow is then diverted around the southern tip of Greenland and turns northwest into the main part of the Labrador Sea.

The Eirik Ridge is a depositional feature associated with the flow of NSOW around the southwestern side of Greenland. The deeper part of the NSOW, which flows along the Charlie Gibbs Fracture Zone to the west, appears near the western end of the fracture zone and flows northwest, forming a cyclonic (counterclockwise) gyre. The movement of this gyre was perhaps initially (after Chron C24) controlled by the western flank of the Reykjanes Ridge on the east, the extinct Labrador Sea Ridge on the north, and the western Thulean Rise (Egloff and Johnson, 1975) on the west. From sediment waves in the upper part, Jones et al. (1970) recognized a thick sedimentary body in this area. Egloff and Johnson (1975) named this the Gloria Drift and mapped the arcuate shape of this sedimentary drift deposit. Site 647 lies about 100 km south of the main axis of this deposit, but the effects of the strong bottom currents that influenced the drift deposit can still be seen on the seafloor topography in the form of sediment waves near the site (Fig. 7).

Site 647 was purposely located off the main axis of Gloria Drift because we wanted to avoid sampling the thicker drift sequence developed there and instead sample the underlying older sedimentary units that occur at shallower depth south of the drift. Therefore, although we cannot directly observe the history of the main younger drift deposits in the cores from Site 647, we can carry the ages of the depositional units and reflectors into the main drift deposit using the network of seismic profiles that exists for this region.

Objectives

In addition to the general paleoclimatic and tectonic objectives outlined in the "Introduction" chapter (this volume), our major objectives at Site 647 were as follows:

1. Recover a glacial sequence to date the inception of ice rafting in the area and compare it with those from Sites 646 and 645 further north. We also expected the interglacial parts of glacial-interglacial cycles (more North Atlantic influence) to show a warmer character and perhaps some influence of the cold Labrador Current to the west.
2. Develop a better understanding of the history of deep circulation and construction of Gloria Drift. Constraining the ages of sedimentary units within the drift and obtaining possible evidence of strengths of deep currents from the textures and structures in the cores could provide this history.
3. Examine evidence of the evolution of the NAMOC system by dating the influx of terrigenous detritus from NAMOC to the site and carrying reflectors of known age into the axis of maximum deposition. The system is thought to have originated by increased sediment supply, largely from glacial erosion, beginning some time in the late Pliocene (Chough and Hesse, in press).
4. Recover a possibly complete, relatively shallow-burial Eocene–Oligocene sequence above oceanic crust that we expected would contain well-preserved calcareous and siliceous biogenic material and would provide important paleoclimatic and paleoceanographic information on the Paleogene at a relatively high latitude.
5. Provide an age for the R4 reflector, which is of regional extent and is thought to represent the beginning of a major change in bottom-water-mass properties near the Eocene/Oligocene boundary. At nearby DSDP Site 112, the reflector is now interpreted as being a middle lower Oligocene (about 34 Ma) horizon (about 365 mbsf) that marks a change from calcareous pelagic facies below to siliceous, current-influenced deposits above, as well as a change from a dominantly agglutinated benthic foraminiferal fauna to a more calcareous one (Miller et al., 1982).
6. To penetrate, recover, and date oceanic crust of probable Chron 24 (55–58.6 Ma) age to provide a firmer constraint on tectonic models of the evolution of the Labrador Sea and surrounding areas.

OPERATIONS

Approach to Site 647

The transit to Site 647 began at about 0000 hr UTC on 14 October 1985, when *JOIDES Resolution* got under way from Site 646. To save on transit time, we decided not to stream any gear and to proceed at full speed to Site 647. However, a few hours after leaving Site 646, we realized that we could not proceed along the most direct route to the site because of the strong winds and large swells that had developed, which caused the ship to roll excessively. The storm necessitated following a suitable course at reduced speed that took more time than originally planned.

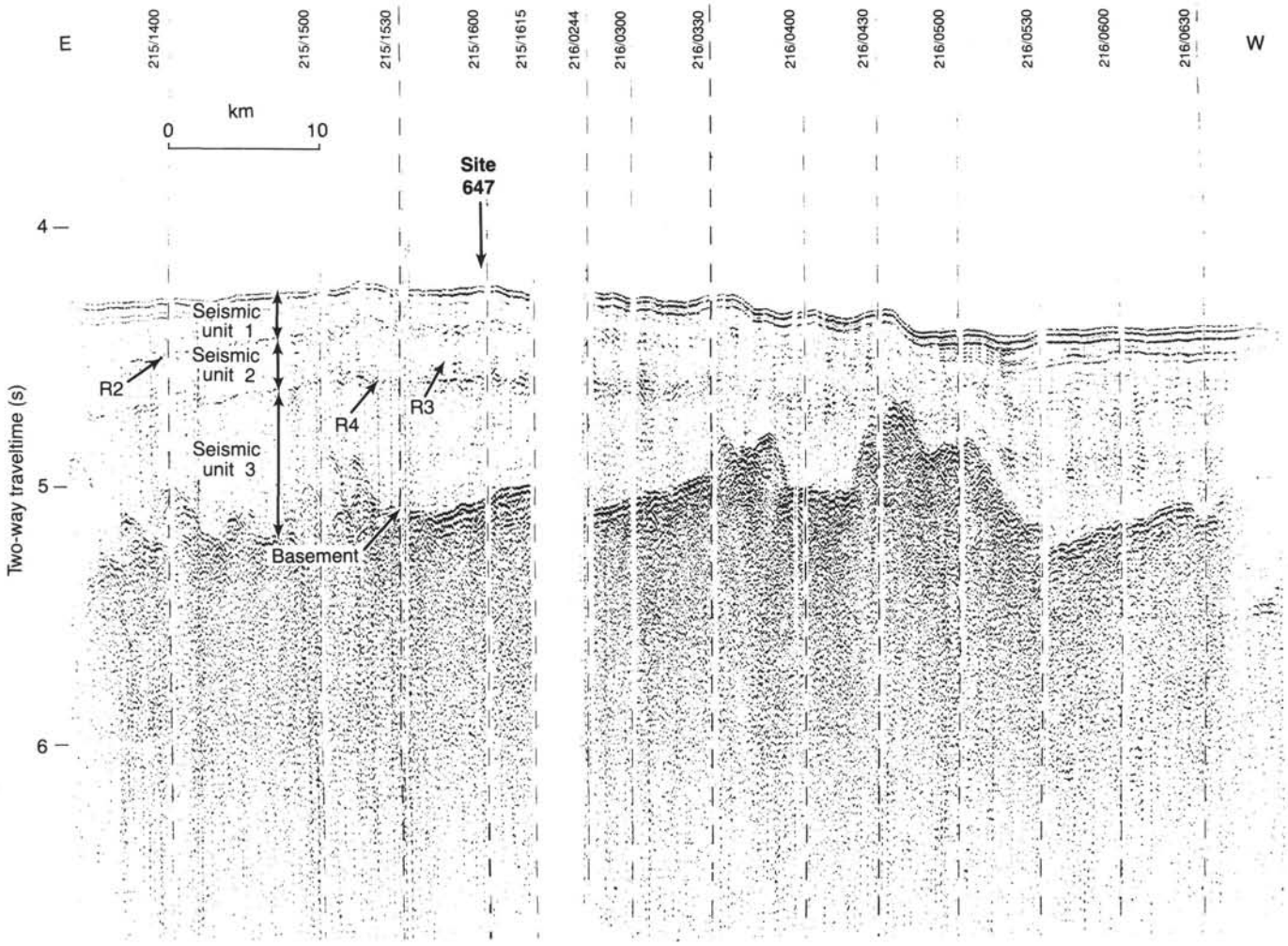

Figure 8. Part of seismic profile (HD 84-30, line 4) across Site 647. For location, see Figure 3.

About 0430 hr UTC on 15 October, we were within 3 hr of our proposed site; we therefore slowed to 5 kt to stream seismic gear and proceeded southeast along *Hudson* 84-30 line 8, preparing the beacon drop at the proposed site LA-9 (Fig. 10). Despite the strong winds and heavy seas, we were able to record reasonably good quality data (see "Underway Geophysics" chapter, this volume) along this line (Fig. 10). As soon as we were certain that we were at our chosen location, we dropped a beacon (0710 hr UTC, 15 October). However, the beacon failed to work. To deploy another beacon, we immediately retrieved the seismic gear and returned on thrusters to the position of the first beacon deployed, using satellite navigation to find the location. While the ship remained on position waiting for a good satellite fix, we prepared (1100 hr UTC) to make up a bottom-hole assembly (BHA). Satellite fixes indicated that we were only 0.5 mi from our chosen location, so we decided to drop another beacon and to begin drilling. We decided to rotary-core drill initially because of the limited time to reach our primary objective of the Paleogene sequence and the basement target at this site.

As usual, we established the corrected water depth, using precision depth recorder (PDR) measurements, below the dual elevator stool (DES) and found it to be 3872.3 m. The actual bottom was felt at 3869.0 m (length of the drill string). After we encountered a small problem with the initial plugging of one of the drill collars during the trip into the hole, drilling started at about 2100 hr UTC 15 October (Site 645 drilling mud had not been swabbed out, but we removed it now by circulating).

The first core arrived on board at about 2300 hr UTC, 15 October. Coring continued at a fair pace despite strong winds (up to 50 kt) and large seas (waves up to 18 ft). Except for the first four to five cores, recovery was good above 250 mbsf. Below this depth, recovery fluctuated, and we decided to pump down some highly viscous drilling mud to make drilling easier. Drilling subsequently continued at a high recovery rate until about 290 mbsf, when the penetration rate again decreased (Fig. 11), where we expected the mid-sediment reflector. Again we pumped down some drilling mud, and continued drilling at a faster pace. Some of the roughest weather on this leg was encountered on 18 October while drilling this hole. Winds gusted up to 56 kt and waves rose up to 25 ft. The ship had no difficulty keeping station during this time.

Except for two occasions, when the center bit had to be dropped to improve bottom-hole conditions (at 588 and 675 mbsf levels), drilling continued at a normal pace until basalt was encountered at 699 mbsf (Table 1). Five cores of basalt were collected before terminating the drilling operation. After the last core arrived on deck at 1900 hr UTC 22 October, we prepared to log Hole 647A.

Hole 647A preparation involved a wiper trip for conditioning the hole, release of the drill bit (hydraulic bit release), and tripping pipe out to the 130-mbsf level. The logging line was rigged up through the wireline heave compensator because of the rough weather that persisted at this site, and the first logging run began at 0250 hr UTC on 23 October. This run con-

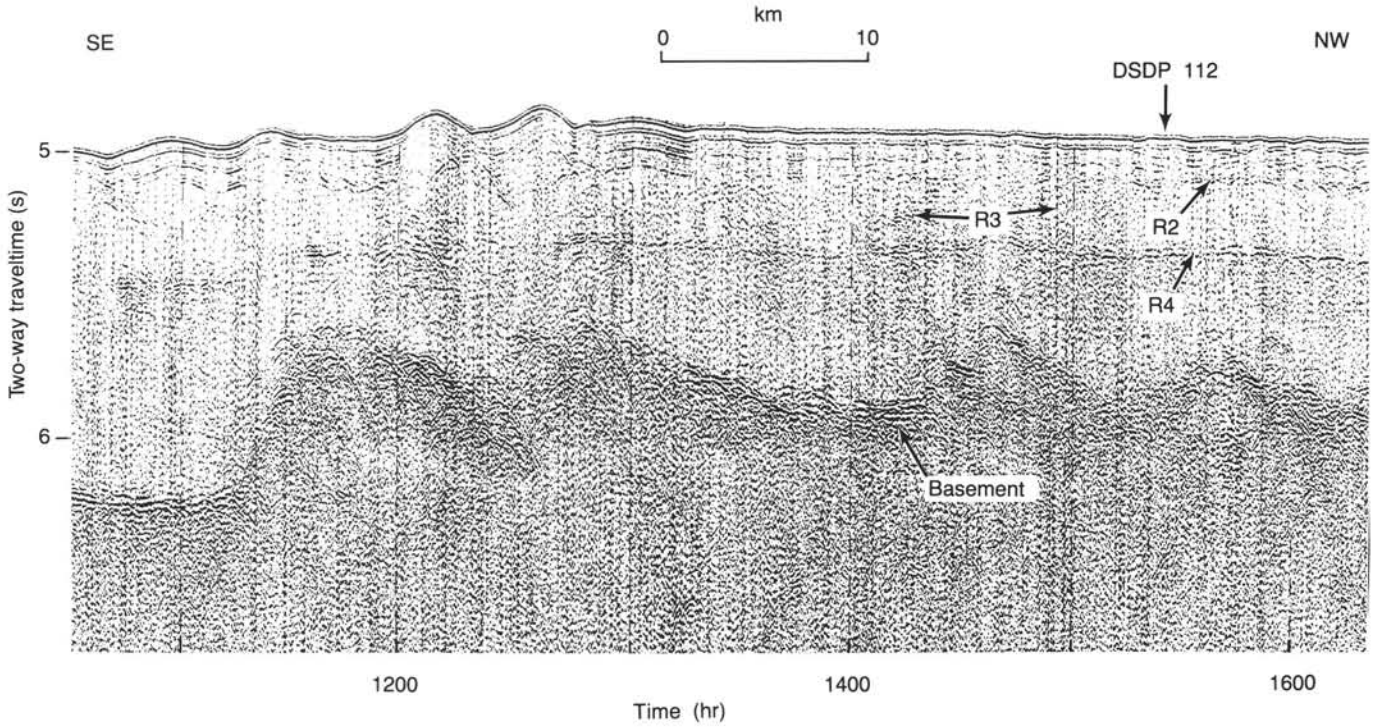

Figure 9. Seismic profile across DSDP Site 112, showing the presence of mid-sediment R4 reflector below 0.41 s depth. For location, see Figure 1.

sisted of the LSS-DIL-MCD-GR tools. Logging continued to a depth of 227 mbsf, when a bridge, which could not be penetrated, stopped further logging.

The logging tools were then retrieved and rigged down so that pipe could be lowered down to the 257-mbsf level, near the beginning of another formation (Unit IIIC) having potentially better hole conditions. Before lowering the logging tools, the caliper was taped off to reduce maximum tool diameter. Several bridges were encountered within a short distance from the pipe, and logging had to be terminated at 283 mbsf.

As soon as the logging tools were brought in and rigged down, the drill string was lowered to the bottom of the hole for filling the hole with 11.4-pounds-per-gallon mud. Hole 647A ended when the trip out was completed at approximately 0015 hr UTC, 24 October.

Hole 647B

We decided to APC core for the time remaining before required departure for St. John's. Another BHA was made up for APC coring, and Hole 647B was spudded at about 1000 hr UTC, 24 October. Eleven cores were collected before a large boulder forced us to terminate further coring at this site at about 0430 hr UTC, 25 October. As soon as the drill string was brought in at 1215 hr UTC on 25 October, we started on our way to St. John's.

SEDIMENTOLOGY

Four lithologic units are recognized at Site 647 (Fig. 41, "Summary and Conclusions" section, this chapter and Table 2). Unit I (0–116 mbsf), of late Pliocene to Holocene age, is characterized by interbedded silty clays, clayey muds, and clayey silts (Fig. 12) containing variable amounts of biogenic constituents, detrital carbonate grains, and scattered gravel-sized rock fragments. Unit II (116–135.4 mbsf) is a condensed sequence containing, in descending order, upper Miocene olive-yellow silty clay and nannofossil clay, lower Miocene olive-yellow silty clay, and lower Miocene grayish green clay. Unit III (135.4–530.3 mbsf) is characterized by lower Oligocene to middle Eocene nannofossil clay (claystone) and clayey oozes (chalks, diatomites), having the biogenic silica concentrated in the lower Oligocene sediments (212.3–241.1 mbsf). Unit IV (530.3–699 mbsf) is dominated by middle to lower Eocene, greenish gray and dusky red claystone, with low biogenic carbonate content. This unit rests on basaltic basement ("Basement Rocks" section, this chapter).

Description of Units

Unit I: Hole 647A (Cores 105-647A-1R to 105-647A-12R), Hole 647B (Cores 105-647B-1H to 105-647B-11H); late Pliocene to Holocene; 0–116 mbsf

The uppermost unit at Site 647 extends from the seafloor to a depth of 116 mbsf. This unit was penetrated by Holes 647A and 647B. Hole 647B, however, was drilled at the very end of the cruise, so that much of the description presented here and all the statistics for Unit I are derived from Hole 647A. Where important, observations of Hole 647B are included as part of the general description of the unit.

Unit I is characterized by interbedded silty clays, clayey muds, and clayey silts, containing variable amounts of biogenic components and scattered pebbles and cobbles. The base of Unit I (Fig. 13) occurs at the unconformity separating upper Pliocene from upper Miocene sediments ("Sediment-Accumulation Rates," this chapter). This unconformity is defined by the disappearance of the gravel and detrital carbonate components and by a color change from gray to the yellow sediments of Unit II. Recovery averaged 65% in Hole 647A (rotary) and 90% in Hole 647B (APC). In Hole 647A, drilling disturbance was generally moderate but greatest near the top of the hole. The first few APC cores of Hole 647B showed considerable deformation from flow-in; deeper cores generally were undeformed and showed facies characteristics much more clearly than did the cores from Hole 647A.

Unit I is characterized by terrigenous silty and clayey sediments, with variable amounts of detrital carbonate and calcareous skeletal material (Fig. 14). The major lithofacies (Fig. 12)

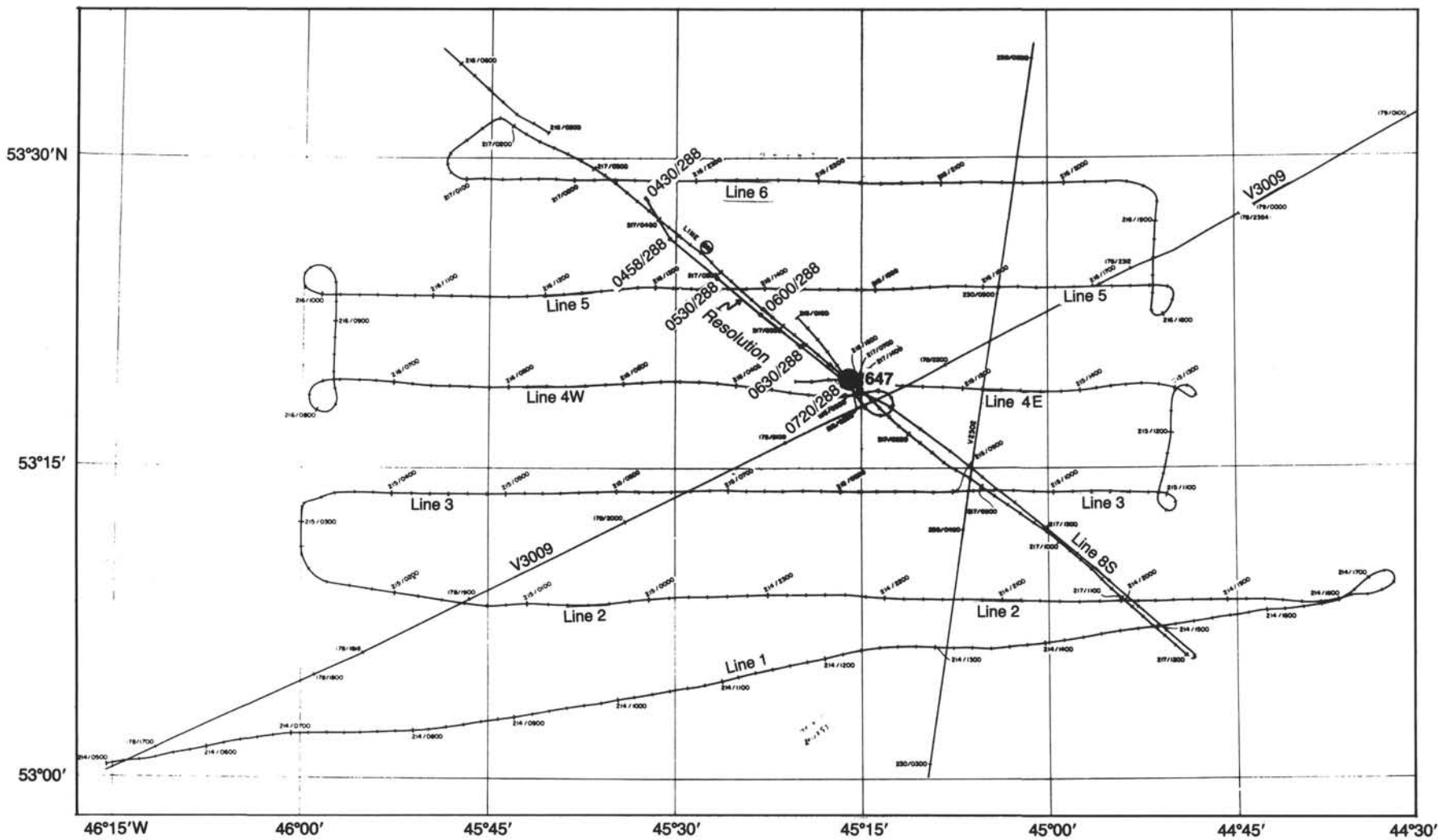

Figure 10. Map showing *JOIDES Resolution* track to Site 647. Shown also are tracks of other cruises to this region.

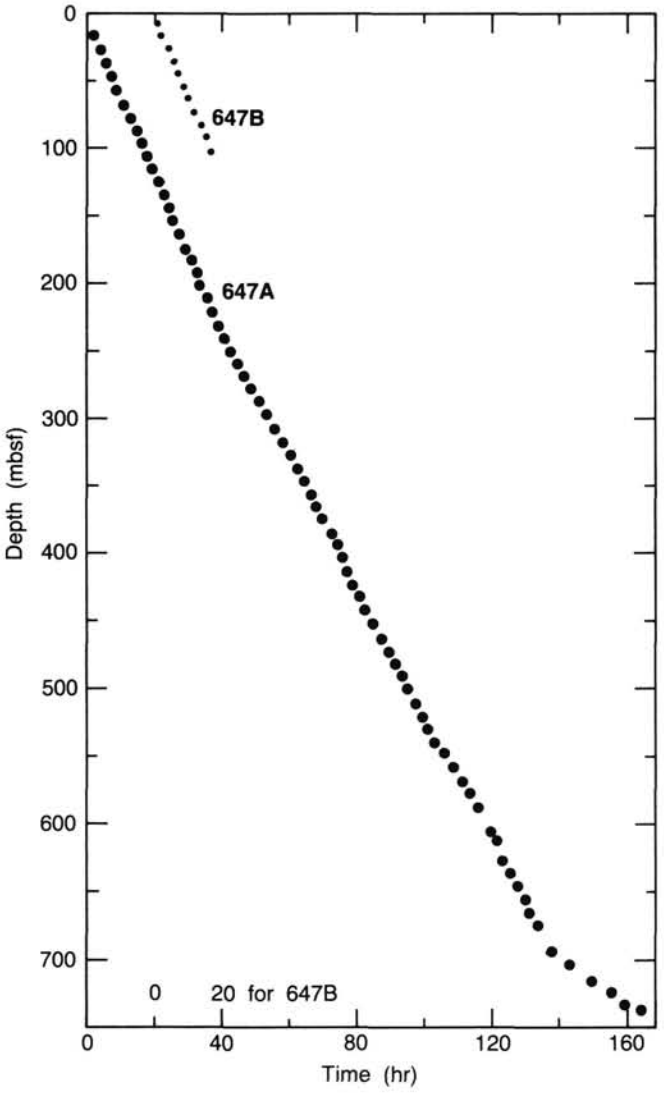

Figure 11. Penetration rate, Site 647.

are gray silty clay (32% of the recovered section); gray to brown clayey mud (27%); gray to light brownish gray clayey silt (19%); and gray to light brownish gray foraminifer-nannofossil silty clay or clayey silt (16%). In the latter facies, biogenic content ranges to a maximum of 40%–50%. A minor lithology is gray to light brownish gray silty mud (6% of recovery). These lithofacies are interbedded on a scale of from 10 cm to 3 m and have both sharp and gradational contacts.

Silty clays and clayey muds are commonly structureless except for color mottling or local color banding, the result in some places of glauconite-rich or clay-rich layers. Green glauconite-rich pockets probably mark burrows. Clayey silts are structureless or mottled.

The foraminifer-nannofossil silty clays or clayey silts are homogeneous except for local color banding and local pockets enriched in foraminifer tests. Tops of units are also commonly enriched in foraminifers. In some places (Fig. 15), the top is sharp; nannofossils are apparently depleted in the upper few centimeters.

Two styles of occurrence of detrital carbonate can be distinguished in Unit I. In the first style, detrital carbonate grains are dispersed within the major lithofacies, especially in the more

Table 1. Coring summary, Site 647.

Core No.	Date (Oct. 1985)	Time (local)	Sub-bottom depths (m)	Length cored (m)	Length recovered (m)	Recovery (%)
Hole 647A						
105-647A-1R	15	2000	0.0–9.2	9.2	9.2	100.4
105-647A-2R	15	2145	9.2–18.9	9.7	9.2	94.8
105-647A-3R	15	2330	18.9–28.6	9.7	0.0	0.0
105-647A-4R	16	0115	28.6–38.1	9.5	9.8	103.6
105-647A-5R	16	0300	38.1–48.6	10.5	0.3	2.9
105-647A-6R	16	0445	48.6–58.3	9.7	9.2	94.5
105-647A-7R	16	0630	58.3–68.0	9.7	9.6	99.3
105-647A-8R	16	0815	68.0–77.6	9.6	3.9	40.9
105-647A-9R	16	1015	77.6–87.3	9.7	4.9	50.6
105-647A-10R	16	1145	87.3–97.0	9.7	6.6	67.7
105-647A-11R	16	1330	97.0–106.7	9.7	5.3	54.9
105-647A-12R	16	1300	106.7–116.0	9.3	5.7	61.3
105-647A-13R	16	1645	116.0–125.7	9.7	7.6	78.1
105-647A-14R	16	1830	125.7–135.4	9.7	3.4	35.0
105-647A-15R	16	2000	135.4–145.1	9.7	3.8	39.4
105-647A-16R	16	2130	145.1–154.8	9.7	3.4	35.0
105-647A-17R	16	2300	154.8–164.1	9.3	7.9	84.5
105-647A-18R	17	0045	164.1–173.8	9.7	2.4	24.9
105-647A-19R	17	0230	173.8–183.5	9.7	8.9	91.2
105-647A-20R	17	0415	183.5–193.1	9.6	8.0	83.2
105-647A-21R	17	0545	193.1–202.7	9.6	5.6	58.3
105-647A-22R	17	0730	202.7–212.3	9.6	0.2	1.7
105-647A-23R	17	0930	212.3–221.9	9.6	9.5	99.1
105-647A-24R	17	1115	221.9–231.5	9.6	5.6	58.3
105-647A-25R	17	1245	231.5–241.1	9.6	8.6	90.0
105-647A-26R	17	1430	241.1–250.4	9.3	1.2	13.2
105-647A-27R	17	1630	250.4–260.1	9.7	9.6	99.4
105-647A-28R	17	1845	260.1–269.7	9.6	9.7	101.1
105-647A-29R	17	2045	269.7–279.4	9.7	9.0	92.8
105-647A-30R	17	2300	279.4–289.0	9.6	9.7	101.3
105-647A-31R	18	0115	289.0–298.6	9.6	2.8	28.9
105-647A-32R	18	0330	298.6–308.3	9.7	2.0	21.0
105-647A-33R	18	0600	308.3–318.0	9.7	2.4	24.3
105-647A-34R	18	0830	318.0–327.6	9.6	1.5	15.2
105-647A-35R	18	1030	327.6–337.2	9.6	5.1	53.1
105-647A-36R	18	1215	337.2–346.7	9.5	6.0	63.1
105-647A-37R	18	1415	346.7–356.4	9.7	5.6	58.0
105-647A-38R	18	1600	356.4–366.1	9.7	9.7	100.4
105-647A-39R	18	1745	366.1–375.7	9.6	4.1	42.9
105-647A-40R	18	1930	375.7–385.4	9.7	0.3	2.6
105-647A-41R	18	2130	385.4–395.1	9.7	8.9	92.0
105-647A-42R	18	2330	395.1–404.8	9.7	9.6	99.3
105-647A-43R	19	0130	404.8–414.5	9.7	9.4	97.2
105-647A-44R	19	0330	414.5–424.1	9.6	9.0	93.5
105-647A-45R	19	0530	424.1–433.8	9.7	4.5	46.2
105-647A-46R	19	0730	433.8–443.5	9.7	9.7	99.7
105-647A-47R	19	0930	443.5–453.2	9.7	9.3	95.8
105-647A-48R	19	1145	453.2–462.8	9.6	9.7	100.7
105-647A-49R	19	1400	462.8–472.5	9.7	9.6	98.4
105-647A-50R	19	1545	472.5–482.1	9.6	9.2	95.8
105-647A-51R	19	1745	482.1–491.8	9.7	8.9	91.7
105-647A-52R	19	1930	491.8–501.4	9.6	9.5	99.1
105-647A-53R	19	2130	501.4–511.1	9.7	9.7	99.7
105-647A-54R	19	2330	511.1–520.7	9.6	8.1	83.8
105-647A-55R	20	0130	520.7–530.3	9.6	9.7	101.0
105-647A-56R	20	0330	530.3–540.0	9.7	0.2	1.7
105-647A-57R	20	0600	540.0–549.7	9.7	0.0	0.0
105-647A-58R	20	0815	549.7–559.4	9.7	0.2	1.7
105-647A-59R	20	1130	559.4–569.1	9.7	0.5	4.6
105-647A-60R	20	1345	569.1–578.8	9.7	9.7	99.6
105-647A-61R	20	1600	578.8–588.4	9.6	0.6	6.6
105-647A-62R	20	2000	598.1–607.8	9.7	8.1	83.7
105-647A-63R	20	2130	607.8–617.5	9.7	2.5	25.7
105-647A-64R	20	2330	617.5–627.2	9.7	4.5	46.1
105-647A-65R	21	0130	627.2–636.8	9.6	4.4	45.6
105-647A-66R	21	0330	636.8–646.5	9.7	3.9	39.7
105-647A-67R	21	0545	646.5–656.2	9.7	5.0	51.0
105-647A-68R	21	0745	656.2–665.9	9.7	5.9	61.2
105-647A-69R	21	0945	665.9–675.5	9.6	0.4	4.1
105-647A-70R	21	1430	685.2–694.8	9.6	5.3	54.7
105-647A-71R	21	1900	694.8–704.5	9.7	3.9	40.2
105-647A-72R	22	0145	704.5–714.0	9.5	4.4	46.4
105-647A-73R	22	0715	714.0–723.5	9.5	9.0	94.8
105-647A-74R	22	1130	723.5–733.0	9.5	9.6	101.5
105-647A-75R	22	1600	733.0–736.0	3.0	4.6	154.3
Hole 647B						
105-647B-1H	24	0700	0.0–6.8	6.8	6.8	100.2
105-647B-2H	24	0845	6.8–16.5	9.7	10.1	104.3
105-647B-3H	24	1045	16.5–26.1	9.6	9.6	99.7
105-647B-4H	24	1215	26.1–35.8	9.7	9.9	101.9
105-647B-5H	24	1330	35.8–45.5	9.7	9.2	95.1
105-647B-6H	24	1515	45.5–55.1	9.6	9.8	102.3
105-647B-7H	24	1615	55.1–64.7	9.6	8.5	88.1
105-647B-8H	24	1815	64.7–74.3	9.6	9.2	95.5
105-647B-9H	24	2030	74.3–83.9	9.6	7.6	78.6
105-647B-10H	24	2145	83.9–93.5	9.6	7.2	75.2
105-647B-11H	24	2315	93.5–103.3	9.8	5.3	54.5

Table 2. Lithostratigraphic summary, Site 647A.

Unit	Lithology	Primary and secondary structures	Interval (mbsf)	Age	Occurrence
I	Interbedded silty clays, clayey silts, and clayey muds with scattered granules and pebbles. Biogenic carbonate, 0%–40%. Detrital carbonate, as much as 75%.	Alternation of facies on scale of centimeters to 1–2 m. Dropstones, slight color banding, and mottling. A few beds, rich in detrital carbonate, are laminated.	0–116	late Pliocene–Holocene	105-647A-1R to -12R 105-647B-1H to -11H
IIA	Silty clay underlain by nannofossil clay.	Homogeneous.	116–119	late Miocene	105-647A-13R-1 to 105-647A-13R-2, 148 cm
IIB	Silty clay and clay with iron-manganese-phosphate nodules.	Homogeneous, except some nodules.	119–135.4	early Miocene	105-647A-13R-2, 148 cm to 105-647A-14R, base
IIIA	Nannofossil clay (claystone) and nannofossil ooze (chalk).	Moderately to strongly bioturbated; color banding.	135.4–212.3	early Oligocene	105-647A-15R to 105-647A-22R
IIIB	Clayey diatomite, clayey nannofossil diatomite, and nannofossil diatomaceous claystone.	Same as above.	212.3–241.1	early Oligocene	105-647A-23R to 105-647A-25R
IIIC	Nannofossil claystone.	Same as above, with carbonate concretions.	241.1–530.3	middle Eocene–early Oligocene	105-647A-26R to 105-647A-55R
IV	Claystone.	Moderately to weakly bioturbated. Alternation of reddish and greenish intervals.	530.3–699	early–middle Eocene	105-647A-56R to 105-647A-71R-2, 75 cm

silty upper part of Unit I (Fig. 14), and occur throughout intervals containing scattered gravel-sized clasts. The second occurrence is characterized by detricarbonate silty clay or clayey silt (carbonate content as much as 75%), which may display distinct physical sedimentary structures, most notably parallel lamination. The stratigraphic position of such beds in Hole 647A is plotted in Figure 13. These beds have sharp bases and grade upward into a more homogeneous, burrowed top. A shipboard X-radiograph of a thin slab (Fig. 16) shows a detricarbonate bed about 20 cm thick that consists of thinner, graded, very fine sand and silt layers with fine internal laminations. Individual graded units are <3 cm thick. The carbonate in all detricarbonate units has a calcite/dolomite ratio of about 1.5:1.0.

Hole 647B contains more numerous and better-preserved examples of the laminated, detricarbonate silty clay and clayey silt beds. Table 3 lists locations of these beds. The beds have sharp bases and commonly overlie (1) nannofossil-foraminiferal silty clays or (2) silty muds, having scattered gravel-sized clasts and visible foraminifers in their upper part.

All facies in Unit I, except the laminated detricarbonate silty clay layers, may contain variable amounts of sand- and gravel-sized material, grading to cobble size (Fig. 13). Core 105-647A-11R contains the most pebbles in Hole 647A: eight pebbles with diameters of 1–5 cm. White and dark silt or sand pockets (Fig. 17) and soft mud clasts are also observed. This material occurs mainly in the clayey muds and clayey silts, either dispersed or concentrated within distinct intervals. Pebbles consist of a variety of lithofacies, including granite, diorite, basalt, limestone, gneiss, quartzite, and amphibolite.

According to examination of approximately 70 smear slides from Hole 647A, the sand- and silt-sized terrigenous fraction of the sediments consists primarily of quartz (as much as 50%), detrital carbonate (as much as 50%), and small amounts of feldspar (plagioclase and microcline). Accessory minerals include glauconite (as much as 5%), pyrite (as much as 2%), garnet, tourmaline, amphibole, zircon, epidote, green and brown biotite, and white mica.

Throughout Unit I, the proportion of biogenic-rich sediments varies little. The overall texture, however, is siltier (Fig. 41, "Summary and Conclusions" section, this chapter), having more sand-size grains and detrital carbonate, in the upper middle part of Unit I. On the scale of single cores, intervals containing gravel and those rich in biogenic constituents appear to alternate cyclically but irregularly (Fig. 13). APC cores from Hole 647B indicate that laminated, detricarbonate beds are also an important part of the lithologic cyclicity.

Unit II: Hole 647A (Cores 105-647A-13R to 105-647A-14R), early to late Miocene, 116.0–135.4 mbsf

Unit II is a condensed stratigraphic sequence, which probably includes surfaces of nondeposition. The unit ranges in age from early to late Miocene ("Sediment-Accumulation Rates" section, this chapter). No middle Miocene sediments have been identified ("Biostratigraphy" section, this chapter). The varying lithofacies (Fig. 18) consist of silty clay, nannofossil clay, and brown, yellow, and green clay (Fig. 12). The upper contact of the unit is between Cores 105-647A-12R and 105-647A-13R and is defined by a hiatus and change in lithofacies from upper Pliocene, gray, silty clays and muds of Unit I to upper Miocene, mottled, olive-yellow, silty clays and nannofossil clays of Unit II (Fig. 18). The base of Unit II is in the unrecovered interval between Cores 105-647A-14R and 105-647A-15R and is defined by the change in lithofacies from the condensed sequence of silica-bearing clays to the Oligocene nannofossil-bearing clays of the underlying Unit III.

Unit II is subdivided at 119 mbsf (Section 105-647A-13R-2, 148 cm) into two subunits based on the nature of the biogenic constituents. Subunit IIA contains a significant proportion of nannofossils, whereas Subunit IIB lacks carbonate microfossils but locally contains as much as 15% biosiliceous material. Subunit IIB is also distinguished by the presence of concretionary nodules (Fig. 19) in its upper part. The precise composition of these nodules is not known, but probably includes phosphates and iron and manganese oxides.

Subunit IIA is characterized by two lithofacies (Fig. 18): an olive-yellow silty clay in the upper 40 cm of Section 105-647A-13R-1 and an underlying light yellowish brown nannofossil clay with scattered black grains (iron/manganese nodules) that increase in abundance toward the base (Sections 105-647A-13R-1, 40 cm, to 105-647A-13R-2, 148 cm). Both lithofacies are moderately burrowed and mottled but otherwise homogeneous. The silty clay contains approximately 70% clay, 25% quartz silt grains, and minor amounts of plagioclase feldspar, mica, pyrite, and a trace of zeolite. The nannofossil clay also contains about 70% clay, 25% nannofossil remains, and minor amounts of quartz, mica, pyrite, and a trace of foraminifers.

Subunit IIB is likewise characterized by two lithofacies (Fig. 18). The upper facies consists of an olive-yellow silty clay to diatom- and spicule-bearing silty clay with dark-gray banding. The silty clay becomes increasingly enriched in diatoms and spicules with depth. This lithofacies consists of 65%–75% clay and as much as 30% quartz, traces of feldspar, mica, and pyrite, and

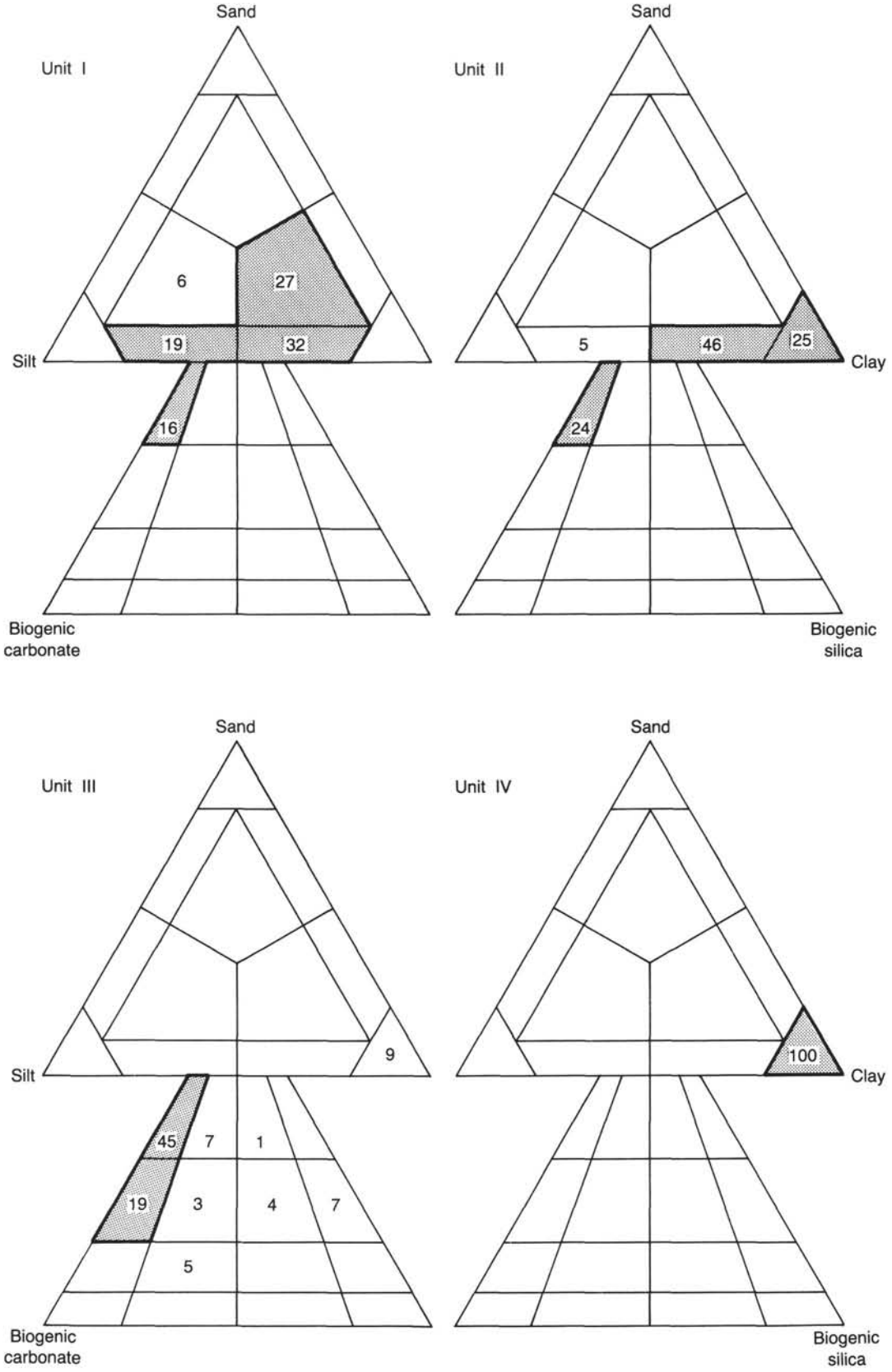

Figure 12. Percentages of recovered sediment from Hole 647A that were assigned to each of the lithologic categories recognized in the classification scheme. The more common lithologies are outlined with a bold line and are stippled. Many of the sediments classified on the terrigenous diagram have biogenic contents of from 10% to 25% and therefore have a name that includes a modifier like "nannofossil bearing."

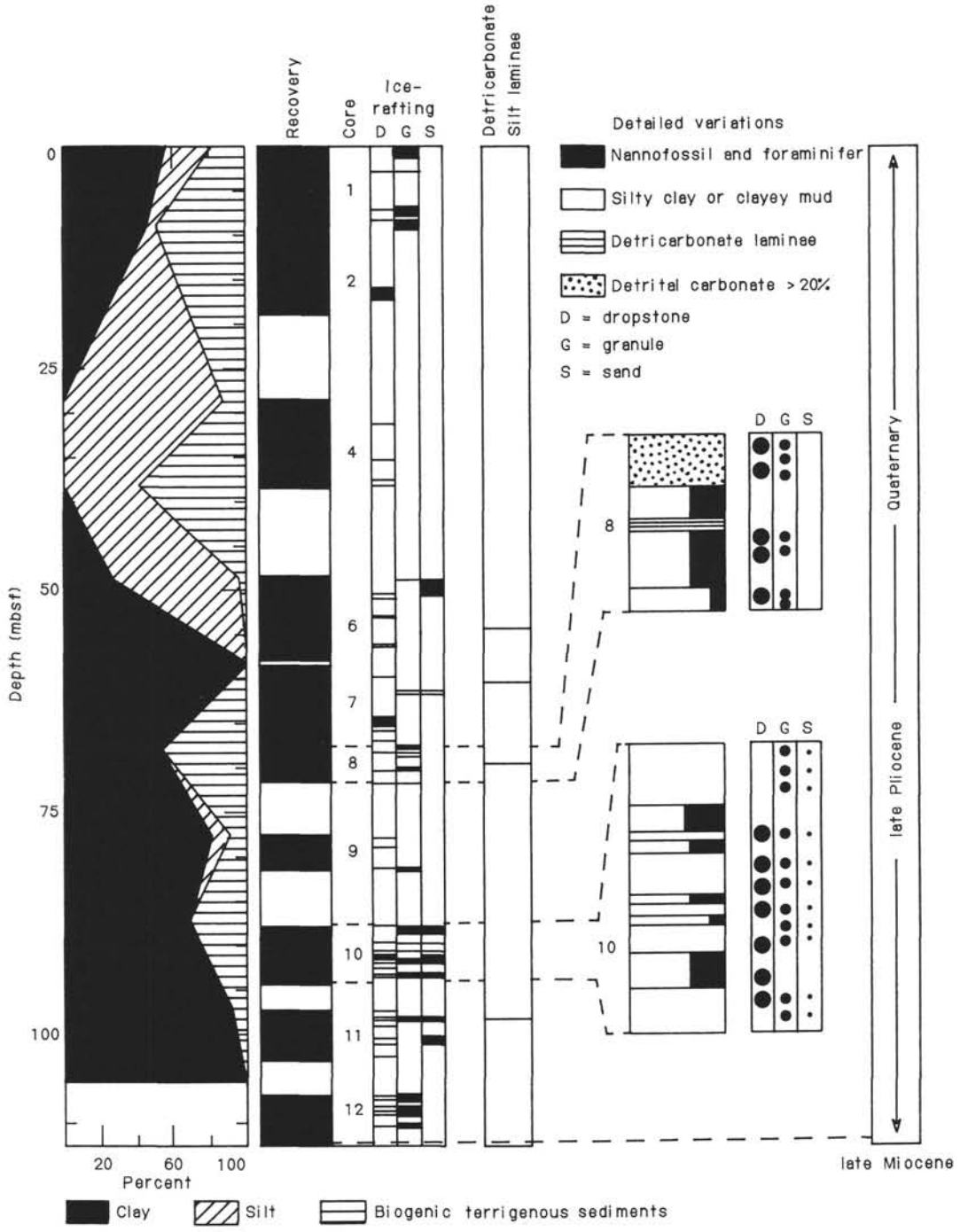

Figure 13. Summary of lithologic variations in Unit I, Hole 647A. The column on the left shows the percentages in single cores of clay-rich lithologies, silt-rich lithologies, and biogenic-rich lithologies. Other columns show the following data: recovery; occurrence of cobbles (D), granules (G), and sand (S); occurrence of laminated detricarbonate silty clays and clayey silts; and details of lithologic variations in Cores 105-647A-8R and 105-647A-10R.

as much as 15% biosiliceous material. No biogenic carbonate was observed in smear slides.

Granule-size nodules (manganese/iron oxides) scattered in variable concentrations throughout the silty clay impart a salt-and-pepper appearance to the sediment. Toward the base, the nodules become both larger and fewer. The largest nodule (Section 105-647A-14R-1, 45 cm; Fig. 19) is a multiple-rimmed concretion, 3.5 cm in diameter. It consists of a nucleus, containing cracks filled with a green clay, and a botryoidal outer zone containing multiple laminations of green clay and black manganese/iron oxides.

The lithofacies at the base of Subunit IIB is grayish green clay, moderately burrowed and mottled but otherwise homogeneous. The sediment contains as much as 90% clay minerals and minor amounts of quartz silt, mica, and accessory minerals. Small amounts of biosiliceous material also occur; biogenic

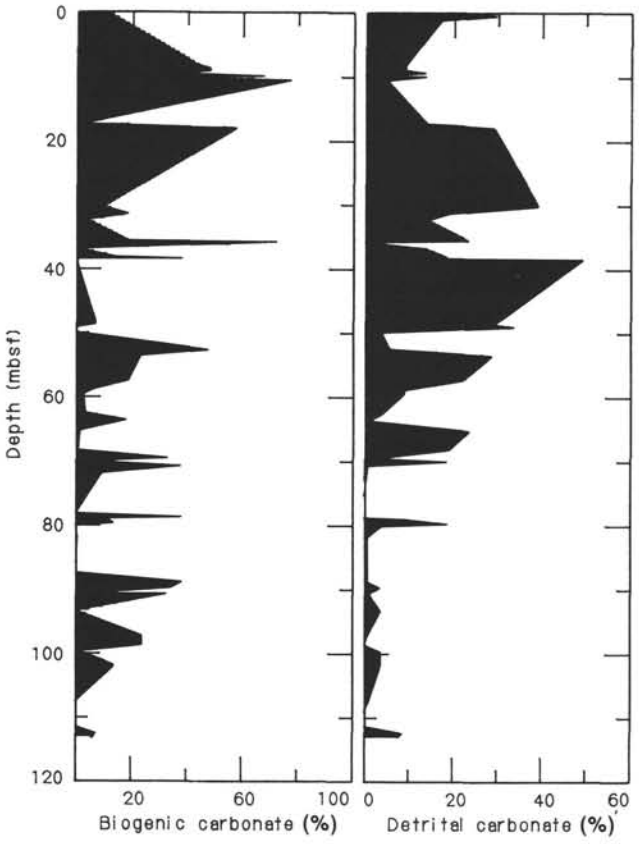

Figure 14. Biogenic carbonate and detrital carbonate content from smear slides, Hole 647A. Smear slide estimates of biogenic carbonate were found to be too high, on the basis of comparison with carbonate-bomb data. Maximum values should be in the range of 40%–50%.

carbonate does not. The lack of biogenic carbonate distinguishes the basal sediments of this subunit from the underlying Unit III.

Unit III Hole 647A (Cores 105-647A-15R to 105-647A-55R), early Oligocene to middle Eocene, 135.4–530.3 mbsf

The top of Unit III is marked by the first occurrence of nannofossil clays below the condensed sequences of Unit II. This boundary is between Cores 105-647A-14R and 105-647A-15R. A hiatus may also occur between these cores, the top of Unit III being probably early Oligocene and certainly no younger than early late Oligocene ("Biostratigraphy" section, this chapter). The base of Unit III is defined as the lowest occurrence of sediments with >25% biogenic constituents and occurs between Cores 105-647A-55R and 105-647A-56R (Fig. 41). Low recovery characterizes this boundary area. The average recovery, on the basis of comparison of total length of sediments described and total thickness of the unit, is 57% (this is not the same as the official ODP average recovery).

Most sediments in Unit III contain 25%–50% biogenic constituents (Fig. 12) and are therefore biogenic clays and clayey oozes. For the entire unit, biogenic carbonate content exceeds biogenic silica content (Fig. 41). In detail, however, the unit can be subdivided into intervals with different biogenic carbonate to biogenic silica ratios. Subunit IIIA (Cores 105-647A-15R to 105-647A-22R, 135.4–212.3 mbsf) contains both nannofossils and diatoms at a carbonate to silica ratio averaging about 2:1. Subunit IIIB (Cores 105-647A-23R to 105-647A-25R, 212.3–241.1 mbsf) contains almost no biogenic carbonate (Fig. 12) but contains 25% to >50% diatom skeletons and sponge spicules. Subunit IIIC (Cores 105-647A-26R to 105-647A-55R, 241.1–530.3 mbsf) contains essentially no biogenic silica but is rich in nannofossils and, locally, foraminifers. Except for differences in the identity of biogenic components, however, the lithofacies in Unit III are similar, being moderately to strongly bioturbated biogenic clay (claystone) or clayey ooze (chalk or diatomite). The color of the sediments is, with the exception of the glauconite-rich layers, shades of greenish gray and light greenish gray. The lighter colored sediments contain the most biogenic carbonate.

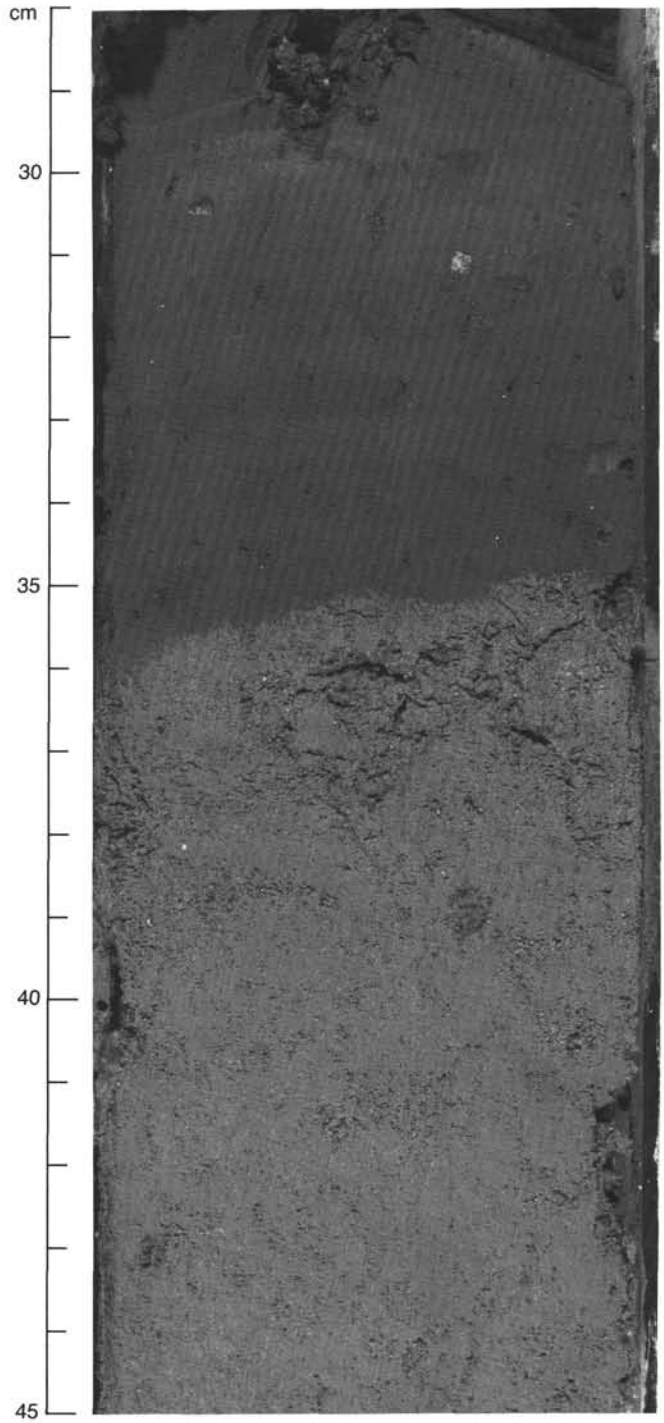

Figure 15. Light-gray nannofossil-foraminifer silty clay with sharp top. Nannofossils are depleted in the upper few centimeters (35.5–45 cm). Interval shown is Sample 105-647A-10R-3, 28–45 cm.

Figure 16. X-radiograph of a thin slab showing the basal part of a sharp-based detricarbonate bed about 20 cm thick that consists of graded intervals based by very fine sand or silt. Sediment shows fine internal laminations. Dark spots are not granules but are authigenic iron-sulfides. Interval shown is Sample 105-647A-11R-1, 50–62 cm.

Table 3. Location of laminated detricarbonate beds, Hole 647B.

Section	Interval (cm)
105-647B-2H-3	5–25
105-647B-3H-3	34–44
105-647B-3H-4	36–54
105-647B-4H-1	74–83
105-647B-5H-5	60–80
105-647B-5H-6	85–105
105-647B-6H-3	88–93
105-647B-6H-4–5	145(S4)–6(S5)
105-647B-7H-3	61–81
105-647B-7H-4	37–50
105-647B-7H-5	17–25
105-647B-7H-6	21–52
105-647B-8H-3–4	141(S3)–14(S4)
105-647B-8H-5	0–6
105-647B-9H-3	56–85
105-647B-9H-4	98–120

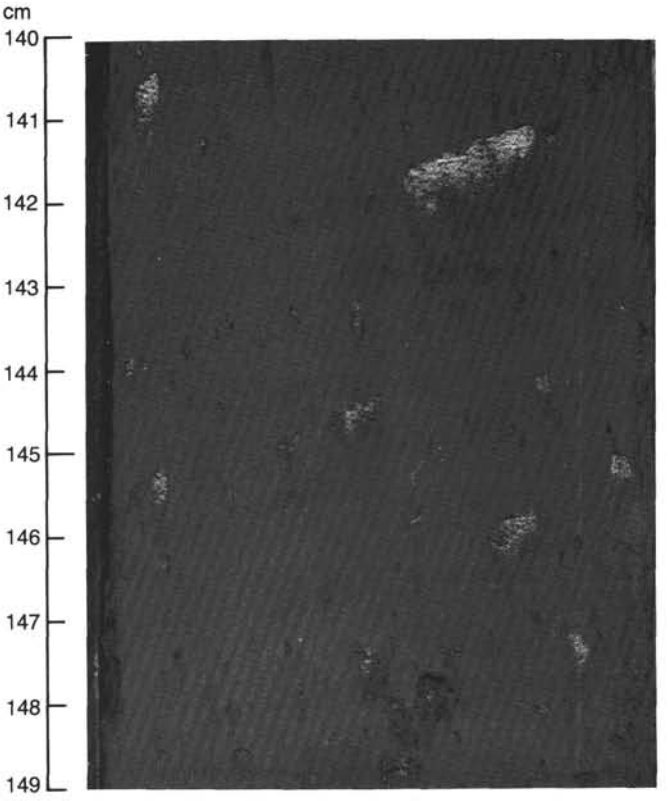

Figure 17. Dark-gray silty clay with scattered granules and sand pockets. Interval shown is Sample 105-647A-10R-2, 140–149 cm.

Burrows, generally darker gray than the surrounding sediments, are predominantly horizontal to subhorizontal *Planolites, Cylindrichnus*, and *Zoophycos* (Figs. 20 and 21) and give the sediment a laminated aspect.

In several places, fine-scale color lamination was identified as a diagenetic feature (Liesegang bands), having no sedimentological implications. In terms of overall diagenesis, sediments below about 165 mbsf are sufficiently indurated to be called claystones, chalks, and diatomites.

Terrigenous components are almost exclusively clays. Authigenic minerals are prevalent, the most common being glauconite, which is concentrated in grayish green bands and in some burrows (Fig. 21). Pyrite occurs as both burrow replacements and nodules as much as about 1 cm in diameter. In some intervals, black smears of monosulfides characterize the sediment. Below about 280 mbsf, white to pale-yellow carbonate concretions (mainly dolomite) become common. This authigenic carbonate acts as a cement in pores of the clayey sediments. In one place, elongate crystals of gypsum are associated with one of the concretions (Fig. 22).

Primary compositional lamination is rare in Unit III and reflects changes in the content of biogenic skeletons. A few intervals show contorted burrows and intraformational brecciation, resulting from either rare downslope movements or deeper deformation. Evidence of such deformation comes from several structural features exhibited by Unit III. Below about 230 mbsf, intact sections of core contain healed microfaults (Fig. 23). Below about 450 mbsf, planar fractures that cut the core commonly exhibit slickensides. These fractures are both faults of minor offset and joint surfaces. Below depths of about 350 mbsf, the original bedding, defined by orientation of burrows, local lamination, and burrow flattening, dips at angles of as much as about 40° (Fig. 23), even in long unbroken sections of

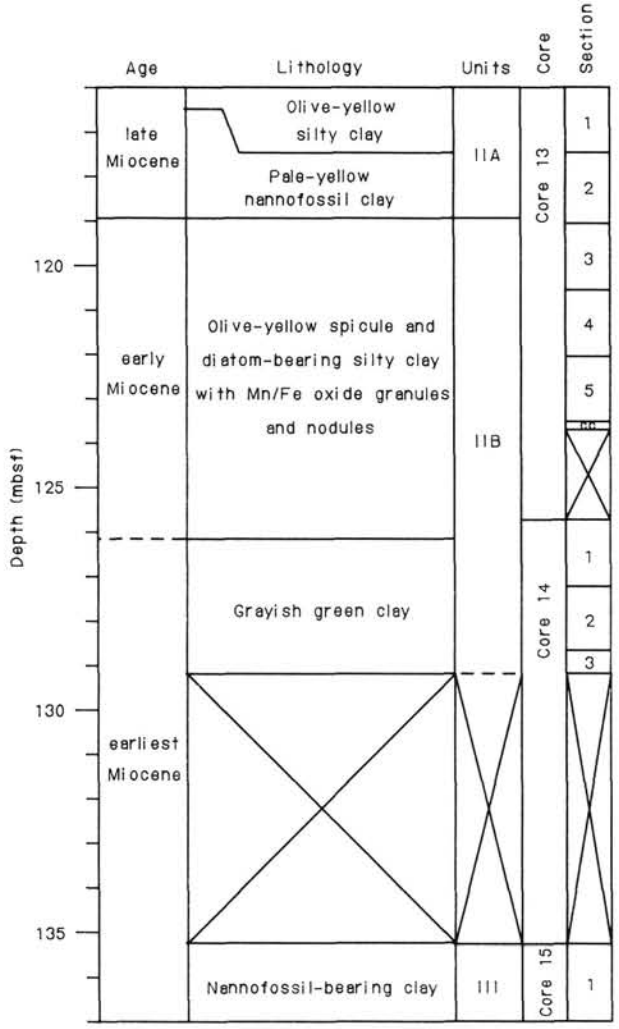

Figure 18. Schematic lithostratigraphic diagram of Unit II, Cores 105-647A-13R and 105-647A-14R.

core that cannot be rotated drilling biscuits. In some places, the maximum apparent dip varies from core to core, suggesting that the section is not just tilted but is broken by faults into blocks with differing orientations.

Unit IV Hole 647A (Cores 105-647A-56R to 105-647A-71R), early to middle Eocene, 530.3–699 mbsf

The top of Unit IV is marked by a net decrease in nannofossil and foraminifer content (Fig. 41, "Summary and Conclusions" section, this chapter) and the first appearance of dusky red to weak red foraminifer-nannofossil-bearing claystone. This contact is not precisely placed because of poor recovery through Cores 105-647A-56R to 105-647A-61R (9% recovery in 58 m of drilling). The base of Unit IV is the contact between sediments and basalts of layer 2. Drilling records show that drilling rate decreased sharply at 699 mbsf, which must represent the top of the basalt sequence.

Most sediments in Unit IV are claystones or foraminifer-nannofossil-bearing claystones (Fig. 12). At the top of the unit, particularly in Core 105-647A-62R, foraminifers are scattered throughout the sediment and are locally concentrated in thin (about 1 cm) layers that may contain as much as about 30% $CaCO_3$ (from carbonate-bomb data).

The most striking characteristic of Unit IV is the alternation of dusky red and light-red claystones with greenish gray claystones having violet shades at the red/green contacts; the result

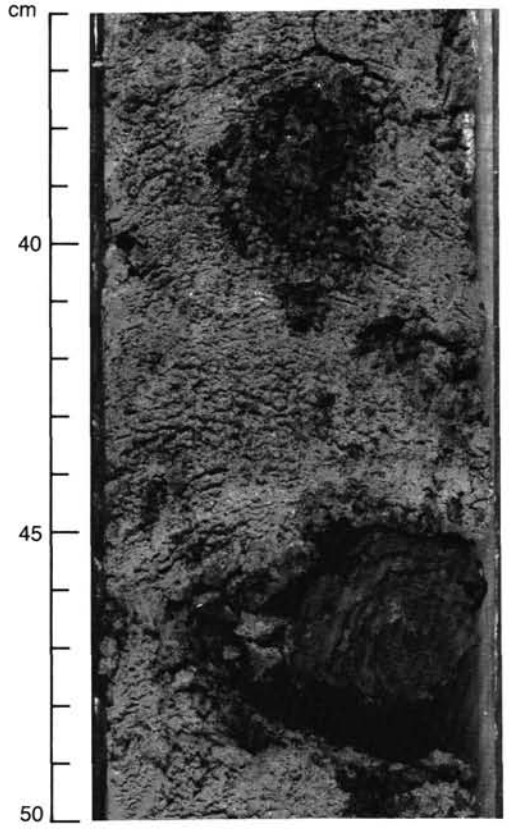

Figure 19. Concentrically banded concretions, the largest being 3.5 cm in diameter (45–48 cm). The contact between the pale-olive-yellow spicule-diatom-bearing silty clay and the underlying grayish green clay occurs at 58 cm. Interval shown is Sample 105-647A-14R-1, 36–50 cm.

is prominent color banding (Sections 105-647A-64R-3, 105-647A-65R-2, and 105-647A-65R-3 and Cores 105-647A-66R and 105-647A-68R). Red claystones are less disturbed by drilling than are the greenish ones. Claystones are slightly to moderately bioturbated; burrows are often flattened in the horizontal plane. In some places, the flattening is severe (inhomogeneous strain), and the sediment has a strong planar fabric. Unit IV also has scattered carbonate concretions, generally as much as 4 cm in diameter; larger concretions cut by the rotary bit, as much as about 15 cm in thickness, are observed in Cores 105-647A-64R, 105-647A-66R, and 105-647A-67R. In some places, the concretions contain chert; one concretion contains gypsum crystals (Section 105-647A-67R-1).

Terrigenous components of Unit IV are almost exclusively clay minerals. Authigenic minerals include iron oxides, as much as 30% in some dark-brown or dusky red claystones. Pyrite and glauconite are very minor constituents.

Joints and slickensided fault surfaces cut the cores at closely spaced intervals (several per section). In the lowermost cores in Unit IV, such fracture surfaces are commonly lined with, or surrounded by envelopes of, calcite or quartz (Fig. 24). The alteration around these fractures is similar to alteration by hydrothermal fluids just above the contact with the basalts (Fig. 25; "Basement Rocks" section, this chapter).

Interpretation

Unit I

Unit I is dominantly terrigenous, having some intervals relatively rich in planktonic microfossils, mostly nannofossils and foraminifers. The alternations between facies containing peb-

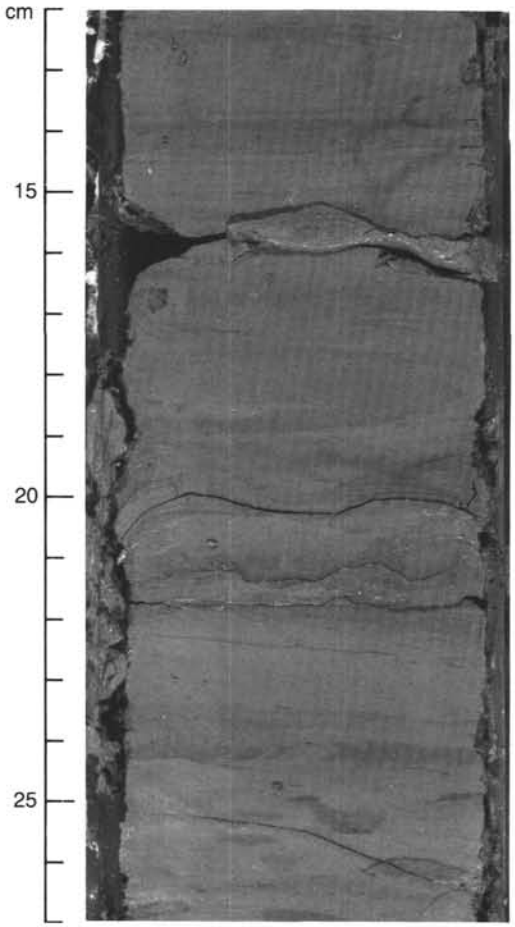

Figure 20. Greenish gray clayey nannofossil chalk. Horizontal burrows flattened by compaction give a laminated aspect to the core. Interval shown is Sample 105-647A-32R-2, 12–27 cm.

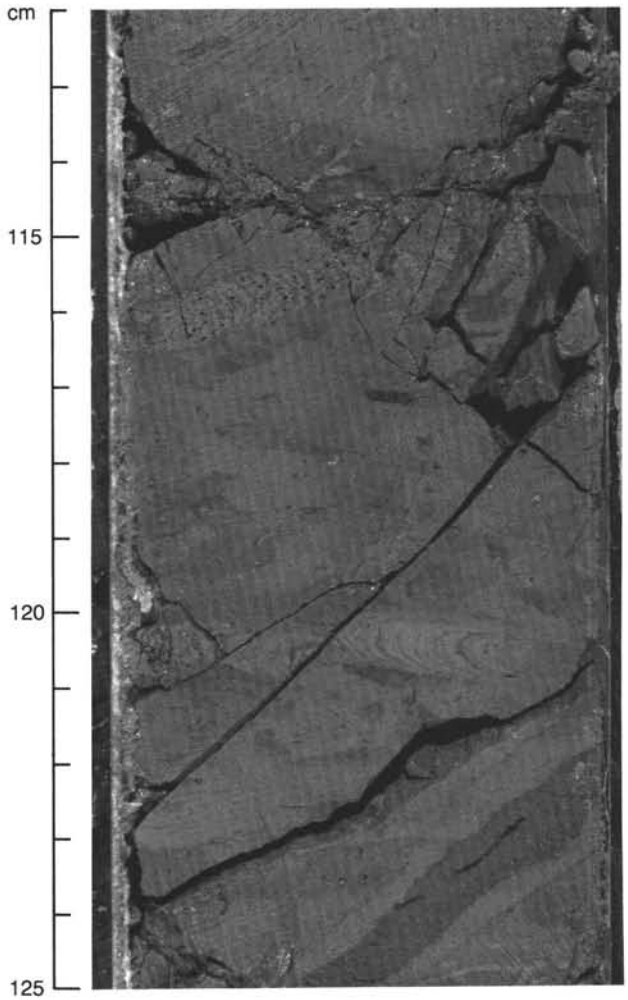

Figure 21. Greenish gray, clayey diatomaceous nannofossil ooze, strongly bioturbated. Glauconite pellets are contained in a *Zoophycos* trace at 116 cm. Interval shown is Sample 105-647A-20R-2, 112–125 cm.

bles and biogenic-rich intervals (Fig. 13) may reflect dissolution and dilution of microfossils or variations between glacial (biocarbonate-poor and pebbly) and interglacial (biocarbonate-rich) climatic stages. Warmer surface waters during interglacial stages may have encouraged a higher rate of biogenic productivity in surface waters, leading to an increased flux of biogenic skeletons to the seafloor. Variations in the production and chemistry of bottom water under different climatic regimes, however, may also have led to varying intensity of dissolution. Cyclicity such as that shown by Unit I characterizes open-ocean North Atlantic sediments formed during the late Pliocene and Pleistocene (Roberts, Schnitker, et al., 1984).

Terrigenous components of all sizes were probably brought to the site by icebergs (Molnia, 1983). Clay-sized components may also have been carried by weak bottom currents as part of a slow-moving nepheloid layer, perhaps the same currents that built Gloria Drift just north of Site 647. No clear primary physical structures are preserved in most of the sequence, perhaps a result of repeated turnover by burrowers. Nevertheless, some evidence of bottom-current winnowing appears at the top of some nannofossil-foraminiferal muds: the tops of these units are sharp, and nannofossils are depleted in the uppermost few centimeters. We interpret these sharp tops as being surfaces of nondeposition and current sorting, the fine-grained nannofossils being preferentially transported away from the site.

The sharp-based, commonly unburrowed, detricarbonate silty clays and clayey silts, some containing a fine sand fraction and showing parallel lamination, are interpreted as being composite turbidite beds. Individual layers (about 1–3 cm thick) are

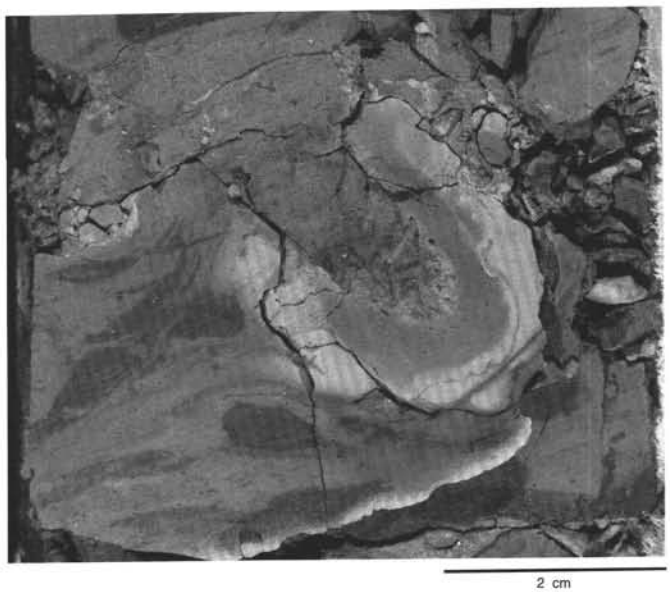

Figure 22. Greenish gray nannofossil claystone with lighter carbonate concretion, horseshoe shaped, containing acicular crystals of gypsum. Interval shown is Sample 105-647A-49R-4, 129–134 cm.

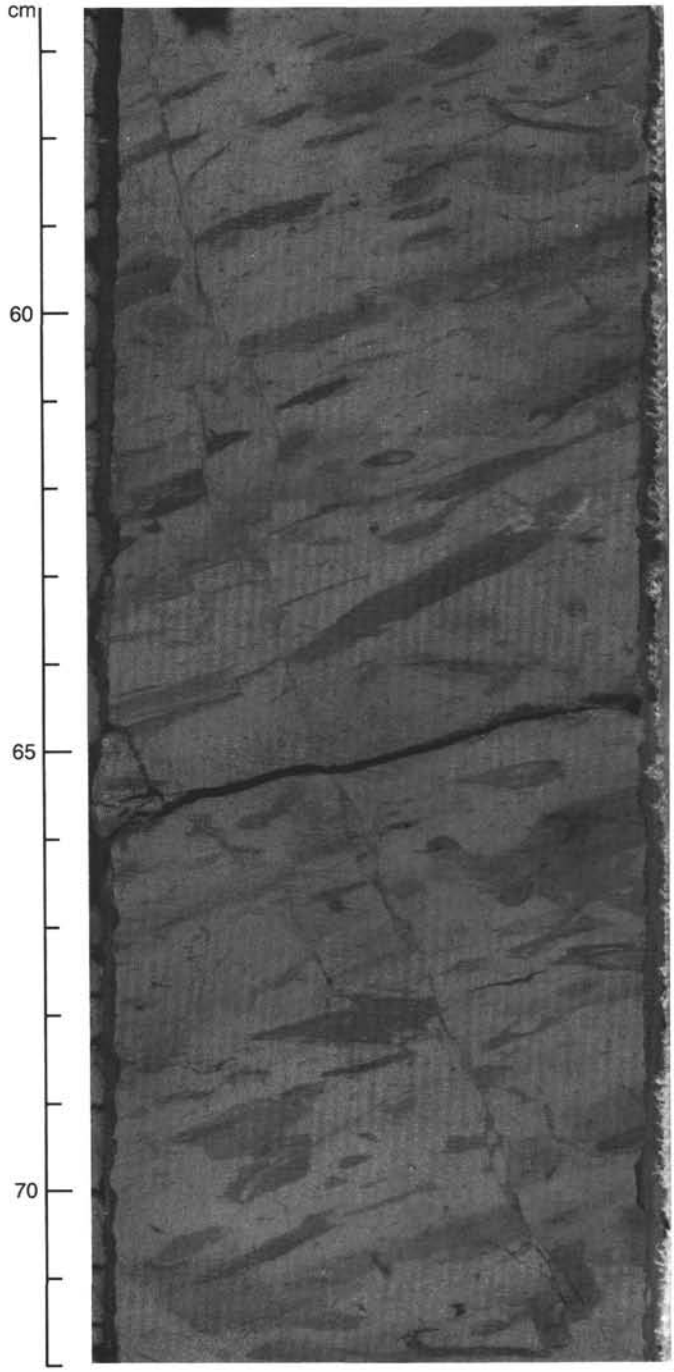

Figure 23. Greenish gray nannofossil claystone, moderately bioturbated, showing a long, subvertical, healed microfault and a bedding dip of about 25°. Interval shown is Sample 105-647A-49R-6, 57–72 cm.

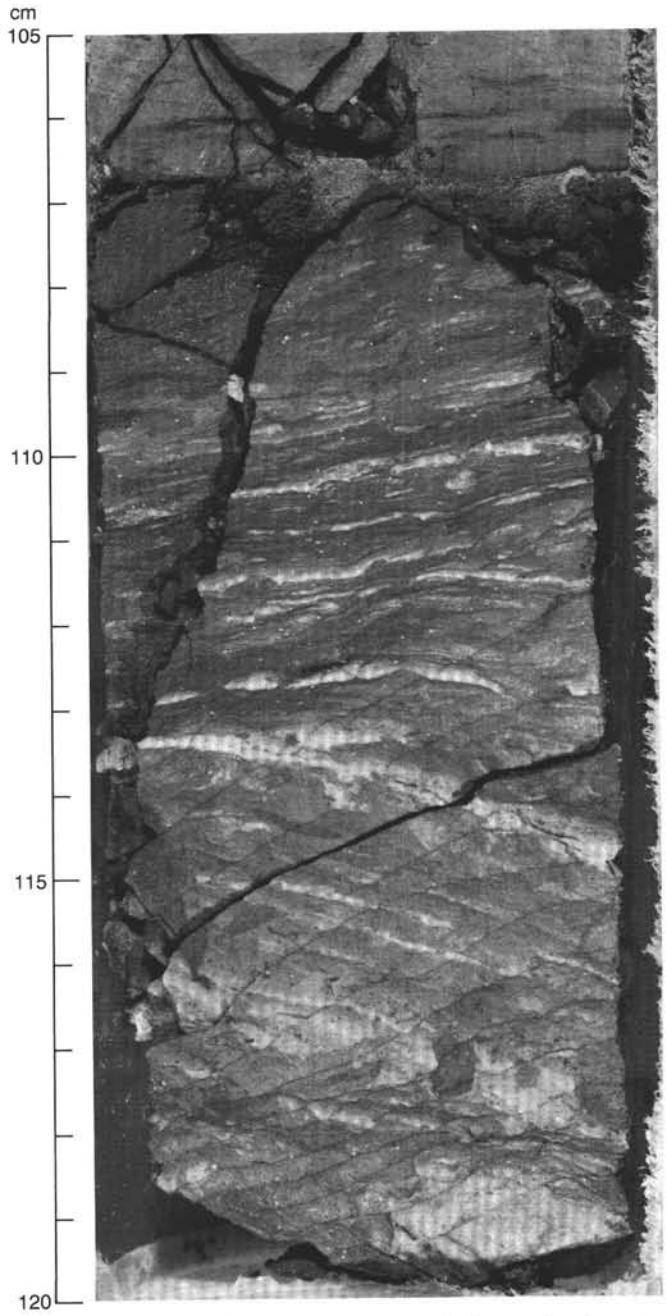

Figure 24. Subhorizontal quartz veins in a band of pervasive alteration associated with fractures in Unit IV. Note the inclined fracture cleavage that postdates vein emplacement. Interval shown is Sample 105-647A-70R-3, 105–120 cm.

graded, as is the entire composite bed, the coarsest grained turbidites being at the base. The mineralogy of these beds, and their internal structures are analogous to similar beds recovered at Site 646, suggesting that they represent spillover facies from the NAMOC. NAMOC is located only 30 km west of the site. According to Chough and Hesse (in press), NAMOC turbidites are rich in detrital carbonate, and NAMOC was most active during glacial episodes. From preliminary observations at Hole 647B, the biogenic carbonate content of the lithologies that immediately underlie the laminated detricarbonate beds appears to increase upward toward the sharp base of these beds. This observation suggests that vigorous spillover from NAMOC occurred after the beginning of postglacial climatic warming and not during the glacial maxima. We therefore tentatively associate periods of major activity of NAMOC with times of deglaciation and climatic amelioration.

Detrital carbonate is also dispersed in all major lithologies of Unit I. The highest percentages are in nonbiogenic intervals. This detrital carbonate may have been carried to the site by icebergs from Baffin Bay. At Site 645, Subunit IB is rich in detrital carbonate of inferred ice-rafted origin. Icebergs calving from

the same glaciers in northern Baffin Bay could easily have passed over Site 647 and dropped material of the same mineralogy.

Unit II

The sediments of Unit II are a complicated series of remnant and condensed sequences that incompletely represent the transition from the hemipelagic nannofossil and biosiliceous clays of Unit III (Oligocene to middle Eocene) to the interbedded terrigenous and biogenic clays of the glacial Pliocene–Pleistocene. Overall, Unit II consists of an upper Miocene remnant of hemipelagic sediment (nannofossil clay) and an upper to lower Miocene condensed sequence (Fig. 18).

The basal lithology of Unit II, a grayish green clay, may also represent a condensed transition to the hemipelagic nannofossil-bearing sediments of Unit III. The absence of biogenic carbonate, in contrast to the sediments of Unit III immediately below, suggests that changing deep-water flow, possibly with concomitant intensification of dissolution, may have begun during the deposition of this sediment. The basal clay of Unit II is characterized by minor biosiliceous content and slight burrowing. These features suggest deposition by predominantly pelagic and nepheloid-layer processes associated with weak bottom currents moving over an oxygenated seabed.

Resting immediately above the basal clay is a diatom- and spicule-bearing silty clay, distinguished by prominent iron/manganese oxide granules and nodules. The concentrically zoned nodules (Fig. 19), which may also contain phosphates, suggest very low rates of sediment accumulation and are similar to those found associated with other major unconformities (Jehanno et al., 1984). Apparently, the nodule-bearing silty clays of Subunit IIB represent a condensed section deposited slowly, probably with several breaks, between the early Miocene and the late Miocene ("Sediment-Accumulation Rates" section, this chapter).

Immediately overlying the condensed section of Subunit IIB is a 2.6-m remnant of upper Miocene, hemipelagic, nannofossil clay (Subunit IIA), showing slight burrowing; manganese/iron oxide granules decrease in abundance moving upward through the lower part of Subunit IIA. The presence of nannofossil clay suggests a period of relatively normal hemipelagic deposition subsequent to the frequent periods of nondeposition and/or erosion that characterized early to late Miocene time. The decreasing size of manganese/iron nodules through the basal part of the sequence also suggests an increasing rate of sediment accumulation, probably because of a long-term decrease in the strength of bottom currents. The origin of the bottom currents is unclear but may be associated with opening of the Charlie Gibbs Fracture Zone during early to late Miocene time, allowing efficient penetration of deep bottom waters to the site.

The unconformity between upper Miocene sediments and the upper Pliocene/Pleistocene glacial sequence occurs between Cores 105-647A-12R and 105-647A-13R, the first dated interval below the unconformity being 40 cm below the top of Core 105-647A-13R. The onset of major northern hemisphere glaciation at 2.4 m.y. (Shackleton et al., 1984) coincides with the age determined for the base of Unit I ("Sediment-Accumulation Rates" section, this chapter). Therefore, the unconformity between Units I and II may represent a prolonged period of nondeposition and/or erosion associated with an intensification of bottom-water flow driven by the deteriorating climatic regime of the early Pliocene.

Unit III

The relatively high amount of terrigenous clay, averaging >50%, relegates the sediments of Unit III to the category of hemipelagic sediments. This conclusion is consistent with the relatively high sedimentation rate of about 40 m/m.y. ("Sediment-Accumulation Rates" section, this chapter). The clay was probably supplied from both North America and Greenland, with weak bottom currents transporting a dilute, suspended load to the site.

Calcareous and siliceous biogenic components characterize Subunit IIIA, whereas Subunit IIIB contains only siliceous biogenic components, indicating either (1) no primary production of calcareous biogenic components or (2) dissolution of carbonate skeletons, either in the water column, on the seafloor, or in the shallow subsurface. If the dissolution rate exceeded the sedimentation rate, then the carbonate compensation depth (CCD) must have been shallower than this site's water depth. Throughout Subunit IIIC, no siliceous biogenic components are found. That no primary production occurred seems rather unlikely. Instead, biogenic silica probably dissolved during diagenesis.

Extremely thin laminae, consisting of color variations with very sharp boundaries, are interpreted as being Liesegang bands. These color bands also surround burrows, mimicking the shape of the burrow, and probably relate to pore-water migration, leading to precipitation along chemical fronts of sulfides or manganese oxides. The burrows probably contained organic material, which produced a slightly different geochemical environment (e.g., different pH and Eh). Carbonate concretions, mainly dolomite, pyrite nodules, and glauconitic bands and fecal pellets, indicate diagenetic reactions involving oxidation/reduction and dissolution/reprecipitation. Carbonate precipitation was probably controlled by subtle variations in composition or by chemical gradients around dispersed organic matter.

The microfractures observed below about 230 mbsf (in lower Oligocene and older rocks); the joints and faults, often with slickensides, below 450 mbsf; and the dips of as much as 40° below about 350 mbsf suggest an episode of tectonic faulting. In the seismic sections, no major faults are identified; the scale of faulting is therefore thought to be less than the resolution of seismic profiles (i.e., about 20 m). The reason for this faulting is unresolved but may be the result of differential compaction or subsidence of the underlying basaltic basement. It is noteworthy, however, that sediments younger than the cessation of seafloor spreading in the Labrador Sea (early Oligocene; Srivastava et al., 1981) are not affected by the faulting.

Unit IV

The basal sediment sequence at this site rests on basaltic crust and is distinguished by its intense red and green banding, high content of authigenic iron oxides, and hydrothermal alteration.

Unit IV was deposited in a hemipelagic regime at relatively low sediment-accumulation rates. The absence of primary physical structures precludes firm conclusions concerning the operation of bottom currents, but the presence of bioturbation indicates deposition under oxygenated bottom water. The generally low and variable content of biogenic carbonate suggests variable productivity in surface waters and/or dissolution on, or below, the seafloor.

A high degree of diagenetic activity is displayed in Cores 105-647A-64R to 105-647A-68R, where iron-oxide-bearing claystones, dolomite concretions, and some chert and gypsum crystals are observed. These occurrences differ significantly from the hydrothermal quartz and calcite found in the sediments directly overlying the basement rocks (Cores 105-647A-70R and 105-647A-71R). These quartz and calcite associations appear to be influenced directly by hot fluids emanating from the basement ("Basement Rocks" section, this chapter), whereas the diagenetic mineral assemblage in Cores 105-647A-64R to 105-647A-68R is more probably associated with uncommonly low sedimentation rates ("Sediment-Accumulation Rates" section, this chapter). Postdepositional compaction was locally severe in Unit IV, perhaps in association with incipient fracture formation and dewatering. Differential movements in the basement

during its cooling and movement away from the ridge crest probably faulted and tilted the strata.

Similarities to Site 112

Results from Site 647 can be compared to earlier cores taken at Site 112, Leg 12, in the Labrador Sea (Laughton, Berggren, et al., 1972). In Hole 112, the five recognized lithologic units are of similar age to Units I through IV and similarly rest on basaltic basement (revised age assignments of Miller et al., 1982, and Berggren and Schnitker, 1983, are used in the following discussion). From the top to the base, the sedimentary units are as follows:

Unit 5. middle Pliocene to Pleistocene gray terrigenous silty to muddy clay with ice-rafted pebbles, interbedded with hemipelagic silty nannofossil clay and marl (115 m thick). The sedimentation rate in the Pleistocene was about 45 m/m.y.

Unit 4. lower Pliocene gray, pelagic, silty to sandy foraminiferal nannofossil marl and ooze and an intercalation of terrigenous sandy clay (about 35 m thick).

Unit 3. lower to upper Oligocene and upper lower to middle Miocene gray, pelagic, burrow-mottled, siliceous nannofossil clay and silt and siliceous ooze (about 220 m thick). Miocene sediments are bounded by unconformities.

Unit 2. middle Eocene to lower Oligocene indurated gray, pelagic, nannofossil clay and marl, burrow mottled with an intercalation of burrowed dusky red clay (about 270 m thick). Sedimentation rates in this part of the sequence were about 15 m/m.y.

Unit 1. lower Eocene (originally specified as Paleocene(?), but < 56 Ma) indurated red clay and claystone and two palagonite sills, each only a few centimeters thick (about 45 m thick).

Site 112 penetrated all but the lower 200 m of a mound-shaped sediment body (Gloria Drift), interpreted by Davies and Laughton (1972) as being a ridge molded by thermohaline bottom currents. Evidence of bottom currents includes broken and hydraulically sorted diatom valves. Inferred turbidite beds at Site 112 are rich in detrital dolomite.

The upper Pliocene–Pleistocene sections at Sites 112 and 647 are similar in both facies and thickness (both about 115 m thick). No lower Pliocene sediments were recovered at Site 647. The Miocene sections at the two sites are different in that Site 112 records only upper lower to middle Miocene strata, whereas Site 647 has upper Miocene and lower Miocene sediments and no currently defined middle Miocene record. Note, however, that about a 30-m coring gap occurs at Site 112 between lower Pliocene and middle Miocene sediments—upper Miocene sediments at Site 647 are at most about 5 m thick and could easily have been missed at Site 112. The upper lower to middle Miocene section, which is at least 60 m thick at Site 112, is definitely not present at Site 647.

The Eocene and Oligocene sediments at Sites 112 and 647 are similar, except for the indication of a higher depositional rate at Site 647 ("Sediment-Accumulation Rates" section, this chapter). The Oligocene at both sites contains biogenic silica, locally in great enough abundance to allow sediment names like siliceous ooze or diatomite. In the Eocene, nannofossils are the only significant biogenic component, and at both sites the sediments become color banded in shades of greenish gray and red near the basement.

BASEMENT ROCKS

The contact between lower Eocene sediments and the basalts of layer 2 occurs at a depth of 699 mbsf, according to drilling records of the depth at which drilling rate decreased sharply. The top of the basalt is at 75 cm in Section 105-647A-72R-2. The last core taken (105-647A-75R) ends within a unit of medium-crystalline basalt. We drilled 31 m of basalt (699–730 mbsf), recovering an average of 77.5%.

Description

The basalts are generally massive, aphyric to moderately pyroxene-phyric, fine- to medium-crystalline, thick flow units. The contact with the sediments is sharp (Fig. 25) but is characterized by (1) large calcite- and chlorite-filled vesicles (amygdules) to about 0.8 × 2.0 cm, (2) stockwork veins in the basalt (Fig. 26), and (3) hydrothermal precipitates and reaction products in the overlying flow-top breccia and sediments (Fig. 26). The crystal size in what appears to be a thick flow unit increases with depth to about 1 mm. In these deeper basalts are 5–10-cm-spaced subhorizontal veins, < 1 cm thick, of massive serpentine (antigorite?).

Interpretation

No shipboard chemical analyses were performed, because the X-ray fluorescence unit was not calibrated for trace elements. Thin sections were not cut because of time constraints and lack of sufficient experience among the sedimentologists in the petrographic description of oceanic basalts to justify sampling the core. Nevertheless, we can say that the basalts represent thick, relatively homogeneous flows, perhaps a single thick flow, having an uppermost chilled contact. Hydrothermal alteration is restricted to the margins of stockwork veins near the top of the basalt sequence. Otherwise, the basalt appears relatively fresh and is probably suitable for radiometric dating. The oldest sediments above the basalt are of early Eocene age (nannofossil zone NP11, 55–56 Ma), providing a minimum age for eruption. Site 647 is situated above anomaly 24 crust, which is believed to have an age of about 55–56 Ma as well (see "Introduction" chapter, this volume).

BIOSTRATIGRAPHY

Hole 647A was drilled to a sub-bottom depth of 736.0 m. Both core-catcher samples and samples from selected intervals were analyzed for diatoms, dinocysts, foraminifers, nannofossils, and radiolarians. The abundance and preservation of microfossil groups are presented in Figures 27 and 28, respectively.

The major chronostratigraphic subdivisions are as follows:

Pliocene/Pleistocene boundary:	~70 mbsf
Oligocene/Miocene boundary:	~135 mbsf
Eocene/Oligocene boundary:	~290 mbsf
late Eocene/middle Eocene:	~450 mbsf

The faunal data suggest that Hole 647A bottomed out in the upper part of the early Eocene nannofossil zone NP11 (about 56 Ma).

Planktonic Foraminifers

Results

The relative abundances of faunal data at Site 647 are presented in Figure 27. According to foraminiferal stratigraphy, Hole 647A can be divided into five intervals.

Interval 1 (0–116.0 mbsf) is characterized by a highly abundant and diverse foraminiferal assemblage. The fauna is dominated by *Globigerina bulloides, G. quinqueloba*, and *Globorotalia inflata* and lesser amounts of sinistral and dextral *Neogloboquadrina pachyderma, N. dutertrei, N.* "du-pac" (*dutertrei-pachyderma* transitional form), *Globigerinita glutinata, Globigerinita uvula*, and *Orbulina universa*. Several *Globorotalias* are also found in the samples as auxiliary species, such as *G. truncatulinoides, G. scitula, G. crassaformis, G. hirsuta, G. menar-*

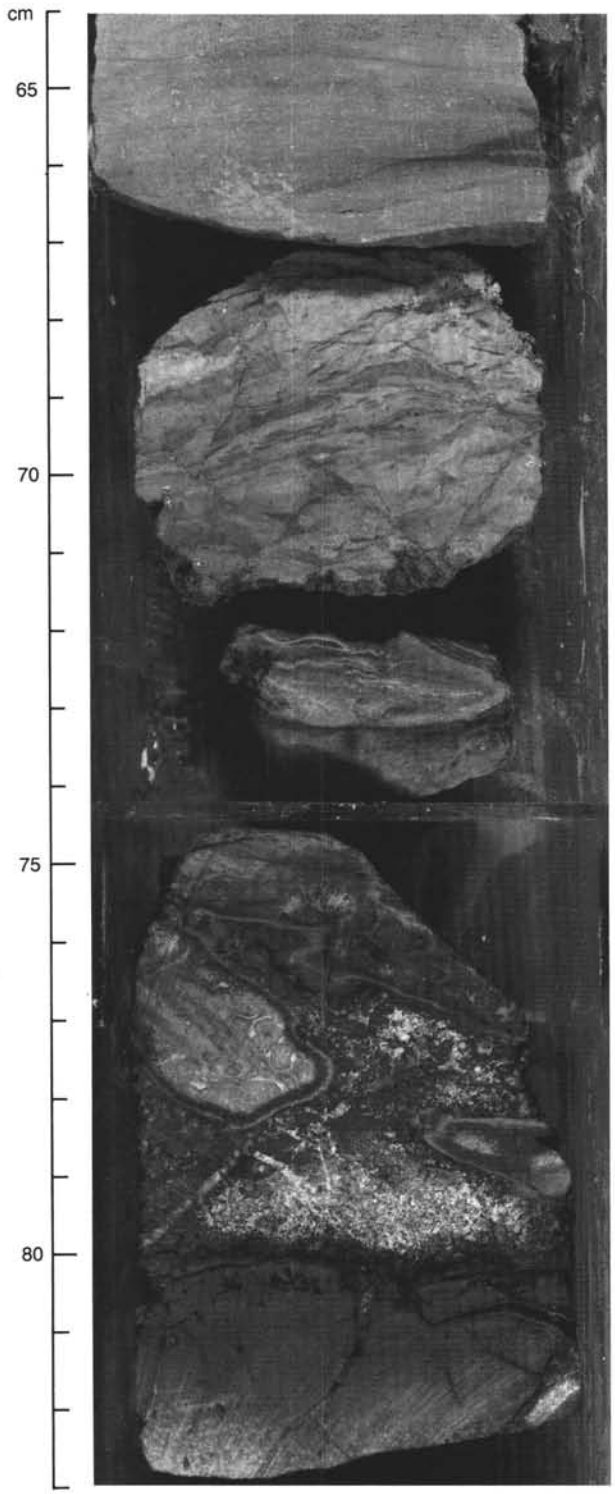

Figure 25. Contact between Unit IV sediments and basement basalts. The dark basalt is cut by a chlorite-filled vein. The reverse side of this piece has calcite-filled vesicles as large as 0.8 × 2.0 cm. The top of the basalt flow is aphanitic, resulting from chilling against water, and is covered by a botryoidal laminated crust (80 cm). The very pale rock above the basalt (76–80 cm) consists of hydrothermal precipitates in the pores of a flow-top breccia. The breccia fragments are devitrified glass with spherulitic crystal masses (77 cm). The overlying sediment is bleached and altered by hydrothermal fluids. Some of the soft clay-rich material between the breccia fragments may have originally been infiltrated sediment. Interval shown is Sample 105-647A-71R-2, 64–83 cm.

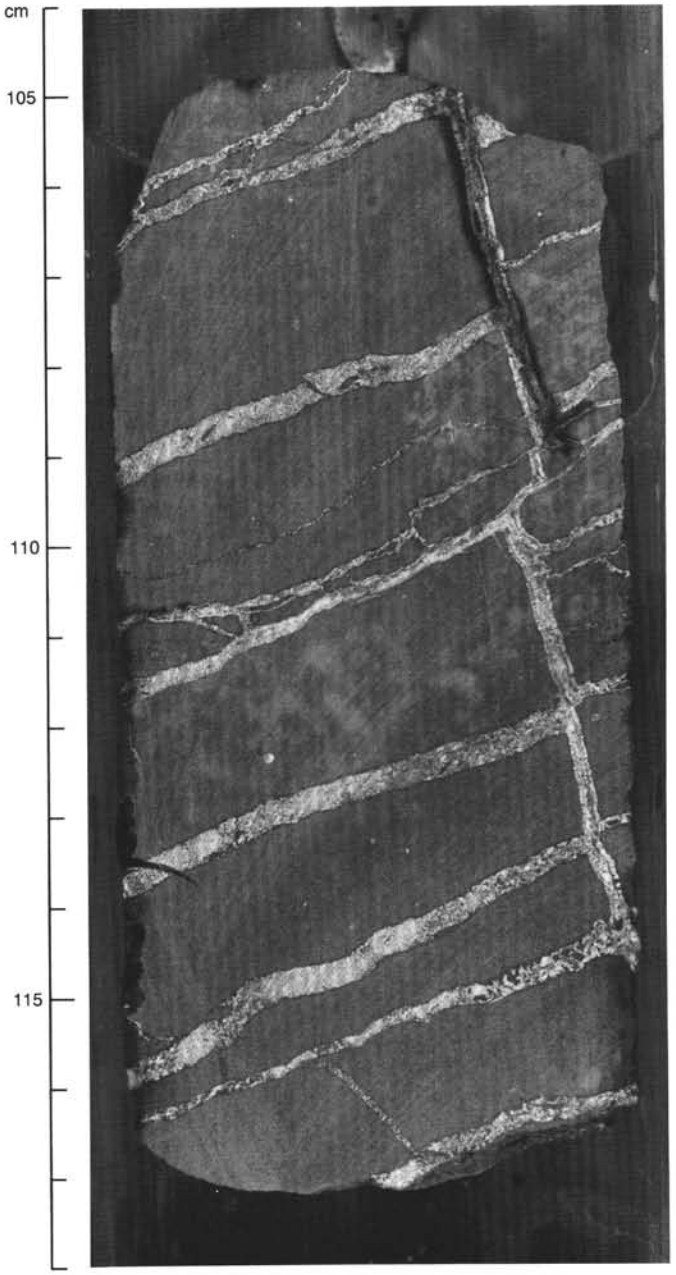

Figure 26. Stockwork veins in finely crystalline basalt. The veins contain calcite, chlorite, and locally pyrite. Note the small amygdules in the basalt. Interval shown is Sample 105-647A-71R-2, 104–118 cm.

dii, and *G. tumida tumida*. Smaller percentages of *Globigerinella aquilateralis, Globigerinoides sacculifer, Globigerinoides ruber, Globigerinoides conglobatus, Globorotalia obesa*, and *Planulina obliquiloculata* are also found occurring sporadically in the samples.

Interval II (116.0–135.4 mbsf) is barren of planktonic foraminifers.

Interval III (135.4–289.0 mbsf) is characterized by a major change in the planktonic foraminiferal assemblage. The fauna is much less diverse than that observed in Interval I. This interval is dominated by *Catapsydrax unicavus, C. dissimilis*, and smaller but consistent occurrences of *Globorotalia postcretacea, Globorotalia munda, G. permicra, Globigerina pseudovenezuelana, Catapsydrax cryptomphala*, and sporadic occurrences of *Globi-*

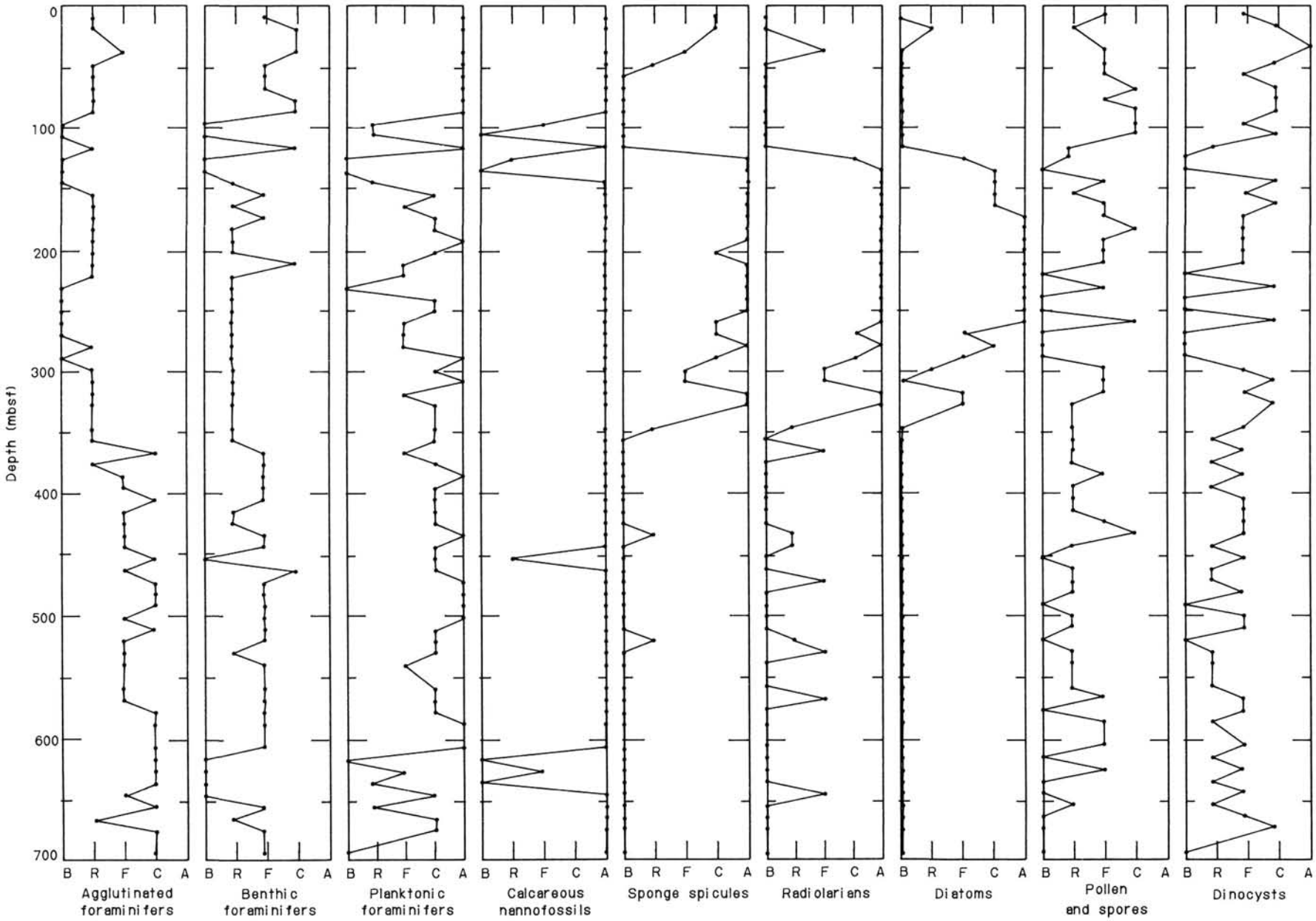

Figure 27. Microfossil abundance, Hole 647A: barren (B), rare (R), few (F), common (C), and abundant (A). Spore and dinocyst abundances are calculated excluding the reworked specimens; reworked palynomorphs include spores, pollen grains, and dinocysts.

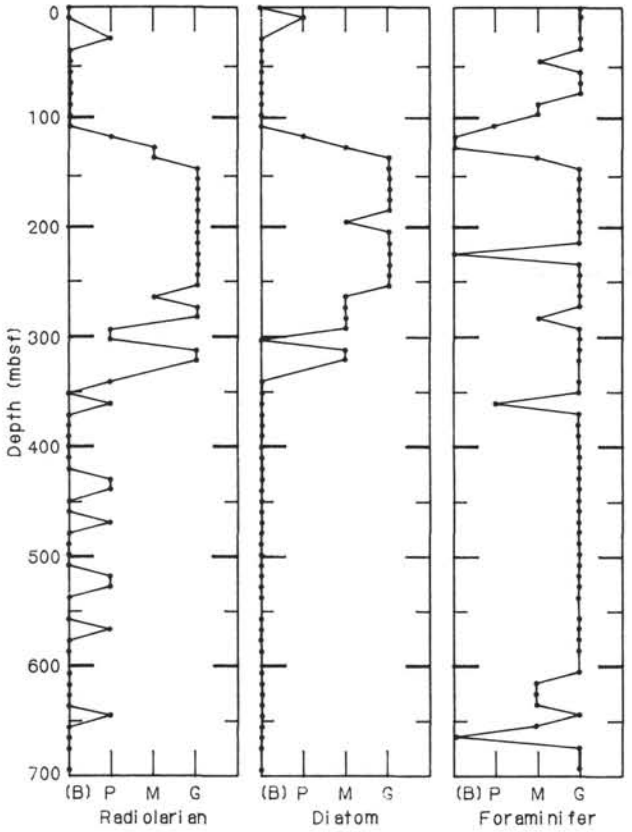

Figure 28. Microfossil preservation, Hole 647A: barren (B), poor (P), moderate (M), good (G).

gerina angiporoides, Globigerina ampliapertura, and *Globorotaloides variabilis*.

Interval IV (289.0–462.8 mbsf) shows an increase in species diversity and abundance. In addition to the fauna cited in Interval III, Interval IV includes *Turborotalia cerroazulensis cerroazulensis, T. cerroazulensis pomeroli, Pseudohastigerina micra, Chiloguembelina cubensis, Globigerina galavisi, Globigerina tripartita, Globigerina increbescens, Globigerina officinalis, Globigerina linaperta, Globigerinatheka index tropicalis*, and *Globigerinatheka index index*.

Interval V (462.8–~697 mbsf) is characterized by a planktonic foraminiferal assemblage that displays higher diversity and abundance than in Interval IV. In addition to the fauna described in Interval IV, this interval also includes *Subbotina frontosa*, several *Acarinina* and *Truncorotaloides* species, *Pseudohastigerina wilcoxensis*, and sporadic occurrences of *Hantkenina alabamensis*. The *Acarininas* are dominated by *A. densa*, and the *Truncorotaloides* by *T. rohri* and *T. collactea*. In Section 105-647A-68R, CC, *Acarinina soldadoensis/pentacamerata* and *Morozovella lensiformis* are observed. In Section 105-647A-70R, CC, a sudden change in fauna to one dominated by *Subbotina patagonica* is observed.

Chronostratigraphy

The first-appearance datum (FAD) of *Globoratalia truncatulinoides* is generally accepted to occur at the 1.9-Ma level, immediately below the Olduvai event (Berggren et al., 1986a). This datum was found in Section 105-647B-7H, CC, and suggests that the upper 68 m of Site 647 correlates with foraminiferal Zone N22-N23. The Pliocene/Pleistocene boundary is extrapolated, using the *G. truncatulinoides* datum, to occur at approximately 58 mbsf. Note, however, that this species is reported to have a diachronous FAD in the North Atlantic. Weaver and Clement (in press) demonstrated that the first appearance of *G. truncatulinoides* in the North Atlantic is clearly a migrational event and occurs at 1.4 Ma at Site 611. Therefore, the aforementioned Pliocene/Pleistocene boundary requires confirmation by the magnetostratigraphy and other biostratigraphic data. The FAD of *G. inflata* occurs at 3.0 Ma in the Mammoth event (Berggren et al., 1986a). According to the first occurrence of *G. inflata*, the base of Interval I is correlated with Zone PL-5.

Both *Catapsydrax dissimilis* and *C. unicavus* range from middle Eocene to lower Miocene. Oligocene age is assigned to Interval III on the basis of the absence of diagnostic Miocene fauna and the similarity of the observed low-diversity assemblage to those described on Legs 12, 49, 80, and 81 (Berggren, 1972; Poore, 1979; Snyder and Waters, 1985). The last-appearance datums (LAD) of *Pseudohastigerina micra* and *Chiloguembelina cubensis* are reported to occur at 34 and 30 Ma, respectively (Berggren et al., 1986b). The last occurrence of these species is found in Sections 105-647A-28R, CC, and 105-647A-27R, CC, respectively, confirming the early Oligocene assignment for Interval III. The faunal assemblage in Sample 105-647A-15R, CC, through 105-647A-19R, CC, is assigned to Zone P21-P22, whereas the section from Sample 105-647A-20R-4, 84–87 cm, through 105-647A-30R, CC, appears to include Zones P21a to P18, based on sporadic occurrences of *Globigerina angiporoides* and *G. ampliapertura*. Berggren et al. (1986b) report the LAD of these species as being 32.0 and 32.8 Ma, respectively.

The Oligocene/Eocene boundary is placed at about 289.0 mbsf (base of Section 105-647A-30R, CC) according to the last occurrence of *Globigerina linaperta* in Sample 105-647A-31R-2, 34–37 cm, and *T. cerroazulensis* s.l. in Section 105-647A-31R, CC (LAD 36.6 Ma; Berggren et al., 1986b). The last occurrence of *Globigerinapsis index* s.l. in Section 105-647A-35R, CC, suggests that the section between 105-647A-31R, CC, and 647A-35R, CC, correlates with Zone P17. The upper/middle Eocene boundary is placed at about 462.8 mbsf according to the LAD of *Acarinina* and *Truncorotaloides* groups, which occur at 40.6 Ma (Berggren et al., 1986b). This boundary also partly defines the P15/P14 zonal transition. On DSDP Leg 80, the last occurrence of *P. wilcoxensis* defines the top of the P12 planktonic foraminiferal zone. Based on the last occurrence of this species, the P13/P12 transition is tentatively placed at about 588 mbsf (Section 105-647A-61R, CC). Between Section 105-647A-61R, CC, and 105-647A-67R, CC, the planktonic fauna is rather sparse and displays lower diversity, but the co-occurrence of *Subbotina frontosa* and *Catapsydrax* spp. supports the P12 zonal assignment for Sample 105-647A-62R-6, 22–25 cm. The occurrence of *Acarinina soldadoensis/pentacamerata* and *Morozovella lensiformis* in Sample 105-647A-68R-1, 129–152 cm, suggests a P8 zonal assignment for this sample.

Fauna in Section 105-647A-70R, CC, includes common *Subbotina patagonica*. The occurrence of this species in sediments of the Norwegian–Greenland Sea, North Sea, and Labrador Margin is restricted to Zones P2 through P8.

Paleoenvironment

Considering the geographic location of Site 647, the fauna observed in Interval I can be described as a cool-temperate to temperate North Atlantic Drift assemblage. No significant faunal variations are observed in the upper 116 m of the site.

The Oligocene was generally a time of low diversity of planktonic foraminiferal faunas. Late Oligocene assemblages can be subdivided into high-latitude *Catapsydrax* and small *Globigerina* fauna and a more diverse low-latitude fauna of large *Globigerina* (Berggren, 1978). Berggren (1978) distinguishes a mid-latitude fauna in the lower Oligocene dominated by *Chiloguembelina*. The foraminiferal assemblage observed in Interval III

suggests a cool-temperate to temperate water mass in the Labrador Sea during the Oligocene.

Fauna in Intervals IV to V represent temperate-water-mass assemblages, on the basis of the scarcity of low-latitude forms such as *Acarinina, Globigerinapsis, Hantkenina*, and the *Turborotalia cerroazulensis* group. Eocene climatic optima are observed in Sections 105-647A-39R, CC, and 105-647A-50R, CC, possibly suggesting a subtropical water mass in the area, on the basis of the rare occurrence of the tropical genus *Hantkenina*.

Benthic Foraminifers

Site 647, Hole 647A

Benthic foraminifers are found in 66 of the 70 core-catcher samples examined from Hole 647A. Five major assemblages can be distinguished in this hole on the basis of faunal composition.

Fauna 1 (Postglacial Pliocene–Holocene, 0.0–116.0 mbsf)

Faunal assemblage 1 is found in Sections 105-647A-1R, CC, to 105-647A-12R, CC. The dominant species are *Pullenia bulloides, Epistominella exigua, Eggerella bradyi, Eponides tener, Pullenia quinqueloba, Melonis pompilioides, Planulina wuellerstorfi*, and *Nuttallides umbonifera*. Sections 105-647A-9R, CC, and 105-647A-6R, CC, contain *Triloculina frigida*, a form restricted to the Pleistocene at Rockall margin Sites 552A, 553A, 554, and 555 (Murray, 1984). This fauna displays closer North Atlantic Deep Water (NADW) affinities than the coeval fauna at Site 646 and resembles the fauna described from the Rockall margin by Murray (1984). As in Site 646, *Nuttallides umbonifera* increases in relative abundance downcore. This species dominates the faunal assemblage in Section 105-647A-12R, CC, suggesting the presence of old bottom water of Antarctic Bottom Water (AABW) affinities.

Fauna 2 (Late Miocene, 116.0–119.0 mbsf)

The benthic assemblage of Unit IIA (Sample 105-647A-13R-2, 102–104 cm) contains *Globocassidulina subglobosa, Oridorsalis umbonatus, Nuttallides umbonifera, Melonis barleeanum, Pullenia quinqueloba, Bulimina aculeata, Laticarinina pauperata*, and *Valvulina haeringensis*. The planktonic microfossil *Bolboforma laevis* is also present.

Fauna 3 (Oligocene, 145.1–298.6 mbsf)

Samples 105-647A-13R, CC, and 105-647A-14R, CC, are barren of foraminifers. The Oligocene fauna occurs in Samples 105-647A-15R, CC, to 105-647A-29R, CC (145.1–279.4 mbsf) and displays lower diversity and abundance of taxa than either Fauna 1 or the Eocene faunas deeper in the core. The numerically dominant forms are bathymetrically wide-ranging and stratigraphically long-ranging species such as *Globocassidulina subglobosa, Pullenia bulloides, P. quinqueloba, Oridorsalis umbonatus, Nodosaria/Stilostomella* spp., *Dentalina* spp., and *Gyroidinoides*. Some floods of *Spirosigmoilinella* are also observed in this interval. This assemblage resembles the Oligocene faunas from the Rockall margin (Murray, 1984) and Goban Spur region (Miller et al., 1984). These taxa have been interpreted as being tolerant of environmental changes because they are survivors of the benthic foraminiferal crisis of the late Eocene (Miller et al., 1984). Many taxa have last occurrences in this interval, including *Bolivinopsis cubensis*, a form restricted to the Oligocene, *Anomalina* cf. *spissiformis*, and *Uvigerina* cf. *rippensis*, which range into the Eocene.

Fauna 4 (Late Eocene, 298.6–453.2 mbsf)

Because the Eocene assemblage at this site contains a mixture of calcareous and agglutinated species, both the calcareous zonation of Tjalsma and Lohmann (1983) and the agglutinated zonation of Geroch and Nowak (1983) can be employed with a good degree of accuracy. A significant faunal turnover occurs between Sections 105-647A-31R, CC, and 105-647A-47R, CC, in the upper Eocene. Throughout the interval, the diversity of benthic taxa steadily increases downcore, and the faunal composition changes from predominantly calcareous to predominantly agglutinated. The calcareous component of the upper Eocene fauna is a typical late Eocene abyssal assemblage, dominated by the "second Q-mode principal component fauna" of Tjalsma and Lohmann (1983): *Oridorsalis umbonatus, Cibicidoides ungerianus, Globocassidulina subglobosa*, and *Gyroidinoides* spp. This fauna occurs at a paleodepth of 2000–3000 m in the western Atlantic. The agglutinated foraminiferal assemblage is dominated by the tubular genera *Rhabdammina, Rhizammina, Bathysiphon*, and *Hyperammina*, and common occurrences of *Ammodiscus, Glomospira, Saccammina, Lituotuba, Reophax, Haplophragmoides, Cyclammina, Spiroplectammina, Bigenerina, Arenobulimina, Karreriella*, and *Gaudryina*.

The Eocene/Oligocene boundary, based on benthic foraminifers, was placed at the last common occurrence (LCO) of flysch-type agglutinated foraminifers, which was found between Sections 105-647A-29R, CC, and 105-647A-32R, CC. The upper Eocene can be distinguished at this site using the zonation of Geroch and Nowak (1983). Although this zonation has not been calibrated to magnetostratigraphy, it is nevertheless useful because all Geroch and Nowak's Eocene marker species are found in the samples examined. *Cyclammina rotundidorsata*, the marker for the latest Eocene, occurs in Section 105-647A-32R, CC. The base of the upper Eocene in the Carpathians is defined by the first occurrence of *Ammodiscus latus* and the LCO of *Cyclammina amplectens*. The last appearance of *C. amplectens* is also used in the North Sea and Labrador Shelf wells to define the top of the middle Eocene. The first occurrence of *A. latus* is found in Section 105-647A-47R, CC (453.2 mbsf), and the LCO of *A. amplectens* occurs in Section 105-647A-46R, CC. A useful datum within the upper Eocene is the last occurrence of *Nuttallides trumpyi*, which was dated at 38.5 Ma at Site 549 (Miller et al., 1984) and occurs in Section 105-647A-41R, CC.

Fauna 5 (Early–Middle Eocene, 453.2–694.8 mbsf)

Cyclammina amplectens, the nominate taxon of the middle Eocene zone of Geroch and Nowak (1983), commonly occurs in this interval. Other common species include *C. ungerianus, Nuttallides trumpyi, Ammodiscus cretaceus, Glomospira charoides*, and *Haplophragmoides walteri*. The last occurrence of *Osangularia mexicana*, which is reported to have an LCO in the Atlantic in Zone P14 (Tjalsma and Lohmann, 1983), is found in Section 105-647-50R, CC.

The lower/middle Eocene boundary (P9/P10 boundary of Blow, 1969) is more difficult to define using benthic foraminifers because it is based on rare or poorly defined markers or on changes in relative abundance of taxa. The last occurrence of *Aragonia semireticulata*, listed by Tjalsma and Lohmann (1983) as being in Zone P8, is found in Section 105-647A-68R, CC. In the zonation of Geroch and Nowak (1983), the base of the middle Eocene is defined by the first appearance of *Cyclammina amplectens*, found in Section 105-647A-67R, CC. The early Eocene in the Carpathians is characterized by increased abundances of *Glomospira* spp. compared with the middle Eocene. The first noticeably greater downhole abundances of *Glomospira* occur in Section 105-647A-63R, CC, and a *Glomospira*-dominated assemblage continues to the base of the hole. The lowermost sample examined (105-647A-73R, CC) contains a benthic fauna that is no older than latest Paleocene Zone P6a.

The absence of deep abyssal calcareous and agglutinated species as well as upper bathyal markers suggests a paleodepth between 2000 and 3000 m in the lower Eocene part of the hole.

Nannofossils

Nannofossils are abundant and moderately to well-preserved in most samples examined from Hole 647A. The interval from the top of Hole 647A down through Sample 105-647A-1R-6, 130–132 cm, is assigned to Zone NN21 of Martini (1971), on the basis of the occurrence of *Emiliania huxleyi*.

The LAD of *Pseudoemiliania lacunosa*, the NN19/NN20 zonal boundary marker, occurs in Sample 105-647A-4R-1, 138–140 cm. The interval between this datum and the FAD of *E. huxleyi* in Sample 105-647A-1R-6, 130–132 cm, is assigned to Zone NN20. Zone NN19 extends from Sample 105-647A-4R-1, 138–140 cm, down to Sample 105-647A-10R-3, 39 cm.

The LAD of *Discoaster brouweri* and *D. pentaradiatus* occur in Samples 105-647A-10R-3, 39 cm, and 105-647A-12R-1, 93–95 cm, respectively. This interval, therefore, is assigned to Zone NN18 (upper Pliocene). Zone NN17 extends from Sample 105-647A-12R-1, 93–95 cm, down to Sample 105-647A-12R-3, 39–41 cm, on the basis of the occurrence of *D. pentaradiatus*.

The LAD of *Discoaster surculus* occurs in Sample 105-647A-12R-3, 39–41 cm, indicating the NN16/NN17 zonal boundary at this level. Sample 105-647A-12R, CC, contains *D. surculus,* but does not contain *Reticulofenestra pseudoumbilica*, which has a LAD that marks the NN15/NN16 zonal boundary. This sample, therefore, is also assigned to Zone NN16.

The nannofossil assemblages in the upper 12 cores of Hole 647A are dominated by *Gephyrocapsa* spp., and *Coccolithus pelagicus*.

The interval from Sample 105-647A-13R-1, 45 cm, through Sample 105-647A-13R-2, 53–55 cm, is assigned to Zone NN11 (upper Miocene) of Martini (1971), on the basis of the presence of *Discoaster quinqueramus. D. berggrenii* and *D.* cf. *berggrenii* are rare in this interval, whereas *Coccolithus pelagicus* and *Reticulofenestra pseudoumbilica* dominate the assemblage. A hiatus, encompassing Zones NN12 through NN15 (upper Miocene–lower Pliocene) occurs between Sections 105-647A-12R, CC, and 105-647A-13R-1, 45 cm.

Sample 105-647A-14R-1, 59–61 cm, contains rare, poorly preserved specimens of *Dictyococcites bisectus*. An interval barren of nannofossils extends below this sample through Section 105-647A-14R, CC. If the specimens of *D. bisectus* in Sample 105-647A-14R-1, 59–61 cm, were not reworked, they would indicate an Oligocene age for this sample. Well-preserved nannofossil assemblages containing typical Oligocene species such as *Dictyococcites bisectus* and *Cyclicargolithus abisectus* first occur in Sample 105-647A-15R-1, 68–70 cm. Sample 105-647A-16R-3, 36–38 cm, contains a single specimen of *Sphenolithus ciperoensis* and is assigned to Zones NP24 and NP25.

The interval between Sample 105-647A-16R-3, 36–38 cm, and the LAD of *Reticulofenestra umbilica* in Sample 105-647A-23R-4, 91–93 cm, is assigned to Zone NP23. This interval contains rare *Sphenolithus predistentus* and *S. distentus*.

Zone NP22 extends from Sample 105-647A-23R-4, 91–93 cm, down through Sample 105-647A-26R, CC, on the basis of the occurrence of *R. umbilica* and the absence of *Ericsonia formosa*. The LAD of *E. formosa* in Sample 105-647A-27R-1, 51–53 cm, marks the top of Zone NP21. The lowermost Oligocene Zone NP 21 occurs from this sample down to Sample 105-647A-30R-7, 48 cm.

The LAD of *Discoaster barbadiensis*, which marks the NP20/NP21 zonal boundary (approximately the Eocene/Oligocene boundary), occurs in Sample 105-647A-30R-7, 48 cm. *D. saipanensis* has its last occurrence in Section 105-647A-30R, CC. These indicate a zonal assignment of NP19–NP20 (upper Eocene) from Sample 105-647A-30R-7, 48 cm, down to the FAD of *Isthmolithus recurvus* in Sample 105-647A-45R-1, 42–44 cm. Zone NP20 is not distinguishable because the zonal marker species, *Sphenolithus pseudoradians*, is not observed. The interval between Sample 105-647A-45R-1, 42-44 cm, and the FAD of *Chiasmolithus oamaruensis* in Sample 105-647A-46R-2, 101-103 cm, is assigned to Zone NP18. The interval represented by this zone appears anomalously narrow, compared with its reported duration by Berggren et al. (1986b). Okada and Thierstein (1979) reported a similar narrow or even nonexistent Zone NP18 at Site 386 of DSDP Leg 43 in the western North Atlantic. This may result from diachroneity of one or both of the zonal boundary markers. Delineation of Zone NP18 in Hole 647A, therefore, may not be useful.

The interval between Samples 105-647A-46R-2, 101–103 cm, and 105-647A-48R-1, 91–93 cm, is assigned to the middle Eocene Zone NP17 of Martini (1971). The dominant species within this interval are *Chiasmolithus expansus* and *Reticulofenestra umbilica*.

The interval between the LAD of *Chiasmolithus solitus* in Sample 105-647A-48R-1, 91–93 cm, and the FAD of *Reticulofenestra umbilica* in Sample 105-647A-63R-1, 36–38 cm, is assigned to Zone NP16. The interval between Samples 105-647A-63R-1, 36–38 cm, and 105-647A-66R-2, 49–51 cm, is barren of nannofossils. The co-occurrence of *Discoaster lodoensis* and *Tribrachiatus orthostylus* from Sample 105-647A-66R-2, 49–51 cm, through Section 105-647A-69R, CC, indicates a zonal assignment of NP12 (lower Eocene).

The interval between Section 105-647A-69R, CC, and Sample 105-647A-71R-2, 41 cm, lies below the FAD of *D. lodoensis* (the NP11/NP12 zonal boundary marker) and above the FAD of *T. orthostylus* (the FAD of which occurs at the NP10/NP11 zonal boundary), thus indicating a zonal assignment of NP11.

Paleoenvironment

The dominance of the assemblages in the top 12 cores of Hole 647A (upper Pliocene to Holocene) by *Coccolithus pelagicus* and *Gephyrocapsa* spp. indicates cool temperatures throughout this interval. Discoasters are present from Sample 105-647A-10R-3, 39 cm, to total depth, but are not abundant, an indication that conditions were not very warm.

The interval from Samples 105-647A-13R-1, 45 cm, through 105-647A-13R-2, 29 cm (upper Miocene), contains slightly higher abundances of discoasters, indicating warmer conditions than in the interval above.

Assemblages in the interval from Samples 105-647A-15R-1, 68–70 cm, through 105-647A-30R-7, 48 cm, (Oligocene) are dominated by *Reticulofenestra* spp. and are generally low in diversity. This indicates cool-water conditions. Additional evidence includes the scarcity of sphenoliths and discoasters (warm-water indicators) and the common occurrence of *Isthmolithus recurvus*, a cool-water indicator, in the lower part of this interval (Section 105-647A-26R, CC, and below).

In the interval from Samples 105-647A-30R-7, 48 cm, through 105-647A-71R-2, 41 cm (Eocene), the assemblages are dominated by *Reticulofenestra* spp. and *Chiasmolithus* spp. Discoasters are more common than in the Oligocene but are not abundant. The high ratio of *Chiasmolithus* spp. to *Discoaster* spp. indicates that water conditions were never very warm, though they may have been temperate. Cool-water indicators commonly present in this interval are *Isthmolithus recurvus* and *Neococcolithes dubius. Lophodolithus* spp., *Rhabdosphaera* spp., *Tribrachiatus orthostylus, Discolithina* spp., *Corannulus germanicus*, and *Zyghrablithus bijugatus*, species that are more common in shelf environments, are present in moderate abundances in this interval. Perhaps these occurrences indicate a redeposition from shelf to basin or an increasing proximity to the shelf edges in early Eocene time.

Hole 647B

The interval from the top of Hole 647B down through Section 105-647B-2H, CC, lies stratigraphically above the LAD of *Pseudoemiliania lacunosa* and is assigned to Zones NN20 and NN21 of Martini (1971). The interval from Sections 105-647B-3H, CC (LAD of *P. lacunosa*), through 105-647B-9H, CC, is assigned to Zone NN19. The interval from Sections 105-647B-10H, CC (LAD of *Discoaster brouweri*), to 105-647B-11H, CC, is assigned to Zone NN18 (upper Pliocene).

Diatoms

The Oligocene diatom assemblage present at Site 647 is composed of high- and low-latitude species and contains a mixture of species observed from the Norwegian–Greenland Sea (Schrader and Fenner, 1976; Dzinoridze et al., 1978), the low-latitude Atlantic (Fenner, 1977, 1984a), the Pacific (Fenner, 1984a; Barron, 1985), and the high-latitude south Atlantic (Gombos and Ciesielski, 1983).

Site 647, Hole 647A

Diatoms are not observed in samples examined from Cores 105-647A-1R through 105-647A-12R. Core 105-647A-13R contains rare to few diatoms (Figs. 27 and 28). The diatom preservation is generally poor. The assemblage is late Oligocene to early Miocene in age, on the basis of the occurrence of *Coscinodiscus lewisianus* in Sample 105-647A-13R-4, 109–111 cm; of *Synedra jousaena, Coscinodiscus oligocenicus*, and one specimen of *Rocella vigilans* in Sample 105-647A-13R-5, 39–41 cm; and of *C. lewisianus* in Sample 105-647A-13R, CC (Fig. 29). These samples also contain numerous reworked species characteristic of the Eocene and lower Oligocene assemblages observed stratigraphically downhole. Species present include *Stephanopyxis spinossima, Pyxilla reticulata, Hemiaulus polycystinorum, Stephanopyxis corona, S. grunowii*, and several *Cestodiscus* species.

Most of the diatoms observed in samples from Core 105-647A-14R are typical of the Eocene–Oligocene and may be reworked. Diatom species present include *Stephanopyxis grunowii, Pyxilla gracilis, P. reticulata, Goniothecium decoratum, G. odontella, Melosira architecturalis, Pterotheca aculeifera, Cymatosira compacta*, and *Synedra jousaena*. Core 105-647A-14R is assigned an early Miocene age, on the basis of radiolarian fauna observed in samples from this core (see "Radiolarians" section, this chapter).

Numerous Oligocene diatoms are present in Cores 105-647A-15R through 105-647A-23R. The sporadic occurrence of *Sceptroneis pupa* and *Cymatosira compacta* in Samples 105-647A-16R-2, 39–41 cm, through 105-647A-25R-2, 120–122 cm, and 105-647A-24R-4, 39–41 cm, respectively, suggests that this interval is early Oligocene to early late Oligocene in age, according to the range of these species in the Norwegian–Greenland Sea (Schrader and Fenner, 1976). The rare occurrence of *Rhizosolenia gravida* in Samples 105-647A-19R-5, 124–126 cm, through 105-647A-26R, CC, suggests that this interval is early Oligocene in age, on the basis of the range of this species in the high-latitudes of the South Atlantic (Gombos and Ciesielski, 1983; Fenner, 1984b). Other stratigraphically useful species in this interval include *Asteromphalus oligocenicus, Rouxia obesa, Coscinodiscus praenitidus, C. oligocenicus, Skeletonema barbadensis, Rutilaria areolata, Sceptroneis mayenica, S. grunowii, Pseudostitodiscus picus, Asterolampra schmidtii, Pyxilla reticulata, P. gracilis, Stephanopyxis marginata, S. grunowii, S. corona, Pseudorocella barbadensis, Melosira architecturalis*, and *Thalassiosira* cf. *irregulata*.

Section 105-647A-23R, CC, through Sample 105-647A-25R-4, 119–121 cm, is assigned to the *Cestodiscus reticulatus* Zone of Fenner (1984b). This zonal assignment is based on the occurrence of *Cestodiscus reticulatus* and *C. robustus* in addition to the assemblage listed above.

The occurrence of *Coscinodiscus excavatus* without *C. reticulatus* in Sections 105-647A-25R, CC, through 105-647A-27R, CC, allows placement of this interval in the *Coscinodiscus excavatus* Zone of Fenner (1984b). Most of the species listed above also occur in this interval.

The diatom abundance and preservation decrease considerably in Cores 105-647A-28R through 105-647A-34R. Nevertheless, the occurrence of *Pyxilla reticulata, P. gracilis, Triceratium unguiculatum, Hemiaulus polycystinorum* (common specimens), *Stephanopyxis grunowii, S. spinossima, Rouxia obesa*, and *Trinacria excavata* suggests an Eocene–Oligocene age.

Except for rare fragments in Section 105-647A-35R, CC, and rare specimens in Section 105-647A-68R, CC, diatoms are not observed in core-catcher samples examined from Cores 105-647A-36R through 105-647A-70R.

Hole 647B

Eleven core-catcher samples were examined from Hole 647B. Of these, only Section 105-647B-2H, CC, contains diatoms. The diatoms observed in this sample are typical pelagic species and are non-age diagnostic. Diatoms are also observed in Sample 105-647B-2H-6, 124 cm. The occurrence of *Rhizosolenia curvirostris* in this sample suggests an age older than 0.25 Ma.

Radiolarians

Pliocene–Pleistocene (Cores 105-647A-1R to 105-647A-12R)

All core-catcher samples are barren of radiolarians except Section 105-647A-4R, CC, which contained rare, poorly preserved specimens. This sample, dated by comparison to other microfossil groups as being Pleistocene in age, consists solely of dissolution-resistant taxa, and most specimens are broken and partly dissolved. The species are typical of the Holocene subpolar assemblage, although the abundance and diversity are abnormally low as a result of dissolution. *Cycladophora davisiana* is the most abundant taxon, suggesting that Section 105-647A-4R, CC, was deposited under glacial conditions. The presence of *C. davisiana* also gives a Pliocene–Holocene age assignment to this sample. No other age indicators are observed.

Early Miocene (Cores 105-647A-13R and 105-647A-14R)

Two sections (105-647A-13R, CC, and 105-647A-14R, CC) contain common to abundant, moderately preserved radiolarians. In the following stratigraphic discussion, unless specifically noted, all first and last occurrences are based on the work of Riedel and Sanfilippo (1978) and on the correlation chart given in the "Introduction" chapter (this volume).

Section 105-647A-13R, CC, contains the stratigraphically useful radiolarians *Cyrtocapsella tetrapera* (FAD, base *C. tetrapera* Zone, 22.5 Ma), *Cyrtocapsella cornuta* (FAD, base *C. tetrapera* Zone, 22.5 Ma; LAD, base *D. antepenultimus* Zone, 8.5 Ma), *Calocycletta robusta* (FAD, upper Oligocene; LAD, lower *S. peregrina* Zone, about 6.0 Ma), *Stichocorys delmontense* (FAD, base *S. delmontense* Zone, 21 Ma; LAD, base *S. peregrina* Zone, 6.2 Ma), *Eucyrtidium diaphanes*(?) (LAD middle *C. costata* Zone, about 17 Ma), and *Velicuculus oddgurneri* (early Oligocene to early Miocene range (Bjørklund, 1976; and Eldholm, Thiede, Taylor, et al., 1987). A stratigraphically significant silicoflagellate is also observed–*Naviculopsis quadratum* (LAD, top of Zone NN3, 17.5 Ma; Martini and Müller, 1976). Although most of the stratigraphic indicators observed are rare, the co-occurrence of several stratigraphically consistent forms in the same sample suggests that reworking and downhole cavings

do not affect the stratigraphic assignment of this sample. Section 105-647A-13R, CC, is thus dated between 17.5 Ma and 21 Ma.

Section 105-647A-14R, CC, contains the following stratigraphically useful radiolarians: *Cyrtocapsella tetrapera, C. cornuta, Velicuculus oddgurneri, Eucyrtidium diaphanes*(?), *Dorcadospyris ateuchus* (FAD, base *D. ateuchus* Zone, 31.2 Ma, LAD, base *S. wolfii* Zone, 19.2 Ma), and *Carpocanopsis cingulata* (FAD, base *Lychnocanoma elongata* Zone, 23.5 Ma; LAD, middle *C. costata* zone, 17 Ma). Because of the rarity of *S. delmontense* in Section 105-647A-13R, CC, the absence of this species in Section 105-647A-14R, CC, may not reflect true biochronology. Age assignment based solely on the presence of species gives an age range for Section 105-647A-14R, CC, of 19.2–22.5 Ma.

Numerous other radiolarians are in Sections 105-647A-13R, CC, and 105-647A-14R, CC. The assemblage is dominated by prunoids, lithelids, and actinommids, all of which are characteristic of high-latitude environments. However, these two samples also contain a significant warmer water component (*Cyrtocapsella, Stichocorys*, and many spyrid species). Identifiable reworked radiolarians consist of a single specimen in Section 105-647A-14R, CC, questionably identified as *Theocotyle cryptocephala*, an Eocene species in the tropical zonation of Riedel and Sanfilippo (1978).

Oligocene (Cores 105-647A-15R to 105-647A-30R)

Core catchers of Cores 105-647A-15R to 105-647A-30R contained abundant, well-preserved radiolarians. The assemblage is dominated by artostrobid species, particularly *Theocampe amphora*, although prunoids, lithelids, and lithomelissids are also common. Many of the standard low-latitude Oligocene stratigraphic indicators such as *Lithocyclia angusta* are absent. The Oligocene–early Miocene species *D. ateuchus* is also missing, despite its presence in the overlying early Miocene section. Assignment of a tentative Oligocene age to these samples is based primarily on similarities in general species composition to Oligocene radiolarian assemblages of the Southern Ocean and Norwegian Sea (Chen, 1975; Bjørklund, 1976; D. Lazarus, pers. comm., 1985). A single specimen of *Cyclampterium pegetrum* (FAD, middle *T. tuberosa* Zone, about 33 Ma, LAD, early *C. tetrapera* Zone, about 22 Ma) is in Section 105-647A-23R, CC. This specimen is broken, has an uncommonly corroded surface, and appears to be reworked from older materials. This gives a maximum age of ~33 Ma to Section 105-647A-23R, CC, although the FAD of *C. pegetrum* in low latitudes is not precisely determined and could well be a bit younger or older than 33 Ma.

Eocene (Core 105-647A-31R to total depth)

Core-catcher Samples 105-647A-31R to 105-647A-34R contain few to abundant, moderate- to well-preserved radiolarians. No stratigraphic indicators are seen, and the age is based on determinations of other microfossil groups. The assemblage appears to be similar to that seen in the Oligocene samples, although dissolution in Cores 105-647A-30R to 105-647A-32R makes direct comparisons difficult. Core 105-647A-34R appears to be most similar to the Oligocene samples uphole, but abundant gravel and clay cobbles in the core-catcher sediment suggest that this sample is, in fact, downhole cavings and not *in-situ* material. Beginning with Core 105-647A-35R and continuing downhole to basement, radiolarians are generally rare and poorly preserved. Virtually all specimens have been fragmented and are pyritized or recrystallized. Identification of taxa is not possible in these samples.

Summary

Radiolarians in Site 647 are abundant and generally well preserved in lower Miocene to upper Eocene sediments and are rare and poorly preserved above and below this interval. Low-latitude stratigraphic indicators are few to rare in the lower Miocene (Cores 105-647A-13R and 105-647A-14R) and virtually absent in the Paleogene (Cores 105-647A-15R to 105-647A-34R). Polar and subpolar taxonomic groups dominate the assemblages in all intervals, although the lower Miocene interval also contains warm-water faunal elements.

Palynology

Neogene Section (0– ~ 135.4 mbsf)

One or two samples per core were analyzed. Pollen, spores, and dinocysts are well preserved, except for some reworked palynomorphs.

Dinoflagellate Cysts

Dinocysts are few to common in most examined samples, except in the lower part of the Neogene section (110–135.4 mbsf), where they are rare to absent.

In the uppermost 100 m, the dinocyst assemblages show a relatively high diversity. The most frequent taxa recorded are *Operculodinium centrocarpum, Nematospharopsis labyrinthea, Bitectadodinium tepikiense*, and several *Spiniferites* spp. (*S. ramosus, S. mirabilis*, and *S. elongatus*) and *Impagidinium* species (*I. aculeatum, I. patulum, I. paradoxum, I. pallidum, I. sphaericum*). *Brigantedinium* species (*B. simplex* notably) are locally common to abundant.

Few of the dinocysts recorded may be used for a chronostratigraphic purpose. However, when calibrating the dinocyst record of Site 647 with the nannofossil stratigraphy or magnetostratigraphy, the stratigraphic ranges of some dinocyst species show discrepancies with those of central North Atlantic sites (Mudie, in press); *Impagidinium pallidum, Impagidinium velorum*, and *Operculodinium* sp. (Piasecki, 1980) have last occurrences in Pliocene sediments from the North Atlantic (Mudie, in press) but are present in Pleistocene deposits at Site 647. *Impagidinium pallidum* and *Operculodinium* sp. (Piasecki, 1980) have been reported as being common in the upper Pleistocene sediments of Site 647 (Core HU-84-003; De Vernal, 1986), pointing to diachronous stratigraphic ranges for several dinoflagellate species.

Nevertheless, the Neogene dinocyst stratigraphy of Site 647 allows a few biostratigraphic interpretations:

1. The presence of *Multispinula minuta* at about 31 mbsf indicates a Pleistocene age (Aksu and Mudie, 1985; Mudie, in press).
2. The occurrence of *Filisphaera filifera* between 55.1 and about 100 mbsf suggests a late Miocene to early Pleistocene age (Bujak, 1984; Mudie, in press); the presence of *Impagidinium japonicum* and *Operculodinium crassum* in this interval may confirm an early Pleistocene or older age (Harland, 1979; Mudie, in press).
3. A slight increase in diversity is observed below 87.3 mbsf. The presence of *Corrudinium harlandii* between 87.3 and about 100 mbsf suggests a late Miocene to late Pliocene age (Harland, 1979; Mudie, in press). This dinocyst assemblage is similar to the assemblage seen in Pliocene sediments at Site 646 and includes the dinocysts *Nematosphaeropsis oblonga, Operculodinium wallii, Tectadodinium* sp. I, and common cf. *Labyrinthodinium* sp.

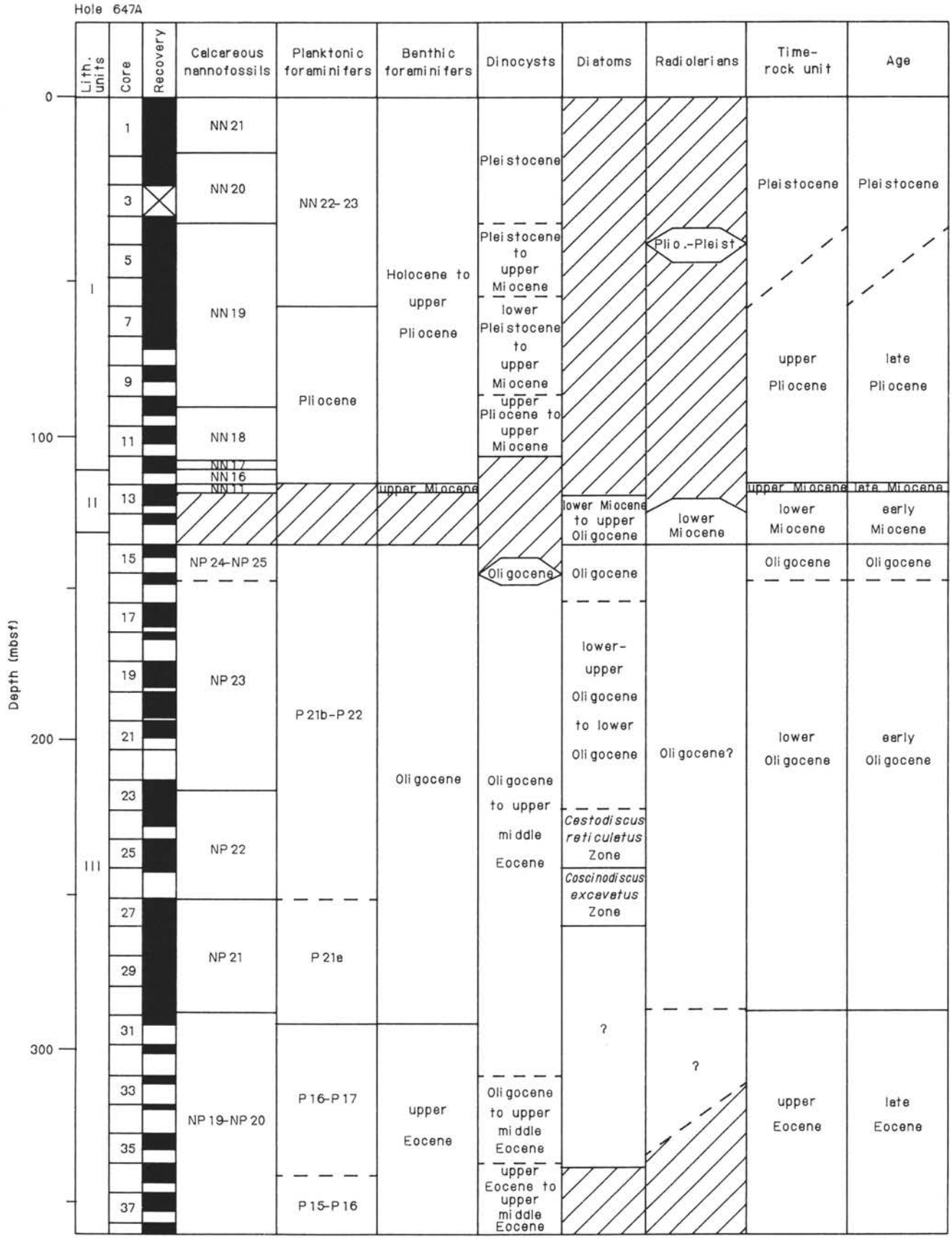

Figure 29. Biostratigraphic summary chart, Site 647. Dashed lines indicate that boundaries are uncertain; diagonal lines indicate an interval barren of microfossils; asterisk indicates drilling breccia found within the basalt.

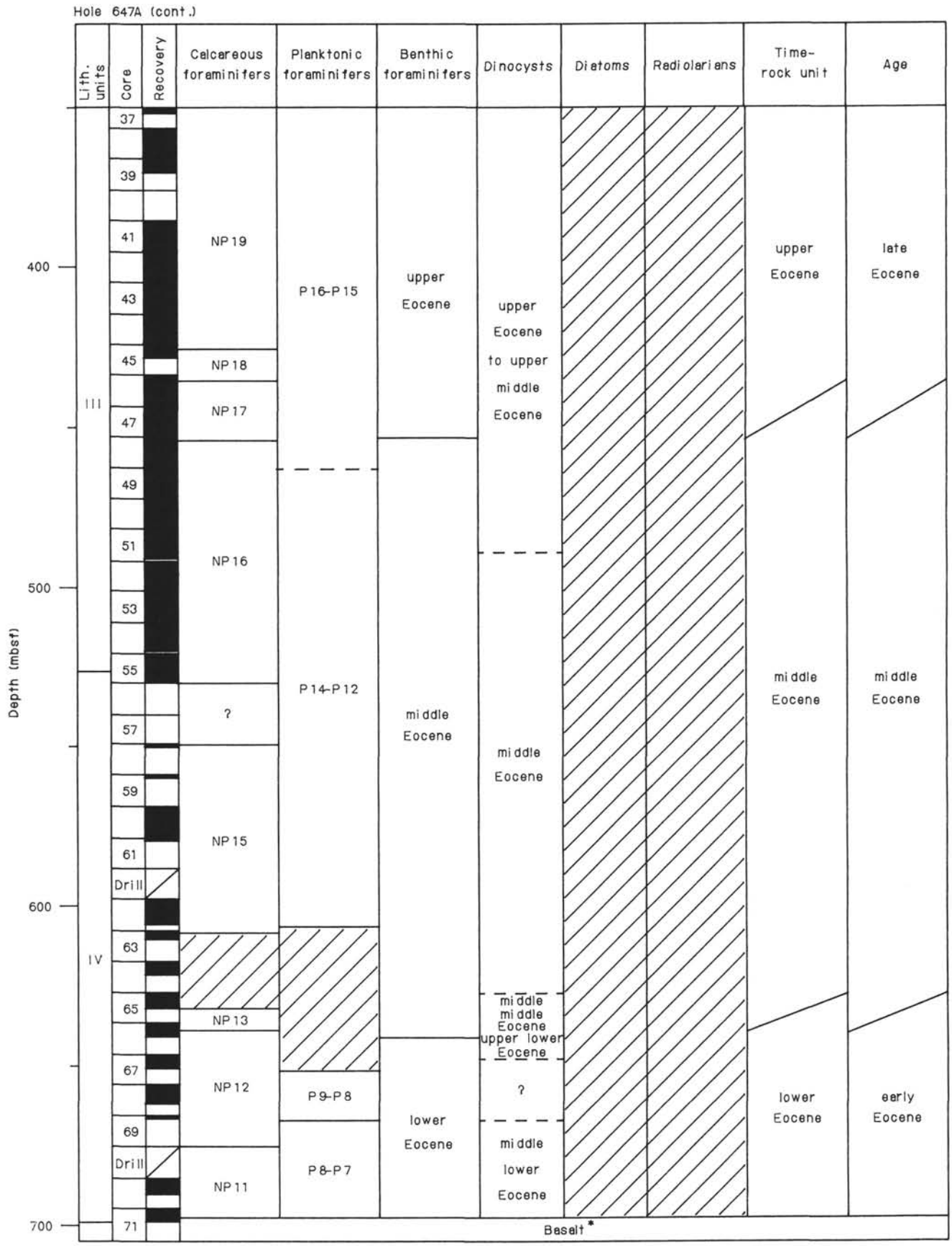

Figure 29 (continued).

The dinocyst associations in the Neogene section reflect cool-temperate surficial water masses, as indicated by the dominance of *Nematosphaeropsis labyrinthea, Operculodinium centrocarpum*, and *Bitectadodinium tepikiense*. The occurrence of warm-temperate to tropical species such as *Spiniferites mirabilis, Impagidinium patulum, I. aculeatum, I. strialatum*, and *Hemicystodinium zoharii* indicates some Gulf Stream influence. In addition, *Brigantedinium simplex*, which is common or abundant in few samples, may suggest input of freshwater or a transportation from the shelf area. In both associations, *B. simplex* could be related to an increase in the influence of the Labrador Current.

Pollen and Spores

The abundance of pollen and spores is relatively low in most examined samples, probably because of the offshore location of Site 647. The dominance of bisaccate pollen grains (*Pinus* and *Picea*) results from the selective effect of long-distance transportation by atmospheric or oceanic circulation.

Paleogene Section (135.4–694.8 mbsf)

Most core-catcher samples from Cores 105-647A-15R through 105-647A-70R were analyzed on board ship for dinocysts. Replicate shore-based analyses of some of these core-catcher samples were carried out together with analyses of some additional samples. Only one section (105-647A-70R, CC) was found to be barren. Preservation is generally good above Section 105-647A-67R, CC, although below this, palynomorphs are variably preserved and darkened in Cores 105-647A-70R and 105-647A-71R, reflecting the proximity of the basaltic basement. Palynomorphs occur in nearly all samples, although their abundance is low in most, and dinocysts generally dominate the assemblage. Spore and pollen diversity is low, being mainly represented by bisaccate pollen.

Dinocyst Stratigraphy

Most dinocyst zonal schemes of the Paleogene are based on shelf assemblages. The dinocyst assemblages from this site could not be easily compared to published zonal schemes because of the sporadic distribution of diagnostic species. This may be a consequence of the more open-oceanic influences at this site. Nevertheless, some biostratigraphic conclusions can be made based on the following dinocyst occurrences currently known for this hole. These occurrences are compared to first- and last-published occurrences of species, which, where possible, have been correlated with calcareous nannofossil zones (Aubry, 1985; Williams and Bujak, 1985; Berggren et al., 1986b).

Interval of ≈ 704–675 mbsf. First occurrence of *Adnatosphaeridium robustum* in Sample 105-647A-71R-1, 40 cm (upper NP11/NP12; Bujak et al., 1980), and last occurrence of *A. robustum* in Section 105-647A-69R, CC (upper NP12; Bujak et al., 1980; Brown and Downie, 1985a, 1985b), indicate a middle early Eocene age for this interval. The presence of *Dracodinium* sp. in Sample 105-647A-70R-4, 42 cm, indicates an age of no greater than early NP11 and maybe a more reliable datum than *A. robustum*.

Interval of ≈ 656–636 mbsf. First occurrence of *Homotryblium oceanum* in Sample 105-647A-67R-2, 28 cm (NP13; Brown and Downie, 1985a), and last occurrence of *Eatonicysta ursulae* in Sample 105-647A-65R-1, 117 cm (middle NP16; Chateauneuf, 1980) constrains this interval to late early Eocene to mid-middle Eocene.

Interval of ≈ 491–337 mbsf. First occurrence of *Corrudinium incompositum* in Section 105-647A-51R, CC (NP16; Bujak et al., 1980), and last occurrence of *Heteraulacacysta porosa* in Section 105-647A-35R, CC (late Eocene; M. Head, pers. comm., 1986), and *Areosphaeridium diktyoplokum* (top Eocene; Williams and Bujak, 1985) constrains this interval to upper middle Eocene to late Eocene, though *A. diktyoplokum* has been recorded occasionally from the Oligocene (Benedek and Müller, 1976; Goodman and Ford, 1983).

Interval of ≈ 337–308 mbsf. Last occurrence of *Corrudinium incompositum* in Section 105-647A-32R, CC (lower NP23; Stover, 1977), constrains this interval to earliest Oligocene or older.

Later work will no doubt refine this biostratigraphy, particularly in the lower part of the hole (below 600 mbsf, where stratigraphically useful species of the Wetzeliellaceae occur. This group, together with the *Glaphyrocysta-Areosphaeridium* and *Phthanoperidinium* lineages are however poorly represented above 600 mbsf, and it may not be possible to tie accurately this part of the section with other Paleocene dinocyst zonations, which are mainly based on species of these lineages.

The Paleogene dinocyst assemblages of this hole are comparable to other assemblages described from the North Atlantic and northwest Europe, particularly for the Eocene interval. Some of the differences observed are probably a result of the more bathyal nature of the assemblages from this site.

The common occurrence of *Histiocysta*(?) sp. described by Clowes and Morgans (1985) and the presence of *Hemiplacophora semilunifera* within the late middle to late Eocene interval suggests some affinities with South Atlantic assemblages described by Goodman and Ford (1983).

Environment

The persistent presence of *Impagidinium* spp., today a predominantly oceanic group, and the poor representation of the Wetzeliellaceae and Phthanoperidiniaceae, which flourish on the shelf, indicate a more open-ocean rather than shelf environment, as supported by low dinocyst abundance. The rarity of pollen (mainly *Pinus*, which is prone to long-distance dispersal) suggests a fair distance from the coastline.

The presence of *Wetzeliellaceae* spp. from Section 105-647A-64R, CC, downhole may indicate shallower conditions. However, among these are *Dracodinium* spp. (Sample 105-647A-70R-4, 42 cm, and Section 105-647A-69R, CC), which appear to favor more open-marine environments than do other genera of the Wetzeliellaceae (Islam, 1984). The lack of observed increase in pollen within this interval implies some distance from the coastline. It is not possible to infer climatic conditions from the sparse pollen assemblages. *Pinus*, which is often the sole constituent, has a broad climatic tolerance.

A number of isolated occurrences of reworked *Aquilapollenites* s.l. pollen species were found through much of the Eocene at this site, indicating that the Late Cretaceous vegetational source belonged to the *Aquilapollenites* phylogeographic province. This province was circumpolar in extent during the end of the Late Cretaceous; its southernmost boundary is generally placed near the southern tip of Greenland by extrapolation from eastern Canadian and northwestern European localities.

Summary

Biostratigraphy

The biostratigraphic summary chart is presented in Figure 29. Except for the placement of the lower/upper Oligocene and Oligocene/Miocene boundaries, few uncertainties exist in the composite biostratigraphies. The placement of stage boundaries is discussed below.

The Pliocene/Pleistocene boundary (1.6 Ma) is tentatively placed within Core 105-647A-8R, or approximately 70 mbsf, on the basis of extrapolation of the sedimentation-rate curve. This placement is between the FAD of *Globoratalia truncatulinoides* in Section 105-647A-7R, CC, and the LAD of *Discoaster brou-*

weri in Sample 105-647A-10R-3, 39 cm. Both datums are reported at 1.9 Ma by Berggren et al. (in press), which suggests that one or both of these datums are diachronous at this site. However, because of the rarity of *D. brouweri* in Sample 105-647A-10R-3, 39 cm, the true last occurrence may be higher. Additional samples will further constrain the exact placement of the Pliocene/Pleistocene boundary.

Section 105-647A-12R, CC, is placed within Zone NN16 (upper Pliocene), whereas Samples 105-647A-13R-1, 45 cm, and 105-647A-13R-2, 53–55 cm, are assigned to Zone NN11 (upper Miocene). This indicates the existence of a hiatus of at least 2 Ma, which corresponds to the boundary between Lithologic Unit I and Subunit IIA.

On the basis of the radiolarian stratigraphy, Section 105-647A-13, CC, is older than 17.5 Ma. This indicates that another hiatus, having a duration of no less than 9 Ma, exists between Sample 105-647A-13R-2, 24 cm, and Section 105-647A-13R, CC (approximating the Subunit IIA/IIB boundary).

Calcareous nannofossil and diatom stratigraphies indicate that the upper Oligocene may be condensed or missing from Hole 647A. The presence of the nannofossil *Sphenolithus ciperoensis* in Sample 105-647A-16R-3, 36–38 cm, indicates an age no older than the base of Zone NP24, or 30.3 Ma. In the interval above and up to Sample 105-647A-15R-1, 68–70 cm, nannofossils indicate only an Oligocene age, not necessarily younger than the 30-Ma age assigned to the lower/upper Oligocene boundary (Berggren et al., 1986a).

Diatom evidence suggests an early Oligocene age for Core 105-647A-22R, and the LAD of the nannofossil *Reticulofenestra umbilica* in Sample 105-647A-23R4, 91–93 cm, indicates the NN22/NN23 zonal boundary (34.6 Ma).

The placement of the Eocene/Oligocene boundary is well bracketed by nannofossil and planktonic and benthic foraminifers. The first rare downcore occurrence of a flysch-type agglutinated foraminifer is observed in Section 105-647A-29R, CC. This event was correlated with the Eocene/Oligocene boundary at Site 112 (Miller et al., 1982). The LAD of *Discoaster barbadiensis*, which marks the NP20/21 zonal boundary, occurs in Sample 105-647A-30R-7, 48 cm. Section 105-647A-31R, CC, contains *Globigerina linaperta* and *Turborotalia cerroazulensis* s.l. as well as common agglutinated species, indicating a late Eocene age.

The middle/upper Eocene boundary is defined by the FAD of *Chiasmolithus oamaruensis* and the *Acarinina/Turborotalia* group. The *C. oamuruensis* datum (NP17/NP18) occurs in Sample 105-647A-46R-2, 101–103 cm. This agrees well with two agglutinated foraminiferal zonal markers that mark the middle/upper Eocene boundary in deep-water sediments in the Carpathians. The first occurrence of *Ammodiscus latus* is found in Section 105-647A-47R, CC, and the LCO of *Cyclammina amplectens* occurs in Section 105-647A-46R, CC.

Nannofossil stratigraphy suggests the presence of a hiatus or condensed section between Core 105-647A-63R and Sample 105-647A-66R-2, 49–51 cm. Sample 105-647A-63R-1, 36–38 cm, is assigned to Zone NP16 on the basis of the presence of *Reticulofenestra umbilica*. The co-occurrence of *Discoaster lodoensis* and *Tribrachiatus orthostylus* in Sample 105-647A-66R-2, 49–51 cm, indicates a zonal assignment of NP12 (lower Eocene). An interval barren of calcareous microfossils between these samples represents a period of approximately 8 Ma. This interpretation is corroborated by planktonic foraminiferal evidence, which gives a P12 zonal assignment to Sample 105-647A-62R-6, 22–25 cm, but a P8 zonal assignment to Sample 105-647A-68R-1, 129–132 cm. *Homotryblium oceanicum* has a lowest reported occurrence at Zone NP13 (Brown and Downie, 1985a) from the Rockall Plateau. Its presence in Sample 105-647A-67R-2, 28 cm, suggests a zonal age of NP13 or younger, which conflicts with the NP12 nannofossil zonal assignment.

The age of the oldest sediment recovered in Hole 647A is well constrained by nannofossils, dinocysts, and foraminifers. The presence of *Dracodinium*(?) *condylos* and *Subbotina patagonica* in Section 105-647A-69R, CC, suggests an age no older than about 56 Ma (P7–P8; uppermost NN11). Section 105-647A-70R, CC, and Sample 105-647A-71R-2, 41 cm, lie below the FAD of *Discoaster lodoensis* and are assigned to Zone NN11.

The occurrence of dinocyst *Dracodinium* sp. in Sample 105-647A-70R-4, 42 cm, indicates an age of no greater than 56.5 Ma, and the presence of *Adnatosphaeridium robustum* in Sample 105-647A-71R-1, 40 cm, indicates an age of no greater than 56 Ma, though this latter datum is probably less reliable than the former.

Preservation

Calcareous microfossil preservation is generally good throughout Hole 647A, except for two short intervals near major unconformities. Core-catcher samples from the base of Lithologic Unit I (Cores 105-647A-10R and 105-647A-11R) contain rare foraminifers and nannofossils (Fig. 27). Unit IIB (Sample 105-647A-13R-2, 148 cm, to Section 105-647A-14R, CC) displays poor preservation of calcareous microfossils (on the basis of examination of core-catcher samples) (Fig. 28). From the upper part of Unit IIIA (in Core 105-647A-15R) to the base of Hole 647A, foraminiferal and nannofossil preservation is good except for a short interval bracketing the hiatus between Cores 105-647A-67R and 105-647A-68R.

Siliceous microfossils are well-preserved in Subunits IIIA and IIIB and moderately preserved in the upper part of Subunit IIIC (Cores 105-647A-26R to 105-647A-35R). The higher total organic content in the Oligocene supports the interpretation that good biogenic silica preservation is related to high surface productivity of siliceous plankton. From Core 105-647A-35R, CC, and continuing downhole to basement, siliceous microfossils are generally rare and poorly preserved or absent. The poor siliceous microfossil preservation and abundance in the Eocene may result from dissolution, according to the analysis of silica concentration in the pore water (J. Zachos, pers. comm., 1985).

Environmental Interpretation

Foraminiferal and nannofossil evidence suggests a predominance of cool surface-water temperatures in the late Pliocene–Pleistocene. Calcareous plankton assemblages are more diverse than in the coeval interval at Site 646 and are dominated by subpolar to cool-temperate forms, such as *Neogloboquadrina* spp., *Globorotalia inflata, Coccolithus pelagicus*, and *Gephyrocapsa* spp. Dinocysts are similar to the present-day North Atlantic Drift assemblage. In addition, the presence of *Brigantedinium* species in a few samples suggests the influence of the Labrador Current. The benthic foraminiferal assemblage reflects deposition at upper-abyssal depths. In the Pleistocene, the benthic assemblage resembles a typical NADW fauna, but the increased abundance of *Nuttallides umbonifera* in the upper Pliocene suggests the presence of older bottom water.

Lower Miocene to upper Eocene nannofossil, foraminifer, and radiolarian assemblages are dominated by high-latitude taxa, although the lower Miocene radiolarian fauna also has a significant temperate to tropical component.

The diatom species observed in the Oligocene are characteristic of both low and high latitudes. The assemblage present has some affinities to the assemblage observed in the high-latitude South Atlantic (Gombos and Ciesielski, 1983), with that observed in the Norwegian Sea (Schrader and Fenner, 1976) but

containing less benthic species, and with assemblages observed by Fenner (1984a) in the South Atlantic, Equatorial Pacific, and Indian oceans.

The upper Oligocene planktonic foraminiferal fauna is the high-latitude "small *Globigerina* and *Catapsydrax* fauna" of Berggren (1978). The nannofossil assemblage displays low diversity and is dominated by *Reticulofenestra*, indicating cool-water conditions. The lower Oligocene and upper Eocene fauna displays increased abundances of *Chiloquembelina*, which is a mid-latitude marker, but the paucity of sphenoliths and discoasters argues against warm-water conditions.

Nannofossils and planktonic foraminifers display an increase in diversity from late to middle Eocene time. Discoasters are more common than in the Oligocene. Spinose planktonic foraminifers, which are warm-water indicators, are common in the late middle Eocene (below Core 105-647A-48R). *Hantkenina*, a reliable tropical indicator, is found in Core 105-647A-50R.

The low-diversity abyssal benthic foraminifer faunas of the Oligocene are subtly replaced by an agglutinated foraminiferal assemblage in the upper Eocene. This change appears to have been gradual, occurring over an interval of about 4 m.y., and was attributed by Miller et al. (1982) to a change in hydrographic properties associated with the development of cold bottom-water circulation and the formation of the psychrosphere. The Eocene calcareous benthic assemblage is a lower bathyal to abyssal fauna similar to faunas described by Tjalsma and Lohmann (1983) from the southwestern Atlantic and by Miller et al. (1984) from Site 549. A reasonable estimate of the middle to late Eocene paleodepth is 2000–3000 m, based on the similarity between these faunas. The dinocyst assemblage favors an open-marine environment throughout the Paleogene, and the scarcity of pollen suggests some distance from the coastline. The increased presence of *Wetzeliellaceae* spp. near the base of the hole may imply less open-marine conditions.

SEDIMENT-ACCUMULATION RATES

Sedimentation-Rate Curve

The biostratigraphic and magnetostratigraphic data used in constructing the sedimentation-rate curve (Fig. 30) are summarized in Table 4. Available stratigraphic data for Site 647 indicate moderate sediment-accumulation rates of 16–47 m/m.y. The sedimentation at Site 647 is interrupted by three hiatuses, the longest having a minimum duration of about 9.3 m.y. Five main intervals may be distinguished. Key stratigraphic data, as follows, were used to construct the age–depth curve for each of these intervals:

1. *0–116.0 mbsf (0–2.5 Ma).* In this interval, six biostratigraphic and seven paleomagnetic datums are recorded. A relatively good agreement among the stratigraphic data is observed, except between the first occurrence of *G. truncatulinoides* (Fig. 30, no. 3) and the last occurrence of *D. brouweri* (Fig. 30, no. 4). Both indicate an age of 1.9 Ma but are recorded at different depths (68.0–76.0 mbsf and 92.2 mbsf, respectively). The base of the 0–116 mbsf interval lies below the LAD of *Discoaster surculus* (Fig. 30, no. 6) and above the LAD of *Reticulofenestra pseudoumbilica*. The age at 116.0 mbsf is therefore older than 2.5 Ma. The best-fitting curve drawn through the data gives a mean sedimentation rate at this interval of 46 m/m.y. from 0 to 2.5 Ma.

2. *116.0–135.0 mbsf (2.5 to 22.5 Ma).* Biostratigraphic data suggest that two hiatuses occurred in this interval. The occurrence of *D. quinqueramus* (Fig. 30, no. 7) from 116.5 to 118.0 mbsf indicates a late Miocene age (5.6–8.2 Ma). A minimum period of 3.1 m.y. thus separates the sediments between 116.0 and 116.5 mbsf. This hiatus may correspond to an apparently sharp lithological contact between Cores 105-647A-12R and 105-647A-13R.

A second hiatus occurs in Core 105-647A-13R. On the basis of radiolarian stratigraphy, a lower Miocene age (17.5–22.5 Ma) is assigned to the interval from Sections 105-647A-13R, CC, through 105-647A-14R, CC (123.9–135.4 mbsf). A minimum gap of 9.3 m.y. therefore occurs between 118.0 and 121.0 mbsf. The exact depth of the hiatus is uncertain but probably occurs at the lithologic break recorded at 119.3 mbsf (between Subunits IIA and IIB).

3. *135.0–215.0 mbsf (>22.5 Ma–34.6 Ma).* In Sample 105-647A-15R-1, 68–70 cm, an Oligocene age is indicated on the basis of nannofossil evidence. However, no biostratigraphic events are observed in this core that would have indicated a precise age for Core 105-647A-15R.

The occurrence of *Sphenolithus ciperoensis* (Fig. 30, no. 13) in Sample 105-647A-16R-3, 36–38 cm, denotes an age younger than 30.3 Ma at this level. The LAD of *Reticulofenestra umbilica* occurs in Sample 105-647A-23R-4, 91–93 cm, indicating an age older than 34.6 Ma for this sample. Upward extrapolation of a sedimentation-rate curve drawn between these two points suggests an age of 29.5 Ma for the top of Core 105-647A-15R. A hiatus of as much as 7.0 m.y. is thereby indicated between Section 105-647A-14R, CC, and Sample 105-647A-15R-1, 68–70 cm. The average sedimentation rate over the 135.0–215.0-m interval is 16 m/m.y.

4. *215.0–608.0 mbsf (34.6–45.5 Ma).* Twenty-four biostratigraphic and magnetostratigraphic datums occur within this interval. Few of these datums are confidently considered to be true biozone events. Rather, they may represent only shortened local ranges. For this reason, few tightly constrained points occur in this interval through which we can fit a detailed, multisegmented sedimentation-rate curve. The data, however, strongly constrain a simple best-fit straight line. The average sedimentation rate determined from this curve is 36 m/m.y.

5. *608.0 mbsf to total depth (45.5–55.8 Ma).* Nine biostratigraphic datums are recorded within the lower part of this interval. None of these datums strongly restrict the placement of the sedimentation-rate curve, although evidence of four events occurs between 640 and 696.6 mbsf that can be used to infer an age–depth correlation: the occurrence of the planktonic foraminifer *Subbotina patagonica* at 696.6 mbsf (53.4–56.1 Ma); the FAD of the nannofossil *Discoaster lodoensis* between 675.5 and 685 mbsf (55.3 Ma); the occurrence of the dinocyst *Homotryblium oceanicum* at 648 mbsf (53.6 Ma); and the occurrence of the nannofossil *Tribrachiatus orthostylus* at 638.5 mbsf.

The first two of these datums define the lower end of a correlation line (>53.7 Ma). The latter two datums, however, conflict with each other. To minimize this discrepancy, the sedimentation-rate curve is placed midway between these two points. The average sedimentation rate thus determined for this interval (640–696.6 mbsf) is 25 m/m.y. No data were obtained within the interval from 608.0 to 642 mbsf. Therefore, placement of the sedimentation-rate curve is tentative and indicated by a dashed line. Sedimentation over this interval could have been either continuous, although at a reduced rate, or interrupted by one or more hiatuses.

INORGANIC GEOCHEMISTRY

Results of shipboard analyses of Site 647 interstitial waters are reported in Table 5 and Figure 31. We took 18 interstitial-water samples from the sediment/water interface to 650 mbsf. Several large gaps in the sampling interval occur as a result of poor recovery in various sections of the hole. Analytical methods are summarized in the "Explanatory Notes" chapter (this volume).

Besides calcium- (Ca-) and magnesium- (Mg-) ion gradients, most chemical parameters show either a slow rate of change or no variation with depth. Alkalinity values, which decrease slightly with depth, are relatively low, generally falling below 4.0 meq/dm^3 (Fig. 31A). These low levels can be attributed to the reduced rates of organic carbon oxidation plus the uptake of excess bicarbonate ion into authigenic carbonate mineral phases. Sulfate concentrations, which are uncommonly high (15–26 mmol), decline by 8–10 mmol from the top of the hole to 400 mbsf (Fig. 31B). This decrease indicates that some sulfate reduction has occurred. However, the absence of a true subsurface minimum suggests that the levels of reduction have been minimal. This is supported by the apparent lack of methane production within the sediment column at this site ("Organic Geochemistry" section, this chapter). The presence of authigenic sulfate minerals (gypsum and barite) around the margins of isolated carbonate concretions in Subunit IIIC and Unit IV sediments suggests an additional supply of sulfate possibly by leaching of sulfur from basement basalts, followed by precipitation in overlying sediments. During low-temperature oxidative alteration of basalts, igneous sulfides are transformed to SO_4, which may be gradually removed from the basement basalts by upward advection of fluids (Andrews, 1979).

Calcium contents display a linear increase with depth from 10 mmol near the top of the hole to 47 mmol at 600 mbsf (Fig. 31C). This coincides with a linear decrease of similar magnitude in magnesium values but only to 430 mbsf, after which magnesium concentrations show no change (Fig. 31D). The trends in these concentration gradients show little or no correlation with changes in sediment lithology at Site 647, which indicates that upward migration of calcium-rich and magnesium-poor interstitial waters from layer 2 basalts has primarily caused the observed gradients. The change in slope of the magnesium gradient below 430 mbsf possibly may have resulted from a diagenetic overprint. Slight inflections in both concentration gradients at 257 and 430 mbsf were produced by contamination from drilling fluids.

In contrast to results from Sites 645 and 646, chlorinity and salinity contents both display little variation with depth to 200 mbsf and average 19.5 and 34.2 ‰, respectively. Both concentration gradients become slightly depleted by about 1 ‰ from 200 to 350 mbsf, after which chlorinity values remain relatively constant and salinity values fluctuate between 32.5 and 34.0 ‰.

ORGANIC GEOCHEMISTRY

At Site 647, 27 vacutainer samples were analyzed for hydrocarbons, and 156 physical property (PP) and organic geochemistry (CO) samples were analyzed for organic and inorganic carbon.

Hydrocarbon Gases

No gas pockets were observed throughout the entire sediment section down to the basement at 699 mbsf. Thus, vacutainer samples were taken from small gaps, found in various places in the cores. Hydrocarbon gases were found only in two of the vacutainer samples. In Cores 105-647A-1R and 105-647A-41R, small amounts of methane were measured (115 and 113 ppm, respectively).

Organic and Inorganic Carbon

The total organic carbon (TOC) content was obtained by direct measurements on acidified samples, using the Perkin Elmer 240C elemental analyzer. The inorganic carbon (expressed as $CaCO_3$ percentage) was either calculated by the difference between total carbon (measured by elemental analyzer on the whole sample) and TOC or determined by the carbonate bomb (see "Explanatory Notes" chapter, this volume).

In general, all TOC values at Site 647 are very low, ranging between 0.05% and 0.50% (Fig. 32, Table 6). The higher values occur in the upper 300 m, reaching a maxima of about 0.5% in the upper Pliocene and the lower Oligocene. The short, intercalated upper Miocene section, which is separated by hiatuses from the intervals below and above (see "Sediment-Accumulation Rates" section, this chapter), is characterized by very low organic carbon contents of about 0.1%. The lower Oligocene TOC maximum coincides with a maximum occurrence of biogenic opal (Lithologic Subunit IIIB, see "Sedimentology" section, this chapter), which could indicate increased oceanic productivity. However, Rock-Eval analyses show low hydrogen index values of <50 mg HC/g C_{org} and high oxygen values of >400 mg CO_2/g C_{org} (T. Cederberg, pers. comm., 1985). The Eocene section (i.e., the interval below 290 mbsf) is characterized by constantly low TOC values between 0.1% and 0.3%. The reddish, greenish, and blackish sediments (see "Sedimentology" section, this chapter) show no difference in organic carbon content. In the 60-m-thick interval just above the basement (635 to 695 mbsf), minimum organic carbon of <0.1% was recorded (Fig. 32). The carbonate values fluctuate between 0% and 55% (Fig. 32). Carbonate contents of <20% dominate in the upper 145 m (Lithologic Units I and II), between 202 and 240 mbsf (Subunit IIIB), and between 610 and 670 mbsf. The intervals between 145 and 202 mbsf and between 240 and 610 mbsf are characterized by carbonate values ranging from about 20% to 55%. The high carbonate value of 80% at 517.8 mbsf (Sample 105-647A-54R-5, 66 cm) is from a dolomite concretion (see "Sedimentology" section, this chapter).

PALEOMAGNETICS

Paleomagnetic studies of sediments cored at Site 647 consisted of both pass-through and discrete-sample measurements, as described in the "Explanatory Notes" chapter (this volume). Discrete samples were taken at nominal intervals of 1.5 m (one per core section). In general, the rotary cores obtained from the upper part of Hole 647A were mechanically disturbed by the drilling process and therefore were not well suited for paleomagnetic study. With depth, the sediments are more indurated, and biscuits or broken fragments that clearly had not rotated about a horizontal axis were sampled for paleomagnetic measurements. Sediments from Site 647 are characterized by lower magnetization intensities (1×10^{-3} Am^{-1}) than those encountered at Site 646, most likely because of the decrease in terrigenous material in these sediments. In the lower intervals of Hole 647A, some magnetization intensities dropped to values near or below the cryogenic noise level, making interpretation of these data tenuous at best. Discrete samples from these intervals were not subjected to partial demagnetization studies because the natural remanent magnetizations were at or below the noise level of the spinner magnetometer.

Results

Hole 647A

Cores 105-647A-10R, 105-647A-11R, and 105-647A-12R exhibit few signs of drilling disturbance and instead are characterized by nearly horizontal bedding. The inclination records from pass-through and discrete-sample measurements of these three cores allow a magnetic-polarity stratigraphy to be established. Shipboard biostratigraphic results place these cores in the upper Pliocene. Given this constraint, the observed polarity record is correlated with the base of the Olduvai Subchron to the top of

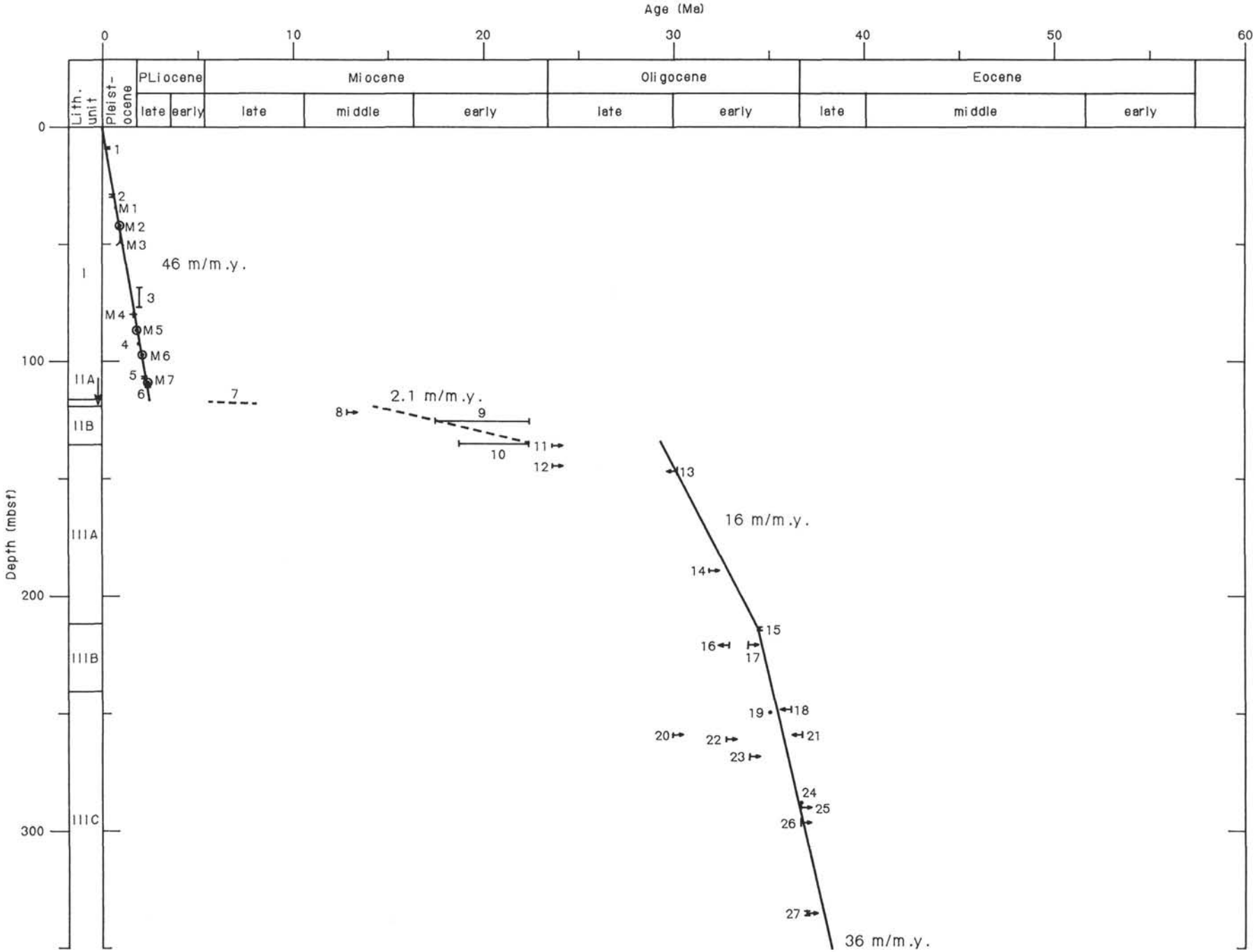
Age (Ma)
0
10
20
30
40
50
60
Lith. unit
Pleist-ocene
PLiocene
Miocene
Oligocene
Eocene
late
early
late
middle
early
late
early
late
middle
early
Depth (mbsf)
0
100
200
300
I
IIA
IIB
IIIA
IIIB
IIIC
M1
M2
M3
M4
M5
M6
M7
46 m/m.y.
2.1 m/m.y.
16 m/m.y.
36 m/m.y.

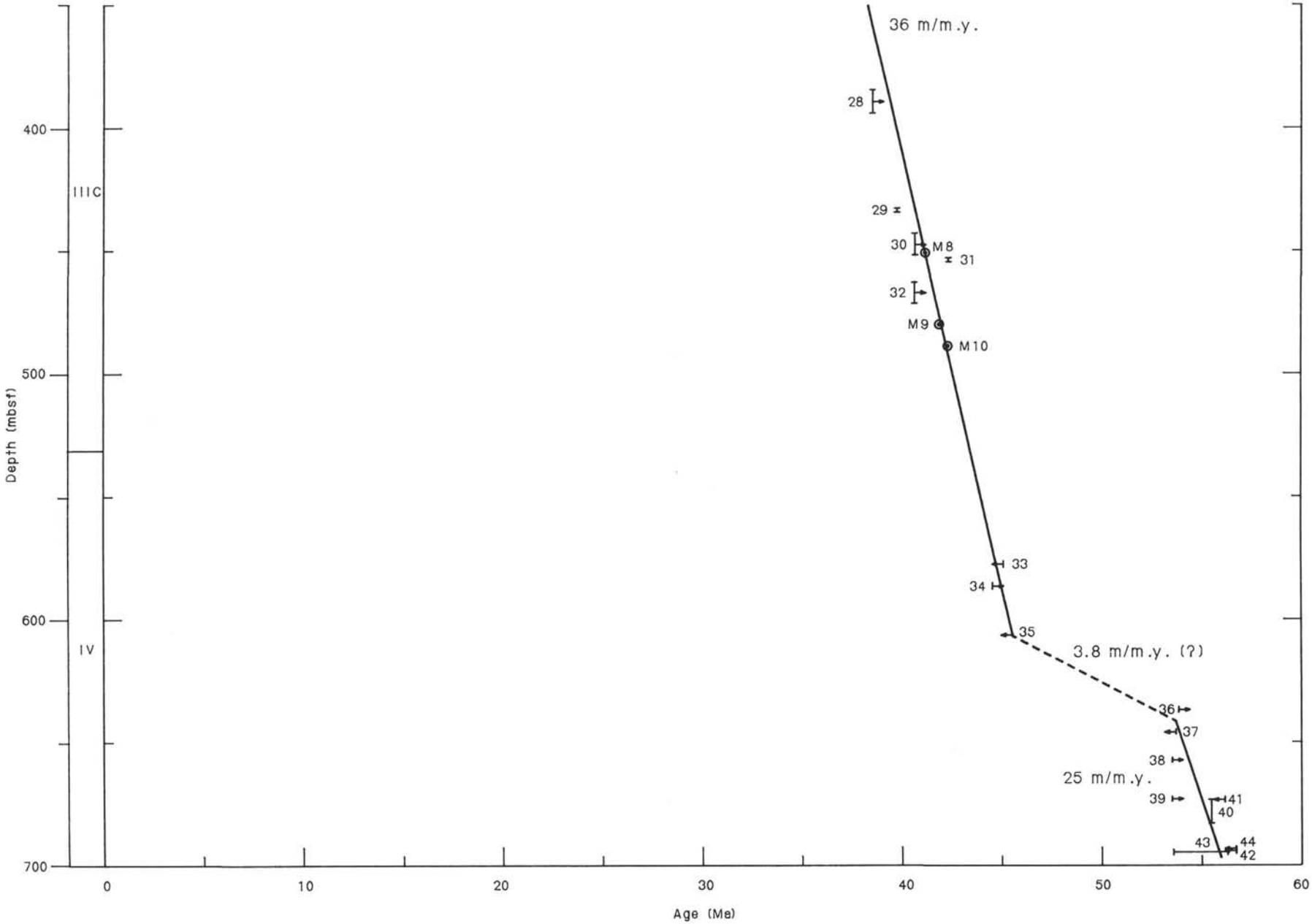

Figure 30. Sedimentation rates, Hole 647A.

Table 4. Datums used in constructing the sedimentation-rate curve.

Fossil group	Datum/event	Zone/age	Depth (mbsf)
1. Nannofossils	FAD *Emiliana huxleyi*	NN20/21, 0.247 Ma	8.8–9.5
2. Nannofossils	LAD *Pseudoemiliana lacunosa*	NN19/20, 0.475 Ma	28.5–30.0
3. Foraminifers	FAD *Globorotalia truncatulinoides*	1.9 Ma	68.0–77.6
4. Nannofossils	LAD *Discoaster brouweri*	NN18/19, 1.9 Ma	92.2
5. Nannofossils	LAD *Discoaster pentaradiatus*	NN17/18, 2.2 Ma	106.7–107.5
6. Nannofossils	LAD *Discoaster surculus*	NN16/17, 2.4 Ma	109.5–111.0
7. Nannofossils	Occurrence *Discoaster quinqueramus*	NN11, 5.6–8.2 Ma	116.5–118.0
8. Diatoms	Occurrence *Coscinodiscus lewisianus*	>12.9 Ma	121.5
9. Radiolarians	Occurrence *Stichocorys delmontense* and *Naviculopsis quadratum* (silicoflagellate)	17.5–21.0 Ma	125.7
10. Radiolarians	Occurrence *Cyrtocapsella tetrapera* and absence *Stichocorys delmontense*	19.2–22.5 Ma	135.4
11. Nannofossils	LCO *Dictyococcites bisectus*	>23.7 Ma	135.4–136.1
12. Dinocysts	Occurrence *Pentadinium imaginatum*	>23.7 Ma	145.1
13. Nannofossils	FAD *Sphenolithus ciperoensis*	<30.3 Ma	147.5
14. Foraminifers	LAD *Globigerina angiporoides*	>32.0 Ma	190.0
15. Nannofossils	LAD *Reticulofenestra umbilica*	NP22/23, 34.6 Ma	214.0–215.5
16. Radiolarians	Occurrence *Cyclamperium pegetrum*	<33 Ma	221.9
17. Diatoms	LO *Cestodiscus reticulatus*	34 Ma	221.9
18. Diatoms	FO *Cestodiscus reticulatus*	36.2 Ma	239.0
19. Nannofossils	LAD *Ericsonia formosa*	35.1 Ma	250.5–251
20. Foraminifers	LAD *Chiloguembelina*	30.0 Ma	260.1
21. Diatoms	Occurrence *Coscinodiscus excavatus*	36.8 Ma	260.1
22. Foraminifers	Occurrence *Globigerina ampliapertura*	>32.8 Ma	262.0
23. Foraminifers	LAD *Pseudohastigerina*	34 Ma	269.7
24. Nannofossils	LAD *Discoaster barbadiensis*	NP20/21, 36.7 Ma	288.8
25. Foraminifers	LO *Globigerina linaperta*	36.7 Ma	291.0
26. Foraminifers	LAD *Turborotalia cerroazulensis* s.l.	36.7 Ma	298.6
27. Foraminifers	LAD *Globigerinatheka*	37.0 Ma	335.0–337.2
28. Foraminifers	LAD *Nuttallides truempyi*	38.5 Ma	385.4–395.1
29. Nannofossils	FAD *Chiasmolithus oamaruensis*	NP17/18, 39.7 Ma	433.5–435.0
30. Foraminifers	LAD *Truncorotaloides*	40.6 Ma	443.5–453.2
31. Nannofossils	LAD *Chiasmolithus solitus*	NP16/17, 42.3 Ma	453.2–454.0
32. Foraminifers	LAD *Acarinina*	40.6 Ma	463.5–472.5
33. Foraminifers	LAD *Globigerinatheka* index	45.0 Ma	578.8
34. Foraminifers	LO *Pseudohastigerina wilcoxensis*	mid P12, 44.5 Ma	588.4
35. Nannofossils	FAD *Reticulofenestra umbilica*	<45.5 Ma	608
36. Nannofossils	Occurrence *Tribrachiatus orthostylus* and *Discoaster lodoensis*	>55.3 Ma	638.5
37. Dinocysts	FO *Homotryblium oceanicum*	<53.6 Ma	648.0
38. Foraminifers	Occurrence of *Morozovella lensiformis*	>53.4 Ma	659.0
39. Foraminifers	LO *Aragonia semireticulata*	>53.4 Ma	675.5
40. Nannofossils	FAD *Discoaster lodoensis*	55.3 Ma	675.5–685.0
41. Dinocysts	FO ?*Dracodinium condylos*	56.0 Ma	675.5
42. Nannofossils	Occurrence *Tribrachiatus orthostylus*	<56.6 Ma	696.6
43. Foraminifers	Occurrence *Subbotina patagonica*	P7-P8, 53.4–56.1 Ma	696.6
44. Dinocysts	FO *Dracodinium*	<56.6 Ma	696.6
M1	Brunhes/Matuyama boundary	0.73	32.06–33.88
M2	Top Jaramillo	0.91	42.06–42.68
M3	Base Jaramillo	0.98	44.18–49.80
M4	Top Olduvai	1.66	80.1–80.55
M5	Base Olduvai	1.88	86.2–87.22
M6	Reunion	2.10	97.25–97.55
M7	Matuyama/Gauss boundary	2.47	109.84–109.94
M8	Base Chron C17	41.11	450.75–453.25
M9	Top N2 event of Chron C18	41.80	481.45–482.15
M10	Base N2 event of Chron C18	42.23	490.15–490.25

the Gauss Chron, as indicated in Table 7 (Berggren et al., 1986a). The very short normal subchronozone observed at 97 mbsf may correlate with the Reunion Subchron (2.01 Ma).

Poor recovery and drilling disturbance in the cores make it difficult to interpret results from the lower intervals of Hole 647A for a polarity stratigraphy. Measurement of Cores 105-647A-43R through 105-647A-53R, however, yielded a well-defined polarity-reversal sequence. Biostratigraphic results ("Biostratigraphy" section, this chapter) place this interval in the upper Eocene. Based on this age determination, the reversals observed in Cores 105-647A-42R through 105-647A-53R are correlated with Chron C17 and the second-youngest normal-polarity subchron in Chron C18 (Table 7). This correlation agrees with the shipboard biostratigraphic data but calls for a significant change in sedimentation rate because of the lack of normally magnetized material below the base of the polarity zone correlated with Chron C18N2. Further shore-based measurements of discrete samples may yield a more detailed polarity record from this hole.

The occurrence of red sediment in cores from the lower section of Hole 647A suggests the presence of hematite, limonite, or some other iron-oxide material. Samples from these intervals exhibit very high coercitivities, as evidenced by high median destructive fields, suggesting the presence of hematite in these sediments. For this reason, an interpretation of the polarity record of Cores 105-647A-63R through 105-647A-70R will await the results of shore-based thermal demagnetization studies.

Hydraulic piston cores taken at Hole 647B are relatively undisturbed compared with the rotary cores from this same interval in Hole 647A, although several of the cores exhibit several

Table 5. Summary of interstitial-water chemistry results, Site 647. Alkalinity and pH measurements were not conducted for those samples having a recovery volume of <20 mL.

Sample interval (cm)	Depth (mbsf)	pH	Alkalinity (meq/DM^3)	Salinity (‰)	Chlorinity (‰)	Ca^{++} (mmol)	Mg^{++} (mmol)	$Sulfate^{=}$ (mmol)
105-647A-1R-5, 140–150	7.4	7.45	3.298	34.5	19.13	10.79	50.18	26.63
105-647A-6R-5, 140–150	56.0	7.66	2.175	34.2	19.70	12.81	46.06	21.09
105-647A-9R-3, 140–150	82.0	7.67	2.425	34.2	19.97	14.08	43.47	22.05
105-647A-12R-3, 140–150	111.1	7.57	4.014	34.0	19.68	15.36	43.28	21.33
105-647A-15R-2, 140–150	138.3	7.51	3.345	33.9	19.34	16.11	45.41	23.36
105-647A-19R-5, 140–150	181.2	6.20	3.032	34.1	19.63	19.47	41.96	23.00
105-647A-23R-2, 140–150	215.2	7.15	4.819	34.4	19.70	22.37	41.32	22.40
105-647A-27R-5, 140–150	257.8	7.57	2.654	34.0	19.86	19.26	41.24	23.32
105-647A-30R-5, 140–150	286.8	6.98	3.106	33.9	19.20	26.40	38.45	20.81
105-647A-36R-3, 140–150	341.6	—	—	33.0	18.79	29.15	33.29	19.30
105-647A-39R-2, 140–150	369.0	—	—	33.1	19.16	31.64	32.04	17.09
105-647A-42R-5, 140–150	402.5	—	—	33.1	19.38	32.86	26.47	15.85
105-647A-45R-4, 140–150	430.0	7.38	1.738	33.7	19.17	24.77	37.44	20.46
105-647A-48R-5, 140–150	460.6	7.58	1.671	34.1	19.05	36.12	28.65	17.23
105-647A-51R-5, 140–150	489.5	—	—	33.0	18.88	34.50	28.10	13.24
105-647A-54R-4, 140–150	517.0	—	—	32.5	19.13	38.53	28.42	14.33
105-647A-64R-2, 140–150	620.4	—	—	33.8	19.27	47.11	27.06	15.70
105-647A-67R-2, 140–150	649.4	—	—	33.1	18.60	43.88	28.86	15.90

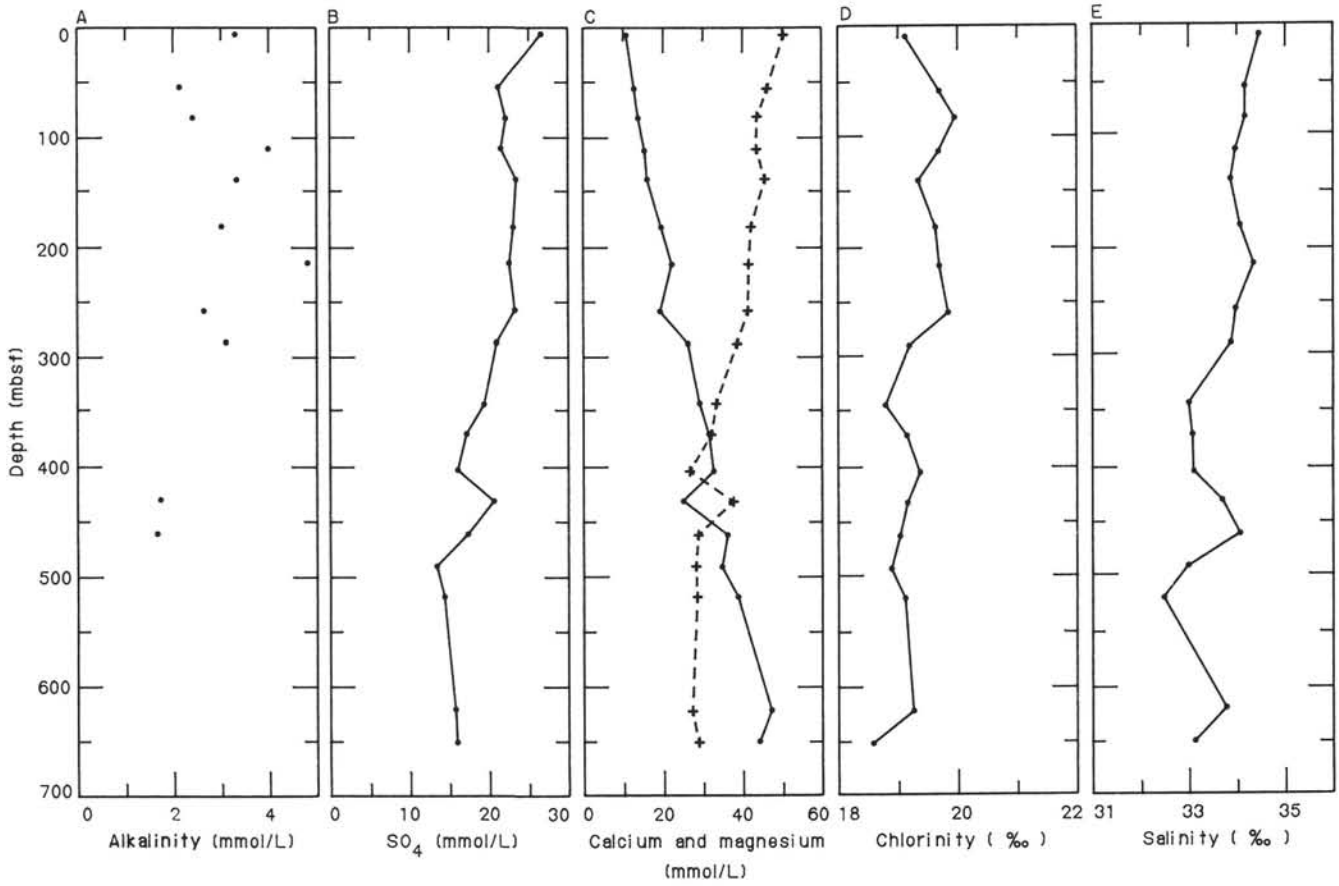

Figure 31. (A) Alkalinity-depth profile, Site 647. (B) Sulfate-depth profile, Site 647. (C) Calcium- and magnesium-depth profiles, Site 647. Calcium values are represented by circles, magnesium by plus (+) symbols. (D) Chlorinity-depth profile, Site 647. (E) Salinity-depth profile, Site 647.

meters of inflow and drilling disturbance. The polarity sequence defined by the discrete-sample record is readily correlated with the magnetic-polarity time scale. The ages and depths of the reversals are indicated in Table 7.

Magnetic Susceptibility

The magnetic susceptibility of 195 samples taken downhole at 647A was measured. Figure 33 is a graph of susceptibility ($10^{-5} \times 4\pi$SI) versus depth. As explained in the "Explanatory Notes" chapter (this volume), these values have not been corrected for volume or mass, and results will be discussed further by Hall and King (this volume, Part B). Lithologic units from Table 2 and geologic boundaries from micropaleontological data are shown.

The Miocene (Unit II) shows a period of decreasing susceptibility into the Oligocene (Subunit IIIA), accompanied by a

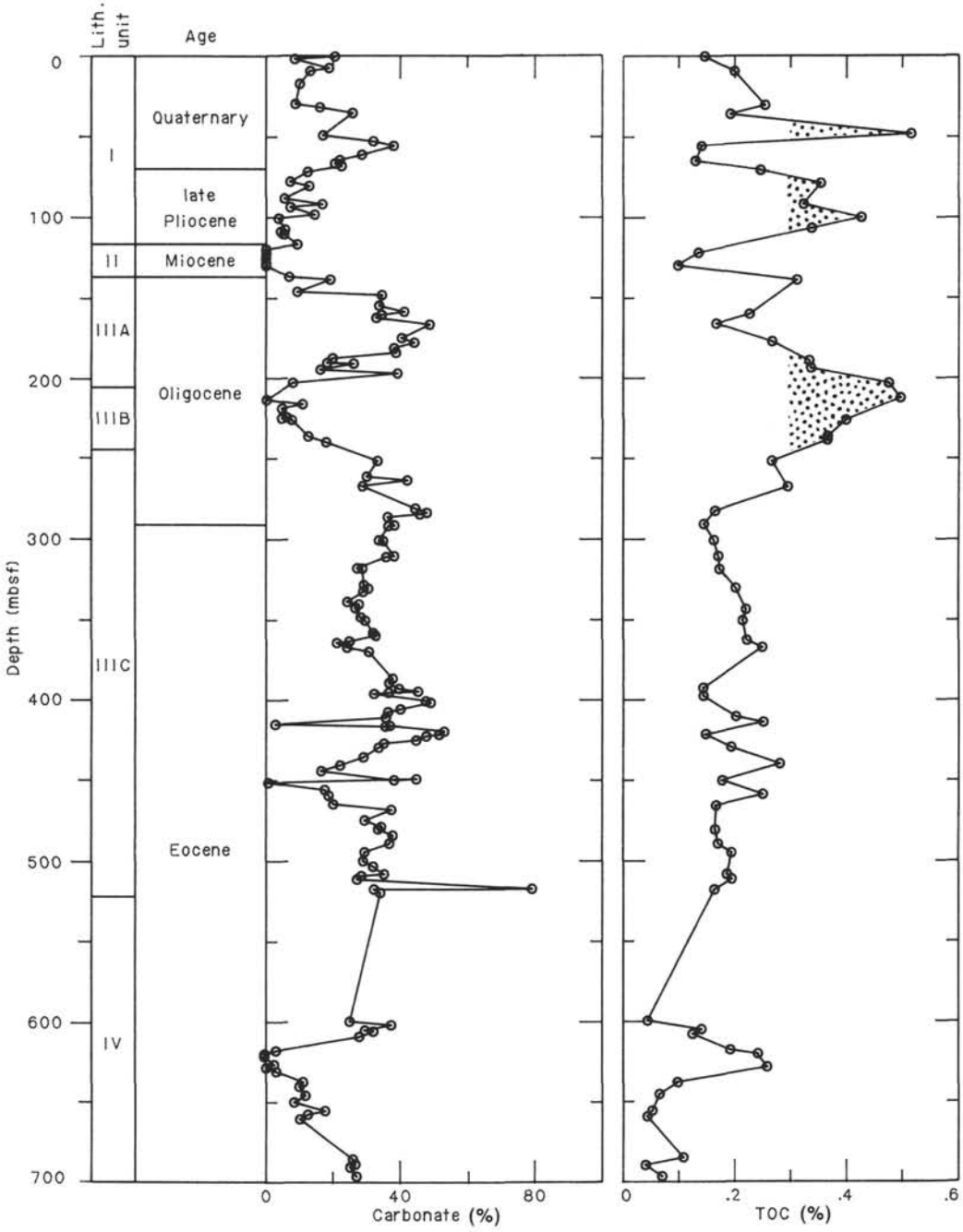

Figure 32. Organic carbon and calcium carbonate contents versus depth. Roman numerals indicate lithologic units. Hatched area marks occurrence of biogenic opal observed in smear slides.

change in sediment composition from clays and silts in the Pleistocene and Pliocene to carbonate oozes, nannofossil muds, and siliceous clays of the Oligocene and lower Eocene. Susceptibility generally increases through the Oligocene and into the Eocene (Subunits IIIB and IIIC), but the susceptibilities never reach values as high as in the Pliocene–Pleistocene sediments. The increase in clay content from 430 mbsf to the base of the hole does not appear to affect this general trend. The peaks near 600 mbsf correspond to red sediments, which may contain hematite, as suggested by the high mean destructive field (40 mT) during alternating-field demagnetization. The low susceptibilities probably result from biogenic sediments diluting the magnetic minerals. This assumes that the magnetic minerals are detrital in origin and that they accumulated at a constant rate.

The reason for the increasing susceptibility through the Oligocene and Eocene is unknown but may result from compaction of sediments.

Whole-core susceptibilities of Hole 647B are plotted in Figure 34. The presence of inflow material in the cores results in numerous data gaps. However, as with Site 646, a direct correlation between carbonate content and magnetic susceptibility does not appear.

PHYSICAL PROPERTIES

GRAPE Wet-Bulk Density

GRAPE density profiles (logs preceding core-description forms, this chapter) from Hole 647A show few distinctive fea-

Table 6. Organic carbon and carbonate contents in sediments, Site 647. Asterisk indicates CO sample. Plus symbol indicates sample measured by both CHN analyzer and carbonate bomb for carbonate content.

Sample	Depth (mbsf)	Carbonate (%)	TOC (%)
105-647A-1R-1, 75-77	0.75	21.8	00.15
105-647A-1R-2, 60-62	2.10	8.0	
105-647A-1R-6, 75-77	8.25	19.0	
105-647A-2R-1, 85-87	10.05	12.7	0.20
105-647A-2R-6, 55-57	17.25	10.0	
105-647A-4R-1, 135-137	29.95	8.1	0.26
105-647A-4R-3, 65-67	32.25	16.0	
105-647A-4R-5, 75-77	35.35	26.2	0.19
105-647A-6R-1, 70-72	49.30	16.6	0.52
105-647A-6R-3, 75-77	52.35	32.0	
105-647A-6R-5, 70-72	55.30	38.3	0.14
105-647A-7R-2, 72-74	60.52	29.0	
105-647A-7R-4, 75-77	63.55	22.0	
105-647A-7R-5, 119-121*	65.49	21.7	0.13
105-647A-7R-6, 75-77	66.55	20.0	
105-647A-8R-1, 74-76	68.74	23.0	
105-647A-8R-3, 65-67	71.65	12.0	0.25
105-647A-9R-1, 77-79	78.37	7.0	
105-647A-9R-2, 80-82+	79.90	13.0	
105-647A-9R-2, 80-82+	79.90	13.7	0.36
105-647A-10R-1, 75-77	88.05	5.0	
105-647A-10R-3, 77-79	91.07	8.0	
105-647A-10R-3, 119-121*	91.49	17.8	0.32
105-647A-10R-5, 40-42	93.70	7.0	
105-647A-11R-1, 80-82	97.80	15.0	
105-647A-11R-3, 80-82	100.80	3.5	0.43
105-647A-12R-1, 70*-72+	107.40	5.8	0.34
105-647A-12R-1, 70*-72+	107.40	4.0	
105-647A-12R-3, 79-81	110.49	5.0	
105-647A-13R-1, 75-77	116.75	10.0	
105-647A-13R-3, 76-78	119.76	0.0	
105-647A-13R-4, 119-121*	121.69	0.1	0.14
105-647A-13R-5, 110-112	123.10	0.0	
105-647A-14R-1, 102-104	126.72	0.0	
105-647A-14R-3, 37-39	129.07	0.0	00.10
105-647A-15R-1, 109-111	136.49	7.0	
105-647A-15R-3, 70-72	139.10	19.4	0.32
105-647A-16R-1, 98-100	146.08	9.0	
105-647A-16R-3, 31-33	148.41	35.0	
105-647A-17R-1, 91-92	155.71	33.0	
105-647A-17R-3, 101-102	158.81	42.0	
105-647A-17R-4, 119-121*	160.49	34.5	0.23
105-647A-17R-5, 129-131	162.09	32.0	
105-647A-18R-2, 93-95	166.53	48.9	0.17
105-647A-19R-1, 84-86	174.64	40.0	
105-647A-19R-3, 88-90	177.68	44.7	0.27
105-647A-19R-5, 121-123	181.01	38.0	
105-647A-20R-1, 50-52	184.00	39.0	
105-647A-20R-3, 48-50	186.98	20.0	
105-647A-20R-4, 119-121*	189.19	18.3	0.34
105-647A-20R-5, 75-77	190.25	27.0	
105-647A-21R-1, 100-102	194.10	16.0	0.34
105-647A-21R-3, 110-112	197.20	40.0	
105-647A-22R-1, 10-12	202.80	7.8	0.48
105-647A-23R-1, 114-116	213.44	0.3	0.50
105-647A-23R-3, 91-93	216.21	12.0	
105-647A-23R-5, 49-51	218.79	5.0	
105-647A-24R-1, 130-132	223.20	6.0	
105-647A-24R-3, 10-12	225.00	4.0	
105-647A-24R-3, 119-121*	226.09	7.3	0.40
105-647A-25R-3, 123-125	235.73	12.8	0.37
105-647A-25R-5, 145-147	238.95	17.9	0.37
105-647A-27R-1, 101-103	251.41	33.8	0.27
105-647A-28R-1, 95-97	261.05	30.0	
105-647A-28R-3, 80-82	263.90	43.0	
105-647A-28R-5, 119-121*	267.29	28.2	0.30
105-647A-30R-1, 75-77	280.15	45.0	
105-647A-30R-3, 73-75	283.13	45.8	0.17
105-647A-30R-3, 73-75	283.13	49.0	
105-647A-30R-5, 75-77	286.15	36.0	
105-647A-31R-2, 75-77+	291.25	39.0	
105-647A-31R-2, 75-77+	291.25	36.3	0.15
105-647A-32R-2, 38-40+	300.48	33.6	0.17
105-647A-32R-2, 38-40+	300.48	35.0	
105-647A-33R-2, 47-49+	310.27	39.0	
105-647A-33R-2, 47-49+	310.27	35.5	0.18
105-647A-34R-1, 50-52+	318.50	27.1	0.18
105-647A-34R-1, 50-52+	318.50	29.0	
105-647A-35R-1, 93-95	328.53	29.0	

Table 6 (continued).

Sample	Depth (mbsf)	Carbonate (%)	TOC (%)
105-647A-35R-2, 119-121*	330.29	30.8	0.21
105-647A-35R-3, 103-105	331.63	30.0	
105-647A-36R-1, 118-120	338.38	24.0	
105-647A-36R-3, 83-85	341.03	28.0	
105-647A-36R-4, 105-107	342.75	26.9	0.23
105-647A-37R-1, 110-112	347.80	28.0	
105-647A-37R-3, 79-81	350.49	29.8	0.22
105-647A-38R-1, 94-96	357.34	32.0	
105-647A-38R-3, 44-46	359.84	33.0	
105-647A-38R-5, 108-110	363.48	25.0	
105-647A-38R-5, 119-121*	363.59	21.0	0.23
105-647A-39R-1, 99-101	367.09	24.2	0.26
105-647A-39R-3, 25-27	369.35	31.0	
105-647A-41R-1, 126-128	386.66	38.0	
105-647A-41R-3, 116-118	389.56	37.0	
105-647A-41R-5, 110-112	392.50	42.0	
105-647A-41R-5, 119-121*	392.59	40.2	0.15
105-647A-41R-6, 128-130	394.18	47.0	
105-647A-42R-1, 57-59	395.67	32.0	
105-647A-42R-1, 75-77	395.85	36.0	
105-647A-42R-3, 85-87	398.95	41.9	0.15
105-647A-42R-4, 113-115	400.73	49.0	
105-647A-42R-5, 76-78	401.86	50.0	
105-647A-43R-1, 62-64	405.42	40.0	
105-647A-43R-2, 71-73	407.01	36.0	
105-647A-43R-5, 65-67	411.45	36.4	0.21
105-647A-44R-1, 57-59	415.07	2.6	0.26
105-647A-44R-2, 25-27	416.25	36.0	
105-647A-44R-2, 50-52	416.50	38.0	
105-647A-44R-4, 50-52	419.50	54.0	
105-647A-44R-5, 75-77	421.25	52.0	
105-647A-44R-5, 119-121*	421.69	47.6	0.15
105-647A-45R-2, 10-12	425.70	45.0	
105-647A-45R-3, 26-28	427.36	35.0	
105-647A-45R-4, 150-152	430.10	33.6	0.20
105-647A-46R-2, 74-76	436.04	29.0	
105-647A-46R-5, 70-72	440.50	21.8	0.29
105-647A-47R-1, 44-46	443.94	16.0	
105-647A-47R-4, 121-123	449.21	38.0	
105-647A-47R-4, 141-143	449.41	45.0	
105-647A-47R-5, 119-121*	450.69	0.3	0.18
105-647A-48R-2, 51-53	455.21	18.0	
105-647A-48R-5, 71-73	459.91	19.3	0.26
105-647A-49R-2, 97-101	465.27	20.8	0.17
105-647A-49R-4, 96-98	468.26	38.0	
105-647A-50R-2, 88-90	474.88	29.0	
105-647A-50R-5, 58-60	479.08	35.0	
105-647A-50R-5, 119-121*	479.69	33.8	0.17
105-647A-51R-2, 32-34	483.92	39.0	
105-647A-51R-6, 64-66	490.24	36.6	0.18
105-647A-52R-3, 59-61	495.39	29.5	0.20
105-647A-52R-6, 91-93	500.21	29.0	
105-647A-53R-2, 69-71	503.59	32.0	
105-647A-53R-5, 64-66	508.04	36.0	
105-647A-53R-5, 119-121*	508.59	28.1	0.19
105-647A-54R-1, 136-138	512.46	26.8	0.20
105-647A-54R-4, 66-68	516.26	80.0	
105-647A-54R-4, 114-116	516.74	31.5	0.17
105-647A-54R-5, 2-4	517.12	35.0	
105-647A-62R-2, 114-116	600.74	24.6	0.05
105-647A-62R-4, 73-75	603.33	38.0	
105-647A-62R-5, 119-121*	605.29	29.6	0.15
105-647A-62R-6, 31-33	605.91	33.0	
105-647A-63R-1, 128-130	609.08	28.7	0.13
105-647A-64R-1, 24-26	617.74	3.0	
105-647A-64R-1, 95-97	618.45	0.0	0.20
105-647A-64R-3, 106-108	621.56	0.0	0.25
105-647A-64R-3, 110-112	621.60	0.0	
105-647A-65R-1, 56-58	627.76	3.0	
105-647A-65R-2, 119-121*	629.89	0.0	0.27
105-647A-65R-3, 135-137	631.55	4.0	
105-647A-66R-1, 94-96	637.74	11.7	0.10
105-647A-66R-3, 77-79	640.57	10.0	
105-647A-67R-1, 27-29	646.77	12.5	0.07
105-647A-67R-4, 2-4	651.02	8.0	
105-647A-68R-1, 31-33	656.51	18.5	0.06
105-647A-68R-1, 52-54	656.72	13.0	
105-647A-68R-2, 111-113	658.81	12.0	
105-647A-68R-4, 28-30	660.98	10.0	0.05
105-647A-70R-1, 71-73	685.91	26.5	0.12
105-647A-70R-3, 119-121*	689.39	27.2	0.04
105-647A-70R-4, 39-41	690.09	25.0	
105-647A-71R-1, 116-118	695.96	27.2	0.08

Table 7. Depths of paleomagnetic-reversal boundaries, Site 647.

Reversal	Age	Bounding samples	Depth (mbsf)
Hole 647A			
Olduvai			
bottom	1.88	105-647A-10R-2, 65-67/105-647A-10R-2, 75-77	89.44-89.54
Reunion	2.10	105-647A-11R-1, 25-27/105-647A-11-1, 55-57	97.25-97.55
Matuyama/Gauss	2.47	105-647A-12R-3, 15/105-647A-12R-3, 25-27	109.84-109.94
Chronozone 17			
bottom	42.73	105-647A-47R-5, 148/105-647A-48R-1, 5-7	450.75-453.25
Chronozone 18			
top N2	41.80	105-647A-50R-6, 145/105-647A-51R-1, 5-7	481.45-482.15
bottom N2	42.23	105-647A-51R-6, 55/105-647A-51R-6, 65-67	490.15-490.25
option 2			
Chronozone 18			
bottom	42.73	105-647A-47R-5, 148	450.75
Chron 19			
top N1	43.60	105-647A-50R-6, 145	481.45
bottom N1	44.06	105-647A-51R-6, 55	490.15
Hole 647B			
Brunhes/Matuyama	0.73	105-647B-4H-5, 86-88/105-647B-4H-6, 28-30	32.06-33.88
Jaramillo			
top	0.91	105-647B-5H-5, 26-28/105-647B-5H-5, 88-90	42.06-42.68
bottom	0.98	105-647B-5H-6, 88-90/105-647B-6H-3, 130-132	44.18-49.80
Olduvai			
top	1.66	105-647B-9H-4, 130-132/105-647B-9H-5, 25-27	80.10-80.55
bottom	1.88	105-647B-10H-2, 80-82/105-647B-10H-3, 32-34	86.20-87.22

tures, partly as a result of drilling disturbance. Disturbance evident in the profiles ranges from slight to extreme. Cores from Hole 647B display less disturbance, and GRAPE profiles are more informative. Intervals of high carbonate concentration, silt layers, and dropstones can be identified in the records. Again, the agreement between the GRAPE-determined and gravimetric-determined wet-bulk density is reasonably good.

All wet-bulk densities of basement rocks were determined by the GRAPE 2-min count technique and are listed in Table 8. Measurements were made on minicores cut from split core sections. Two determinations were made for each sample, one with the minicore axis parallel to the beam path and the other with its axis perpendicular to the beam path. Densities obtained by the latter orientation are consistently lower than those obtained by the former, suggesting that the beam path was not aligned with the diameter of the minicore.

Index Properties

Vertical profiles of the index properties of Holes 647A and 647B (Fig. 35) display three general intervals with differing characteristics. In the upper interval, 0–116 mbsf, wet-bulk density increases from 1.50 to 1.90 g/cm^3, water content decreases from 100% to 35% dry weight, and porosity decreases from 75% to 50%. Below 116 mbsf in the span of 10 m, wet-bulk density sharply decreases to 1.26 g/cm^3, water content increases to 246%, and porosity increases to 87%. This middle interval extends from 116 to approximately 250 mbsf and is characterized by a slight increase and then decrease in wet-bulk density. A similar but inverse trend is displayed by porosity. Water content varies over a greater range but displays the same overall trend as porosity. Mean grain densities between 2.30 and 2.40 g/cm^3 coincide with density minima in the middle interval (Table 9). At the base of the middle interval, wet-bulk density increases abruptly from 1.50 to 1.80 g/cm^3. In the lower interval, 250 mbsf to the base of the sediment at 699 mbsf, density increases relatively uniformly to 2.20 g/cm^3. Slightly higher bulk densities are present immediately below the recovery gap between 519 and 601 mbsf and at the base of the sediment sequence as a result of grain densities of approximately 2.90 g/cm^3 at these depths. Water content and porosity are characterized by smoothly decreasing profiles that extend across the recovery gap with no change in slope. In the lower interval, the variation in water content and porosity is from 50% to 20% and 60% to 40%, respectively.

Changes in the characteristics of the vertical profiles correspond well to changes in lithology and location of major seismic reflectors. The upper interval in the profiles correlates with Lithologic Unit I (Fig. 41), and its base is at the R2 reflector (Fig. 41). This unit is characterized by terrigenous silty and clayey sediments having lesser amounts of biogenic mud. Low wet-bulk density and high water content and porosity in the middle interval correlate with the increase in the amount of biogenic silica in the sediment (Fig. 41). The structural attributes of siliceous microfossils result in an open sediment framework, producing the anomalously low bulk density and high water content and porosity. Siliceous sediments with similarly anomalous properties at sub-bottom depths comparable to those at Site 647 were observed in Deep Sea Drilling Project sites in the equatorial Pacific (Keller and Bennett, 1973; Mayer, 1982). In Hole 647A, low wet-bulk density is also associated with mean grain densities that are as low as 2.32 g/cm^3 at 213.44 mbsf (Table 9), resulting from the abundance of biogenic silica. The depth of this particular density minima roughly corresponds to the location of the R3 reflector (Fig. 41). The bulk-density and grain-density minima between 200 and 225 mbsf correlate with the maxima in estimated biogenic silica (Fig. 41) and a maxima in total organic carbon. This correspondence is not as evident at the bulk- and grain-density minima at 125 mbsf; however, at this depth, calcium carbonate is almost entirely absent. The slight increase and then decrease in wet-bulk density between 125 and 200 mbsf coincides with a similar pattern in the carbonate content. Sediments in the lower interval are a mixture of terrigenous silts, clays, and calcareous oozes. Few clues to the character of material in the no-recovery interval are offered by the physical-property trends, the only difference being the higher grain density and, consequently, bulk density immediately below the gap. Iron and manganese oxides present in the sediment most likely cause the higher densities.

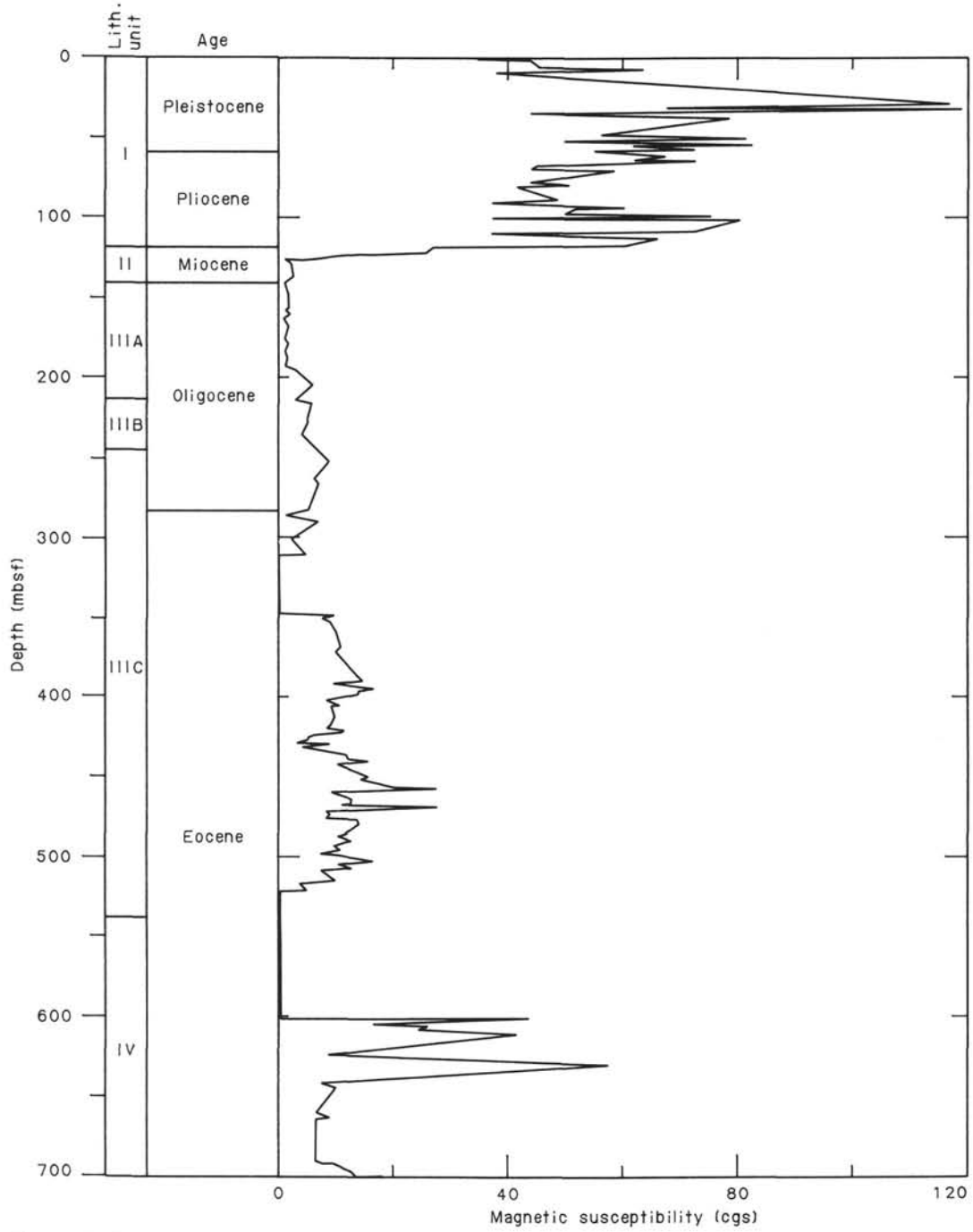

Figure 33. Discrete-sample magnetic susceptibility, Site 647. Magnetic susceptibility measured on 195 samples from Site 647 is plotted versus depth (mbsf). Included with this data are the lithological units (from Table 2) and geological age boundaries (from micropaleontological data). Susceptibility sharply decreases in Lithologic Unit II, and susceptibility stays relatively low from Units II through IV. This decrease can be related directly to the increase in biogenic components in the Miocene to the middle late Eocene. The increase in susceptibility from Unit II through Subunit IIIC does not appear to be directly affected by clay concentrations. This increase may instead be the result of compaction within these units. The peaks in susceptibility at 600 mbsf occur within the zone of red sediments. The red staining indicates hematite formation. Because hematite is formed by low-temperature oxidation of iron oxides, it can form *in situ* at sufficiently high concentrations to increase the susceptibility.

Vane-Shear Strength

Vane-shear-strength testing was performed at Hole 647A, despite recognition of the considerable degree of disruption created by rotary drilling in soft sediments (Bennett and Keller, 1973). Comparatively undisturbed sections were chosen for measurements, but actual values are still regarded with suspicion, and only relative trends are considered valid. Testing was abandoned when drilling biscuits were observed near 150 mbsf (Table 9). In addition, shear-strength analyses were undertaken in the APC cores of Hole 647B (Table 9).

Variations in shear strength above approximately 60 mbsf in Hole 647A bear little relation to concurrent changes in water content (Fig. 35). This is most likely the result of consistently

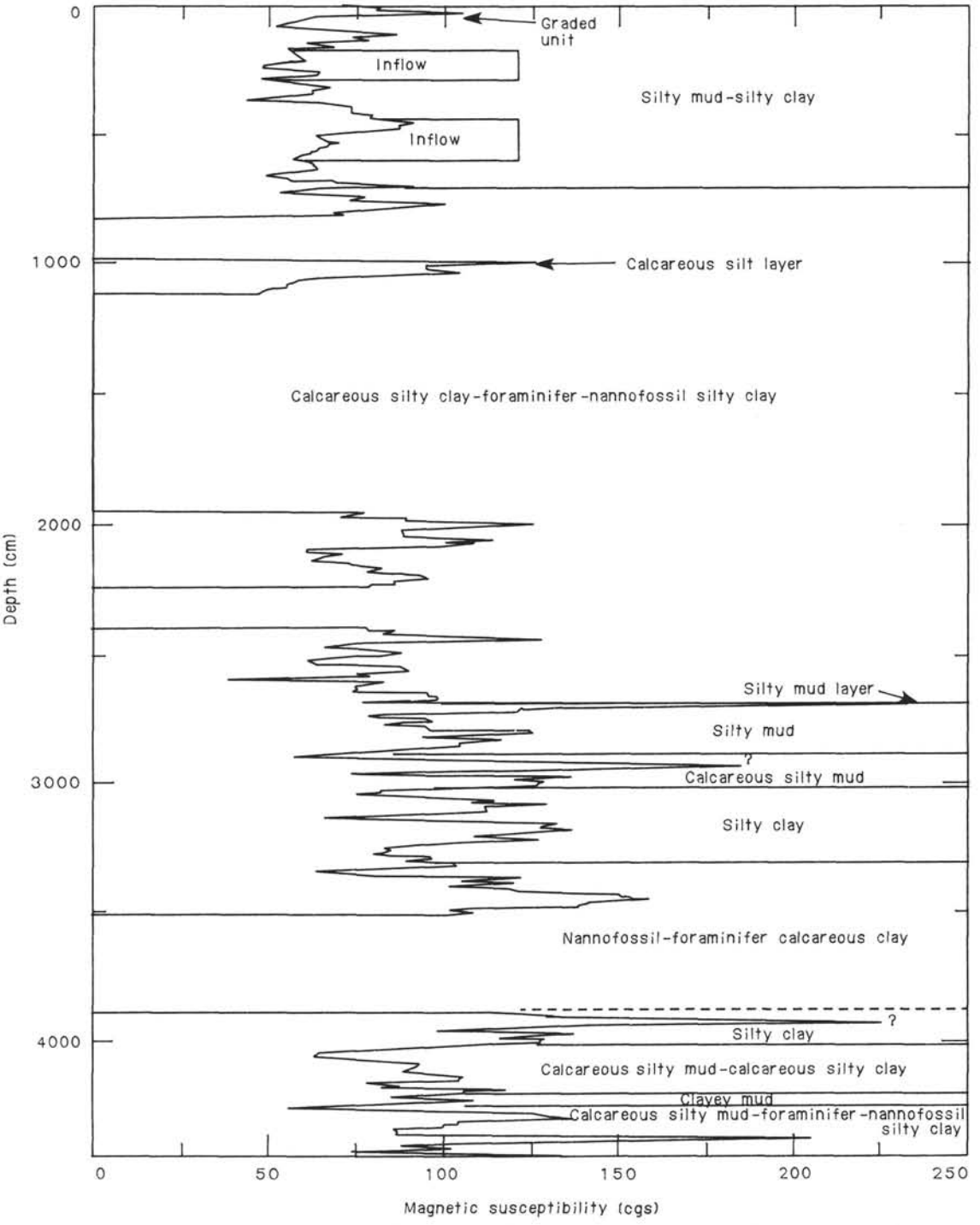

Figure 34. Magnetic susceptibility of Cores 105-647B-1H to 105-647B-5H. Because of core disturbances (mostly inflow, which was not measured), large gaps occur in the record. A relationship between large-scale lithologic variations and susceptibility does not appear. Calcareous units are as strong and vary as much as noncalcareous units. However, some small-scale variations are seen, as indicated.

low shear-strength values caused by the relatively greater degree of disturbance in the shallow section. As expected, values in the APC hole are consistently higher than those in the rotary-drilled hole (Fig. 36). Below 60 mbsf in Hole 647A, overall trends in shear strength can be tied to those in water content. The large increase in shear strength to the maxima at 117 mbsf is not associated with a concordant reduction in water content, but the sharp decrease immediately below coincides with the water-content spike centered at 127 mbsf (Fig. 39). This change in both properties is most likely related to the increase in the biogenic silica content (Bryant et al., 1981) observed in Lithologic Unit II.

A steady increase in shear strength within Lithologic Unit I, from approximately 4 kPa at 63 mbsf to the maxima of 138 kPa at 117 mbsf, is observed. This trend suggests a normal consolidation history, weakly supported by a slight decrease in water

Table 8. Basement-rock wet-bulk density and velocity measurements.

Section	Depth (mbsf)	Bulk density (g/cm^3)	Velocity (m/s)	Minicore orientation[a]
105-647A-71R-2	697.60	2.05		Vertical[b]
105-647A-71R-2	697.60	2.59	3430	Horizontal[c]
105-647A-72R-1	704.85	2.56	5236	Vertical
105-647A-72R-1	704.85	3.00	5562	Horizontal
105-647A-72R-4	707.87	2.52	5580	Vertical
105-647A-72R-4	707.87	3.12	5745	Horizontal
105-647A-72R-4	708.58		4894	Whole round
105-647A-73R-2	716.06		5709	Whole round
105-647A-73R-2	716.06	2.42		Vertical
105-647A-73R-2	716.06	3.13	4936	Horizontal
105-647A-73R-3	717.60		5376	Whole round
105-647A-74R-1	723.66	2.43		Vertical
105-647A-74R-1	723.66	3.13	5940	Horizontal
105-647A-74R-3	727.30		3605	Half round
105-647A-75R-4	736.65	2.37		Vertical
105-647A-75R-4	736.65	3.09	5878	Horizontal
105-647A-75R-4	737.23		4888	Half round

[a] Orientation for 2-min GRAPE density measurement and velocity determination.
[b] Parallel to bedding, minicore axis perpendicular to beam path.
[c] Perpendicular to bedding, minicore axis parallel to beam path.

content and porosity over the same depth interval. Unit II is characterized by low shear-strength values, averaging 28 kPa. An underconsolidated state is strongly suggested, possibly resulting from a long period of nondeposition and absence of dewatering when sedimentation began again. Further evidence of this hypothesis is indicated by the large percentage of low-permeability clay present in Units I and II.

Thermal Conductivity

Thermal-conductivity measurements were performed on the cores from Hole 647A to a depth of 220 mbsf (Table 9), where sediment drilling biscuits became too hard to penetrate with the probes. No testing was done in Hole 647B. A pronounced trend in conductivity with depth is observed (Fig. 35). Although a fairly high degree of scatter exists, values increase steadily in Lithologic Unit I to a depth of approximately 110 mbsf. Between 110 and 130 mbsf, conductivity decreases dramatically to values near 2.1×10^{-3} cal $\times$ °$C^{-1} \times cm^{-1} \times s^{-1}$ in Unit II. Thermal conductivity in Subunit IIIA gradually increases to 2.4×10^{-3} cal $\times$ °$C^{-1} \times cm^{-1} \times s^{-1}$ at 184 mbsf, before decreasing again to about 2.0×10^{-3} cal $\times$ °$C^{-1} \times cm^{-1} \times s^{-1}$ at 220 mbsf, where measurements stop. As at Sites 645 and 646, trends in thermal conductivity closely resemble those of bulk density. A correlation between conductivity and grain density also appears, which is probably the result of the interdependence of bulk density and grain density.

Compressional-Wave Velocity

Compressional-wave-velocity measurements were performed on samples from the rotary-drilled cores of Hole 647A and the APC cores of Hole 647B. Disregarding two measurements well below the speed of sound in water, values range from approximately 1470 m/s to a maxima of 2160 m/s in Hole 647A (Table 9). Velocities remain relatively low to a depth of about 250 mbsf. Values decrease from the surface to the base of the Pleistocene at approximately 70 mbsf. This trend cannot be related to the bulk density, which displays a steady increase over this interval. Velocities rise fairly abruptly but then exhibit a high degree of variability to the bottom of Unit II. Values in Subunits IIIA and IIIB are nearly constant.

Below 250 mbsf, velocities tend to increase with depth, generally paralleling the trend in bulk density. This relationship is evident in Figure 37, in which velocity is plotted versus bulk density. A good correlation ($r = 0.83$) exists between the two properties at bulk densities and velocities >1.8 g/cm^3 and 1600 m/s, respectively. A sharp decrease from the maxima of 2160 m/s to about 1740 m/s appears immediately below the hiatus between 510 and 600 mbsf. Values again increase to approximately 2000 m/s near the top of the basalt.

Velocities within the basalt layer are somewhat variable and highly dependent upon the degree of saturation of the material (Table 8). Samples measured immediately after recovery generated lower values than those measured after splitting and sampling, despite attempts at resaturation, which included soaking the specimens in seawater for up to 2 hr. Values range from 3430 m/s in the upper weathered section to 5710 m/s in a fully saturated whole-round sample at 716 mbsf.

Velocity and density values were used to calculate acoustic impedance and to create a synthetic seismogram and impedance log (Fig. 38). See "Downhole Measurements" section (Site 645 chapter, this volume) for details on the procedure for generating the synthetic product. Significant impedance contrasts signal the depth of acoustic reflectors. The impedance change at 70 mbsf coincides with the mid-Unit I reflector observed in seismic profiles. Reflectors discerned from calculated impedance at approximately 120 and 250 mbsf correspond to seismic reflectors R2 and R4, respectively. The R3 reflector is not readily apparent in the laboratory impedance data, probably because of a paucity of velocity measurements near 200 mbsf for which the bulk-density variation at this depth is fairly substantial (Fig. 35). In addition, a major impedance contrast at 610 mbsf correlates with a prominent seismic reflector within Unit IV. Another reflector is suggested at approximately 460 mbsf but cannot be substantiated on the seismic profiles.

Numerous subordinate reflectors are recognized where minor variations in density and velocity combine to produce distinct changes in acoustic impedance. These are only weakly visible, however, on the seismic sections. Velocity data generated by downhole sonic logging at depths from 114 to 260 mbsf are represented by the solid line in Figure 39. Good agreement between downhole logging and laboratory-measured values is evident at depths from 127 to 236 mbsf, where velocities tend to remain fairly constant. Velocities above 127 mbsf display a weak correlation, disregarding the anomalously low value at 117 mbsf. Trends in the two types of velocity diverge considerably below 216 mbsf, probably because of suspect velocity values in downhole logs.

Summary

Trends in index properties, thermal conductivity, and shear strength exhibited abrupt variations near 120 mbsf, the depth of the R2 reflector and the boundary between lithologic and seismic Units I and II. A substantial change in the mode of deposition is suggested. In addition, index properties display a close correspondence to lithology, particularly the abundance of biogenic silica and calcium carbonate. Silica-rich zones are characterized by high water content and porosity and by low bulk density, shear strength, and grain density. Below seismic reflector R4, at approximately 245 mbsf, values of measured properties become relatively uniform; gradients are low to the base of the sedimentary section near 700 mbsf. The only exception is sonic velocity, which decreases then increases sharply near 600 mbsf, distinguishing a prominent seismic reflector within Unit IV.

DOWNHOLE MEASUREMENTS

Operations

Rig up of the LSS-DIL-MCD-GR tool began at 2350 hr local time on 22 October 1985. The tool was rapidly lowered downhole until open hole was reached. At a depth of 60 m below

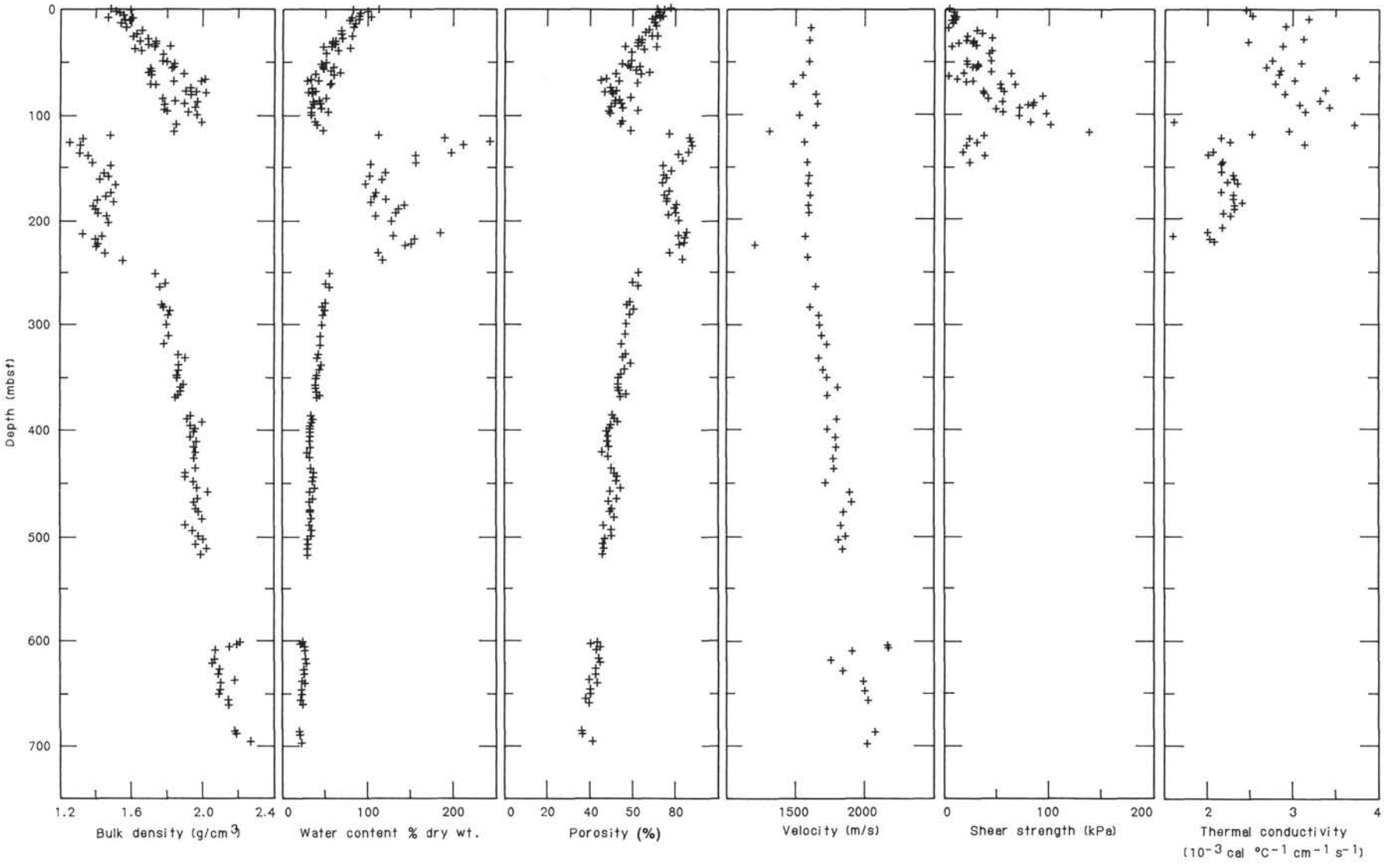

Figure 35. Vertical profiles of the variation of physical properties.

Table 9. Physical-properties summary, Site 647, Hole 647A.

Section	Depth (mbsf)	Bulk density (g/cm^3)	Grain density (g/cm^3)	Water content (dry wt. %)	Porosity (%)	Shear strength (kPa)	Thermal conductivity (10^{-3} cal $°C^{-1}$ cm^{-1} s^{-1})	Velocity (m/s)
105-647A-1R-1	0.75	1.60	2.76	82	70.4			
105-647A-1R-2	2.10	1.52	2.54	100	74.1		2.43	
105-647A-1R-6	8.25	1.61	2.68	80	69.8		2.51	
105-647A-2R-1	9.95						3.18	
105-647A-2R-1	10.05	1.57	2.72	89	72.4	9.99		
105-647A-2R-6	17.25	1.58	2.77	83	70.2	2.70		
105-647A-2R-6	17.40						2.91	
105-647A-2R-7	18.22							1599
105-647A-4R-1	29.35						3.14	
105-647A-4R-1	29.95	1.75	2.75	59	63.6	20.39		
105-647A-4R-2	30.12							1589
105-647A-4R-3	32.25	1.75	2.71	58	62.4	13.38		
105-647A-4R-3	32.35						2.48	
105-647A-4R-5	35.35	1.74	2.74	57	62.1	6.00	2.88	
105-647A-6R-1	49.30	1.79	2.68	51	58.7	20.99		
105-647A-6R-1	49.35						2.75	
105-647A-6R-1	50.07							1586
105-647A-6R-3	52.35	1.85	2.78	44	54.9	21.22	3.10	
105-647A-6R-5	55.30	1.72	2.75	60	62.8	26.76		
105-647A-6R-5	55.35						2.68	
105-647A-7R-1	59.30						2.86	
105-647A-7R-2	60.52	1.71	2.68	68	67.5	17.89		
105-647A-7R-3	62.30						2.85	
105-647A-7R-4	62.82							1540
105-647A-7R-4	63.55	1.73	2.71	60	63.3	4.37		
105-647A-7R-5	65.30						3.76	
105-647A-7R-6	66.55	2.03	2.74	31	46.8	12.07		
105-647A-8R-1	68.74	1.85	2.67	42	53.2	19.76	3.02	
105-647A-8R-3	71.75						2.79	
105-647A-8R-3	71.65	1.75	2.71	56	61.7	53.52		
105-647A-8R-3	71.74							1470
105-647A-9R-1	78.35						3.39	
105-647A-9R-1	78.37	1.98	2.73	35	49.6	36.91		
105-647A-9R-2	79.90	2.04	2.64	30	45.8	37.83		
105-647A-9R-3	81.35						2.91	
105-647A-9R-4	82.13							1640
105-647A-10R-1	87.97						3.33	
105-647A-10R-1	88.05	1.99	2.80	36	51.3	54.90		
105-647A-10R-3	90.33							1650
105-647A-10R-3	91.05						3.09	
105-647A-10R-3	91.07	1.80	2.74	44	54.5	79.81		
105-647A-10R-5	93.70	1.98	2.63	34	49.6	71.67	3.44	
105-647A-11R-1	97.80	1.82	2.79	54	62.5	55.25	3.16	
105-647A-11R-3	100.80	1.99	2.67	34	49.1	70.92		
105-647A-11R-3	101.47							1520
105-647A-12R-1	107.45						1.58	
105-647A-12R-1	107.40	2.02	2.92	38	54.6	81.63		
105-647A-12R-3	110.16						3.74	
105-647A-12R-3	110.49	1.87	2.68	41	53.5	102.62		
105-647A-12R-3	111.17							1635
105-647A-13R-1	116.71							1305
105-647A-13R-1	116.75	1.85	2.61	49	59.2	137.60	2.96	
105-647A-13R-3	119.76	1.50	2.74	114	77.9	37.32	2.50	
105-647A-13R-5	122.80						2.14	
105-647A-13R-5	123.10	1.34	2.77	194	86.6	23.89		
105-647A-14R-1	126.50						2.26	
105-647A-14R-1	126.72	1.26	2.40	246	87.4	31.37		
105-647A-14R-1	127.04							1551
105-647A-14R-3	129.07	1.32	2.67	215	87.7	21.68	3.16	
105-647A-15R-1	136.49	1.32	2.46	202	86.1	17.07		
105-647A-15R-1	136.55						2.05	
105-647A-15R-3	139.10	1.37	2.59	158	81.7	38.29	1.98	
105-647A-16R-1	146.08	1.40	2.75	161	84.3	24.45	2.17	
105-647A-16R-1	146.57							1573
105-647A-16R-2	147.60						2.15	
105-647A-16R-3	148.41	1.50	2.59	104	74.6			
105-647A-17R-1	155.55						2.15	
105-647A-17R-1	155.71	1.46	2.63	123	78.5			
105-647A-17R-3	158.65						2.29	
105-647A-17R-3	158.81	1.49	2.77	105	74.6			1590
105-647A-17R-5	161.55						2.30	
105-647A-17R-5	162.09	1.44	2.65	118	76.1			
105-647A-18R-1	164.75						2.22	
105-647A-18R-2	166.48							1581
105-647A-18R-2	166.53	1.53	2.75	99	74.2			
105-647A-18R-2	166.60						2.35	
105-647A-19R-1	174.64	1.50	2.60	111	77.3		2.14	
105-647A-19R-3	177.50						2.30	
105-647A-19R-3	177.68	1.47	2.59	109	74.8			1591
105-647A-19R-5	180.50						2.29	
105-647A-19R-5	181.01	1.42	2.36	123	76.4			
105-647A-20R-1	184.00	1.52	2.61	105	76.1			
105-647A-20R-1	184.25						2.41	
105-647A-20R-3	186.98	1.40	2.57	144	80.3			1583
105-647A-20R-3	187.00						2.30	
105-647A-20R-5	190.25	1.41	2.61	138	79.5		2.30	

Table 9 (continued).

Section	Depth (mbsf)	Bulk density (g/cm^3)	Grain density (g/cm^3)	Water content (dry wt. %)	Porosity (%)	Shear strength (kPa)	Thermal conductivity (10^{-3} cal $°C^{-1}$ cm^{-1} s^{-1})	Velocity (m/s)
105-647A-21R-1	194.07						2.17	
105-647A-21R-1	194.10	1.43	2.81	136	80.5			1585
105-647A-21R-3	197.10						2.27	
105-647A-21R-3	197.20	1.48	2.63	112	76.6			
105-647A-22R-1	207.77						2.17	
105-647A-22R-1	202.80	1.49	2.65	129	82.0			
105-647A-23R-1	213.25						1.99	
105-647A-23R-1	213.44	1.34	2.32	188	85.6			
105-647A-23R-3	216.05						1.58	
105-647A-23R-3	216.21	1.45	2.58	135	81.5			1560
105-647A-23R-5	218.79	1.41	2.59	159	84.4			
105-647A-23R-5	218.82						2.02	
105-647A-23R-7	221.70						2.07	
105-647A-24R-1	223.20	1.43	2.36	154	84.3			
105-647A-24R-3	225.00	1.42	2.52	147	82.7			1200
105-647A-25R-1	232.18	1.47	2.58	117	77.5			
105-647A-25R-3	235.73							1580
105-647A-25R-5	238.95	1.57	3.13	120	83.8			
105-647A-27R-1	251.41	1.75	2.55	58	62.9			
105-647A-28R-1	261.05	1.81	2.76	51	60.0			
105-647A-28R-3	263.90	1.78	2.74	57	63.1			1640
105-647A-30R-1	280.15	1.79	2.71	51	59.1			
105-647A-30R-3	283.13	1.80	2.67	48	57.3			1594
105-647A-30R-5	286.15	1.84	2.81	51	60.7			
105-647A-31R-2	291.25	1.83	2.63	49	58.7			1662
105-647A-32R-2	300.48	1.82	2.67	48	57.3			1666
105-647A-33R-2	310.27	1.83	2.50	46	56.5			1681
105-647A-34R-1	318.50	1.81	2.57	45	54.7			1713
105-647A-35R-1	328.53	1.89	2.74	44	56.6			
105-647A-35R-3	331.63	1.93	2.77	42	55.9			1660
105-647A-36R-1	338.38	1.89	2.90	48	60.2			
105-647A-36R-4	342.75	1.89	2.71	44	56.0			1690
105-647A-37R-1	347.80	1.88	2.74	42	54.7			
105-647A-37R-3	350.49	1.88	2.72	41	53.5			1720
105-647A-38R-1	357.34	1.92	2.71	40	53.7			
105-647A-38R-3	359.84	1.90	2.72	40	53.1			1800
105-647A-38R-5	363.48	1.90	2.68	41	53.6			
105-647A-39R-1	367.09	1.89	2.69	45	57.0			1720
105-647A-39R-3	369.35	1.87	2.76	42	54.4			
105-647A-41R-1	386.66	1.96	2.62	36	50.7			
105-647A-41R-3	389.56	1.94	2.56	38	51.9			1790
105-647A-41R-5	392.50	2.03	2.87	37	53.5			
105-647A-42R-1	395.85	1.96	2.75	35	50.0			
105-647A-42R-3	398.95	1.99	2.76	34	49.4			1725
105-647A-42R-5	401.86	1.98	2.84	33	48.2			
105-647A-43R-2	407.01	1.96	2.73	34	48.9			1784
105-647A-43R-5	411.45	2.00	2.72	33	48.0			
105-647A-44R-2	416.50	1.98	2.76	34	49.2			1789
105-647A-44R-5	421.25	1.99	2.71	31	45.7			
105-647A-45R-3	426.40	1.98	2.67	34	48.9			1766
105-647A-46R-2	436.04	1.99	2.77	35	50.3			1770
105-647A-46R-5	440.50	1.93	2.73	38	51.8			
105-647A-47R-1	443.94	1.93	2.73	39	52.9			
105-647A-47R-4	449.21	1.98	2.71	37	52.1			
105-647A-47R-4	449.33							1710
105-647A-48R-2	455.21	2.00	2.88	39	54.8			
105-647A-48R-5	458.41	2.06	2.78	33	49.7			1880
105-647A-49R-2	465.27	2.00	2.83	37	53.1			
105-647A-49R-4	468.26	1.98	2.69	34	49.0			1900
105-647A-50R-2	474.88	1.99	2.64	35	50.3			
105-647A-50R-5	477.58	2.01	2.74	34	49.4			1840
105-647A-51R-2	483.92	2.03	2.89	35	51.8			
105-647A-51R-6	490.24	1.93	2.52	32	46.3			1820
105-647A-52R-3	495.39	1.97	2.72	36	50.5			
105-647A-52R-6	500.21	2.00	2.65	35	50.3			1850
105-647A-53R-2	503.59	2.03	2.77	32	47.5			1795
105-647A-53R-5	508.04	1.99	2.59	31	46.3			
105-647A-54R-1	512.46	2.05	2.71	31	46.8			1829
105-647A-54R-5	518.24	2.02	2.65	30	45.8			
105-647A-62R-2	601.49	2.24	2.86	25	43.5			
105-647A-62R-4	603.33	2.22	2.86	23	40.4			2150
105-647A-62R-6	605.91	2.18	2.90	27	45.2			2160
105-647A-63R-1	608.71							1900
105-647A-63R-1	609.08	2.10	2.67	27	43.2			
105-647A-64R-1	617.74	2.10	2.64	28	44.6			1742
105-647A-64R-3	621.60	2.08	2.63	29	45.2			
105-647A-65R-1	627.75	2.12	2.72	26	42.9			1829
105-647A-65R-3	631.55	2.12	2.62	26	42.6			
105-647A-66R-1	637.74	2.21	2.73	23	39.7			1979
105-647A-66R-3	639.97	2.13	2.68	27	44.0			
105-647A-67R-1	646.77	2.13	2.64	24	40.4			1987
105-647A-67R-4	651.02	2.12	2.65	24	40.3			
105-647A-68R-1	656.51	2.18	2.61	22	38.3			2009
105-647A-68R-4	660.98	2.18	2.69	24	40.5			
105-647A-70R-1	685.91	2.21	2.65	20	36.3			2060
105-647A-70R-4	688.60	2.22	2.64	20	36.6			
105-647A-71R-1	695.96	2.30	2.89	22	40.6			2000

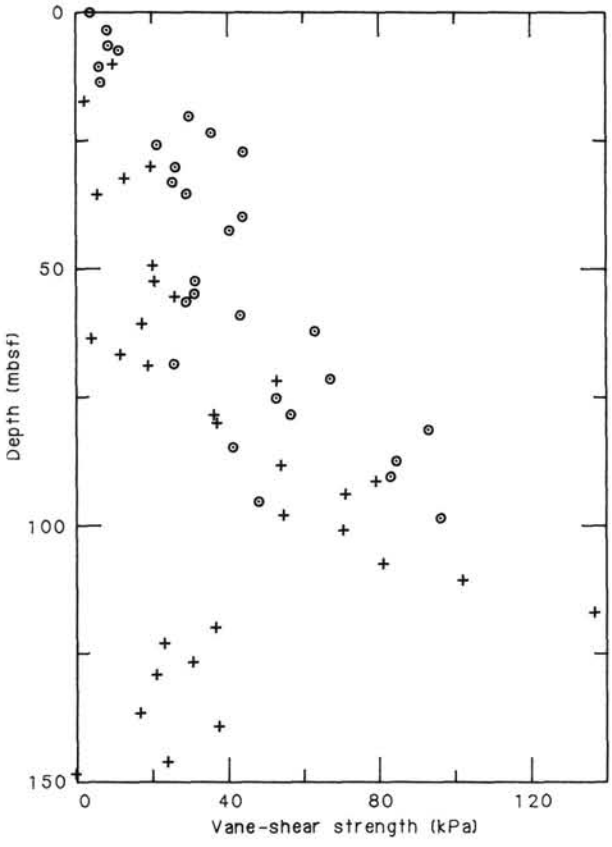

Figure 36. Vane-shear strength versus uncorrelated sub-bottom depth, Holes 647A and 647B. Plus signs represent measurements in Hole 647A; circles correspond to Hole 647B.

pipe, a test of winch minimum speed began by logging up at a decelerating speed. Logging speed was found to be 65–67 m/hr. The wireline heave compensator (WHC) was then turned on and the test repeated. Logging speed was thereby reduced to 44 m/hr, a minimum rate adequate for any logging tool currently on the ship, including both gamma-ray spectrometer (GST) and borehole televiewer. After continuing up into pipe, downhole logging began again at 1800 m/hr. Several bridges were encountered, and others were visible on the caliper before resting at 227 mbsf on an impenetrable bridge. The pipe was therefore raised 28 m and logging out proceeded at 550 m/hr.

The tool was pulled in and rigged down so that pipe could be set to 257 mbsf, near the beginning of another formation (Subunit IIIC) having potentially better hole conditions. Before reentering the pipe with the LSS combination, the caliper was taped off to substantially reduce maximum tool diameter. The second run encountered bridges at 4 and 22 m into open hole, as well as sticky hole conditions. After the pipe was raised 28 m, the tool was unable to reach even the second bridge encountered previously at 283 mbsf. The remaining interval of open hole was logged, and the tool was then pulled out of the hole. Because of the poor hole conditions, further logging was suspended.

We used 11 of the 16 hr allotted for logging, obtaining 146 m of usable open-hole logs in the interval from 114 to 274 mbsf. Quality of the gamma-ray and resistivity logs is good. The caliper quality was fair while logging down on the first pass. As at Sites 645 and 646, the caliper accumulated mud, which caused it to fail for uphole logging. The quality of the initial sonic log varies from good to poor. Through reprocessing (see "Downhole Measurements" section, Site 465 chapter, this volume), the quality of most of the sonic log was improved to good. However, analysis of sonic waveforms will be required for greater log reliability, particularly for the lowest and highest parts of the logged interval.

Log Interpretation

The logged interval from 114 to 274 mbsf spans the lithostratigraphic interval from lowest Unit I to upper Subunit IIIC ("Sedimentology" section, this chapter). Data gaps exist within this interval on all logs (Fig. 40) because of the lack of overlap in the two logging runs and the different depths of tools within the tool string.

The gamma-ray log for Site 647 indicates a dominant trend of a slowly decreasing clay mineral percentage downhole from 118 mbsf to about 175 mbsf, stabilizing at a low clay content from 175 to at least 208 mbsf, then slowly increasing from 232 to 265 mbsf. Superimposed on this broad trend are thin clay-rich layers at 135–137 and 139–142 mbsf. A sudden major reduction in the clay base-line pattern may occur at 265 mbsf.

The clay mineral percentage in the logged interval is probably controlled primarily by dilution effects of siliceous and calcareous ooze. Abundance of sponge spicules, radiolarians, and diatoms increases from 115 to 175 mbsf, then decreases from 260 to 305 mbsf ("Biostratigraphy" section, this chapter). Carbonate percentage increases from 130 to 150 mbsf, decreases from 180 to 210 mbsf, and gradually increases below this depth ("Sedimentology" section, this chapter). Lacking reliable percentages for biogenic silica, we cannot quantitatively compare the gamma-ray clay variations with biogenic component variations.

Comparison of gamma-ray variations with lithostratigraphic variations in clay is hazardous because the former measures clay mineral abundance and the latter measures clay grain-size abundance. Nevertheless, only in the upper part of the logged interval is there an obvious parallel between the two, and both decrease downhole.

A porosity log was calculated from the resistivity log, based on the Archie water-saturation equation. Because the resistivity of formation water (R_w) is unknown but is required in the calculation, porosities from core measurements at six depths were compared with resistivities and consistently yielded an estimated R_w of about 0.38 ohm. This value for R_w was therefore used in the conversion from resistivity to porosity. The resulting porosity log agrees well with porosities from core measurements ("Physical Properties" section, this chapter) throughout the interval (Fig. 40), indicating that the assumption of constant R_w is probably reasonable.

Porosities exhibit a rapid increase throughout lowest Unit I and all of Unit II (114–139 mbsf), rising from 55% to 90% as the quantity of diatoms increases. A gradual decrease occurs throughout Subunits IIIA and IIIB, to a level near 75% at about the Subunit IIIB/IIIC boundary (247 mbsf). A sudden drop to 65% porosity apparently occurs at this depth and changes little between 247 and 274 mbsf. A single excursion to nearly 97% porosity at 191 mbsf over a very thin interval is accompanied by a drop in gamma-ray response. This drop may represent a thin layer of pure diatom ooze, but the unrealistically high porosity value suggests that both log responses probably reflect hole washout.

The entire interval from 139 to 247 mbsf exhibits porosities that are anomalously high for such depths; such porosities are usually encountered only within a few centimeters of the seafloor. The high abundance of diatoms is probably the primary reason for very high porosity, but the minor compaction effect is surprising.

Sonic traveltimes are broadly consistent with porosities, and higher traveltimes are associated with higher porosities, as observed experimentally by Raymer et al. (1980) and in logs at Site

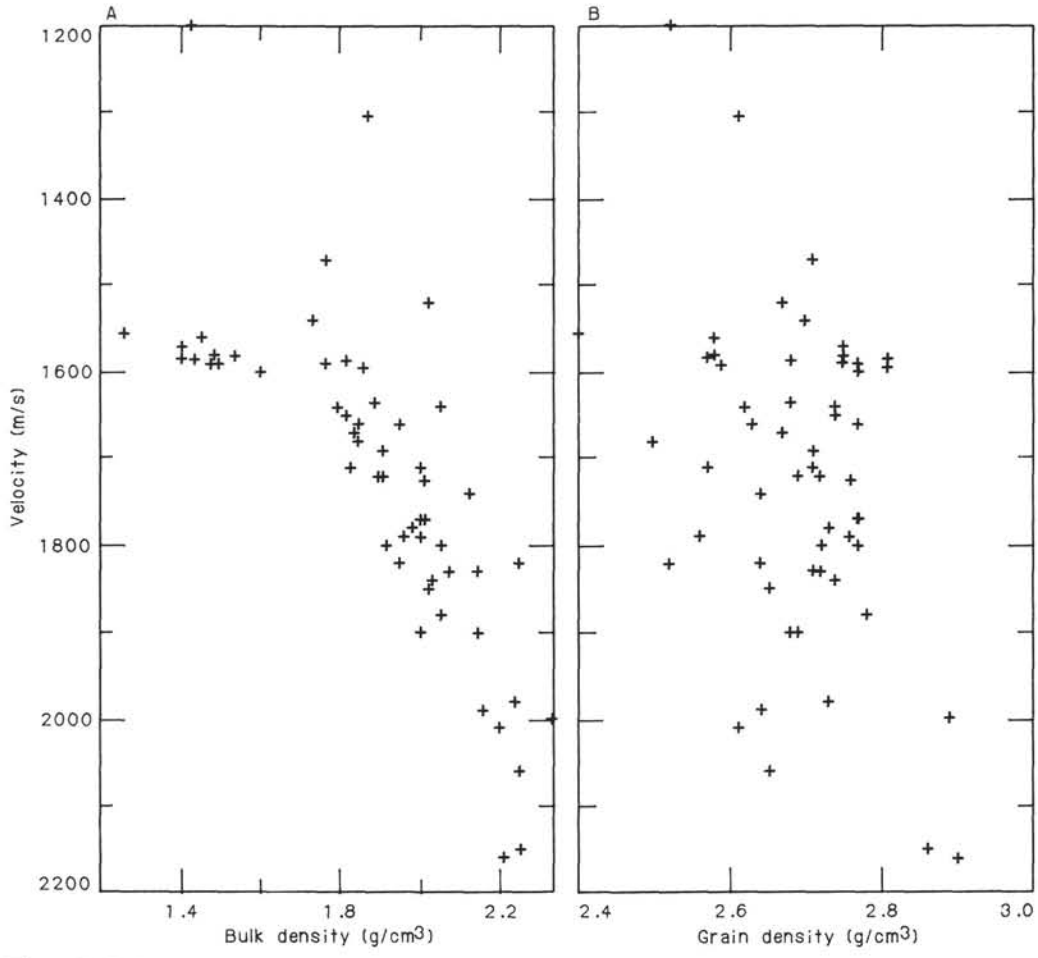

Figure 37. Laboratory-measured compressional-wave velocity versus bulk density.

646 (see Fig. 50, Site 646 chapter, this volume). The porosity/traveltime data of Site 647 extend the relationship observed at Site 646 to velocities almost as slow as water (1.55 km/s), consistent with the data of Raymer et al. (1980). However, caution must be exercised in interpreting the sonic data for three reasons. First, the results shown are from the initial reprocessing of the sonic log, and waveform processing will yield more reliable sonic values. Second, both the sudden increase in traveltime at 128 mbsf and the lower traveltimes below 225 mbsf than near 200 mbsf are not paralleled by similar large changes in porosity. Third, although the traveltimes from 125 to 200 mbsf correspond well to velocity measurements on cores, the traveltimes below 225 mbsf are significantly lower than those from cores ("Physical Properties" section, this chapter).

SEISMIC STRATIGRAPHY

Site 647 is at the intersections of HD 84-30 lines 8 and 4. These and other lines that lie near this site (Fig. 3) show the presence of several prominent reflectors. These reflectors have been grouped into three discrete seismic units based on their uniformity, continuity, and seismic characteristics, as briefly described in the "Background and Objectives" section (this chapter).

Here, we discuss the correlation between drilling results, major seismic reflectors, and seismic units near the site. DSDP Site 112, which was drilled during DSDP Leg 12, lies about 100 km northwest of Site 647. A comparison between these two sites can be made using the seismic lines that cross them, as discussed in detail in the "Summary and Conclusions" section (this chapter). Here, we show the continuation of some of the seismic units between these two sites. A number of reflectors can be recognized within each seismic unit, and we have, tentatively, correlated these with physical- and chemical-properties measurements made on the cores recovered at this site.

For calculations of the depth to each reflector (Table 10), we used an average velocity of 1.62 km/s for the first two units (above 0.32 s two-way traveltime) and 2.0 km/s for seismic unit 3 (0.32–0.77 s two-way traveltime) as obtained from the physical-properties measurements. Comparison of the velocity values obtained from sonic logs with those from the physical-properties measurements of the interval from 100 to 250 mbsf agree very well.

We also correlated each of the seismic units with various lithological units and find, on the whole, a moderate to good correlation between the two sets of units with some minor differences. Comparison of a synthetic seismogram (Fig. 38, "Physical Properties" section, this chapter) based on the physical-properties measurements shows impedance contrasts and reflectors of varying amplitudes that match reasonably well with the reflectors observed in the seismic profiles. The correlation of the calculated reflector depths from the seismic-reflection lines with the changes in lithofacies, physical properties, and biostratigraphy (Fig. 35) is surprisingly good. These correlations are discussed as follows for each seismic unit.

Seismic Unit I

Seismic unit 1 is about 0.12 s thick at Site 647 and comprises a series of moderate- to high-amplitude reflectors that are parallel to the seafloor. The unit varies in thickness over the nearby

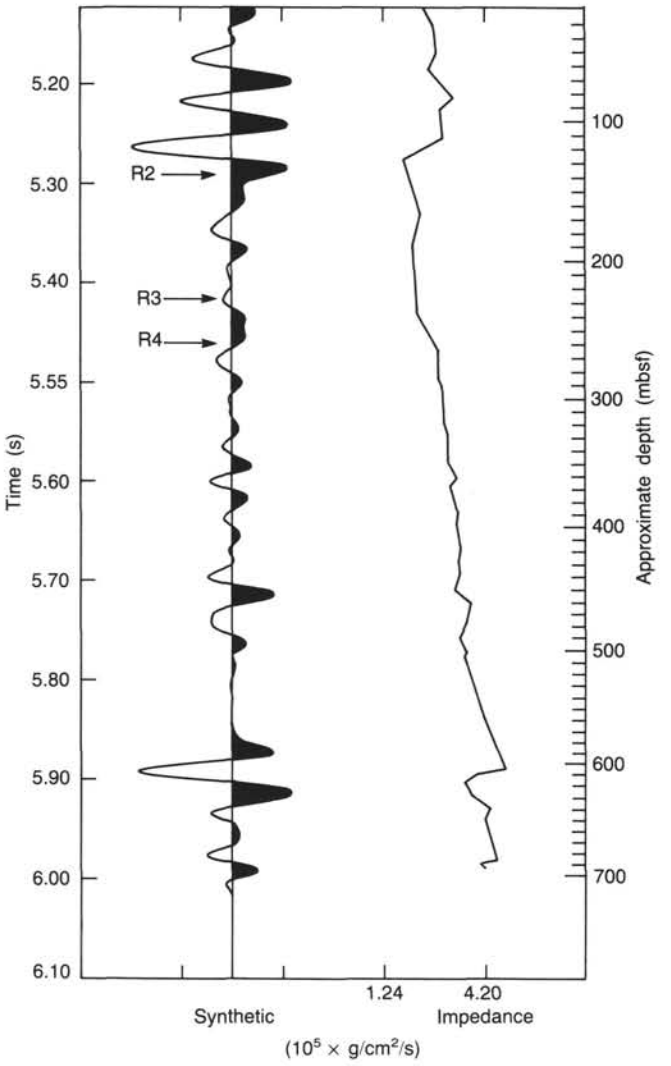

Figure 38. Synthetic seismogram generated from laboratory-measured values of velocity and bulk density. Synthetic impedance is plotted versus synthetic traveltime. An approximate scale of sub-bottom depth is included.

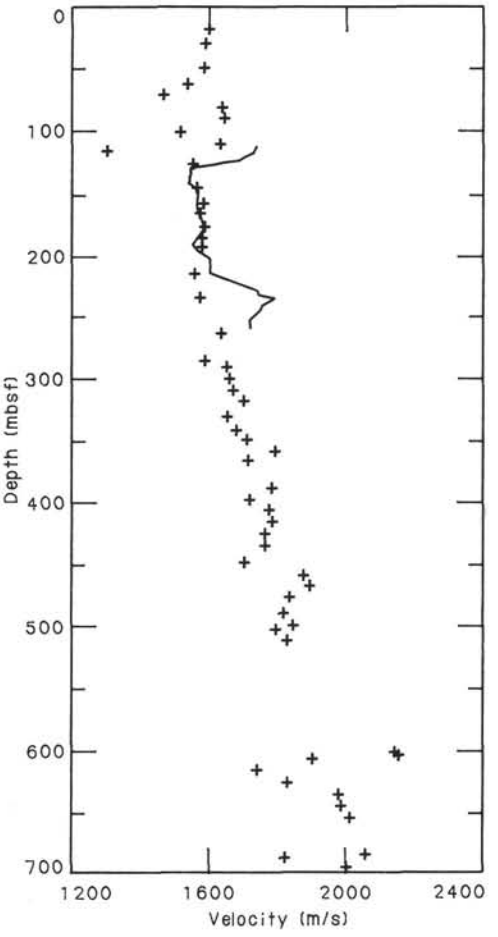

Figure 39. Acoustic velocity versus depth, Hole 647A. Plus signs represent laboratory-measured values; solid line originates from estimates of downhole-logging velocities.

region and has a maximum thickness of about 0.3 s west of Site 647 (Fig. 45, "Summary and Conclusions" section, this chapter), presumably because of the inflow of turbidites from the NAMOC. Reflectors within the unit are generally parallel to subparallel except in regions where the unit thickens. In these thicker regions, the lower reflectors onlap the top of seismic unit 2 (Fig. 6). The base of seismic unit 1 is characterized by a strong, continuous to discontinuous reflector that may represent an unconformity, as indicated by the onlap of seismic unit 1 strata.

Lithologically, this reflector in the base of seismic unit 1 correlates well with the top of Lithologic Unit II (Fig. 41), being of early to late Miocene age and consisting mainly of silty mud, clay, and nannofossil clay and silica-bearing clays lacking calcareous nannofossils in the lower part. A prominent hiatus, encompassing an interval between 5.6 and 2.5 Ma, exists between Lithologic Units I and II. Thus reflector R2, which forms the top of seismic unit 2, corresponds to this hiatus and represents an unconformity. In fact, two parallel reflectors are clearly visible at this level (Fig. 7). If real, they could correlate with the top and bottom of Lithologic Unit II. Parallelism and similarity between these reflectors and those seen at the sea bottom make ascertaining their validity difficult because these reflectors could easily be caused by a large bubble pulse from the sound source used for generating this profile.

Nonetheless, the coincidence between the thickness of Lithologic Unit II and the separation between the two reflectors, as part of the R2 reflector, is interesting. The sediments comprising seismic unit 1 and Lithologic Unit I are terrigenous in nature. Recognizable alternations of relatively nannofossil-rich silty clay and more gravel-rich, silty intervals, marking perhaps glacial-interglacial climatic cycles, form the main part of this seismic unit. Both bottom-current-winnowed beds enriched in biogenic components and turbiditic, detrital carbonate-rich sediment derived from spillover from the NAMOC are also present. What causes prominent reflectors within seismic unit 1 is uncertain, but synthetic seismograms generated from the density and velocity measurements show that some of the reflectors arise from variations in density as the result of changes in relative proportions of carbonate and terrigenous materials (Fig. 38).

Seismic Unit 2

Seismic unit 2 occurs between 0.12 and 0.32 s bsf at Site 647, but it varies between 0.15 to 0.25 s in thickness over the region. In the seismic record across Site 647, the unit appears transparent, except for one fairly prominent reflector near the base (at about 116 mbsf). Northwest of Site 647, the same reflector lies in the middle of seismic unit 2 (Fig. 43, "Summary and Conclusions" section, this chapter). This intraunit reflector was tenta-

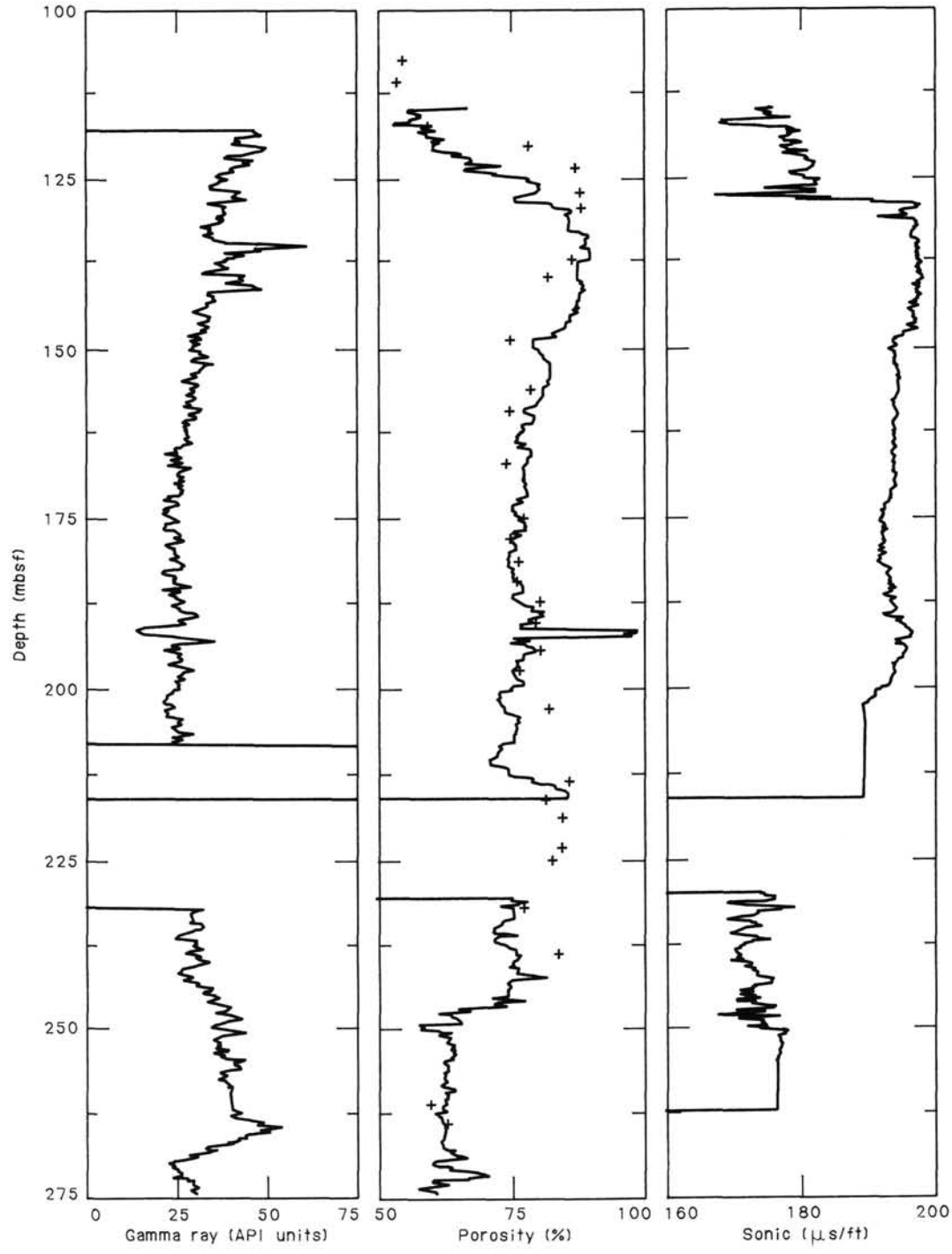

Figure 40. Gamma-ray (GR), porosity (from ILM resistivity), and sonic traveltime logs, Site 647. Pluses on porosity log are measured porosities of discrete-core samples ("Physical Properties" section, this chapter).

Table 10. Depth to reflectors.

Seconds	Velocity (m/s)	Depth (mbsf)	Reflector	Age
0.145	1620	117.45	R2	late Pliocene/early Miocene
0.29	1620	234.9	R3	early Oligocene
0.31	1620	251.1	R4	
0.60	2000	543		
0.67	2000	618		
0.75	2000	693	Basement	early Eocene

tively identified as being the R3 reflector of Miller and Tucholke (1983) in this region. The base of seismic unit 2 is marked by a high-amplitude continuous to discontinuous reflector, which is the most prominent reflector traceable throughout the region. The equivalent reflector was drilled at DSDP Site 112, about 100 km northwest of Site 647 (Fig. 9), and was called a mid-sediment reflector and given a middle Oligocene age by Laughton, Berggren, et al. (1972). Miller and Tucholke (1983) later identified this as the R3 and R4 reflectors of mid-early Oligocene age; they argued that it is equivalent to the Oligocene–Eocene R4 re-

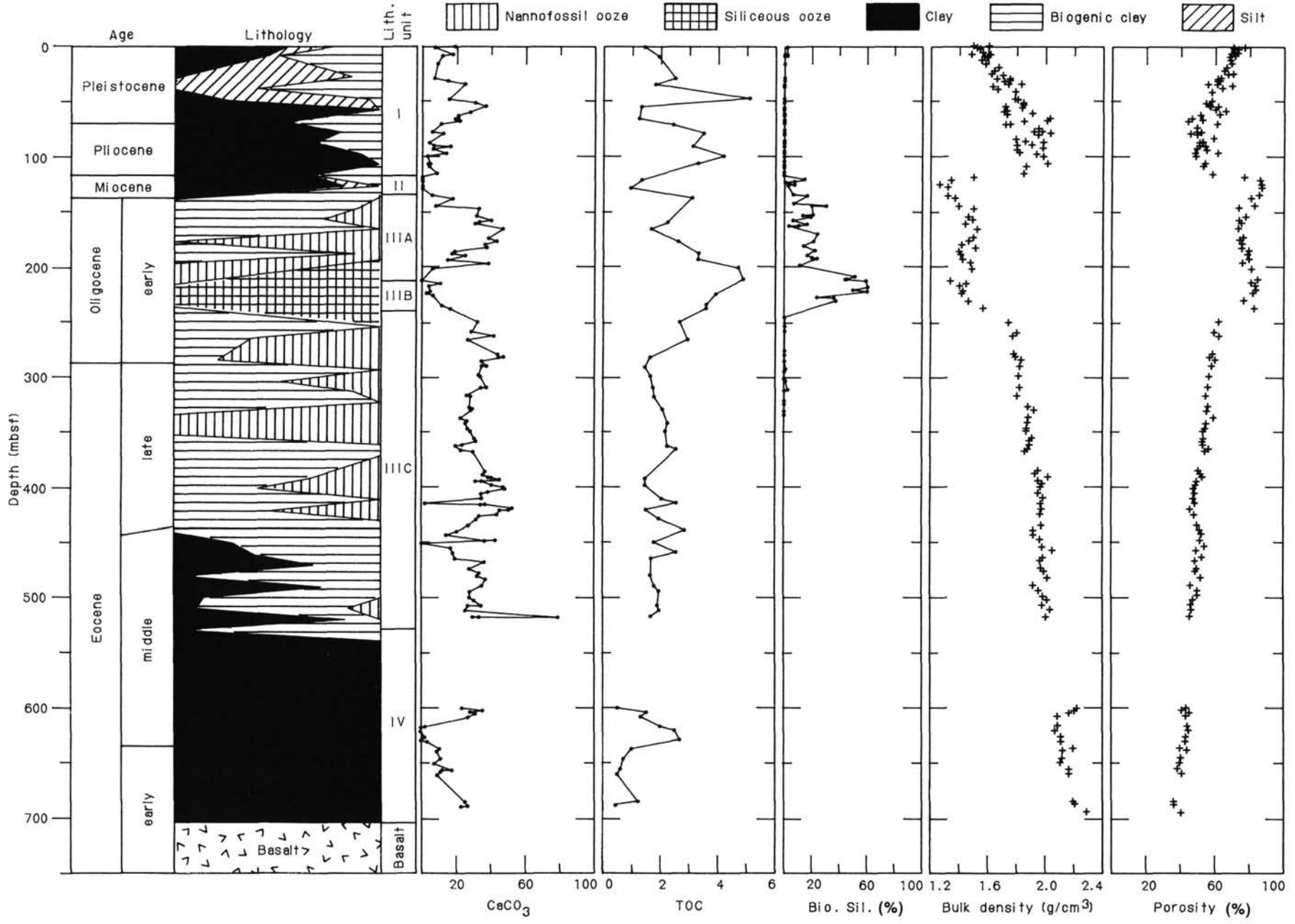

Figure 41. Lithology, $CaCO_3$ (carbonate bomb), lithologic units, and calcareous and siliceous biogenic material observed in smear slides, total organic carbon (TOC), and age of sediments at Site 647.

flector in the northeast Atlantic. Reflector R4 in the northeast Atlantic is associated with a major erosional unconformity at the Oligocene/Eocene boundary (Roberts et al., 1979). Correlation of this seismic unit with lithologic units at Site 647 suggests that seismic unit 3 should correspond to Lithologic Subunits IIIA and IIIB (134–240 mbsf). Thus, seismic unit 2 is early Oligocene through late Miocene in age.

Lithologic Subunits IIIA and IIIB contain mainly bioturbated biogenic claystones and clayey ooze, which are predominantly nannofossil rich but which also contain biogenic opal in the upper Eocene through lower Oligocene part. The lower Oligocene strata between 212.3 and 241.1 mbsf are particularly biogenic opal rich. The unit is devoid of any hiatuses that could be regarded as unconformities. Thus, the only prominent lithologic boundary that can be matched to the calculated depth to reflector R4 is the change from siliceous to calcareous biogenic claystones. The reflector thus appears to bear no direct relationship to changes in bottom-water circulation.

A major but somewhat gradual change in the benthic foraminiferal fauna, from agglutinated to calcareous dominated, occurred during the late Eocene through earliest Oligocene, which is below the level of R4 (Table 10). Sonic velocity measurements from discrete samples in Lithologic Subunits IIIA and IIIB exhibit a decrease from those obtained in Unit I. A similar behavior is also seen in the density values (Fig. 38). The largely transparent nature of seismic unit 2 probably relates to the consistently low densities and velocities observed in this interval. These characteristics persist on a regional basis.

Seismic Unit 3

Seismic unit 3, the deepest unit defined in the records crossing Site 647 (Figs. 38 and 43), lies below 0.32 s and extends to the top of the fairly prominent basement reflector that marks the top of the oceanic crust at roughly 0.77 s depth near the site. Except for a few reflectors near the bottom of the unit that have attitudes conformable with the inferred basement surface, the unit is more or less transparent but has higher reflectivity than does seismic unit 2. The bottommost reflector in seismic unit 3 abuts against the basement highs, indicating that the sediments at or below that reflector were deposited in the basement valleys.

Correlation of this unit with lithology at Site 647 shows that it encompasses strata belonging to Lithologic Subunit IIIC and Unit IV (240–699 mbsf) and therefore is early Eocene to early Oligocene in age. Sediments within Subunit IIIC are similar to those in the overlying lithologic units, except that they contain relatively little biogenic silica and are relatively rich in calcareous nannofossils. One of the reflectors that lies near the base of seismic unit 3 appears to correspond in depth to the base of Lithologic Subunit IIIC (525 mbsf). No major changes could be observed at this depth in the physical-properties measurements (Fig. 38). A prominent interval of very slow sedimentation was observed in Lithologic Unit IV (composed of mainly claystone). The top of this interval occurs at a depth (about 615 mbsf) that corresponds well to the calculated depth (618 mbsf) to the second reflector seen above the base of seismic unit 3 (Fig. 38). This is also supported by the reflector generated in the synthetic seismogram (Fig. 38).

In general, a good correlation between the lithostratigraphy, biostratigraphy, physical-properties, and seismic-reflection data exists at Site 647. None of the reflectors appear to correspond to the major onset of strong bottom-water circulation at or near the Oligocene/Eocene boundary, in contrast to what was observed in the northeast Atlantic. This undoubtedly has strong implications for hypotheses of deep-water activity in the North Atlantic during the Oligocene and Eocene.

SUMMARY AND CONCLUSIONS

Background

Site 647 in the southern Labrador Sea completes a transect of three sites, from Baffin Bay through the Labrador Sea drilled during ODP Leg 105. The transect was designed to examine latitudinal gradients in high-latitude Paleogene through Quaternary paleoclimates, to study changes in water-mass exchange between the Arctic and the North Atlantic that accompanied the paleoclimatic changes, and to investigate the changing pattern and intensity of deep oceanic circulation in the Labrador Sea during the Paleogene and Neogene. Site 647 lies in a position that should provide a record of the repeated penetrations of warm, temperate North Atlantic surface-water masses into a region that has been dominated by cooler subarctic to arctic water masses during the late Neogene to Holocene.

The possible beginnings of major southward flow of arctic waters in the middle Miocene were observed in Site 645, and we thought that the effects of the resulting cold Labrador Current might be observed in the region of Site 647, also in and above the middle to upper Miocene. In addition, the site is located on the south flank of a large drift deposit, Gloria Drift (Fig. 1), formed by bottom-currents that originate in the Norwegian–Greenland Sea and that flow through the Charlie Gibbs Fracture Zone.

We hoped to develop a better understanding of the timing and pattern of drift formation for comparison with that of Eirik Ridge at Site 646, where the inception of major drift sedimentation was dated as late Miocene to early Pliocene but where the influence of bottom currents on sedimentation may have begun earlier. Furthermore, because we were unable to recover a high-latitude Paleogene sequence at either Sites 645 or 646 and because recovery at nearby DSDP Site 112 was inadequate for important high-resolution paleoceanographic studies, Site 647 offered us the best opportunity to obtain a complete middle Eocene through Oligocene pelagic sequence that had not been deeply buried and diagenetically altered. We also hoped to recover and date the top of oceanic crust at Site 647, thus constraining tectonic models of the Labrador Sea. Therefore, we drilled Site 647 in a water depth of 3869 m, at 53°19.876′N and 45°15.717′W, south of Gloria Drift, north of the Charlie Gibbs Fracture Zone and east of the NAMOC. The total depth of penetration was 736.0 mbsf, and average recovery during rotary drilling at Hole 647A was 62% (90% during APC coring at Hole 647B).

Lithologic Units and General Features

Four major sedimentary units were encountered at Site 647 between the seafloor and 699 mbsf. Basalt was recovered from 699 to 736 mbsf. The lithologic units are described in the "Sedimentology" section (this chapter). The sequence is dominated by terrigenous material in the upper 116 mbsf (Pliocene–Pleistocene) and again below about 530 mbsf (lower and middle Eocene). Coarse-grained terrigenous material occurs only in the Pliocene–Pleistocene strata and is dominated by quartz with subordinate amounts of feldspar and heavy minerals. Terrigenous clay minerals are the primary constituent in the lower to middle Eocene. Biogenic carbonate and opal together compose 50% or more of the sediment in the middle Eocene through upper Miocene interval. Carbonate contents in Unit I range from 0% to 40% (Fig. 41), divided between detrital carbonate silt grains and biogenic carbonate. Biogenic opal is rare. In Unit II, carbonate contents are below 5%, and biogenic opal is an important component, as it is for Subunit IIIB. However, Subunits IIIA and IIIC contain as much as 50% biogenic carbonate, averaging about 35%, and have lower biogenic opal concentrations. Unit IV is characterized by carbonate contents between

0% and 30%, mostly <10%, and contains no biogenic opal. Organic carbon contents are <0.52% over the entire sequence (Fig. 41); values of organic carbon are highest in the middle Oligocene and again in parts of the Pliocene and Pleistocene. In the Eocene and lower Oligocene section, organic carbon values are <0.3%.

Stratigraphy and Sedimentation Rates

We were fortunate at Site 647 to find planktonic and benthic foraminifers and calcareous nannofossils throughout the sequence, thus providing numerous biostratigraphic datums. In addition, radiolarians and diatoms were common to abundant in the interval from 116 to about 340 mbsf, allowing additional biostratigraphic control. Dinoflagellate cysts were also helpful in zonation of the sequence, especially in the Eocene interval of low biogenic carbonate and opal contents below 525 mbsf. At this site, a continuous middle Eocene through lower Oligocene sequence containing both calcareous and siliceous microfossils will undoubtedly provide an important stratigraphic reference section in the North Atlantic. Unfortunately, the lack of continuous core recovery and the highly disturbed, biscuited cores from much of the section did not allow establishment of a complete magnetostratigraphy at the site. Major stratigraphic boundaries established using provisional results from biostratigraphic and magnetostratigraphic studies are as follows:

1. 33 mbsf: lower Pleistocene/upper Pleistocene (top of Matuyama Chron at 0.73 Ma).
2. 75 mbsf: Pliocene/Pleistocene boundary (1.6 Ma).
3. 116 mbsf: unconformity between upper Pliocene (2.5 Ma) and upper Miocene (5.6 Ma).
4. 119.3 mbsf: unconformity between upper Miocene (8.2 Ma) and lower Miocene (17.5 Ma).
5. 135 mbsf: unconformity between lower Miocene and upper Oligocene (23.7 Ma).
6. 143 mbsf: upper Oligocene/lower Oligocene boundary (29.5 Ma).
7. 143–215 mbsf: slow deposition during early Oligocene (29.5 Ma–34.5 Ma).
8. 290 mbsf: Oligocene/Eocene boundary (36.6 Ma).
9. 412 mbsf: upper Eocene/middle Eocene boundary (40 Ma).
10. 608–643 mbsf: slow deposition during middle Eocene and early Eocene (45.5–53.5 Ma), no firm evidence of a hiatus.
11. 699 mbsf: lower Eocene (55–56 Ma) at top of basement.

Sedimentation rates were calculated on the basis of these datums and additional stratigraphic information and are shown in Figure 30. Rates of sediment accumulation average about 46 m/m.y. in the Pliocene–Pleistocene, about 2.3 m/m.y. in the hiatus-ridden interval between the middle Miocene and the upper Oligocene, and about 36 m/m.y. in much of the rest of the Oligocene and the Eocene; some intervals of lower accumulation rate appear in the lower Oligocene (16 m/m.y.) and the lower to middle Eocene (25 m/m.y.).

The sedimentation rates and bulk-density and porosity information were used to calculate the accumulation rates of carbonate, organic carbon, and noncarbonate material (including both terrigenous material and biogenic opal) shown in Figure 42. The results are intended to give only a general picture; the details await more firm biostratigraphic data. Nevertheless, bulk-accumulation rates are high only during the last 2.5 m.y. of deposition, and during the intervals from 46 to 34 Ma and 56 to 54 Ma. Much of the relatively high bulk-accumulation rate is the result of high supply rates of terrigenous sediment. Biogenic carbonate accumulation rates are less than half of those of noncarbonate material. Organic carbon accumulation rates are uniformly low but increase slightly in the high-sedimentation-rate interval from 46 to 34 Ma. A maximum in biogenic opal concentrations from 34 to 32 Ma is not considered as being a high accumulation rate of either opal or organic carbon. Part of the high carbonate-accumulation rates above 2.5 Ma results from detrital carbonate supply (turbidites, ice-rafted detritus).

Paleoenvironmental Evolution

Glacial History

Rotary and APC cores provide a nearly complete sequence over the last 2.5 m.y. of deposition (late Pliocene–Pleistocene). Recognizable alternations of relatively nannofossil-rich silty clay and more gravel-rich, silty intervals appear to represent depositional cycles related to glacial-interglacial climatic cycles. Average sedimentation rates are about 46 m/m.y. (4.6 cm/k.y.). Sediment deposited over the last 1.2 m.y. contains more silt, sand, and detrital carbonate than does the older part of Unit I. Both (1) bottom-current-winnowed beds enriched in biogenic components and (2) turbiditic, detricarbonate sediment derived from spillover of the NAMOC occur in the Pliocene–Pleistocene sequence. A suite of ice-rafted pebbles, including intrusive and extrusive igneous rocks, high-grade metamorphic rocks, and a variety of sedimentary clasts, could have been derived from a broad region, such as carbonate terrains in the northern Baffin Bay region.

As at Site 646, the earliest evidence of glacial ice rafting suggests onset at about 2.5 Ma. Strata of this age, dominated by terrigenous input, directly overlie a hiatus at 116 mbsf, which encompasses the interval between at least 5.6 and 2.5 Ma. The hiatus lies at the level of a prominent regional reflector (R2) and may correspond to an apparently sharp lithologic contact between Cores 105-647A-12R and 105-647A-13R. However, the results of Site 647 studies cannot precisely constrain the age of R2 because of another prominent hiatus spanning the 8.2–17.5-Ma interval, only 3 m below the late Miocene–Pliocene hiatus.

Planktonic foraminifers and calcareous nannofossils are relatively abundant and preservation is good throughout the Pliocene–Pleistocene interval. Radiolarians and diatom remains are rare. The flora and fauna indicate general dominance of surface-water conditions by typical North Atlantic Drift conditions similar to those of today but with some probable colder and perhaps less saline conditions at times. Perhaps the area near the site was periodically influenced by the cold Labrador Current during the Pliocene and Pleistocene.

Neogene to Paleogene Paleoclimates and Paleoceanography

A condensed sedimentary sequence represents the early to late Miocene deposition (Unit II) and contains at least one hiatus between the upper Miocene (8.2 Ma) and the lower Miocene (17.5 Ma). iron/manganese and phosphate nodules, streaks, and bands characterize much of the interval. The hiatuses and slow sedimentation <1 m/m.y. for the intervening interval (116–119.3 mbsf) probably indicate scour by strong bottom currents and/or nondeposition in conjunction with low sediment supply during much of the early to late Miocene. This episode approximately coincides with the beginning of major drift sedimentation in the North Atlantic. An additional hiatus of 7.0 m.y. may be present between the lower Miocene and upper Oligocene between Cores 105-647A-14R and 105-647A-15R (135 mbsf).

A particularly important feature of the recovery at Site 647 is the continuous, upper middle Eocene through lower Oligocene sequence, which shows a high sedimentation rate. The sedimentation rate, however, decreased to 16 m/m.y. between the early middle Oligocene and late Oligocene (135–215 mbsf). The biogenic claystones and clayey oozes were deposited at average rates of about 36 m/m.y. in the late middle Eocene to early Oligocene

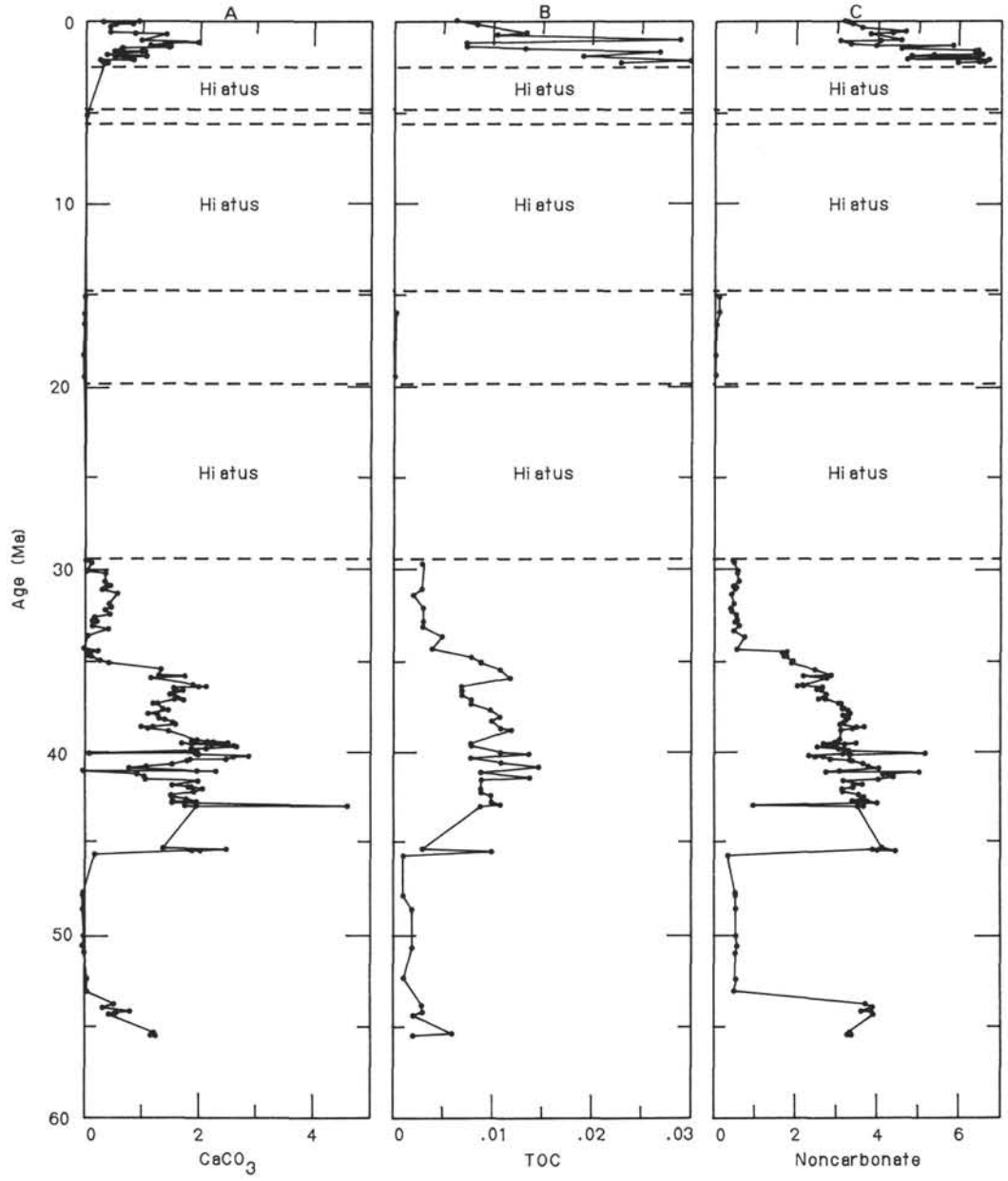

Figure 42. Accumulation rates of (A) carbonate, including Pliocene and Pleistocene detrital material, (B) organic carbon (TOC), and (C) noncarbonate material, including biogenic opal at Site 647.

and are predominantly nannofossil rich, but biogenic opal occurs in the upper Eocene through lower Oligocene strata. Lower Oligocene strata between 212.3 and 241.1 mbsf are particularly biogenic opal rich.

A prominent regional seismic reflector identified as R4 corresponds to the change from siliceous- to calcareous-biogenic claystones in the lower Oligocene at about 240 mbsf, corresponding to the previous identification of R4 at DSDP Site 112 nearby (Figs. 43 through 45). The reflector appears to bear no direct relationship to changes in bottom-water circulation at Site 647.

A major but somewhat gradual change in the benthic foraminiferal fauna, from agglutinated to calcareous dominated, occurred during the late Eocene through earliest Oligocene (essentially complete by the formation of the Eocene/Oligocene boundary at 290 mbsf), which is below the level of R4. The benthic faunal transition may indicate a change in bottom-water characteristics and, coupled with high rates of deposition and supply of terrigenous clay, may signify increased rates of deep circulation. However the sediment textures and structures provide no indication of strong abyssal currents at the site during this time.

The seafloor at the site apparently subsided below the CCD during the early to early middle Eocene, when lithologic Unit IV was deposited. An approximate 8–10.5-m.y. hiatus (45.5–53.5 Ma) or a change in the rate of deposition occurs within this unit at about 630 mbsf; poor core recovery causes difficulty in assigning an exact depth to this slow-sedimentation-rate event. The CCD apparently descended during the middle to late Eocene and into the early Oligocene, as indicated by the predominance of biogenic carbonate-rich facies and fair to good preservation of calcareous microfossils. Carbonate productivity may also have increased over that time. A climatic optimum characterized by highest diversity of calcareous plankton occurred during the late middle Eocene (about 41 Ma). The early Oligocene episode of biosiliceous sediment deposition probably represents

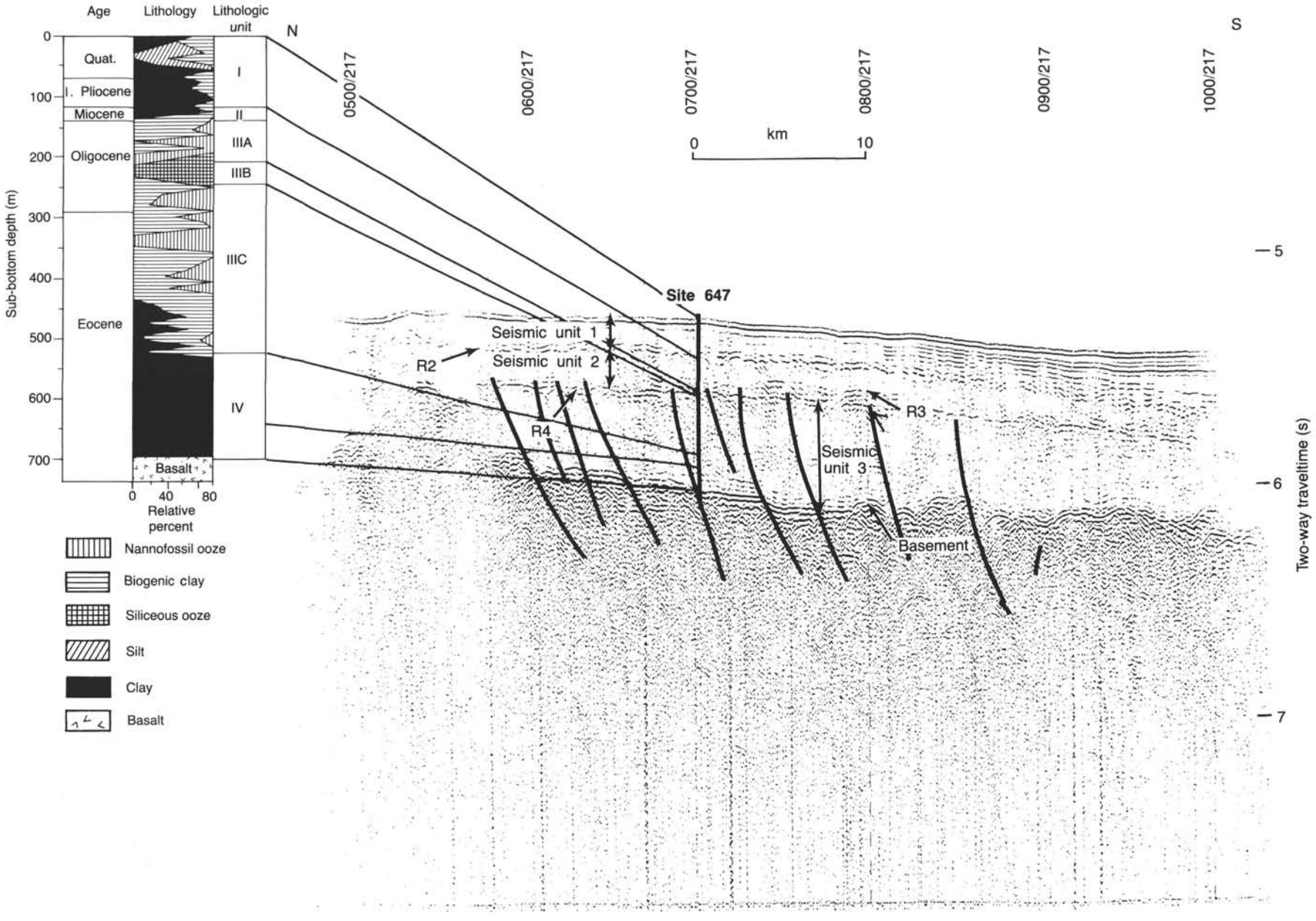

Figure 43. Single-channel seismic line (*Hudson* 84-30, line 4) showing character of major reflectors, seismic units, and correlation to lithology and age at Site 647. Note faults cutting basement and strata below reflector R4.

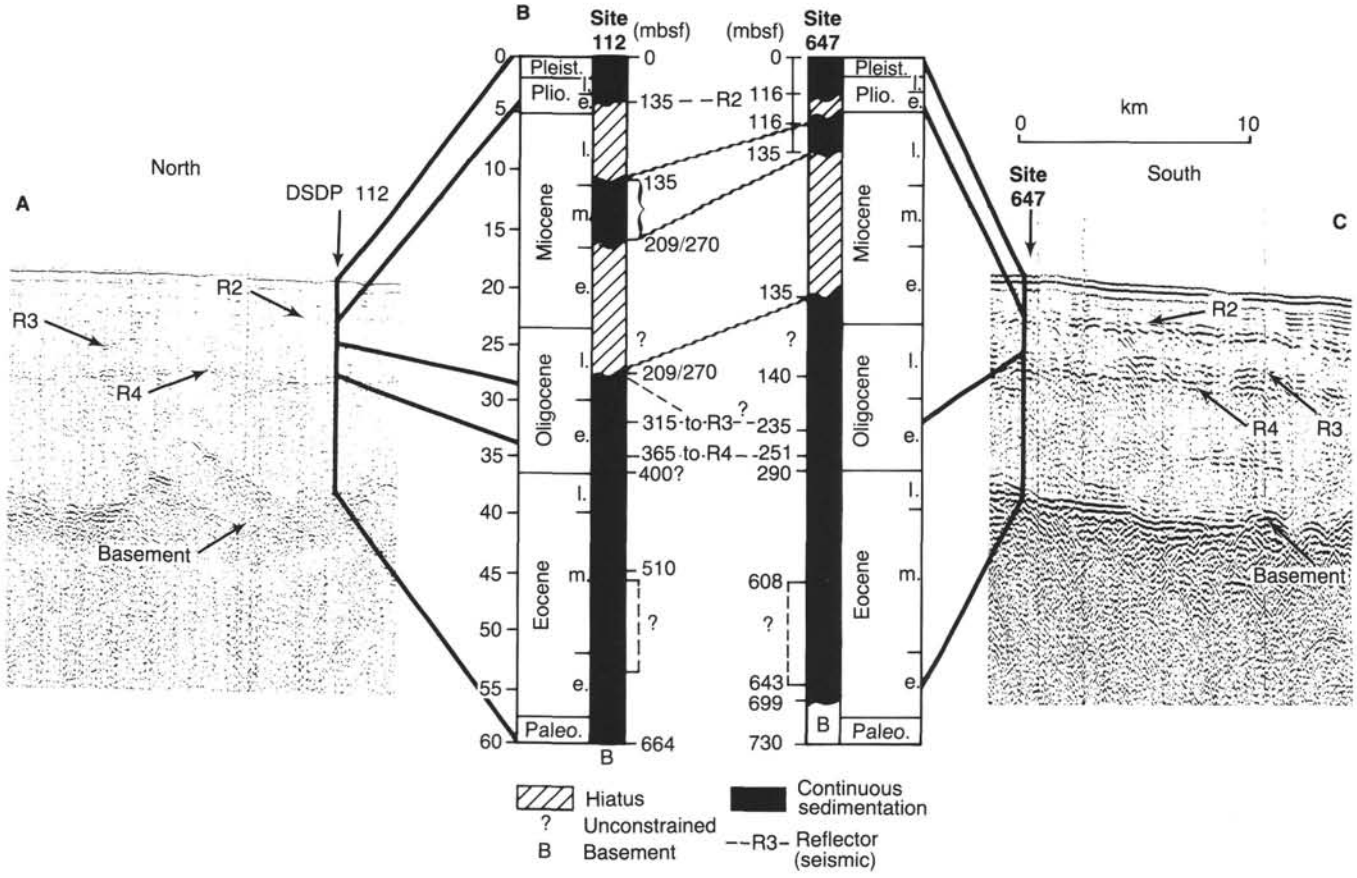

Figure 44. Seismic character (A) near DSDP Site 112 correlated to age and lithology at Site 112 (B), and (C) seismic character near Site 647 correlated with age and lithology at Site 647.

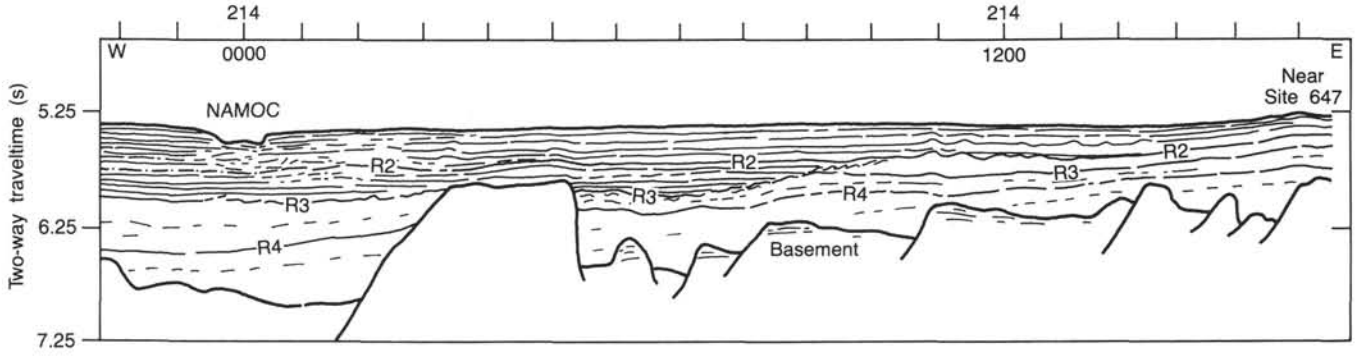

Figure 45. Line drawing of *Hudson* 84-30 line 1 across NAMOC west and south of Site 647, showing correlation of seismic reflection identified at Site 646.

increased opal and decreased carbonate production in surface waters, a trend that began during the late Eocene accompanied by cooling of surface waters. Opal-accumulation rates increased in that interval, while the carbonate-accumulation rate decreased. Organic-carbon-accumulation rates (Fig. 41) are at a maximum in the middle Eocene in conjunction with high abundance of agglutinated benthic foraminifers.

Sediment Supply and Bottom Circulation in the Southern Labrador Sea

Drilling results from Site 647, comparisons with DSDP Site 112, and correlations through selected single-channel seismic lines across the region allow us to draw some preliminary conclusions regarding the development of both the NAMOC (Fig. 55) and the Gloria Drift (Figs. 46 and 47).

Chough and Hesse (in press) suggested that deposition of the sequence of turbidites in the NAMOC, which is as much as 0.5 s (perhaps 425 m) thick, probably began about 2.5 Ma, coincident with the beginning of northern hemisphere glaciation. This inferred timing was based on the reasonable assertion that a major increase in the supply of terrigenous sediment to the region would have taken place with the advent of glacial erosion of surrounding continents. Indeed, the correlation of our drilling results to a network of seismic lines demonstrates that a major

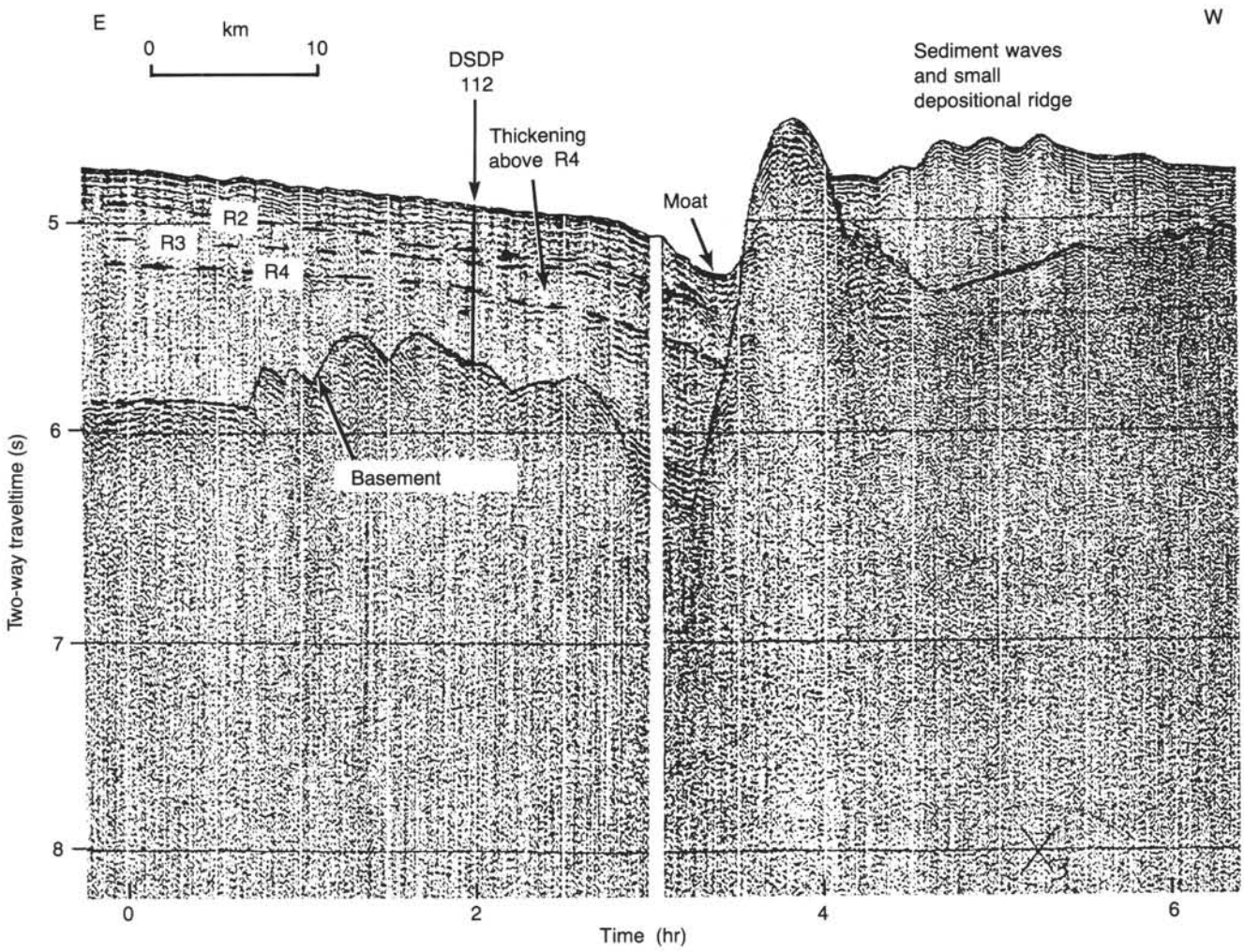

Figure 46. Segment of seismic-reflection profile *Vema* 3009, across DSDP Site 112 (see Fig. 1 for location).

part of the NAMOC deposits are 2.5 Ma or younger. Figure 45 illustrates that reflector R2, an unconformity above upper Miocene strata overlain by terrigenous sediments dated at 2.4–2.5 Ma, passes beneath much of the acoustically well-laminated NAMOC deposits west of Site 647. However, according to their seismic character, an equivalent thickness of probable turbidites clearly occurs below R2 in the NAMOC area (Fig. 45). These deposits are laterally less extensive than the upper unit, but probably represent an earlier phase of turbidite deposition in the NAMOC. The lower boundary of this second depositional unit is the reflector we have termed R3; at Site 647, this horizon (at about 210 mbsf) marks a change from low-carbonate claystone (<10%) below to nannofossil claystone above (20%–50% $CaCO_3$). The reflector occurs in the upper lower Oligocene, which indicates that turbidite sedimentation in the NAMOC could have begun by the early Miocene. This horizon also coincides with a decrease in the sedimentation rate and a possible 7-m.y. hiatus spanning the late Oligocene–earliest Miocene. We cannot definitely state that sedimentation was continuous. The average estimated sedimentation rate is only 16 m/m.y., but much of the deposition between R2 and R3 could have occurred in a limited period. For the upper 0.26 s above R2, the rates are a maximum of 85 m/m.y. The latter value is similar to that estimated for NAMOC deposits by Chough and Hesse (in press), who extrapolated sedimentation rates over the last glacial-interglacial cycle. Thus it appears that important terrigenous sediment supply to the region occurred from at least 2.5 Ma to the present through NAMOC but that terrigenous influx could have begun earlier.

In the Imarssuak Mid-Ocean Channel (IMOC) (Egloff and Johnson, 1975) north of Gloria Drift, the drilling results from DSDP Site 113 (Laughton, Berggren, et al., 1972) indicate that high terrigenous sediment supply began as early as the latest Miocene to early Pliocene. The IMOC is currently the major source of detritus to the lower NAMOC (Egloff and Johnson, 1975); therefore, the results of DSDP Site 113 studies also suggest an earlier phase of terrigenous supply to NAMOC.

In seismic records over the southern part of Gloria Drift (Figs. 43 and 44), the highly reflective NAMOC deposits progressively onlap more transparent units below. An observable transition exists from the highly reflective western units to the less reflective, nearly transparent eastern units. The acoustically transparent strata occur at somewhat shallower depths than the age-equivalent, highly reflective units. At least above reflector R3, these relationships suggest that Gloria Drift, on the margin of which Site 647 was drilled, consists primarily of fine-grained sediment that has been reworked, transported, and deposited by bottom currents. Well-developed sediment waves (hyperbolic echoes and reflectors) occur in the sequence above reflector R2, but discernment of such features is difficult below R2 in most seismic records (Figs. 46 and 47). However, the diffractive returns

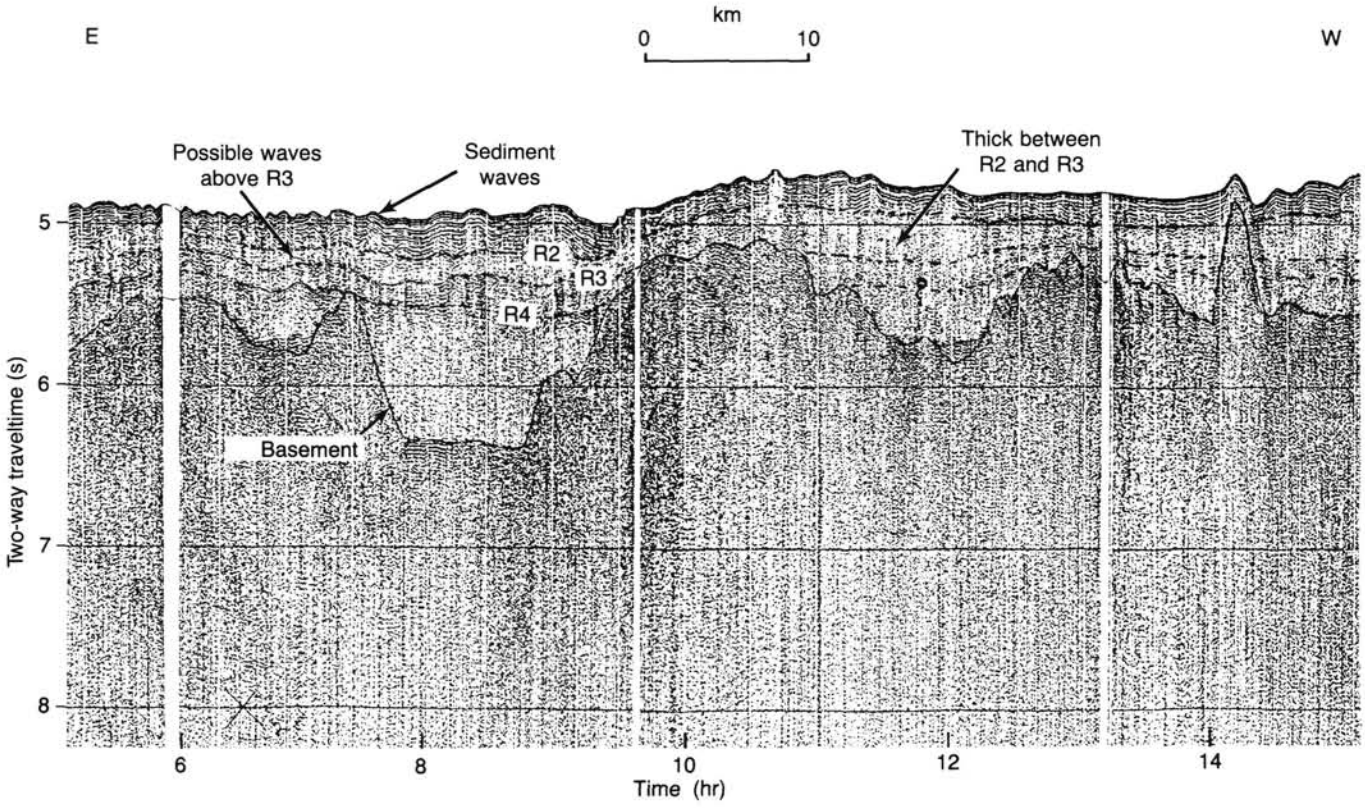

Figure 47. Segment of seismic-reflection profile *Vema* 3009, across Gloria Drift (see Fig. 1 for location).

above R4 in the main part of Gloria Drift probably represent sediment waves or otherwise irregular deposits resulting from bottom-current activity. These sediment waves and the shape of ridges on Gloria Drift (Egloff and Johnson, 1975) attest to the influence of deep currents in the construction of Gloria Drift.

Clearly much of the drift sequence has been formed above R2 (Figs. 46 and 47), which gives it a minimum age of late Miocene (5.6 Ma) and a maximum age of 17.5 Ma. However, the records at ODP Site 647 and DSDP Site 112 suggest mainly upper Pliocene and Pleistocene sediment above R2; thicknesses of the upper recognizable drift unit of up to 0.26 s (300 m) occur in the middle to southern part of Gloria Drift above R2, averaging about 160 m (110 m at Site 647; 135 m at Site 112, both located in regions of thinner sediment). The interval between R2 and R3 in the seismic records is of variable thickness over the region and is generally thickest along the axes of the sediment ridges built by bottom-current deposition.

No clear features suggest deposition by currents within the sediments bounded by R2 and R3 at either Site 647 or DSDP Site 112, and no unequivocal features appear in seismic lines across the sites themselves that might suggest current activity. Nonetheless, small depositional ridges probably formed above R3 (Figs. 46 and 47). At DSDP Site 112, either R3 represents an unconformity between the middle Miocene and upper Oligocene strata at about 220 mbsf (0.24 s) (Fig. 44)—therefore, what we identified as the R3 surface there is somewhat younger than at Site 647—or R3 perhaps represents the same change from biogenic carbonate to opal-rich sediment in the lower Oligocene. In the latter possibility, however, the depth to R3 at Site 112 (about 315 mbsf) would be significantly greater than calculated using a reasonable range of seismic velocities (i.e., the reflector should occur at a depth between 240 and 270 mbsf). Therefore, the R3 reflector at Site 647 may not correlate with that at Site 112. Nevertheless, drift deposition occurred above R3 in the region and therefore mainly after the middle Oligocene. The topography above R3 that appears in seismic records (Figs. 46 and 47) suggests that this is a reasonable hypothesis.

Basement Age and Tectonics

We recovered 37 m of one or more thick flows of fine- to medium-crystalline, aphyric to phyric basalt at the base of Hole 647A. We are reasonably certain that this represents recovery of the top of layer 2 basalts and that no interbedded sediments occur. The age of the uppermost basaltic basement is 55–56 Ma, on the basis of the oldest sediment immediately overlying it. Preservation of microfossils is good, and the age represents agreement of all major microfossil groups. This age closely agrees with the age of basement initially assigned according to magnetic-anomaly correlations (Fig. 1; anomaly 24; Srivastava et al., 1981), thus supporting the geophysical data. The results also validate the tectonic model of Labrador Sea evolution (Srivastava et al., 1981), which calls for a major change in seafloor-spreading orientation at Chron 24. Spreading in the Labrador Sea continued until Chron 13 (earliest Oligocene, 36.5 Ma; Fig. 3).

Evidence of some late hydrothermal activity and associated faults and fractures occurs in Eocene-age strata overlying the basement to depths as shallow as 250 mbsf in the cores. The evidence of faulting occurs only in strata older than early Oligocene. Faulting is also observed in the seismic lines near the site (Fig. 43) and appears to affect strata at and below reflector R4. Such deformation may indicate that differential basement subsidence occurred until the cessation of seafloor spreading in the region and that sediments draped the area after the early Oligocene without deformation.

REFERENCES

Aksu, A. E., and Mudie, P. J., 1985. Magnetostratigraphy and palynology demonstrate at least 4 million years of Arctic Ocean sedimentation. *Nature*, 318:280–283.

Andrews, A. J., 1979. On the effect of low temperature seawater-basalt interaction on the distribution of sulfur in oceanic crust, Layer 2. *Earth Planet. Sci. Lett.*, 46:68–80.

Aubry, M. P., 1985. Northwestern European Paleogene magnetostratigraphy, biostratigraphy and paleogeography: calcareous nannofossil evidence. *Geology*, 13(3):198–202.

Barron, J. A., 1985. Late Eocene to Holocene diatom biostratigraphy of the equatorial Pacific Ocean, Deep Sea Drilling Project Leg 85. *In* Mayer, L., Theyer, F., et al., *Init. Repts. DSDP*, 85: Washington (U.S. Govt. Printing Office), 413–456.

Benedek, P. N., and Müller, C., 1974. Nannoplankton-phytoplankton-korrelation im Mittel- und Ober-Oligozän von NW-Deutschland. *N. Jahrb. Geol. und Paläontol. Monatsh.*, 385–397.

Benedek, P. N., and Müller, C., 1976. Die Grenze Unter/Mittel-Oligozän am Doberg bei Bünde/Westfalen. 1 Phyto- und Nannoplankton. *Jahrb. Geol. Paläontol. Monatsh.*, 3:129–144.

Bennett, R. H., and Keller, G. H., 1973. Physical properties evaluation. *In* van Andel, T. H., Heath, G. R., et al., *Init. Repts. DSDP*, 16: Washington (U.S. Govt. Printing Office), 513–519.

Berggren, W. A., 1972. Cenozoic biostratigraphy and paleobiogeography of the North Atlantic. *In* Laughton, A. S., Berggren, W. A., et al., *Init. Repts. DSDP*, 12: Washington (U.S. Govt. Printing Office), 965–1002.

_____, 1978. Recent advances in Cenozoic planktonic foraminiferal biostratigraphy, biochronology and biogeography: Atlantic Ocean. *Micropaleontology*, 24:337–370.

Berggren, W. A., and Schnitker, D., 1983. Cenozoic marine environments in the North Atlantic and Norwegian-Greenland Sea. *In* Bott, M.H.P., Saxov, S., Talwani, M., Thiede, J. (Eds.), *Structure and Development of the Greenland-Scotland Ridge — New Methods and Concepts*. NATO Conference Series IV: New York (Plenum), 8:495–548.

Berggren, W. A., Kent, D. V., and van Couvering, J. A., 1986a [1985]. Neogene geochronology and chronostratigraphy. *In* Snelling, N. J., *Geochronology and the Geologic Time Scale*. Geol. Soc. London, Mem. 10, 211–250.

Berggren, W. A., Kent, D. V., and Flynn, J. J., 1986b [1985]. Paleogene geochronology and chronostratigraphy. *In* Snelling, N. J., *Geochronology and the Geologic Time Scale*. Geol. Soc. London, Mem. 10, 141–195.

Bjørklund, K. R., 1976. Radiolarians from the Norwegian Sea, Leg 38 of the Deep Sea Drilling Project. *In* Talwani, M., Udintsev, G., et al., *Init. Repts. DSDP*, 38: Washington (U.S. Govt. Printing Office), 1101–1168.

Blow, W. H., 1969. Late middle Eocene to Recent planktonic foraminiferal biostratigraphy. *In* Bronnimann, P., and Renz, H. H. (Eds.), *Proc. First Init. Conf. Planktonic Microfossils*, Geneva, 1967: Leiden (E. J. Brill), 689–702.

Brown, S., and Downie, C., 1985a. Dinoflagellate cyst biostratigraphy of late Paleocene and early Eocene sediments from Holes 552, 553A, and 555, Leg 81, Deep Sea Drilling Project (Rockall Plateau). *In* Roberts, D. G., Schnitker, D., et al., *Init. Repts. DSDP*, 81: Washington (U.S. Govt. Printing Office), 565–579.

_____, 1985b. Dinoflagellate cyst stratigraphy of Paleocene to Miocene sediments from the Goban Spur (Sites 548–550, Leg 80). *In* de Graciansky, P. C., Poag, C. W., et al., *Init. Repts. DSDP*, 80: Washington (U.S. Govt. Printing Office), 643–651.

Bryant, W. R., Bennett, R. H., and Katherman, C. E., 1981. Shear strength, consolidation, porosity and permeability of oceanic sediments. *In* Emiliani, C. (Ed.), *The Oceanic Lithosphere (Vol. 7), The Sea*: New York (Wiley), 1555–1616.

Bujak, J. P., 1984. Cenozoic dinoflagellate cysts and acritarchs from the Bering Sea and northern North Pacific, DSDP Leg 19. *Micropaleontology*, 30:180–212.

Bujak, J. P., Downie, C., Eaton, G. L., and Williams, G. L., 1980. Dinoflagellate cysts and acritarchs from the Eocene of southern England. *Spec. Pap. Palaeontol.*, 24:1–100.

Chateauneuf, J.-J., 1980. Palynostratigraphie et paléoclimatologie de l'Eocene supérieur et de l'Oligocene du bassin de Paris (France). *Bureau de Recherches Géologiques et Minières Mém.*, 116.

Chateauneuf, J. -J., and Gruas-Cavagnetto, C., 1978. Les zones de Wetzeliellaceae (Dinophyceae) du bassin de Paris. *Bull. Bureau de Recherches Géologiques et Minières*, 2nd Ser., Sect. IV, 2-1978, 59–93.

Chen, P. -H. 1975. Antarctic radiolaria. *In* Hayes, D. E., and Frakes, L. A., et al., *Init. Repts. DSDP*, 28: Washington (U.S. Govt. Printing Office), 437–513.

Chough, S. K., and Hesse, R., in press. The northwest Atlantic Mid-Ocean Channel of the Labrador Sea: V. morphology, sedimentary facies, stratigraphy and processes of a giant deep-sea channel. Submitted to *Can. J. Earth Sci.*

Chough, S. K., Hesse, R., and Muller, J., in press. The Northwest Atlantic Mid-Ocean Channel of the Labrador Sea: IV, petrography and provenance of the sediments. Submitted to *Can. J. Earth Sci.*

Clowes, C. D., and Morgans, H.E.G., 1985. Micropaleontology of the Whamgaroan (Eocene–Oligocene) Totara limestone. *New Zealand Geol. Sur.*, Record 3, 30–40.

Davies, T. A., and Laughton, A. S., 1972. Sedimentary processes in the North Atlantic. *In* Laughton, A. S., Berggren, W. A., et al., *Init. Repts. DSDP*, 12: Washington (U.S. Govt. Printing Office), 905–934.

De Vernal, A., 1986. Analyses palynologiques et isotopiques de sediments de la baie de Baffin et de la mer du Labrador: Éléments d'une climatostratigraphie du Pléistocene supérieur dans l'est du Canada [Ph.D. dissert.]. Université de Montreal, Canada.

Dzinoridze, R. N., Jousé, A. P., Koroleva-Golikova, G. S., Kozlova, G. E., Nagaeva, G. S., Petrushevskaya, M. G., and Strelnikova, N. I., 1978. Diatom and radiolarian Cenozoic stratigraphy, Norwegian Basin; DSDP Leg 38. *In* Talwani, M., Udintsev, G., et al., *Init. Repts. DSDP*, Suppl. to Vols. 38, 39, 40, and 41: Washington (U.S. Govt. Printing Office), 289–427.

Egloff, J., and Johnson, G. L., 1975. Morphology and structure of the southern Labrador Sea. *Can. J. Earth Sci.*, 12:2111–2133.

Eldholm, O., Thiede, J., Taylor, E., et al., in press. *Proc. Init. Repts., ODP*, 104.

Fenner, J., 1977. Cenozoic diatom biostratigraphy of the Equatorial and Southern Atlantic Ocean. *In* Perch-Nielsen, K., Supko, P. R., et al., *Init. Repts. DSDP*, Suppl. to Vols. 38, 39, 40, and 41: Washington (U.S. Govt. Printing Office), 491–624.

_____, 1984a. Middle Eocene to Oligocene planktonic diatom stratigraphy from Deep Sea Drilling sites in the South Atlantic, equatorial Pacific and Indian oceans. *In* Hay, W. W., Sibuet, J. -C., et al., *Init. Repts. DSDP*, 75: Washington (U.S. Govt. Printing Office), 1245–1271.

_____, 1984b. Eocene-Oligocene planktic diatom stratigraphy in the low latitudes and in the high southern latitudes. *Micropaleontology*, 30(4):319–342.

_____, 1985. Late Cretaceous to Oligocene planktic diatoms. *In* Bolli, H. M., Saunders, J. B., and Perch-Nielsen, K. (Eds.), *Plankton Stratigraphy*, Cambridge (Cambridge Univ. Press), 713–762.

Geroch, S., and Nowak, W., 1983. Proposal of zonation for the Late Tithonian–late Eocene based upon arenaceous foraminifera from the outer Carpathians, Poland. *Benthos '83: Proc., Second Int. Symp. Benthic Foraminifera*, 225–239.

Gombos, A. M., Jr., and Ciesielski, P. F., 1983. Late Eocene to early Miocene diatoms from the southwest Atlantic. *In* Ludwig, W. J., Krasheninnikov, V. A., et al., *Init. Repts. DSDP*, 71, Pt. 2: Washington (U.S. Govt. Printing Office), 583–634.

Goodman, D. K., and Ford, L. N., Jr., 1983. Preliminary dinoflagellate biostratigraphy for the middle Eocene to lower Oligocene from the southwest Atlantic Ocean. *In* Ludwig, W. J., Krasheninnikov, V. A., et al., *Init. Repts. DSDP*, 71, Pt. 2: Washington (U.S. Govt. Printing Office), 859–887.

Harland, R., 1978. Quaternary and Neogene dinoflagellate cysts. *In* Thusu, B. (Ed.), *Distribution of Diagnostic Dinoflagellate Cysts and Miospores from the Northwest European Continental Shelf and Adjacent Areas*: (Norway Continental Shelf Institute), 100.

_____, 1979. Dinoflagellate biostratigraphy of Neogene and Quaternary sediments at Holes 400/400A in the Bay of Biscay (DSDP Leg 48). *In* Montadert, L., Roberts, D. G., et al., *Init. Repts. DSDP*, 48: Washington (U.S. Govt. Printing Office), 531–545.

Islam, M. A., 1984. A study of early Eocene paleoenvironments in the Isle of Sheppey as determined from microplankton assemblage composition. *Tertiary Res.* 6(1), 11–21.

Jehanno, C., Lallier-Verges, E., Bonnot-Courtois, C., Desprairies, A., Bijon, J., and Riviere, M., 1984. Fossil polymetallic concretions from

Deep Sea Drilling Project Leg 81: mineralogical, geochemical, and statistical studies. *In* Roberts, D. G., Schnitker, D., et al., *Init. Repts. DSDP*, 81: Washington (U.S. Govt. Printing Office), 701–723.

Johnson, G. L., and Schneider, E. D., 1969. Depositional ridges in the North Atlantic. *Earth Planet. Sci. Lett.*, 6:416–422.

Jones, E. J., Ewing, M., Ewing, J. I., and Eittreim, S. L., 1970. Influences of Norwegian Sea overflow on sedimentation in the northern North Atlantic and the Labrador Sea. *J. Geophys. Res.*, 75:1655–1680.

Keller, G. H., and Bennett, R. H., 1973. Sediment mass physical properties–Panama Basin and northeastern equatorial Pacific. *In* van Andel, T. H., Heath, G. R., et al., *Init. Repts. DSDP*, 16: Washington (U.S. Govt. Printing Office), 499–512.

Kristoffersen, Y., and Talwani, M., 1977. Extinct triple junction south of Greenland and the Tertiary motion of Greenland relative to North America. *Geol. Soc. Am. Bull.*, 88:1037–1049.

Laughton, A. S., 1972. The southern Labrador Sea—a key to the Mesozoic and early Tertiary evolution of the North Atlantic. *In* Laughton, A. S., Berggren, W. A., et al., *Init. Repts. DSDP*, 12: Washington (U.S. Govt. Printing Office), 1155–1179.

Laughton, A. S., Berggren, W. A., et al., 1972. *Init. Repts. DSDP*, 12: Washington (U.S. Govt. Printing Office).

Martini, E., 1971. Standard Tertiary and Quaternary calcareous nannoplankton zonation. *In* Farinaci, A. (Ed.), *Proc. Second Plankton. Conf.*, 2:739–785.

Martini, E., and Müller, C., 1976. Eocene to Pleistocene silicoflagellates from the Norwegian-Greenland Sea (DSDP Leg 38). *In* Talwani, M., Udintsev, G., et al., *Init. Repts. DSDP*, 38: Washington (U.S. Govt. Printing Office), 857–896.

Mayer, L. A., 1982. Physical properties of sediment recovered on Deep Sea Drilling Project Leg 68 with the hydraulic piston corer. *In* Prell, W. L., Gardner, J. V., et al., *Init. Repts. DSDP*, 68: Washington (U.S. Govt. Printing Office), 365–382.

Mayhew, M. A., 1969. Marine geophysical measurements in the Labrador Sea: relations to Precambrian geology and sea-floor spreading [Ph.D. dissert.]. Columbia University, New York.

Miller, K. G., and Tucholke, B. E., 1983. Development of Cenozoic abyssal circulation south of the Greenland-Scotland Ridge. *In* Bott, M.H.P., Saxov, S., Talwani, M., and Thiede, J. (Eds.), *Structure and Development of the Greenland-Scotland Ridge*: New York (Plenum), 549–589.

Miller, K. G., Gradstein, F. M., and Berggren, W. A., 1982. Late Cretaceous to early Tertiary agglutinated foraminifera in the Labrador Sea. *Micropaleontology*, 28:1–30.

Miller, K. G., Currey, W. B., and Ostermann, D. R., 1984. Late Paleogene (Eocene to Oligocene) benthic foraminiferal oceanography of the Goban Spur region, Deep Sea Drilling Project Leg 80. *In* de Graciansky, P. C., Poag, C. W., et al., *Init. Repts. DSDP*, 80: Washington (U.S. Govt. Printing Office), 505–538.

Molnia, B. F., 1983. Distal glacial-marine sedimentation: abundance, composition, and distribution of North Atlantic Ocean Pleistocene ice-rafted sediment. *In* Molnia, B. F. (Ed.), *Glacial-Marine Sedimentation*: New York (Plenum), 593–626.

Mudie, P. J., in press. Palynology and dinoflagellate biostratigraphy of DSDP Leg 94, Sites 607 and 611, North Atlantic Ocean. *In* Rudiman, W. T., Kidd, R., et al., *Init. Repts. DSDP*, 94: Washington (U.S. Govt. Printing Office).

Murray, J. W., 1984. Paleogene and Neogene benthic foraminifers from Rockall Plateau. *In* Roberts, D. G., Schnitker, D., et al., *Init. Repts. DSDP*, 81: Washington (U.S. Govt. Printing Office), 503–539.

Okada, H., and Bukry, D., 1980. Supplementary modification and introduction of code numbers to the low-latitude coccolith biostratigraphic zonation (Bukry 1973, 1975). *Mar. Micropaleontol.*, 5:321–325.

Okada, H., and Thierstein, H. R., 1979. Calcareous nannoplankton—Leg 43, Deep Sea Drilling Project. *In* Tucholke, B. E., Vogt, P. R., et al., *Init. Repts. DSDP*, 43: Washington (U.S. Govt. Printing Office), 507–573.

Piasecki, S., 1980. Dinoflagellate cyst stratigraphy of the Miocene Hoddle and Gram Formations. *Bull. Geol. Soc. Denmark*, 29:53–76.

Poore, R. Z., 1979. Oligocene through Quaternary planktonic foraminiferal biostratigraphy of the North Atlantic: DSDP Leg 49. *In* Luyendyk, B. P., Cann, J. R., et al., *Init. Repts. DSDP*, 49: Washington (U.S. Govt. Printing Office), 447–518.

Raymer, L. L., Hunt, E. R., and Gardner, J. S., 1980. An improved sonic transit time to porosity transform. *Trans. SPWLA, Annu. Logging Symp.*, Pap. P.

Riedel, W. R., and Sanfilippo, A., 1978. Stratigraphy and evolution of tropical Cenozoic radiolarians. *Micropaleontology*, 23:61–96.

Roberts, D. G., Montadert, L., and Searle, R. C., 1979. The western Rockall Plateau: stratigraphy and structural evolution. *In* Montadert, L., Roberts, D. G., et al., *Init. Repts. DSDP*, 48: Washington (U.S. Govt. Printing Office), 1061–1088.

Roberts, D. G., Schnitker, D., et al., 1984. *Init. Repts. DSDP*, 81: Washington (U.S. Govt. Printing Office).

Schrader, H. -J., and Fenner, J., 1976. Part I Norwegian Sea Cenozoic diatom biostratigraphy. *In* Talwani, M., Udintsev, G., et al., *Init. Repts. DSDP*, 38: Washington (U.S. Govt. Printing Office), 921–962.

Shackleton, N. J., Backman, J., Zimmerman, H. B., Kent, D. V., Hall, M. A., Roberts, D. G., and Schnitker, D., 1984. Oxygen isotope calibration of the onset of icerafting in DSDP Site 552A: history of glaciation in the North Atlantic region. *Nature*, 307:620–623.

Snyder, S. W., and Waters, V. J., 1985. Cenozoic planktonic foraminiferal biostratigraphy of the Goban Spur region, DSDP Leg 80. *In* de Graciansky, P. C., Poag, C. W., et al., *Init. Repts. DSDP*, 80: Washington (U.S. Govt. Printing Office), 439–472.

Srivastava, S. P., 1978. Evolution of the Labrador Sea and its bearing on the early evolution of the North Atlantic. *Geophy. J. R. Astron. Soc.*, 52:313–357.

Srivastava, S. P., Falconer, R.K.H., and Maclean, B., 1981. Labrador Sea, Davis Strait, Baffin Bay: geology and geophysics–a review. *In* Kerr, J. W., Fergusson, A. J., and Machan, L. C. (Eds.), *Geology of the North Atlantic Borderlands*: Can. Soc. Pet. Geol. Mem. 7:333–398.

Stacey, F. D., and Banerjee, S. K., 1974. *The Physical Principles of Rock Magnetism*: The Netherlands (Elsevier).

Stover, L. E., 1977. Oligocene and early Miocene dinoflagellates from the Atlantic Corehole 5/5B, Blake Plateau. Am. Assoc. of Stratigraph. Palynol., Contrib. Ser. 5A, 66–89.

Tjalsma, R. C., and Lohmann, G. P., 1983. Paleocene-Eocene bathyal and abyssal benthic foraminifera from the Atlantic ocean. *Micropaleontology spec. Publ.* 4.

Vogt, P. R., and Avery, O. E., 1974. Detailed magnetic surveys in the Northeast Atlantic and Labrador Sea. *J. Geophys. Res.*, 79:363–389.

Weaver, P.P.E., and Clement, B. M., in press. Magnetobiostratigraphy of planktonic foraminiferal datums: DSDP Leg 94, North Atlantic. *In* Ruddiman, W. F., Kidd, R., et al., *Init. Repts. DSDP*, 94: Washington (U.S. Govt. Printing Office).

Williams, G. L., and Bujak, J. P., 1985. Mesozoic and Cenozoic dinoflagellates. *In* Bolli, H. M., Saunders, J. B., and Perch-Nielsen, K. (Eds.), *Plankton Stratigraphy*: Cambridge (Cambridge Univ. Press), 847–964.

Worthington, L. V., and Volkmann, G. H., 1965. The volume transport of the Norwegian Sea overflow water in the North Atlantic. *Deep-Sea Res.*, 12:667–676.

Worthington, L. V., and Wright, W. R., 1970. North Atlantic Ocean atlas of potential temperature and salinity in the deep water including temperature, salinity and oxygen profiles from the Erica Dan cruise of 1962. *Woods Hole Oceanographic Institution Atlas Series*, 2.

Summary log for Hole 647A

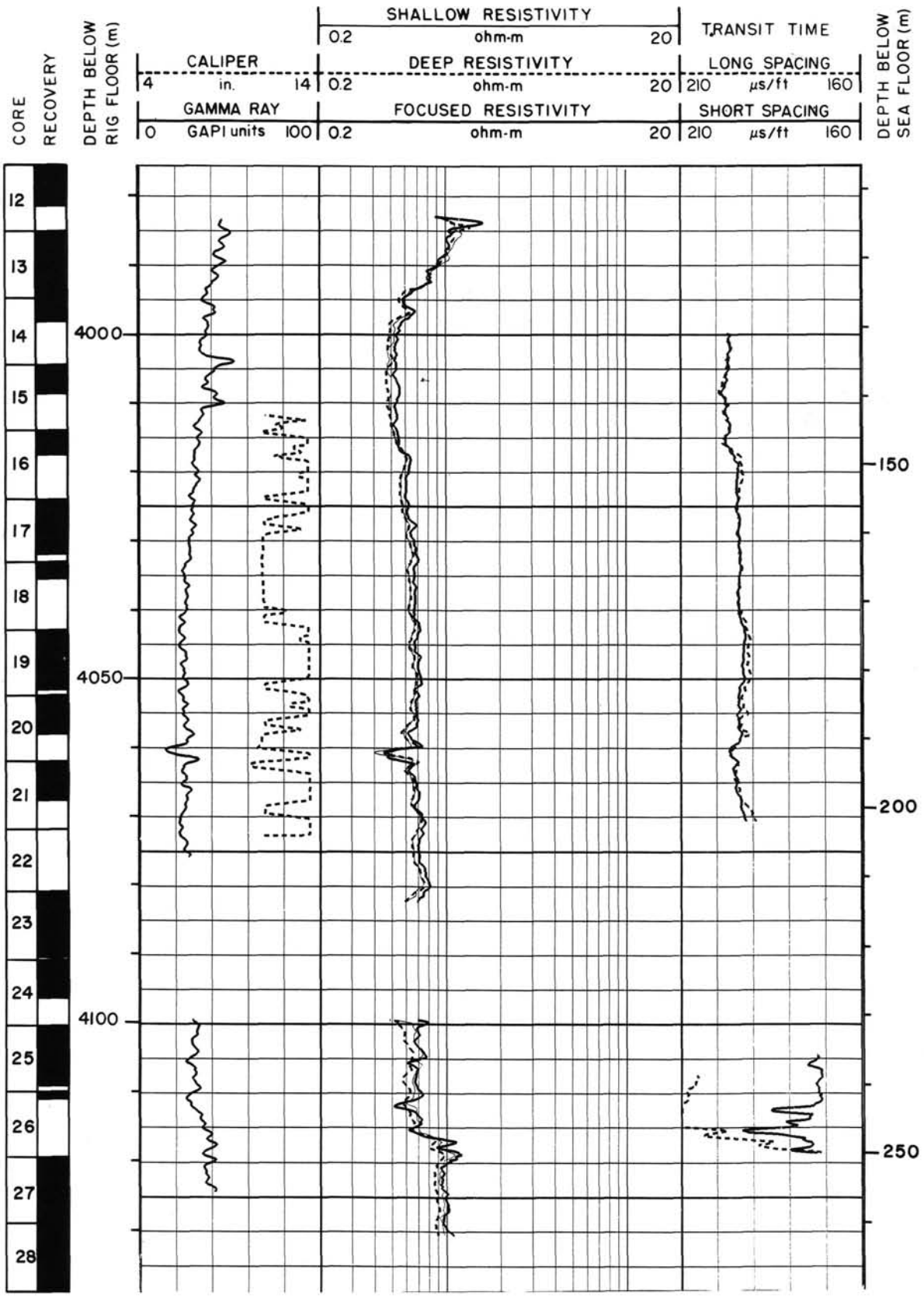

SITE 647 HOLE A CORE 1 R CORED INTERVAL 3858.5-3867.7 mbsl; 0.0-9.2 mbsf

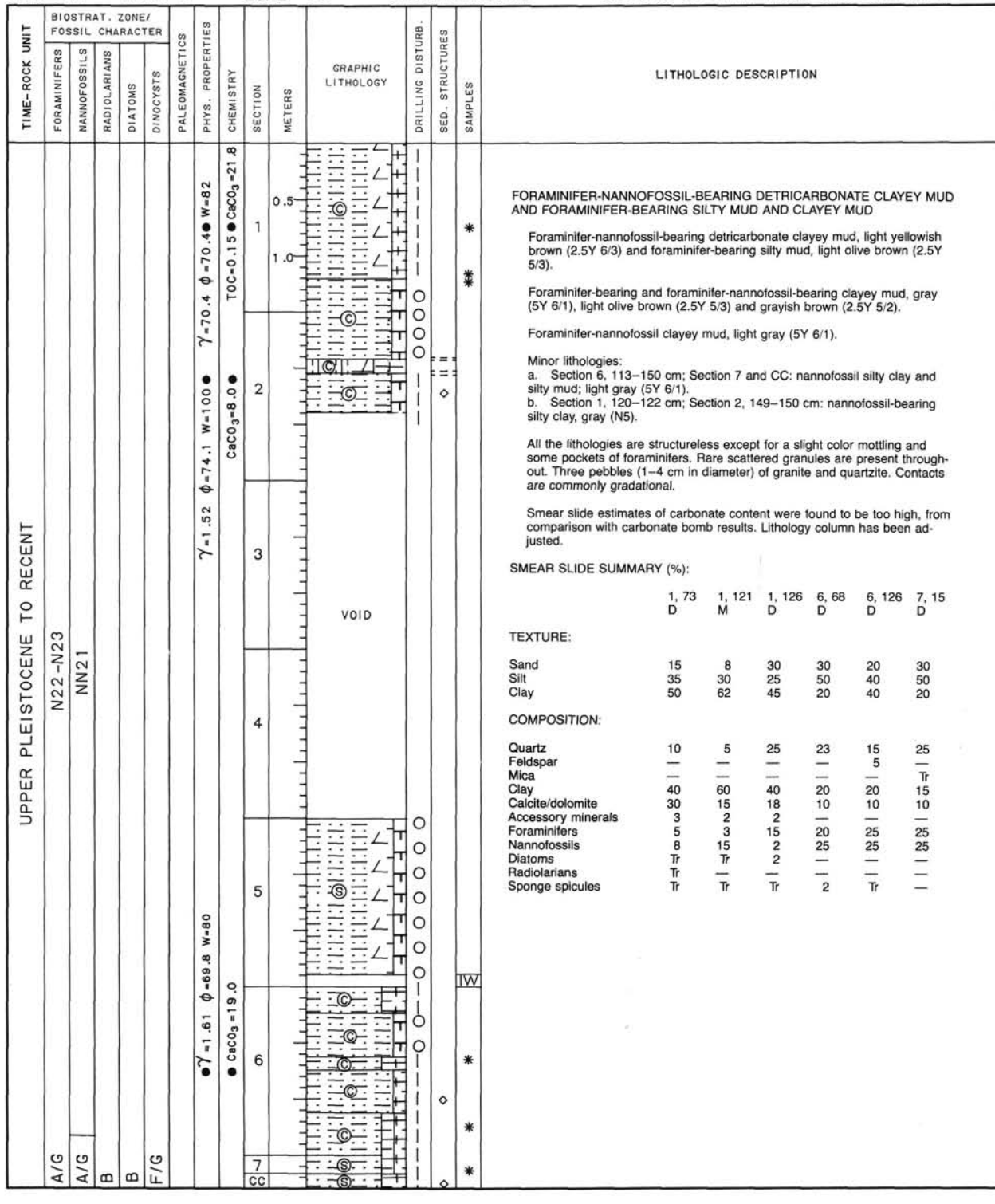

FORAMINIFER-NANNOFOSSIL-BEARING DETRICARBONATE CLAYEY MUD AND FORAMINIFER-BEARING SILTY MUD AND CLAYEY MUD

Foraminifer-nannofossil-bearing detricarbonate clayey mud, light yellowish brown (2.5Y 6/3) and foraminifer-bearing silty mud, light olive brown (2.5Y 5/3).

Foraminifer-bearing and foraminifer-nannofossil-bearing clayey mud, gray (5Y 6/1), light olive brown (2.5Y 5/3) and grayish brown (2.5Y 5/2).

Foraminifer-nannofossil clayey mud, light gray (5Y 6/1).

Minor lithologies:
a. Section 6, 113–150 cm; Section 7 and CC: nannofossil silty clay and silty mud; light gray (5Y 6/1).
b. Section 1, 120–122 cm; Section 2, 149–150 cm: nannofossil-bearing silty clay, gray (N5).

All the lithologies are structureless except for a slight color mottling and some pockets of foraminifers. Rare scattered granules are present throughout. Three pebbles (1–4 cm in diameter) of granite and quartzite. Contacts are commonly gradational.

Smear slide estimates of carbonate content were found to be too high, from comparison with carbonate bomb results. Lithology column has been adjusted.

SMEAR SLIDE SUMMARY (%):

	1, 73 D	1, 121 M	1, 126 D	6, 68 D	6, 126 D	7, 15 D
TEXTURE:						
Sand	15	8	30	30	20	30
Silt	35	30	25	50	40	50
Clay	50	62	45	20	40	20
COMPOSITION:						
Quartz	10	5	25	23	15	25
Feldspar	—	—	—	—	5	—
Mica	—	—	—	—	—	Tr
Clay	40	60	40	20	20	15
Calcite/dolomite	30	15	18	10	10	10
Accessory minerals	3	2	2	—	—	—
Foraminifers	5	3	15	20	25	25
Nannofossils	8	15	2	25	25	25
Diatoms	Tr	Tr	2	—	—	—
Radiolarians	Tr	—	—	—	—	—
Sponge spicules	Tr	Tr	Tr	2	Tr	—

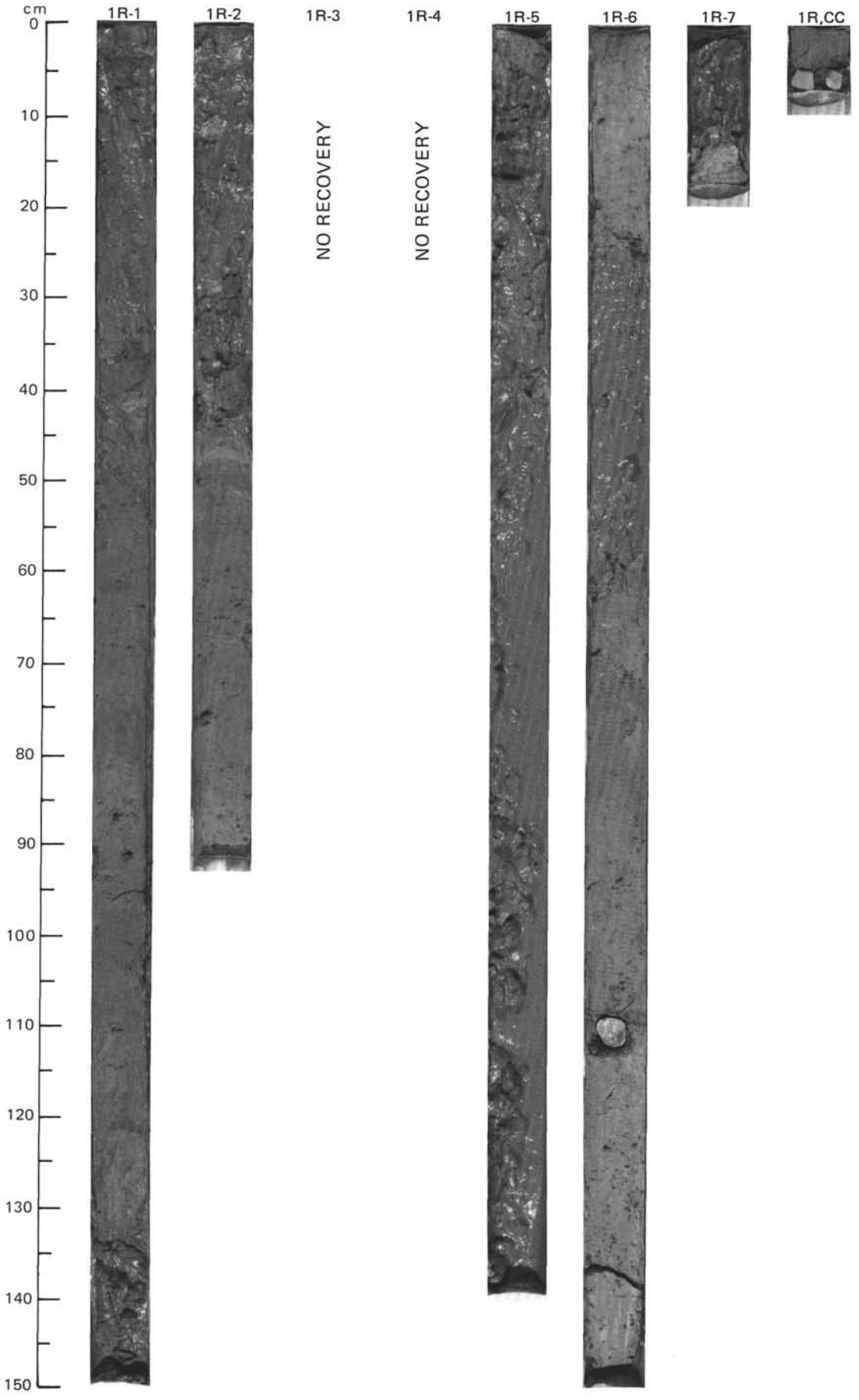
cm
0
10
20
30
40
50
60
70
80
90
100
110
120
130
140
150
1R-1
1R-2
1R-3
NO RECOVERY
1R-4
NO RECOVERY
1R-5
1R-6
1R-7
1R,CC

SITE 647 HOLE A CORE 2 R CORED INTERVAL 3867.7-3877.4 mbsl; 9.2-18.9 mbsf

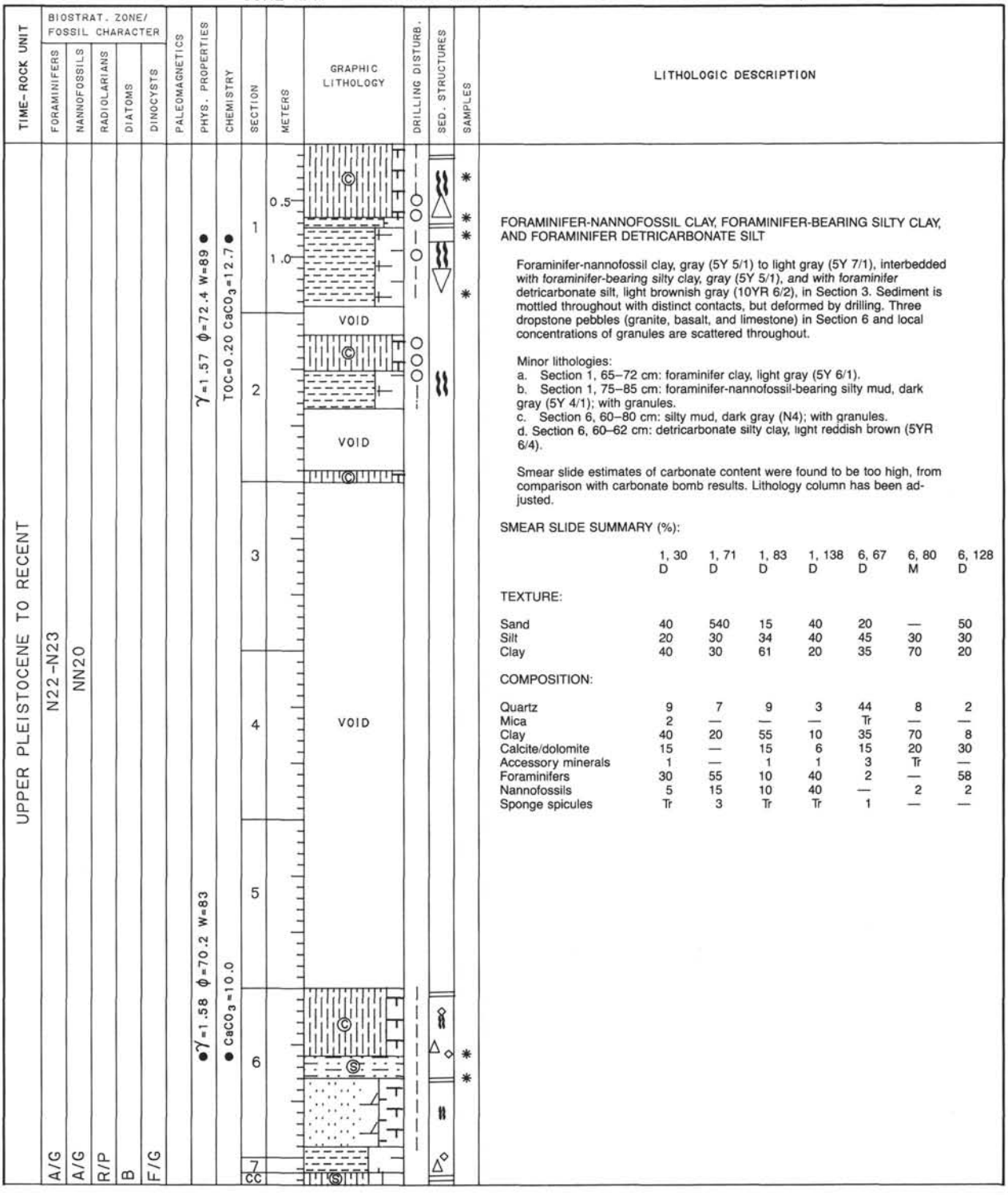

LITHOLOGIC DESCRIPTION

FORAMINIFER-NANNOFOSSIL CLAY, FORAMINIFER-BEARING SILTY CLAY, AND FORAMINIFER DETRICARBONATE SILT

Foraminifer-nannofossil clay, gray (5Y 5/1) to light gray (5Y 7/1), interbedded with *foraminifer-bearing silty clay, gray* (5Y 5/1), *and with foraminifer* detricarbonate silt, light brownish gray (10YR 6/2), in Section 3. Sediment is mottled throughout with distinct contacts, but deformed by drilling. Three dropstone pebbles (granite, basalt, and limestone) in Section 6 and local concentrations of granules are scattered throughout.

Minor lithologies:
a. Section 1, 65–72 cm: foraminifer clay, light gray (5Y 6/1).
b. Section 1, 75–85 cm: foraminifer-nannofossil-bearing silty mud, dark gray (5Y 4/1); with granules.
c. Section 6, 60–80 cm: silty mud, dark gray (N4); with granules.
d. Section 6, 60–62 cm: detricarbonate silty clay, light reddish brown (5YR 6/4).

Smear slide estimates of carbonate content were found to be too high, from comparison with carbonate bomb results. Lithology column has been adjusted.

SMEAR SLIDE SUMMARY (%):

	1, 30 D	1, 71 D	1, 83 D	1, 138 D	6, 67 D	6, 80 M	6, 128 D
TEXTURE:							
Sand	40	540	15	40	20	—	50
Silt	20	30	34	40	45	30	30
Clay	40	30	61	20	35	70	20
COMPOSITION:							
Quartz	9	7	9	3	44	8	2
Mica	2	—	—	—	Tr	—	—
Clay	40	20	55	10	35	70	8
Calcite/dolomite	15	—	15	6	15	20	30
Accessory minerals	1	—	1	1	3	Tr	—
Foraminifers	30	55	10	40	2	—	58
Nannofossils	5	15	10	40	—	2	2
Sponge spicules	Tr	3	Tr	Tr	1	—	—

CORE 3R NO RECOVERY

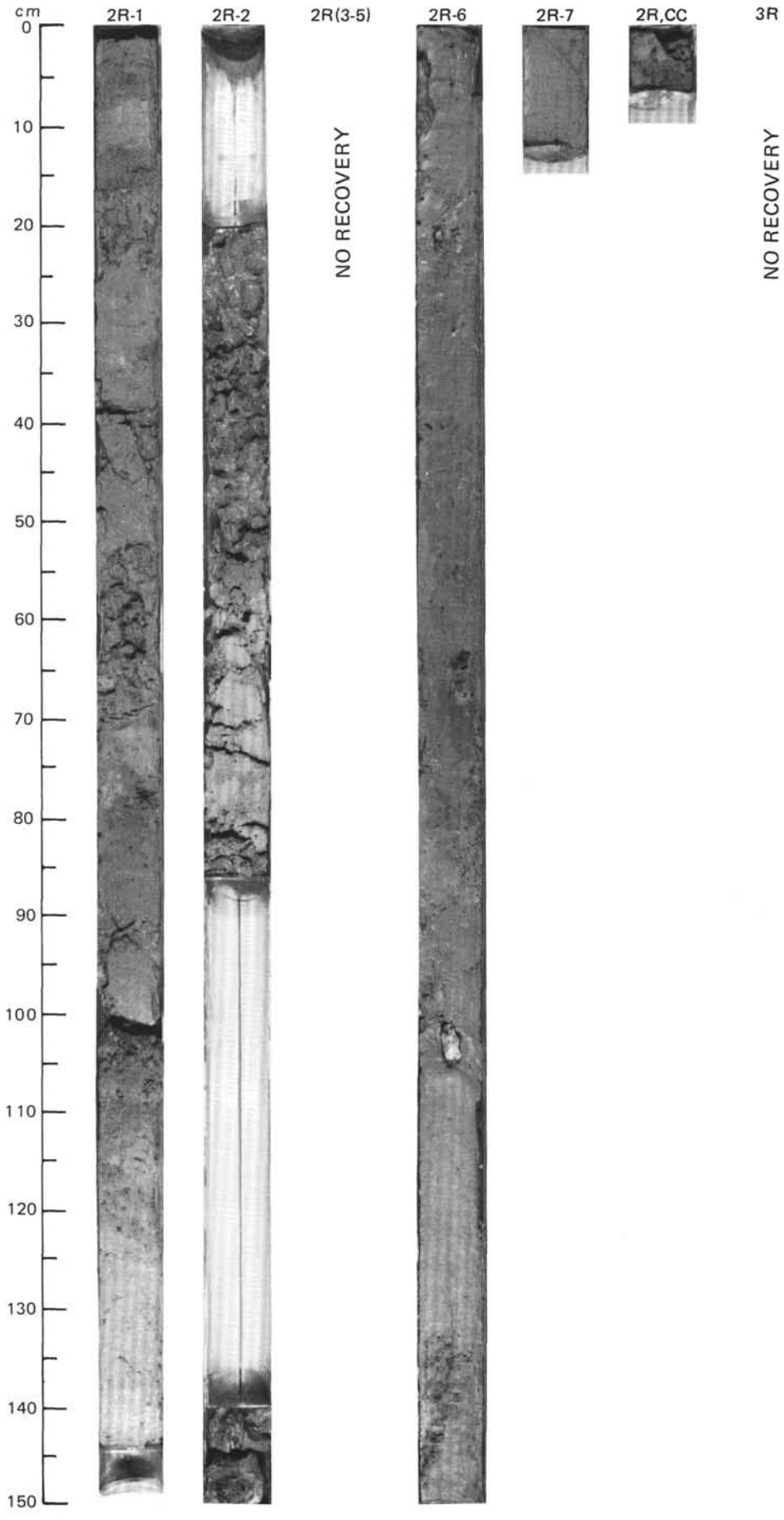
cm
0
10
20
30
40
50
60
70
80
90
100
110
120
130
140
150
2R-1
2R-2
2R(3-5)
NO RECOVERY
2R-6
2R-7
2R,CC
3R
NO RECOVERY

SITE 647 HOLE A CORE 4 R CORED INTERVAL 3887.1-3896.6 mbsl; 28.6-38.1 mbsf

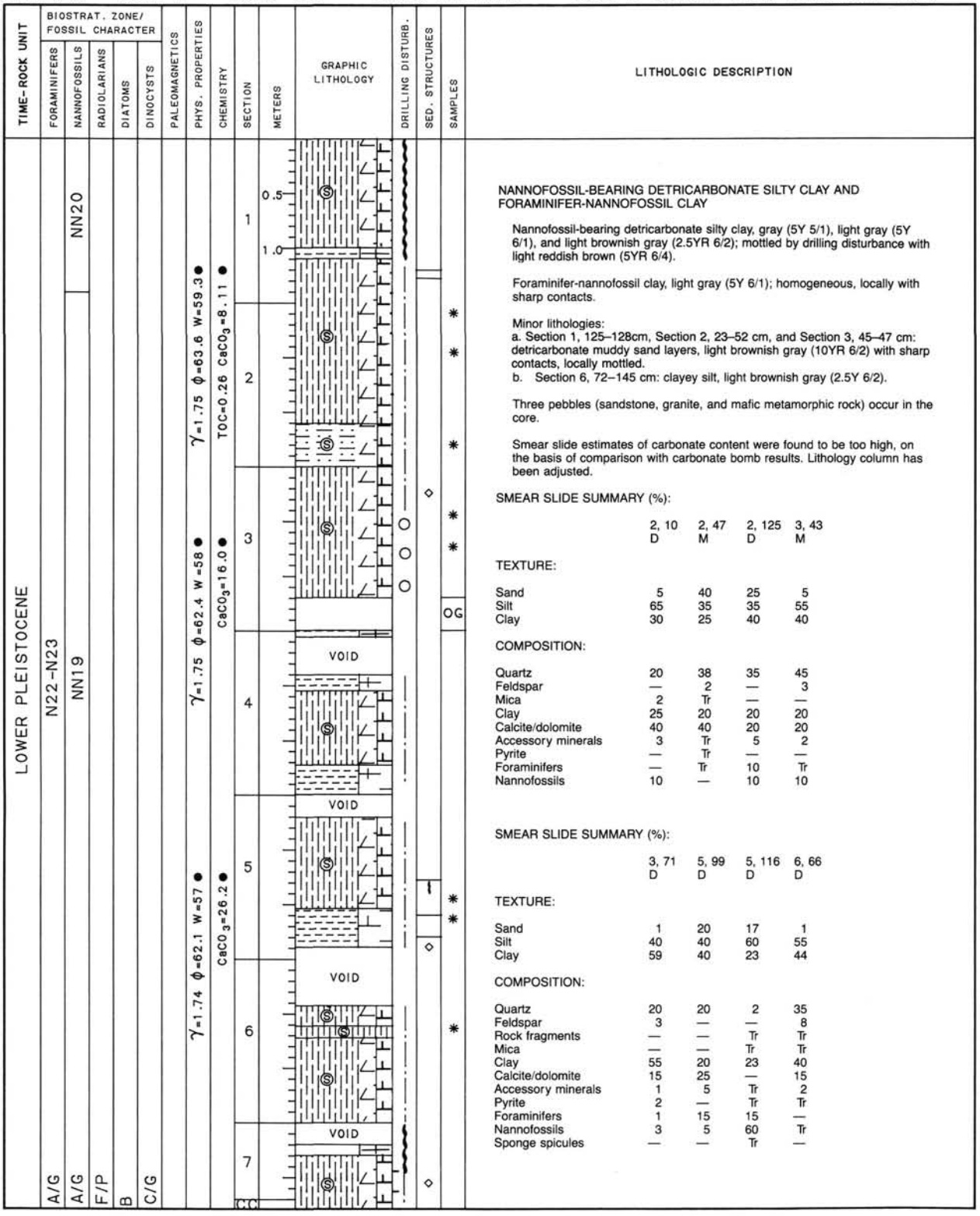

NANNOFOSSIL-BEARING DETRICARBONATE SILTY CLAY AND FORAMINIFER-NANNOFOSSIL CLAY

Nannofossil-bearing detricarbonate silty clay, gray (5Y 5/1), light gray (5Y 6/1), and light brownish gray (2.5YR 6/2); mottled by drilling disturbance with light reddish brown (5YR 6/4).

Foraminifer-nannofossil clay, light gray (5Y 6/1); homogeneous, locally with sharp contacts.

Minor lithologies:
a. Section 1, 125–128cm, Section 2, 23–52 cm, and Section 3, 45–47 cm: detricarbonate muddy sand layers, light brownish gray (10YR 6/2) with sharp contacts, locally mottled.
b. Section 6, 72–145 cm: clayey silt, light brownish gray (2.5Y 6/2).

Three pebbles (sandstone, granite, and mafic metamorphic rock) occur in the core.

Smear slide estimates of carbonate content were found to be too high, on the basis of comparison with carbonate bomb results. Lithology column has been adjusted.

SMEAR SLIDE SUMMARY (%):

	2, 10 D	2, 47 M	2, 125 D	3, 43 M
TEXTURE:				
Sand	5	40	25	5
Silt	65	35	35	55
Clay	30	25	40	40
COMPOSITION:				
Quartz	20	38	35	45
Feldspar	—	2	—	3
Mica	2	Tr	—	—
Clay	25	20	20	20
Calcite/dolomite	40	40	20	20
Accessory minerals	3	Tr	5	2
Pyrite	—	Tr	—	—
Foraminifers	—	Tr	10	Tr
Nannofossils	10	—	10	10

SMEAR SLIDE SUMMARY (%):

	3, 71 D	5, 99 D	5, 116 D	6, 66 D
TEXTURE:				
Sand	1	20	17	1
Silt	40	40	60	55
Clay	59	40	23	44
COMPOSITION:				
Quartz	20	20	2	35
Feldspar	3	—	—	8
Rock fragments	—	—	Tr	Tr
Mica	—	—	Tr	Tr
Clay	55	20	23	40
Calcite/dolomite	15	25	—	15
Accessory minerals	1	5	Tr	2
Pyrite	2	—	Tr	Tr
Foraminifers	1	15	15	—
Nannofossils	3	5	60	Tr
Sponge spicules	—	—	Tr	—

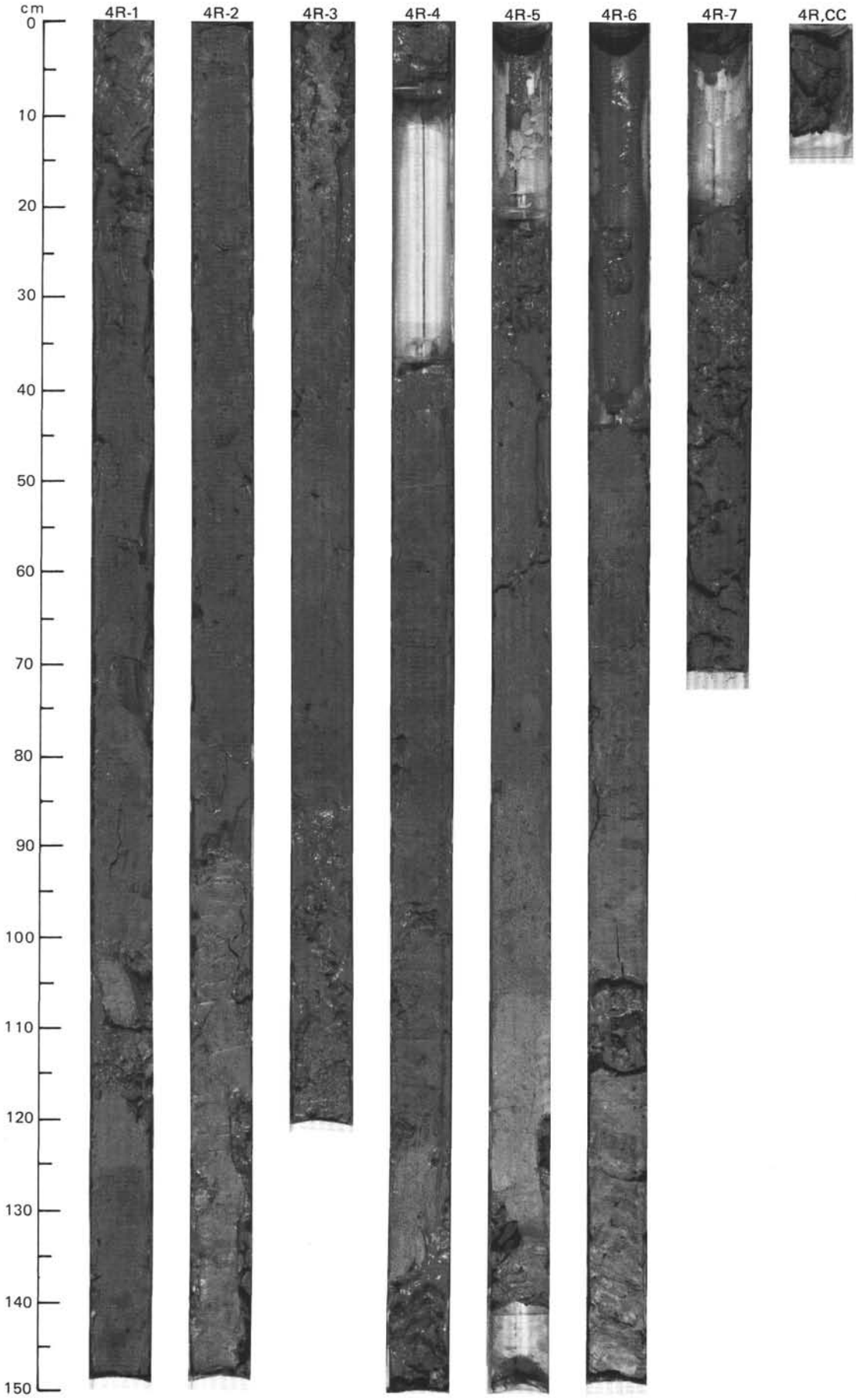
cm
0
10
20
30
40
50
60
70
80
90
100
110
120
130
140
150
4R-1
4R-2
4R-3
4R-4
4R-5
4R-6
4R-7
4R,CC

SITE 647 HOLE A CORE 5 R CORED INTERVAL 3896.6-3097.1 mbsl; 38.1-48.6 mbsf

TIME-ROCK UNIT	BIOSTRAT. ZONE/ FOSSIL CHARACTER: FORAMINIFERS	NANNOFOSSILS	RADIOLARIANS	DIATOMS	DINOCYSTS	PALEOMAGNETICS	PHYS. PROPERTIES	CHEMISTRY	SECTION	METERS	GRAPHIC LITHOLOGY	DRILLING DISTURB.	SED. STRUCTURES	SAMPLES	LITHOLOGIC DESCRIPTION
LOWER PLEISTOCENE	A/G	A/G	B	B	F/G				1				◇	***	DETRICARBONATE NANNOFOSSIL-BEARING CLAYEY SILT, NANNOFOSSIL SILT, AND CALCAREOUS SILTY MUD
	N22-N23	NN19													

Detricarbonate nannofossil-bearing clayey silt, gray (5Y 5/1), nannofossil silt, light gray (5Y 6/1) and detricarbonate silty mud, brown (7.5YR 5/2) occurring in "mud balls." Sediments are very disturbed. One quartzite pebble was observed.

SMEAR SLIDE SUMMARY (%):

	1, 6 D	1, 20 D	1, 29 D
TEXTURE:			
Sand	Tr	5	10
Silt	60	35	50
Clay	40	60	40
COMPOSITION:			
Quartz	34	15	15
Mica	Tr	—	Tr
Clay	30	30	34
Calcite/dolomite	20	15	50
Accessory minerals	Tr	Tr	1
Pyrite	Tr	—	—
Foraminifers	Tr	5	—
Nannofossils		5	—

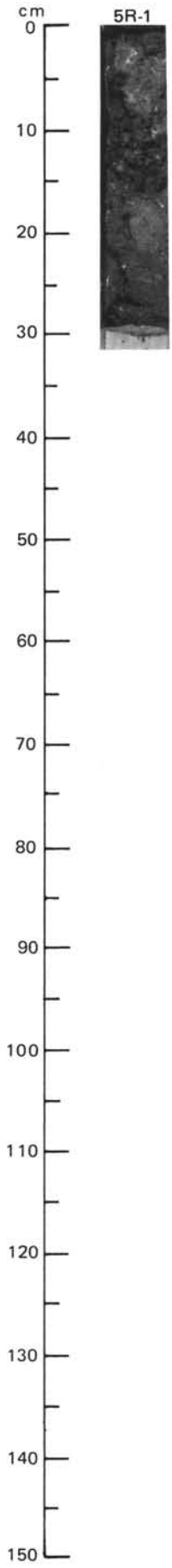
cm
0
10
20
30
40
50
60
70
80
90
100
110
120
130
140
150
5R-1

SITE 647 HOLE A CORE 6 R CORED INTERVAL 3907.1-3916.8 mbsl; 48.6-58.3 mbsf

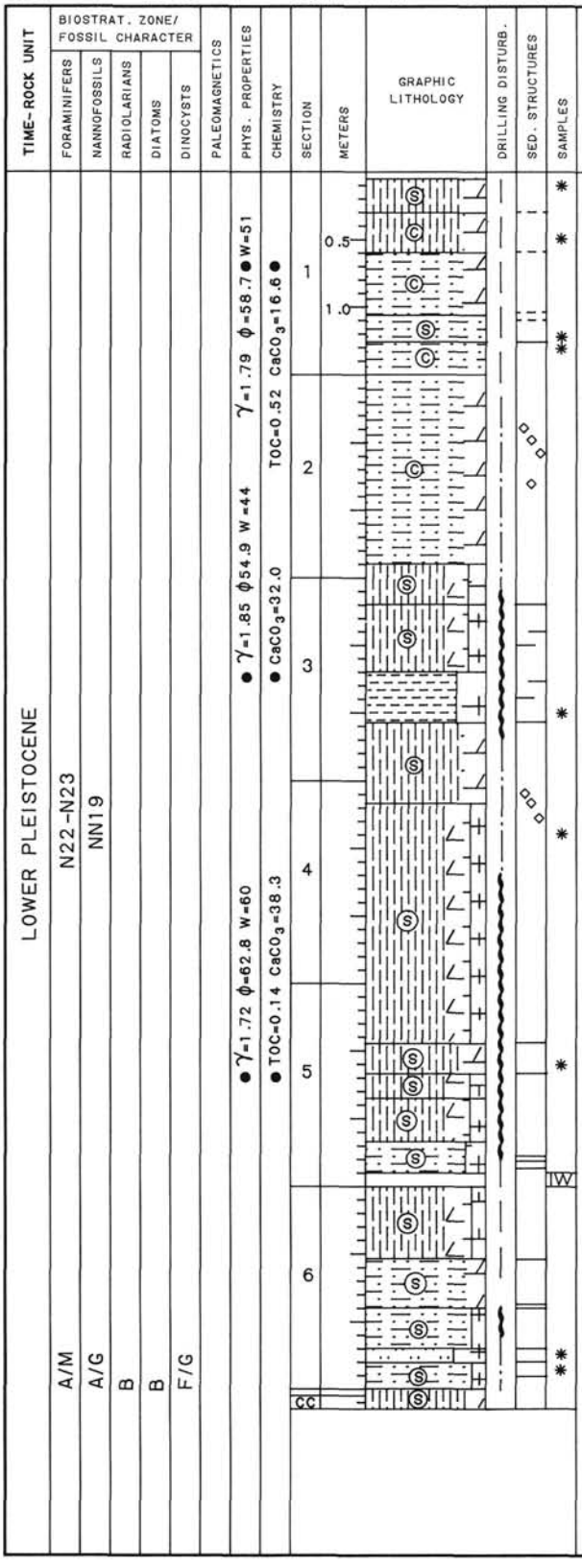

LITHOLOGIC DESCRIPTION

DETRICARBONATE CLAYEY MUD, DETRICARBONATE CLAYEY SILT, FORAMINIFER-NANNOFOSSILBEARING DETRICARBONATE CLAYEY SILT, AND FORAMINIFER-NANNOFOSSIL-BEARING DETRICARBONATE SILTY MUD

Detricarbonate clayey mud and detricarbonate clayey silt, gray (5Y 5/1) and greenish gray (5GY 5/1); foraminifer-nannofossil-bearing detricarbonate clayey silt and foraminifer-nannofossil-bearing detricarbonate silty mud, gray (5Y 5/1), greenish gray (5GY 5/1), and grayish brown (10YR 5/1).

The core presents a succession of these different lithologies with rather sharp contacts. Scattered basalt pebbles (approximately 10), dark silt pockets and muddy clasts are found in detricarbonate mud and clayey silt. Indistinct layering and clean quartz and foraminifer pockets characterize the biogenic-bearing clayey silt and ooze.

Minor lithologies:
a. Section 1, 32–60 cm: detricarbonate silty clay, olive gray (5Y 4/2).
b. Section 1, 107–112 cm: silty clay, gray (5Y 5/1).
c. Section 1, 112–125 cm: silty mud, gray (5Y 5/1) and dark gray (N4) with dark silt pockets.
d. Section 6, 55–82 cm: silty mud, light brownish gray (2.5Y 6/2).
e. Section 1, 60–107 cm: clayey mud, gray (5Y 5/1).
f. Section 3, 70–80 cm: nannofossil-foraminifer clay, light brownish gray (2.5Y 6/2) to light yellowish brown (2.5Y 6/4).
g. Section 6, 121–128 cm: foraminifer-nannofossil silt, light gray (5Y 6/1).

Smear slide estimates of carbonate content were found to be too high, on the basis of comparison with carbonate-bomb results. Lithology column has been adjusted.

SMEAR SLIDE SUMMARY (%):

	1, 12 D	1, 49 D	1, 123 D	1, 128 D	3, 97 D
TEXTURE:					
Sand	2	—	15	30	20
Silt	53	45	65	15	45
Clay	45	55	20	55	35
COMPOSITION:					
Quartz	17	13	45	30	10
Feldspar	—	—	8	2	—
Mica	3	2	10	5	1
Clay	40	50	20	55	30
Calcite/dolomite	30	35	5	5	7
Pore space	—	—	5	—	—
Accessory minerals	2	—	—	3	2
Glauconite	—	—	5	—	—
Pyrite	—	—	2	—	—
Foraminifers	1	—	—	—	20
Nannofossils	7	Tr	—	Tr	30
Plant debris	—	—	Tr	—	—

SMEAR SLIDE SUMMARY (%):

	4, 41 D	5, 63 M	5, 127 M	6, 131 D	6, 127 M
TEXTURE:					
Sand	20	—	25	5	20
Silt	60	98	45	60	40
Clay	20	2	30	35	40
COMPOSITION:					
Quartz	25	20	25	30	10
Feldspar	—	—	5	2	—
Mica	—	—	5	—	—
Clay	20	—	20	20	20
Calcite/dolomite	30	75	10	23	15
Accessory minerals	1	5	5	3	Tr
Pyrite	—	—	—	2	—
Foraminifers	19	—	15	5	30
Nannofossils	5	—	15	15	25
Sponge spicules	—	—	—	—	Tr

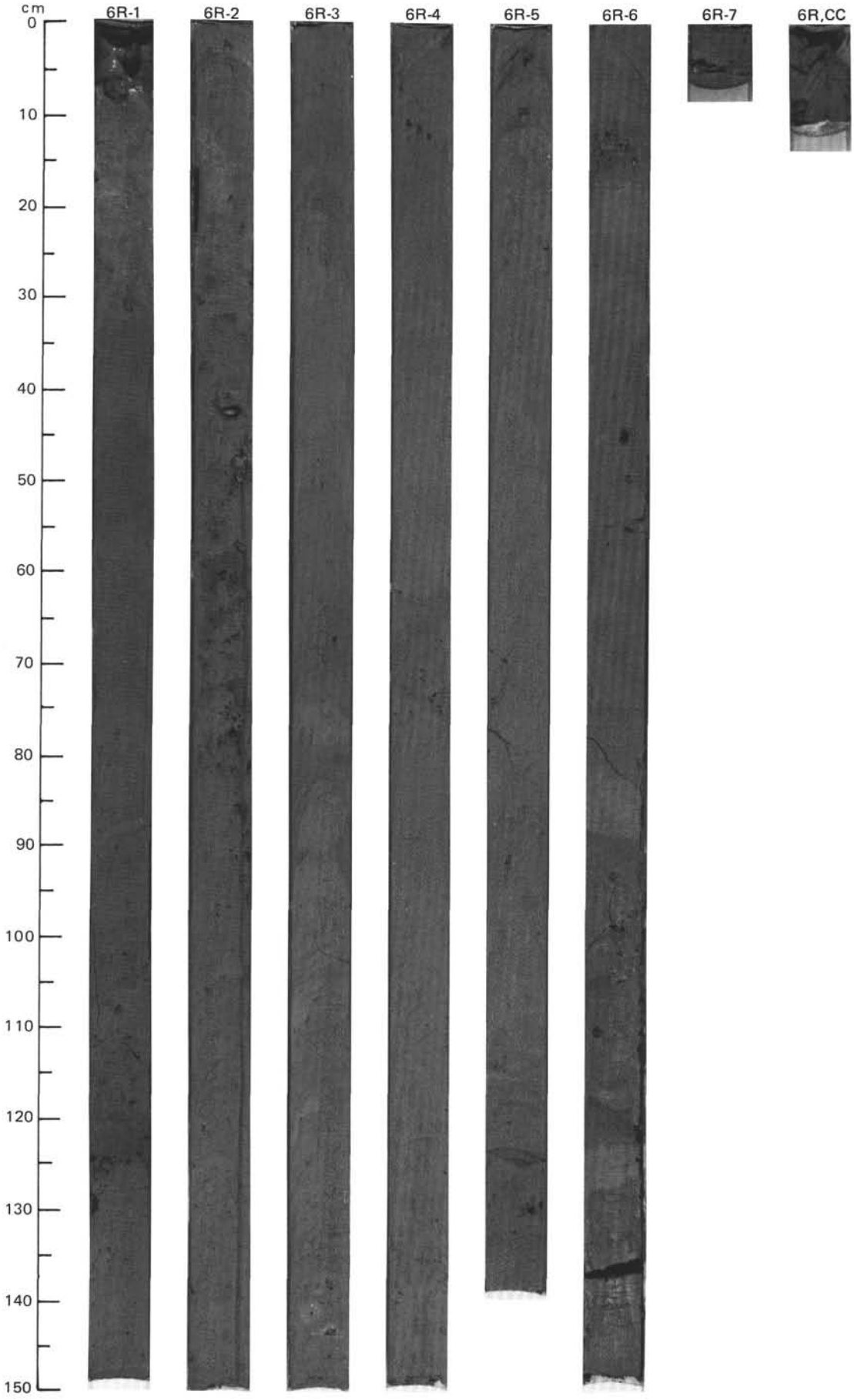
cm
0
10
20
30
40
50
60
70
80
90
100
110
120
130
140
150
6R-1
6R-2
6R-3
6R-4
6R-5
6R-6
6R-7
6R,CC

SITE 647 HOLE A CORE 7 R CORED INTERVAL 3916.8-3926.5 mbsl; 58.3-68.0 mbsf

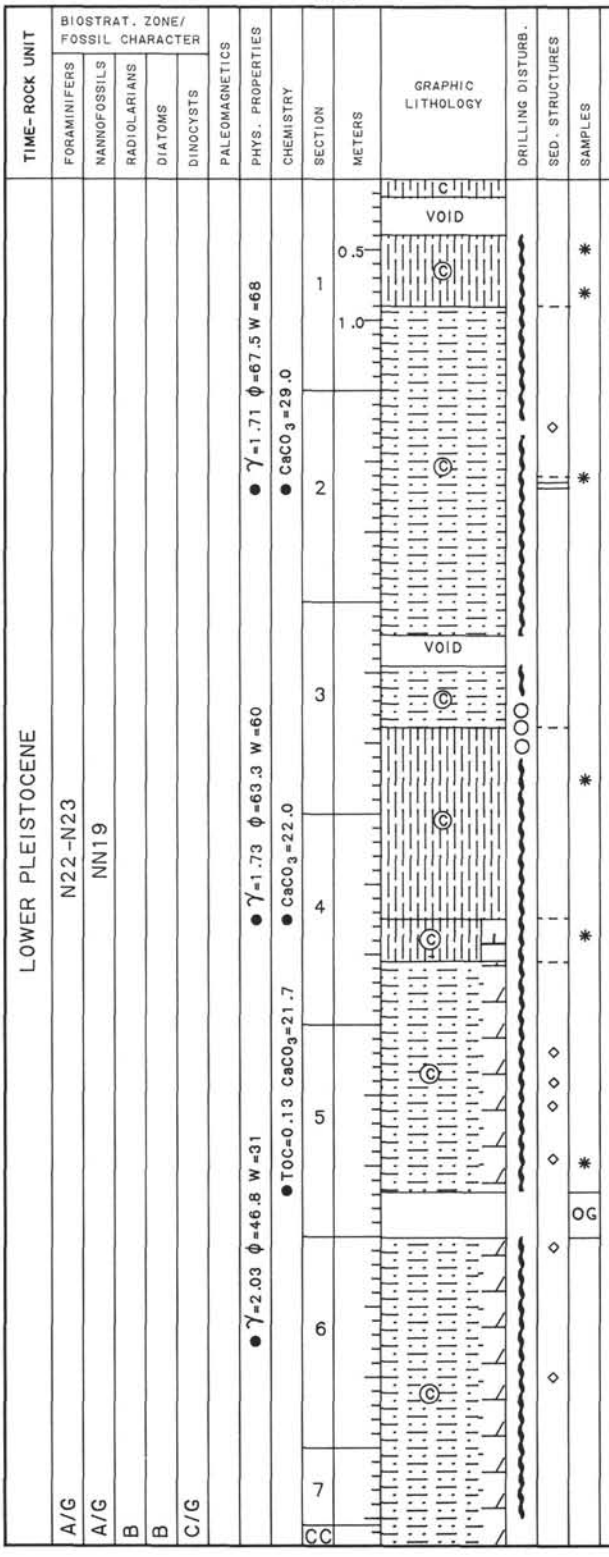

LITHOLOGIC DESCRIPTION

SILTY CLAY, DETRICARBONATE CLAYEY MUD, AND NANNOFOSSIL-FORAMINIFER-BEARING SILTY CLAY

Silty clay, greenish gray (5GY 5/1) to gray (5Y 5/1), interbedded with clayey mud; mottled by drilling disturbance, blebs and smears of sulfide, and scattered granules and pebbles.

Detricarbonate clayey mud greenish gray (5GY 5/1) to gray (5Y 5/1), mottled with smears of sulfide and a few pyritic burrows. Scattered granules and pebbles. In the lower part are 3-mm pockets of very fine sand.

Nannofossil-foraminifer-bearing silty clay, greenish gray (5Y 5/1), mottled, with pocket (4 cm in diameter) of well-sorted detrital calcareous silt.

Minor lithologies:
a. Section 2, 57–63 cm: nannofossil-foraminifer silty clay, gray (N5) with greenish sand grains.
b. Section 2, 66–70 cm: well-sorted detricarbonate silt, gray (5GY 6/1), interbedded with clayey mud and silty clay.

SMEAR SLIDE SUMMARY (%):

	1, 51 D	1, 127 D	2, 61 M	3, 128 D	4, 87 D	5, 98 D
TEXTURE:						
Sand	8	15	15	2	20	20
Silt	30	35	25	30	25	30
Clay	62	50	60	58	55	50
COMPOSITION:						
Quartz	30	40	15	25	30	30
Feldspar	1	2	Tr	Tr	Tr	2
Mica	Tr	Tr	Tr	Tr	Tr	Tr
Clay	53	45	53	56	48	41
Calcite/dolomite	10	10	2	5	2	25
Accessory minerals	Tr	Tr	Tr	Tr	Tr	Tr
Foraminifers	5	3	20	1	15	
Nannofossils	2	Tr	10	3	5	

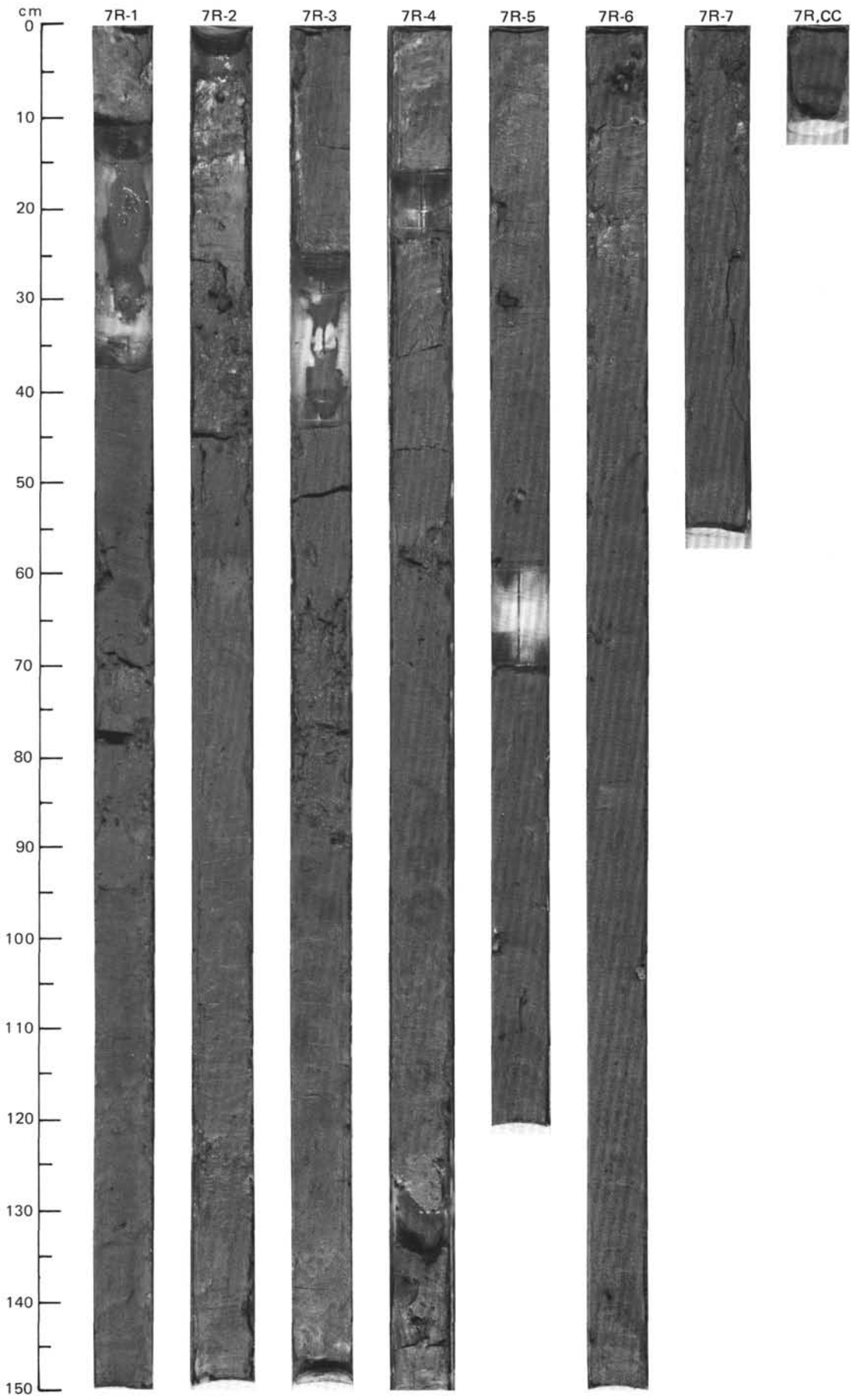
cm
0
10
20
30
40
50
60
70
80
90
100
110
120
130
140
150
7R-1
7R-2
7R-3
7R-4
7R-5
7R-6
7R-7
7R,CC

SITE 647 HOLE A CORE 8 R CORED INTERVAL 3926.5-3936.1 mbsl; 68.0-77.6 mbsf

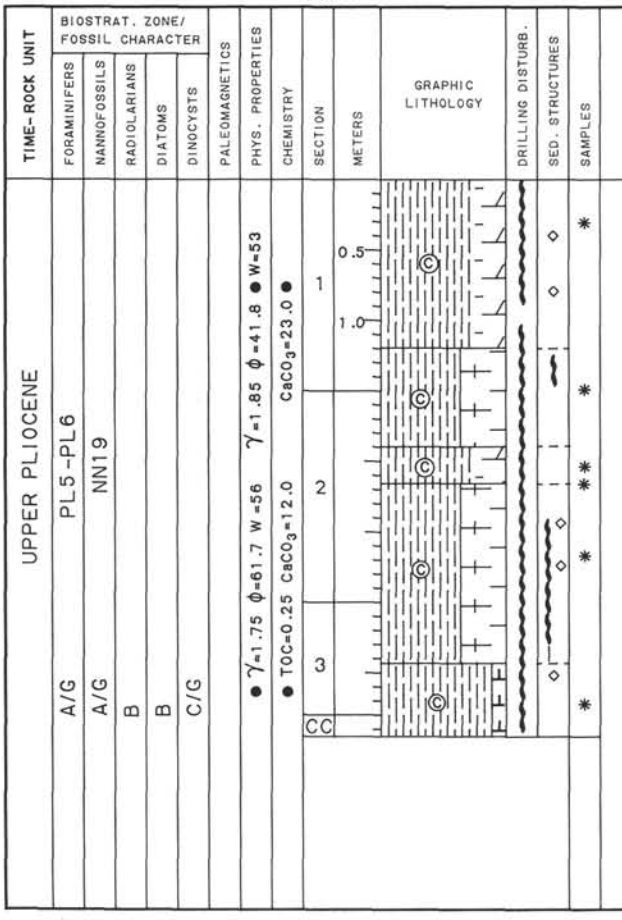

LITHOLOGIC DESCRIPTION

FORAMINIFER-NANNOFOSSIL SILTY CLAY, DETRICARBONATE CLAYEY MUD, DETRICARBONATE SILTY CLAY, AND NANNOFOSSIL-BEARING SILTY CLAY

Foraminifer-nannofossil silty clay, gray to light gray (5Y 6/1), slightly bioturbated, scattered sulfide smears, locally containing scattered granules and pebbles.

Detricarbonate clayey mud, gray (5Y 5/1) with scattered granules and fine pebbles, one piece of coal. Black sulfide smears.

Detricarbonate silty clay, greenish gray (5GY 5/1) with pockets and thin laminae of detricarbonate silt just above a sharp base. Silt is light brownish gray (10YR 6/2).

Nannofossil-bearing silty clay, gray (5Y 5/1), with scattered granules (mud clasts) and a 3-cm plutonic pebble.

SMEAR SLIDE SUMMARY (%):

	1, 30 D	1, 143 D	2, 54 D	2, 66 M	2, 112 D	3, 72 D
TEXTURE:						
Sand	20	10	—	—	10	5
Silt	35	35	35	95	40	25
Clay	45	55	65	5	50	70
COMPOSITION:						
Quartz	40	10	15	45	15	20
Feldspar	5	2	Tr	1	Tr	2
Mica	Tr	—	Tr	Tr	Tr	—
Clay	34	50	62	3	43	66
Volcanic glass	—	—	—	—	—	Tr
Calcite/dolomite	20	3	20	50	2	—
Accessory minerals	Tr	Tr	Tr	1	Tr	Tr
Foraminifers	Tr	10	Tr	—	10	—
Nannofossils	1	25	3	—	30	10

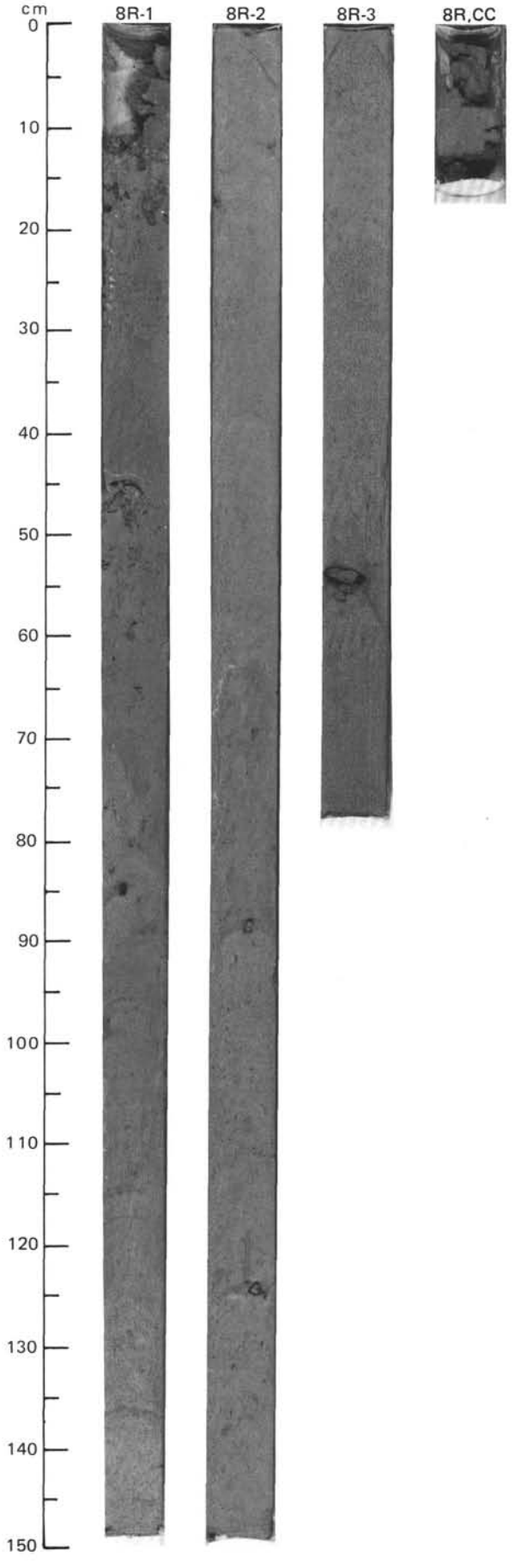
cm
8R-1
8R-2
8R-3
8R,CC
0
10
20
30
40
50
60
70
80
90
100
110
120
130
140
150

SITE 647 HOLE A CORE 9 R CORED INTERVAL 3936.1-3945.8 mbsl; 77.6-87.3 mbsf

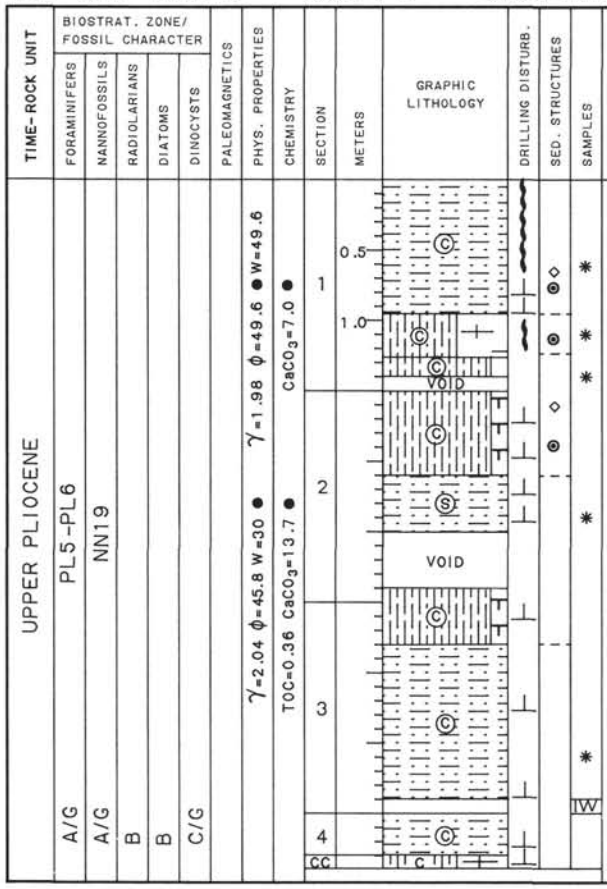

LITHOLOGIC DESCRIPTION

CLAYEY MUD, FORAMINIFER-BEARING SILTY CLAY, NANNOFOSSIL-FORAMINIFER SILTY CLAY, AND SILTY MUD

Clayey mud, dark gray to gray (5Y 4/1–5Y 5/1) with sulfide smears, pockets of foraminifers and few pebbles.

Foraminifer-bearing silty clay and nannofossil-foraminifer silty clay, greenish gray (5GY 5/1); homogeneous to slightly mottled.

Nannofossil-bearing detricarbonate silty clay, greenish gray to gray (5GY 5/1–5Y 5/1); color banded, some pyrite-cemented burrows.

Silty mud, greenish gray to gray (5GY 5/1–5Y 5/1); smears of sulfide, color banded and mottled.

SMEAR SLIDE SUMMARY (%):

	1, 60 D	1, 110 D	1, 135 D	2, 51 D	2, 98 D	3, 110 M
TEXTURE:						
Sand	15	30	10	5	10	85
Silt	30	20	20	45	50	15
Clay	55	50	70	50	40	—
COMPOSITION:						
Quartz	45	15	10	20	55	80
Feldspar	5	—	Tr	Tr	5	15
Mica	Tr	—	—	—	—	—
Clay	47	45	69	45	34	—
Volcanic glass	Tr	—	—	—	—	—
Calcite/dolomite	1	Tr	10	20	5	2
Accessory minerals	2	Tr	Tr	Tr	1	2
Foraminifers	—	30	10	5	—	1
Nannofossils	Tr	10	1	10	—	—

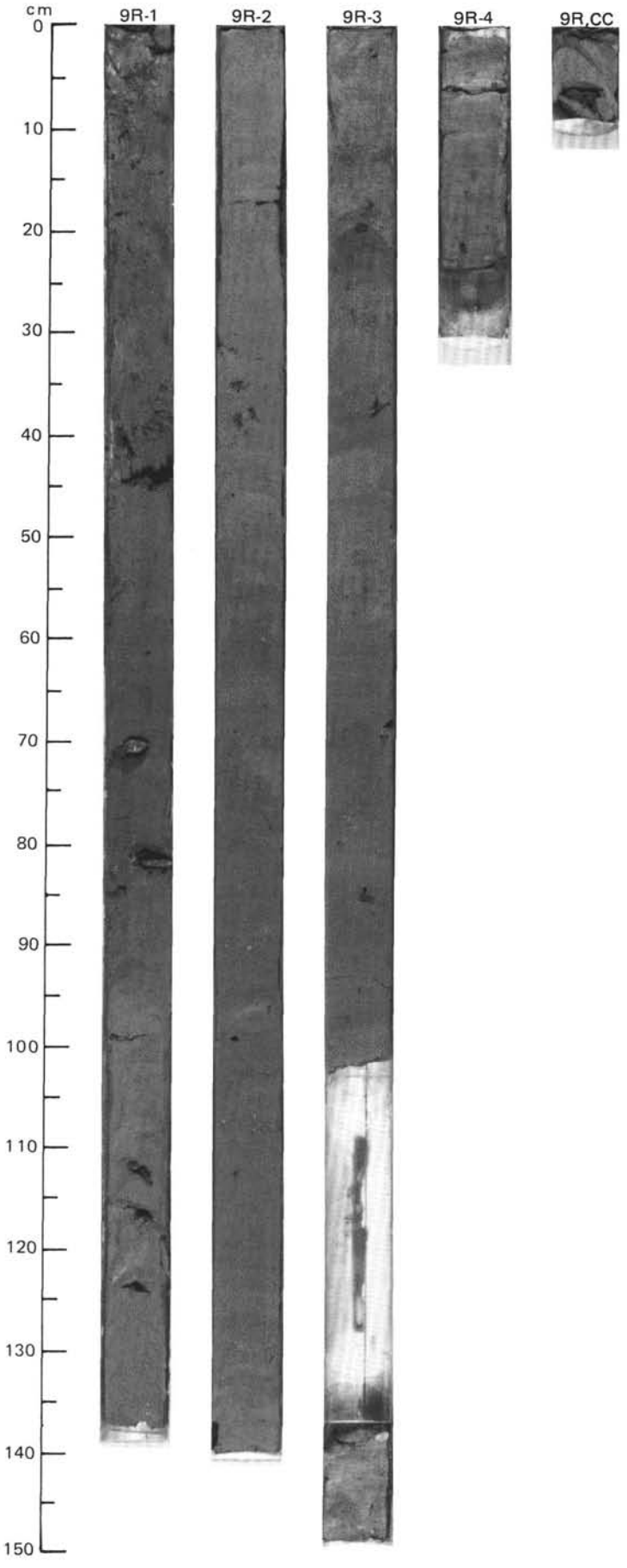
cm
0
10
20
30
40
50
60
70
80
90
100
110
120
130
140
150
9R-1
9R-2
9R-3
9R-4
9R,CC

SITE 647 HOLE A CORE 10 R CORED INTERVAL 3945.8-3955.5 mbsl; 87.3-97.0 mbsf

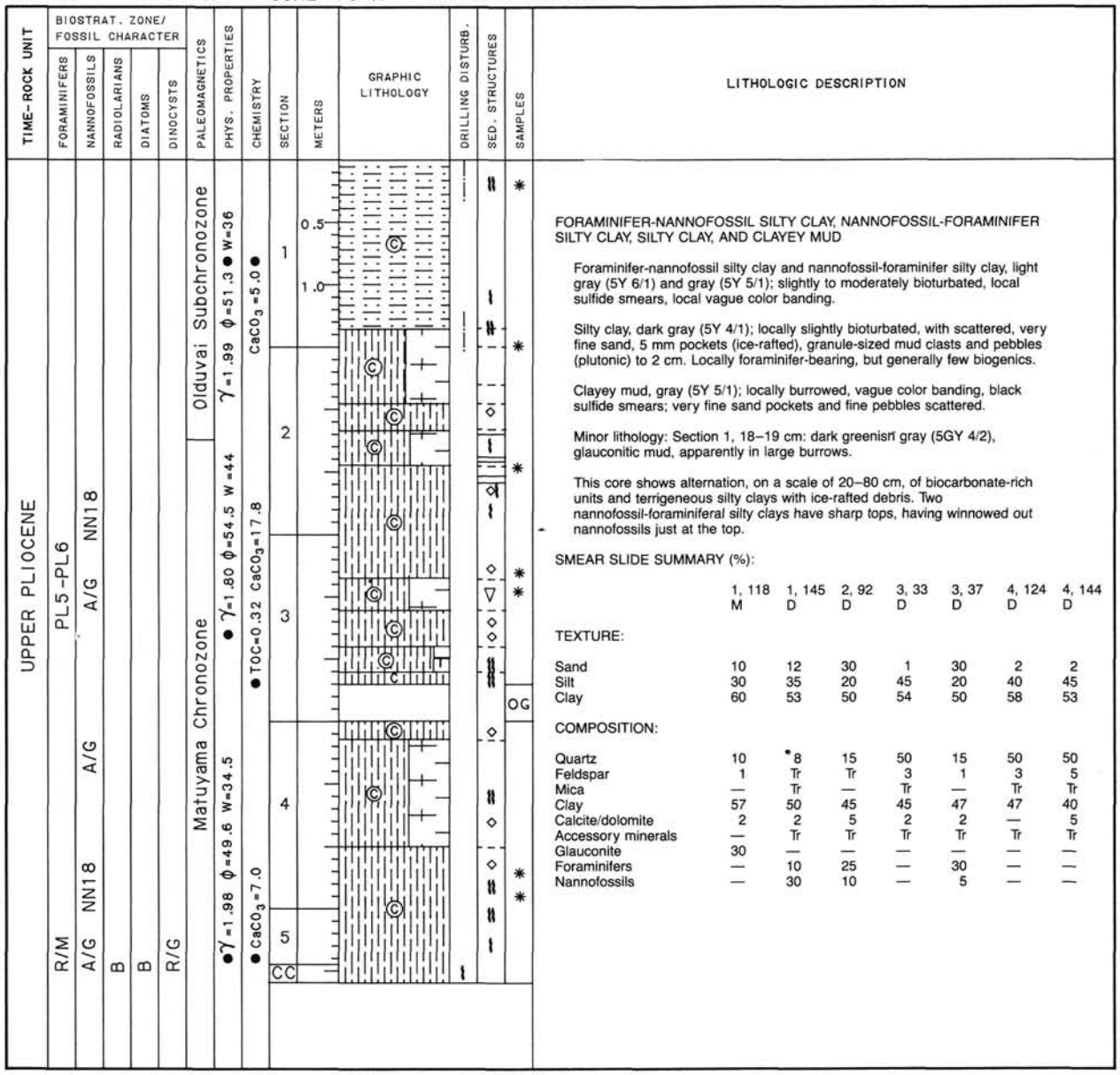

FORAMINIFER-NANNOFOSSIL SILTY CLAY, NANNOFOSSIL-FORAMINIFER SILTY CLAY, SILTY CLAY, AND CLAYEY MUD

Foraminifer-nannofossil silty clay and nannofossil-foraminifer silty clay, light gray (5Y 6/1) and gray (5Y 5/1); slightly to moderately bioturbated, local sulfide smears, local vague color banding.

Silty clay, dark gray (5Y 4/1); locally slightly bioturbated, with scattered, very fine sand, 5 mm pockets (ice-rafted), granule-sized mud clasts and pebbles (plutonic) to 2 cm. Locally foraminifer-bearing, but generally few biogenics.

Clayey mud, gray (5Y 5/1); locally burrowed, vague color banding, black sulfide smears; very fine sand pockets and fine pebbles scattered.

Minor lithology: Section 1, 18–19 cm: dark greenish gray (5GY 4/2), glauconitic mud, apparently in large burrows.

This core shows alternation, on a scale of 20–80 cm, of biocarbonate-rich units and terrigeneous silty clays with ice-rafted debris. Two nannofossil-foraminiferal silty clays have sharp tops, having winnowed out nannofossils just at the top.

SMEAR SLIDE SUMMARY (%):

	1, 118 M	1, 145 D	2, 92 D	3, 33 D	3, 37 D	4, 124 D	4, 144 D
TEXTURE:							
Sand	10	12	30	1	30	2	2
Silt	30	35	20	45	20	40	45
Clay	60	53	50	54	50	58	53
COMPOSITION:							
Quartz	10	8	15	50	15	50	50
Feldspar	1	Tr	Tr	3	1	3	5
Mica	—	Tr	—	Tr	—	Tr	Tr
Clay	57	50	45	45	47	47	40
Calcite/dolomite	2	2	5	2	2	—	5
Accessory minerals	—	Tr	Tr	Tr	Tr	Tr	Tr
Glauconite	30	—	—	—	—	—	—
Foraminifers	—	10	25	—	30	—	—
Nannofossils	—	30	10	—	5	—	—

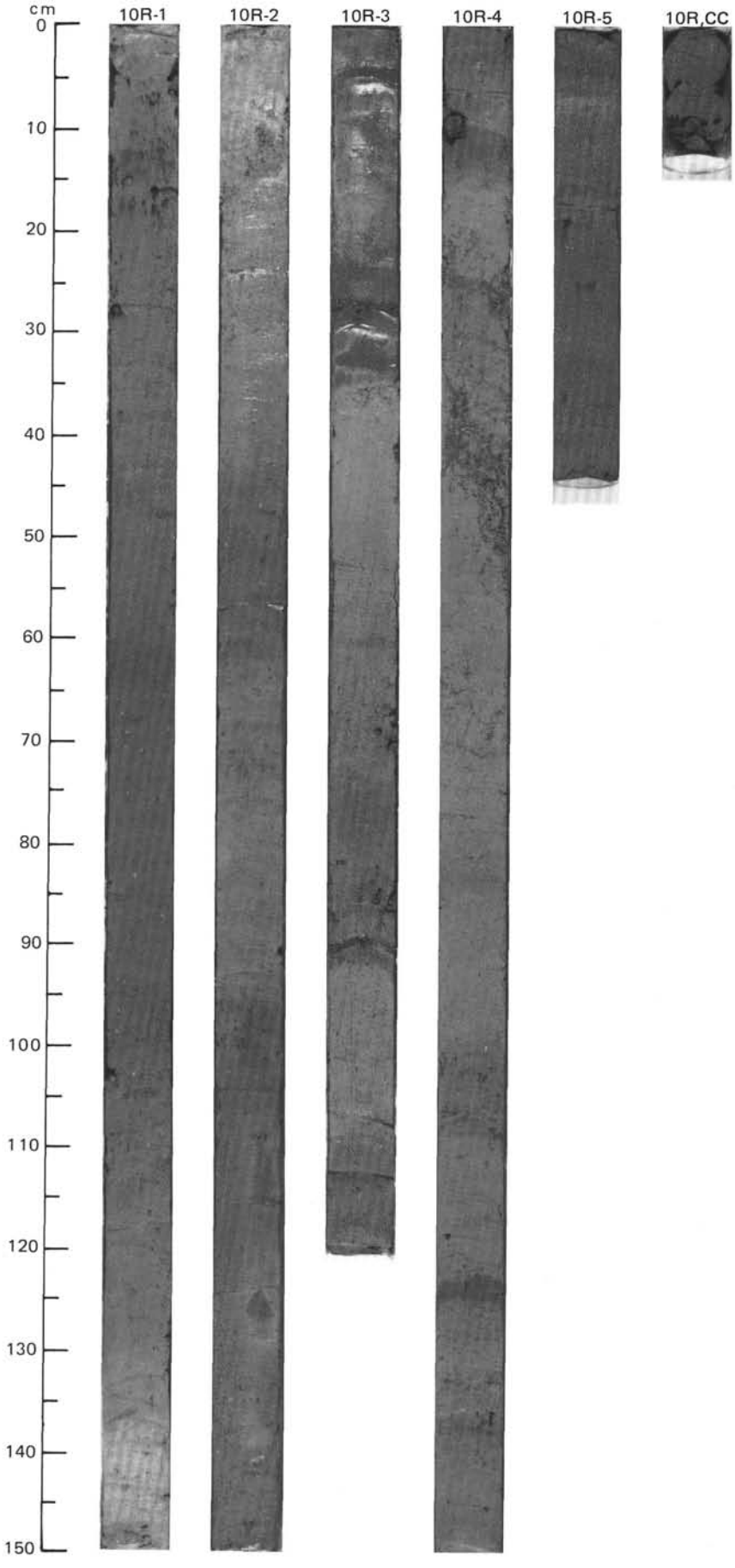
cm
0
10
20
30
40
50
60
70
80
90
100
110
120
130
140
150
10R-1
10R-2
10R-3
10R-4
10R-5
10R,CC

SITE 647 HOLE A CORE 11 R CORED INTERVAL 3955.5-3965.2 mbsl; 97.0-106.7 mbsf

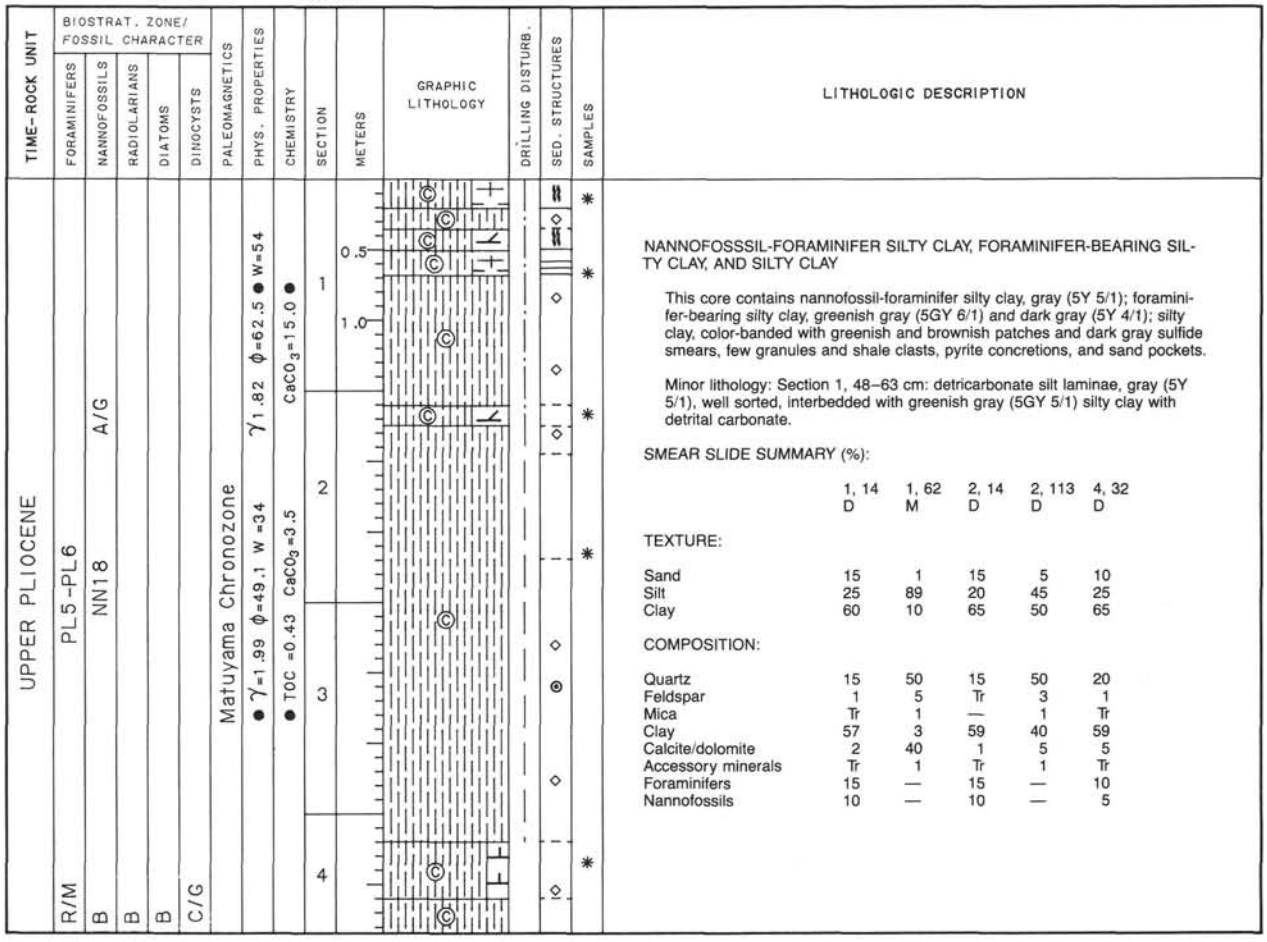

NANNOFOSSSIL-FORAMINIFER SILTY CLAY, FORAMINIFER-BEARING SILTY CLAY, AND SILTY CLAY

This core contains nannofossil-foraminifer silty clay, gray (5Y 5/1); foraminifer-bearing silty clay, greenish gray (5GY 6/1) and dark gray (5Y 4/1); silty clay, color-banded with greenish and brownish patches and dark gray sulfide smears, few granules and shale clasts, pyrite concretions, and sand pockets.

Minor lithology: Section 1, 48–63 cm: detricarbonate silt laminae, gray (5Y 5/1), well sorted, interbedded with greenish gray (5GY 5/1) silty clay with detrital carbonate.

SMEAR SLIDE SUMMARY (%):

	1, 14 D	1, 62 M	2, 14 D	2, 113 D	4, 32 D
TEXTURE:					
Sand	15	1	15	5	10
Silt	25	89	20	45	25
Clay	60	10	65	50	65
COMPOSITION:					
Quartz	15	50	15	50	20
Feldspar	1	5	Tr	3	1
Mica	Tr	1	—	1	Tr
Clay	57	3	59	40	59
Calcite/dolomite	2	40	1	5	5
Accessory minerals	Tr	1	Tr	1	Tr
Foraminifers	15	—	15	—	10
Nannofossils	10	—	10	—	5

cm
0
10
20
30
40
50
60
70
80
90
100
110
120
130
140
150
11R-1
11R-2
11R-3
11R-4

SITE 647 HOLE A CORE 12 R CORED INTERVAL 3965.2-3974.5 mbsl; 106.7-116.0 mbsf

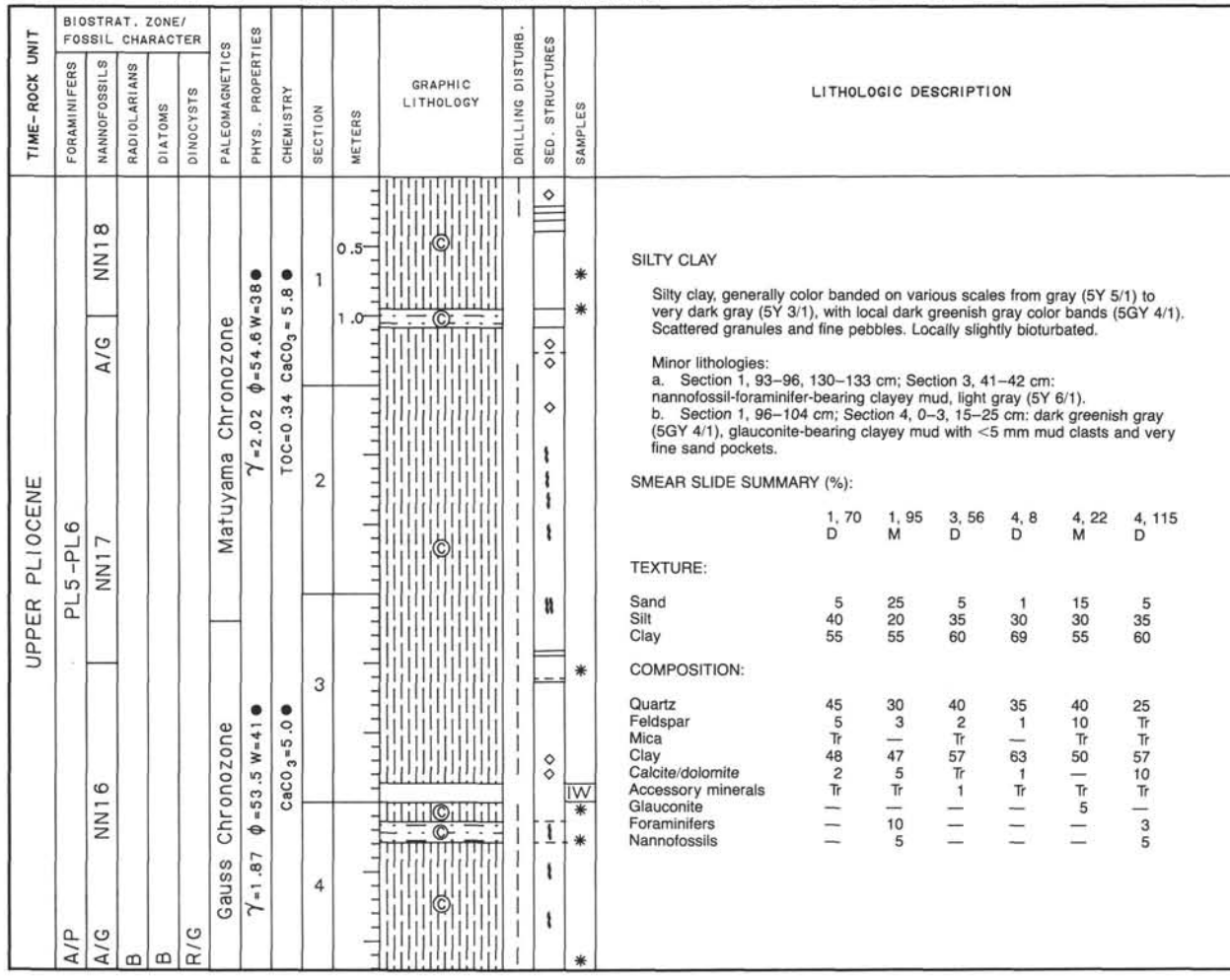

LITHOLOGIC DESCRIPTION

SILTY CLAY

Silty clay, generally color banded on various scales from gray (5Y 5/1) to very dark gray (5Y 3/1), with local dark greenish gray color bands (5GY 4/1). Scattered granules and fine pebbles. Locally slightly bioturbated.

Minor lithologies:
a. Section 1, 93–96, 130–133 cm; Section 3, 41–42 cm: nannofossil-foraminifer-bearing clayey mud, light gray (5Y 6/1).
b. *Section 1, 96–104 cm; Section 4, 0–3, 15–25 cm:* dark greenish gray (5GY 4/1), glauconite-bearing clayey mud with <5 mm mud clasts and very fine sand pockets.

SMEAR SLIDE SUMMARY (%):

	1, 70 D	1, 95 M	3, 56 D	4, 8 D	4, 22 M	4, 115 D
TEXTURE:						
Sand	5	25	5	1	15	5
Silt	40	20	35	30	30	35
Clay	55	55	60	69	55	60
COMPOSITION:						
Quartz	45	30	40	35	40	25
Feldspar	5	3	2	1	10	Tr
Mica	Tr	—	Tr	—	Tr	Tr
Clay	48	47	57	63	50	57
Calcite/dolomite	2	5	Tr	1	—	10
Accessory minerals	Tr	Tr	1	Tr	Tr	Tr
Glauconite	—	—	—	—	5	—
Foraminifers	—	10	—	—	—	3
Nannofossils	—	5	—	—	—	5

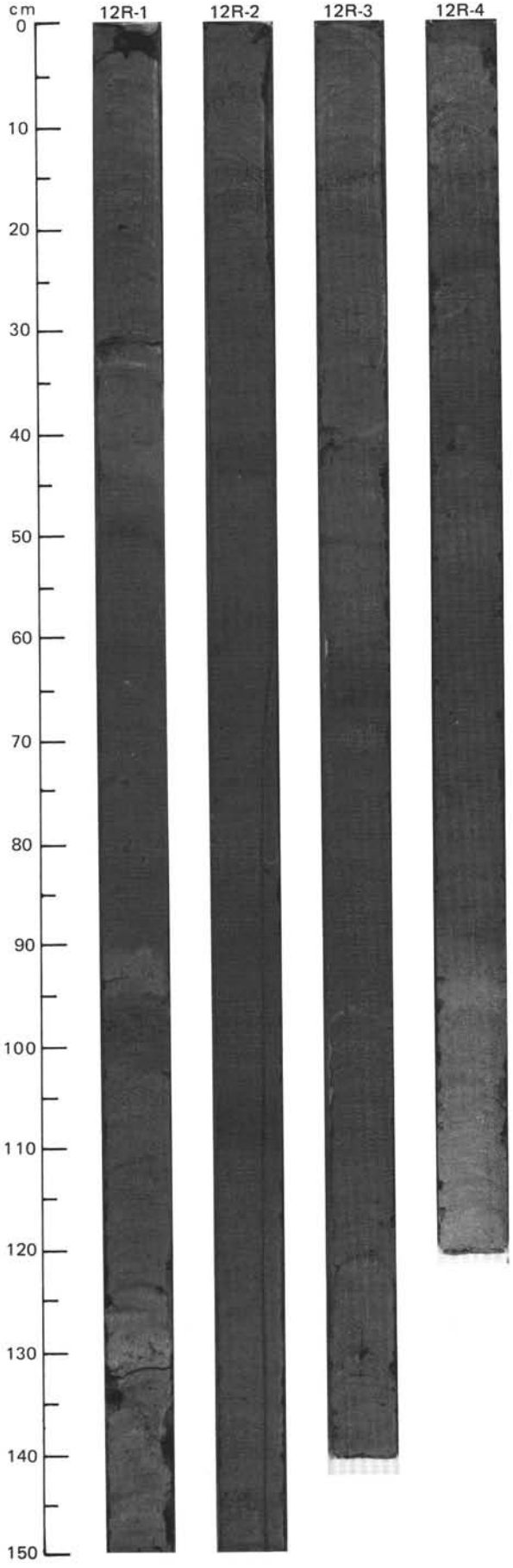
cm
12R-1
12R-2
12R-3
12R-4
0
10
20
30
40
50
60
70
80
90
100
110
120
130
140
150

SITE 647 HOLE A CORE 13 R CORED INTERVAL 3974.5-3984.2 mbsl; 116.0-125.7 mbsf

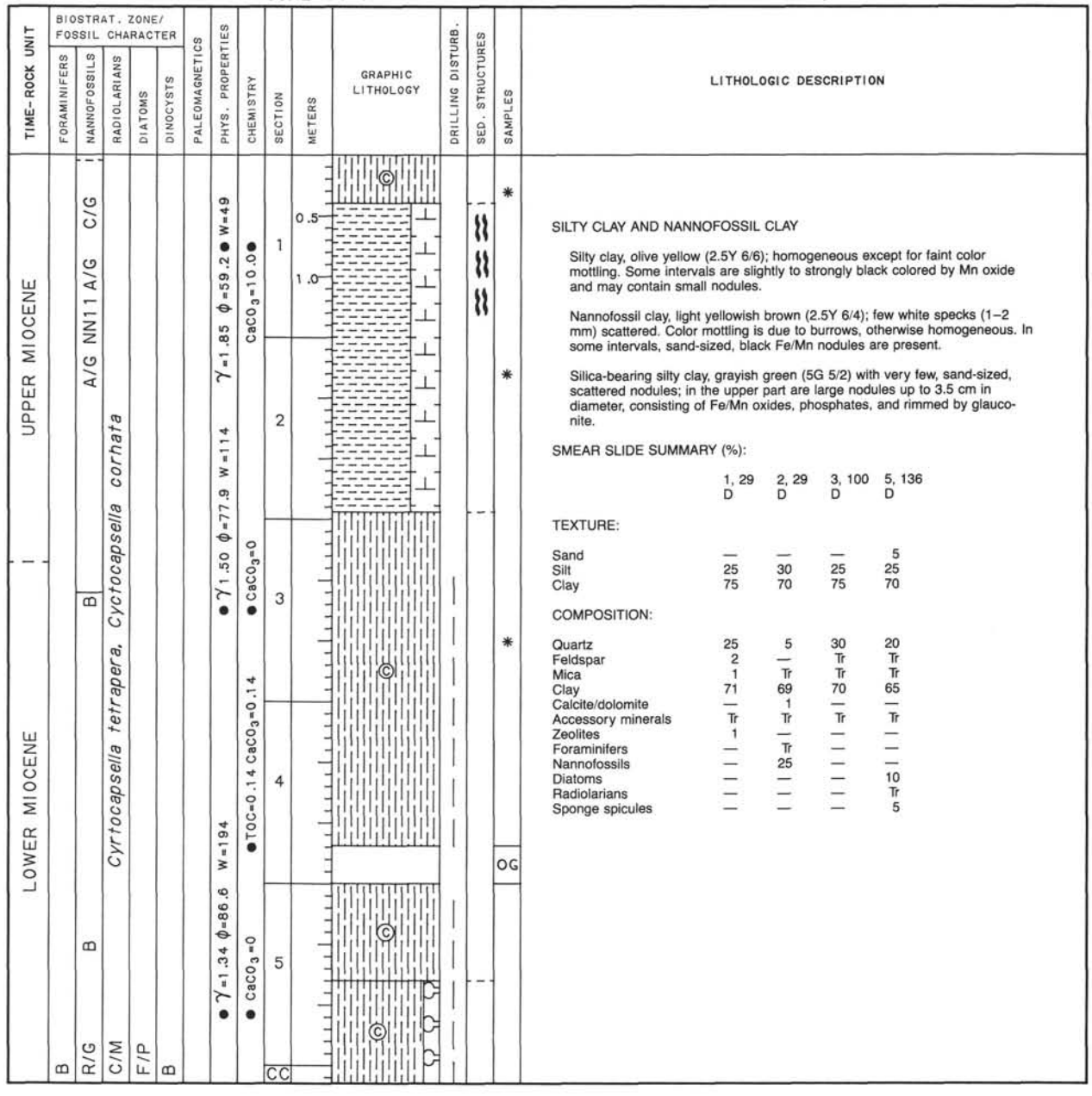

SILTY CLAY AND NANNOFOSSIL CLAY

Silty clay, olive yellow (2.5Y 6/6); homogeneous except for faint color mottling. Some intervals are slightly to strongly black colored by Mn oxide and may contain small nodules.

Nannofossil clay, light yellowish brown (2.5Y 6/4); few white specks (1–2 mm) scattered. Color mottling is due to burrows, otherwise homogeneous. In some intervals, sand-sized, black Fe/Mn nodules are present.

Silica-bearing silty clay, grayish green (5G 5/2) with very few, sand-sized, scattered nodules; in the upper part are large nodules up to 3.5 cm in diameter, consisting of Fe/Mn oxides, phosphates, and rimmed by glauconite.

SMEAR SLIDE SUMMARY (%):

	1, 29 D	2, 29 D	3, 100 D	5, 136 D
TEXTURE:				
Sand	—	—	—	5
Silt	25	30	25	25
Clay	75	70	75	70
COMPOSITION:				
Quartz	25	5	30	20
Feldspar	2	—	Tr	Tr
Mica	1	Tr	Tr	Tr
Clay	71	69	70	65
Calcite/dolomite	—	1	—	—
Accessory minerals	Tr	Tr	Tr	Tr
Zeolites	1	—	—	—
Foraminifers	—	Tr	—	—
Nannofossils	—	25	—	—
Diatoms	—	—	—	10
Radiolarians	—	—	—	Tr
Sponge spicules	—	—	—	5

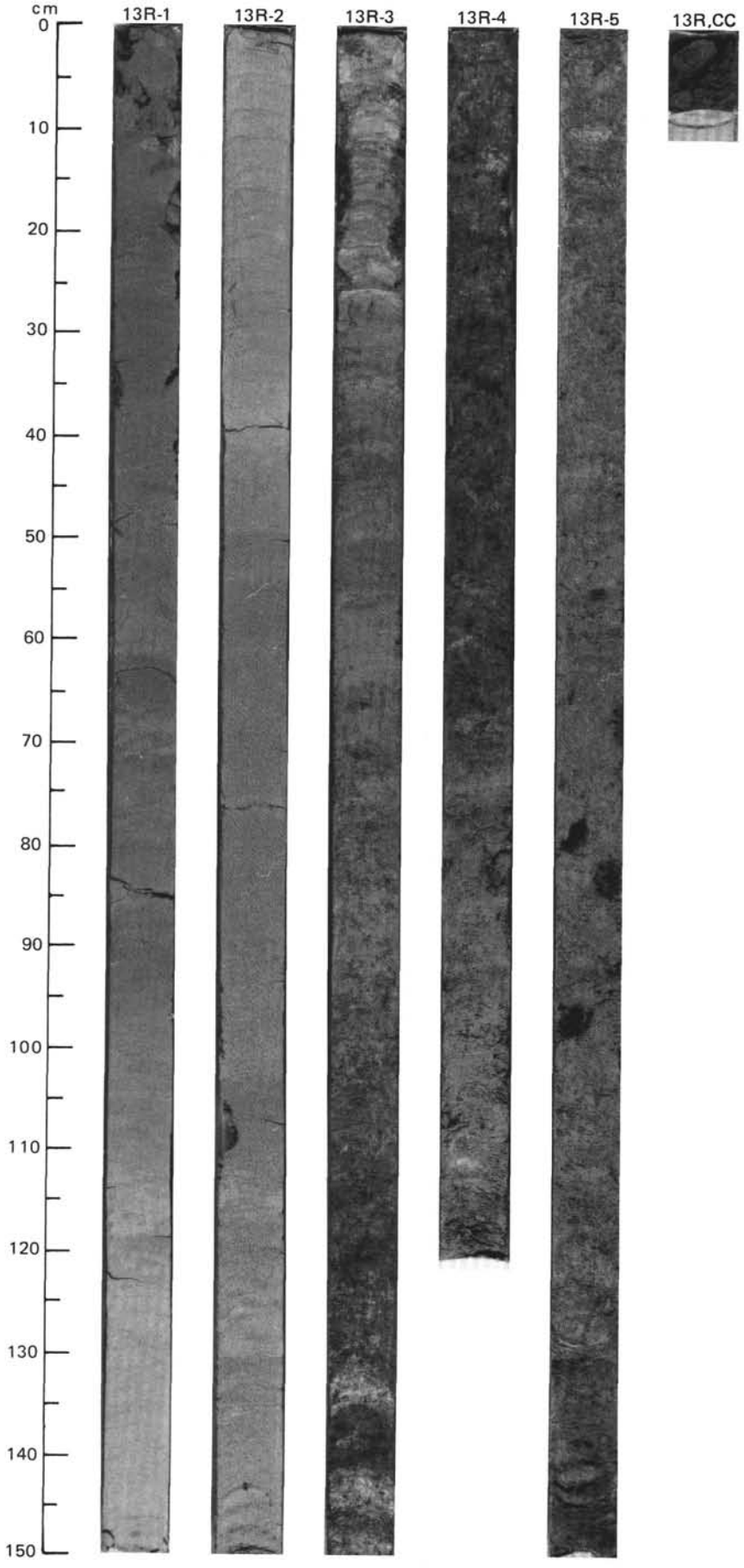
cm
0
10
20
30
40
50
60
70
80
90
100
110
120
130
140
150
13R-1
13R-2
13R-3
13R-4
13R-5
13R,CC

SITE 647 HOLE A CORE 14 R CORED INTERVAL 3984.2-3993.9 mbsl; 125.7-135.4 mbsf

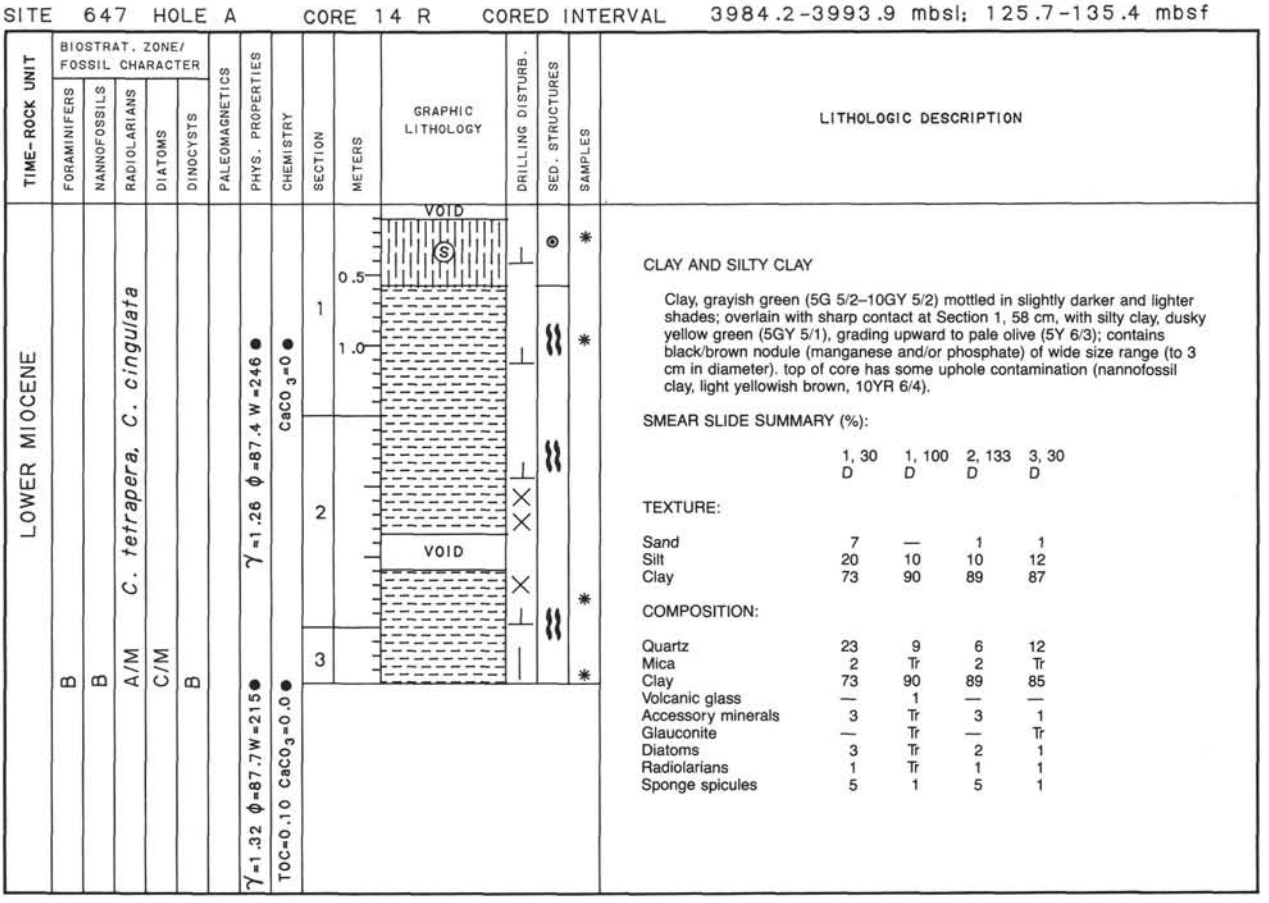

CLAY AND SILTY CLAY

Clay, grayish green (5G 5/2–10GY 5/2) mottled in slightly darker and lighter shades; overlain with sharp contact at Section 1, 58 cm, with silty clay, dusky yellow green (5GY 5/1), grading upward to pale olive (5Y 6/3); contains black/brown nodule (manganese and/or phosphate) of wide size range (to 3 cm in diameter). top of core has some uphole contamination (nannofossil clay, light yellowish brown, 10YR 6/4).

SMEAR SLIDE SUMMARY (%):

	1, 30 D	1, 100 D	2, 133 D	3, 30 D
TEXTURE:				
Sand	7	—	1	1
Silt	20	10	10	12
Clay	73	90	89	87
COMPOSITION:				
Quartz	23	9	6	12
Mica	2	Tr	2	Tr
Clay	73	90	89	85
Volcanic glass	—	1	—	—
Accessory minerals	3	Tr	3	1
Glauconite	—	Tr	—	Tr
Diatoms	3	Tr	2	1
Radiolarians	1	Tr	1	1
Sponge spicules	5	1	5	1

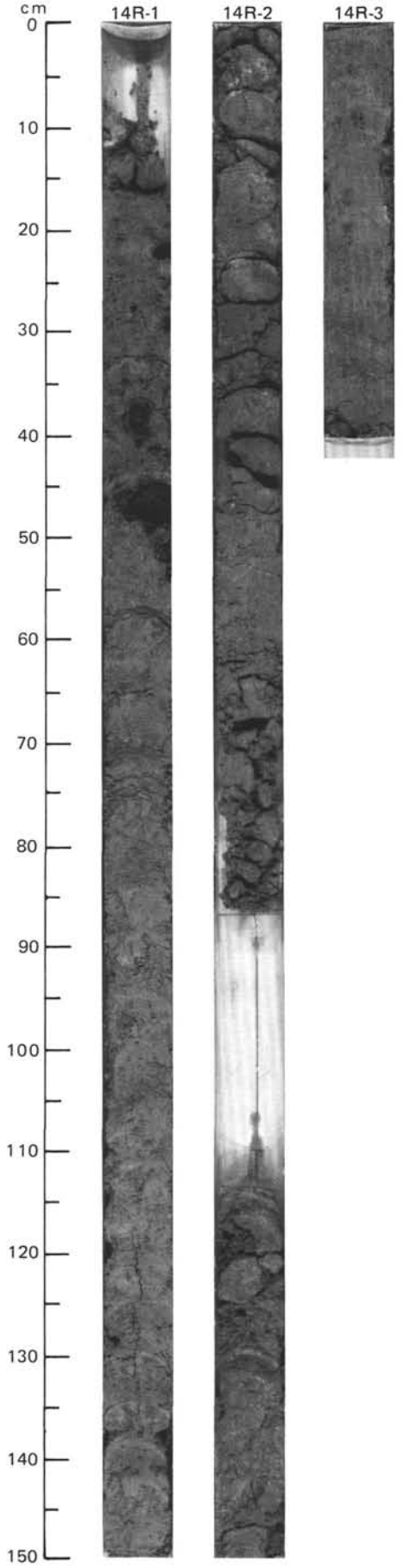
cm
14R-1
14R-2
14R-3
0
10
20
30
40
50
60
70
80
90
100
110
120
130
140
150

SITE 647 HOLE A CORE 15 R CORED INTERVAL 3993.9-4003.6 mbsl; 135.4-145.1 mbsf

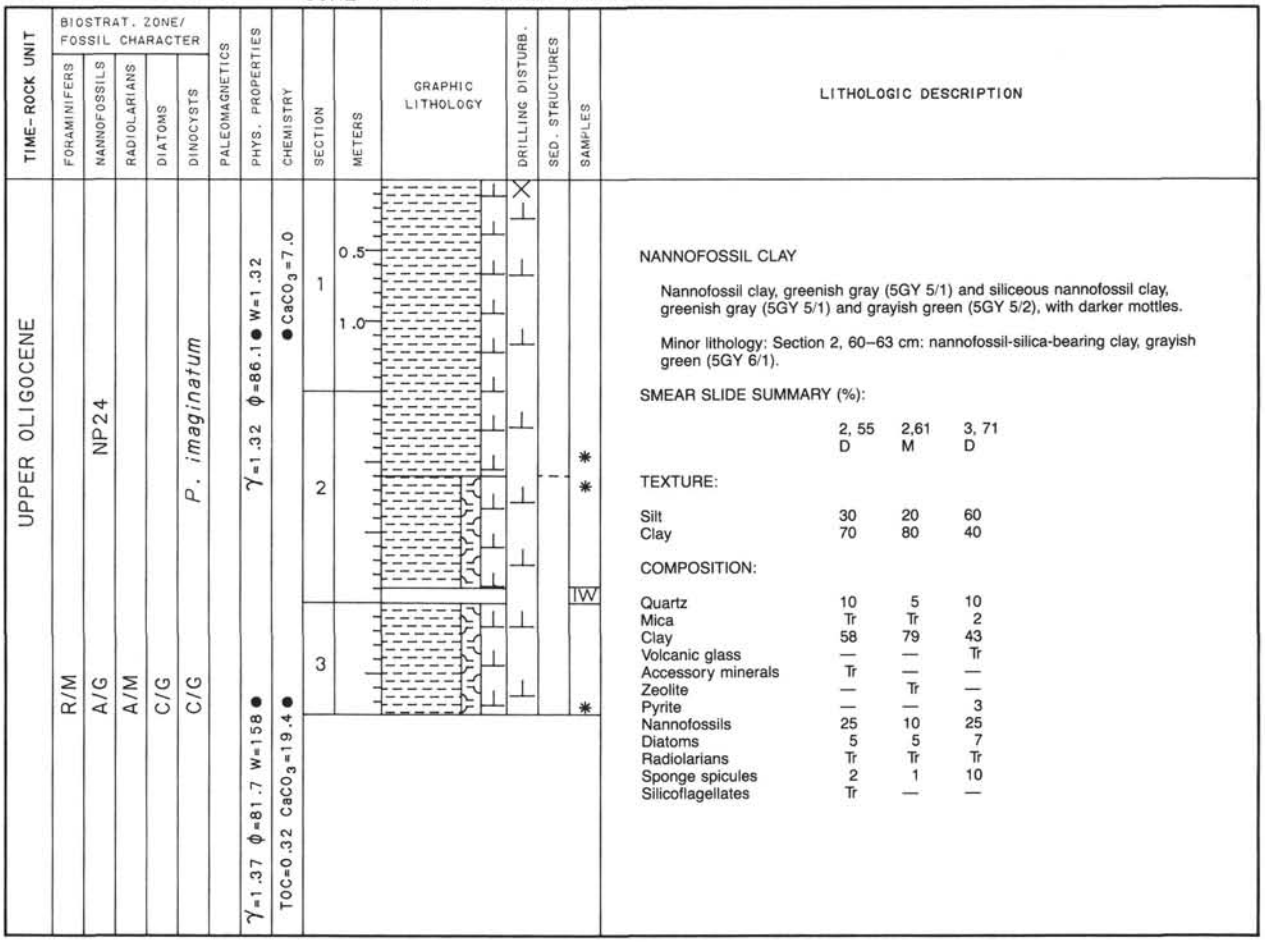

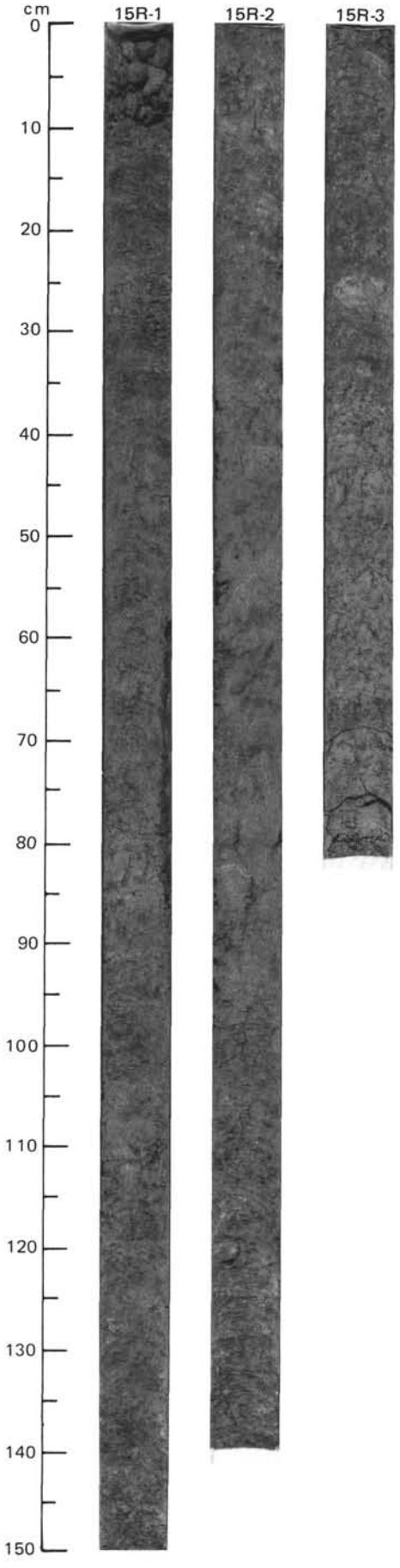
cm
15R-1
15R-2
15R-3
0
10
20
30
40
50
60
70
80
90
100
110
120
130
140
150

SITE 647 HOLE A CORE 16 R CORED INTERVAL 4003.6-4013.3 mbsl; 145.1-154.8 mbsf

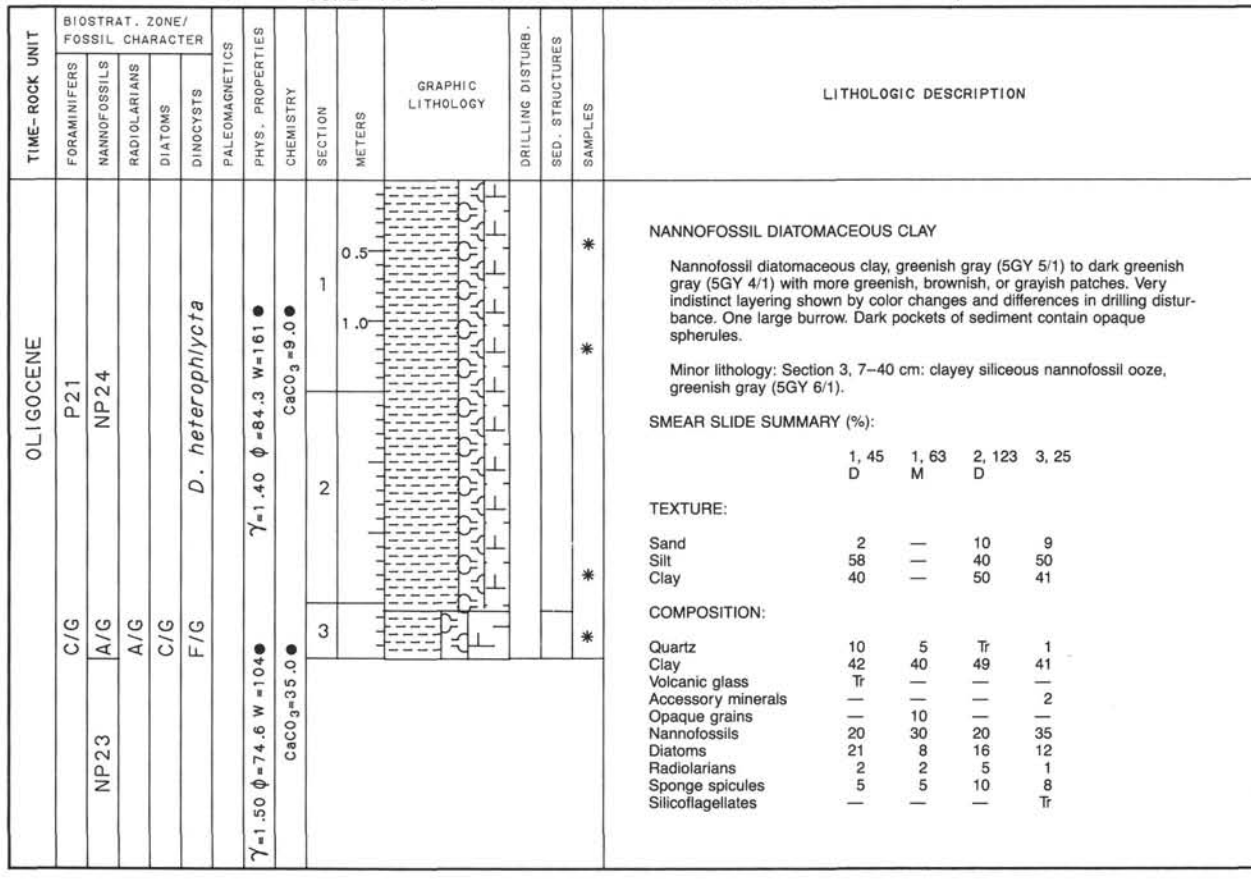

NANNOFOSSIL DIATOMACEOUS CLAY

Nannofossil diatomaceous clay, greenish gray (5GY 5/1) to dark greenish gray (5GY 4/1) with more greenish, brownish, or grayish patches. Very indistinct layering shown by color changes and differences in drilling disturbance. One large burrow. Dark pockets of sediment contain opaque spherules.

Minor lithology: Section 3, 7–40 cm: clayey siliceous nannofossil ooze, greenish gray (5GY 6/1).

SMEAR SLIDE SUMMARY (%):

	1, 45 D	1, 63 M	2, 123 D	3, 25
TEXTURE:				
Sand	2	—	10	9
Silt	58	—	40	50
Clay	40	—	50	41
COMPOSITION:				
Quartz	10	5	Tr	1
Clay	42	40	49	41
Volcanic glass	Tr	—	—	—
Accessory minerals	—	—	—	2
Opaque grains	—	10	—	—
Nannofossils	20	30	20	35
Diatoms	21	8	16	12
Radiolarians	2	2	5	1
Sponge spicules	5	5	10	8
Silicoflagellates	—	—	—	Tr

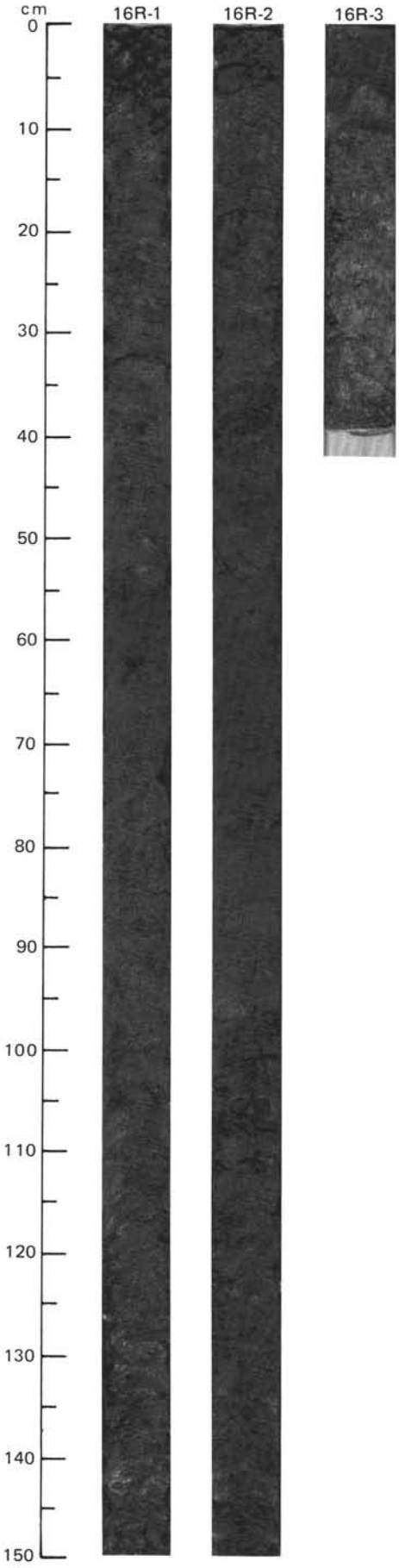
cm
16R-1
16R-2
16R-3
0
10
20
30
40
50
60
70
80
90
100
110
120
130
140
150

SITE 647 HOLE A CORE 17 R CORED INTERVAL 4013.3-40.22.6 mbsl; 154.8-164.1 mbsf

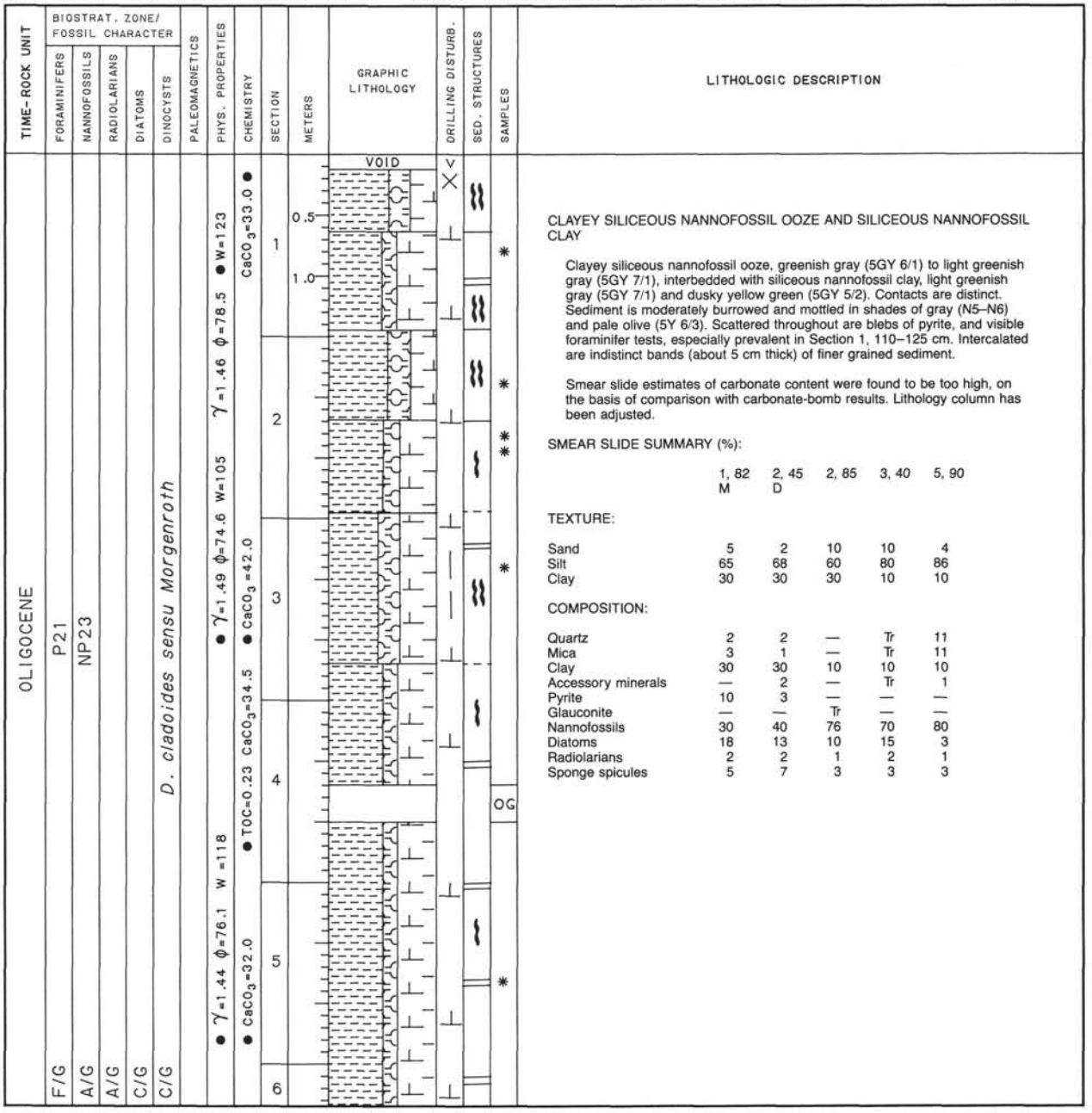

CLAYEY SILICEOUS NANNOFOSSIL OOZE AND SILICEOUS NANNOFOSSIL CLAY

Clayey siliceous nannofossil ooze, greenish gray (5GY 6/1) to light greenish gray (5GY 7/1), interbedded with siliceous nannofossil clay, light greenish gray (5GY 7/1) and dusky yellow green (5GY 5/2). Contacts are distinct. Sediment is moderately burrowed and mottled in shades of gray (N5–N6) and pale olive (5Y 6/3). Scattered throughout are blebs of pyrite, and visible foraminifer tests, especially prevalent in Section 1, 110–125 cm. Intercalated are indistinct bands (about 5 cm thick) of finer grained sediment.

Smear slide estimates of carbonate content were found to be too high, on the basis of comparison with carbonate-bomb results. Lithology column has been adjusted.

SMEAR SLIDE SUMMARY (%):

	1, 82 M	2, 45 D	2, 85	3, 40	5, 90
TEXTURE:					
Sand	5	2	10	10	4
Silt	65	68	60	80	86
Clay	30	30	30	10	10
COMPOSITION:					
Quartz	2	2	—	Tr	11
Mica	3	1	—	Tr	11
Clay	30	30	10	10	10
Accessory minerals	—	2	—	Tr	1
Pyrite	10	3	—	—	—
Glauconite	—	—	Tr	—	—
Nannofossils	30	40	76	70	80
Diatoms	18	13	10	15	3
Radiolarians	2	2	1	2	1
Sponge spicules	5	7	3	3	3

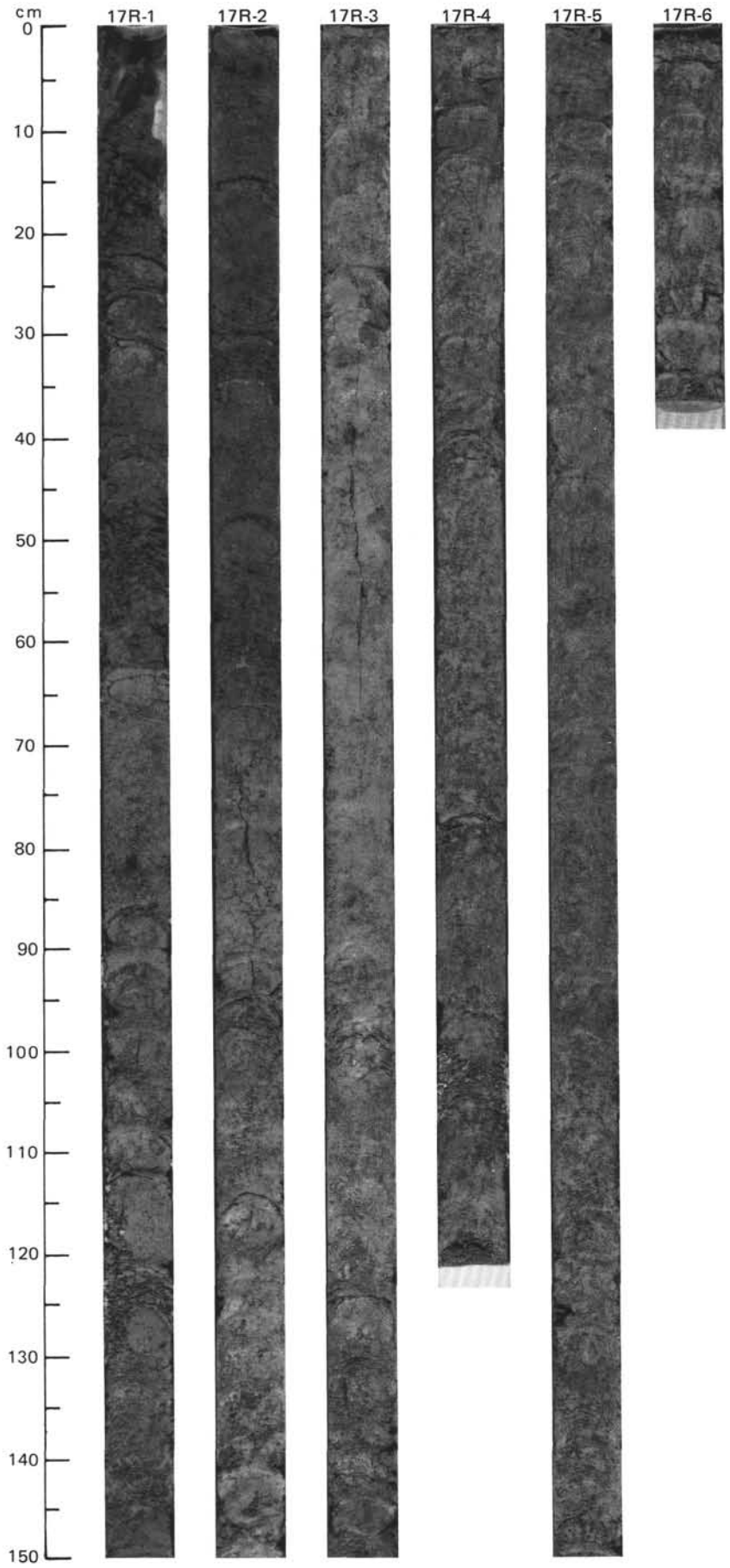
cm
17R-1
17R-2
17R-3
17R-4
17R-5
17R-6
0
10
20
30
40
50
60
70
80
90
100
110
120
130
140
150

SITE 647 HOLE A CORE 18 R CORED INTERVAL 4022.6-4032.3 mbsl; 164.1-173.8 mbsf

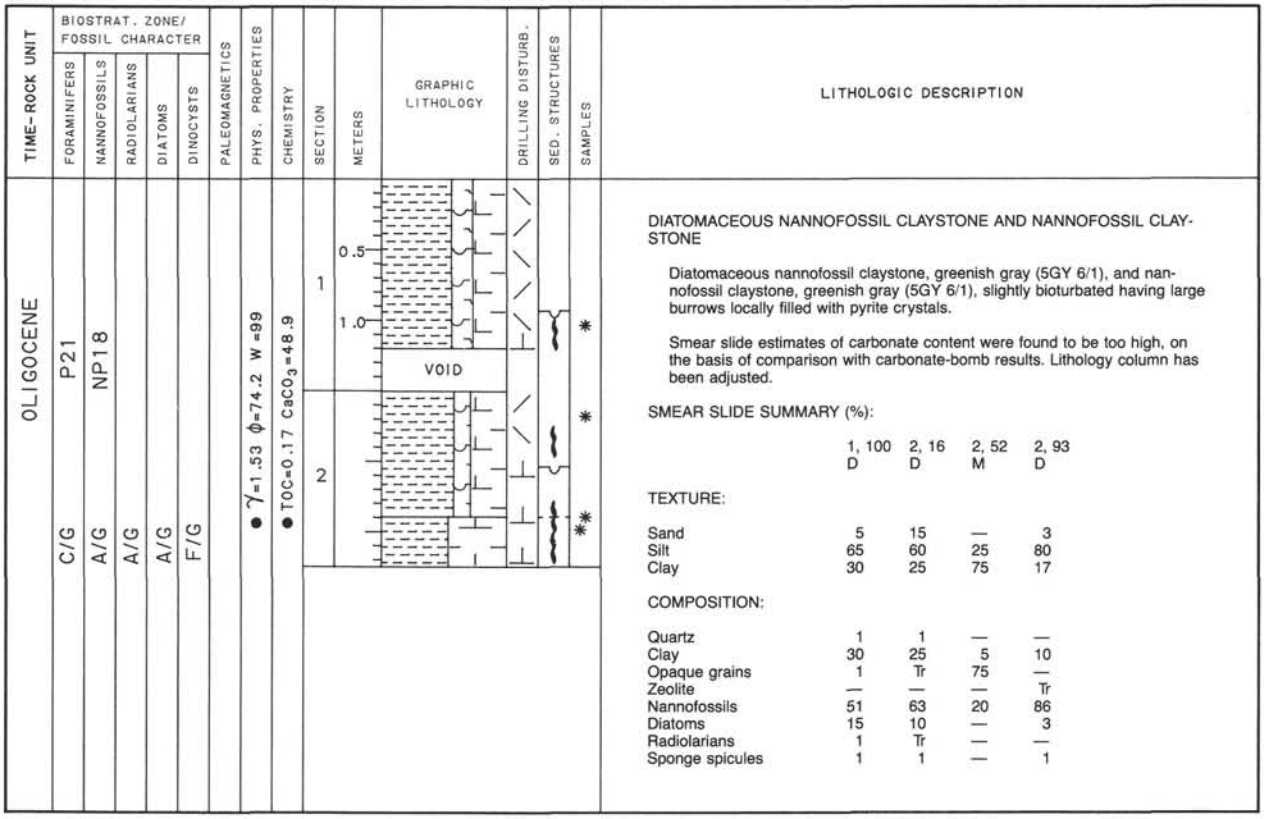

DIATOMACEOUS NANNOFOSSIL CLAYSTONE AND NANNOFOSSIL CLAYSTONE

Diatomaceous nannofossil claystone, greenish gray (5GY 6/1), and nannofossil claystone, greenish gray (5GY 6/1), slightly bioturbated having large burrows locally filled with pyrite crystals.

Smear slide estimates of carbonate content were found to be too high, on the basis of comparison with carbonate-bomb results. Lithology column has been adjusted.

SMEAR SLIDE SUMMARY (%):

	1, 100 D	2, 16 D	2, 52 M	2, 93 D
TEXTURE:				
Sand	5	15	—	3
Silt	65	60	25	80
Clay	30	25	75	17
COMPOSITION:				
Quartz	1	1	—	—
Clay	30	25	5	10
Opaque grains	1	Tr	75	—
Zeolite	—	—	—	Tr
Nannofossils	51	63	20	86
Diatoms	15	10	—	3
Radiolarians	1	Tr	—	—
Sponge spicules	1	1	—	1

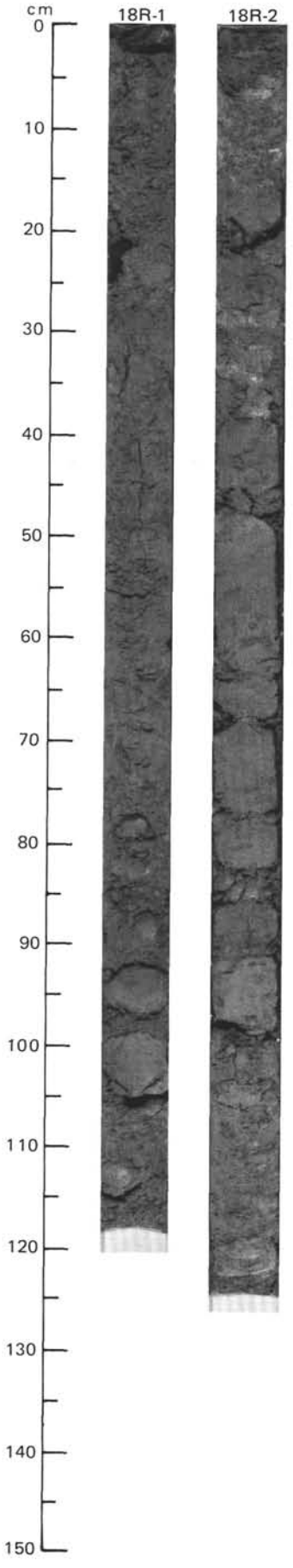
cm
18R-1
18R-2
0
10
20
30
40
50
60
70
80
90
100
110
120
130
140
150

SITE 647 HOLE A CORE 19 R CORED INTERVAL 4032.3-4042.0 mbsl; 173.8-183.5 mbsf

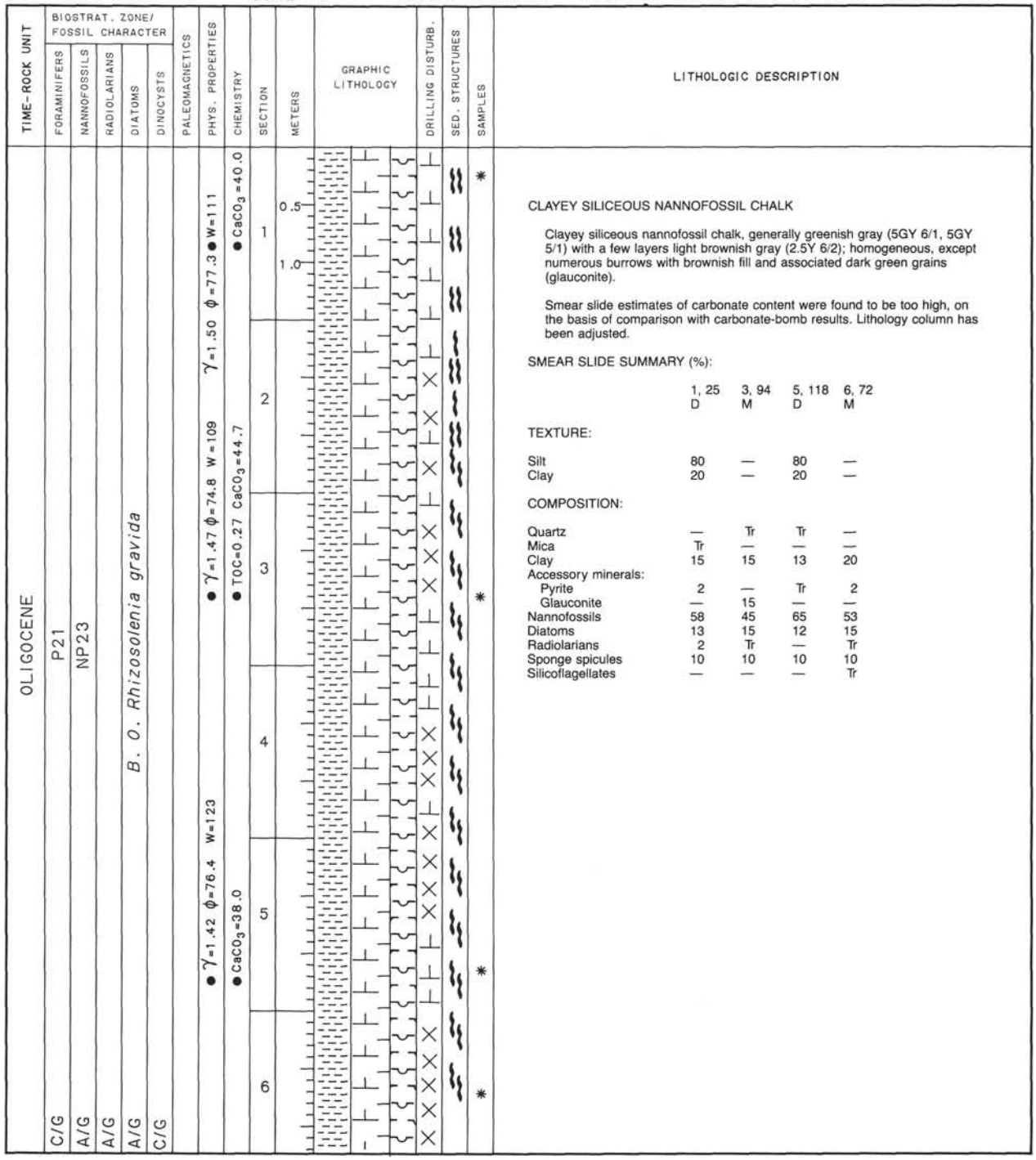

CLAYEY SILICEOUS NANNOFOSSIL CHALK

Clayey siliceous nannofossil chalk, generally greenish gray (5GY 6/1, 5GY 5/1) with a few layers light brownish gray (2.5Y 6/2); homogeneous, except numerous burrows with brownish fill and associated dark green grains (glauconite).

Smear slide estimates of carbonate content were found to be too high, on the basis of comparison with carbonate-bomb results. Lithology column has been adjusted.

SMEAR SLIDE SUMMARY (%):

	1, 25 D	3, 94 M	5, 118 D	6, 72 M
TEXTURE:				
Silt	80	—	80	—
Clay	20	—	20	—
COMPOSITION:				
Quartz	—	Tr	Tr	—
Mica	Tr	—	—	—
Clay	15	15	13	20
Accessory minerals:				
Pyrite	2	—	Tr	2
Glauconite	—	15	—	—
Nannofossils	58	45	65	53
Diatoms	13	15	12	15
Radiolarians	2	Tr	—	Tr
Sponge spicules	10	10	10	10
Silicoflagellates	—	—	—	Tr

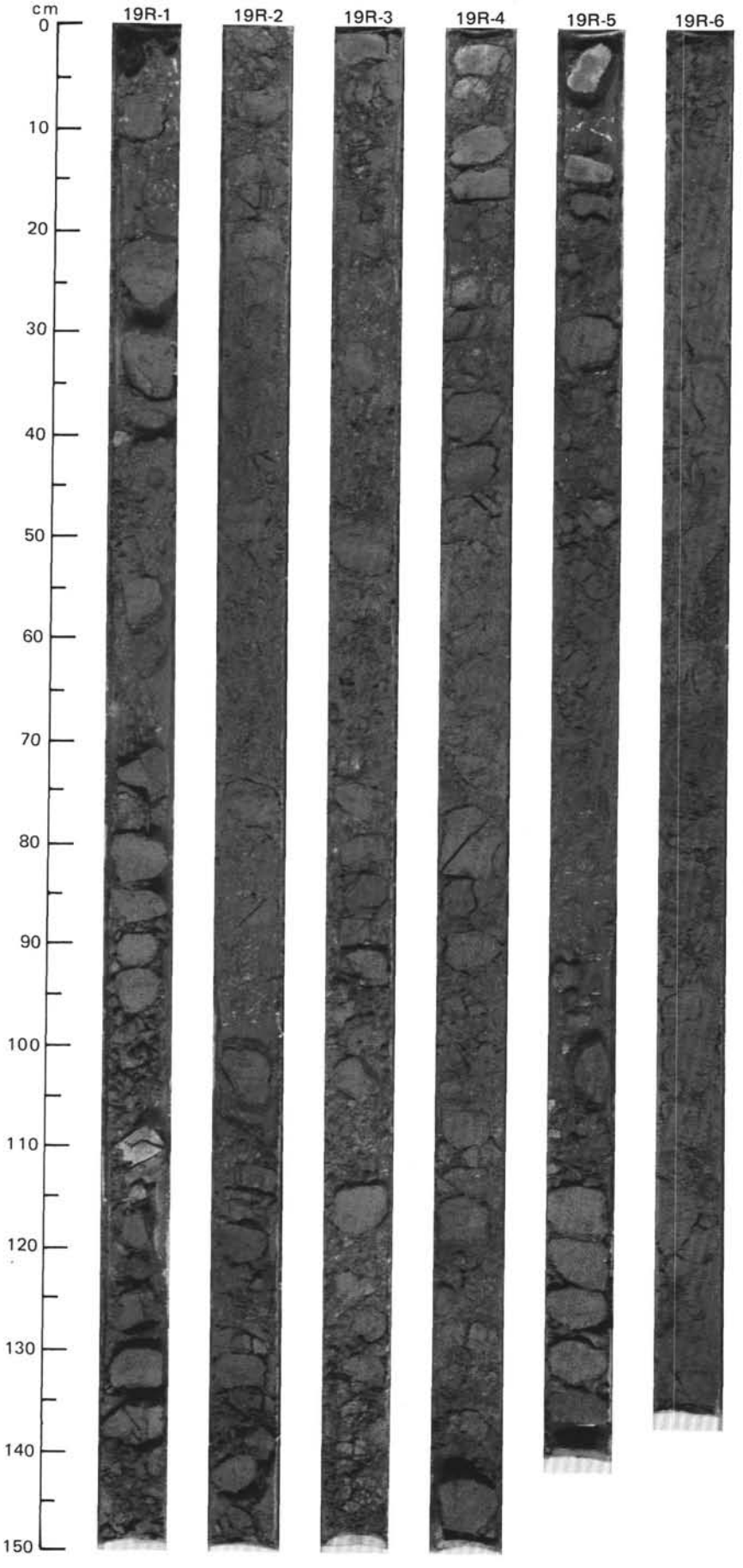
cm
0
10
20
30
40
50
60
70
80
90
100
110
120
130
140
150
19R-1
19R-2
19R-3
19R-4
19R-5
19R-6

SITE 647 HOLE A CORE 20 R CORED INTERVAL 4042.0-4051.6 mbsl; 183.5-193.1 mbsf

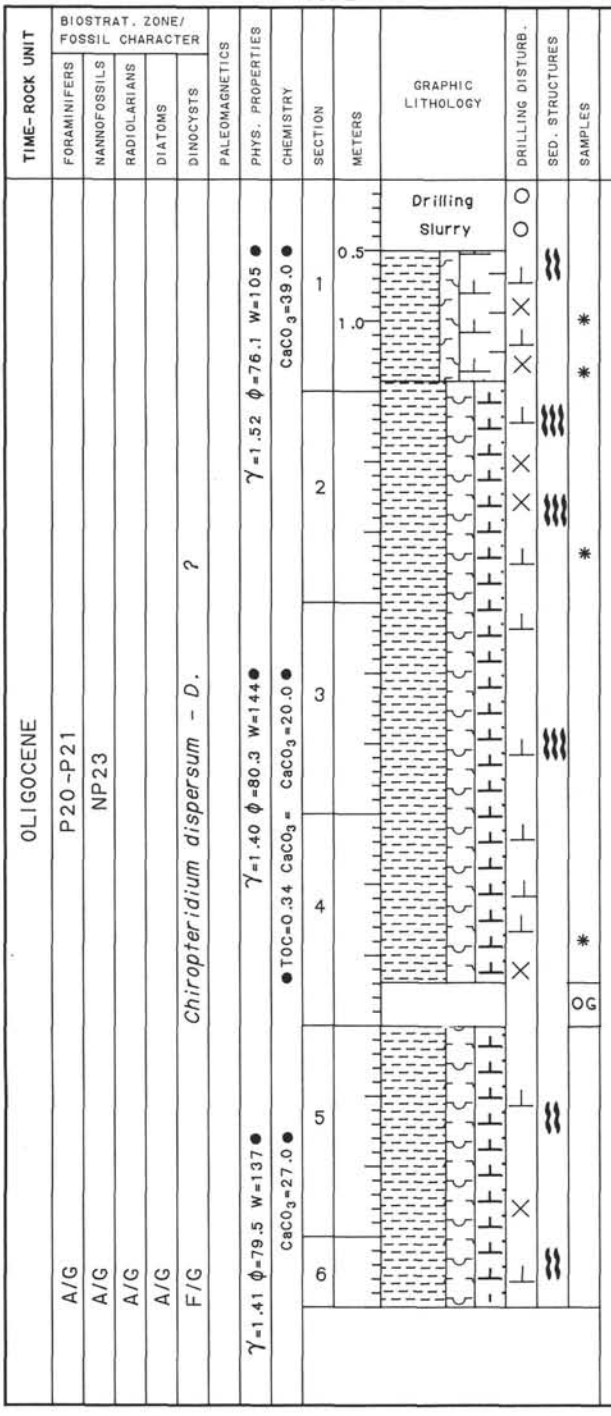

LITHOLOGIC DESCRIPTION

DIATOMACEOUS NANNOFOSSIL CLAYSTONE AND CLAYEY DIATOMACEOUS NANNOFOSSIL CHALK

Diatomaceous nannofossil claystone, greenish gray (5GY 5/1); grading upward into clayey diatomaceous nannofossil chalk, light greenish gray (5GY 7/1); throughout bioturbated with very prominent burrows of various types (*Zoophycos, Chondrites*), depicted in greenish gray (5G 5/1), pale brown (10YR 6/3), gray (N5), and light gray (5Y 7/1); horizontal to subhorizontal burrows are dominant. Section 1, 125 cm, to Section 4, 20 cm, exhibits very prominent sets of microfaults, indicating normal displacement of a few cm with dip angle from 40° to vertical. Vague layering and lamination are disrupted by burrowing, but suggest relict bedding.

Minor lithology: Section 2, 116 cm: glauconite grains within *Zoophycos* burrow.

Smear slide estimates of carbonate content were found to be too high, on the basis of comparison with carbonate-bomb results. Lithology column has been adjusted.

SMEAR SLIDE SUMMARY (%):

	1, 104 D	1, 137 M	2, 115 M	4, 84 D
TEXTURE:				
Sand	5	5	100	15
Silt	75	65	—	50
Clay	20	30	—	35
COMPOSITION:				
Quartz	—	Tr	—	Tr
Mica	—	Tr	—	—
Clay	15	26	—	30
Volcanic glass	—	—	—	—
Accessory minerals	—	Tr	—	—
Glauconite	—	—	100	Tr
Zeolite	—	—	—	Tr
Foraminifers	—	Tr	—	47
Nannofossils	70	55	—	47
Diatoms	13	8	—	20
Radiolarians	1	3	—	—
Sponge spicules	1	7	—	2
Silicoflagellates	Tr	1	—	1

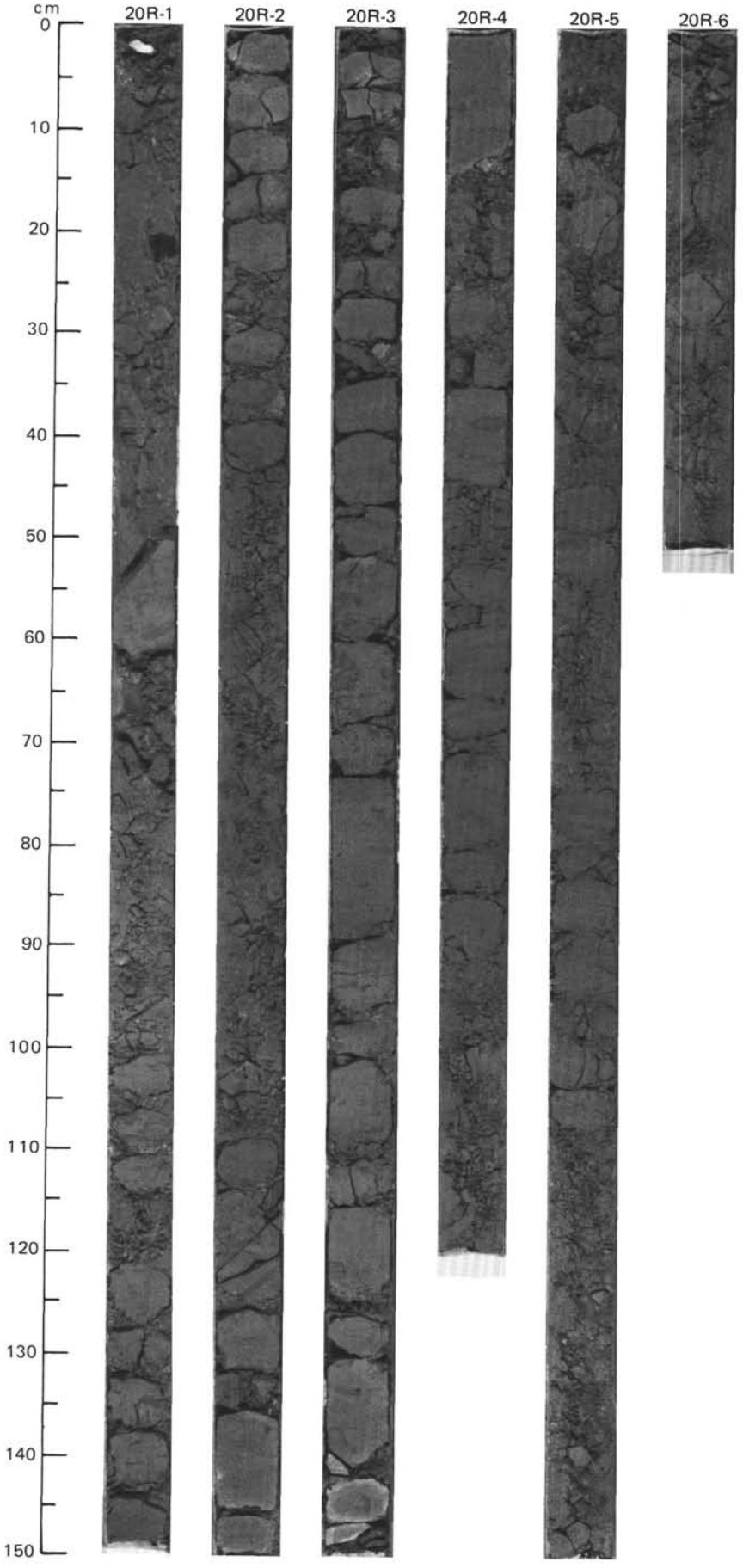
cm
0
10
20
30
40
50
60
70
80
90
100
110
120
130
140
150
20R-1
20R-2
20R-3
20R-4
20R-5
20R-6

SITE 647 HOLE A CORE 21 R CORED INTERVAL 4051.6-4061.2 mbsl; 193.1-202.7 mbsf

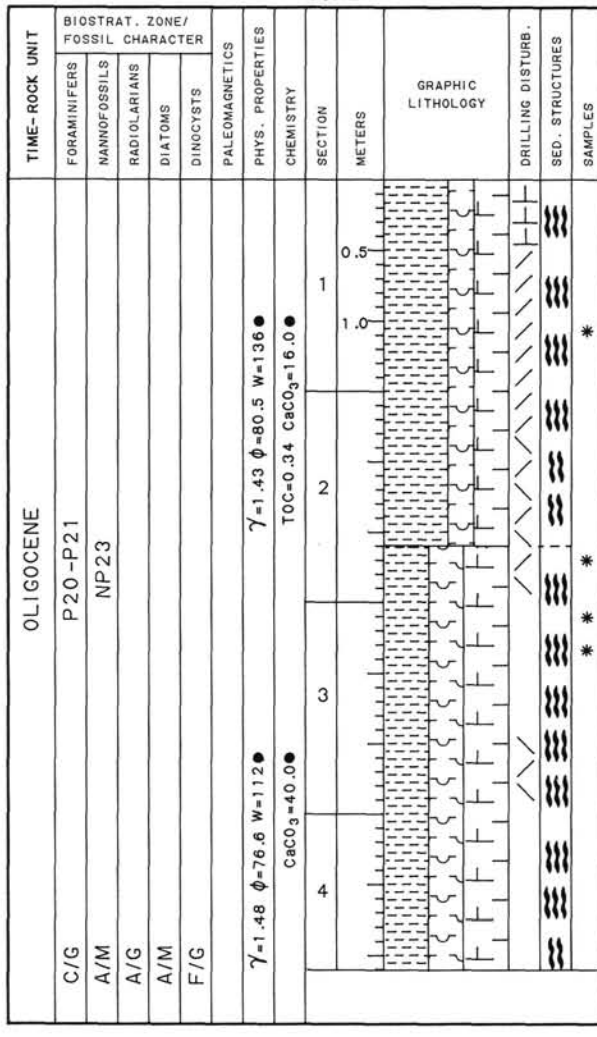

LITHOLOGIC DESCRIPTION

DIATOM NANNOFOSSIL CLAYSTONE AND CLAYEY DIATOM NANNOFOSSIL CHALK

Diatom nannofossil claystone, greenish gray (5GY 5/1); moderately to strongly bioturbated with local concentrations of black glauconite pellets.

Clayey diatom nannofossil chalk, greenish gray (5GY 6/1); strongly bioturbated with local concentrations of glauconite.

Minor lithlogy: Section 3, 6–12 cm: light greenish gray (5GY 7/1), clay-bearing nannofossil chalk, strongly bioturbated, with some glauconite.

Burrows are widely varied, with *Planolites*, *Zoophycos*, *Cylindrichnus*, and others.

Comparison with carbonate-bomb data shows smear slide estimates of carbonate to be too high. Lithologic column has been adjusted to reflect total carbonate content better.

SMEAR SLIDE SUMMARY (%):

	1, 108 D	2, 123 D	3, 10 M	3, 36 D
TEXTURE:				
Sand	15	15	5	20
Silt	50	65	65	65
Clay	35	20	30	15
COMPOSITION:				
Quartz	Tr	Tr	Tr	Tr
Clay	33	19	24	14
Accessory minerals	Tr	Tr	Tr	Tr
Foraminifers	—	Tr	—	—
Nannofossils	50	60	70	60
Diatoms	15	20	5	25
Radiolarians	Tr	—	Tr	Tr
Sponge spicules	2	1	1	1
Silicoflagellates	—	Tr	—	—

SITE 647 HOLE A CORE 22 R CORED INTERVAL 4061.2-4070.8 mbsl; 202.7-212.3 mbsf

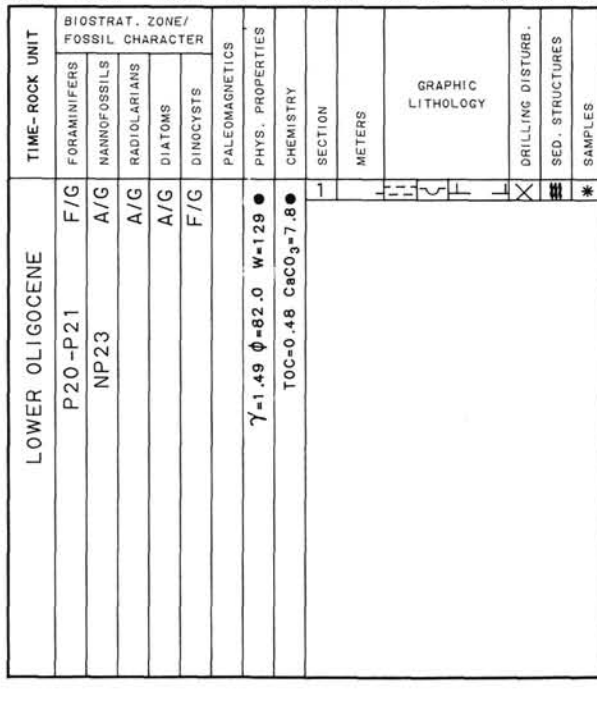

LITHOLOGIC DESCRIPTION

NANNOFOSSIL CHALK

Nannofossil chalk, greenish gray (5GY 5/1 to 5GY 6/1), with abundant sand-sized glauconite grains, more concentrated in irregular pockets.

SMEAR SLIDE SUMMARY (%):

	1, 10 D
TEXTURE:	
Sand	10
Silt	60
Clay	30
COMPOSITION:	
Quartz	Tr
Clay	27
Accessory minerals	1
Nannofossils	50
Diatoms	10
Radiolarians	Tr
Sponge spicules	2

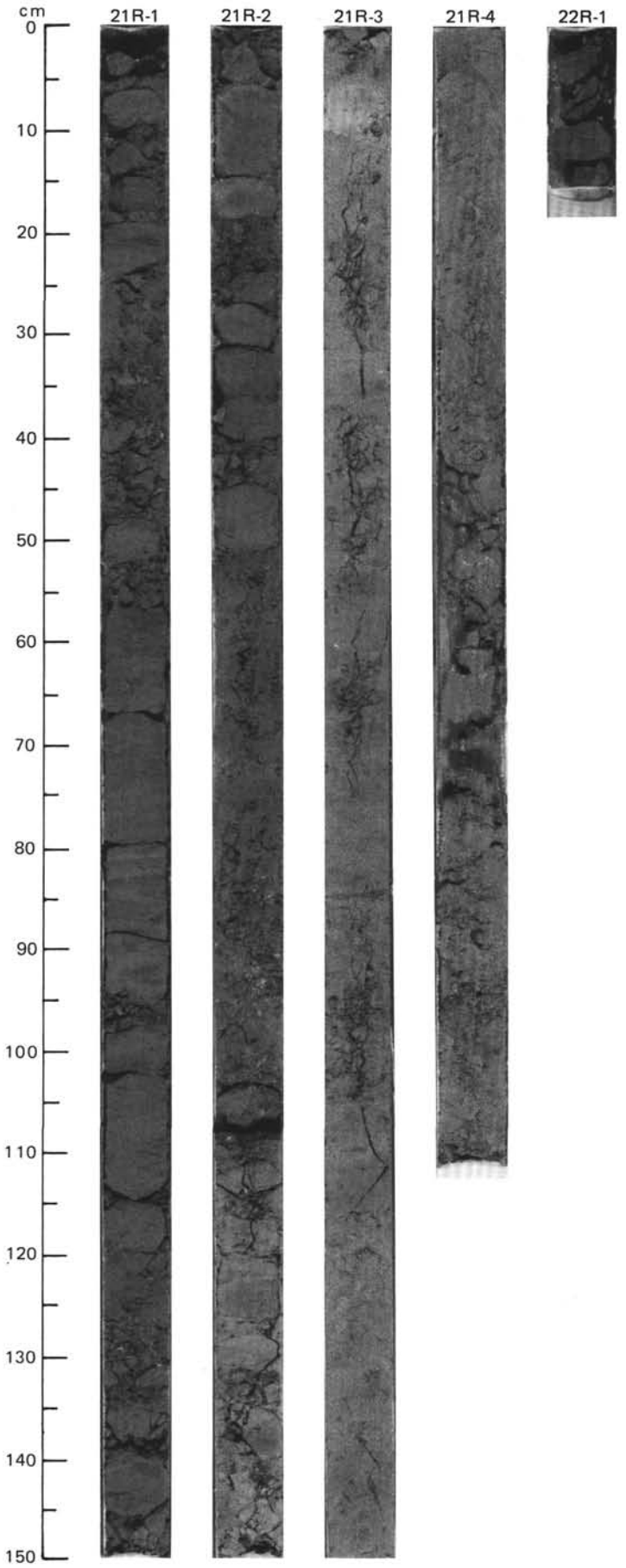
cm
0
10
20
30
40
50
60
70
80
90
100
110
120
130
140
150
21R-1
21R-2
21R-3
21R-4
22R-1

SITE 647 HOLE A CORE 23 R CORED INTERVAL 4070.8- 4080.4 mbsl; 212.3-221.9 mbsf

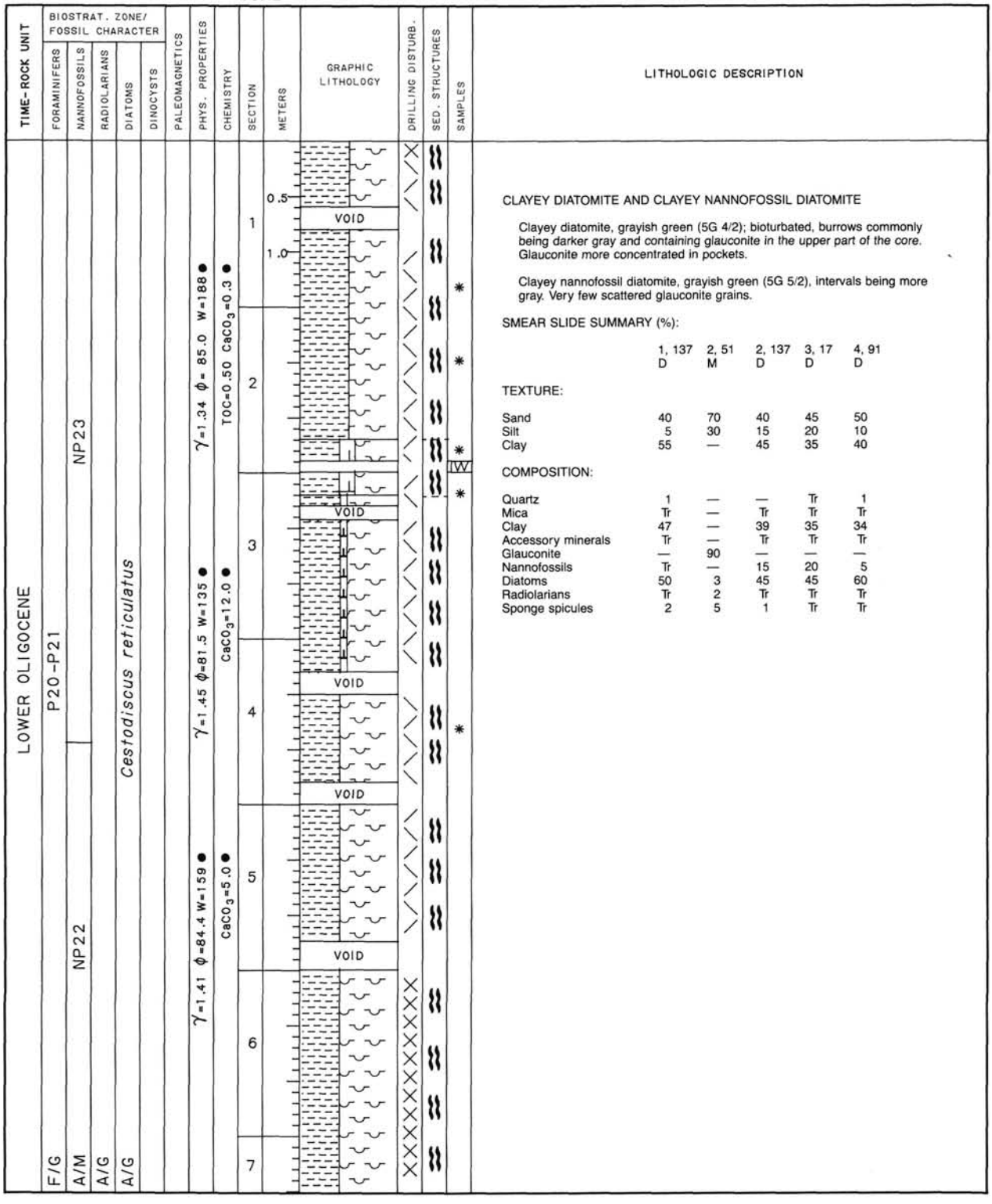

CLAYEY DIATOMITE AND CLAYEY NANNOFOSSIL DIATOMITE

Clayey diatomite, grayish green (5G 4/2); bioturbated, burrows commonly being darker gray and containing glauconite in the upper part of the core. Glauconite more concentrated in pockets.

Clayey nannofossil diatomite, grayish green (5G 5/2), intervals being more gray. Very few scattered glauconite grains.

SMEAR SLIDE SUMMARY (%):

	1, 137 D	2, 51 M	2, 137 D	3, 17 D	4, 91 D
TEXTURE:					
Sand	40	70	40	45	50
Silt	5	30	15	20	10
Clay	55	—	45	35	40
COMPOSITION:					
Quartz	1	—	—	Tr	1
Mica	Tr	—	Tr	Tr	Tr
Clay	47	—	39	35	34
Accessory minerals	Tr	—	Tr	Tr	Tr
Glauconite	—	90	—	—	—
Nannofossils	Tr	—	15	20	5
Diatoms	50	3	45	45	60
Radiolarians	Tr	2	Tr	Tr	Tr
Sponge spicules	2	5	1	Tr	Tr

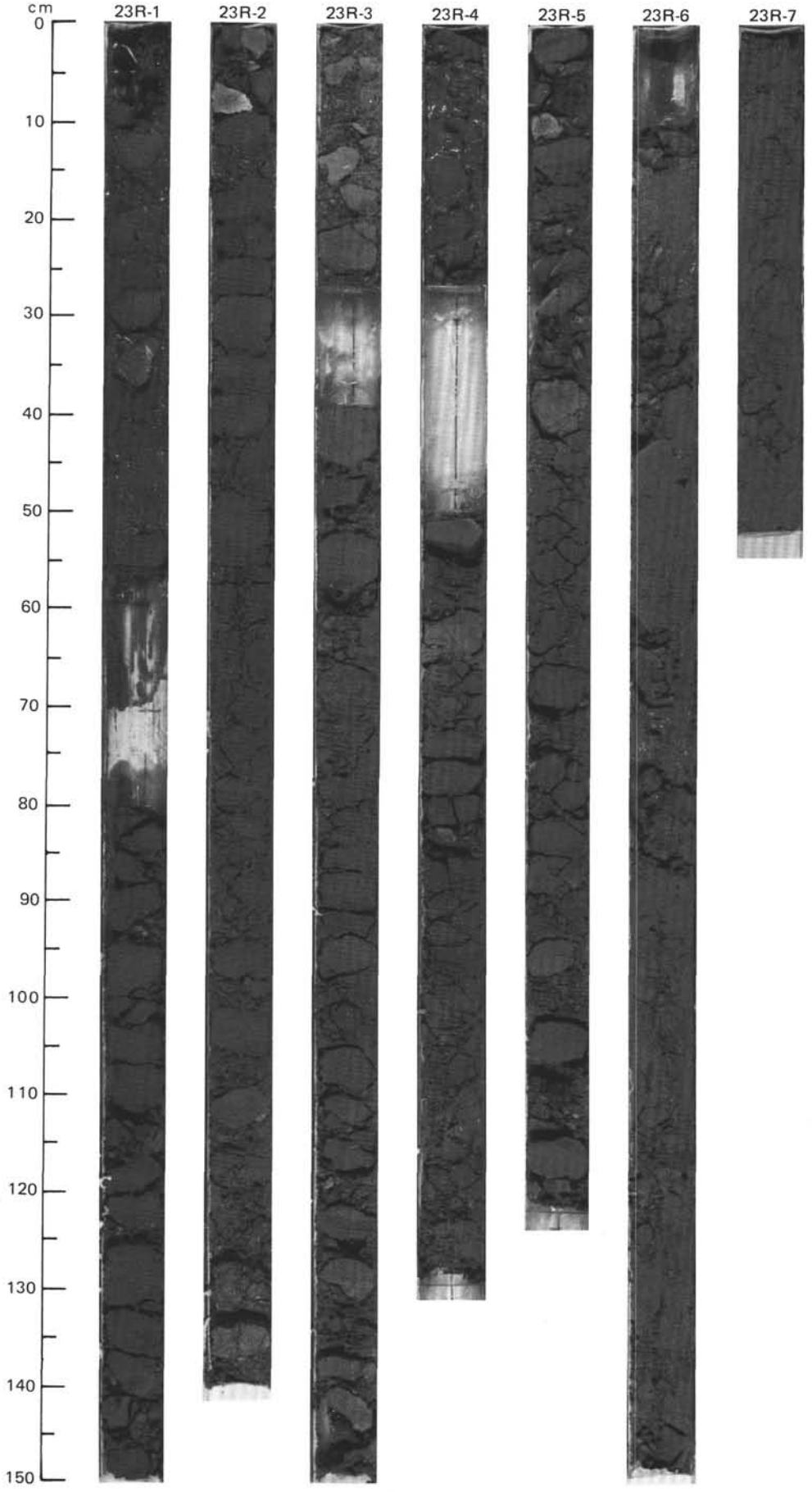
cm
0
10
20
30
40
50
60
70
80
90
100
110
120
130
140
150
23R-1
23R-2
23R-3
23R-4
23R-5
23R-6
23R-7

SITE 647 HOLE A CORE 24 R CORED INTERVAL 4080.4-4090.0 mbsl; 221.9-231.5 mbsf

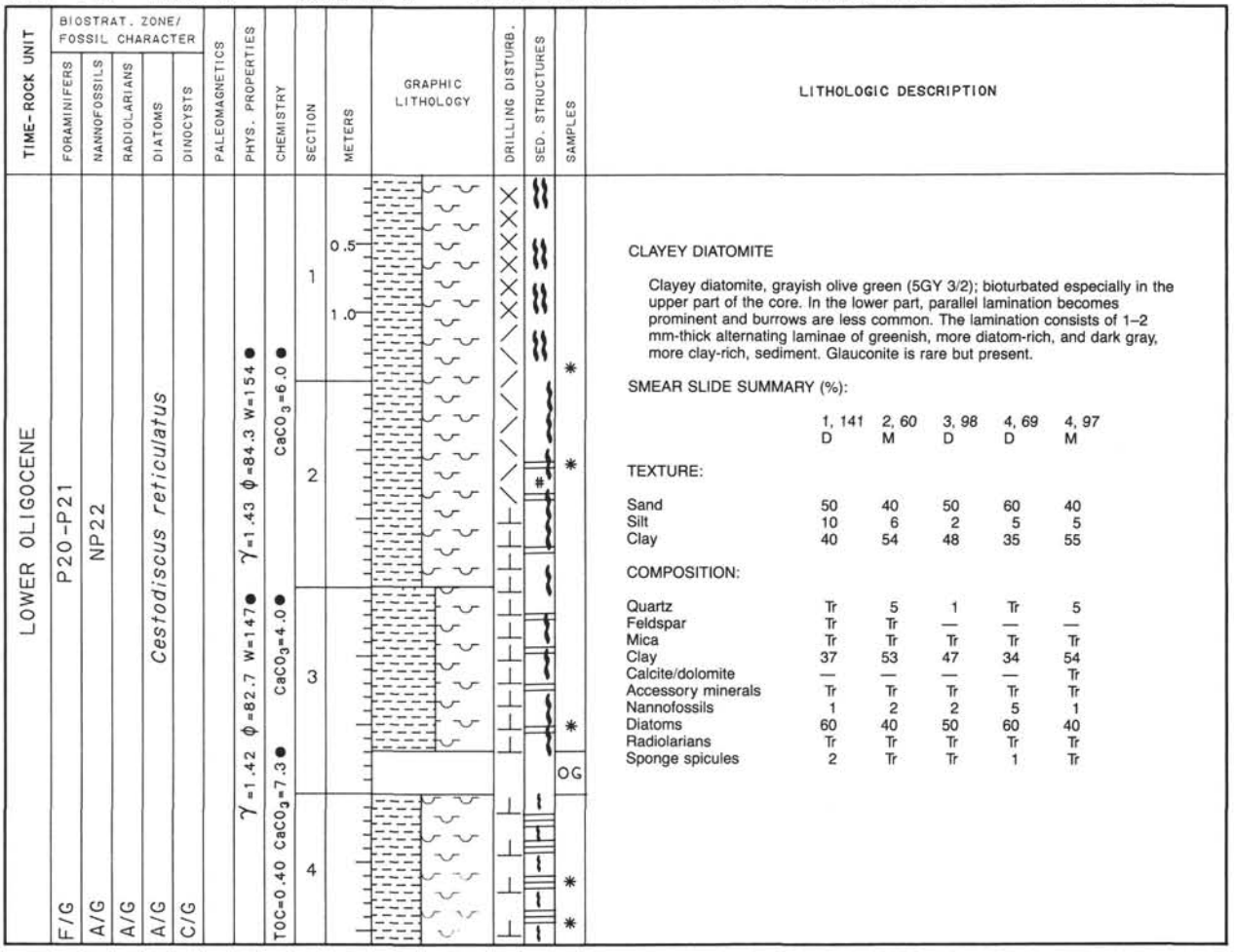

CLAYEY DIATOMITE

Clayey diatomite, grayish olive green (5GY 3/2); bioturbated especially in the upper part of the core. In the lower part, parallel lamination becomes prominent and burrows are less common. The lamination consists of 1–2 mm-thick alternating laminae of greenish, more diatom-rich, and dark gray, more clay-rich, sediment. Glauconite is rare but present.

SMEAR SLIDE SUMMARY (%):

	1, 141 D	2, 60 M	3, 98 D	4, 69 D	4, 97 M
TEXTURE:					
Sand	50	40	50	60	40
Silt	10	6	2	5	5
Clay	40	54	48	35	55
COMPOSITION:					
Quartz	Tr	5	1	Tr	5
Feldspar	Tr	Tr	—	—	—
Mica	Tr	Tr	Tr	Tr	Tr
Clay	37	53	47	34	54
Calcite/dolomite	—	—	—	—	Tr
Accessory minerals	Tr	Tr	Tr	Tr	Tr
Nannofossils	1	2	2	5	1
Diatoms	60	40	50	60	40
Radiolarians	Tr	Tr	Tr	Tr	Tr
Sponge spicules	2	Tr	Tr	1	Tr

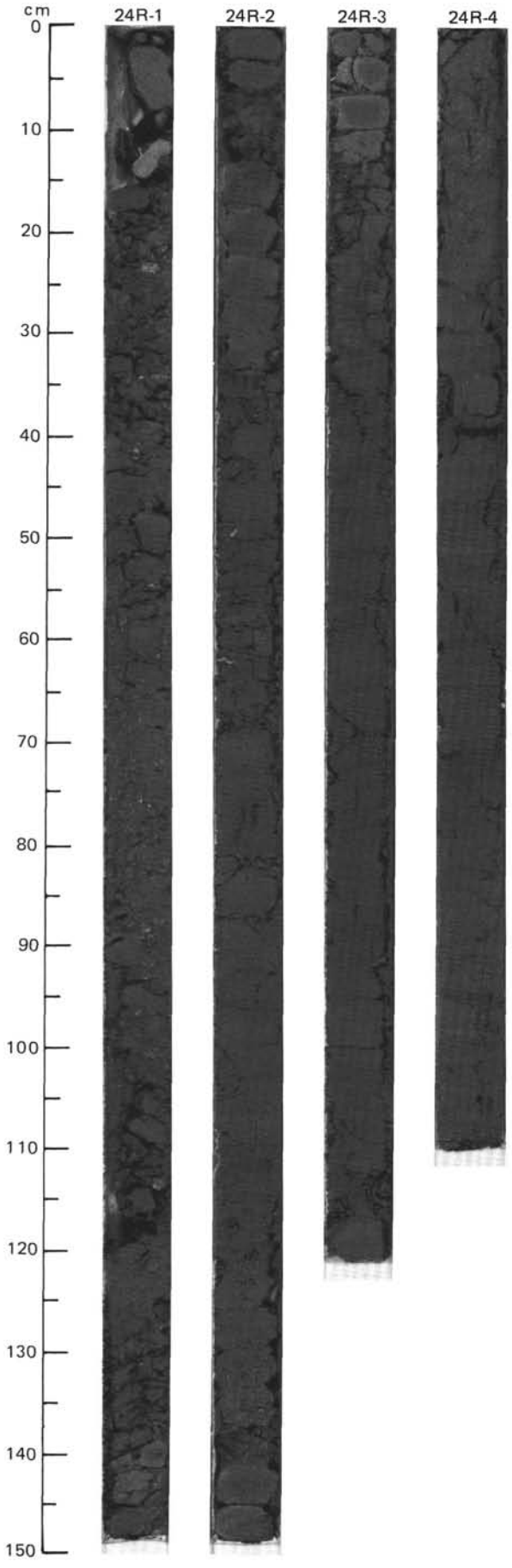
cm
0
10
20
30
40
50
60
70
80
90
100
110
120
130
140
150
24R-1
24R-2
24R-3
24R-4

SITE 647 HOLE A CORE 25 R CORED INTERVAL 4090.0–4099.6 mbsl; 231.5–241.1 mbsf

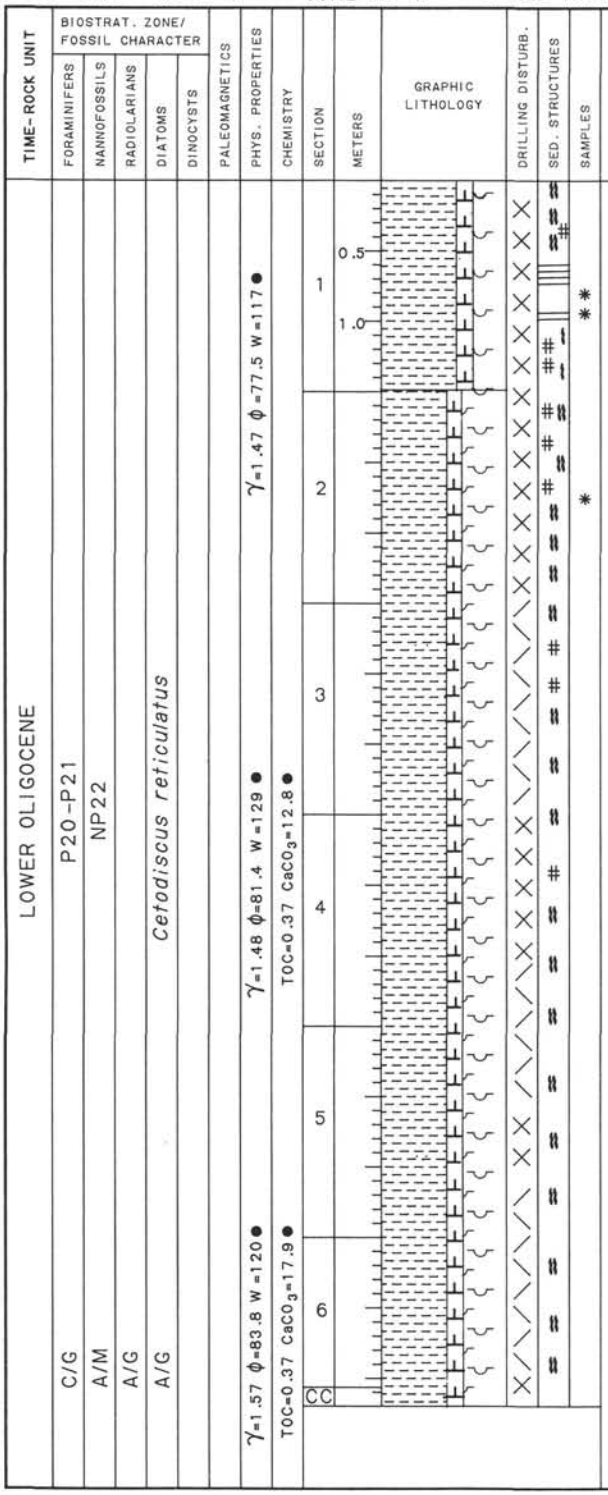

LITHOLOGIC DESCRIPTION

NANNOFOSSIL DIATOMACEOUS CLAYSTONE

Nannofossil diatomaceous claystone, greenish gray (5GY 5/1), generally moderately bioturbated (e.g., *Planolites*, *Zoophycos*), with local fine lamination (Section 1, 60–75 cm) and local concentrations of glauconitic pellets. Scattered microfaults.

Minor lithology: Section 1, 93–97 cm: vaguely laminated fine pebble to granule conglomerate, with all clasts being of glauconitic mud. Thin black Fe sulfide laminae. Probable disconformity.

Much of this core is strongly brecciated by drilling.

SMEAR SLIDE SUMMARY (%):

	1, 74 D	1, 97 M	2, 72 D	4, 44 D
TEXTURE:				
Sand	25	5	35	35
Silt	10	95	10	10
Clay	65	—	55	55
COMPOSITION:				
Quartz	Tr	1	Tr	Tr
Mica	Tr	—	Tr	Tr
Clay	64	—	53	52
Accessory minerals	Tr	—	Tr	Tr
Glauconite	—	5	—	—
Pyrite	—	84	—	—
Foraminifers	—	Tr	8	Tr
Nannofossils	10	Tr	10	10
Diatoms	25	—	35	37
Radiolarians	Tr	—	Tr	1
Sponge spicules	1	10	2	Tr
Silicoflagellates	Tr	—	Tr	Tr

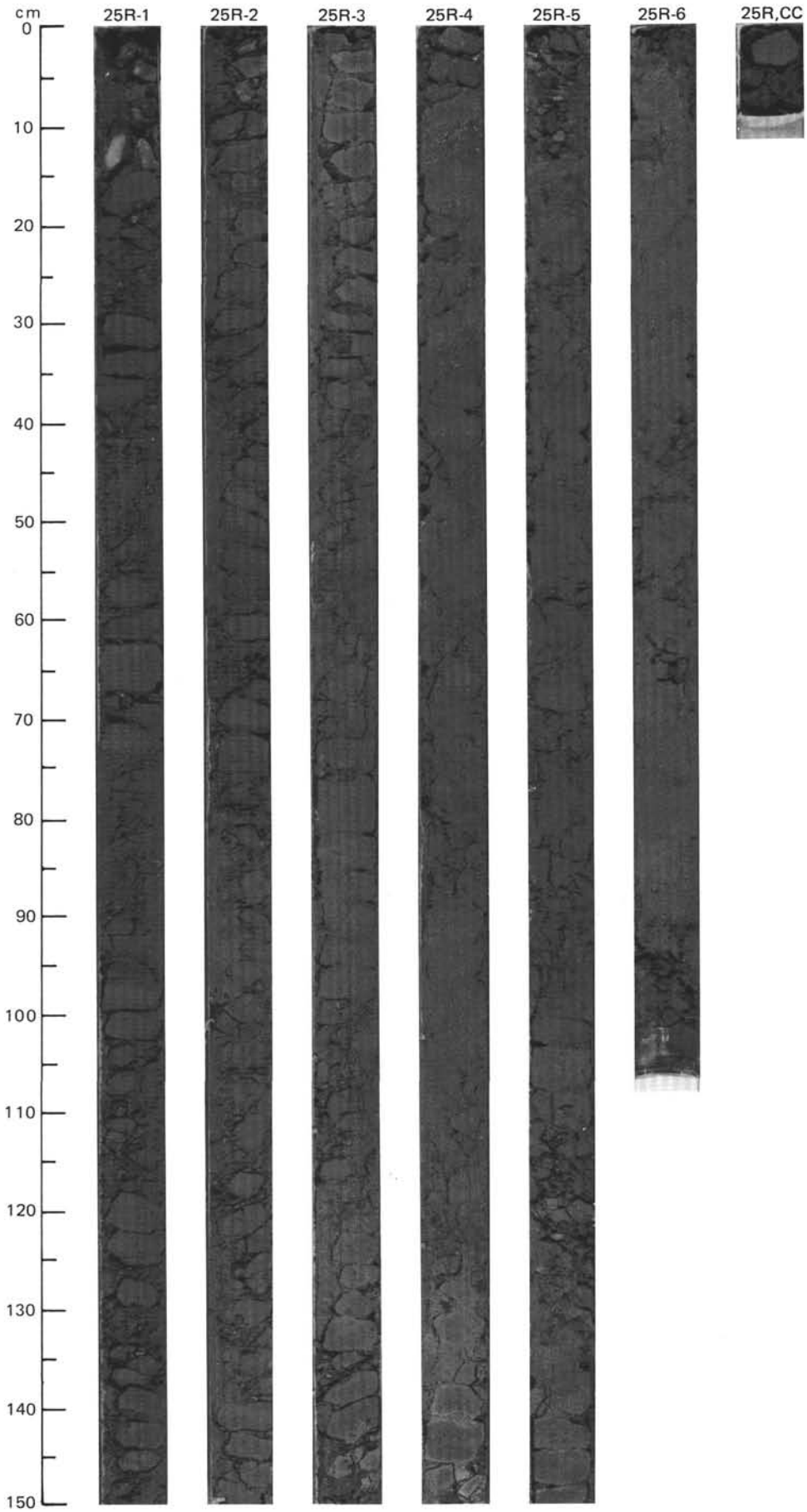
cm
25R-1
25R-2
25R-3
25R-4
25R-5
25R-6
25R,CC
0
10
20
30
40
50
60
70
80
90
100
110
120
130
140
150

SITE 647 HOLE A CORE 26 R CORED INTERVAL 4099.6-4108.9 mbsl; 241.1-250.4 mbsf

TIME-ROCK UNIT	BIOSTRAT. ZONE/ FOSSIL CHARACTER: FORAMINIFERS	NANNOFOSSILS	RADIOLARIANS	DIATOMS	DINOCYSTS	PALEOMAGNETICS	PHYS. PROPERTIES	CHEMISTRY	SECTION	METERS	GRAPHIC LITHOLOGY	DRILLING DISTURB.	SED. STRUCTURES	SAMPLES	LITHOLOGIC DESCRIPTION
LOWER OLIGOCENE	P20-P21 C/G	NP22 A/M	A/G	*Coscinodiscus excavatus* A/G					1	0.5 1.0	Drilling Slurry	X X X X			DIATOM NANNOFOSSIL CLAYSTONE Core is entirely drilling slurry with caved pebbles and probable brecciated in-place lithology that is Diatom Nannofossil Claystone.

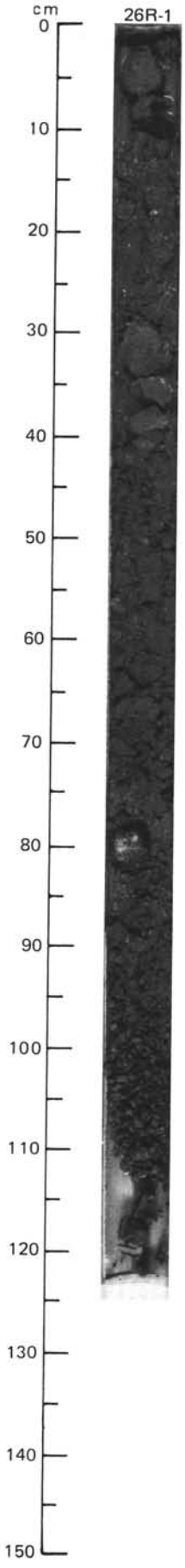
cm
26R-1
0
10
20
30
40
50
60
70
80
90
100
110
120
130
140
150

SITE 647 HOLE A CORE 27 R CORED INTERVAL 4108.9-4118.6 mbsl; 250.4-260.1 mbsf

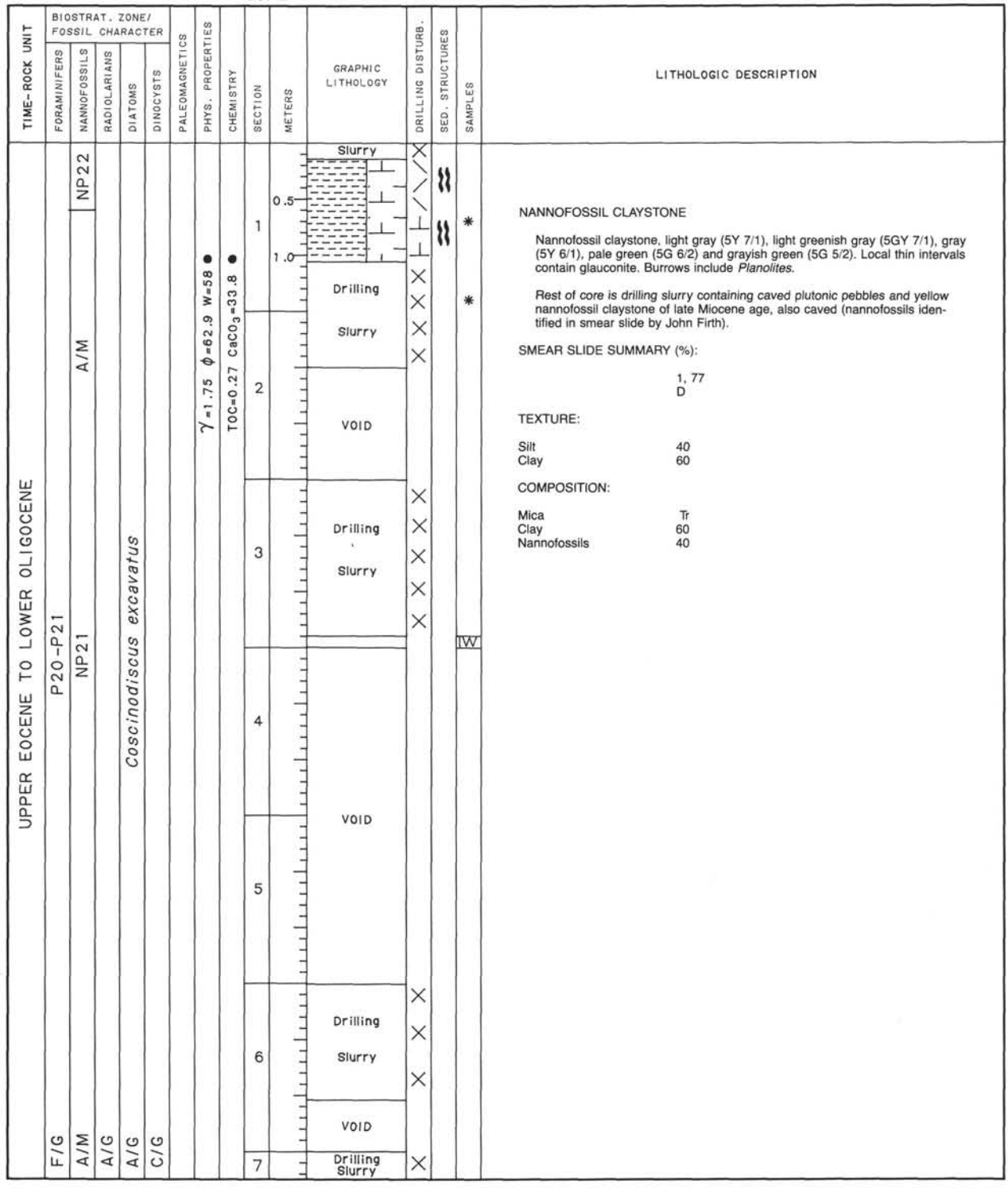

NANNOFOSSIL CLAYSTONE

Nannofossil claystone, light gray (5Y 7/1), light greenish gray (5GY 7/1), gray (5Y 6/1), pale green (5G 6/2) and grayish green (5G 5/2). Local thin intervals contain glauconite. Burrows include *Planolites*.

Rest of core is drilling slurry containing caved plutonic pebbles and yellow nannofossil claystone of late Miocene age, also caved (nannofossils identified in smear slide by John Firth).

SMEAR SLIDE SUMMARY (%):

	1, 77 D
TEXTURE:	
Silt	40
Clay	60
COMPOSITION:	
Mica	Tr
Clay	60
Nannofossils	40

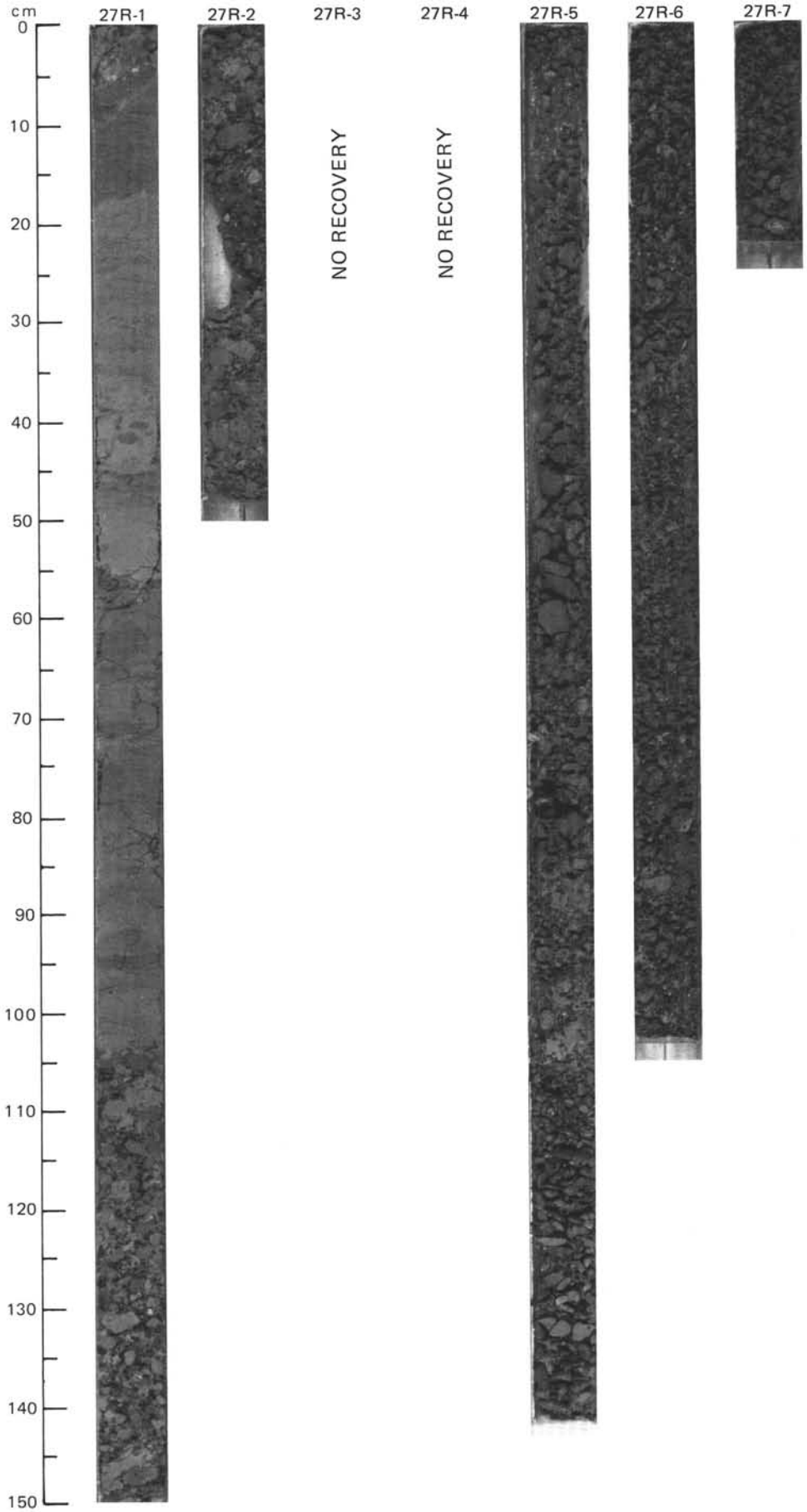
cm
0
10
20
30
40
50
60
70
80
90
100
110
120
130
140
150
27R-1
27R-2
27R-3
NO RECOVERY
27R-4
NO RECOVERY
27R-5
27R-6
27R-7

SITE 647 HOLE A CORE 28 R CORED INTERVAL 4118.6-4128.2 mbsl, 260.1-269.7 mbsf

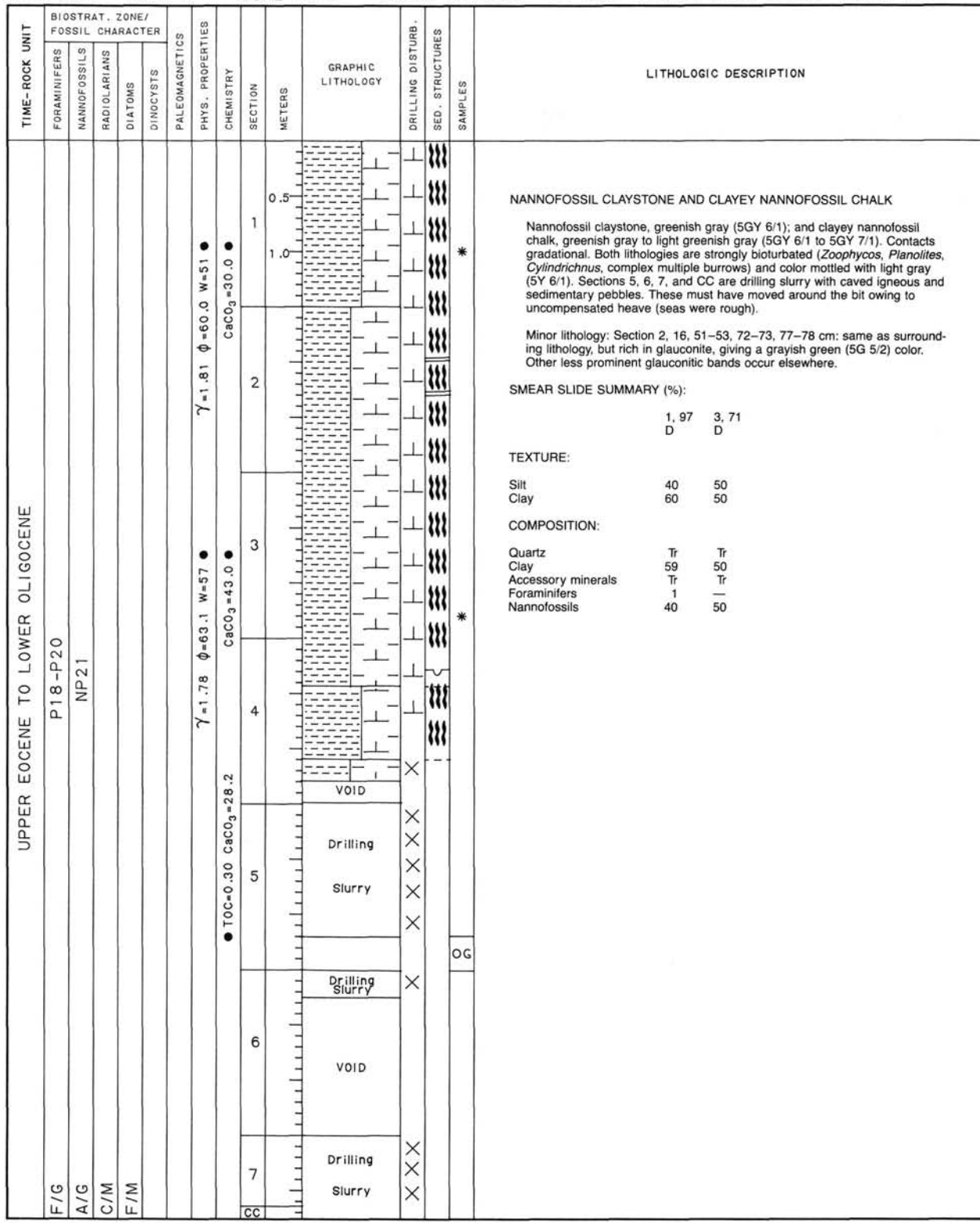

NANNOFOSSIL CLAYSTONE AND CLAYEY NANNOFOSSIL CHALK

Nannofossil claystone, greenish gray (5GY 6/1); and clayey nannofossil chalk, greenish gray to light greenish gray (5GY 6/1 to 5GY 7/1). Contacts gradational. Both lithologies are strongly bioturbated (*Zoophycos*, *Planolites*, *Cylindrichnus*, complex multiple burrows) and color mottled with light gray (5Y 6/1). Sections 5, 6, 7, and CC are drilling slurry with caved igneous and sedimentary pebbles. These must have moved around the bit owing to uncompensated heave (seas were rough).

Minor lithology: Section 2, 16, 51–53, 72–73, 77–78 cm: same as surrounding lithology, but rich in glauconite, giving a grayish green (5G 5/2) color. Other less prominent glauconitic bands occur elsewhere.

SMEAR SLIDE SUMMARY (%):

	1, 97 D	3, 71 D
TEXTURE:		
Silt	40	50
Clay	60	50
COMPOSITION:		
Quartz	Tr	Tr
Clay	59	50
Accessory minerals	Tr	Tr
Foraminifers	1	—
Nannofossils	40	50

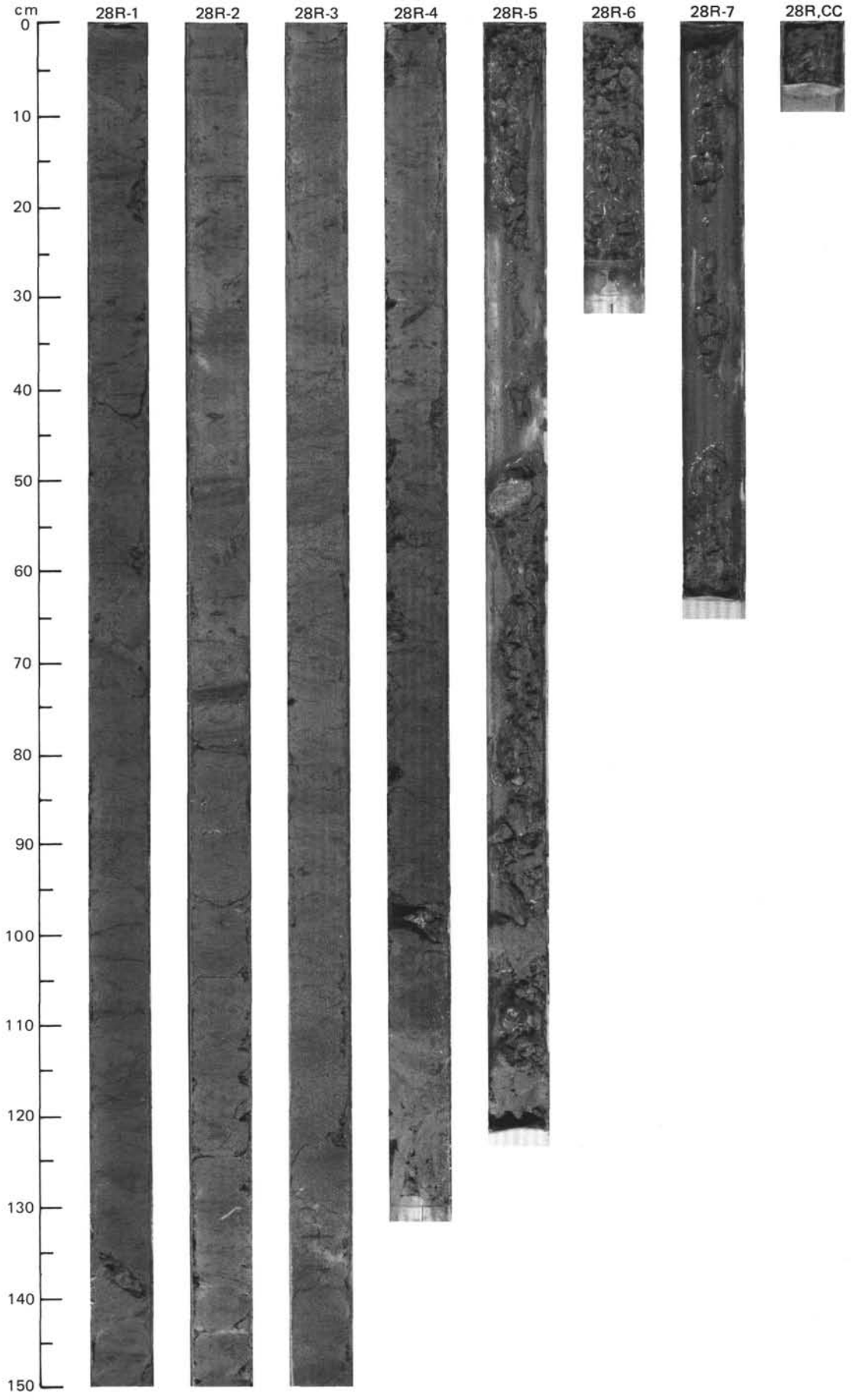
cm
0
10
20
30
40
50
60
70
80
90
100
110
120
130
140
150
28R-1
28R-2
28R-3
28R-4
28R-5
28R-6
28R-7
28R,CC

SITE 647 HOLE A CORE 29 R CORED INTERVAL 4128.2-4137.9 mbsl; 269.7-279.4 mbsf

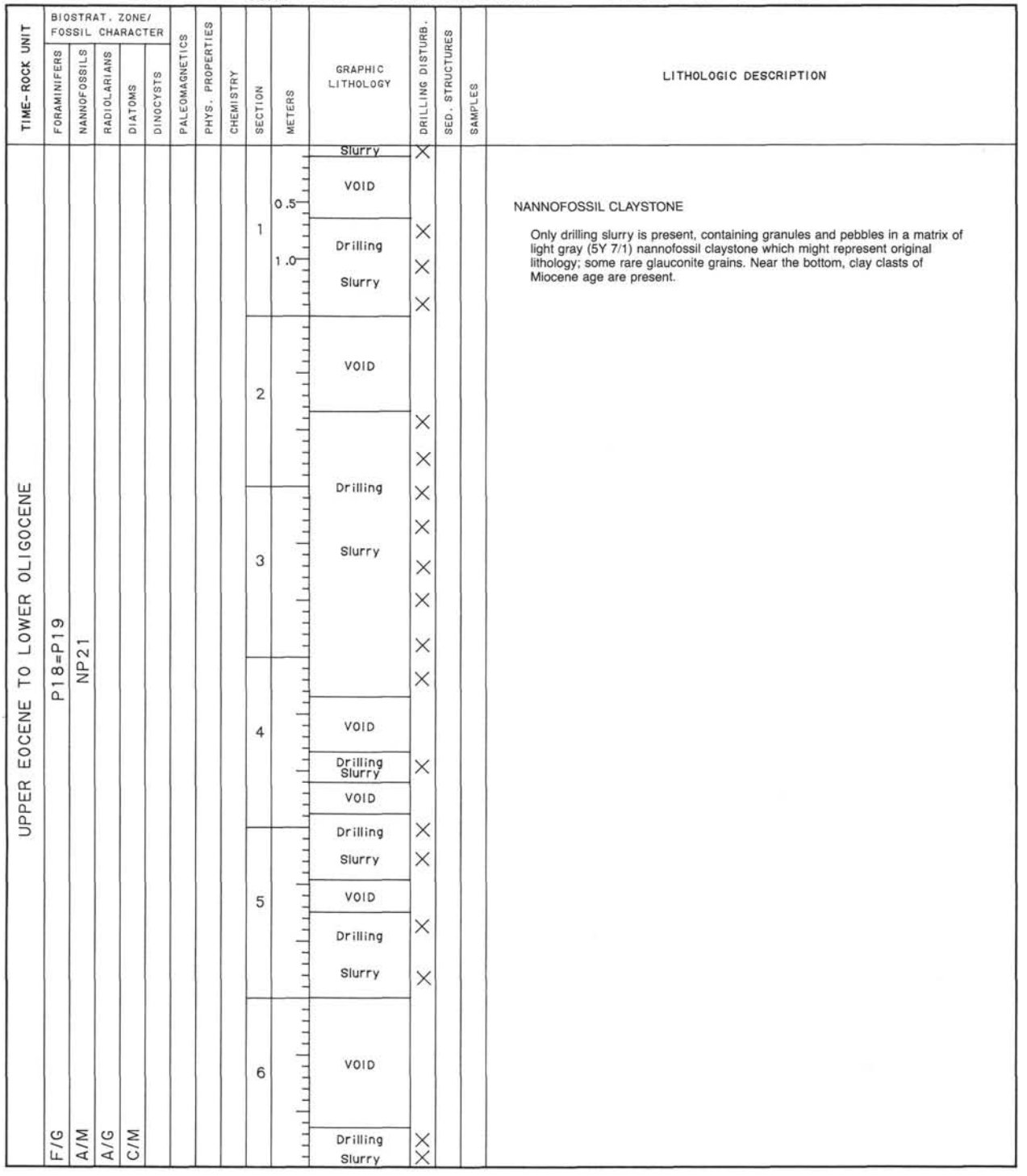

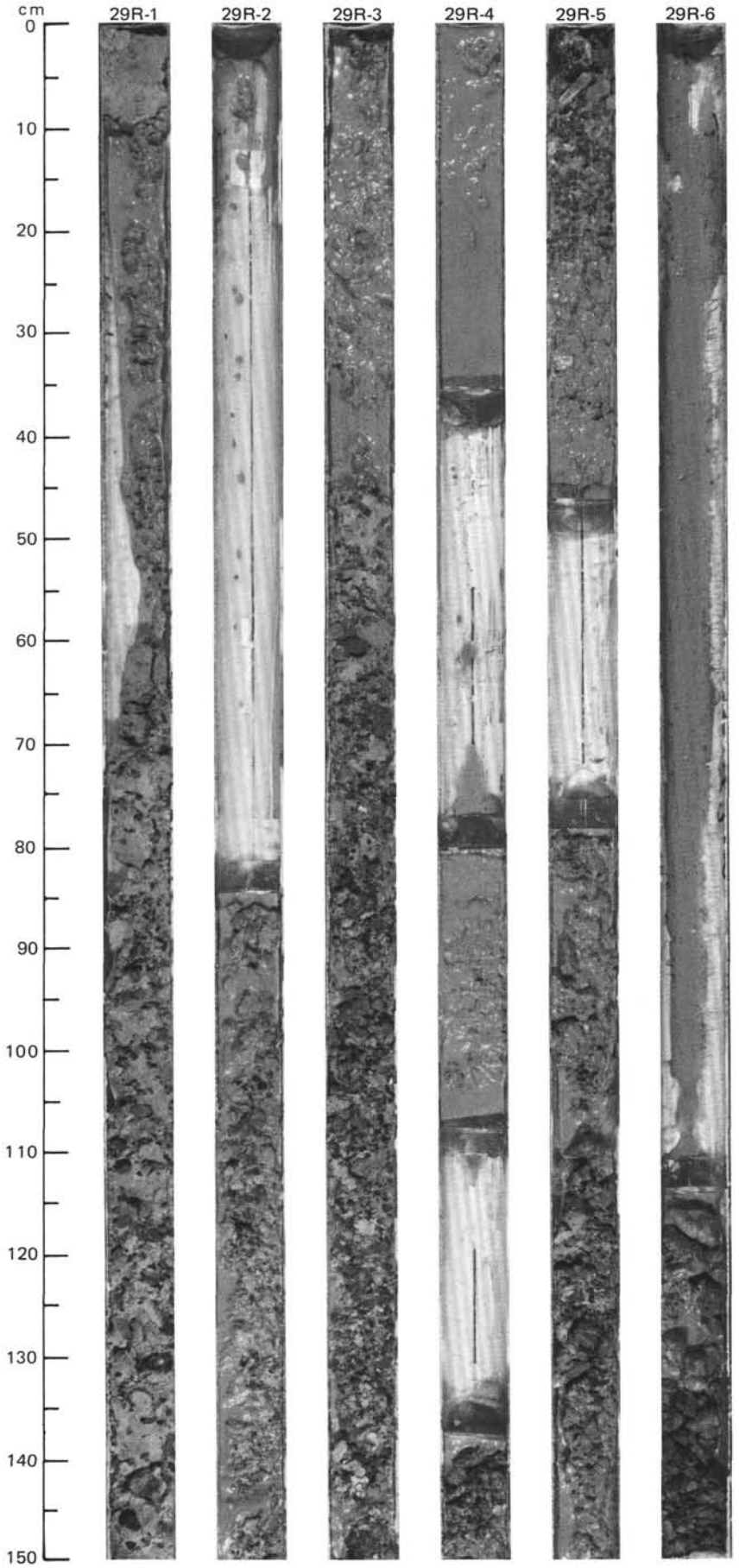
cm
29R-1
29R-2
29R-3
29R-4
29R-5
29R-6
0
10
20
30
40
50
60
70
80
90
100
110
120
130
140
150

SITE 647 HOLE A CORE 30 R CORED INTERVAL 4137.9-4147.5 mbsl; 279.4-289.0 mbsf

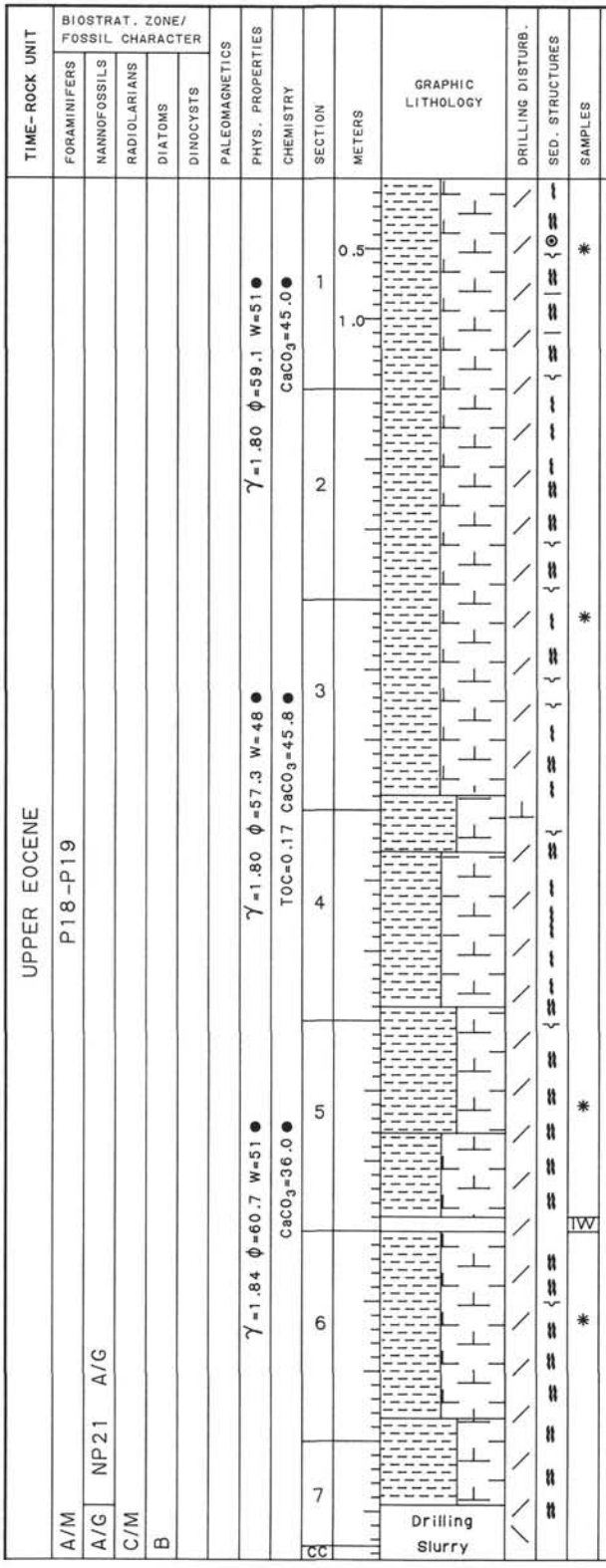

LITHOLOGIC DESCRIPTION

CLAYEY NANNOFOSSIL CHALK AND NANNOFOSSIL CLAYSTONE

Clay-bearing nannofossil chalk, light greenish gray (5GY 7/1) and greenish gray (5GY 6/1); and nannofossil claystone, greenish gray (5GY 6/1–5GY 5/1). Bioturbation is mainly moderate with grayish green (10GY 5/2) and gray (5Y 5/1) burrows locally containing opaque minerals. Large burrows like *Zoophycos*, *Planolites* and halo burrows are widely present. Microfaults seem to have been produced by drilling disturbance.

Minor lithology: Section 1, 50–52 cm: light gray (5Y 7/1) chalk layer with gradational contacts, composed dominantly of authigenic carbonate.

SMEAR SLIDE SUMMARY (%):

	1, 52 M	3, 15 D	5, 52 D	6, 58 M
TEXTURE:				
Silt	20	55	50	60
Clay	80	45	50	40
COMPOSITION:				
Quartz	—	—	5	—
Clay	10	45	50	40
Cement/micrite	70	—	—	—
Pyrite	-	—	—	5
Nannofossils	20	55	45	55

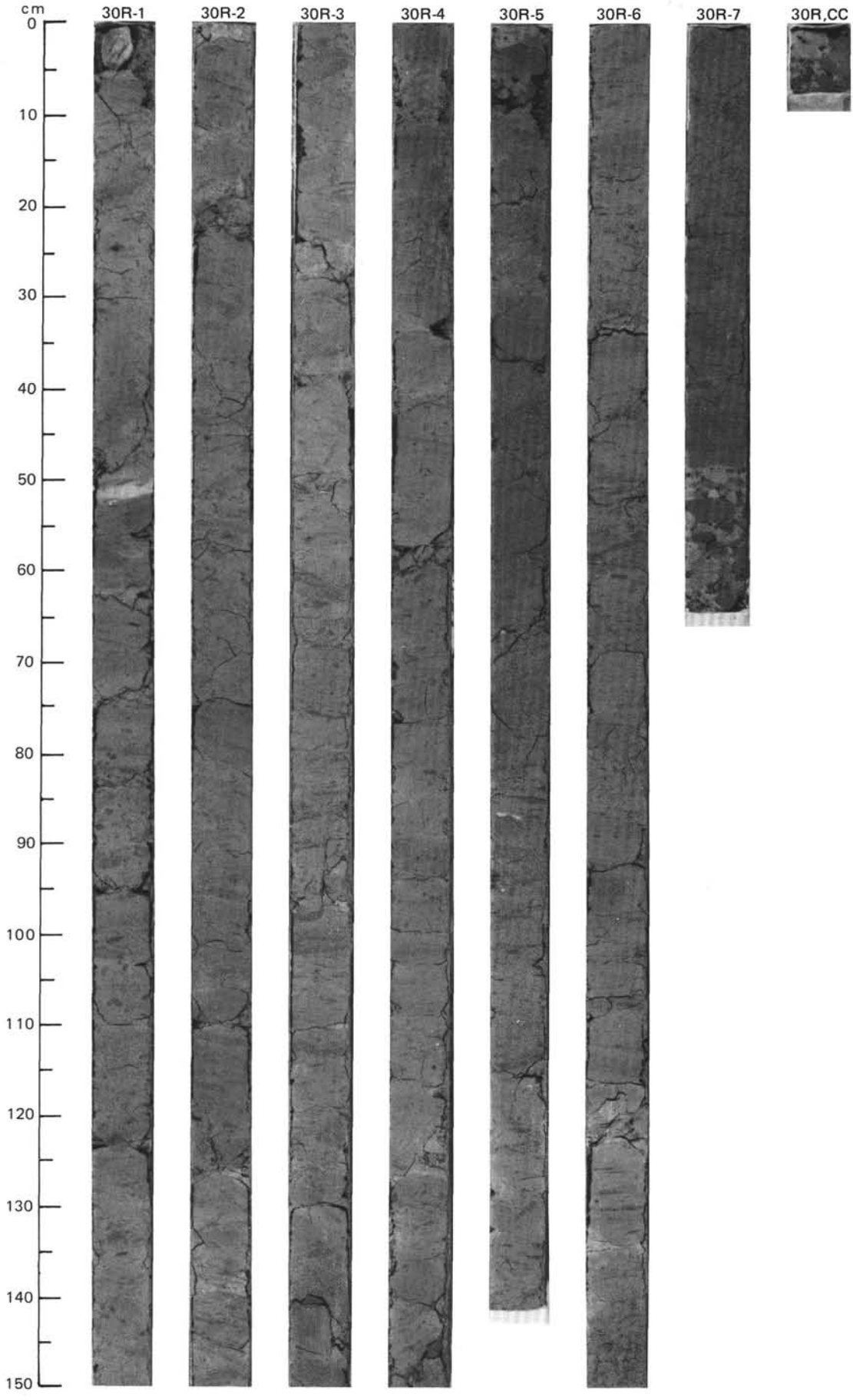
cm
0
10
20
30
40
50
60
70
80
90
100
110
120
130
140
150
30R-1
30R-2
30R-3
30R-4
30R-5
30R-6
30R-7
30R,CC

SITE 647 HOLE A CORE 31 R CORED INTERVAL 4147.5-4157.1 mbsl; 289.0-298.6 mbsf

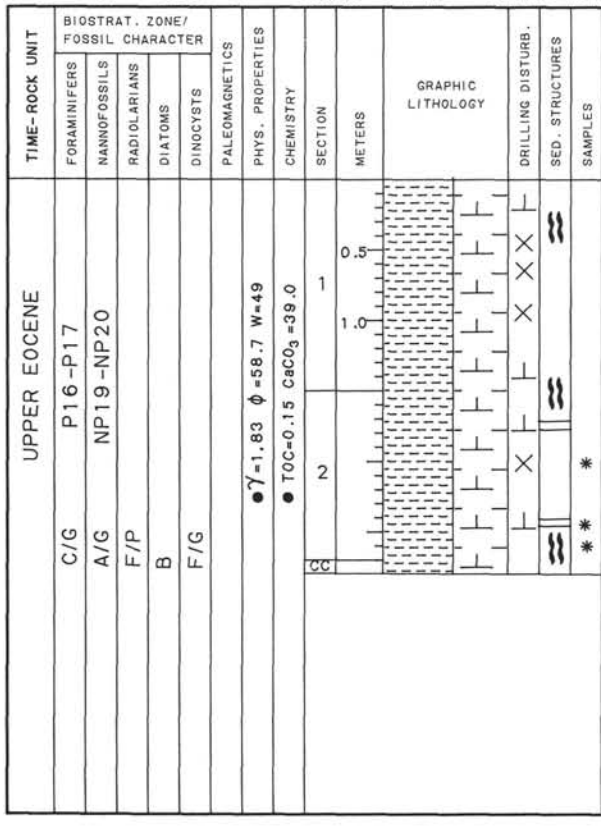

LITHOLOGIC DESCRIPTION

NANNOFOSSIL CLAYSTONE

Nannofossil claystone, lighter and darker shades of grayish green (5GY 6/1 and 5GY 5/1 respectively); shade appears to follow content of pyrite and varies on scale of about 50–100 cm. Sediment is moderately bioturbated with burrows depicted in shades of gray (5Y 5/1) to grayish green (5G 5/2) and dominantly horizontal to subhorizontal. Sediment appears to contain relict laminae or banding.

Minor lithology: Section 2, 100–116 cm: three white layers or pockets (about 3–5 mm thick) of dolomite.

SMEAR SLIDE SUMMARY (%):

	2, 62 D	2, 105 M	2, 111 D
TEXTURE:			
Sand	2	—	—
Silt	47	100	50
Clay	51	—	50
COMPOSITION:			
Mica	2	—	—
Clay	51	—	50
Calcite/dolomite	—	100	—
Accessory minerals	Tr	—	—
Opaque minerals	2	—	5
Foraminifers	Tr	—	—
Nannofossils	45	—	45

SITE 647 HOLE A CORE 32 R CORED INTERVAL 4157.1-4166.8 mbsl; 298.6-308.3 mbsf

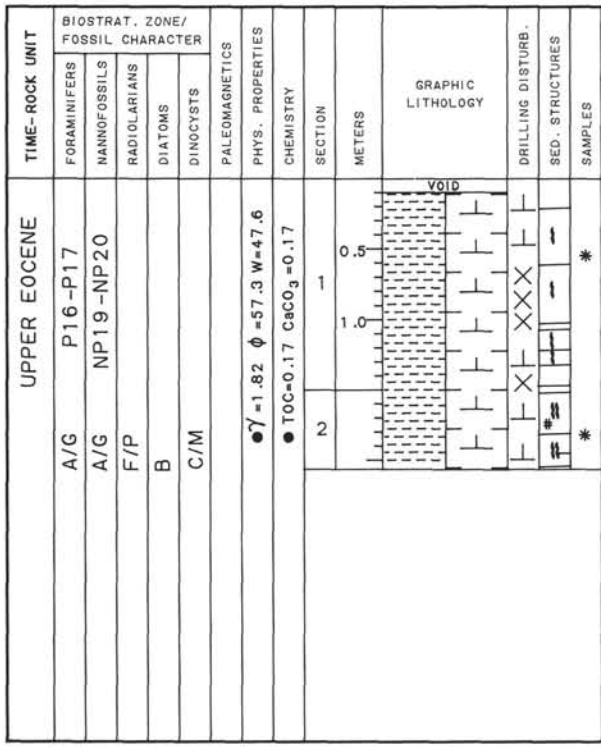

LITHOLOGIC DESCRIPTION

CLAYEY NANNOFOSSIL CHALK AND NANNOFOSSIL CLAYSTONE

Interlayered clay-bearing nannofossil chalk, greenish gray (5GY 5/1); and nannofossil claystone, olive gray (5Y 4/2). Parts of sediment are homogeneous, locally bioturbated; others contain thin numerous laminae of different colors. These may be caused by burrowing (horizontal rimmed burrows) rather than by primary lamination.

SMEAR SLIDE SUMMARY (%):

	1, 64 D	2, 32 D
TEXTURE:		
Silt	60	50
Clay	40	50
COMPOSITION:		
Quartz	1	1
Mica	1	—
Clay	40	47
Accessory minerals	—	1
Pyrite	1	1
Foraminifers	1	2
Nannofossils	55	48
Diatoms	Tr	Tr
Sponge spicules	1	Tr

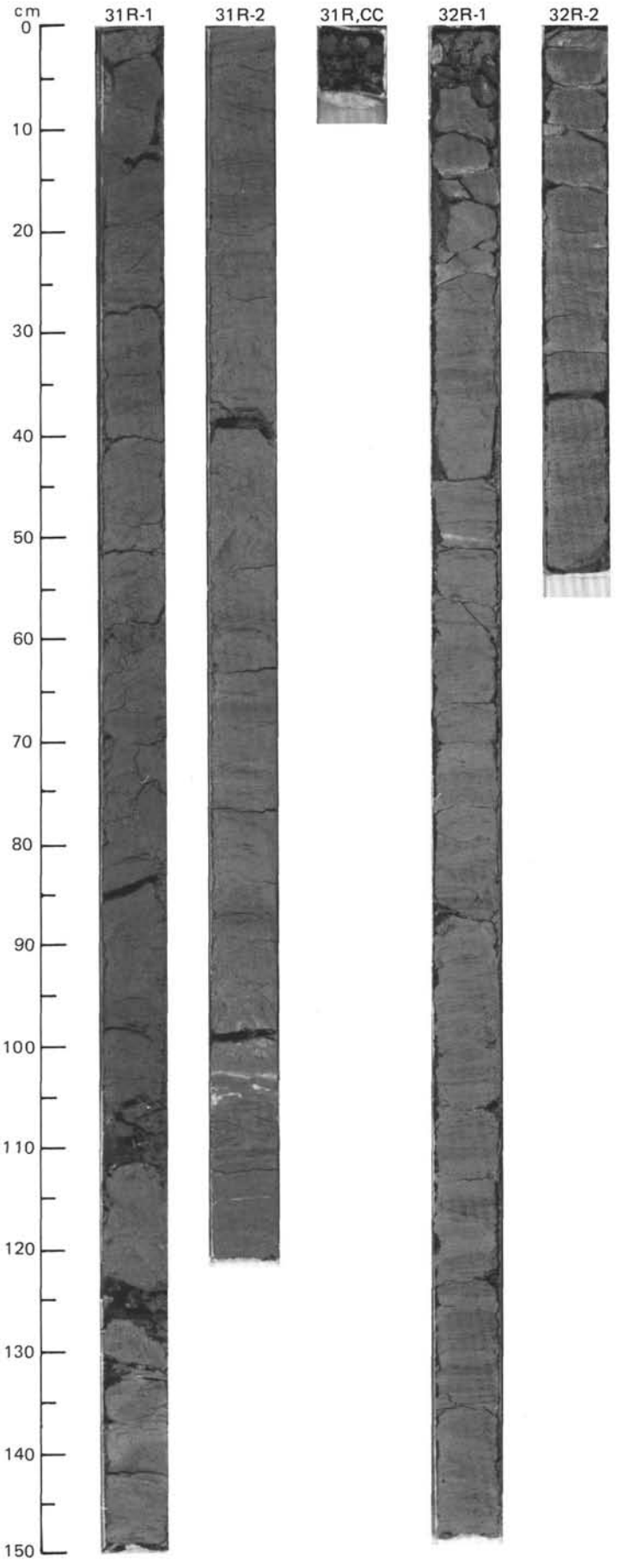
cm
31R-1
31R-2
31R,CC
32R-1
32R-2
0
10
20
30
40
50
60
70
80
90
100
110
120
130
140
150

SITE 647 HOLE A CORE 33 R CORED INTERVAL 4166.8-4176.5 mbsl; 308.3-318.0 mbsf

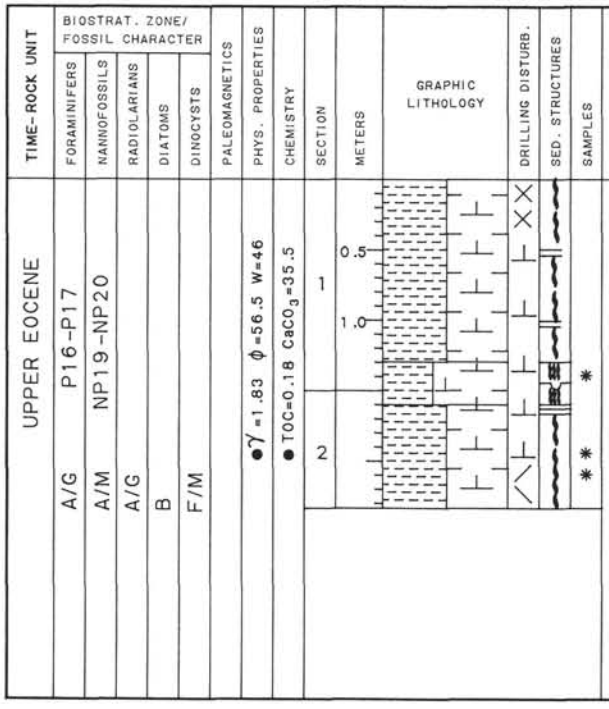

LITHOLOGIC DESCRIPTION

NANNOFOSSIL CLAYSTONE AND CLAYEY NANNOFOSSIL CHALK

Nannofossil claystone, gray to light gray (5Y 6/1) and gray (5Y 5/1); slightly bioturbated with mostly subhorizontal burrows and few poorly defined laminae. One distinct 30-cm-thick bed of light gray (5Y 7/1) clayey nannofossil chalk is intercalated. This sediment is strongly bioturbated and has sharp upper and lower contacts. Below it is a laminated interval of approximately 3 cm.

SMEAR SLIDE SUMMARY (%):

	1, 133 D	2, 48 D	2, 58 M
TEXTURE:			
Silt	63	52	49
Clay	37	48	51
COMPOSITION:			
Clay	37	48	51
Opaque minerals	1	1	1
Foraminifers	—	—	Tr
Nannofossils	60	48	44
Diatoms	2	2	2

SITE 647 HOLE A CORE 34 R CORED INTERVAL 4176.5- 4186.1 mbsl; 318.0-327.6 mbsf

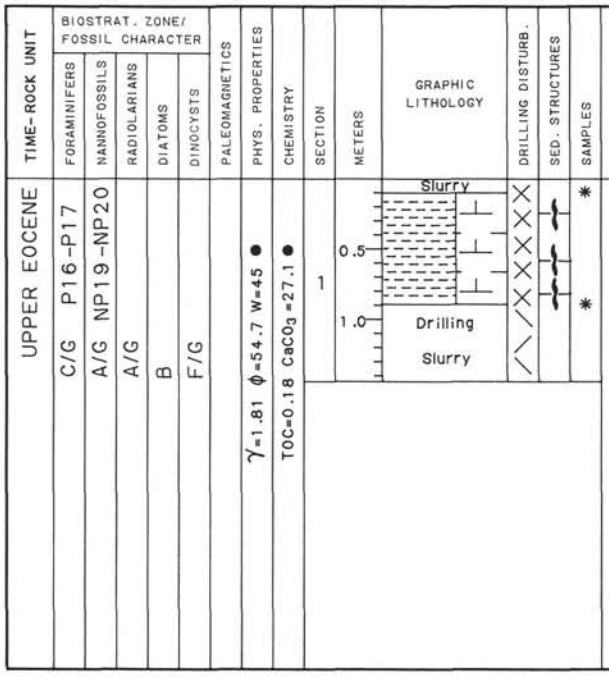

LITHOLOGIC DESCRIPTION

NANNOFOSSIL CLAYSTONE

Nannofossil claystone, greenish gray and olive gray (5GY 5/1, 5Y 5/2). The small amount of undisturbed sediment, as drilling biscuits, shows moderate bioturbation in horizontal narrow burrows, giving a laminated aspect to the sediment.

SMEAR SLIDE SUMMARY (%):

	1, 11 D	1, 83 D
TEXTURE:		
Silt	51	54
Clay	49	46
COMPOSITION:		
Quartz	—	2
Clay	49	46
Pyrite	1	2
Nannofossils	47	50
Diatoms	3	—

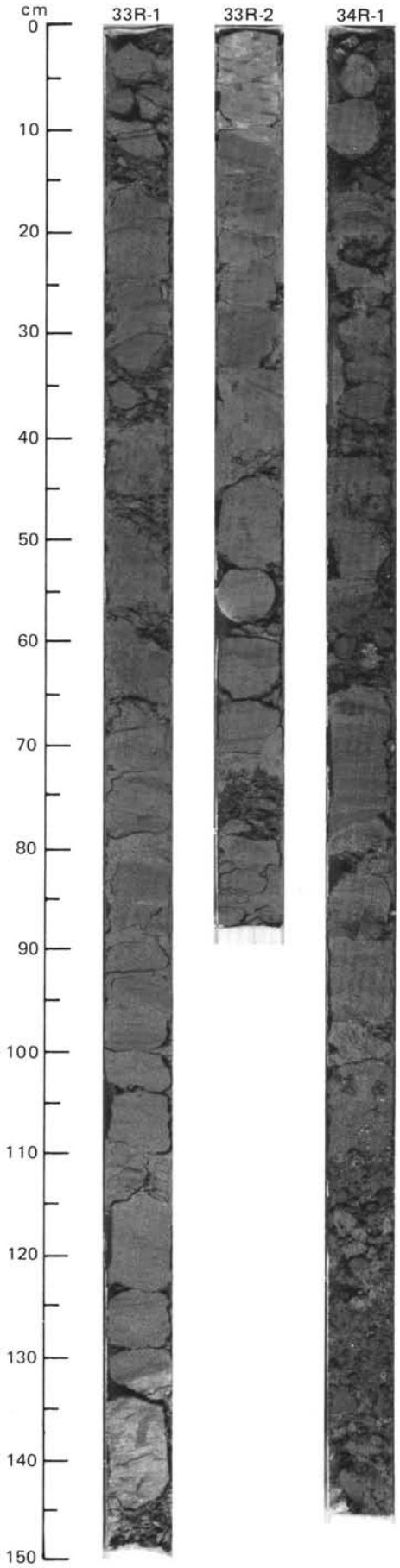
cm
33R-1
33R-2
34R-1
0
10
20
30
40
50
60
70
80
90
100
110
120
130
140
150

SITE 647 HOLE A CORE 35 R CORED INTERVAL 4186.1-4195.7 mbsl; 327.6-337.2 mbsf

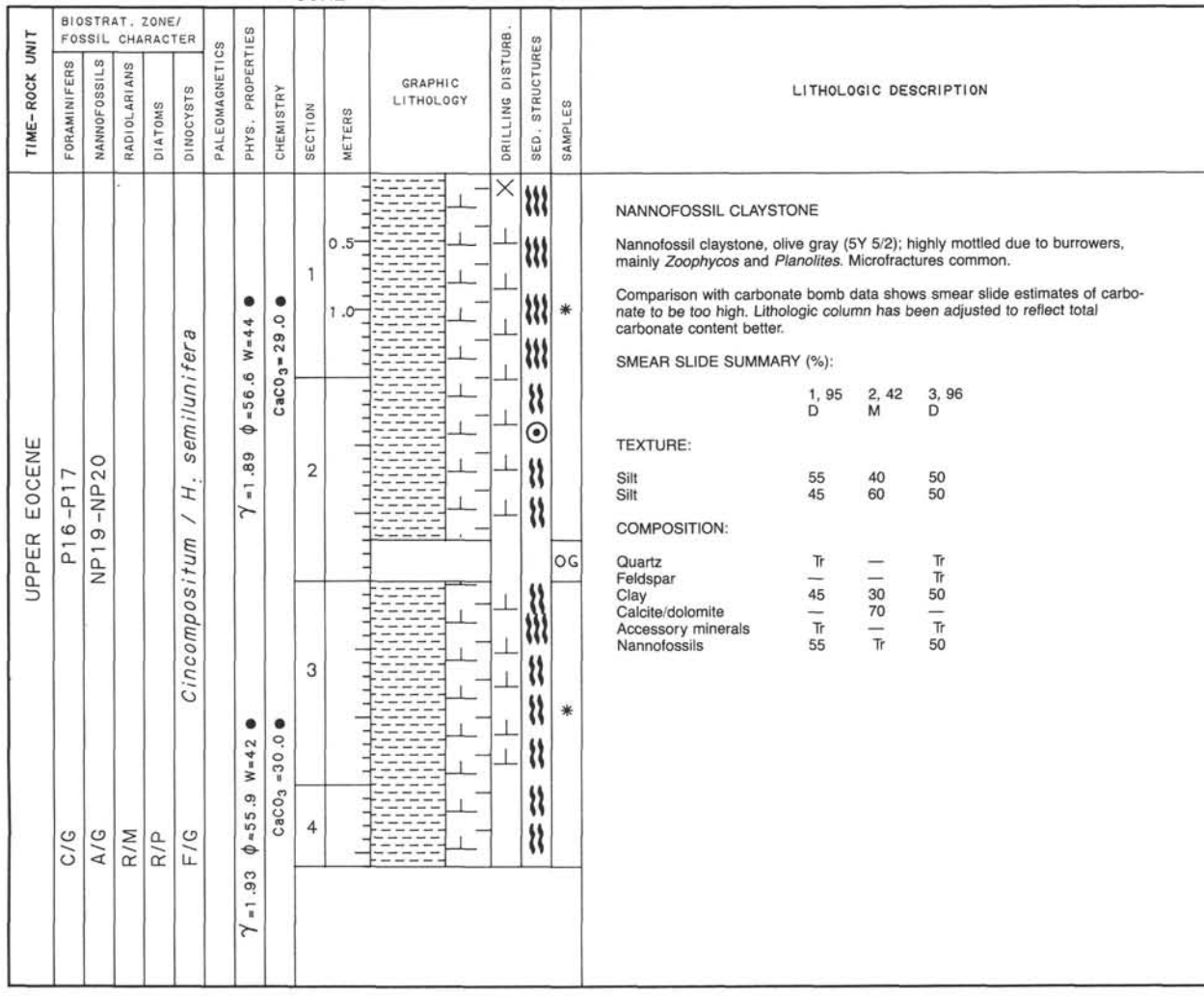

NANNOFOSSIL CLAYSTONE

Nannofossil claystone, olive gray (5Y 5/2); highly mottled due to burrowers, mainly *Zoophycos* and *Planolites*. Microfractures common.

Comparison with carbonate bomb data shows smear slide estimates of carbonate to be too high. *Lithologic column has been adjusted to reflect* total carbonate content better.

SMEAR SLIDE SUMMARY (%):

	1, 95 D	2, 42 M	3, 96 D
TEXTURE:			
Silt	55	40	50
Silt	45	60	50
COMPOSITION:			
Quartz	Tr	—	Tr
Feldspar	—	—	Tr
Clay	45	30	50
Calcite/dolomite	—	70	—
Accessory minerals	Tr	—	Tr
Nannofossils	55	Tr	50

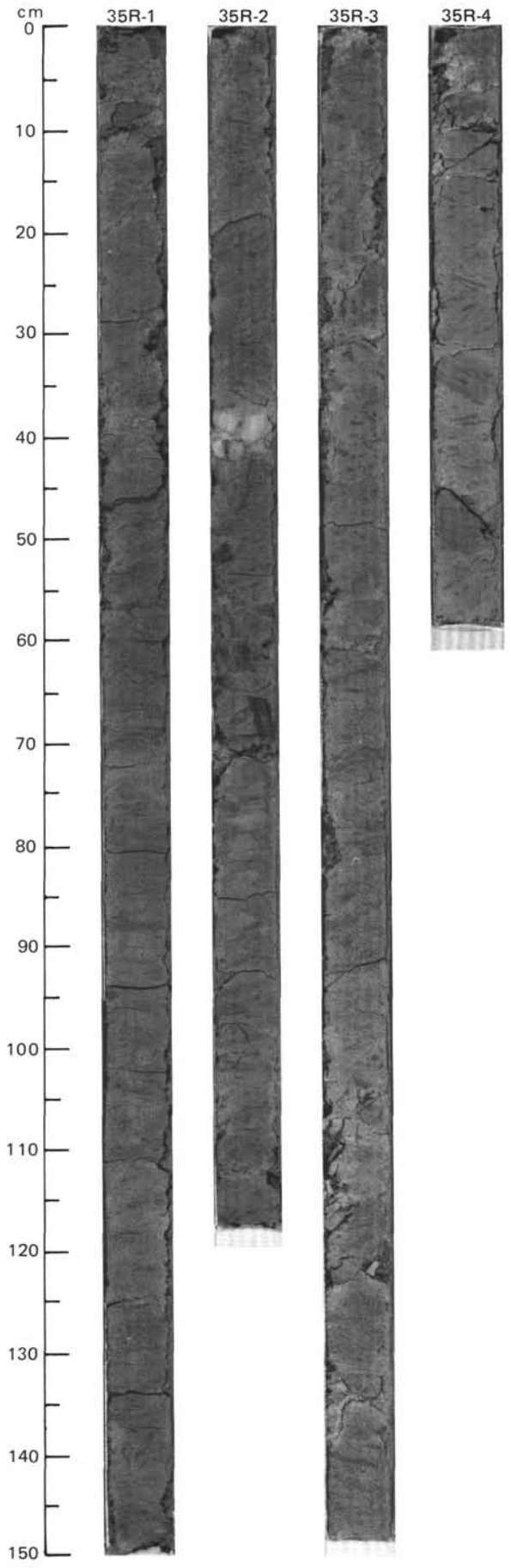
cm
35R-1
35R-2
35R-3
35R-4
0
10
20
30
40
50
60
70
80
90
100
110
120
130
140
150

SITE 647 HOLE A CORE 36 R CORED INTERVAL 41957-4205.2 mbsl; 337.2-346.7 mbsf

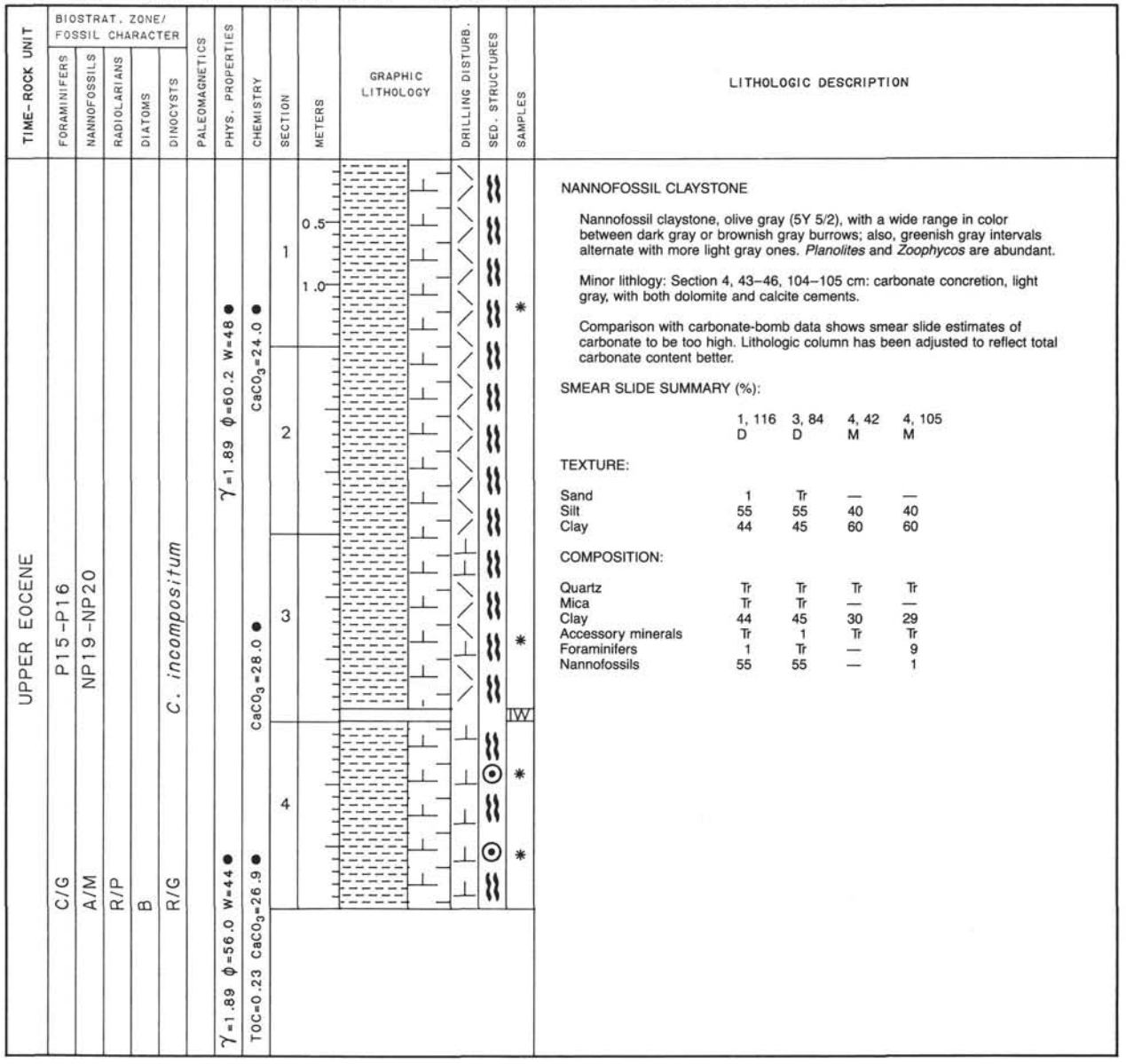

NANNOFOSSIL CLAYSTONE

Nannofossil claystone, olive gray (5Y 5/2), with a wide range in color between dark gray or brownish gray burrows; also, greenish gray intervals alternate with more light gray ones. *Planolites* and *Zoophycos* are abundant.

Minor lithlogy: Section 4, 43–46, 104–105 cm: carbonate concretion, light gray, with both dolomite and calcite cements.

Comparison with carbonate-bomb data shows smear slide estimates of carbonate to be too high. Lithologic column has been adjusted to reflect total carbonate content better.

SMEAR SLIDE SUMMARY (%):

	1, 116 D	3, 84 D	4, 42 M	4, 105 M
TEXTURE:				
Sand	1	Tr	—	—
Silt	55	55	40	40
Clay	44	45	60	60
COMPOSITION:				
Quartz	Tr	Tr	Tr	Tr
Mica	Tr	Tr	—	—
Clay	44	45	30	29
Accessory minerals	Tr	1	Tr	Tr
Foraminifers	1	Tr	—	9
Nannofossils	55	55	—	1

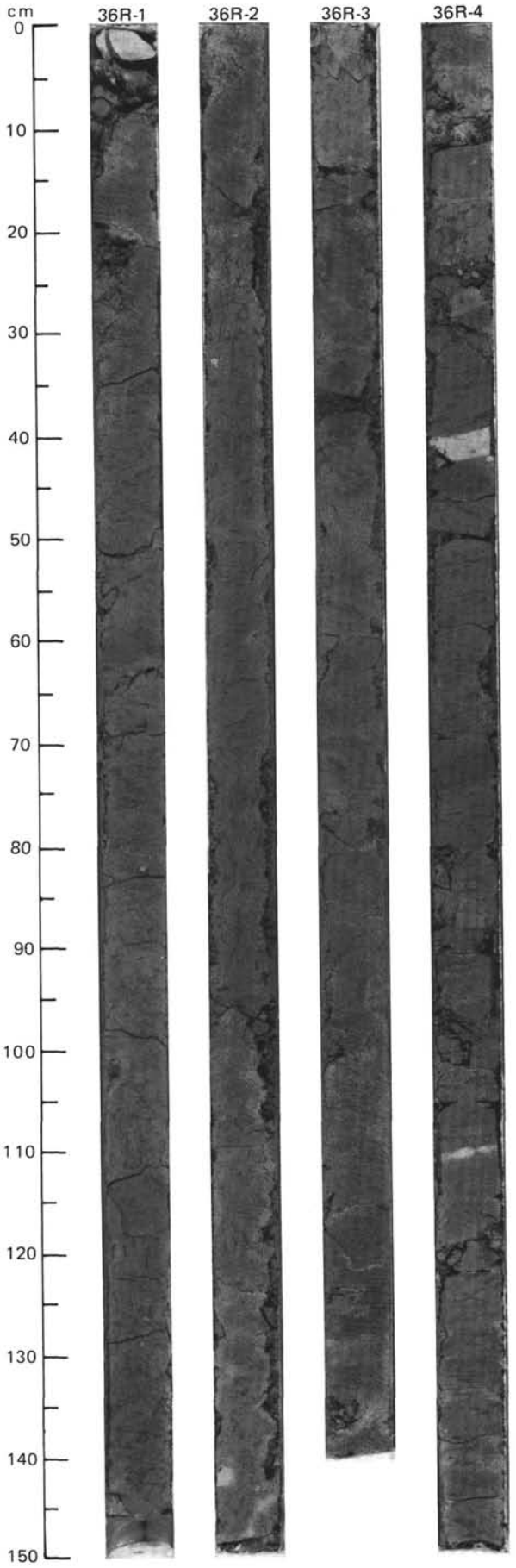
cm
36R-1
36R-2
36R-3
36R-4
0
10
20
30
40
50
60
70
80
90
100
110
120
130
140
150

SITE 647 HOLE A CORE 37 R CORED INTERVAL 4205.2-4214.9 mbsl; 346.7-356.4 mbsf

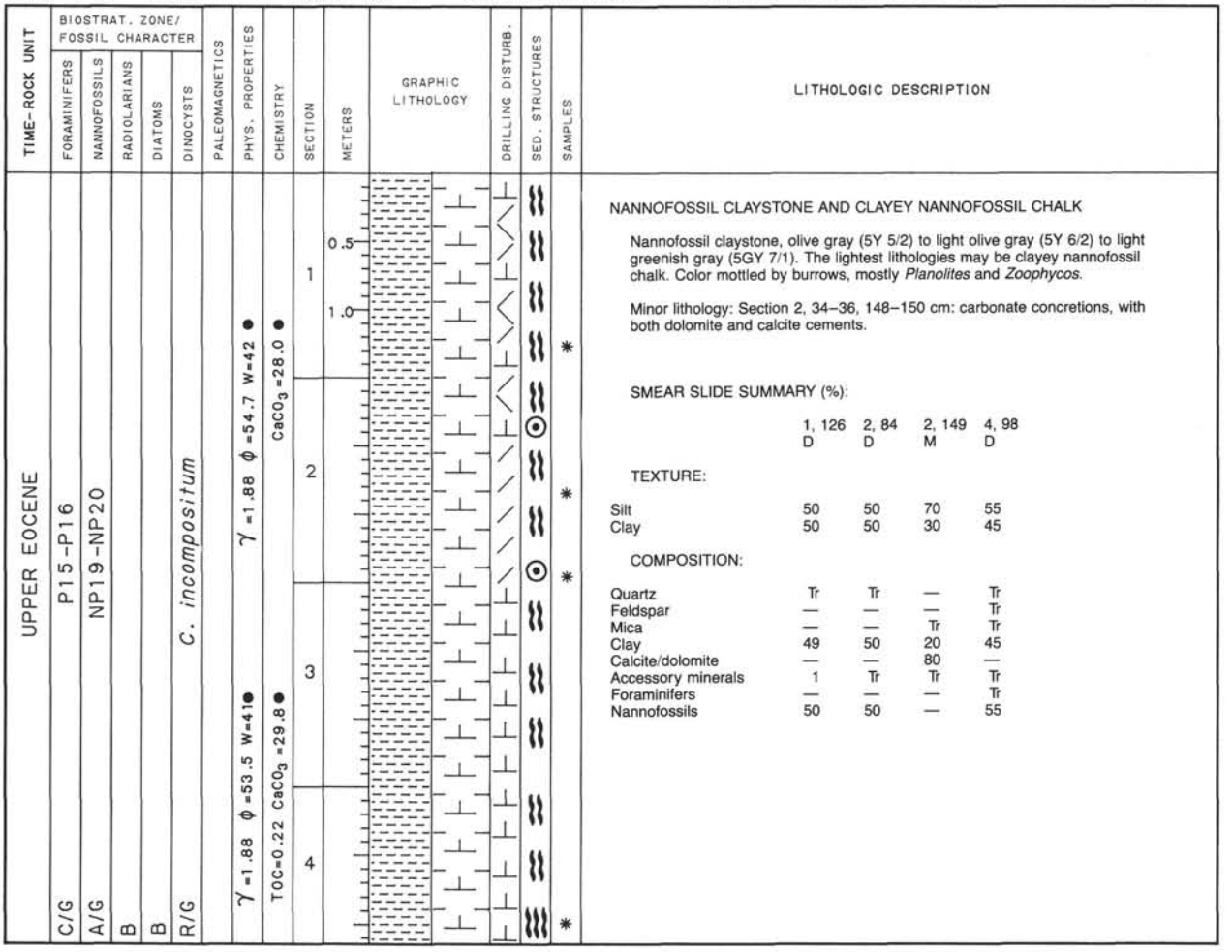

NANNOFOSSIL CLAYSTONE AND CLAYEY NANNOFOSSIL CHALK

Nannofossil claystone, olive gray (5Y 5/2) to light olive gray (5Y 6/2) to light greenish gray (5GY 7/1). The lightest lithologies may be clayey nannofossil chalk. Color mottled by burrows, mostly *Planolites* and *Zoophycos*.

Minor lithology: Section 2, 34–36, 148–150 cm: carbonate concretions, with both dolomite and calcite cements.

SMEAR SLIDE SUMMARY (%):

	1, 126 D	2, 84 D	2, 149 M	4, 98 D
TEXTURE:				
Silt	50	50	70	55
Clay	50	50	30	45
COMPOSITION:				
Quartz	Tr	Tr	—	Tr
Feldspar	—	—	—	Tr
Mica	—	—	Tr	Tr
Clay	49	50	20	45
Calcite/dolomite	—	—	80	—
Accessory minerals	1	Tr	Tr	Tr
Foraminifers	—	—	—	Tr
Nannofossils	50	50	—	55

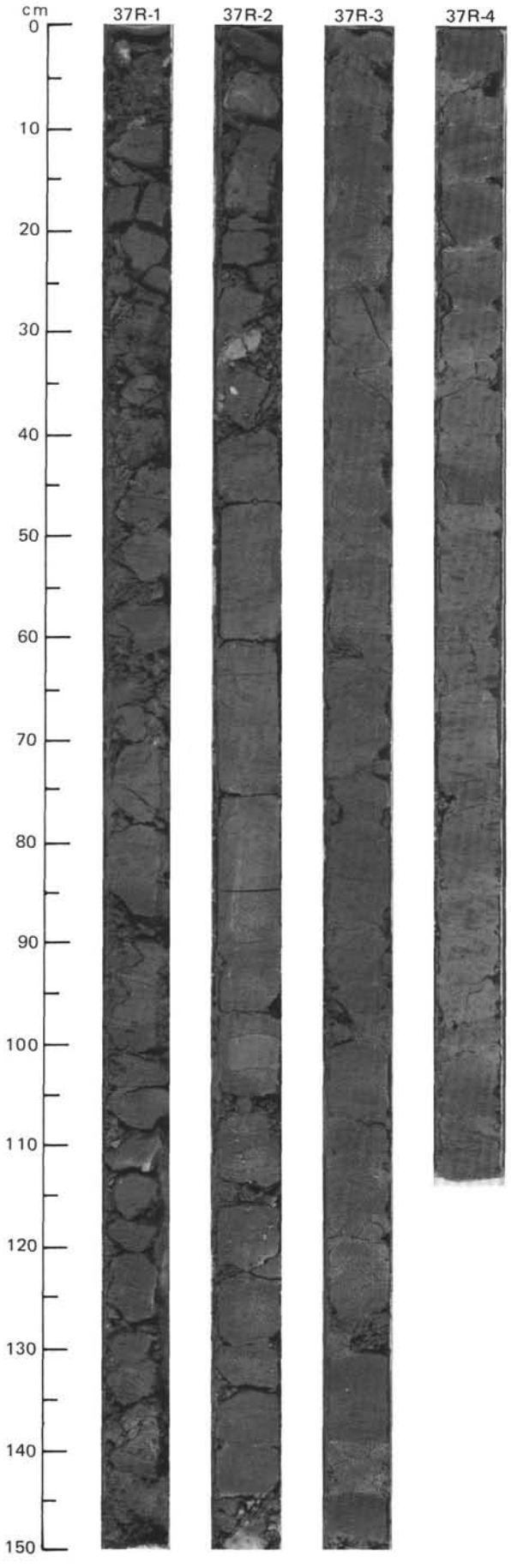
cm
37R-1
37R-2
37R-3
37R-4
0
10
20
30
40
50
60
70
80
90
100
110
120
130
140
150

SITE 647 HOLE A CORE 38 R CORED INTERVAL 4214.9-4224.6 mbsl; 356.4-366.1 mbsf

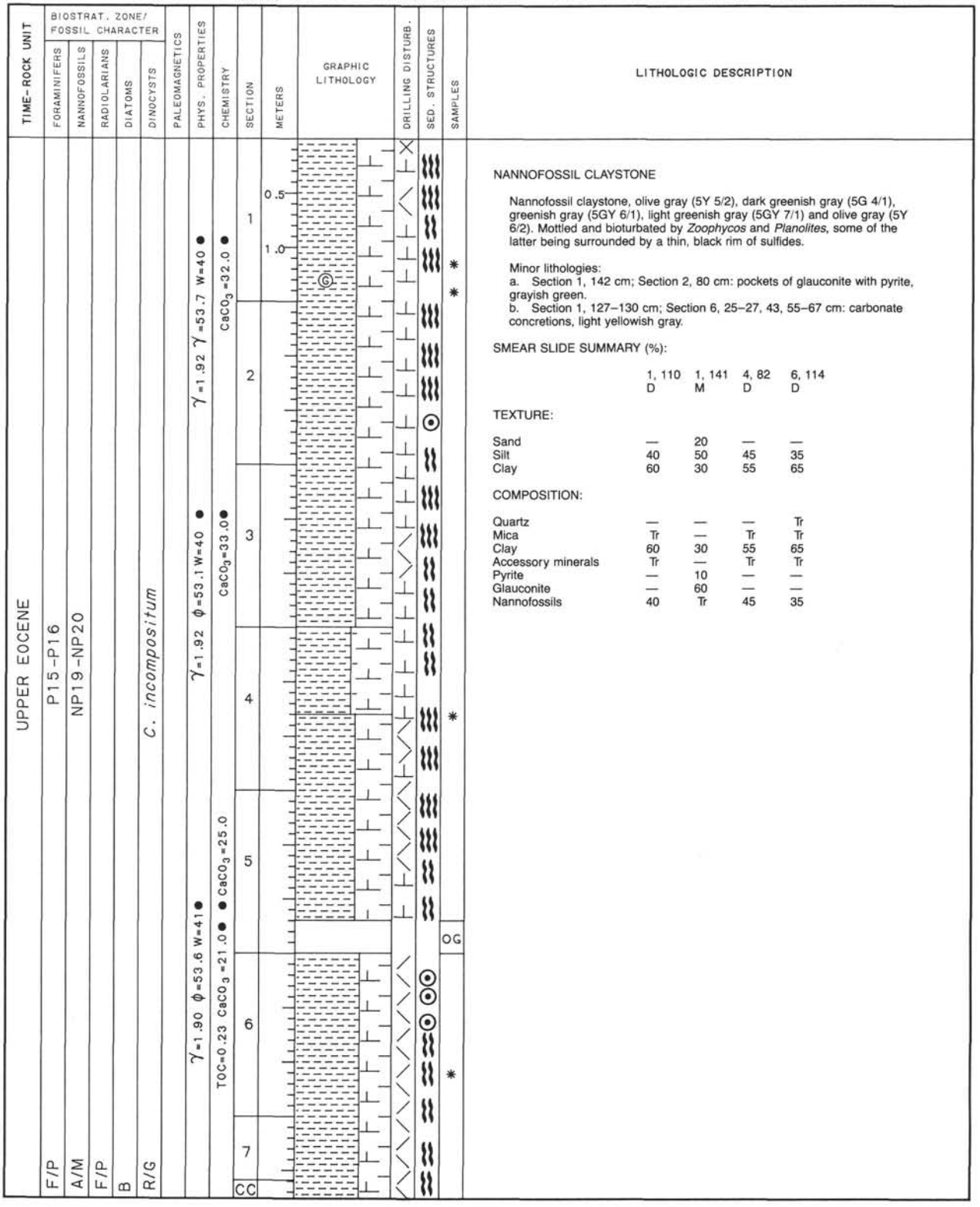

NANNOFOSSIL CLAYSTONE

Nannofossil claystone, olive gray (5Y 5/2), dark greenish gray (5G 4/1), greenish gray (5GY 6/1), light greenish gray (5GY 7/1) and olive gray (5Y 6/2). Mottled and bioturbated by *Zoophycos* and *Planolites*, some of the latter being surrounded by a thin, black rim of sulfides.

Minor lithologies:
a. Section 1, 142 cm; Section 2, 80 cm: pockets of glauconite with pyrite, grayish green.
b. Section 1, 127–130 cm; Section 6, 25–27, 43, 55–67 cm: carbonate concretions, light yellowish gray.

SMEAR SLIDE SUMMARY (%):

	1, 110 D	1, 141 M	4, 82 D	6, 114 D
TEXTURE:				
Sand	—	20	—	—
Silt	40	50	45	35
Clay	60	30	55	65
COMPOSITION:				
Quartz	—	—	—	Tr
Mica	Tr	—	Tr	Tr
Clay	60	30	55	65
Accessory minerals	Tr	—	Tr	Tr
Pyrite	—	10	—	—
Glauconite	—	60	—	—
Nannofossils	40	Tr	45	35

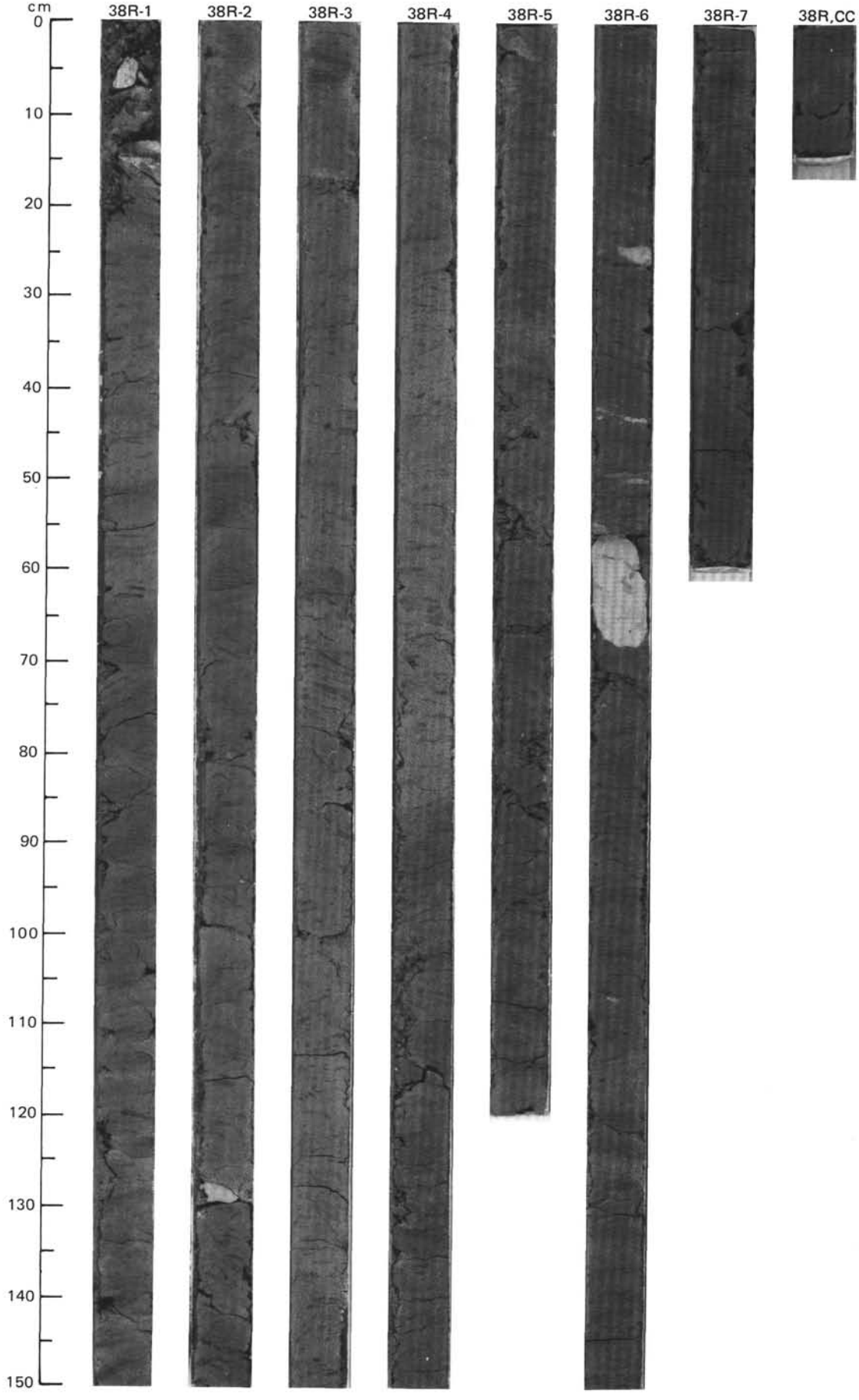
cm
0
10
20
30
40
50
60
70
80
90
100
110
120
130
140
150
38R-1
38R-2
38R-3
38R-4
38R-5
38R-6
38R-7
38R,CC

SITE 647 HOLE A CORE 39 R CORED INTERVAL 4224.6-4234.2 mbsl; 366.1-375.7 mbsf

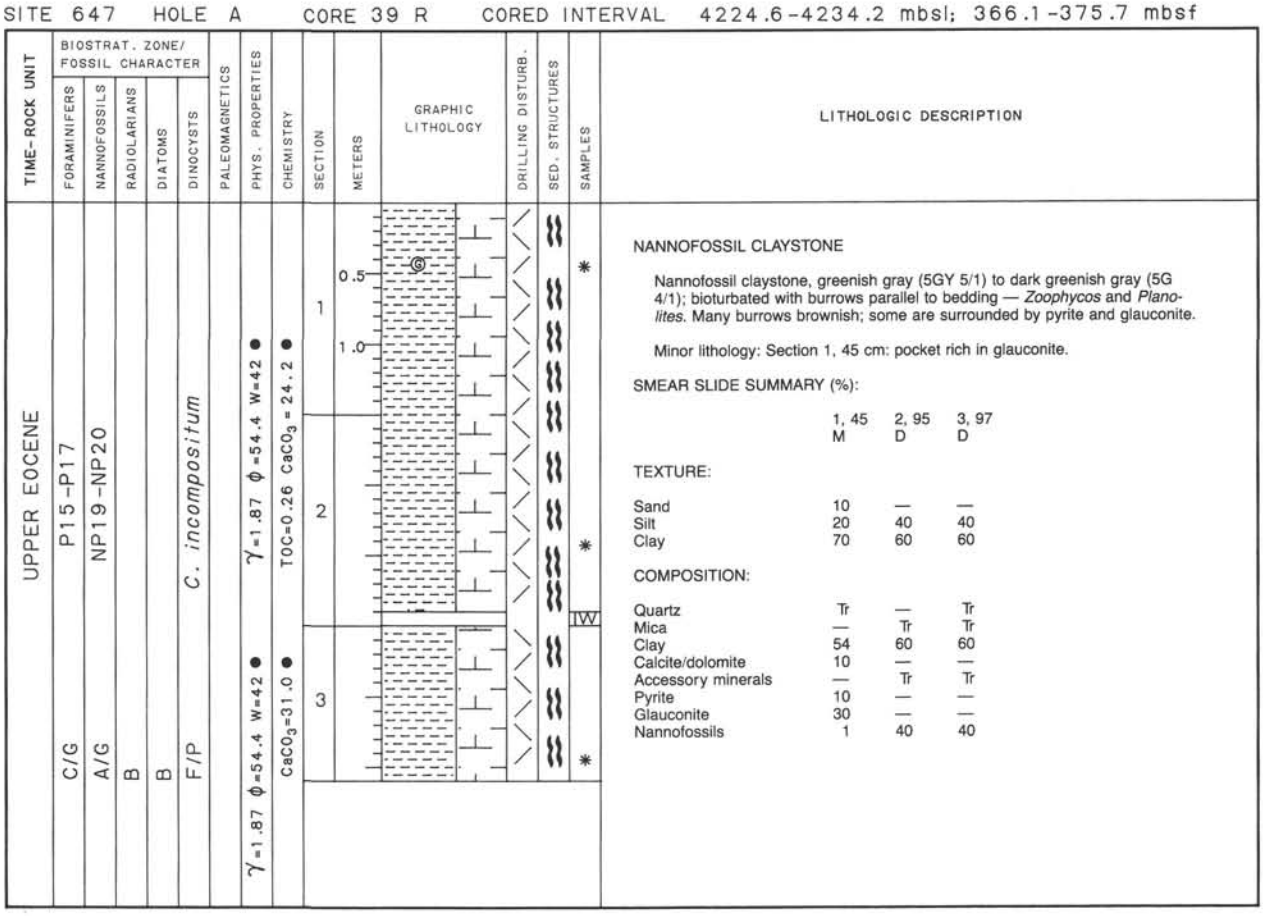

NANNOFOSSIL CLAYSTONE

Nannofossil claystone, greenish gray (5GY 5/1) to dark greenish gray (5G 4/1); bioturbated with burrows parallel to bedding — *Zoophycos* and *Planolites*. Many burrows brownish; some are surrounded by pyrite and glauconite.

Minor lithology: Section 1, 45 cm: pocket rich in glauconite.

SMEAR SLIDE SUMMARY (%):

	1, 45 M	2, 95 D	3, 97 D
TEXTURE:			
Sand	10	—	—
Silt	20	40	40
Clay	70	60	60
COMPOSITION:			
Quartz	Tr	—	Tr
Mica	—	Tr	Tr
Clay	54	60	60
Calcite/dolomite	10	—	—
Accessory minerals	—	Tr	Tr
Pyrite	10	—	—
Glauconite	30	—	—
Nannofossils	1	40	40

SITE 647 HOLE A CORE 40 R CORED INTERVAL 4234.2-4243.9 mbsl; 375.7-385.4 mbsf

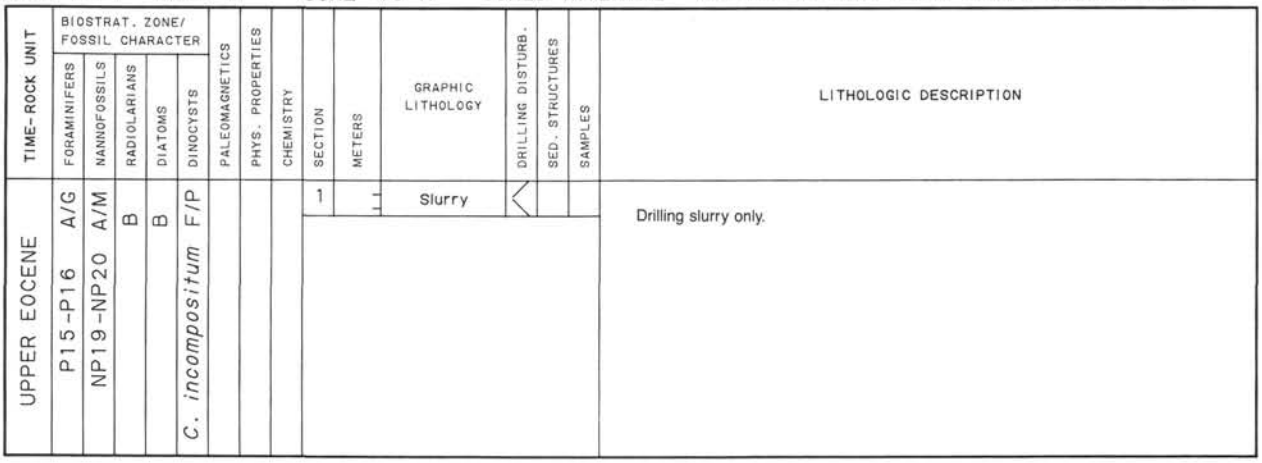

Drilling slurry only.

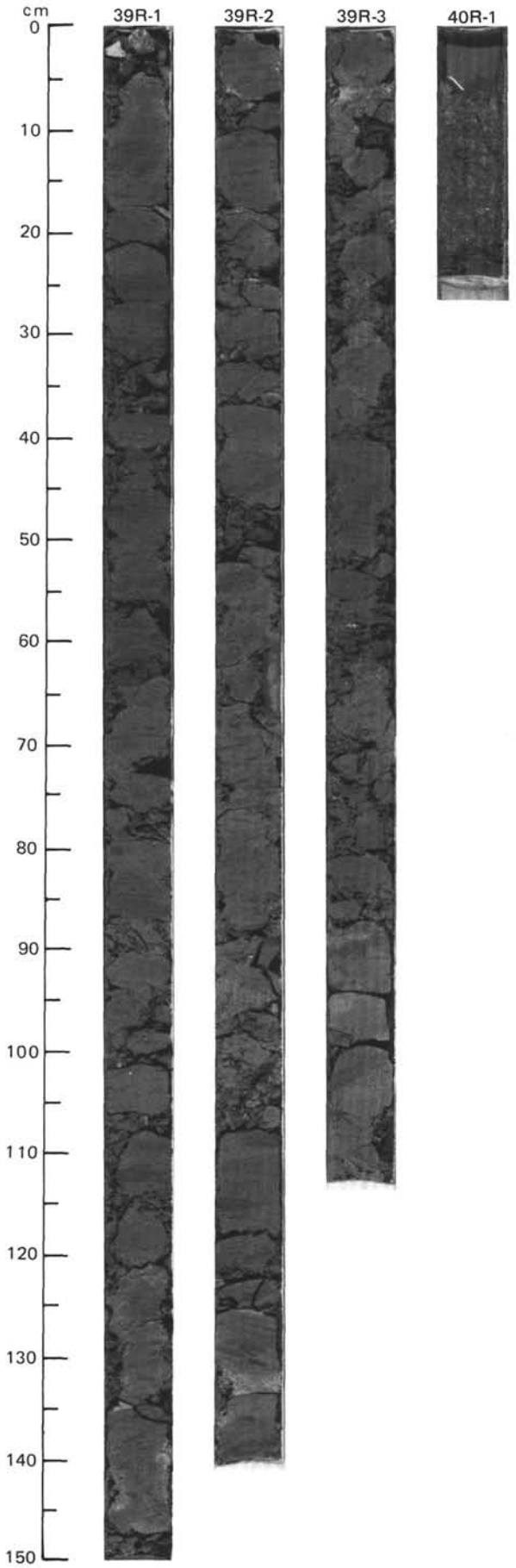
cm
39R-1
39R-2
39R-3
40R-1
0
10
20
30
40
50
60
70
80
90
100
110
120
130
140
150

SITE 647 HOLE A CORE 41 R CORED INTERVAL 4243.9–4253.6 mbsl; 385.4–395.1 mbsf

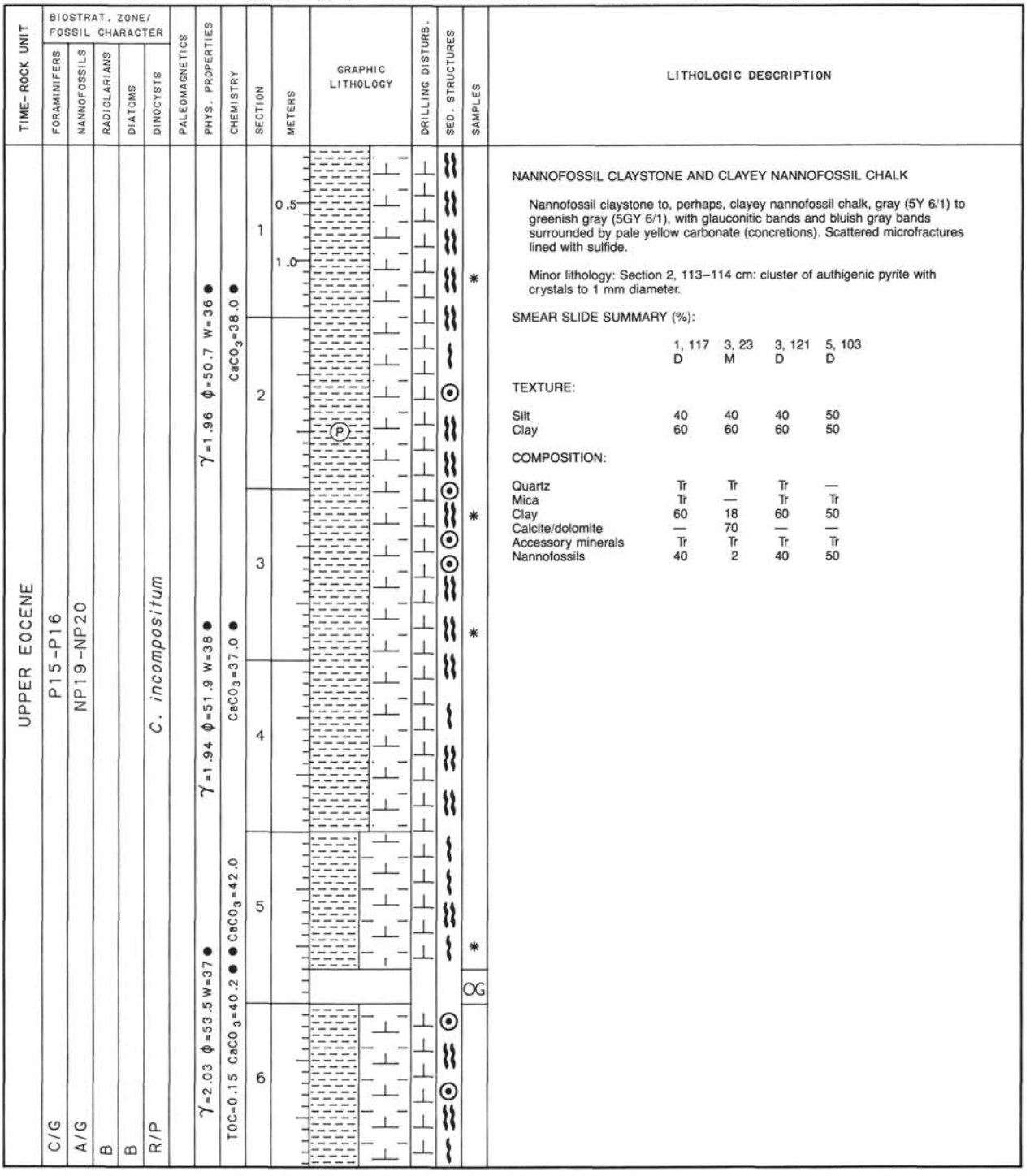

NANNOFOSSIL CLAYSTONE AND CLAYEY NANNOFOSSIL CHALK

Nannofossil claystone to, perhaps, clayey nannofossil chalk, gray (5Y 6/1) to greenish gray (5GY 6/1), with glauconitic bands and bluish gray bands surrounded by pale yellow carbonate (concretions). Scattered microfractures lined with sulfide.

Minor lithology: Section 2, 113–114 cm: cluster of authigenic pyrite with crystals to 1 mm diameter.

SMEAR SLIDE SUMMARY (%):

	1, 117 D	3, 23 M	3, 121 D	5, 103 D
TEXTURE:				
Silt	40	40	40	50
Clay	60	60	60	50
COMPOSITION:				
Quartz	Tr	Tr	Tr	—
Mica	Tr	—	Tr	Tr
Clay	60	18	60	50
Calcite/dolomite	—	70	—	—
Accessory minerals	Tr	Tr	Tr	Tr
Nannofossils	40	2	40	50

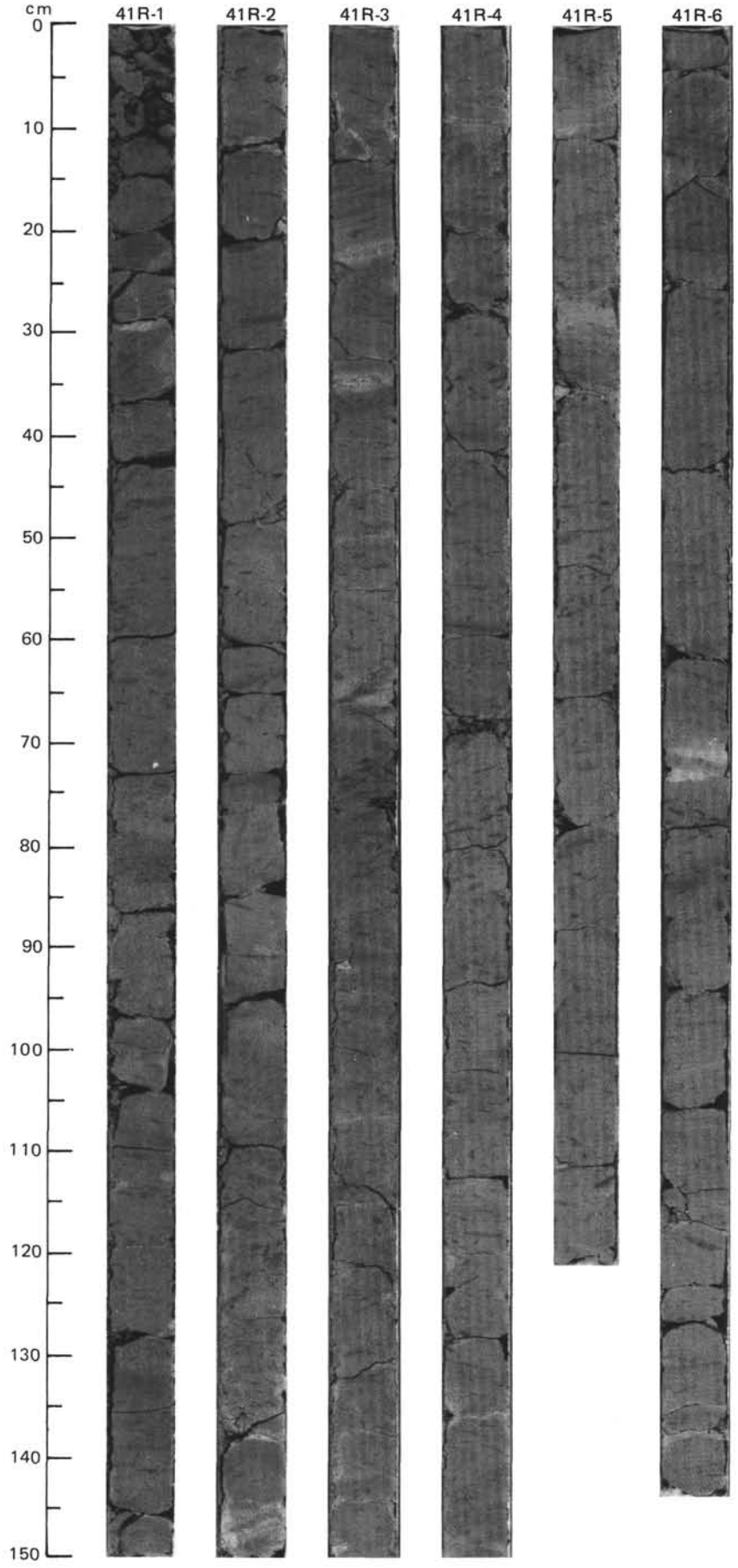
cm
0
10
20
30
40
50
60
70
80
90
100
110
120
130
140
150
41R-1
41R-2
41R-3
41R-4
41R-5
41R-6

SITE 647 HOLE A CORE 42 R CORED INTERVAL 4253.6–4263.3 mbsl; 395.1–404.8 mbsf

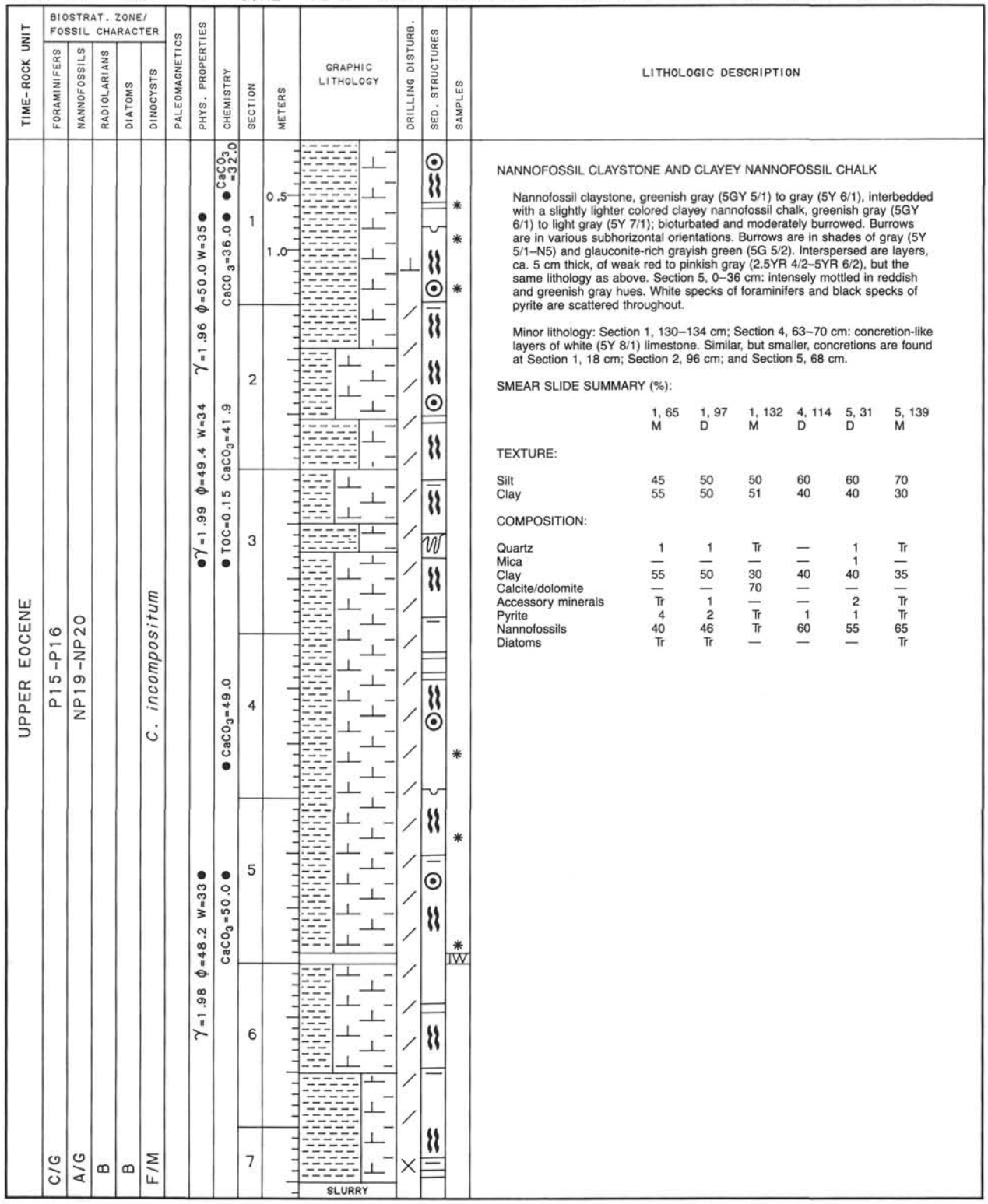

NANNOFOSSIL CLAYSTONE AND CLAYEY NANNOFOSSIL CHALK

Nannofossil claystone, greenish gray (5GY 5/1) to gray (5Y 6/1), interbedded with a slightly lighter colored clayey nannofossil chalk, greenish gray (5GY 6/1) to light gray (5Y 7/1); bioturbated and moderately burrowed. Burrows are in various subhorizontal orientations. Burrows are in shades of gray (5Y 5/1–N5) and glauconite-rich grayish green (5G 5/2). Interspersed are layers, ca. 5 cm thick, of weak red to pinkish gray (2.5YR 4/2–5YR 6/2), but the same lithology as above. Section 5, 0–36 cm: intensely mottled in reddish and greenish gray hues. White specks of foraminifers and black specks of pyrite are scattered throughout.

Minor lithology: Section 1, 130–134 cm; Section 4, 63–70 cm: concretion-like layers of white (5Y 8/1) limestone. Similar, but smaller, concretions are found at Section 1, 18 cm; Section 2, 96 cm; and Section 5, 68 cm.

SMEAR SLIDE SUMMARY (%):

	1, 65 M	1, 97 D	1, 132 M	4, 114 D	5, 31 D	5, 139 M
TEXTURE:						
Silt	45	50	50	60	60	70
Clay	55	50	51	40	40	30
COMPOSITION:						
Quartz	1	1	Tr	—	1	Tr
Mica	—	—	—	—	1	—
Clay	55	50	30	40	40	35
Calcite/dolomite	—	—	70	—	—	—
Accessory minerals	Tr	1	—	—	2	Tr
Pyrite	4	2	Tr	1	1	Tr
Nannofossils	40	46	Tr	60	55	65
Diatoms	Tr	Tr	—	—	—	Tr

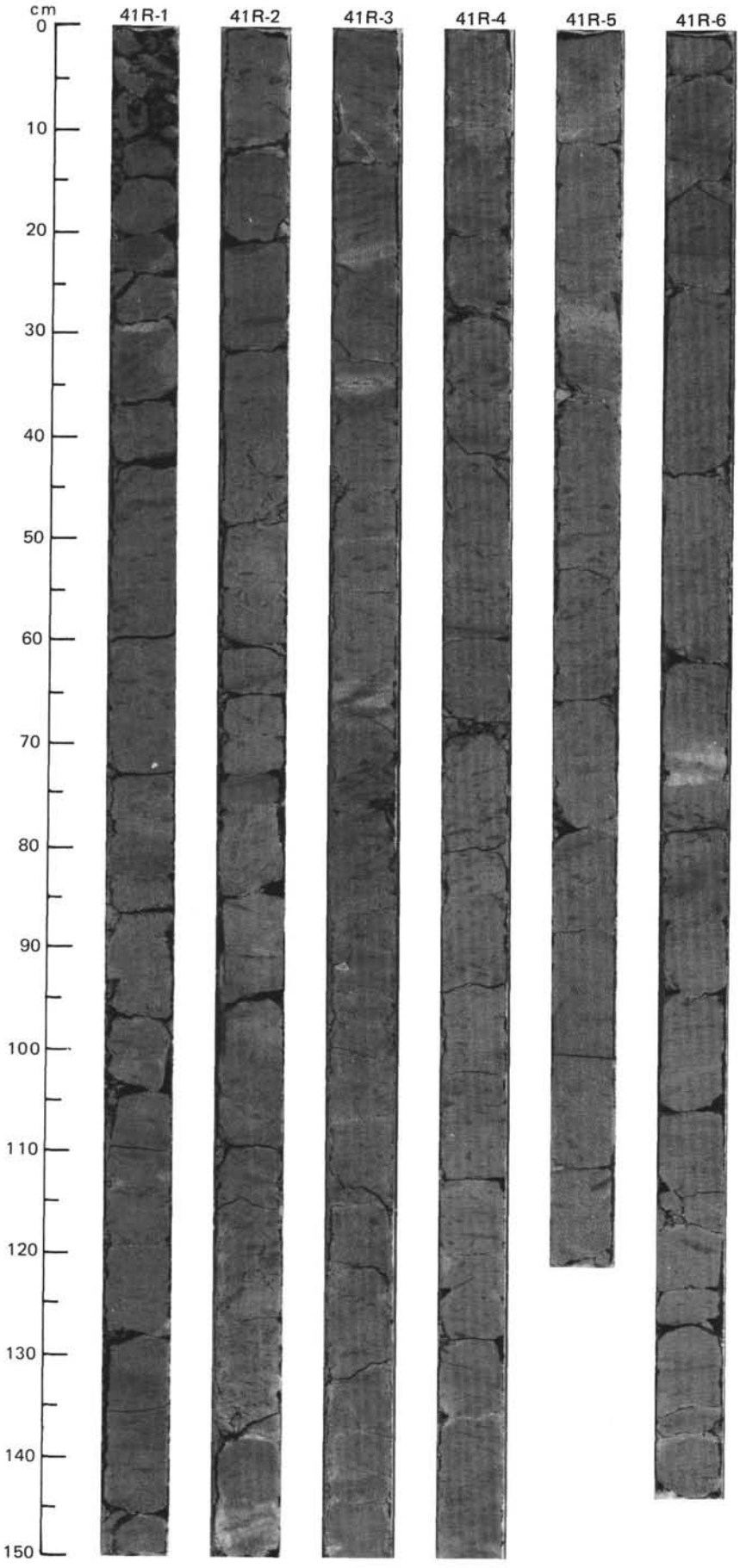
cm
0
10
20
30
40
50
60
70
80
90
100
110
120
130
140
150
41R-1
41R-2
41R-3
41R-4
41R-5
41R-6

SITE 647 HOLE A CORE 42 R CORED INTERVAL 4253.6-4263.3 mbsl; 395.1-404.8 mbsf

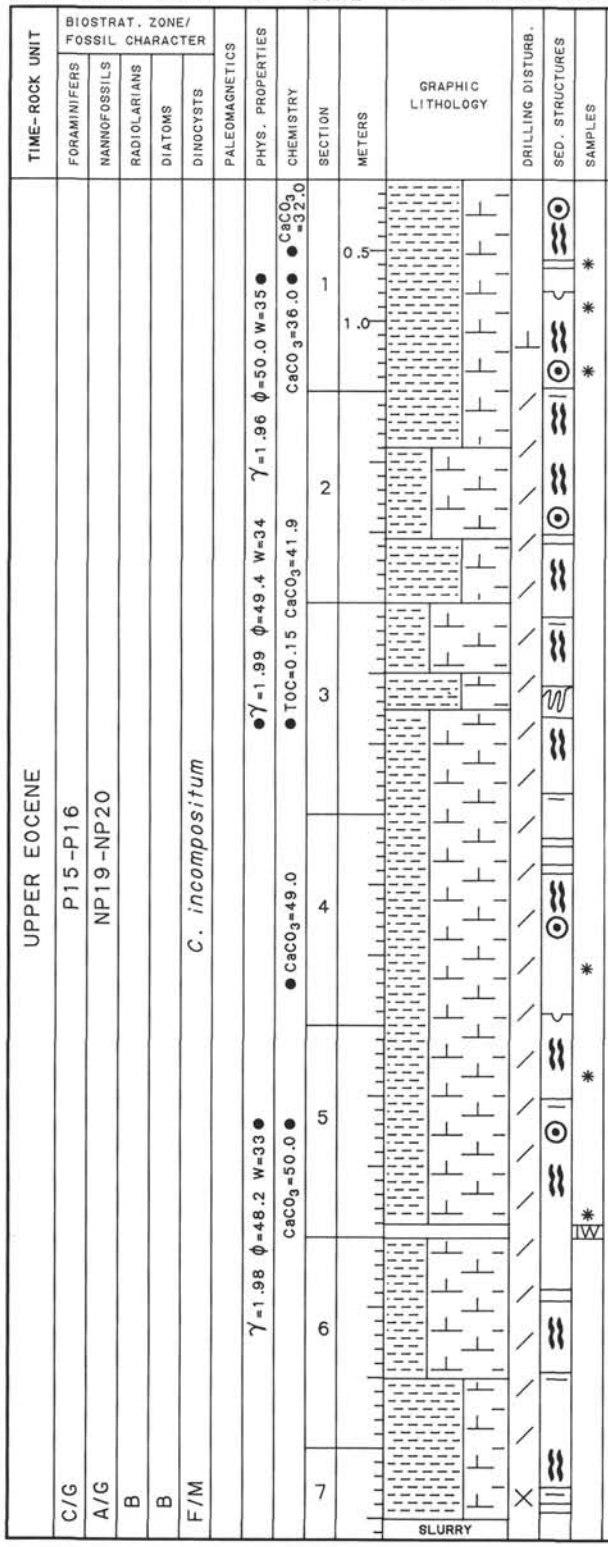

LITHOLOGIC DESCRIPTION

NANNOFOSSIL CLAYSTONE AND CLAYEY NANNOFOSSIL CHALK

Nannofossil claystone, greenish gray (5GY 5/1) to gray (5Y 6/1), interbedded with a slightly lighter colored clayey nannofossil chalk, greenish gray (5GY 6/1) to light gray (5Y 7/1); bioturbated and moderately burrowed. Burrows are in various subhorizontal orientations. Burrows are in shades of gray (5Y 5/1–N5) and glauconite-rich grayish green (5G 5/2). Interspersed are layers, ca. 5 cm thick, of weak red to pinkish gray (2.5YR 4/2–5YR 6/2), but the same lithology as above. Section 5, 0–36 cm: intensely mottled in reddish and greenish gray hues. White specks of foraminifers and black specks of pyrite are scattered throughout.

Minor lithology: Section 1, 130–134 cm; Section 4, 63–70 cm: concretion-like layers of white (5Y 8/1) limestone. Similar, but smaller, concretions are found at Section 1, 18 cm; Section 2, 96 cm; and Section 5, 68 cm.

SMEAR SLIDE SUMMARY (%):

	1, 65 M	1, 97 D	1, 132 M	4, 114 D	5, 31 D	5, 139 M
TEXTURE:						
Silt	45	50	50	60	60	70
Clay	55	50	51	40	40	30
COMPOSITION:						
Quartz	1	1	Tr	—	1	Tr
Mica	—	—	—	—	1	—
Clay	55	50	30	40	40	35
Calcite/dolomite	—	—	70	—	—	—
Accessory minerals	Tr	1	—	—	2	Tr
Pyrite	4	2	Tr	1	1	Tr
Nannofossils	40	46	Tr	60	55	65
Diatoms	Tr	Tr	—	—	—	Tr

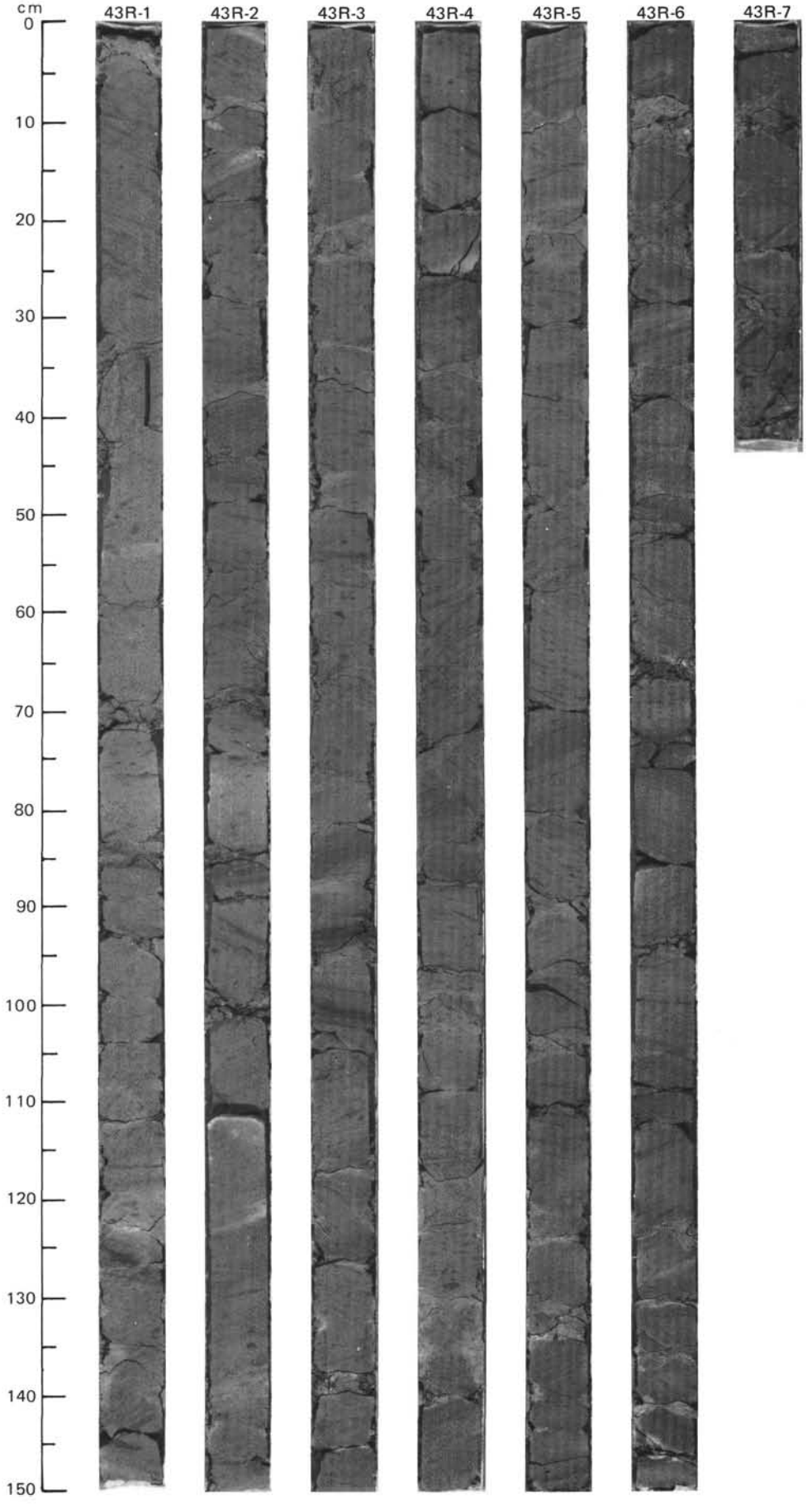
cm
0
10
20
30
40
50
60
70
80
90
100
110
120
130
140
150
43R-1
43R-2
43R-3
43R-4
43R-5
43R-6
43R-7

SITE 647 HOLE A CORE 44 R CORED INTERVAL 4273.0-4282.6 mbsl; 414.5-424.1 mbsf

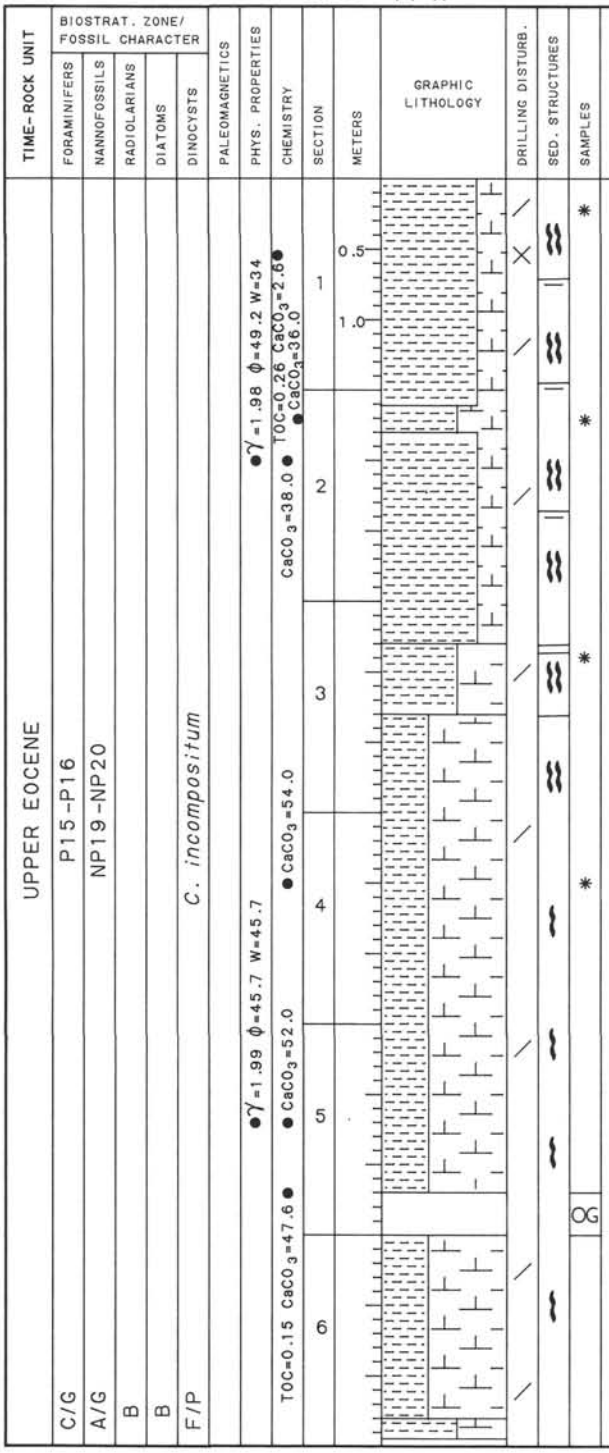

LITHOLOGIC DESCRIPTION

NANNOFOSSIL-BEARING CLAYSTONE, NANNOFOSSIL CLAYSTONE, AND CLAYEY NANNOFOSSIL CHALK

Nannofossil-bearing claystone, dark gray (5Y 4/1), gray (5Y 5/1), and greenish gray (5GY 5/1); interbedded with nannofossil claystone, greenish gray (5GY 6/1); grading downward into clayey nannofossil chalk, light greenish gray (5GY 7/1). Bioturbation is moderate in the upper sections and becomes less intense in the homogeneous chalks. The flattening plane of burrows dips at angles in excess of 10°, but this flattening plane was originally horizontal (i.e., in bedding). The rotation from bedding suggests rotation of rock pieces ahead of the drill. White specks of foraminifer tests are scattered throughout.

Minor lithology: Section 3, 28–35 cm: dolomite-bearing clayey nannofossil chalk, weak red (2.5YR 5/2).

SMEAR SLIDE SUMMARY (%):

	1, 25 D	2, 25 D	3, 37 M	4, 51 D
TEXTURE:				
Silt	48	60	—	77
Clay	52	40	—	23
COMPOSITION:				
Quartz	1	1	—	1
Mica	2	2	—	—
Clay	72	60	35	43
Calcite/dolomite	—	—	5	—
Accessory minerals	2	1	2	1
Pyrite	1	1	2	1
Foraminifers	—	—	—	2
Nannofossils	22	25	56	53
Diatoms	—	—	—	Tr
Sponge spicules	—	Tr	—	—

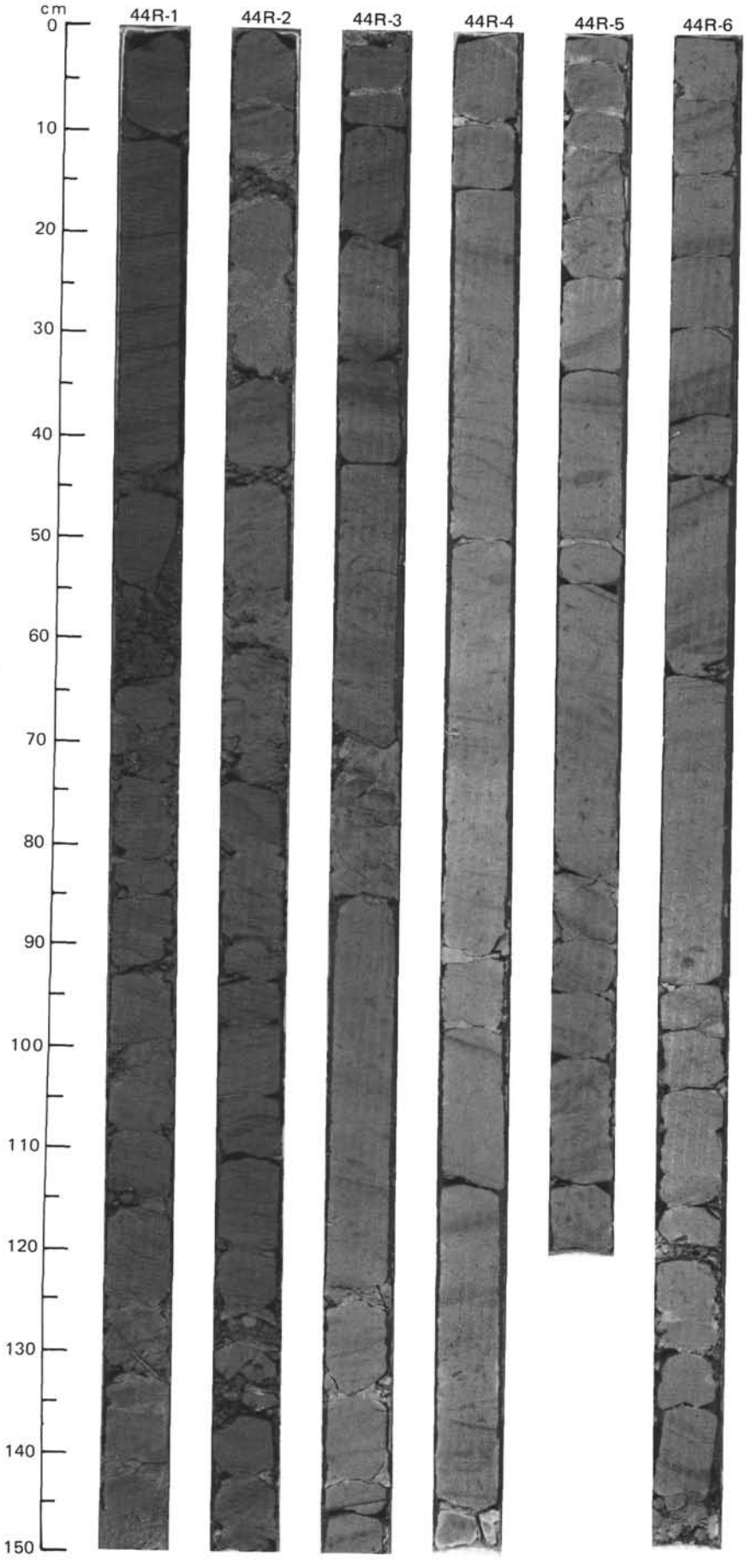
cm
0
10
20
30
40
50
60
70
80
90
100
110
120
130
140
150
44R-1
44R-2
44R-3
44R-4
44R-5
44R-6

SITE 647 HOLE A CORE 45 R CORED INTERVAL 4282.6-4292.3 mbsl; 424.1-433.8 mbsf

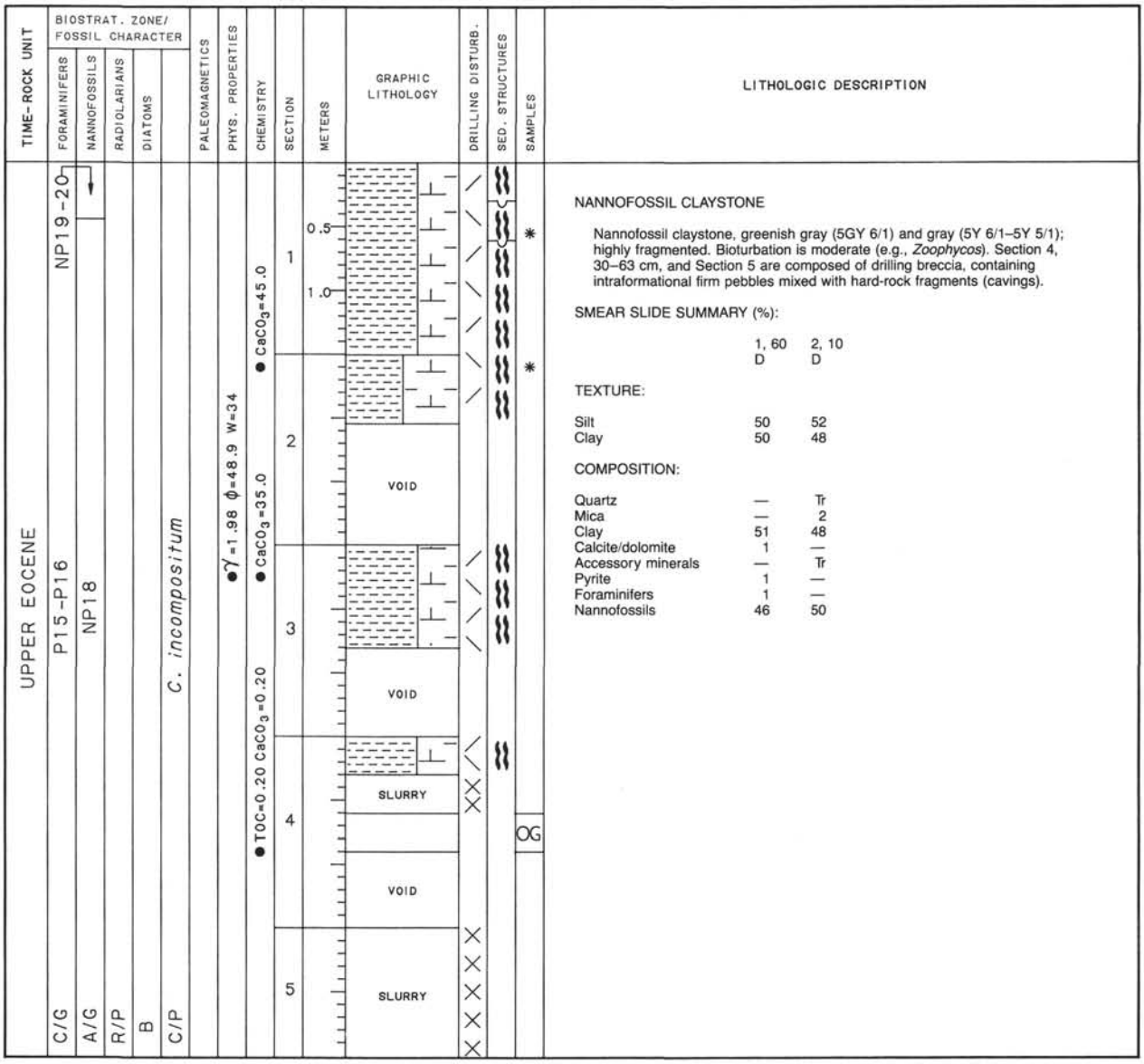

NANNOFOSSIL CLAYSTONE

Nannofossil claystone, greenish gray (5GY 6/1) and gray (5Y 6/1–5Y 5/1); highly fragmented. Bioturbation is moderate (e.g., *Zoophycos*). Section 4, 30–63 cm, and Section 5 are composed of drilling breccia, containing intraformational firm pebbles mixed with hard-rock fragments (cavings).

SMEAR SLIDE SUMMARY (%):

	1, 60 D	2, 10 D
TEXTURE:		
Silt	50	52
Clay	50	48
COMPOSITION:		
Quartz	—	Tr
Mica	—	2
Clay	51	48
Calcite/dolomite	1	—
Accessory minerals	—	Tr
Pyrite	1	—
Foraminifers	1	—
Nannofossils	46	50

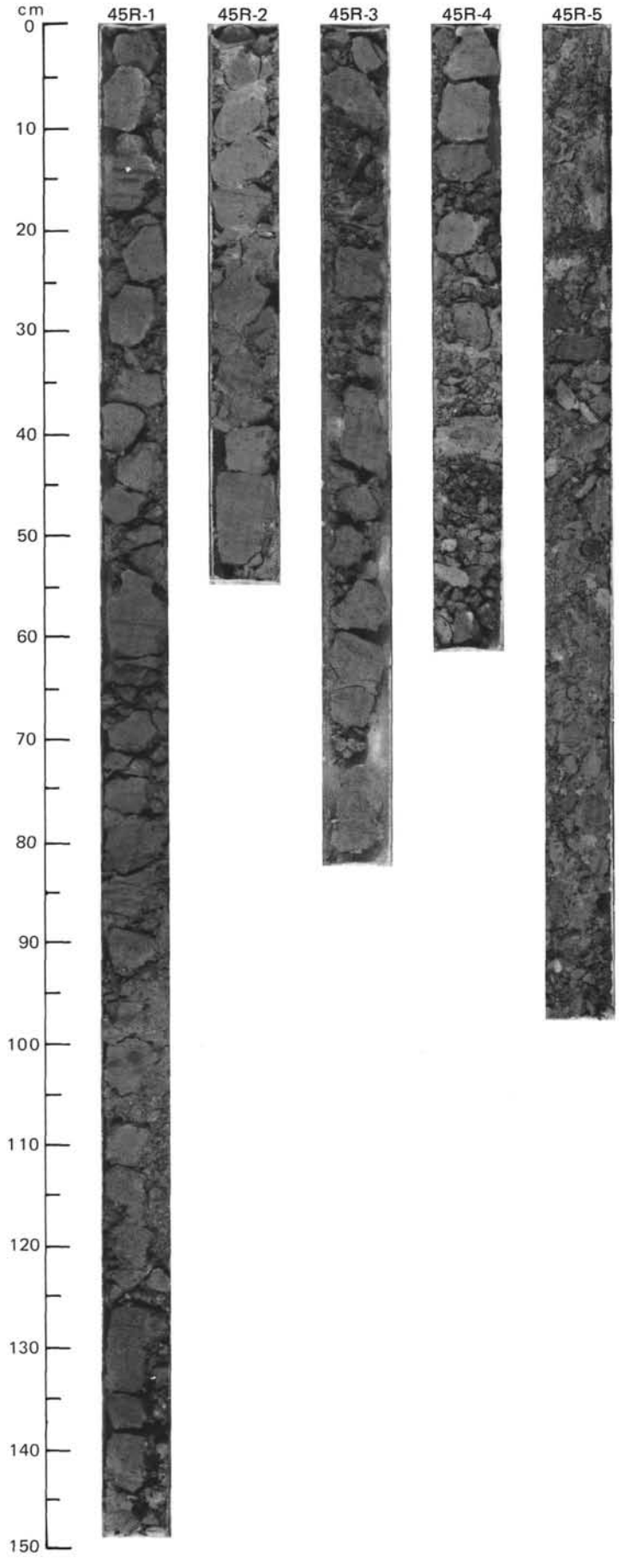
cm
45R-1
45R-2
45R-3
45R-4
45R-5
0
10
20
30
40
50
60
70
80
90
100
110
120
130
140
150

SITE 647 HOLE A CORE 45 R CORED INTERVAL 4282.6-4292.3 mbsl; 424.1-433.8 mbsf

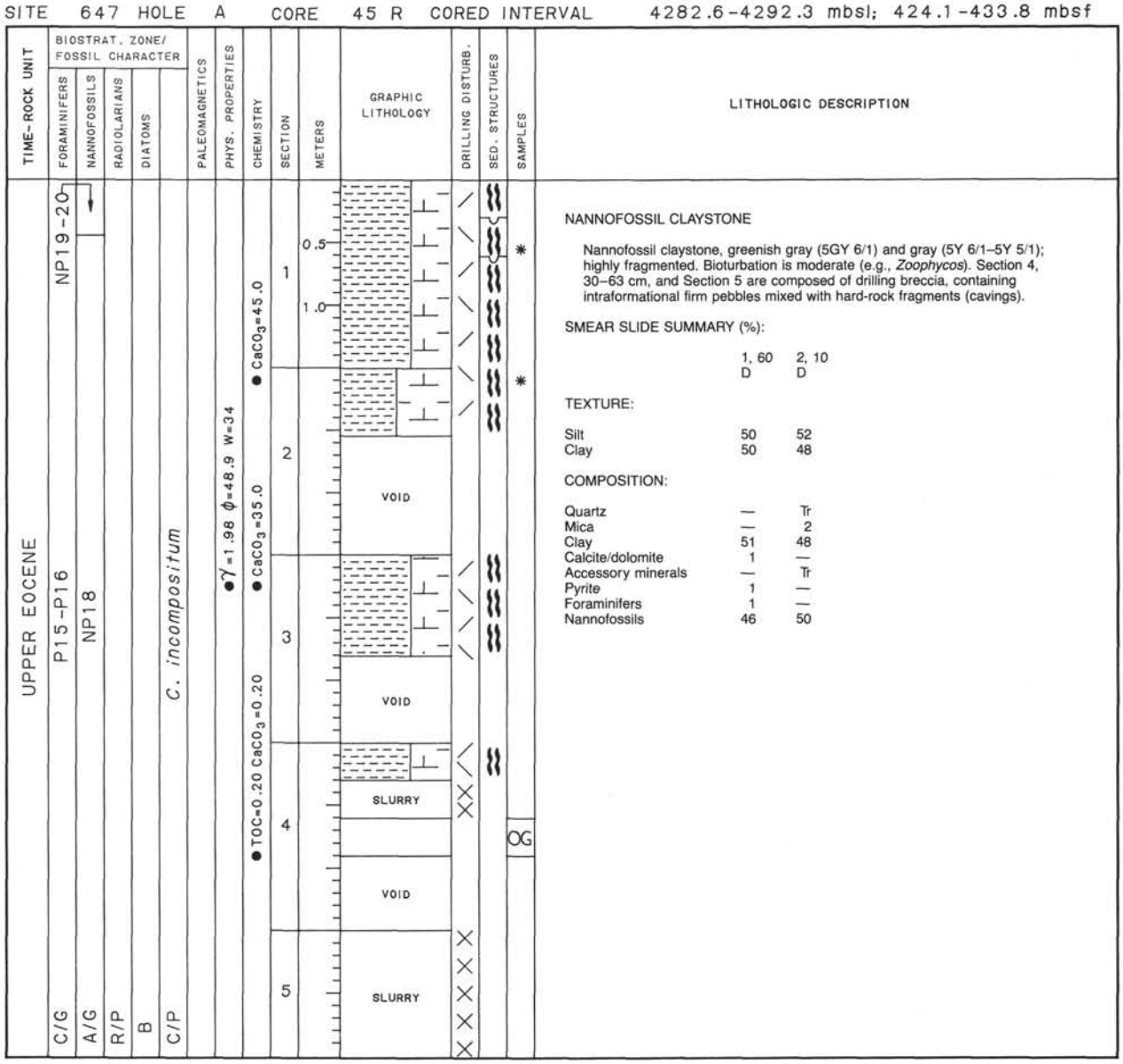

NANNOFOSSIL CLAYSTONE

Nannofossil claystone, greenish gray (5GY 6/1) and gray (5Y 6/1–5Y 5/1); highly fragmented. Bioturbation is moderate (e.g., *Zoophycos*). Section 4, 30–63 cm, and Section 5 are composed of drilling breccia, containing intraformational firm pebbles mixed with hard-rock fragments (cavings).

SMEAR SLIDE SUMMARY (%):

	1, 60 D	2, 10 D
TEXTURE:		
Silt	50	52
Clay	50	48
COMPOSITION:		
Quartz	—	Tr
Mica	—	2
Clay	51	48
Calcite/dolomite	1	—
Accessory minerals	—	Tr
Pyrite	1	—
Foraminifers	1	—
Nannofossils	46	50

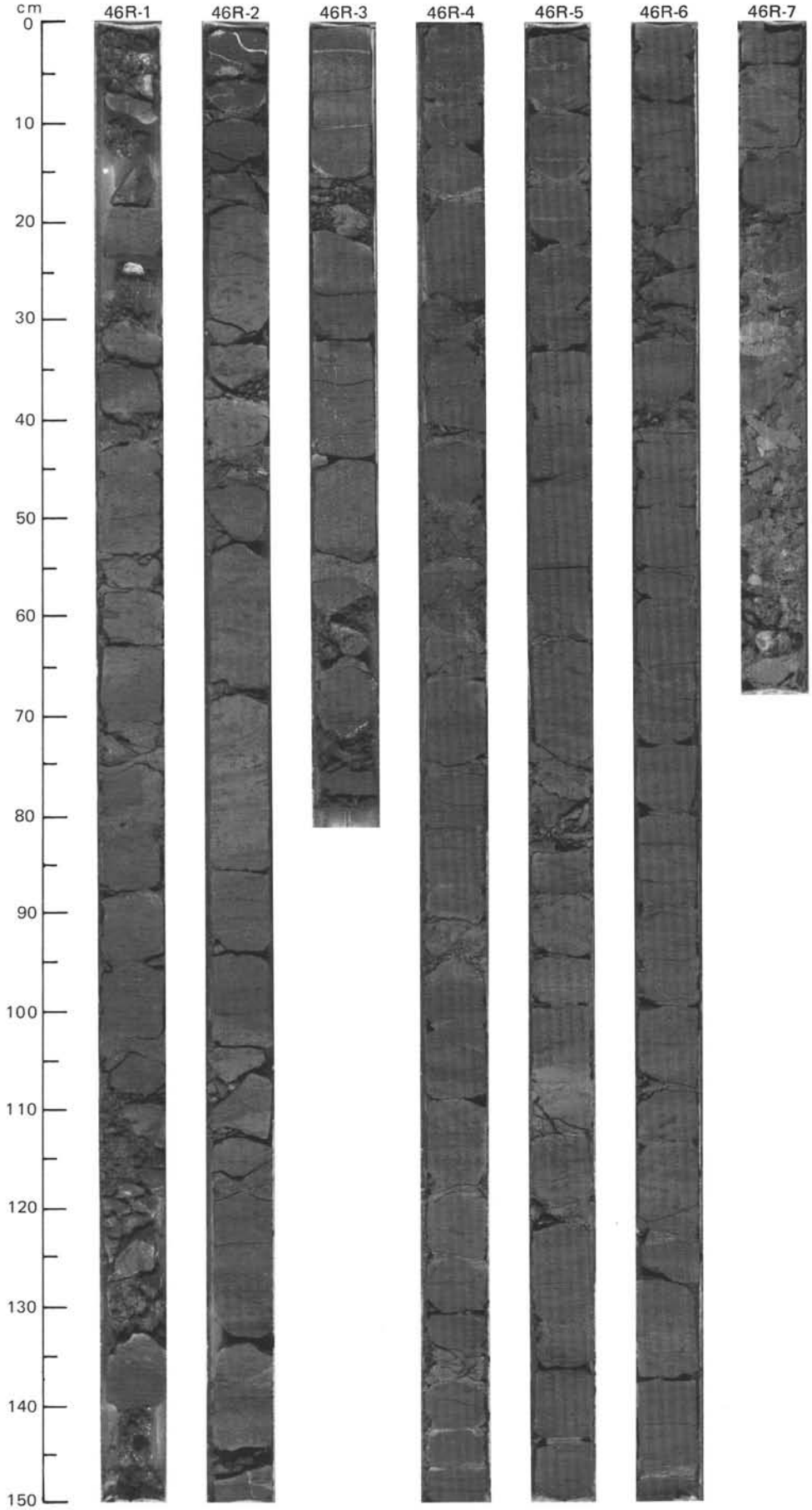
cm
46R-1
46R-2
46R-3
46R-4
46R-5
46R-6
46R-7
0
10
20
30
40
50
60
70
80
90
100
110
120
130
140
150

SITE 647 HOLE A CORE 47 R CORED INTERVAL 4302.0-4311.7 mbsl; 443.5-453.2 mbsf

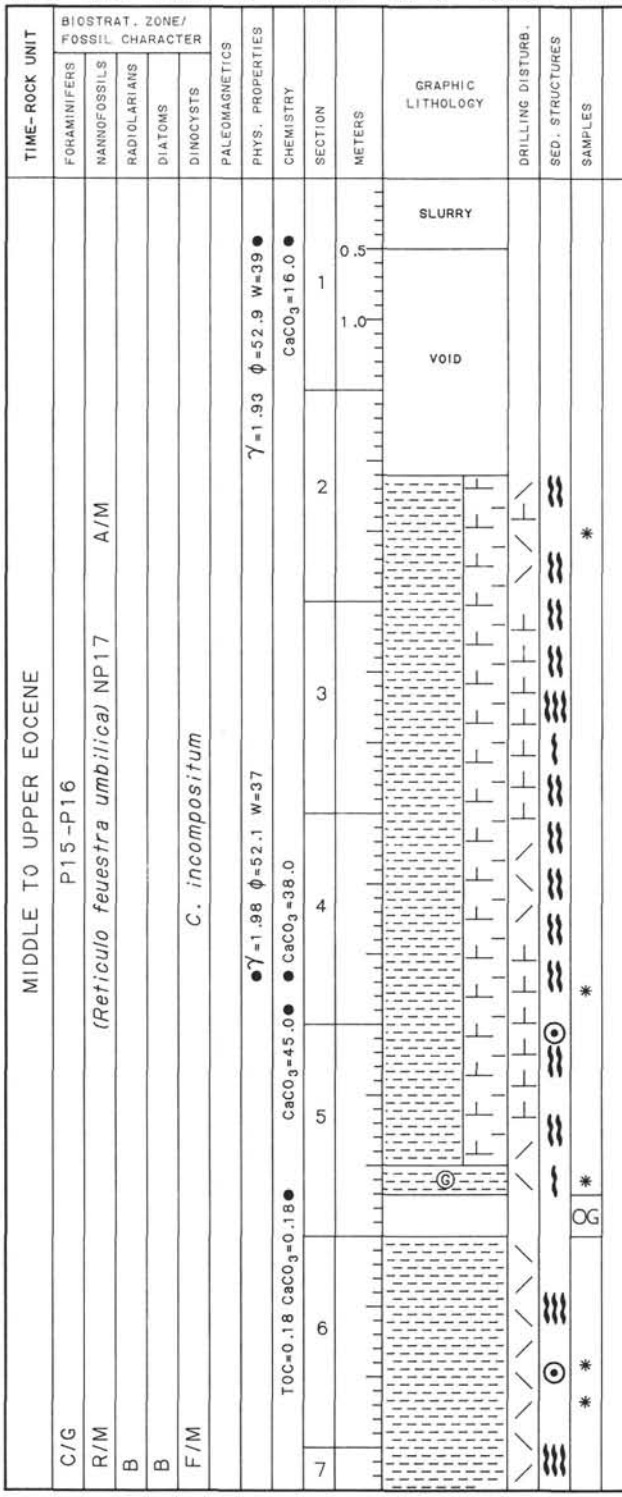

LITHOLOGIC DESCRIPTION

NANNOFOSSIL CLAYSTONE AND CLAYSTONE

Nannofossil claystone, greenish gray (5GY 5/1) to light greenish gray (5GY 6/1). Color mottling by burrows (e.g., *Zoophycos* and *Planolites*) and greenish bands of glauconitic clay. Some burrows are surrounded by dark bands of sulfide. Very few scattered foraminifers are present.

Claystone, dark olive gray (5Y 3/2); mottled with grayish green bands and burrows.

Minor lithology: Section 5, 100–120 cm: glauconite-bearing claystone, grayish green (5GY 5/1).

SMEAR SLIDE SUMMARY (%):

	2, 109 D	4, 163 D	5, 108 M	6, 92 M	6, 106 D
TEXTURE:					
Sand	00	3	5	5	—
Silt	25	43	10	10	5
Clay	75	57	85	85	95
COMPOSITION:					
Quartz	—	Tr	—	—	—
Mica	Tr	Tr	—	—	Tr
Clay	72	—	85	84	95
Calcite/dolomite	1	1	—	1	—
Accessory minerals	Tr	Tr	Tr	Tr	Tr
Glauconite	—	—	15	—	5
Foraminifers	—	3	—	—	—
Nannofossils	27	40	Tr	Tr	—
Sponge spicules					
Silicoflagellates					
Fish remains					
Plant debris					

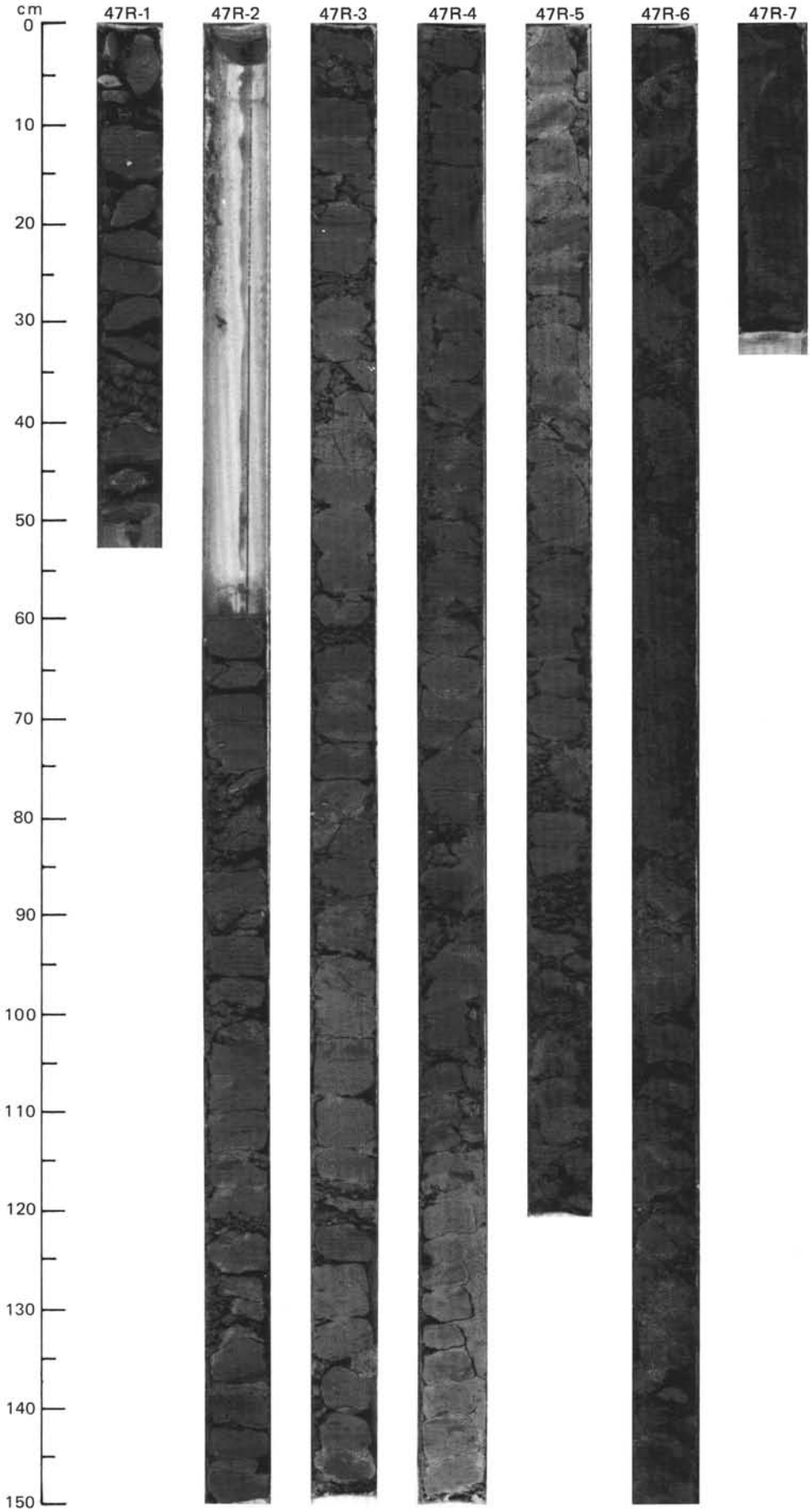
cm
47R-1
47R-2
47R-3
47R-4
47R-5
47R-6
47R-7
0
10
20
30
40
50
60
70
80
90
100
110
120
130
140
150

SITE 647 HOLE A CORE 48 R CORED INTERVAL 4311.7–4321.3 mbsl; 453.2–462.8 mbsf

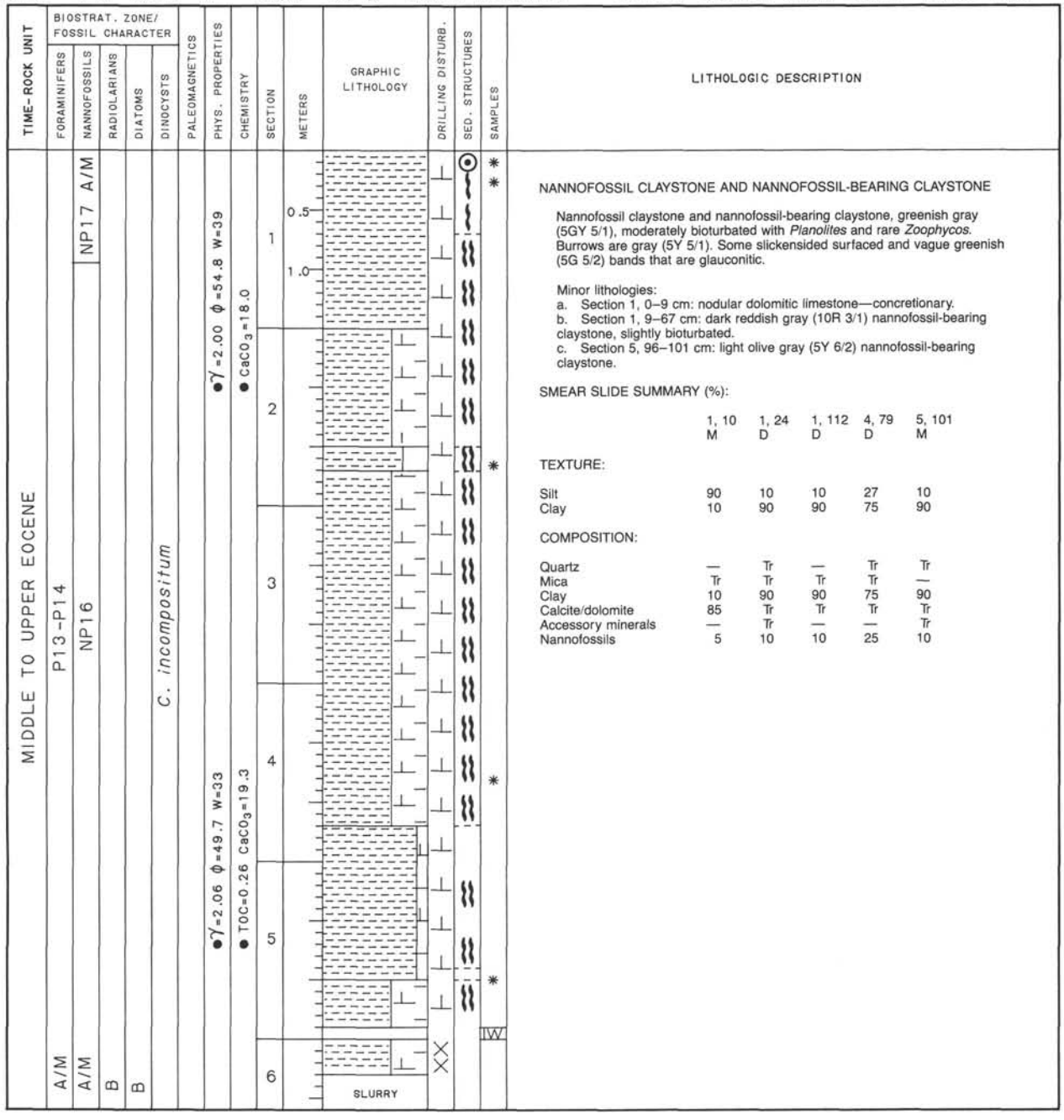

NANNOFOSSIL CLAYSTONE AND NANNOFOSSIL-BEARING CLAYSTONE

Nannofossil claystone and nannofossil-bearing claystone, greenish gray (5GY 5/1), moderately bioturbated with *Planolites* and rare *Zoophycos*. Burrows are gray (5Y 5/1). Some slickensided surfaced and vague greenish (5G 5/2) bands that are glauconitic.

Minor lithologies:
a. Section 1, 0–9 cm: nodular dolomitic limestone—concretionary.
b. Section 1, 9–67 cm: dark reddish gray (10R 3/1) nannofossil-bearing claystone, slightly bioturbated.
c. Section 5, 96–101 cm: light olive gray (5Y 6/2) nannofossil-bearing claystone.

SMEAR SLIDE SUMMARY (%):

	1, 10 M	1, 24 D	1, 112 D	4, 79 D	5, 101 M
TEXTURE:					
Silt	90	10	10	27	10
Clay	10	90	90	75	90
COMPOSITION:					
Quartz	—	Tr	—	Tr	Tr
Mica	Tr	Tr	Tr	Tr	—
Clay	10	90	90	75	90
Calcite/dolomite	85	Tr	Tr	Tr	Tr
Accessory minerals	—	Tr	—	—	Tr
Nannofossils	5	10	10	25	10

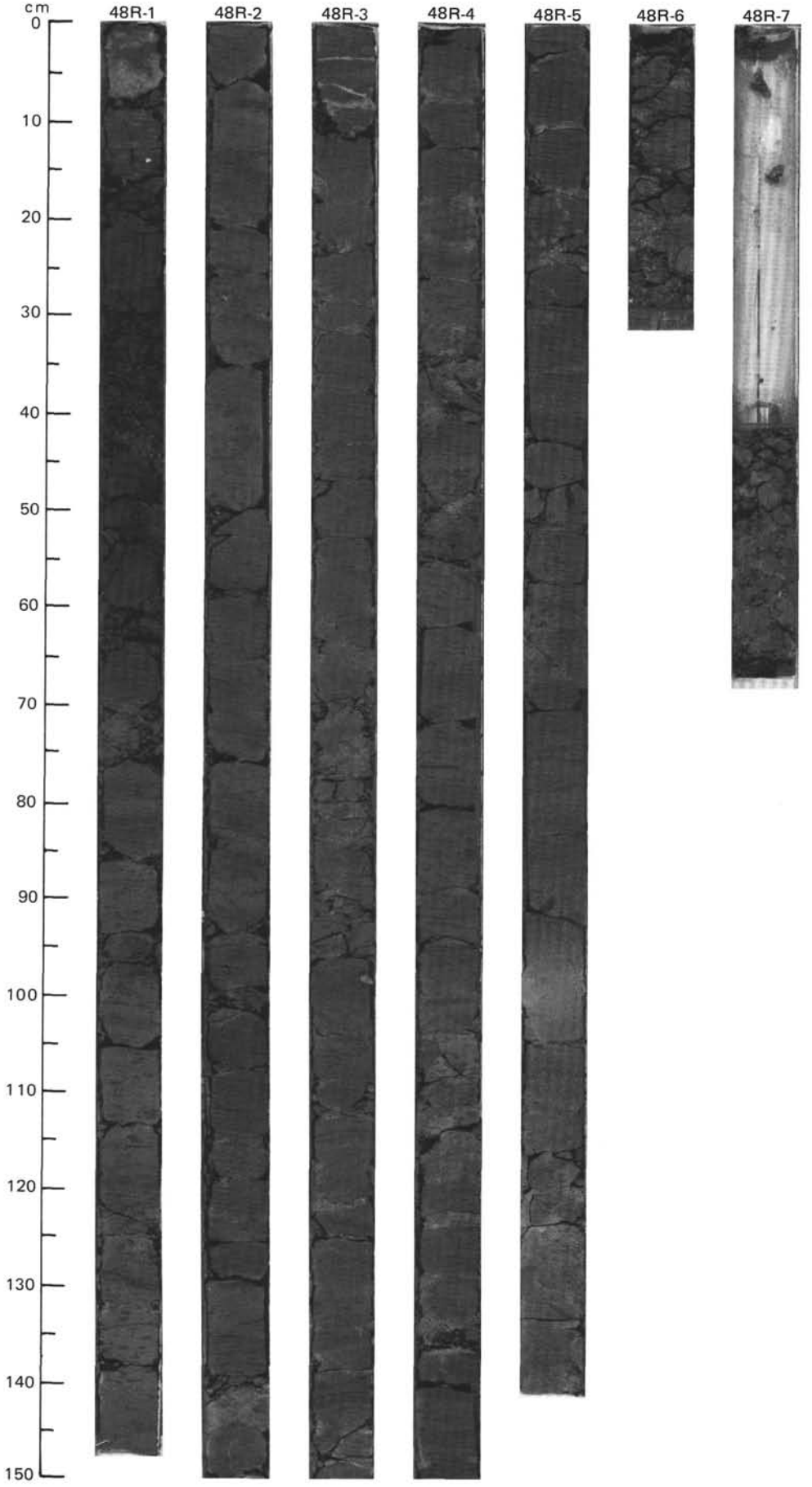
cm
0
10
20
30
40
50
60
70
80
90
100
110
120
130
140
150
48R-1
48R-2
48R-3
48R-4
48R-5
48R-6
48R-7

SITE 647 HOLE A CORE 49 R CORED INTERVAL 4321.3-4331.0 mbsl; 462.8-472.5 mbsf

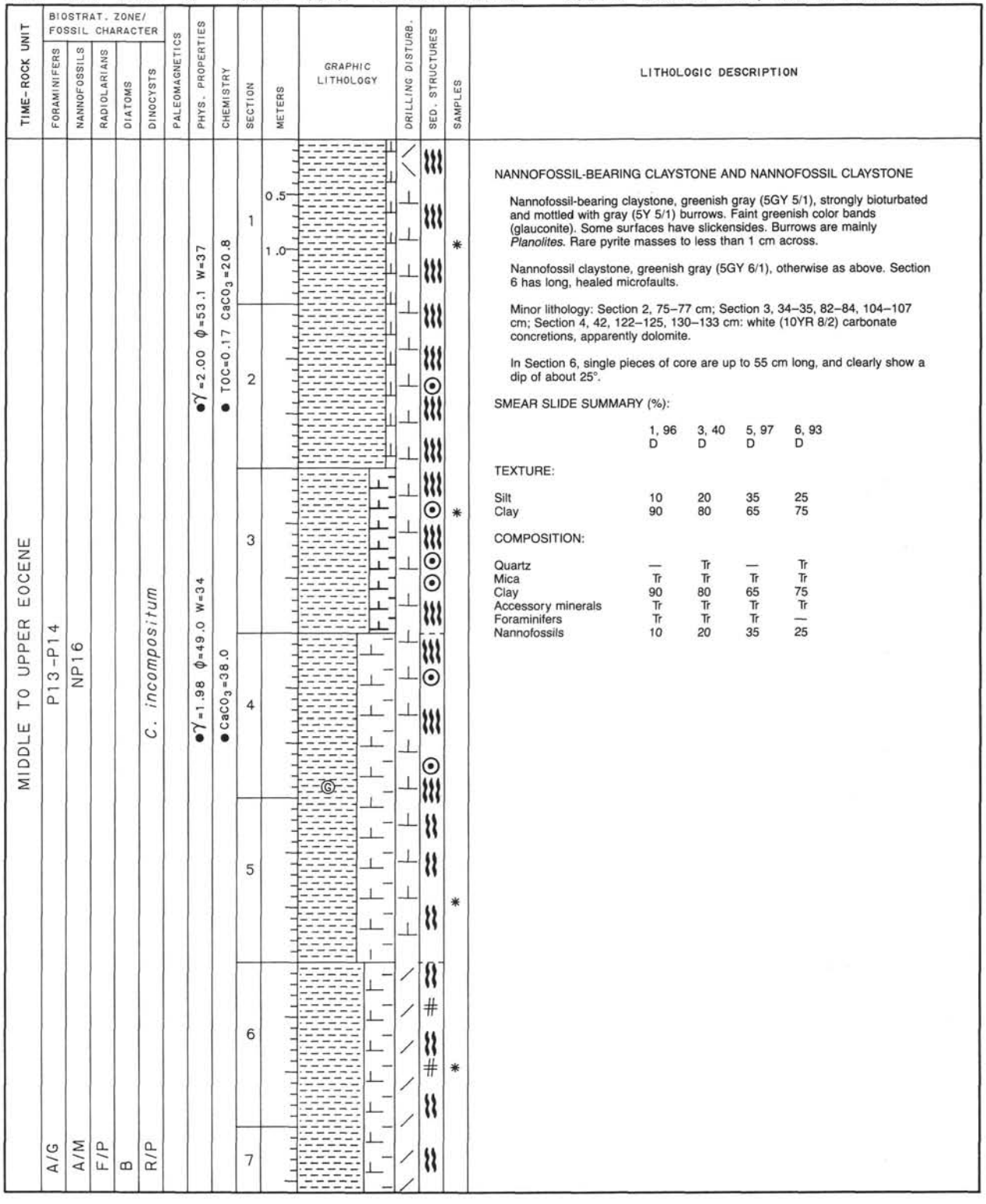

NANNOFOSSIL-BEARING CLAYSTONE AND NANNOFOSSIL CLAYSTONE

Nannofossil-bearing claystone, greenish gray (5GY 5/1), strongly bioturbated and mottled with gray (5Y 5/1) burrows. Faint greenish color bands (glauconite). Some surfaces have slickensides. Burrows are mainly *Planolites*. Rare pyrite masses to less than 1 cm across.

Nannofossil claystone, greenish gray (5GY 6/1), otherwise as above. Section 6 has long, healed microfaults.

Minor lithology: Section 2, 75–77 cm; Section 3, 34–35, 82–84, 104–107 cm; Section 4, 42, 122–125, 130–133 cm: white (10YR 8/2) carbonate concretions, apparently dolomite.

In Section 6, single pieces of core are up to 55 cm long, and clearly show a dip of about 25°.

SMEAR SLIDE SUMMARY (%):

	1, 96 D	3, 40 D	5, 97 D	6, 93 D
TEXTURE:				
Silt	10	20	35	25
Clay	90	80	65	75
COMPOSITION:				
Quartz	—	Tr	—	Tr
Mica	Tr	Tr	Tr	Tr
Clay	90	80	65	75
Accessory minerals	Tr	Tr	Tr	Tr
Foraminifers	Tr	Tr	Tr	—
Nannofossils	10	20	35	25

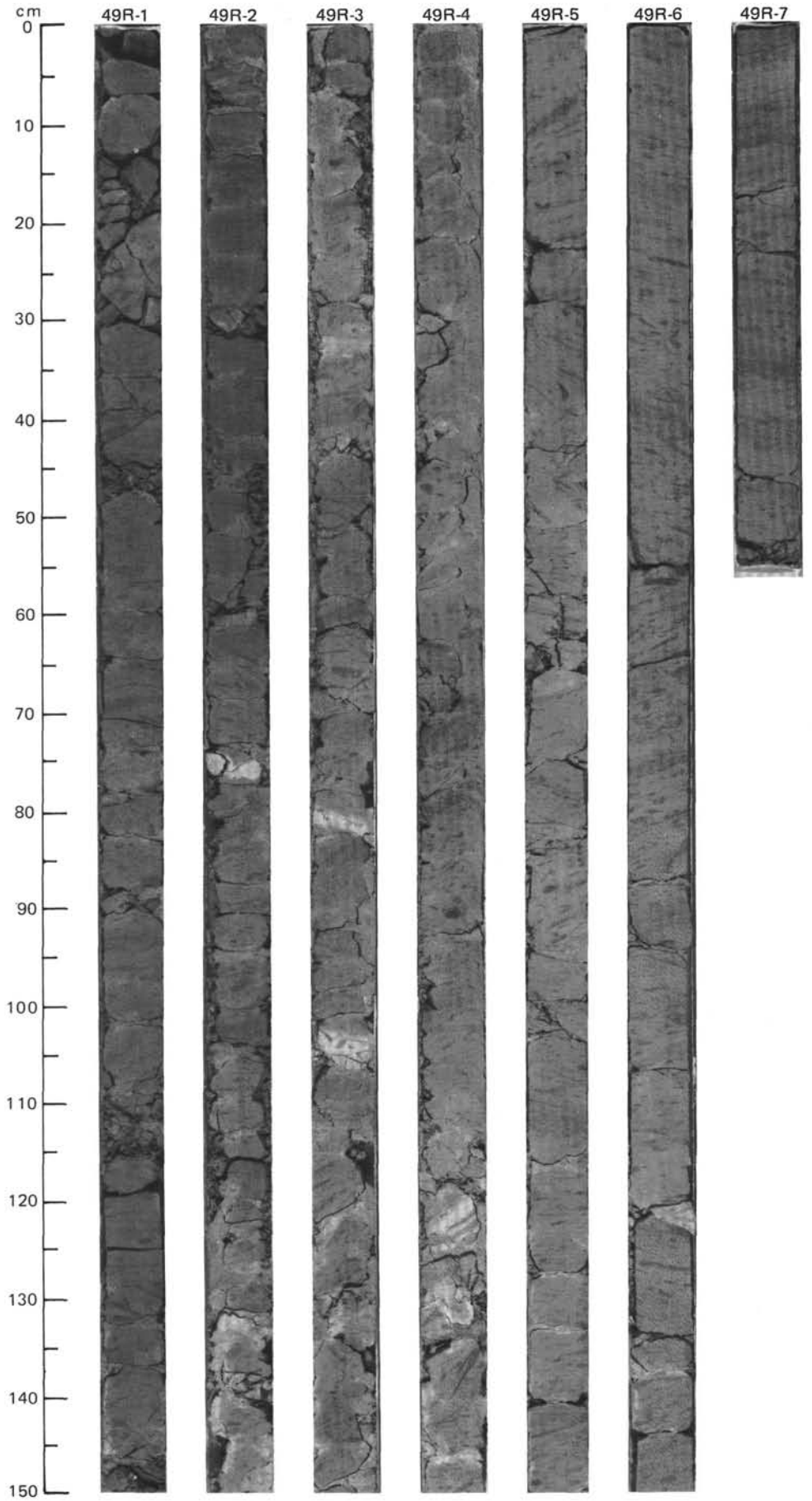
cm
0
10
20
30
40
50
60
70
80
90
100
110
120
130
140
150
49R-1
49R-2
49R-3
49R-4
49R-5
49R-6
49R-7

SITE 647 HOLE A CORE 50 R CORED INTERVAL 4331.0-4340.6 mbsl; 472.5-482.1 mbsf

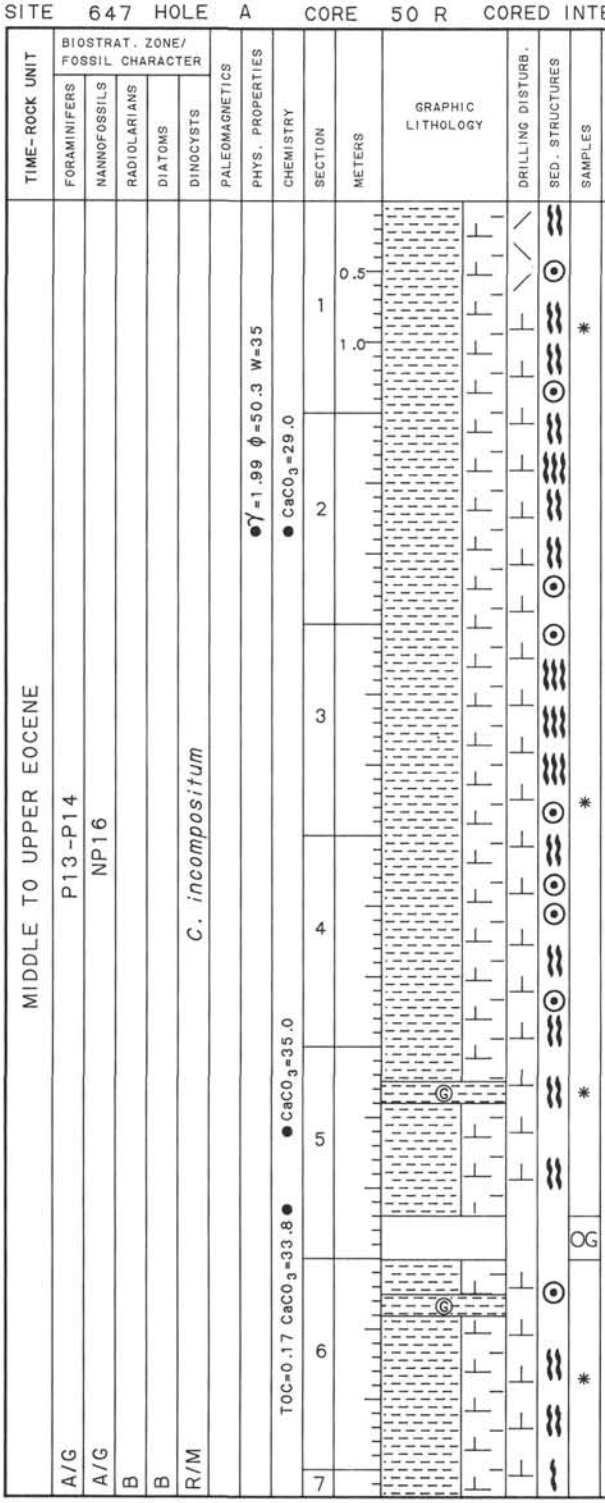

LITHOLOGIC DESCRIPTION

NANNOFOSSIL CLAYSTONE

Nannofossil claystone, greenish gray (5GY 5/1); microfractured. Burrows parallel to bedding of *Zoophycos* and *Planolides*. Some carbonate concretions, mostly dolomite.

Minor lithology: Section 5, 23–40 cm; Section 6, 23–36 cm: glauconite-bearing claystone.

SMEAR SLIDE SUMMARY (%):

	1, 94 D	3, 127 D	5, 39 D	6, 88 D
TEXTURE:				
Sand	—	—	5	—
Silt	25	30	15	35
Clay	75	70	80	65
COMPOSITION:				
Quartz	Tr	—	—	—
Mica	Tr	Tr	—	Tr
Clay	75	70	80	65
Calcite/dolomite	—	—	Tr	Tr
Accessory minerals	Tr	Tr	Tr	Tr
Glauconite	—	—	15	—
Foraminifers	—	Tr	Tr	—
Nannofossils	25	30	5	35

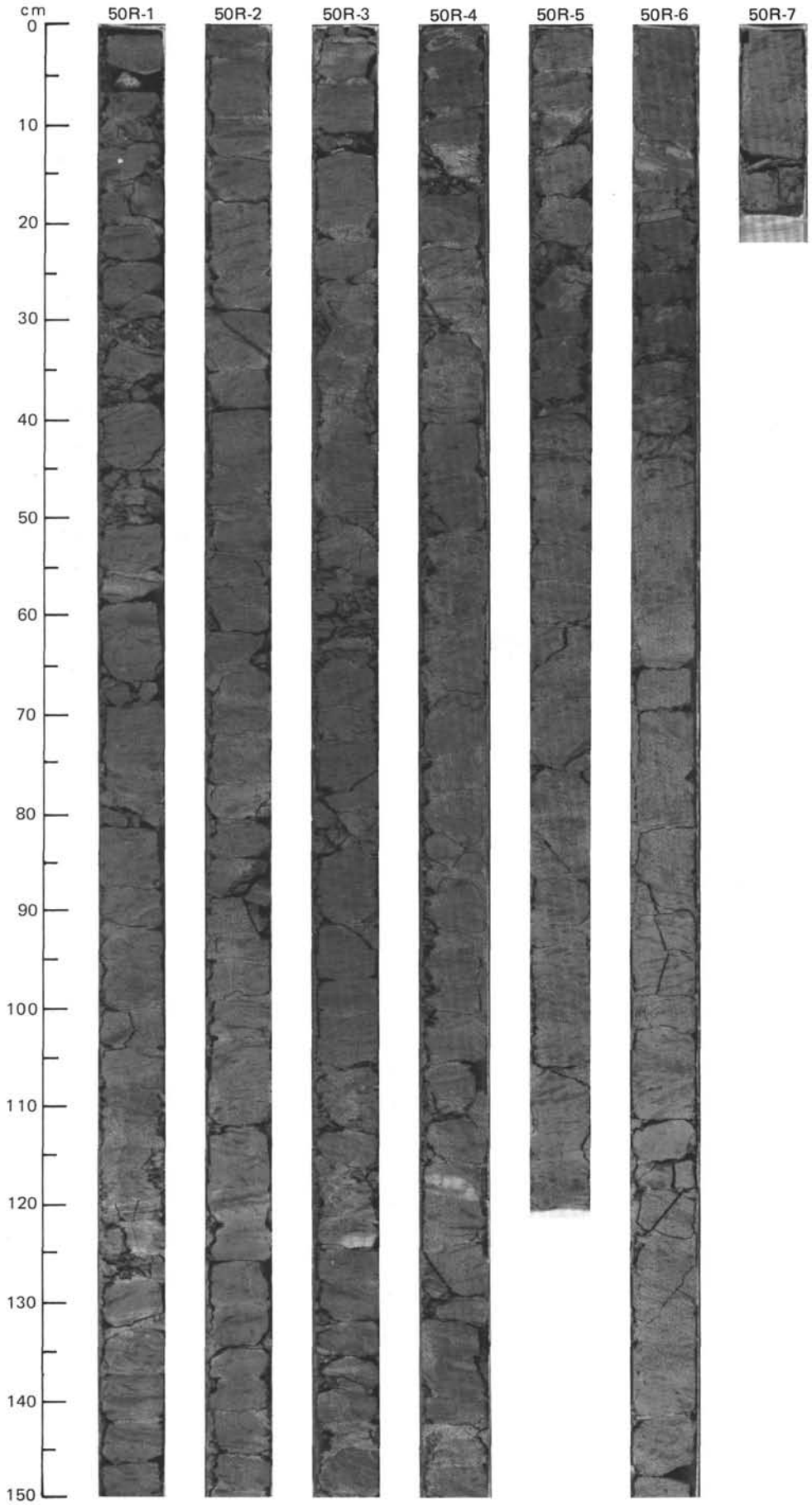
cm
50R-1
50R-2
50R-3
50R-4
50R-5
50R-6
50R-7
0
10
20
30
40
50
60
70
80
90
100
110
120
130
140
150

SITE 647 HOLE A CORE 51 R CORED INTERVAL 4340.6-4350.3 mbsl; 482.1-491.8 mbsf

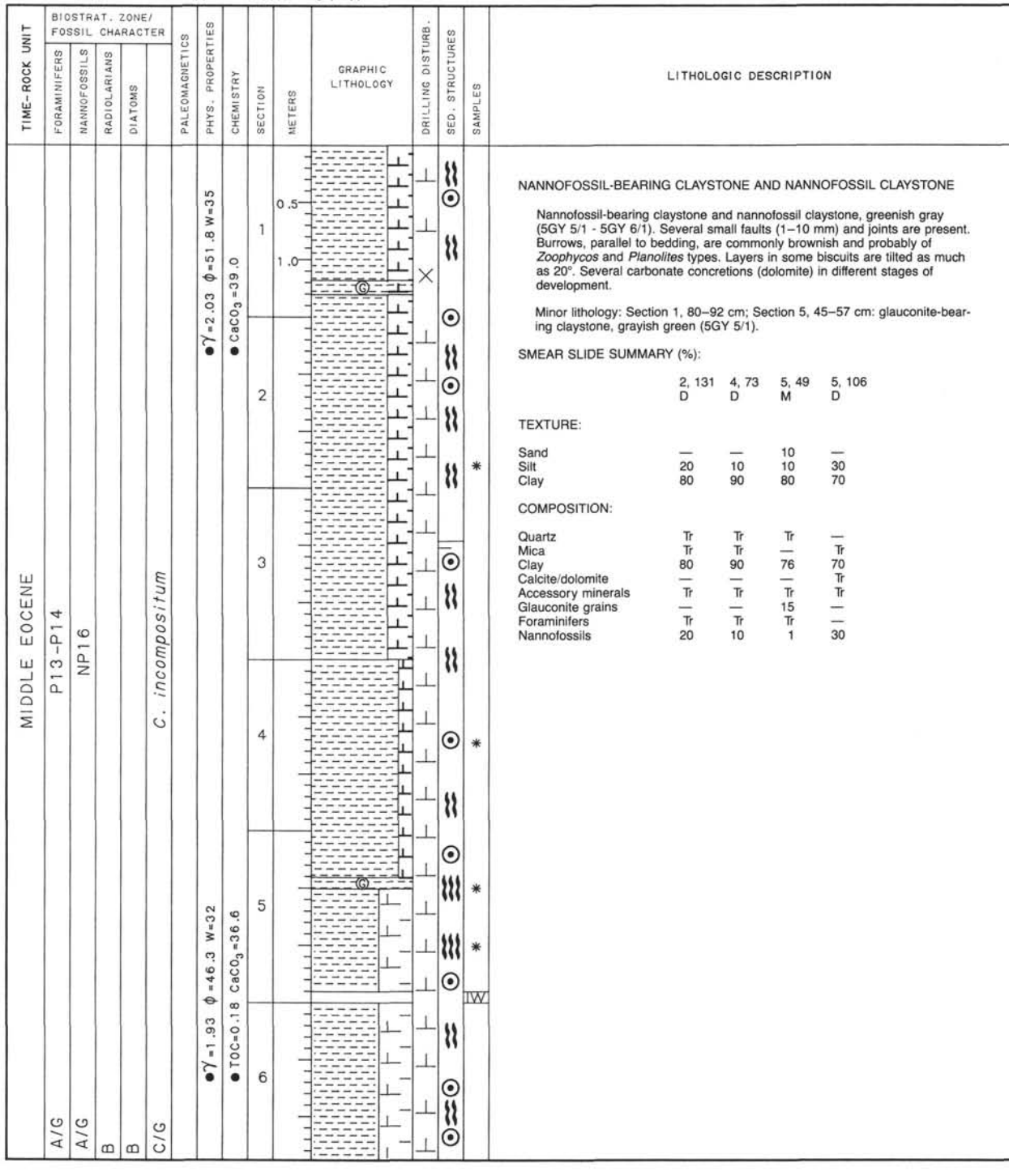

LITHOLOGIC DESCRIPTION

NANNOFOSSIL-BEARING CLAYSTONE AND NANNOFOSSIL CLAYSTONE

Nannofossil-bearing claystone and nannofossil claystone, greenish gray (5GY 5/1 - 5GY 6/1). Several small faults (1–10 mm) and joints are present. Burrows, parallel to bedding, are commonly brownish and probably of *Zoophycos* and *Planolites* types. Layers in some biscuits are tilted as much as 20°. Several carbonate concretions (dolomite) in different stages of development.

Minor lithology: Section 1, 80–92 cm; Section 5, 45–57 cm: glauconite-bearing claystone, grayish green (5GY 5/1).

SMEAR SLIDE SUMMARY (%):

	2, 131 D	4, 73 D	5, 49 M	5, 106 D
TEXTURE:				
Sand	—	—	10	—
Silt	20	10	10	30
Clay	80	90	80	70
COMPOSITION:				
Quartz	Tr	Tr	Tr	—
Mica	Tr	Tr	—	Tr
Clay	80	90	76	70
Calcite/dolomite	—	—	—	Tr
Accessory minerals	Tr	Tr	Tr	Tr
Glauconite grains	—	—	15	—
Foraminifers	Tr	Tr	Tr	—
Nannofossils	20	10	1	30

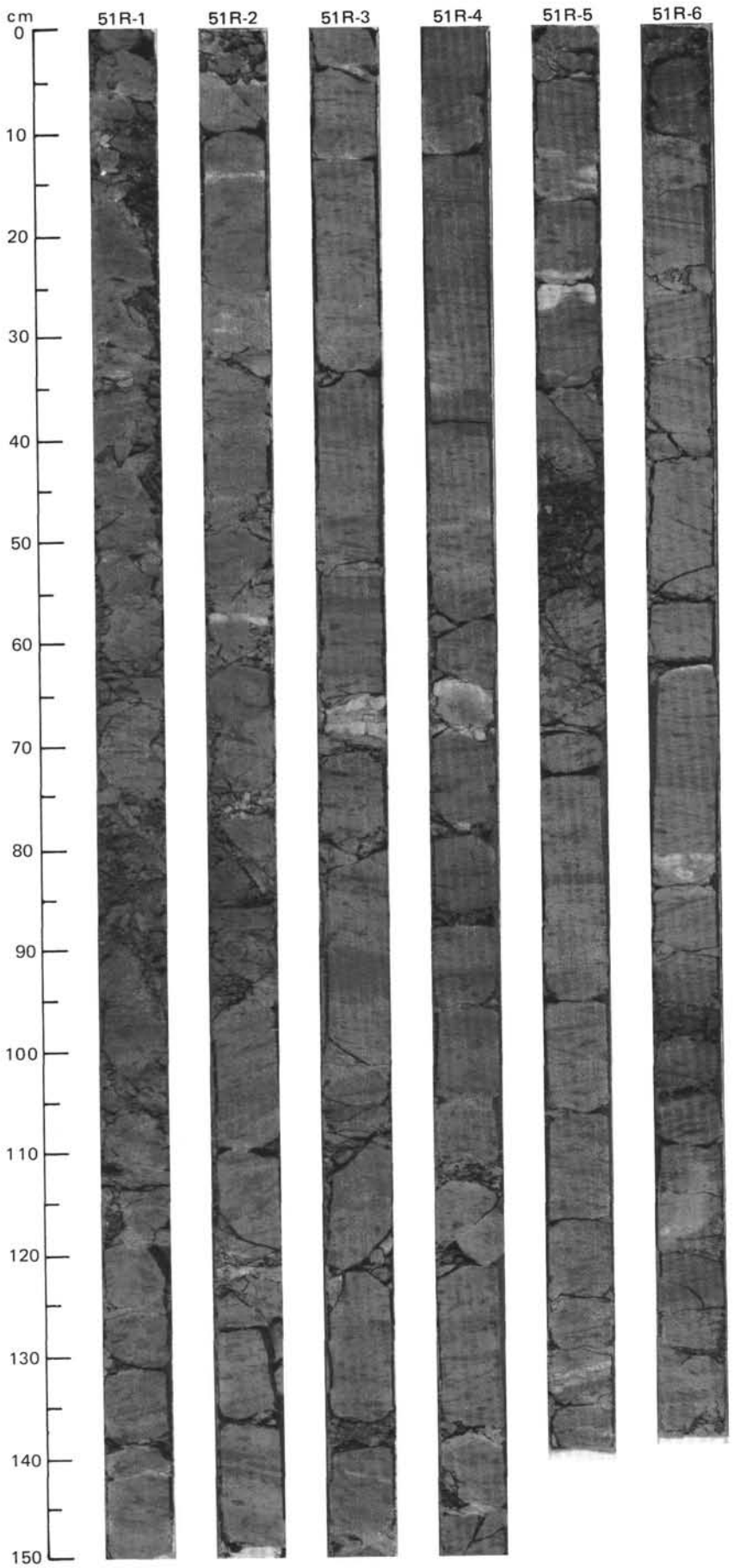
cm
51R-1
51R-2
51R-3
51R-4
51R-5
51R-6
0
10
20
30
40
50
60
70
80
90
100
110
120
130
140
150

SITE 647 HOLE A CORE 52 R CORED INTERVAL 4350.3-4359.9 mbsl; 491.8-501.4 mbsf

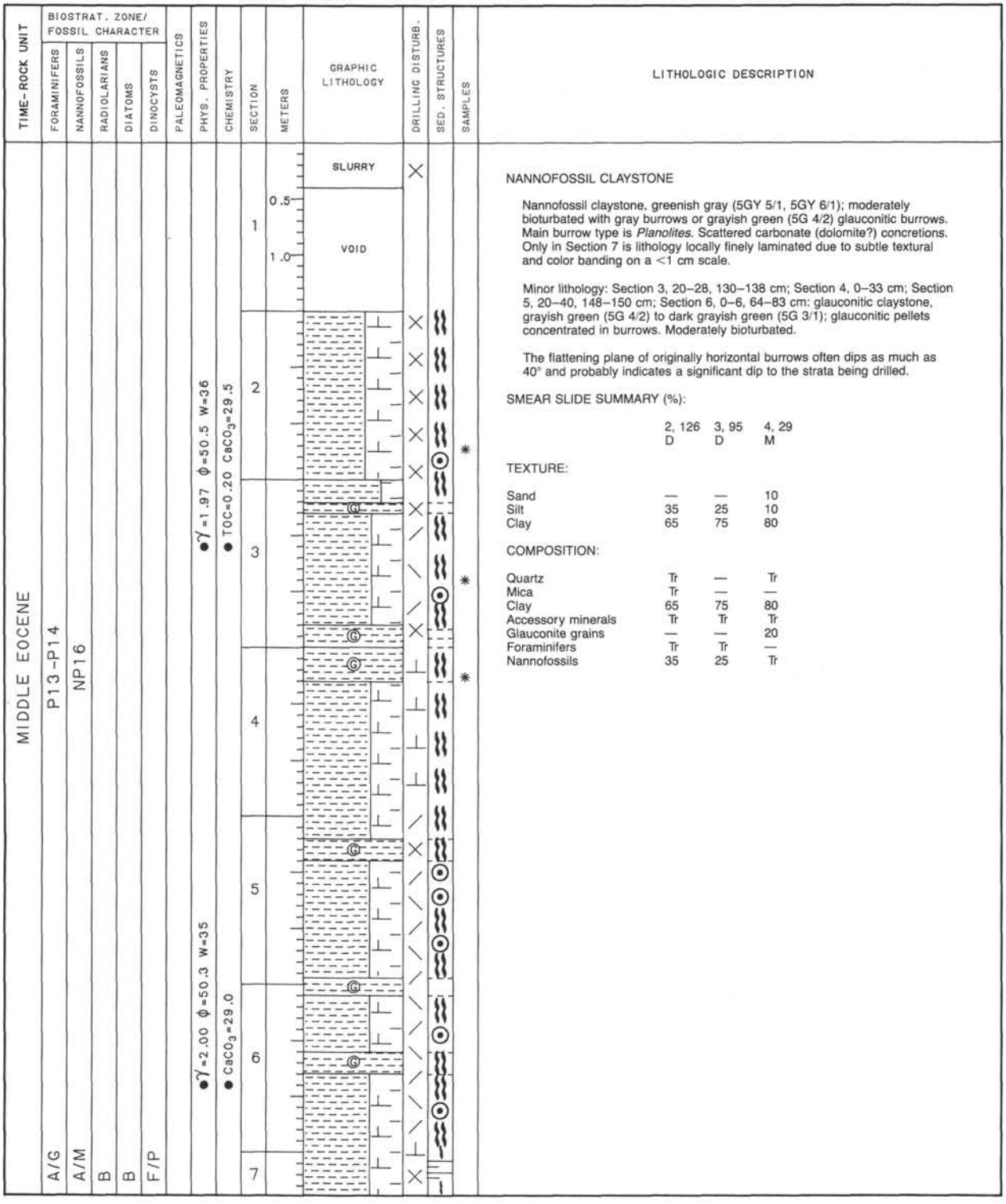

NANNOFOSSIL CLAYSTONE

Nannofossil claystone, greenish gray (5GY 5/1, 5GY 6/1); moderately bioturbated with gray burrows or grayish green (5G 4/2) glauconitic burrows. Main burrow type is *Planolites*. Scattered carbonate (dolomite?) concretions. Only in Section 7 is lithology locally finely laminated due to subtle textural and color banding on a <1 cm scale.

Minor lithology: Section 3, 20–28, 130–138 cm; Section 4, 0–33 cm; Section 5, 20–40, 148–150 cm; Section 6, 0–6, 64–83 cm: glauconitic claystone, grayish green (5G 4/2) to dark grayish green (5G 3/1); glauconitic pellets concentrated in burrows. Moderately bioturbated.

The flattening plane of originally horizontal burrows often dips as much as 40° and probably indicates a significant dip to the strata being drilled.

SMEAR SLIDE SUMMARY (%):

	2, 126 D	3, 95 D	4, 29 M
TEXTURE:			
Sand	—	—	10
Silt	35	25	10
Clay	65	75	80
COMPOSITION:			
Quartz	Tr	—	Tr
Mica	Tr	—	—
Clay	65	75	80
Accessory minerals	Tr	Tr	Tr
Glauconite grains	—	—	20
Foraminifers	Tr	Tr	—
Nannofossils	35	25	Tr

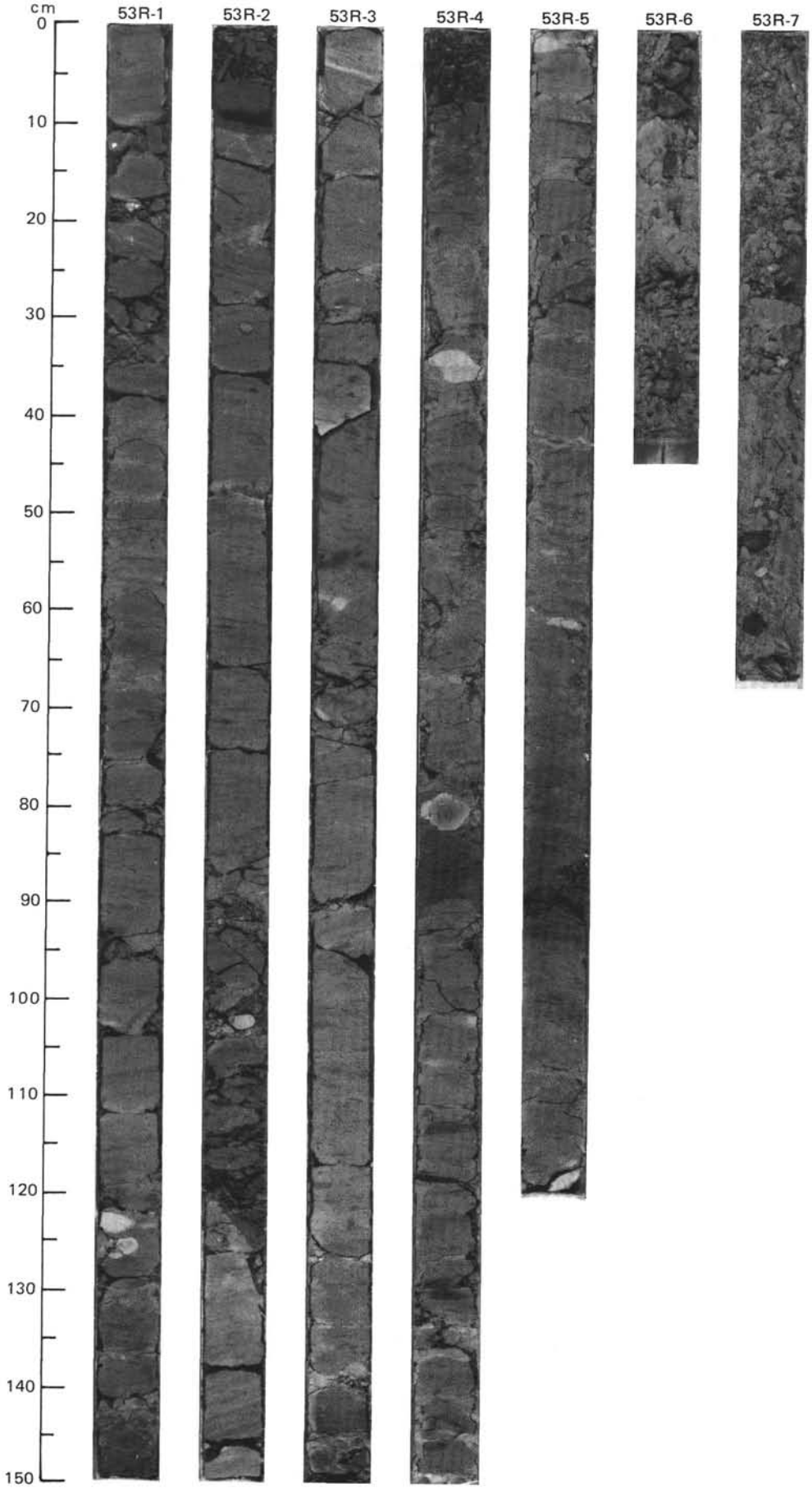
cm
0
10
20
30
40
50
60
70
80
90
100
110
120
130
140
150
53R-1
53R-2
53R-3
53R-4
53R-5
53R-6
53R-7

SITE 647 HOLE A CORE 54 R CORED INTERVAL 4369.6-4379.2 mbsl; 511.1-520.7 mbsf

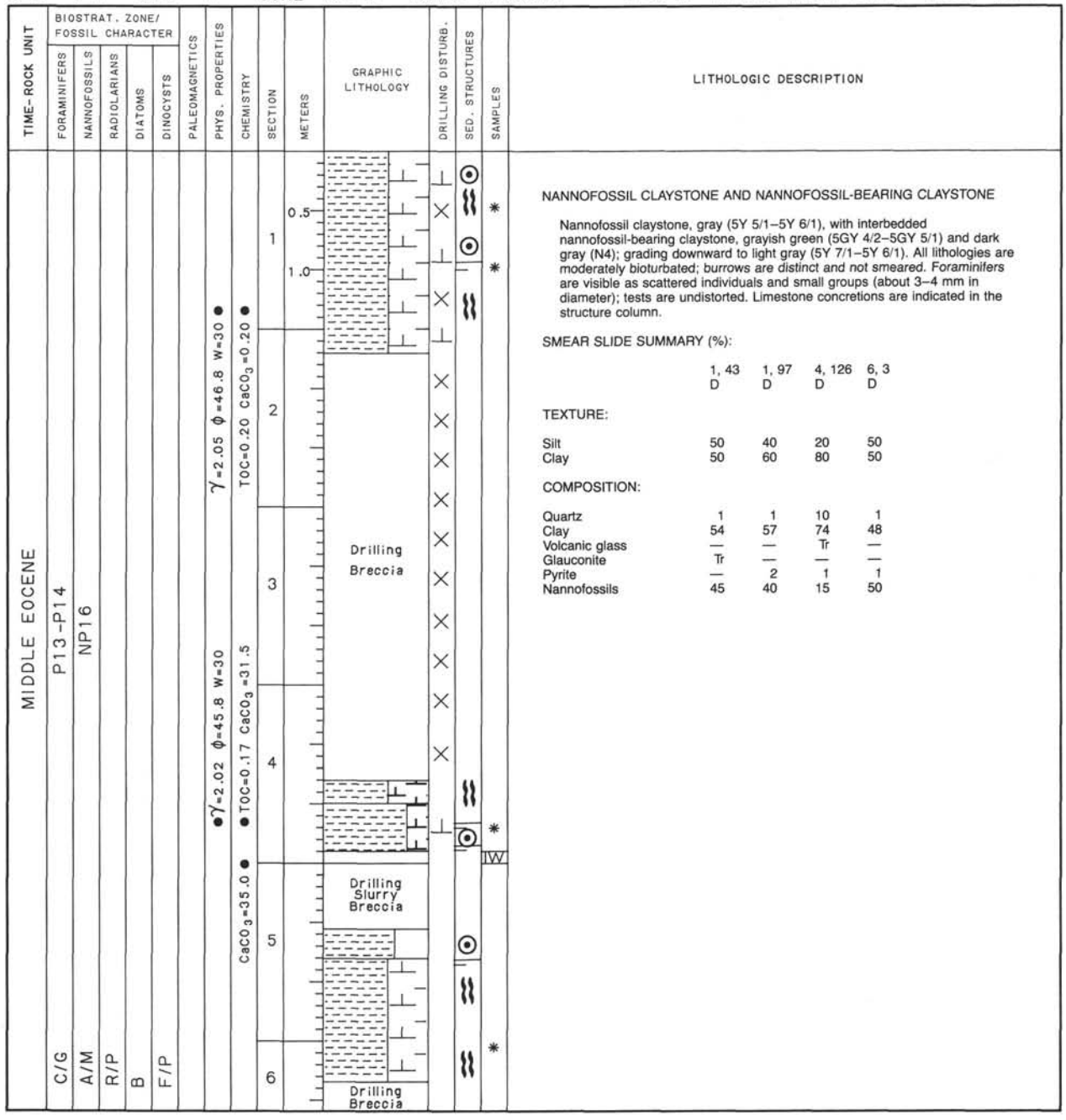

NANNOFOSSIL CLAYSTONE AND NANNOFOSSIL-BEARING CLAYSTONE

Nannofossil claystone, gray (5Y 5/1–5Y 6/1), with interbedded nannofossil-bearing claystone, grayish green (5GY 4/2–5GY 5/1) and dark gray (N4); grading downward to light gray (5Y 7/1–5Y 6/1). All lithologies are moderately bioturbated; burrows are distinct and not smeared. Foraminifers are visible as scattered individuals and small groups (about 3–4 mm in diameter); tests are undistorted. Limestone concretions are indicated in the structure column.

SMEAR SLIDE SUMMARY (%):

	1, 43 D	1, 97 D	4, 126 D	6, 3 D
TEXTURE:				
Silt	50	40	20	50
Clay	50	60	80	50
COMPOSITION:				
Quartz	1	1	10	1
Clay	54	57	74	48
Volcanic glass	—	—	Tr	—
Glauconite	Tr	—	—	—
Pyrite	—	2	1	1
Nannofossils	45	40	15	50

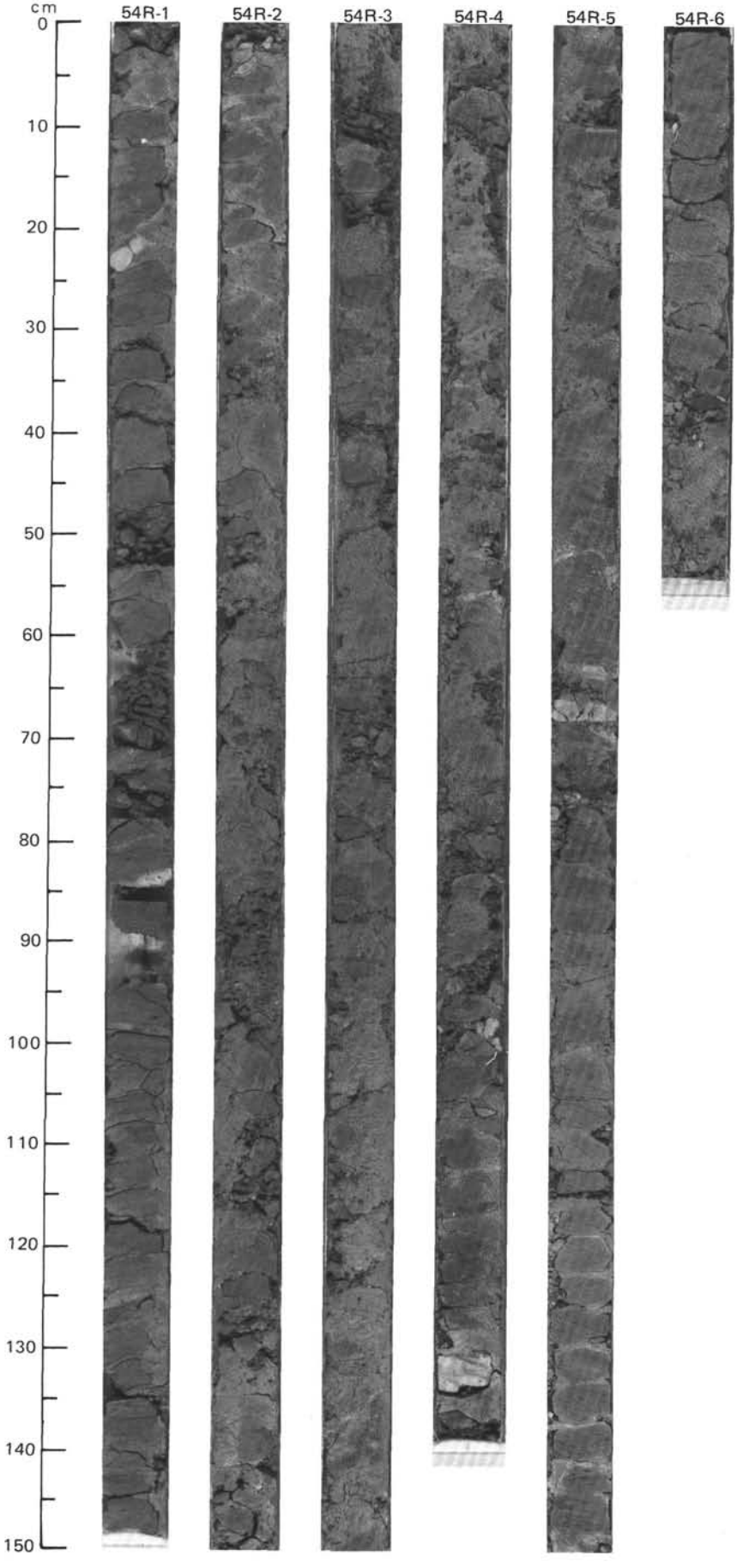
cm
0
10
20
30
40
50
60
70
80
90
100
110
120
130
140
150
54R-1
54R-2
54R-3
54R-4
54R-5
54R-6

SITE 647 HOLE A CORE 55 R CORED INTERVAL 4379.2-4388.8 mbsl; 520.7-530.3 mbsf

TIME-ROCK UNIT	BIOSTRAT. ZONE/ FOSSIL CHARACTER: FORAMINIFERS	NANNOFOSSILS	RADIOLARIANS	DIATOMS	DINOCYSTS	PALEOMAGNETICS	PHYS. PROPERTIES	CHEMISTRY	SECTION	METERS	GRAPHIC LITHOLOGY	DRILLING DISTURB.	SED. STRUCTURES	SAMPLES	LITHOLOGIC DESCRIPTION
MIDDLE EOCENE	C/G	A/G	F/P	B	R/P				1		SLURRY				NANNOFOSSIL CLAYSTONE 15 cm of smeared sediment, similar to previous cores, i.e., nannofossil claystone.
	P13-P14	NP16													

SITE 647 HOLE A CORE 56 R CORED INTERVAL 4388.8-4398.5 mbsl; 530.3-540.0 mbsf

TIME-ROCK UNIT	BIOSTRAT. ZONE/ FOSSIL CHARACTER: FORAMINIFERS	NANNOFOSSILS	RADIOLARIANS	DIATOMS	DINOCYSTS	PALEOMAGNETICS	PHYS. PROPERTIES	CHEMISTRY	SECTION	METERS	GRAPHIC LITHOLOGY	DRILLING DISTURB.	SED. STRUCTURES	SAMPLES	LITHOLOGIC DESCRIPTION
MIDDLE EOCENE	F/G	A/G	B	B	R/P				1					*	NANNOFOSSIL-BEARING CLAYSTONE Drilling breccia (15 cm) of olive gray (5Y 4/2) nannofossil-bearing claystone. SMEAR SLIDE SUMMARY (%): 1, 10 D COMPOSITION: Quartz 1 Clay 76 Volcanic glass Tr Calcite/dolomite 1 Pyrite 2 Nannofossils 20
	P13-P14	NP16													

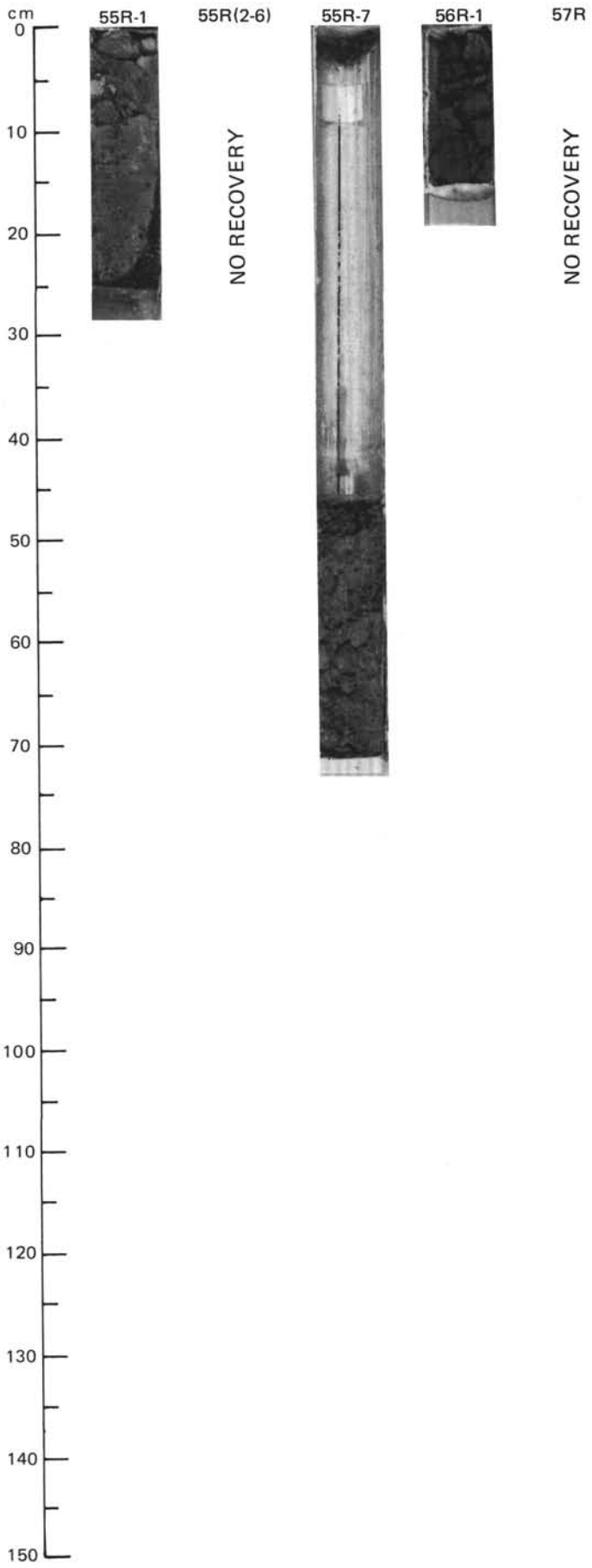
cm
55R-1
55R(2-6)
55R-7
56R-1
57R
0
10
20
30
40
50
60
70
80
90
100
110
120
130
140
150
NO RECOVERY
NO RECOVERY

SITE 647 HOLE A CORE 58 R CORED INTERVAL 4408.2-4417.9 mbsl; 549.7-559.4 mbsf

TIME-ROCK UNIT	BIOSTRAT. ZONE/ FOSSIL CHARACTER: FORAMINIFERS	NANNOFOSSILS	RADIOLARIANS	DIATOMS	PALEOMAGNETICS	PHYS. PROPERTIES	CHEMISTRY	SECTION	METERS	GRAPHIC LITHOLOGY	DRILLING DISTURB.	SED. STRUCTURES	SAMPLES	LITHOLOGIC DESCRIPTION
MIDDLE EOCENE	C/G	A/G	B	B				1		SLURRY	X			Drilling slurry and uphole debris.
P13-P14														

SITE 647 HOLE A CORE 59 R CORED INTERVAL 4417.9-4427.6 mbsl; 559.4-569.1 mbsf

TIME-ROCK UNIT	BIOSTRAT. ZONE/ FOSSIL CHARACTER: FORAMINIFERS	NANNOFOSSILS	RADIOLARIANS	DIATOMS	DINOCYSTS	PALEOMAGNETICS	PHYS. PROPERTIES	CHEMISTRY	SECTION	METERS	GRAPHIC LITHOLOGY	DRILLING DISTURB.	SED. STRUCTURES	SAMPLES	LITHOLOGIC DESCRIPTION
MIDDLE EOCENE	C/G	A/G	F/P	B	F/P				1			X		*	NANNOFOSSIL-BEARING CLAYSTONE Soft drilling slurry and jumbled fragments of nannofossil-bearing claystone. SMEAR SLIDE SUMMARY (%): 1, 35 D TEXTURE: Silt 20 Clay 80 COMPOSITION: Quartz Tr Mica Tr Clay 79 Calcite/dolomite 1 Accessory minerals Tr Nannofossils 20
P13-P14															
NP16															
Phthanoperidinium brooksii															

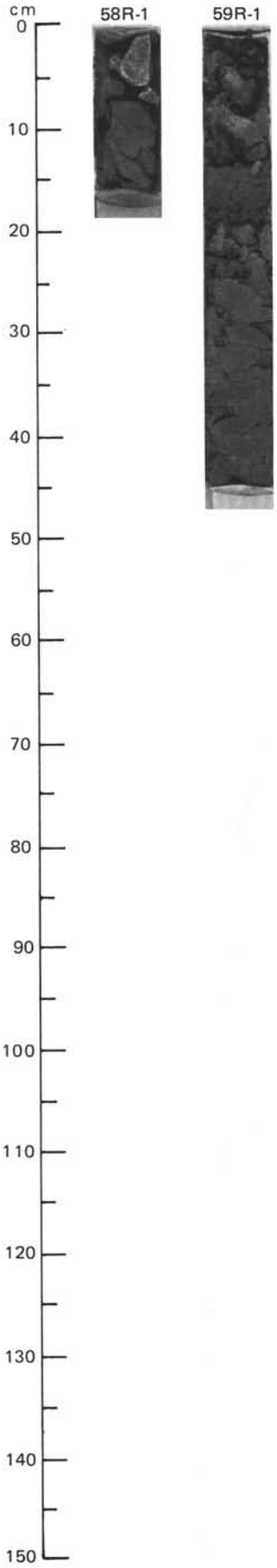
cm
58R-1
59R-1
0
10
20
30
40
50
60
70
80
90
100
110
120
130
140
150

SITE 647 HOLE A CORE 60 R CORED INTERVAL 4427.6-4437.3 mbsl; 569.1-578.8 mbsf

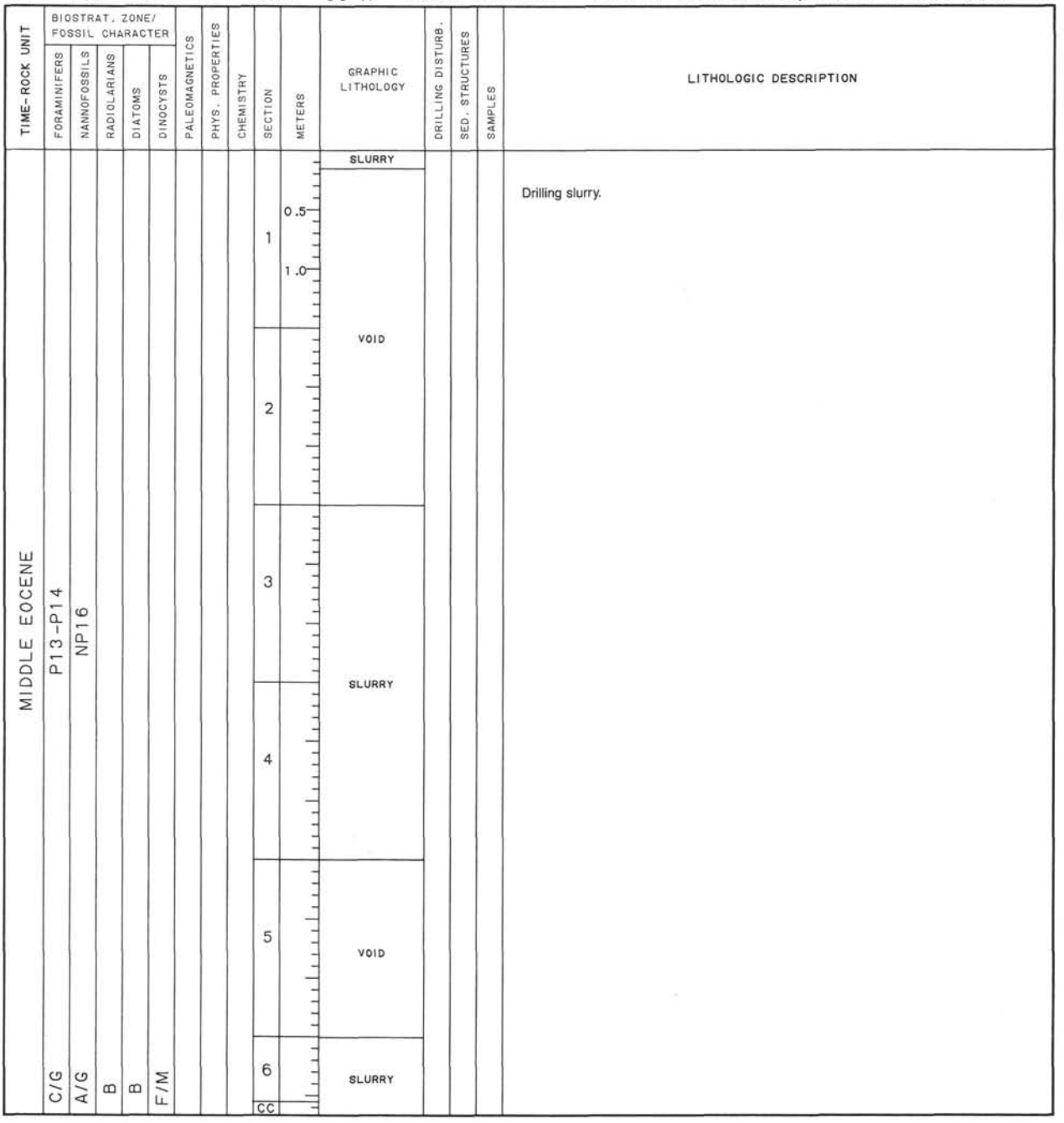

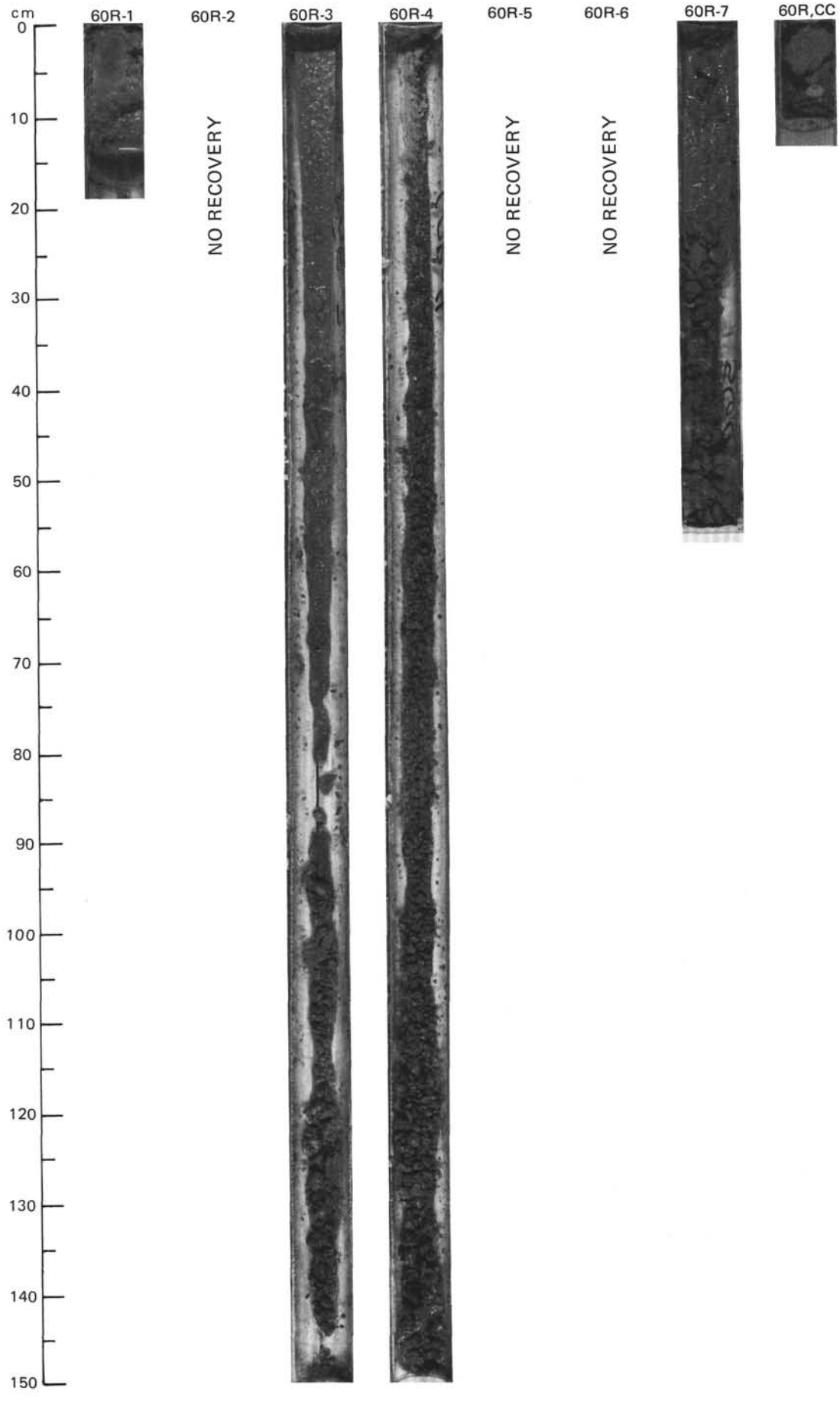
cm
0
10
20
30
40
50
60
70
80
90
100
110
120
130
140
150
60R-1
60R-2
NO RECOVERY
60R-3
60R-4
60R-5
NO RECOVERY
60R-6
NO RECOVERY
60R-7
60R,CC

SITE 647 HOLE A CORE 61 R CORED INTERVAL 4437.3-4446.9 mbsl; 587.8-588.4 mbsf

TIME-ROCK UNIT	BIOSTRAT. ZONE/ OSSIL CHARACTER: FORAMINIFERS	NANNOFOSSILS	RADIOLARIANS	DIATOMS	DINOCYSTS	PALEOMAGNETICS	PHYS. PROPERTIES	CHEMISTRY	SECTION	METERS	GRAPHIC LITHOLOGY	DRILLING DISTURB.	SED. STRUCTURES	SAMPLES	LITHOLOGIC DESCRIPTION
MIDDLE EOCENE	P12? A/G	NP16 A/M	B	B	*P. comatum* F/M				1	0.5		X X		*	NANNOFOSSIL-BEARING CLAYSTONE Nannofossil-bearing claystone, highly deformed. SMEAR SLIDE SUMMARY (%): 1, 48 D TEXTURE: Silt 20 Clay 80 COMPOSITION: Mica Tr Clay 79 Calcite/dolomite Tr Accessory minerals 1 Nannofossils 20

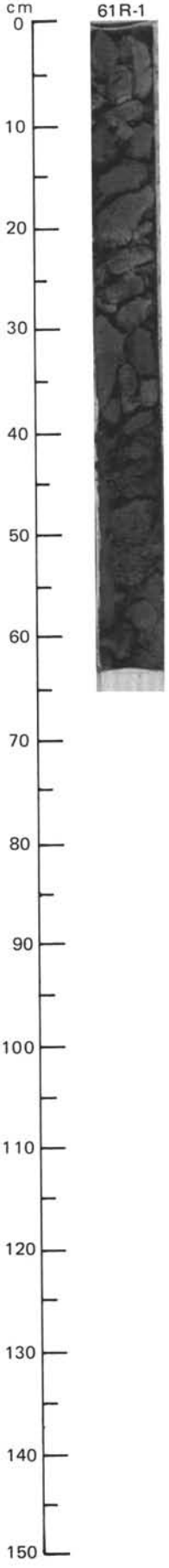
cm
61R-1
0
10
20
30
40
50
60
70
80
90
100
110
120
130
140
150

SITE 647 HOLE A CORE 62 R CORED INTERVAL 4456.6-4466.3 mbsl; 598.1-607.8 mbsf

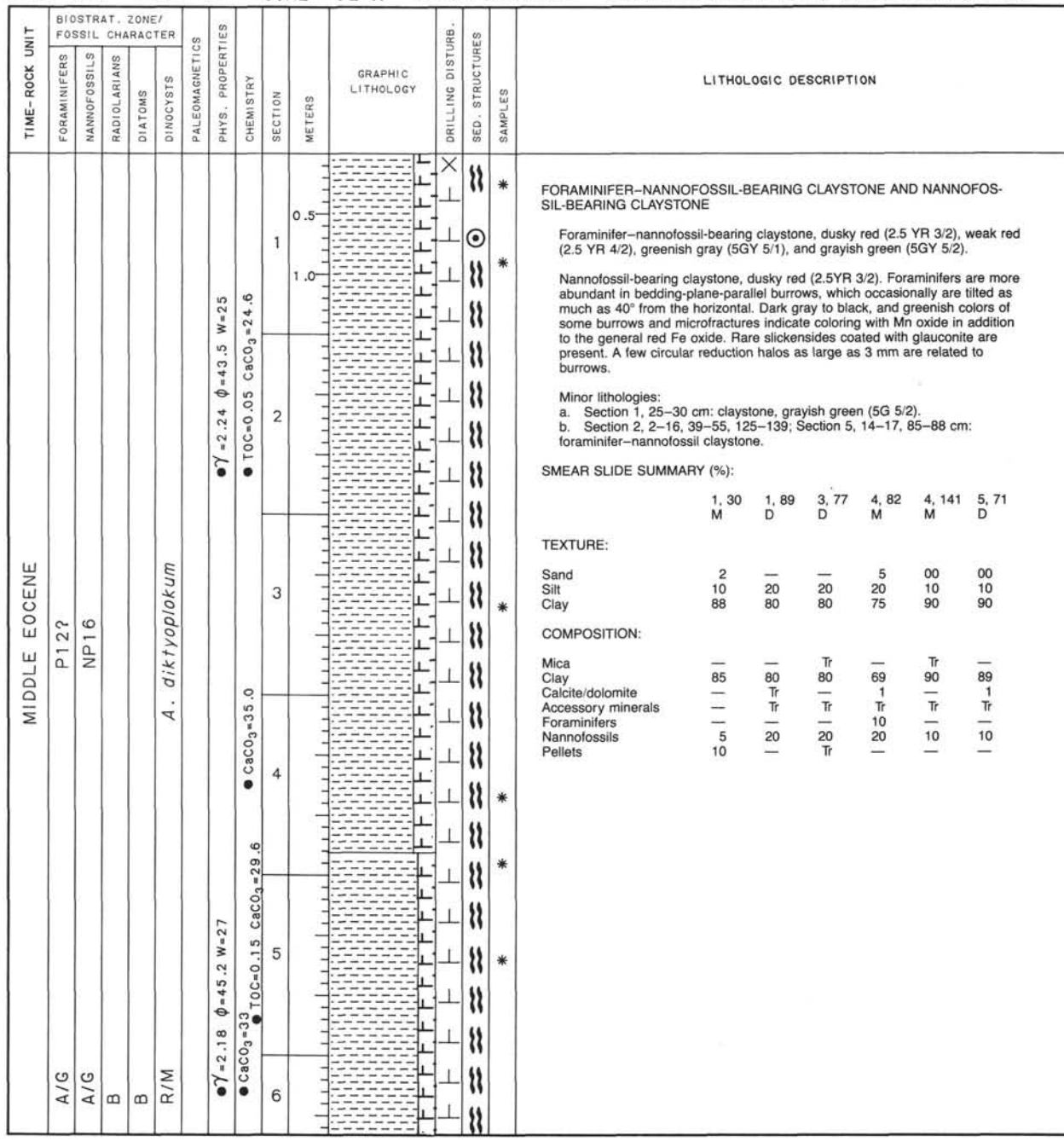

LITHOLOGIC DESCRIPTION

FORAMINIFER–NANNOFOSSIL-BEARING CLAYSTONE AND NANNOFOSSIL-BEARING CLAYSTONE

Foraminifer–nannofossil-bearing claystone, dusky red (2.5 YR 3/2), weak red (2.5 YR 4/2), greenish gray (5GY 5/1), and grayish green (5GY 5/2).

Nannofossil-bearing claystone, dusky red (2.5YR 3/2). Foraminifers are more abundant in bedding-plane-parallel burrows, which occasionally are tilted as much as 40° from the horizontal. Dark gray to black, and greenish colors of some burrows and microfractures indicate coloring with Mn oxide in addition to the general red Fe oxide. Rare slickensides coated with glauconite are present. A few circular reduction halos as large as 3 mm are related to burrows.

Minor lithologies:
a. Section 1, 25–30 cm: claystone, grayish green (5G 5/2).
b. Section 2, 2–16, 39–55, 125–139; Section 5, 14–17, 85–88 cm: foraminifer–nannofossil claystone.

SMEAR SLIDE SUMMARY (%):

	1, 30 M	1, 89 D	3, 77 D	4, 82 M	4, 141 M	5, 71 D
TEXTURE:						
Sand	2	—	—	5	00	00
Silt	10	20	20	20	10	10
Clay	88	80	80	75	90	90
COMPOSITION:						
Mica	—	—	Tr	—	Tr	—
Clay	85	80	80	69	90	89
Calcite/dolomite	—	Tr	—	1	—	1
Accessory minerals	—	Tr	Tr	Tr	Tr	Tr
Foraminifers	—	—	—	10	—	—
Nannofossils	5	20	20	20	10	10
Pellets	10	—	Tr	—	—	—

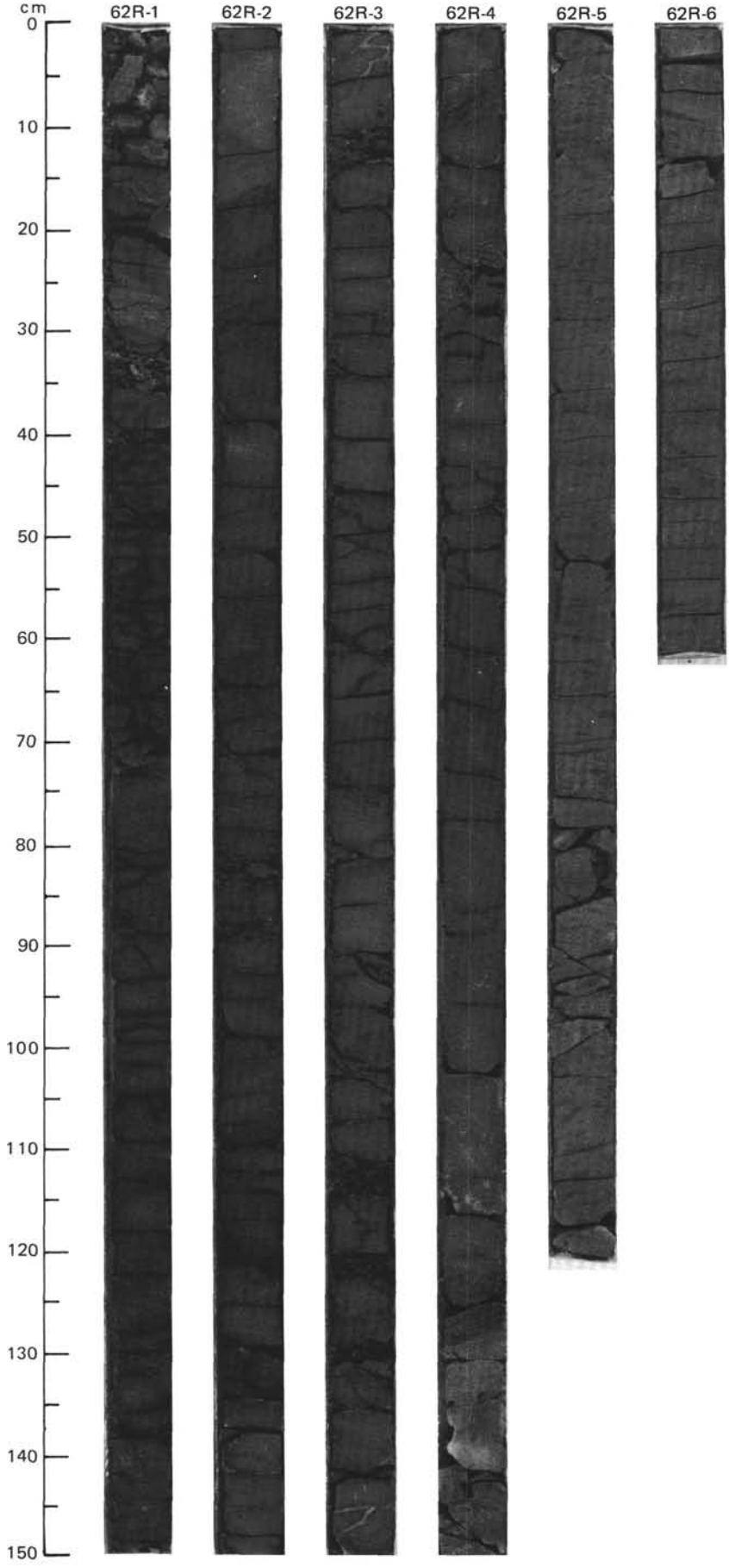
cm
62R-1
62R-2
62R-3
62R-4
62R-5
62R-6
0
10
20
30
40
50
60
70
80
90
100
110
120
130
140
150

SITE 647 HOLE A CORE 63 R CORED INTERVAL 4466.3-4476.0 mbsl; 607.8-617.5 mbsf

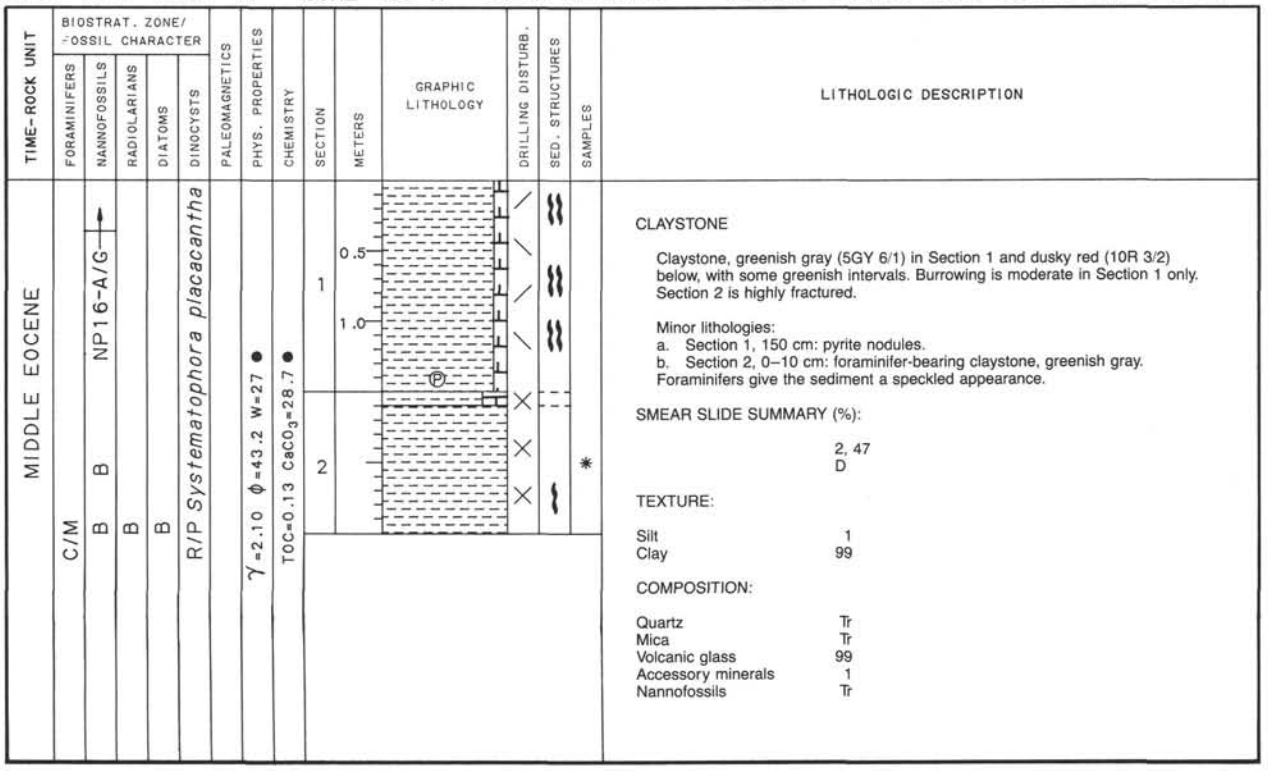

CLAYSTONE

Claystone, greenish gray (5GY 6/1) in Section 1 and dusky red (10R 3/2) below, with some greenish intervals. Burrowing is moderate in Section 1 only. Section 2 is highly fractured.

Minor lithologies:
a. Section 1, 150 cm: pyrite nodules.
b. Section 2, 0–10 cm: foraminifer-bearing claystone, greenish gray. Foraminifers give the sediment a speckled appearance.

SMEAR SLIDE SUMMARY (%):

	2, 47 D
TEXTURE:	
Silt	1
Clay	99
COMPOSITION:	
Quartz	Tr
Mica	Tr
Volcanic glass	99
Accessory minerals	1
Nannofossils	Tr

SITE 647 HOLE A CORE 64 R CORED INTERVAL 4476.0-4485.7 mbsl; 617.5-627.2 mbsf

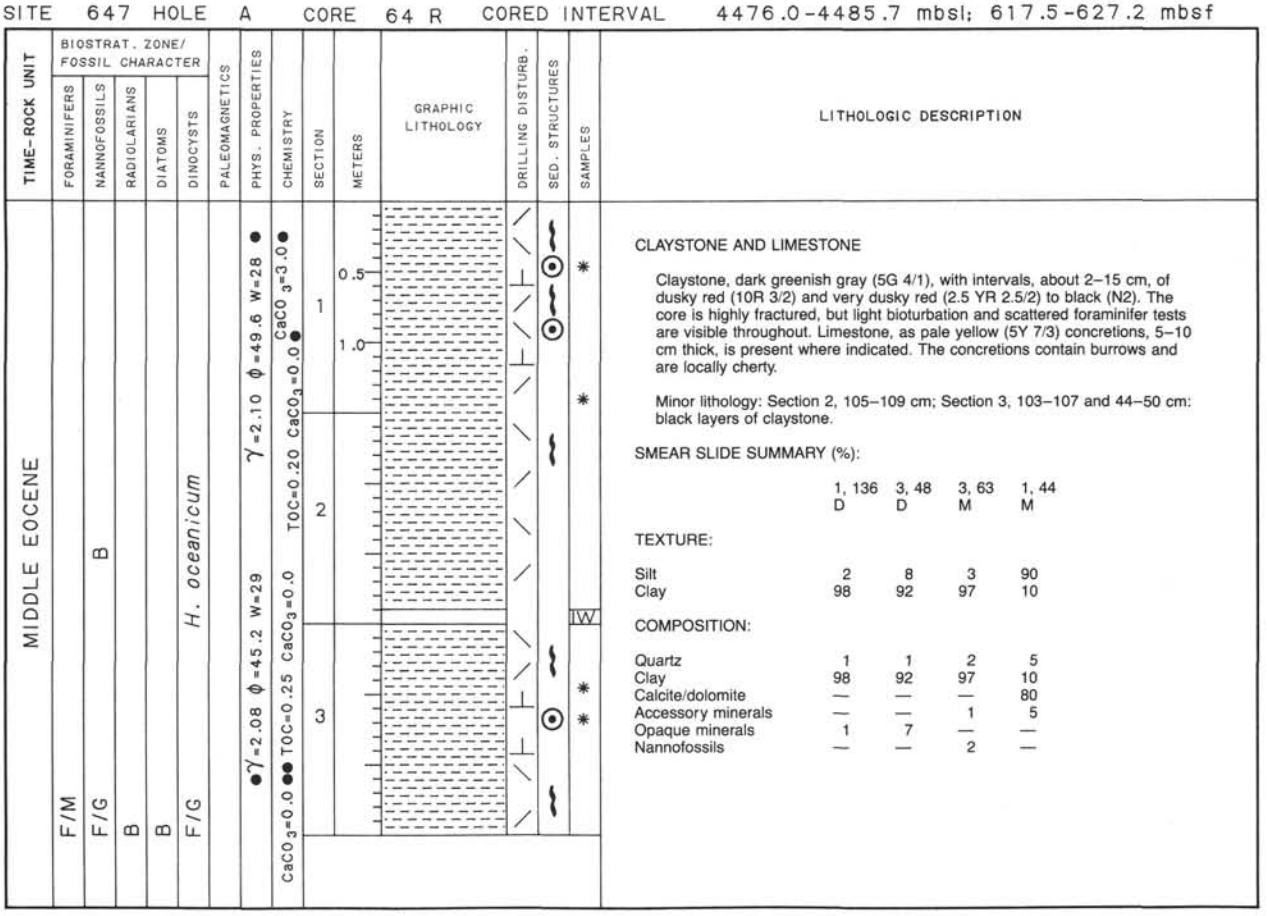

CLAYSTONE AND LIMESTONE

Claystone, dark greenish gray (5G 4/1), with intervals, about 2–15 cm, of dusky red (10R 3/2) and very dusky red (2.5 YR 2.5/2) to black (N2). The core is highly fractured, but light bioturbation and scattered foraminifer tests are visible throughout. Limestone, as pale yellow (5Y 7/3) concretions, 5–10 cm thick, is present where indicated. The concretions contain burrows and are locally cherty.

Minor lithology: Section 2, 105–109 cm; Section 3, 103–107 and 44–50 cm: black layers of claystone.

SMEAR SLIDE SUMMARY (%):

	1, 136 D	3, 48 D	3, 63 M	1, 44 M
TEXTURE:				
Silt	2	8	3	90
Clay	98	92	97	10
COMPOSITION:				
Quartz	1	1	2	5
Clay	98	92	97	10
Calcite/dolomite	—	—	—	80
Accessory minerals	—	—	1	5
Opaque minerals	1	7	—	—
Nannofossils	—	—	2	—

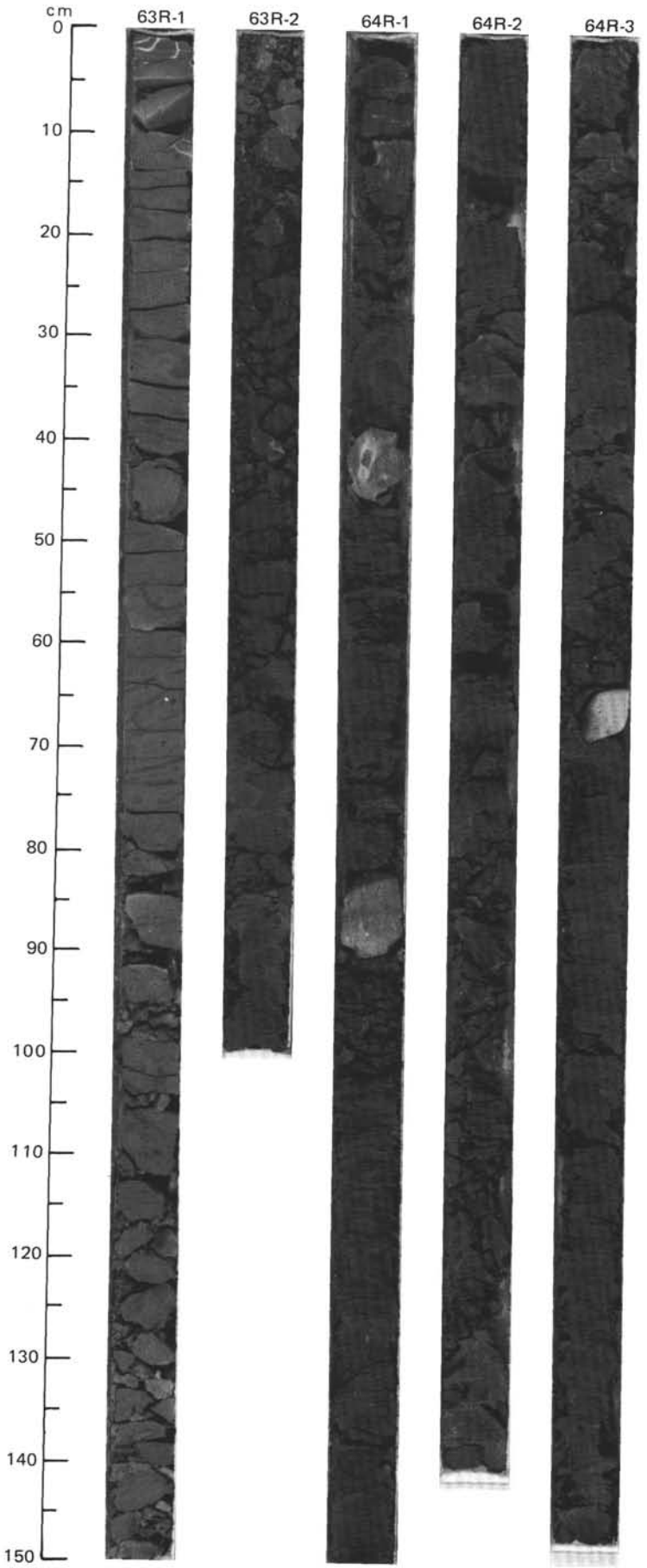
cm
0
10
20
30
40
50
60
70
80
90
100
110
120
130
140
150
63R-1
63R-2
64R-1
64R-2
64R-3

SITE 647 HOLE A CORE 65 R CORED INTERVAL 4485.7-4495.3 mbsl; 627.2-636.8 mbsf

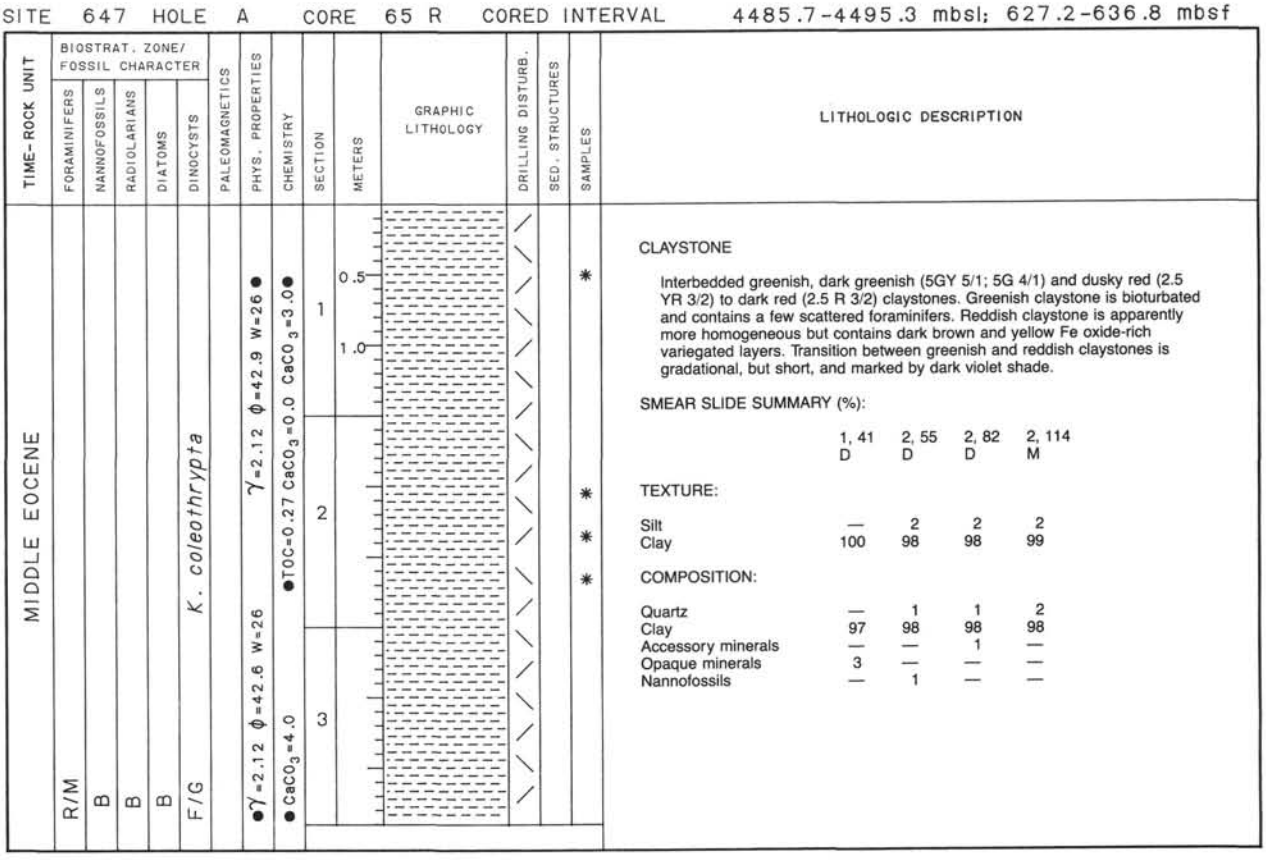

CLAYSTONE

Interbedded greenish, dark greenish (5GY 5/1; 5G 4/1) and dusky red (2.5 YR 3/2) to dark red (2.5 R 3/2) claystones. Greenish claystone is bioturbated and contains a few scattered foraminifers. Reddish claystone is apparently more homogeneous but contains dark brown and yellow Fe oxide-rich variegated layers. Transition between greenish and reddish claystones is gradational, but short, and marked by dark violet shade.

SMEAR SLIDE SUMMARY (%):

	1, 41 D	2, 55 D	2, 82 D	2, 114 M
TEXTURE:				
Silt	—	2	2	2
Clay	100	98	98	99
COMPOSITION:				
Quartz	—	1	1	2
Clay	97	98	98	98
Accessory minerals	—	—	1	—
Opaque minerals	3	—	—	—
Nannofossils	—	1	—	—

SITE 647 HOLE A CORE 66 R CORED INTERVAL 4495.3-4505.0 mbsl; 636.8-646.5 mbsf

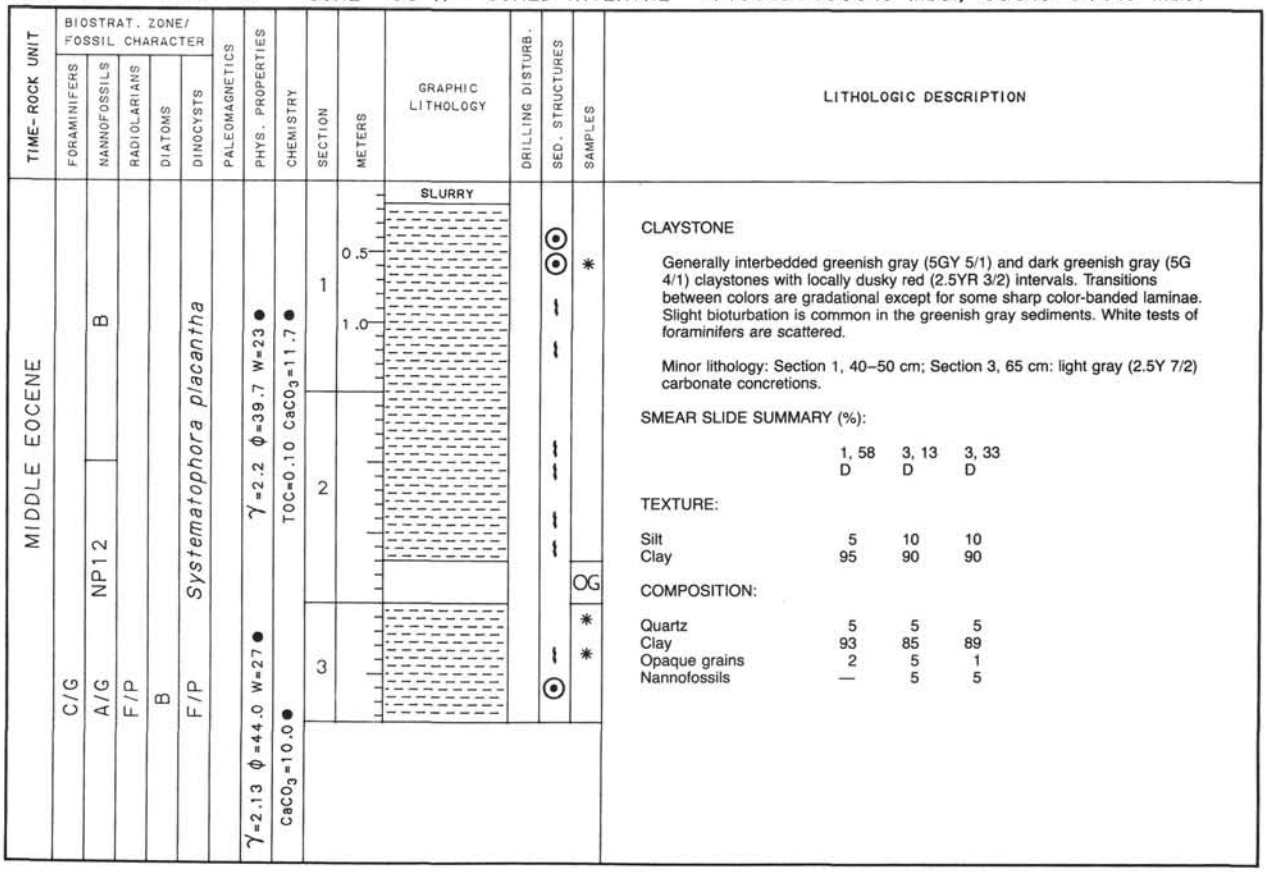

CLAYSTONE

Generally interbedded greenish gray (5GY 5/1) and dark greenish gray (5G 4/1) claystones with locally dusky red (2.5YR 3/2) intervals. Transitions between colors are gradational except for some sharp color-banded laminae. Slight bioturbation is common in the greenish gray sediments. White tests of *foraminifers are scattered.*

Minor lithology: Section 1, 40–50 cm; Section 3, 65 cm: light gray (2.5Y 7/2) carbonate concretions.

SMEAR SLIDE SUMMARY (%):

	1, 58 D	3, 13 D	3, 33 D
TEXTURE:			
Silt	5	10	10
Clay	95	90	90
COMPOSITION:			
Quartz	5	5	5
Clay	93	85	89
Opaque grains	2	5	1
Nannofossils	—	5	5

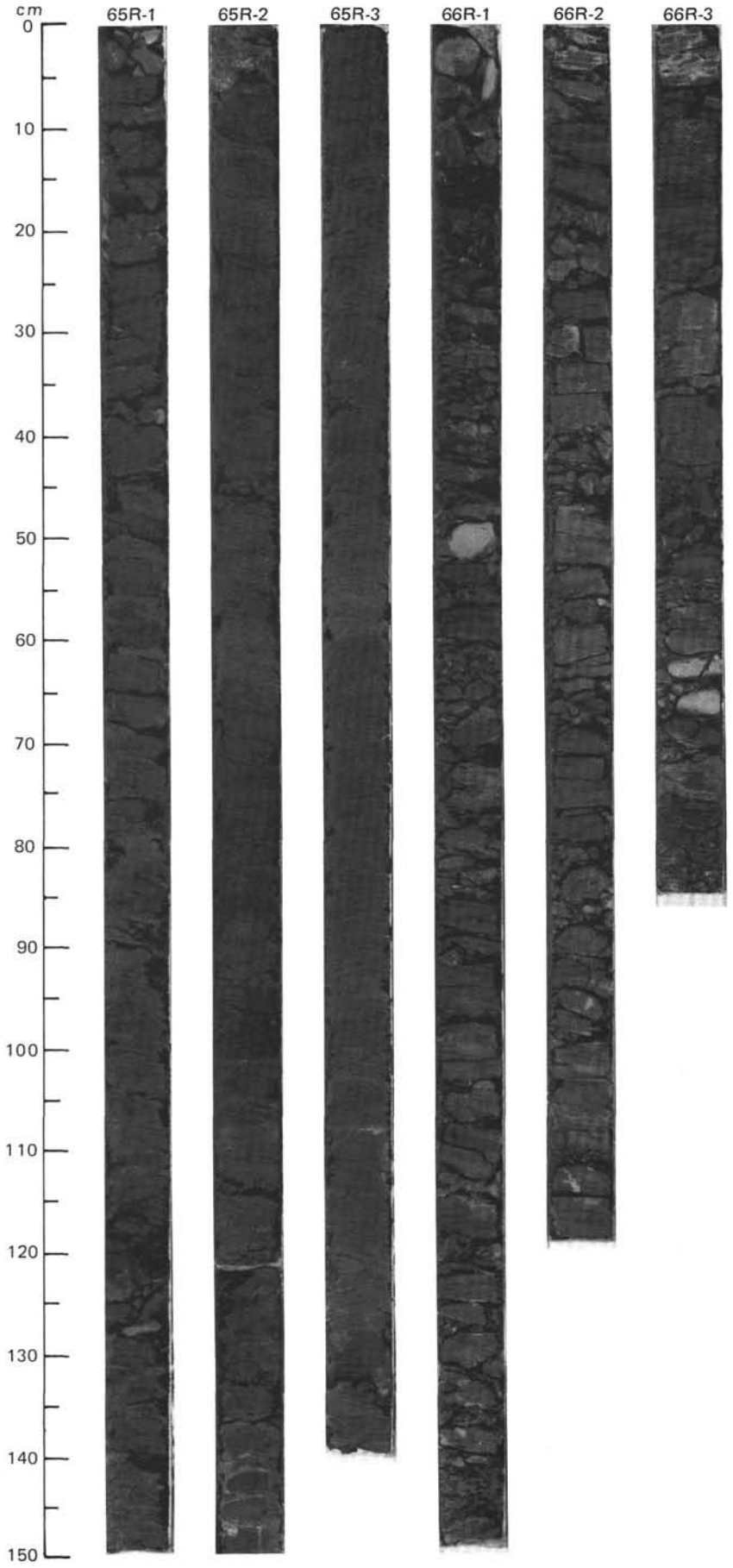
cm
65R-1
65R-2
65R-3
66R-1
66R-2
66R-3
0
10
20
30
40
50
60
70
80
90
100
110
120
130
140
150

SITE 647 HOLE A CORE 67 R CORED INTERVAL 4505.0-4514.7 mbsl; 646.5-656.2 mbsf

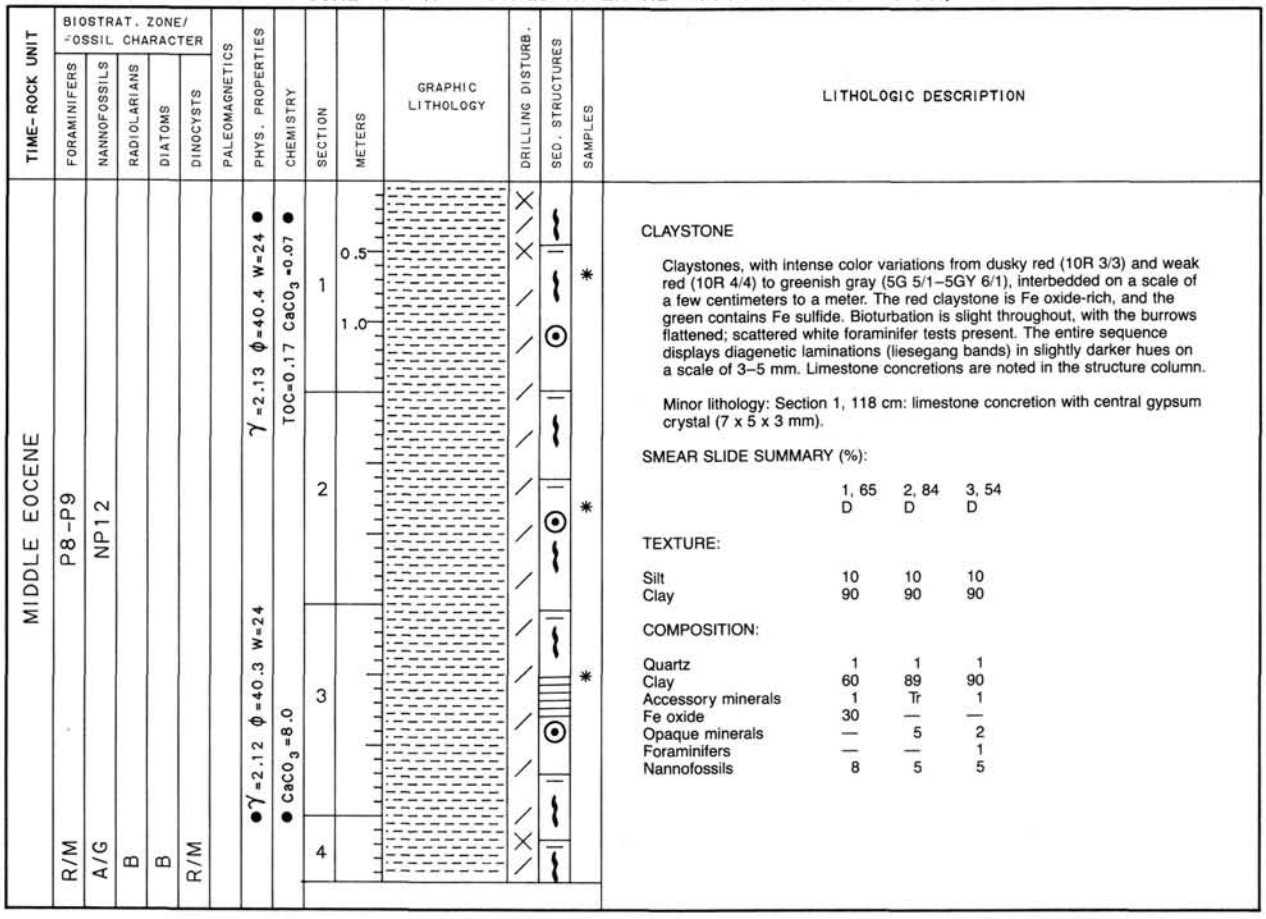

CLAYSTONE

Claystones, with intense color variations from dusky red (10R 3/3) and weak red (10R 4/4) to greenish gray (5G 5/1–5GY 6/1), interbedded on a scale of a few centimeters to a meter. The red claystone is Fe oxide-rich, and the green contains Fe sulfide. Bioturbation is slight throughout, with the burrows flattened; scattered white foraminifer tests present. The entire sequence displays diagenetic laminations (liesegang bands) in slightly darker hues on a scale of 3–5 mm. Limestone concretions are noted in the structure column.

Minor lithology: Section 1, 118 cm: limestone concretion with central gypsum crystal (7 x 5 x 3 mm).

SMEAR SLIDE SUMMARY (%):

	1, 65 D	2, 84 D	3, 54 D
TEXTURE:			
Silt	10	10	10
Clay	90	90	90
COMPOSITION:			
Quartz	1	1	1
Clay	60	89	90
Accessory minerals	1	Tr	1
Fe oxide	30	—	—
Opaque minerals	—	5	2
Foraminifers	—	—	1
Nannofossils	8	5	5

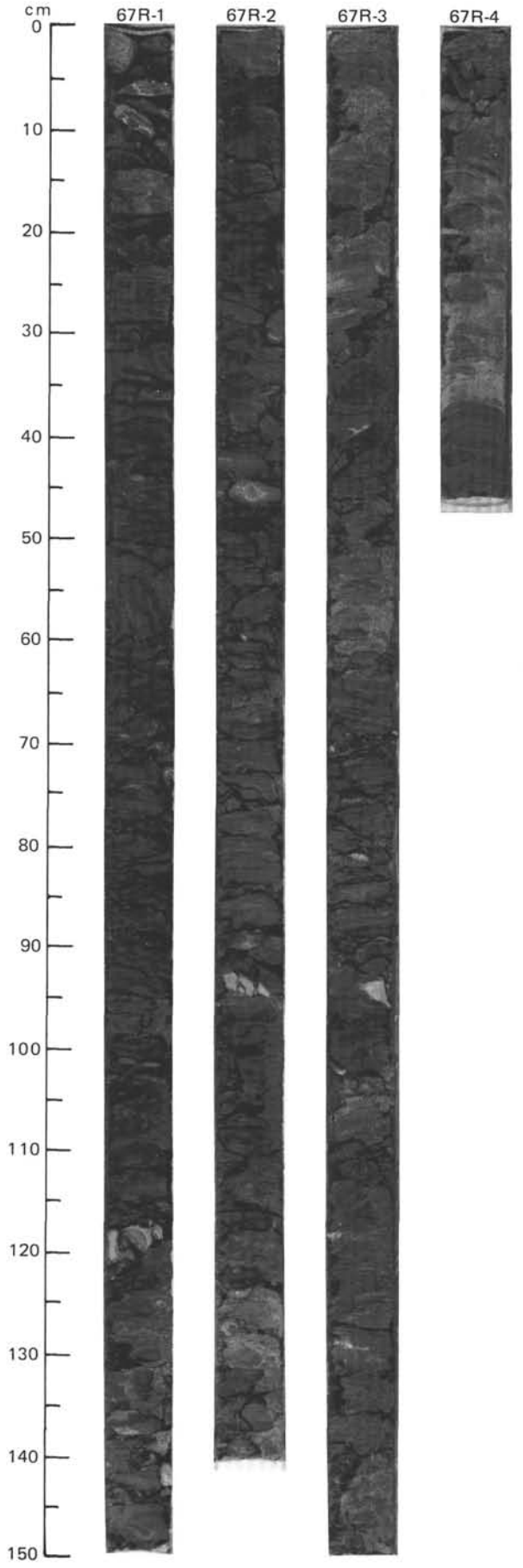
cm
67R-1
67R-2
67R-3
67R-4
0
10
20
30
40
50
60
70
80
90
100
110
120
130
140
150

SITE 647 HOLE A CORE 68 R CORED INTERVAL 4514.7-4524.4 mbsl; 656.2-665.9 mbsf

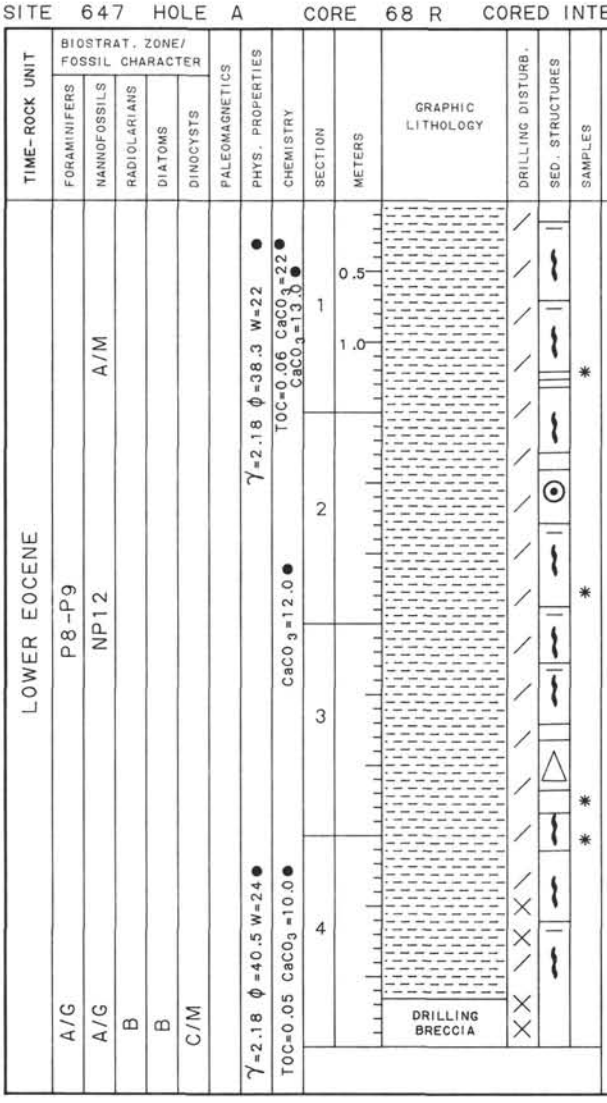

LITHOLOGIC DESCRIPTION

NANNOFOSSIL-BEARING CLAYSTONE

Nannofossil-bearing claystone, with intense color variation from dusky red (10R 3/3) and weak red (10R 4/4) to greenish gray (5G 5/1), interbedded on a scale of a few centimeters to a meter. Minor colors include bluish gray (5B 5/1), white (7.5YR N8/), light gray (7.5YR N7/), and pale green (5G 7/2). Bioturbation is slight; entire sequence displays diagenetic laminations (liesegang bands) and mottles of slightly darker or lighter hues on a scale of 1–5 mm. Foraminifer tests are scattered throughout, but also occur as more concentrated groups; e.g., Section 3, 30–38, 12–18, 0–4 cm. Section 3, 138–191 cm, consists of a sequence with upward decreasing content of foraminifer tests.

SMEAR SLIDE SUMMARY (%):

	1, 122 D	2, 128 D	3, 128 M	4, 7 D
TEXTURE:				
Silt	20	13	20	13
Clay	80	87	80	87
COMPOSITION:				
Quartz	2	1	1	1
Clay	79	87	80	87
Accessory minerals	1	2	1	1
Opaque minerals	1	—	—	—
Foraminifers	4	2	3	1
Nannofossils	13	8	15	10

SITE 647 HOLE A CORE 69 R CORED INTERVAL 4524.4-4534.0 mbsl; 665.9-675.5 mbsf

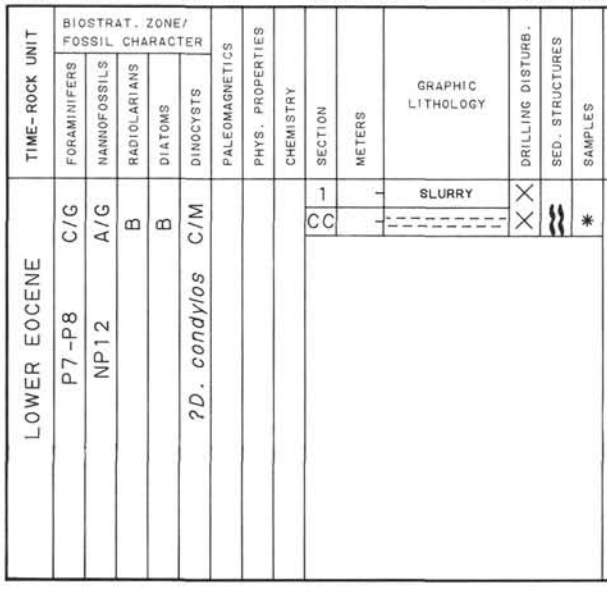

LITHOLOGIC DESCRIPTION

CLAYSTONE

Claystone, mottled weak brownish, grayish and greenish (5G 5/1–5YR 4/1) with scattered foraminifers and pyrite concretions.

SMEAR SLIDE SUMMARY (%):

	CC, 12 D
TEXTURE:	
Silt	4
Clay	96
COMPOSITION:	
Mica	Tr
Clay	96
Calcite/dolomite	1
Accessory minerals	Tr
Nannofossils	3

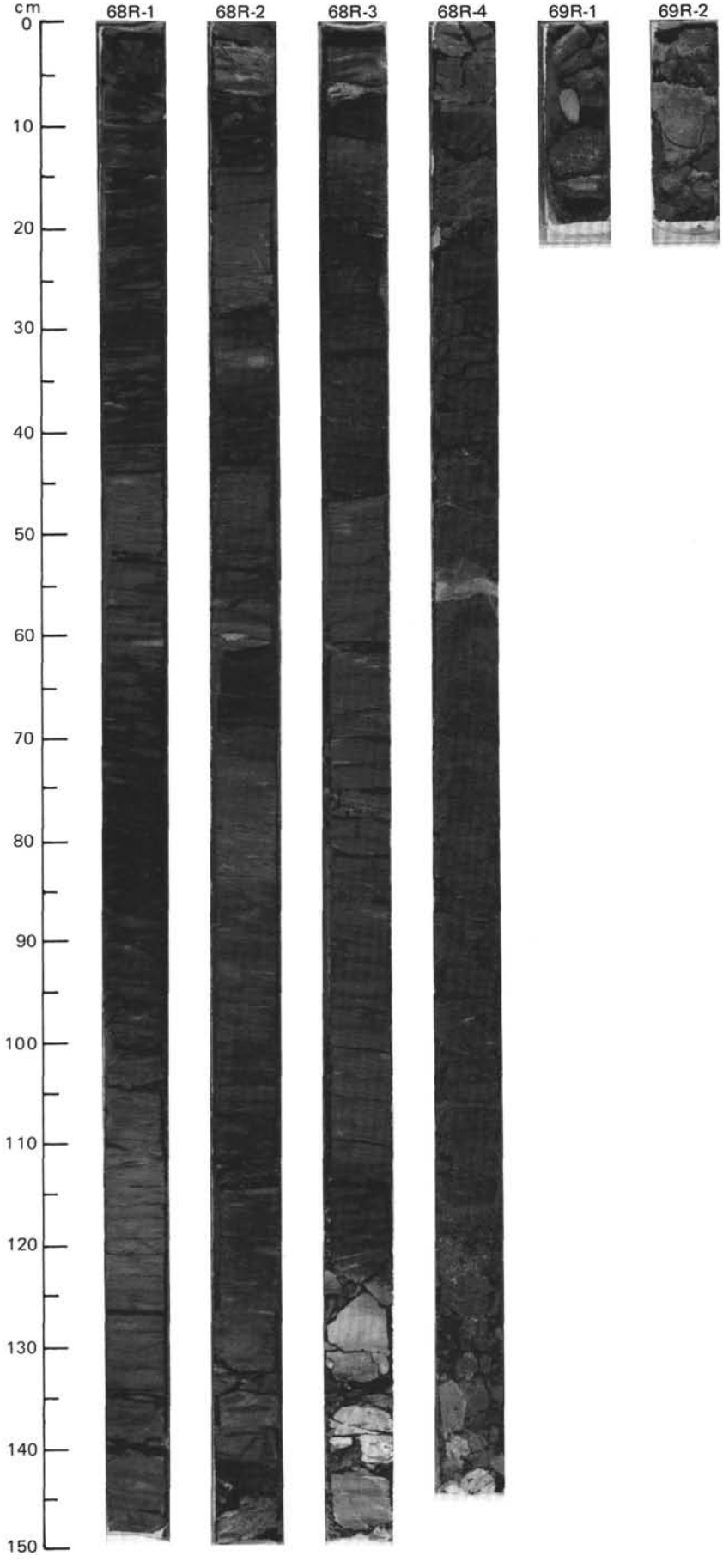
cm
0
10
20
30
40
50
60
70
80
90
100
110
120
130
140
150
68R-1
68R-2
68R-3
68R-4
69R-1
69R-2

SITE 647 HOLE A CORE 70 R CORED INTERVAL 4543.7-4553.3 mbsl; 685.2-694.8 mbsf

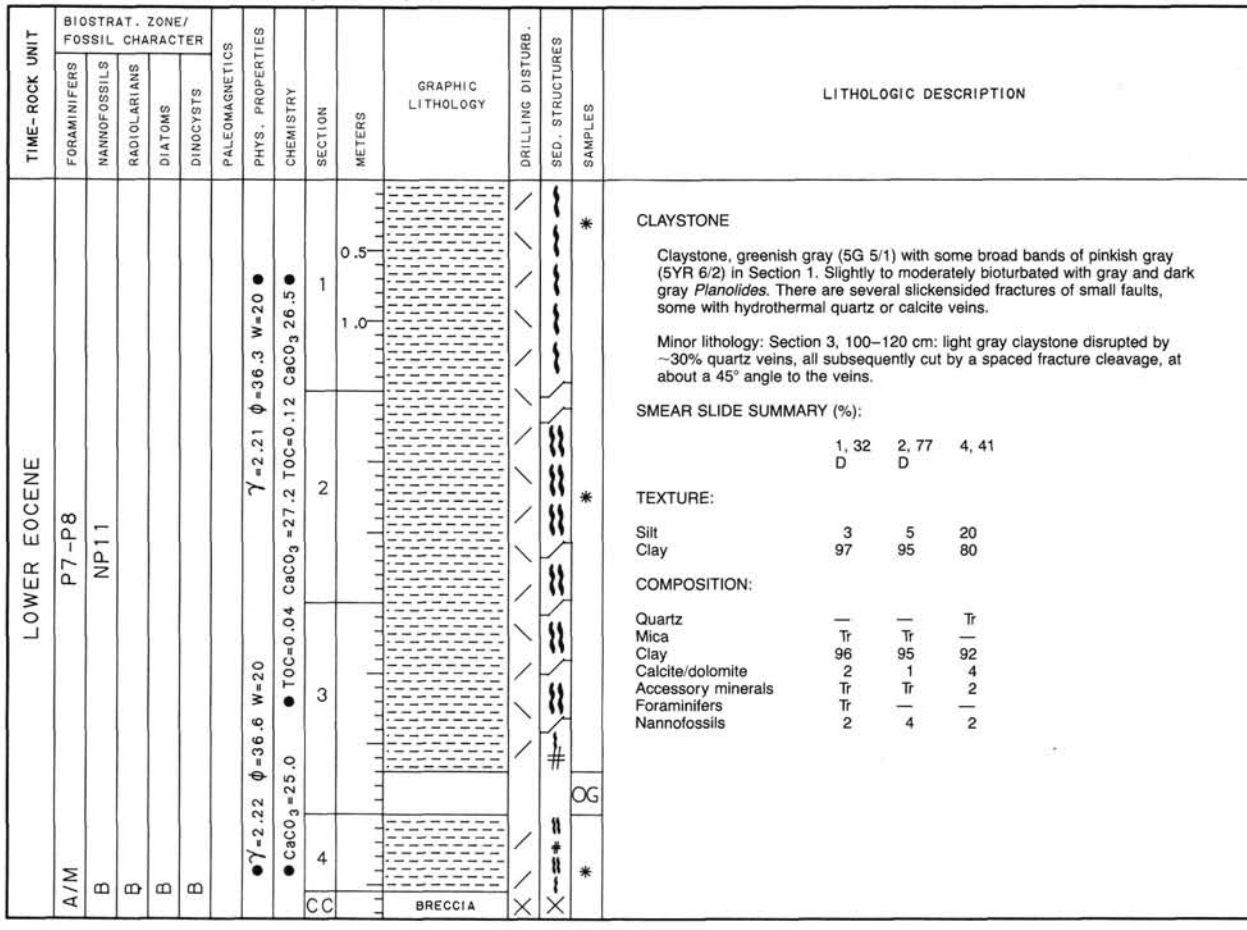

CLAYSTONE

Claystone, greenish gray (5G 5/1) with some broad bands of pinkish gray (5YR 6/2) in Section 1. Slightly to moderately bioturbated with gray and dark gray *Planolides*. There are several slickensided fractures of small faults, some with hydrothermal quartz or calcite veins.

Minor lithology: Section 3, 100–120 cm: light gray claystone disrupted by ~30% quartz veins, all subsequently cut by a spaced fracture cleavage, at about a 45° angle to the veins.

SMEAR SLIDE SUMMARY (%):

	1, 32 D	2, 77 D	4, 41
TEXTURE:			
Silt	3	5	20
Clay	97	95	80
COMPOSITION:			
Quartz	—	—	Tr
Mica	Tr	Tr	—
Clay	96	95	92
Calcite/dolomite	2	1	4
Accessory minerals	Tr	Tr	2
Foraminifers	Tr	—	—
Nannofossils	2	4	2

SITE 647 HOLE A CORE 71 R CORED INTERVAL 4553.5-4563.0 mbsl; 694.8-704.5 mbsf

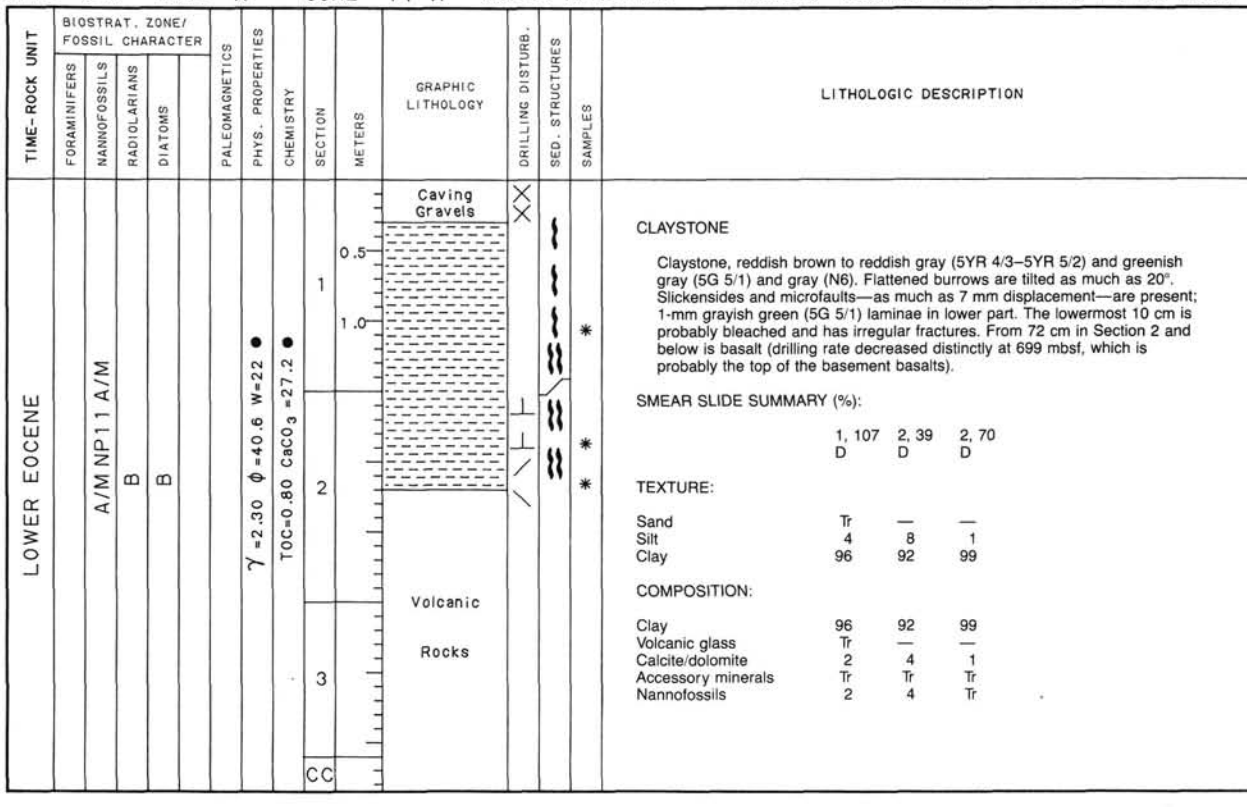

CLAYSTONE

Claystone, reddish brown to reddish gray (5YR 4/3–5YR 5/2) and greenish gray (5G 5/1) and gray (N6). Flattened burrows are tilted as much as 20°. Slickensides and microfaults—as much as 7 mm displacement—are present; 1-mm grayish green (5G 5/1) laminae in lower part. The lowermost 10 cm is probably bleached and has irregular fractures. From 72 cm in Section 2 and below is basalt (drilling rate decreased distinctly at 699 mbsf, which is probably the top of the basement basalts).

SMEAR SLIDE SUMMARY (%):

	1, 107 D	2, 39 D	2, 70 D
TEXTURE:			
Sand	Tr	—	—
Silt	4	8	1
Clay	96	92	99
COMPOSITION:			
Clay	96	92	99
Volcanic glass	Tr	—	—
Calcite/dolomite	2	4	1
Accessory minerals	Tr	Tr	Tr
Nannofossils	2	4	Tr

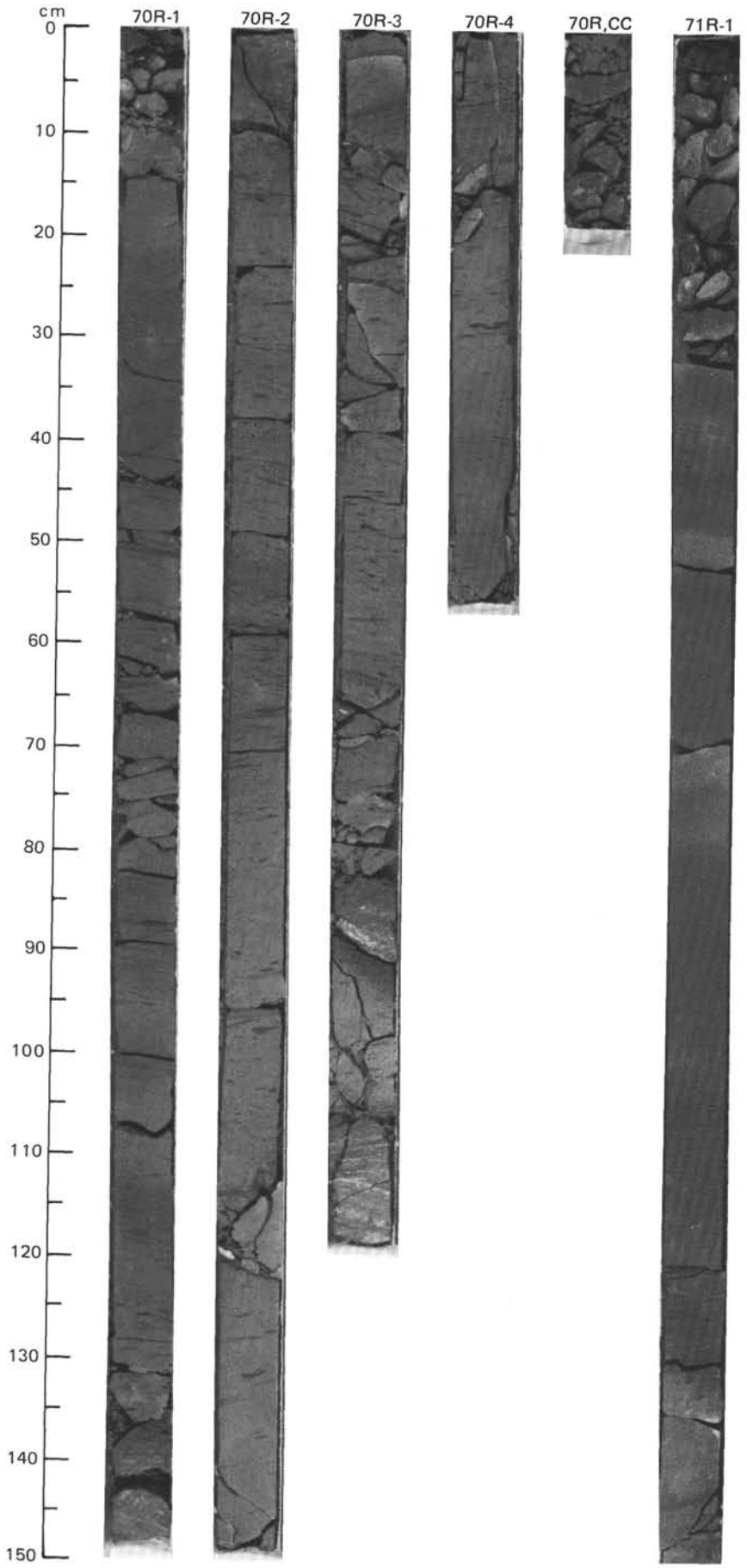
cm
0
10
20
30
40
50
60
70
80
90
100
110
120
130
140
150
70R-1
70R-2
70R-3
70R-4
70R,CC
71R-1

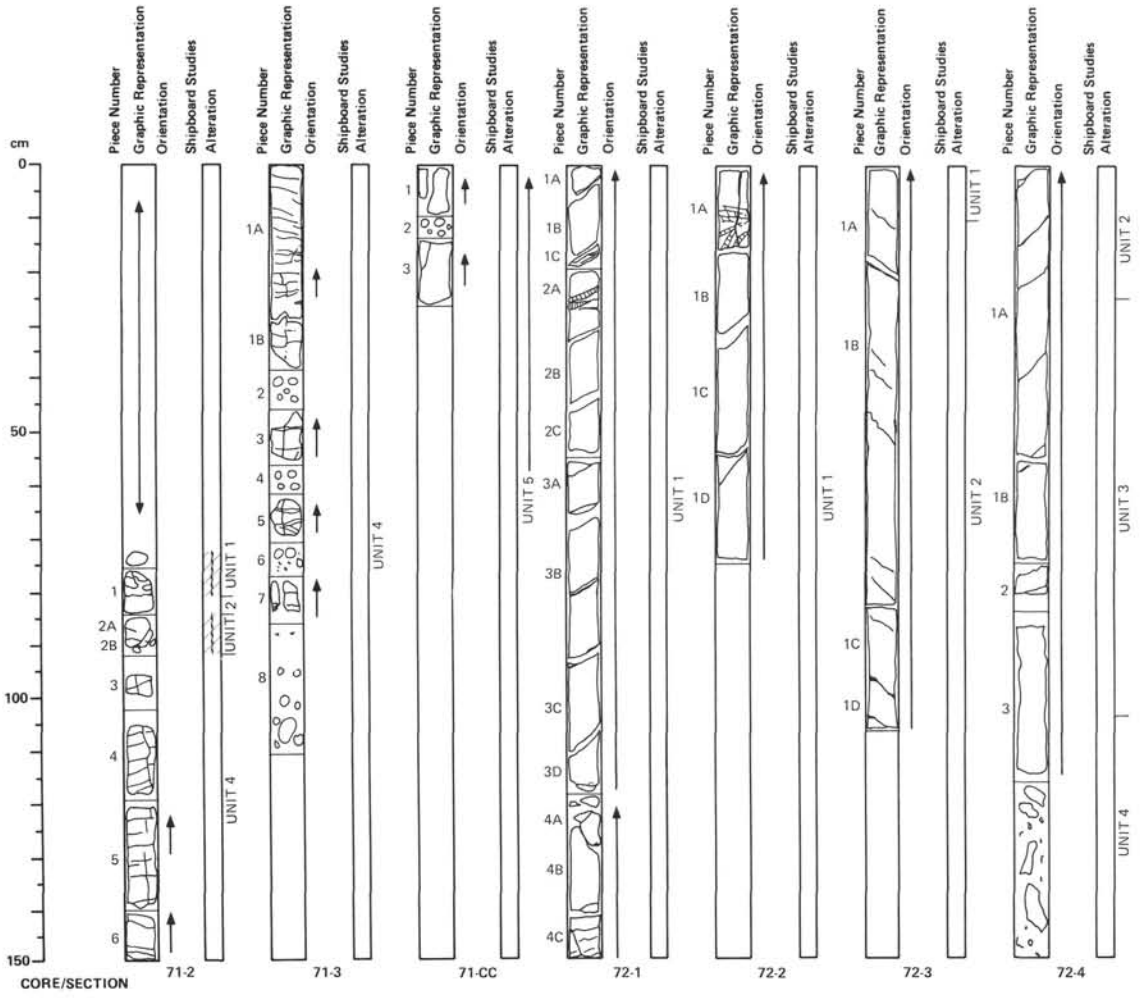

105–647A–72R

4563.0–4572.6 MBSL **704.5–714.0 MBSF**

UNIT 1 **647A–72R–1, 0 cm to 647A–72R–3, 10 cm**

Fine-grained aphyric basalt.
Phenocrysts: pyroxene less than 1% up to 1 mm in diameter.
Color: gray (2.5Y N5)
Alteration: *no visible alteration*
Fracturing: SH = 3; I = 10; SV = 1.
1a: talc-filled vein on the bottom 6 mm
1a: strongly altered, greenish mixture of different minerals strongly fractured.
2a: 2–5 mm subhorizontal veins of talc-rich material.
Inclined veins are dominantly filled by calcite; in some cases with slip striae and pyrite crystals.

Section 647A–72R–2
Phenocrysts: pyroxene less than 1% at 1 mm thickness.
Fracturing: SV1, I4 1a – 8–16 cm; multiple highly fractured veins with different greenish minerals and quartz and pyrite.

UNIT 2 **647A–72R–3, 10 cm to 647A–72R–4, 25 cm**

Fine-grained, sparsely phyric, basalt
Phenocrysts: pyroxene - 2% at 0.5–2 mm.
Color: (2.5Y N5) gray.
Fracturing: V=0; I9; H1; 2 are filled with calcite (0.5 mm).

UNIT 3 **647A–72R–4, 25–113 cm**

Fine-medium-grained moderate phyric basalt
Phenocrysts: Pyroxene less than 10%
Color: (2.5Y N5) gray.
Fracturing: H=0; I=7; V=0

UNIT 4 **647A–72R–4 113–150 cm**

Fine-grained, sparsely phyric, basalt
Phenocrysts: pyroxene; 2 at 0.5–2 mm.

105–647A–71R

4553.3–4563.0 MBSL **694.8–704.5 MBSF**

Basement rock was recovered at the bottom of this core in section 647A–71R–2.

UNIT 1 **647A–71R–2, 73-82 cm**

Coarsely crystalline calcite and chlorite, occurring as a hydrothermal meshwork of radiating white crystals and veins, which surround irregular fragments (2–3 cm in diameter) with internal large-scale spherulitic texture. These appear glassy on uncut surfaces. The color is pale gray to white.
Alteration: Strong, with numerous crosscutting veins, devitrification of fragments, soft chlorite and calcite hydrothermal void filling.
Fractures: I = 2.

UNIT 2 **647A–71R–2, 82–84 cm**

Aphyric finely crystalline (upper contact) to **spherulitic or variolitic** (< 1 mm variolites) basalt with large calcite-filled vesicles (0.7 x 2 cm maximum). Cross-cutting vein breaks through top, which has a botryoidal, laminated crust, 0.1–0.5 mm thick. Top 1 cm seems to be a chilled margin. This unit is probably a flow, with original glassy top. Large fragments in UNIT 1 are probably flow-top breccia.
Phenocrysts: Absent
Vesicles: To 2 cm long and <1 cm high, filled with calcite and chlorite.
Color: Dark greenish gray (5BG 4/1)
Alteration: Little apparent, except for crosscutting vein of chlorite.
Crystallinity: Aphanitic to finely crystalline and variolitic. Top could be pillow salvage.

UNIT 3 **647A–71R–2, 82–93 cm**

Talc-or pyrophyllite - bearing basalt. The rock is strongly altered, is greenish gray (5BG 5/1) in color, and has a chalky luster. Vesicles range up to <5 mm size. The material is strongly altered by veins of calcite. This rock may be the altered equivalent of UNIT 4 below.
Fractures: V = 1.

UNIT 4 **647A–71R–2, 32 cm to 647A–71R–3, 110 cm**

Finely crystalline, aphyric basalt with scattered <1 mm vesicles filled with chlorite and calcite. The most striking feature is stockwork veins of calcite and chlorite which are <5 mm wide. The rocks are greenish gray (5G 5/1). No obvious alteration is observed. This unit is probably part of a thin flow because it is so finely crystalline. No salvages are present.
Fractures: H = 20, V = 3. Section 647A–71R–4, greenish gray (5G 5/1) with very rare vesicles 1 mm in diameter which are partly filled with calcite. Very few altered veins, frequent horizontal veins up to 3 mm thick. A few vertical veins are present with occasional veins up to 1 mm thick. Both types are filled with: a. calcite (dominant) b. chlorite (abundant) c. pyrite (common). Thirty-one horizontal or almost horizontal fractures (veins filled). One to two nearly vertical fractures, some of which are filled (veins). Grain size coarsens *downward.*

UNIT 5 **647A–71R, CC, 0–26cm**

Aphyric, fine-grained basalt, dark gray to dark greenish gray. Very slightly altered to un-altered. One 3 mm thick, horizontal vein filled with calcite. One vertical fracture. No vesicles.

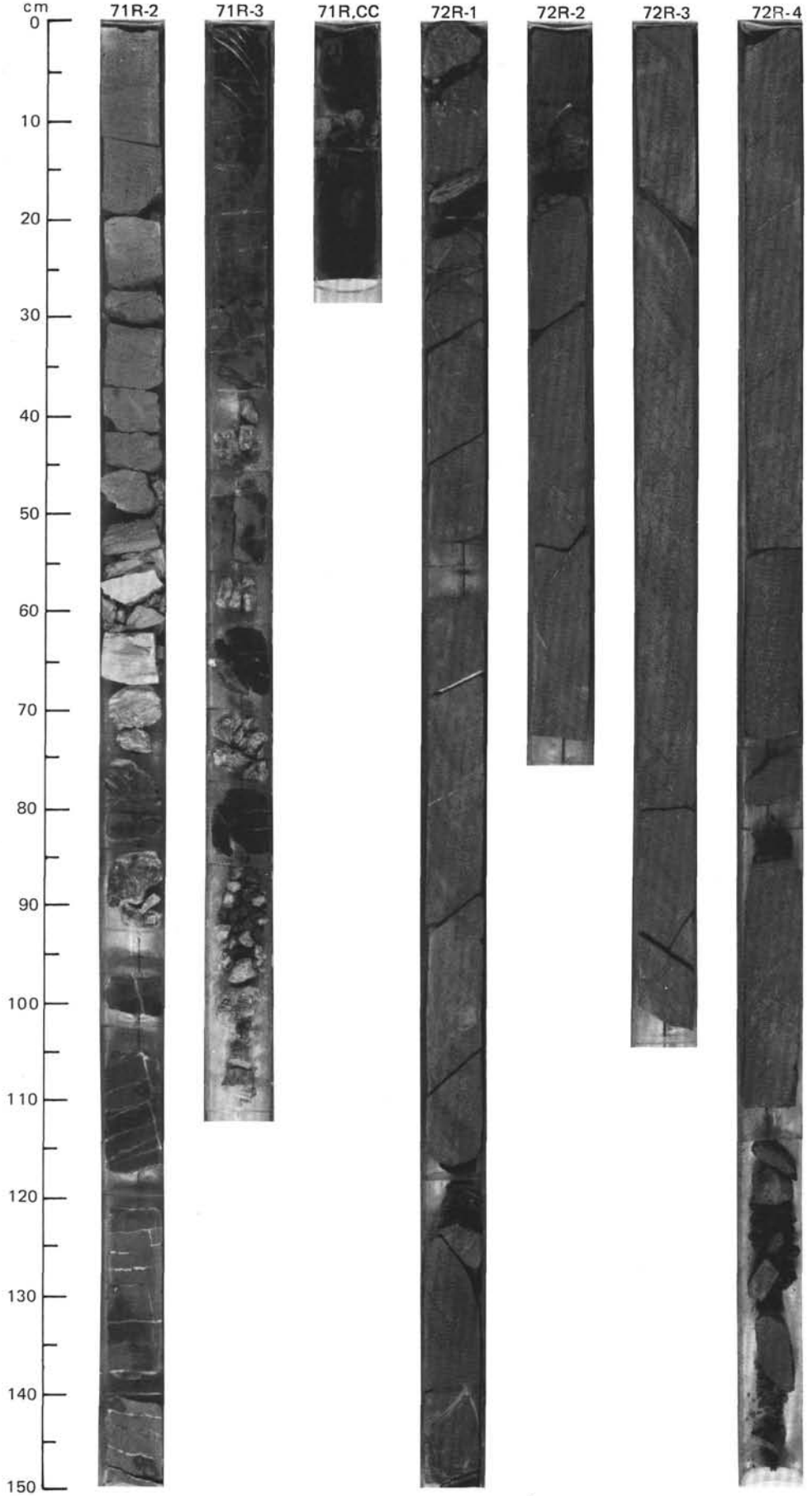
cm
0
10
20
30
40
50
60
70
80
90
100
110
120
130
140
150
71R-2
71R-3
71R,CC
72R-1
72R-2
72R-3
72R-4

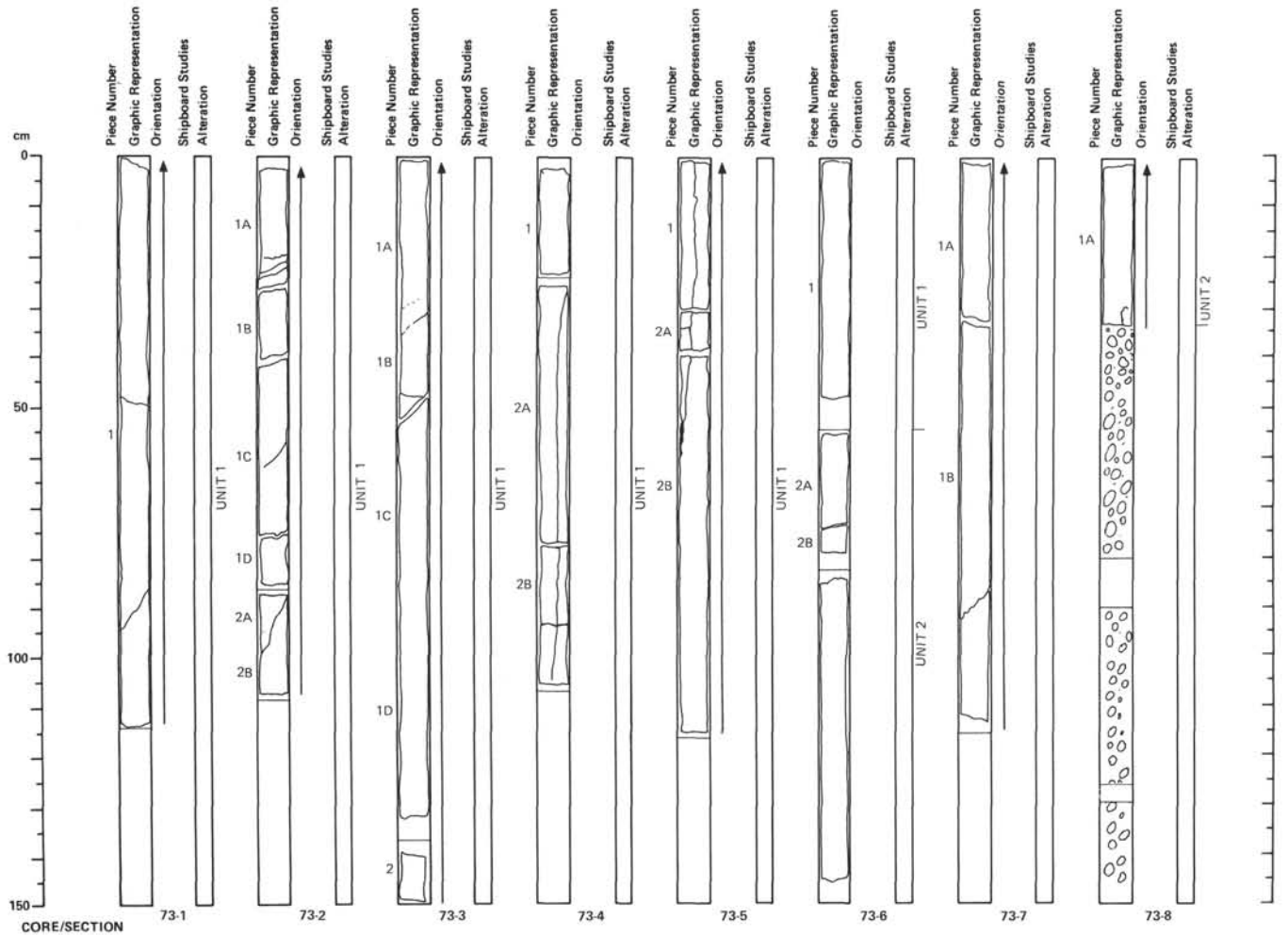

105–647A–73R–1

4572.6–4582.0 MBSL **714.0–723.5 MBSF**

UNIT 1 **647A–73R–1, 0 cm to 647A–73R–6, 54 cm**

Medium-grained, sparsely pyroxene-phyric massive basalt.

Phenocrysts: pyroxene - 2% at 0.5–1.5 mm.

Vesicles: *absent*

Color: gray

Fracturing: numerous fine, irregular, inclined, fractures.

Section 73R–2

Fracturing: Numerous irregular fine fractures mostly inclined to subhorizontal.

1a, 24 cm: 0.5 cm thick fracture (subhorizontal) filled with greenish minerals, possibly chlorite. 42 cm, calcite filled fracture between 1b and 1c.

Section 73R–3

Phenocrysts: pyroxene - 1% at 0.5–1.5 mm

1a, 31 cm: concentrated band of phenocrysts

Fracturing: I = 4

1b, 48 cm, clacite filled, 1 mm thick fracture,horizontal to inclined.

Vesiciles: rare irregular vesicles filled with phyllosilicates and calcite.

Section 73R–4

Fracturing: SH = 3, one vertical fracture in Piece 2a and 2b on top filled with calcite.

Section 73R–5

Phenocrysts: pyroxene; 2% at 1 mm.

Fracturing: some horizontal fine fractures; one large vertical fracture from 0–60 cm.

UNIT 2 **647A–73R–6, 54 cm, to 647A–73R–8, 34 cm**

Medium-grained, moderately pyroxene phyric, massive basalt.

Phenocrysts: pyroxene; 5% at 1–2 mm.

Color: gray

Fracturing: some fine subhorizontal, irregular fractures.

Section 73R–7

Phenocrysts: pyroxene; 3–5% at 1–2 mm.

Fracturing: *some fine irregular subhorizontal fractures.*

1b one irregular inclined fracture.

Section 73R–8

Phenocrysts: pyroxene; 7% at 1–2 mm.

Fracturing: calcite filled fracture (vertical) at the bottom from 33–150 cm; and CC, 0–11 cm (vertical). Drilling breccia containing different pebble-sized sediment fragments from younger lithologies above (cavings). Smear slides show nannofossils from the middle Eocene, which are younger than the oldest ages from the sediment directly above the basement contact.

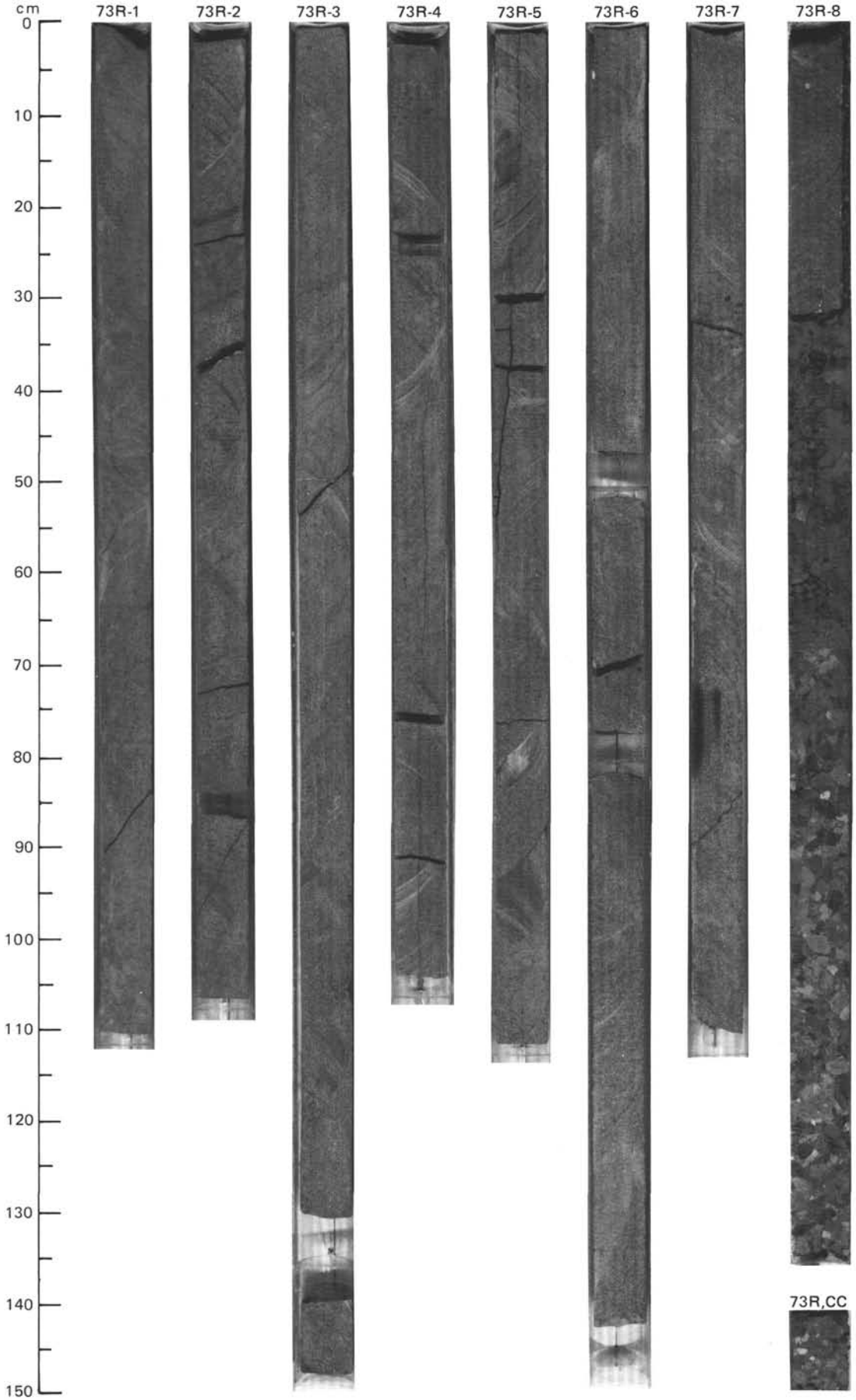
cm
0
10
20
30
40
50
60
70
80
90
100
110
120
130
140
150
73R-1
73R-2
73R-3
73R-4
73R-5
73R-6
73R-7
73R-8
73R,CC

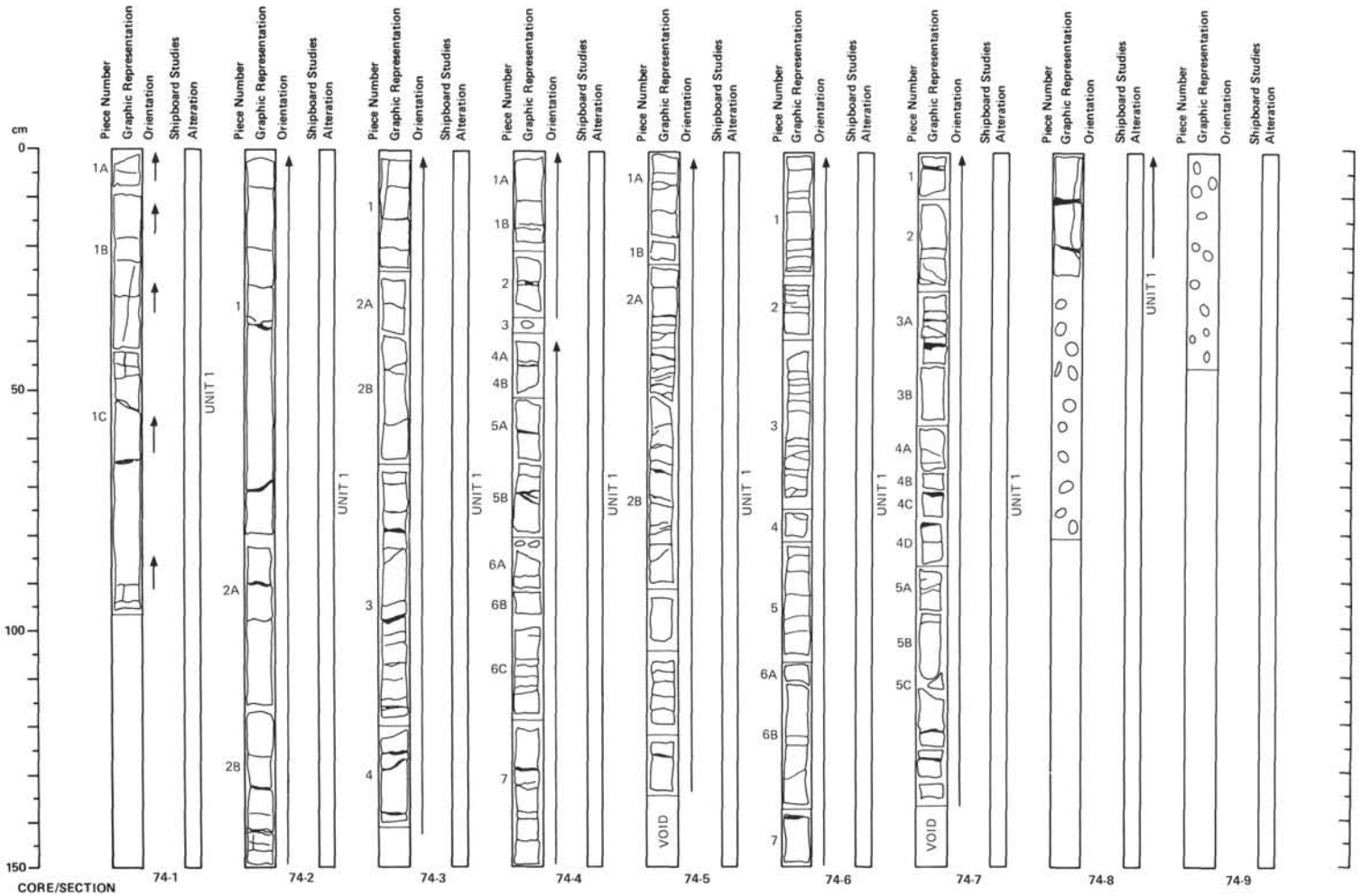

105–647A–74R

4582.0–4591.5 MBSL **723.5–733.0 MBSF**

UNIT 1 **647A–74R–1, 0 cm to 647A–74R–8, 26 cm**

Medium grained, moderately pyroxene-phyric, massive basalt; *fresh pyroxene:* 5%; 1 mm, *pockets of very light gray irregular small* crystals (probably plagioclase) in a very fine black matrix. Pyroxenes occur in the black matrix as well as in the gray pockets.
No Vesicles
H = 9; SB = 3; V = 7.
Most veins (9) less than 1 mm; (2) ca 3 mm thick
The vein material is pyrite (abundant) calcite (very rare) and greenish phyllosilicates. Probably chlorite and/or serpentine (dominant).

Section 74R–2
Pyroxene: 5%; 1–1.5 mm
Small crystals of light gray plagioclase are somewhat concentrated in 5 mm "pockets" surrounded by a black finer grained matrix. Pyroxene-phenocrysts less abundant in these 'pockets".

Horizontal fractures and veins: 14, 7: 2–3 mm thick, 7: 1 mm; one vertical fracture in the bottom is less than 1 mm thick.

Vein material: pyrite (abundant), calcite (very rare), phyllosilicates (dominant), probably chlorite and serpentine.

Isolated grains of pyrite, some millimeters in diameter mm in thick veins. In thin veins, pyrite may be the dominant secondary mineral.

Section 74R–3
Horizontal fractures and veins 15) 9 > 1 mm.
Subhorizontal fractures and veins 5) 11 ≤ 1 mm. Two of the latter complex with *smaller* 'apophyses."
One vertical vein <1 mm.

Vein material: Dominant: chlorite and serpentine
Abundant: pyrite a) as few mm grains in thick veins. b) dominant in some smaller veins.

Section 74R–4
H = 21; SH = 2.
Two of the latter complex with smaller 'apophyses."
Chlorite and serpentine dominant in veins.
Pyrite often concentrated in few mm grains in bigger veins.
Fractures are produced by drilling and are almost entirely located in veins.
Section 74R–5
H = 17; SH = 12.
Section 74R–6
H = 30; SH = 4.
Section 74R–7
H = 15; SH = 3.
Section 74R–8
Two horizontal veins of chlorite/serpentine
One vertical vein of chlorite/serpentine.
26–81 cm: drill, gravel and slurry cavings from younger sediments.
Drill, gravel and slurry cavings: 74R–9, 0–26 *cm.*

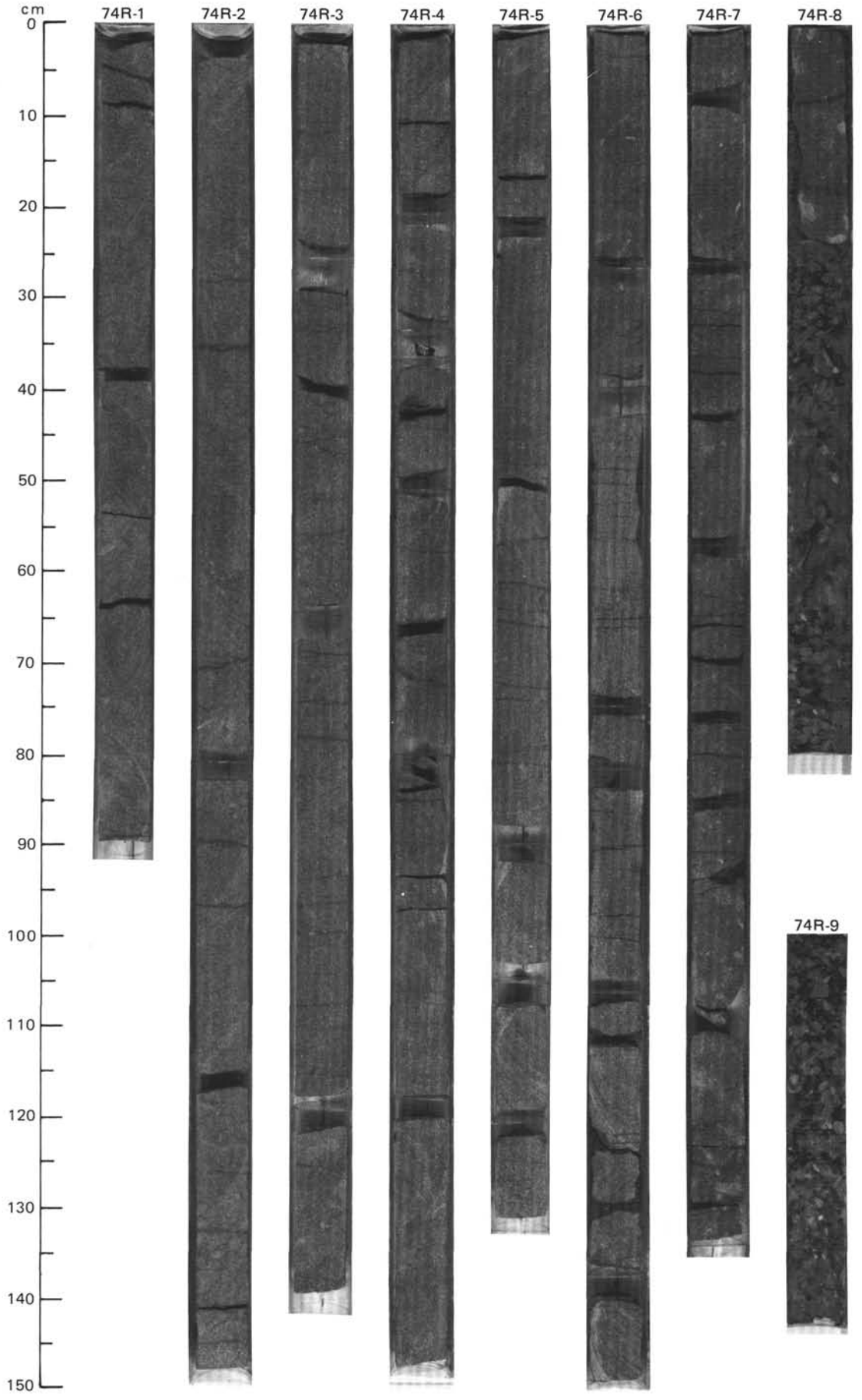
cm
0
10
20
30
40
50
60
70
80
90
100
110
120
130
140
150
74R-1
74R-2
74R-3
74R-4
74R-5
74R-6
74R-7
74R-8
74R-9

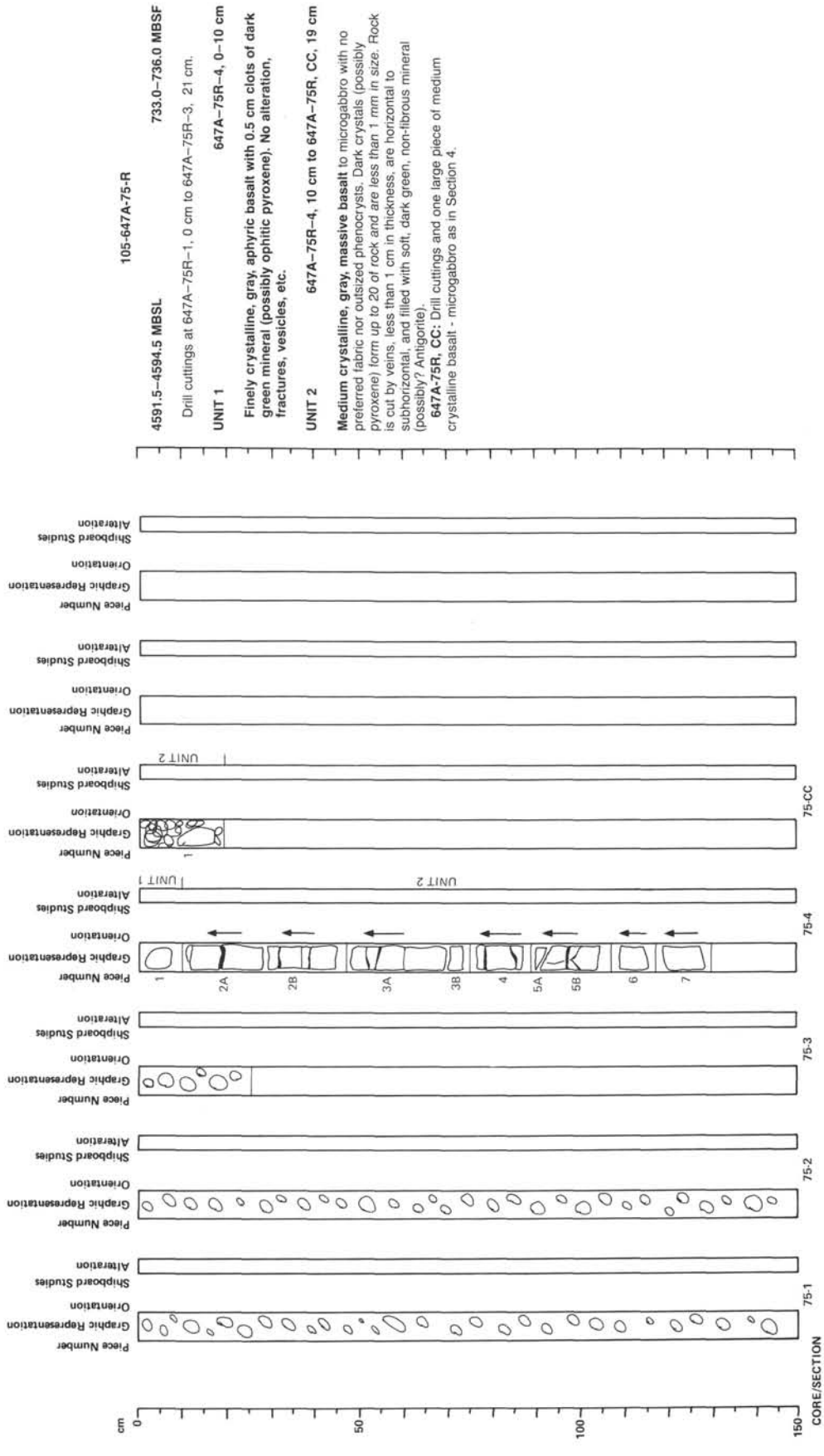
105-647A-75-R
4591.5–4594.5 MBSL
733.0–736.0 MBSF
Drill cuttings at 647A–75R–1, 0 cm to 647A–75R–3, 21 cm.
UNIT 1
647A–75R–4, 0–10 cm
Finely crystalline, gray, aphyric basalt with 0.5 cm clots of dark green mineral (possibly ophitic pyroxene). No alteration, fractures, vesicles, etc.
UNIT 2
647A–75R–4, 10 cm to 647A–75R, CC, 19 cm
Medium crystalline, gray, massive basalt to microgabbro with no preferred fabric nor outsized phenocrysts. Dark crystals (possibly pyroxene) form up to 20 of rock and are less than 1 mm in size. Rock is cut by veins, less than 1 cm in thickness, are horizontal to subhorizontal, and filled with soft, dark green, non-fibrous mineral (possibly? Antigorite).
647A-75R, CC: Drill cuttings and one large piece of medium crystalline basalt - microgabbro as in Section 4.
Piece Number
Graphic Representation
Orientation
Shipboard Studies
Alteration
cm
0
50
100
150
CORE/SECTION
75-1
75-2
75-3
75-4
75-CC
UNIT 1
UNIT 2
1
2A
2B
3A
3B
4
5A
5B
6
7

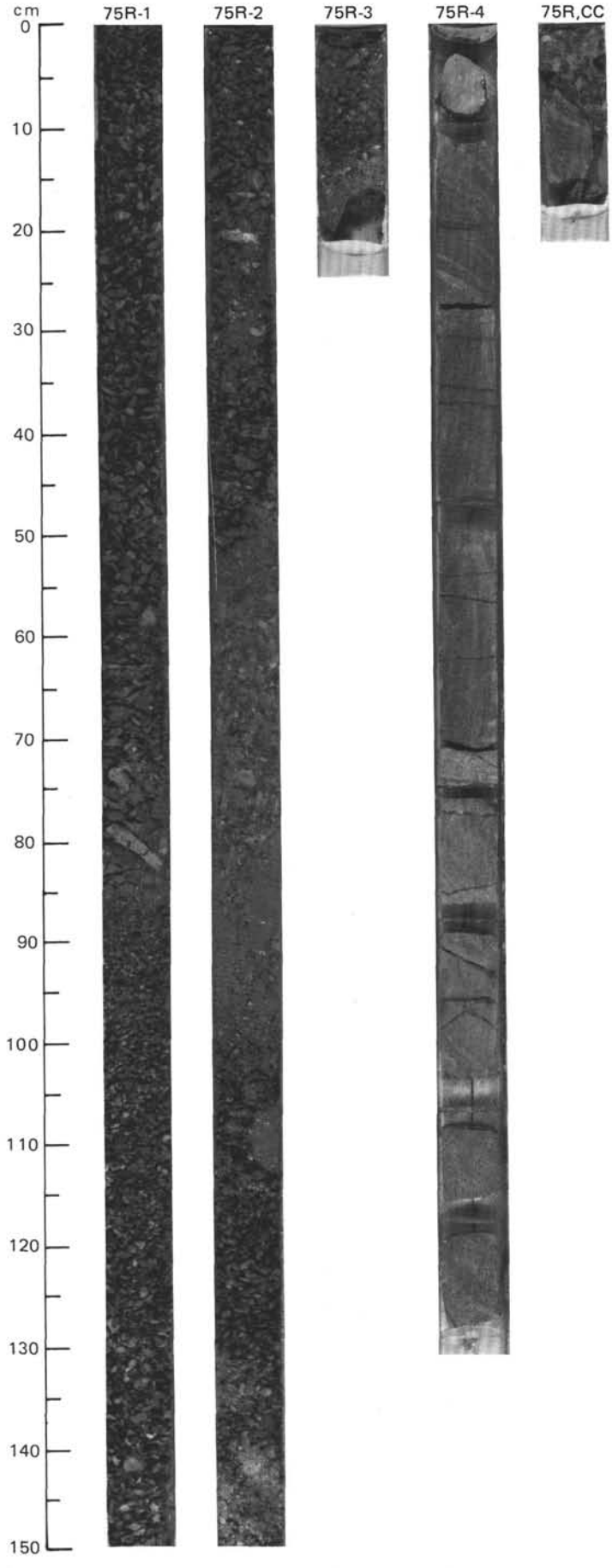
cm
75R-1
75R-2
75R-3
75R-4
75R,CC
0
10
20
30
40
50
60
70
80
90
100
110
120
130
140
150

SITE 647 HOLE B CORE 1 H CORED INTERVAL 3860.2-3867.0 mbsl; 0.0-6.8 mbsf

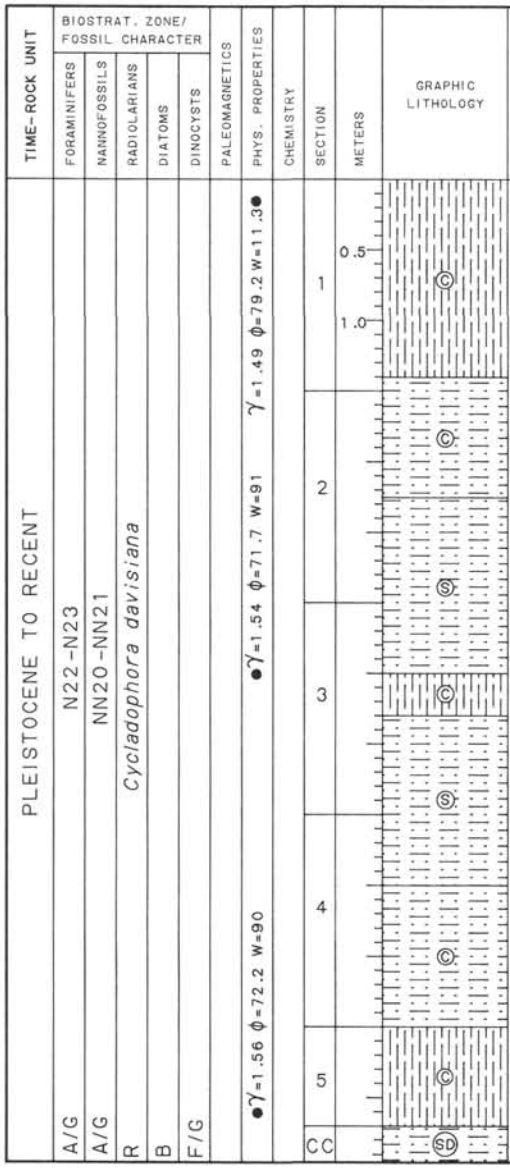

LITHOLOGIC DESCRIPTION

SILTY CLAY, CLAYEY MUD, AND SILTY MUD

Silty clay, light yellowish brown (10YR 6/4), pale brown (10YR 6/3), light brownish gray (10YR 6/1), and light gray (2.5Y 7/2); interbedded with clayey mud, light olive gray (5Y 6/2), light brownish gray (2.5Y 6/2) and greenish gray (5GY 6/1), and silty mud, olive gray (5Y 5/2) to gray (5Y 5/1).

Flow-in: bottom of Section 3 and Section 4. Otherwise distinctly mottled throughout. Silty clay of Section 1 displays subtle color layering and grain-size variations with sharp-based graded unit at Section 1, 39–32 cm. Dropstone pebbles are irregularly distributed and granules are scattered, but locally in groups of greater abundance.

Minor lithology: CC: muddy sand, light gray (5Y 6/1); homogeneous.

SMEAR SLIDE SUMMARY (%):

	1, 80 D	2, 35 D	2, 90 D	3, 72 D	3, 120 D	4, 46 D	4, 51 D
TEXTURE:							
Sand	7	15	20	4	30	11	11
Silt	45	30	45	43	40	50	40
Clay	48	55	35	53	30	39	49
COMPOSITION:							
Quartz	17	40	37	6	39	35	25
Feldspar	2	—	2	1	2	6	5
Rock fragments	—	—	—	—	—	Tr	Tr
Mica	—	—	—	—	—	Tr	Tr
Clay	48	37	35	53	30	35	45
Calcite/dolomite	18	8	3	21	18	15	10
Accessory minerals	3	1	3	3	—	3	1
Opaque minerals	—	1	—	—	2	—	2
Foraminifers	7	12	5	3	5	4	8
Nannofossils	2	2	2	12	4	2	3
Diatoms	1	—	—	Tr	—	—	Tr
Radiolarians	Tr	—	—	Tr	—	—	—
Sponge spicules	2	1	3	1	Tr	—	Tr

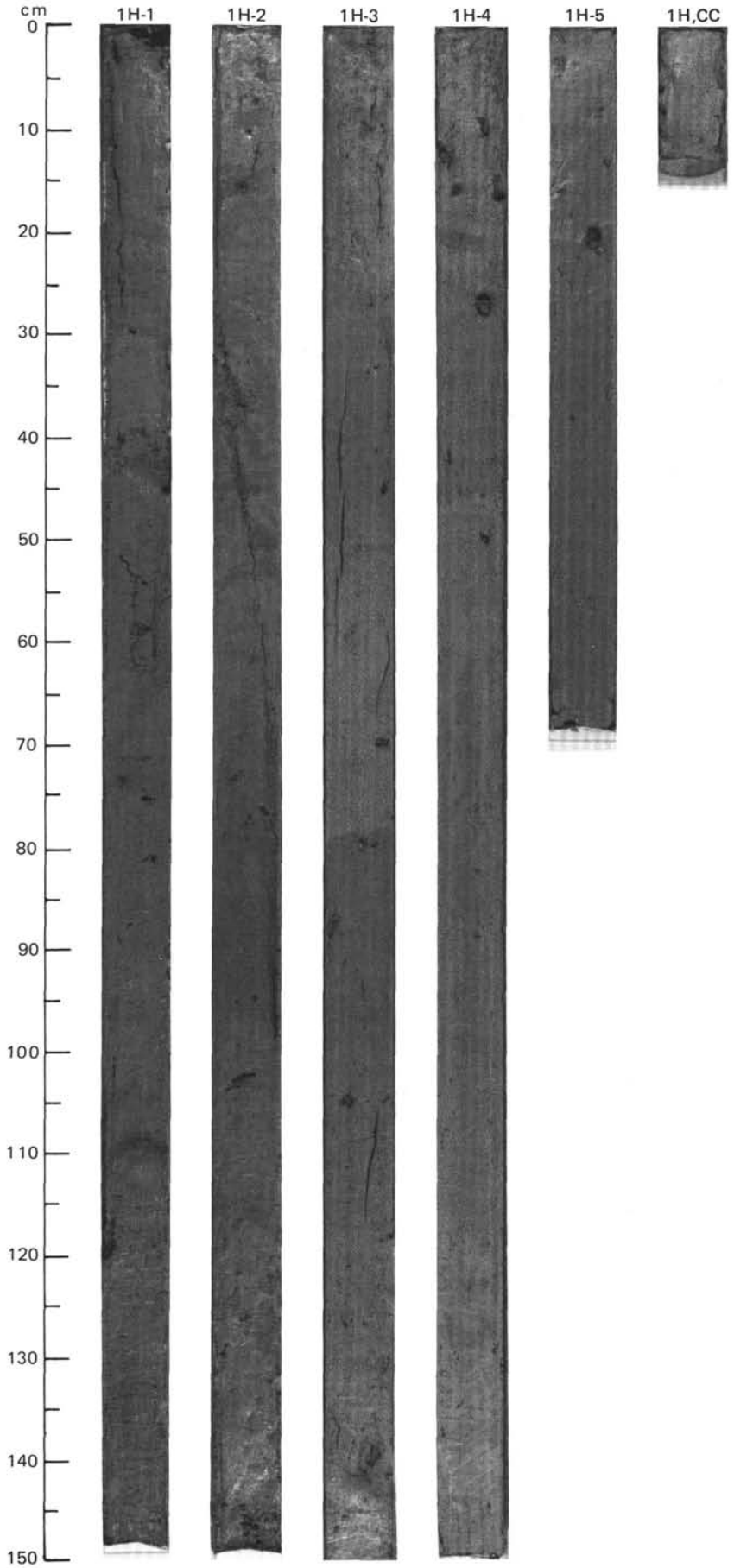
cm
0
10
20
30
40
50
60
70
80
90
100
110
120
130
140
150
1H-1
1H-2
1H-3
1H-4
1H-5
1H,CC

SITE 647 HOLE B CORE 2 H CORED INTERVAL 3867.0-3876.7 mbsl; 6.8-16.5 mbsf

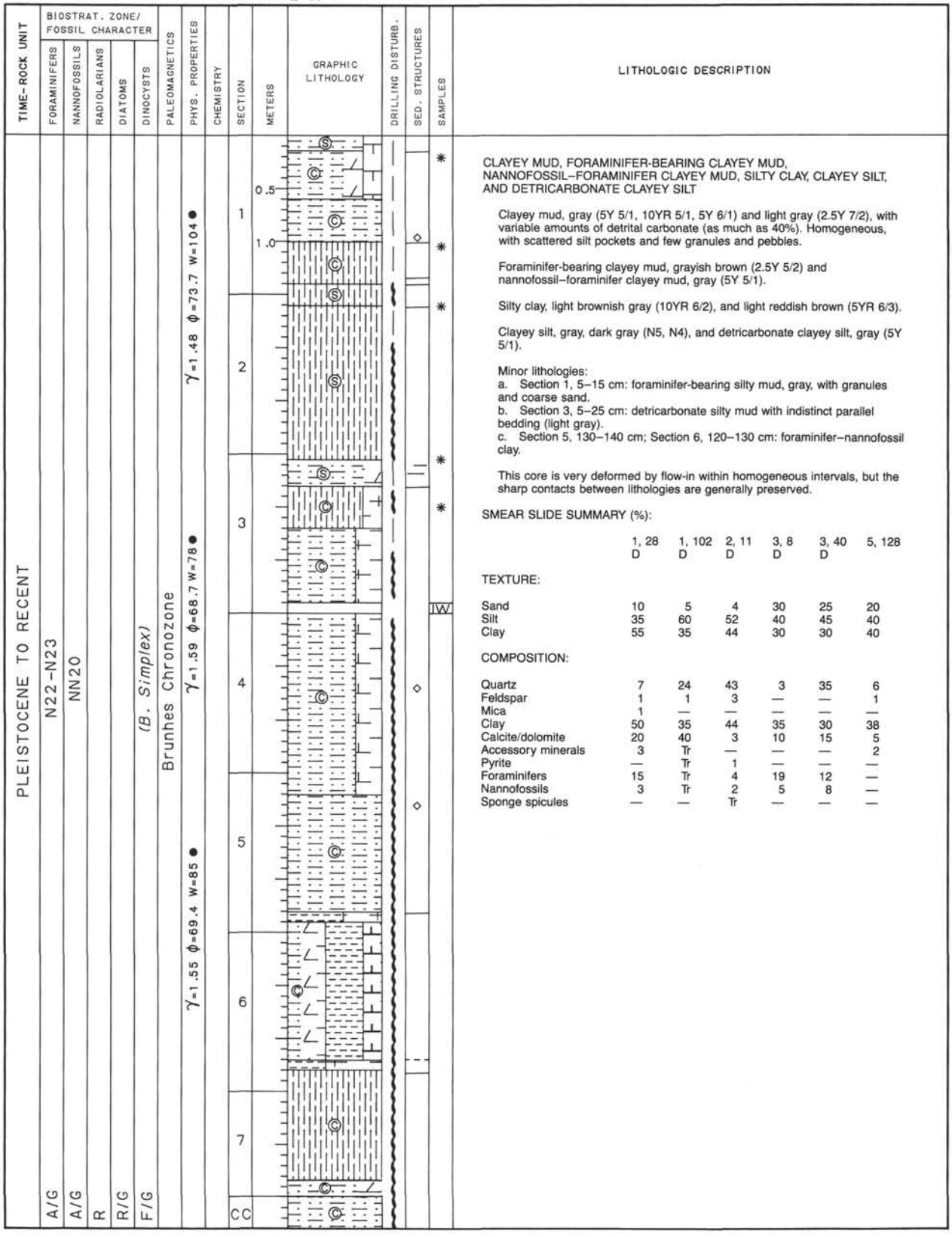

LITHOLOGIC DESCRIPTION

CLAYEY MUD, FORAMINIFER-BEARING CLAYEY MUD, NANNOFOSSIL–FORAMINIFER CLAYEY MUD, SILTY CLAY, CLAYEY SILT, AND DETRICARBONATE CLAYEY SILT

Clayey mud, gray (5Y 5/1, 10YR 5/1, 5Y 6/1) and light gray (2.5Y 7/2), with variable amounts of detrital carbonate (as much as 40%). Homogeneous, with scattered silt pockets and few granules and pebbles.

Foraminifer-bearing clayey mud, grayish brown (2.5Y 5/2) and nannofossil–foraminifer clayey mud, gray (5Y 5/1).

Silty clay, light brownish gray (10YR 6/2), and light reddish brown (5YR 6/3).

Clayey silt, gray, dark gray (N5, N4), and detricarbonate clayey silt, gray (5Y 5/1).

Minor lithologies:
a. Section 1, 5–15 cm: foraminifer-bearing silty mud, gray, with granules and coarse sand.
b. Section 3, 5–25 cm: detricarbonate silty mud with indistinct parallel bedding (light gray).
c. Section 5, 130–140 cm; Section 6, 120–130 cm: foraminifer–nannofossil clay.

This core is very deformed by flow-in within homogeneous intervals, but the sharp contacts between lithologies are generally preserved.

SMEAR SLIDE SUMMARY (%):

	1, 28 D	1, 102 D	2, 11 D	3, 8 D	3, 40 D	5, 128
TEXTURE:						
Sand	10	5	4	30	25	20
Silt	35	60	52	40	45	40
Clay	55	35	44	30	30	40
COMPOSITION:						
Quartz	7	24	43	3	35	6
Feldspar	1	1	3	—	—	1
Mica	1	—	—	—	—	—
Clay	50	35	44	35	30	38
Calcite/dolomite	20	40	3	10	15	5
Accessory minerals	3	Tr	—	—	—	2
Pyrite	—	Tr	1	—	—	—
Foraminifers	15	Tr	4	19	12	—
Nannofossils	3	Tr	2	5	8	—
Sponge spicules	—	—	Tr	—	—	—

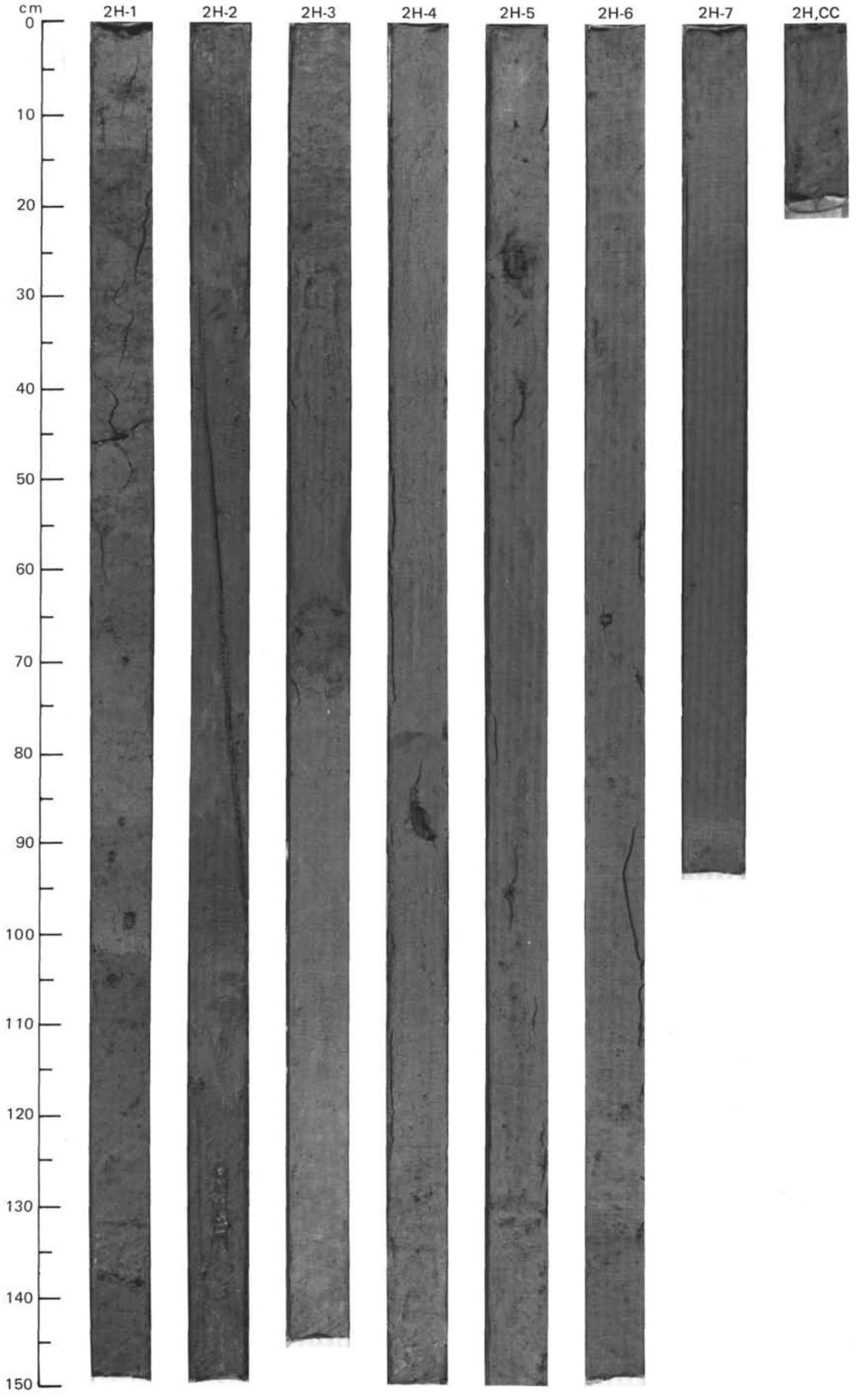
cm
0
10
20
30
40
50
60
70
80
90
100
110
120
130
140
150
2H-1
2H-2
2H-3
2H-4
2H-5
2H-6
2H-7
2H,CC

SITE 647 HOLE B CORE 3 H CORED INTERVAL 3876.7-3886.3 mbsl; 16.5-26.1 mbsf

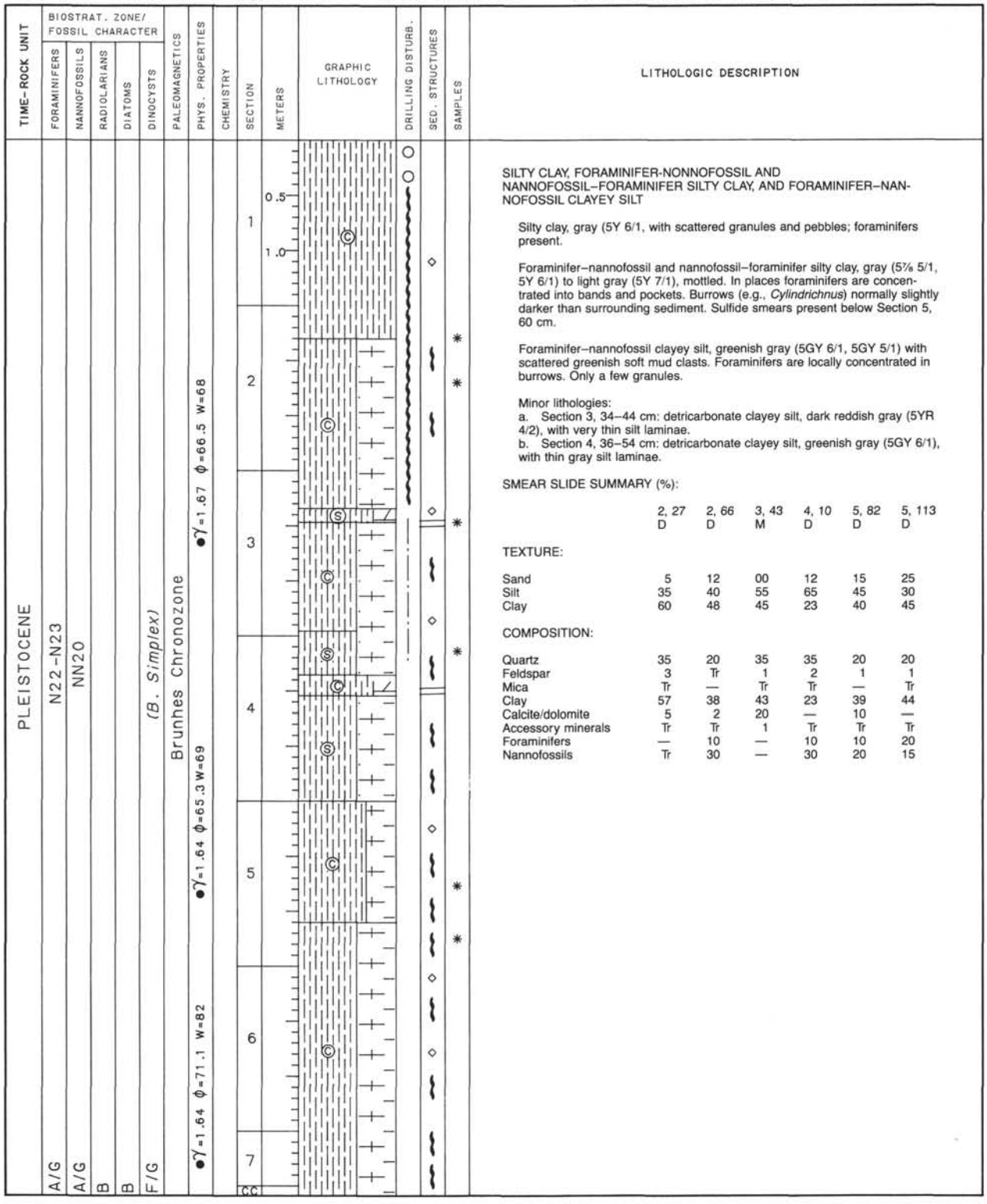

SILTY CLAY, FORAMINIFER-NONNOFOSSIL AND NANNOFOSSIL–FORAMINIFER SILTY CLAY, AND FORAMINIFER–NANNOFOSSIL CLAYEY SILT

Silty clay, gray (5Y 6/1, with scattered granules and pebbles; foraminifers present.

Foraminifer–nannofossil and nannofossil–foraminifer silty clay, gray (5⅞ 5/1, 5Y 6/1) to light gray (5Y 7/1), mottled. In places foraminifers are concentrated into bands and pockets. Burrows (e.g., *Cylindrichnus*) normally slightly darker than surrounding sediment. Sulfide smears present below Section 5, 60 cm.

Foraminifer–nannofossil clayey silt, greenish gray (5GY 6/1, 5GY 5/1) with scattered greenish soft mud clasts. Foraminifers are locally concentrated in burrows. Only a few granules.

Minor lithologies:
a. Section 3, 34–44 cm: detricarbonate clayey silt, dark reddish gray (5YR 4/2), with very thin silt laminae.
b. Section 4, 36–54 cm: detricarbonate clayey silt, greenish gray (5GY 6/1), with thin gray silt laminae.

SMEAR SLIDE SUMMARY (%):

	2, 27 D	2, 66 D	3, 43 M	4, 10 D	5, 82 D	5, 113 D
TEXTURE:						
Sand	5	12	00	12	15	25
Silt	35	40	55	65	45	30
Clay	60	48	45	23	40	45
COMPOSITION:						
Quartz	35	20	35	35	20	20
Feldspar	3	Tr	1	2	1	1
Mica	Tr	—	Tr	Tr	—	Tr
Clay	57	38	43	23	39	44
Calcite/dolomite	5	2	20	—	10	—
Accessory minerals	Tr	Tr	1	Tr	Tr	Tr
Foraminifers	—	10	—	10	10	20
Nannofossils	Tr	30	—	30	20	15

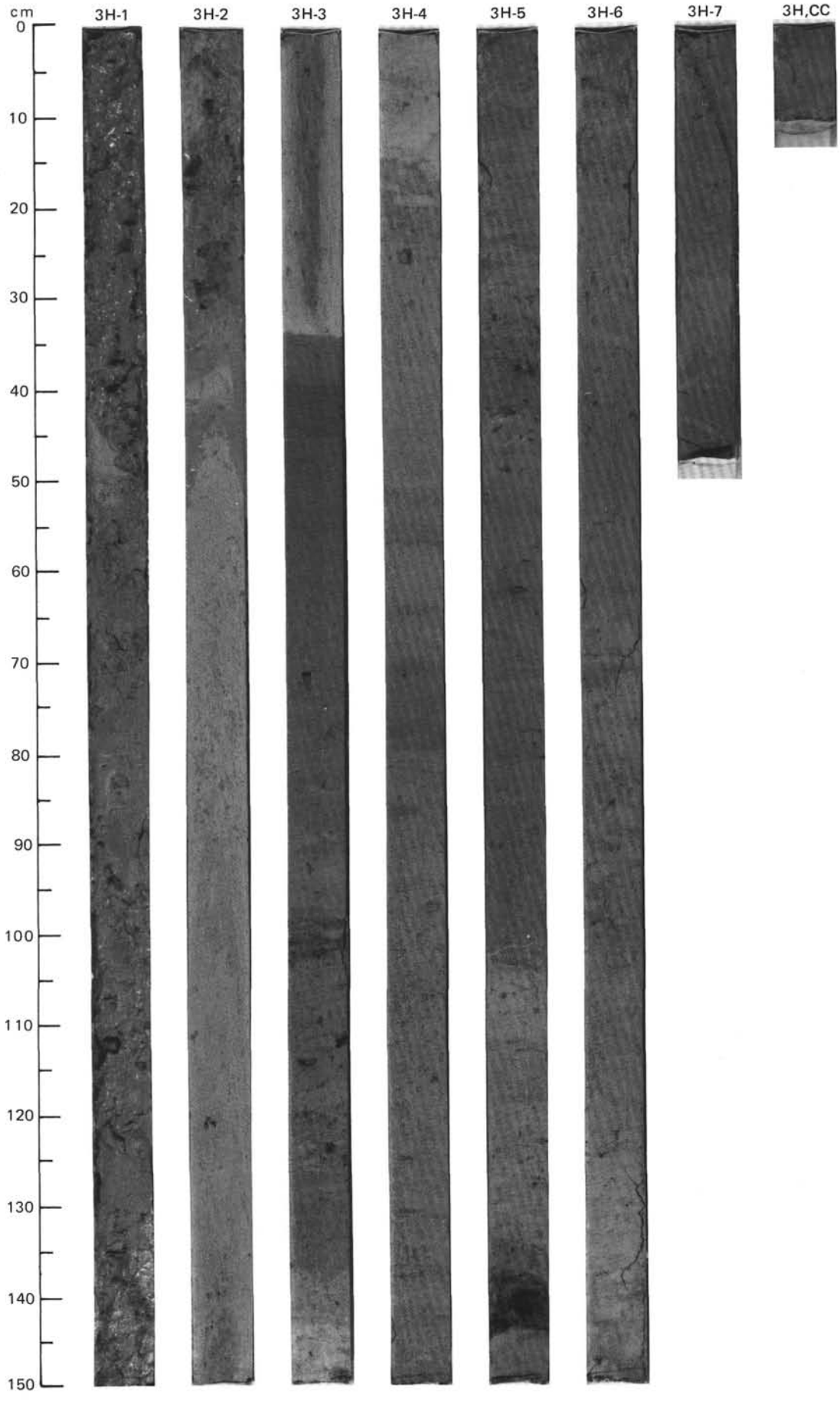
cm
0
10
20
30
40
50
60
70
80
90
100
110
120
130
140
150
3H-1
3H-2
3H-3
3H-4
3H-5
3H-6
3H-7
3H,CC

SITE 647 HOLE B CORE 4 H CORED INTERVAL 3886.3-3896.0 mbsl; 26.1-35.8 mbsf

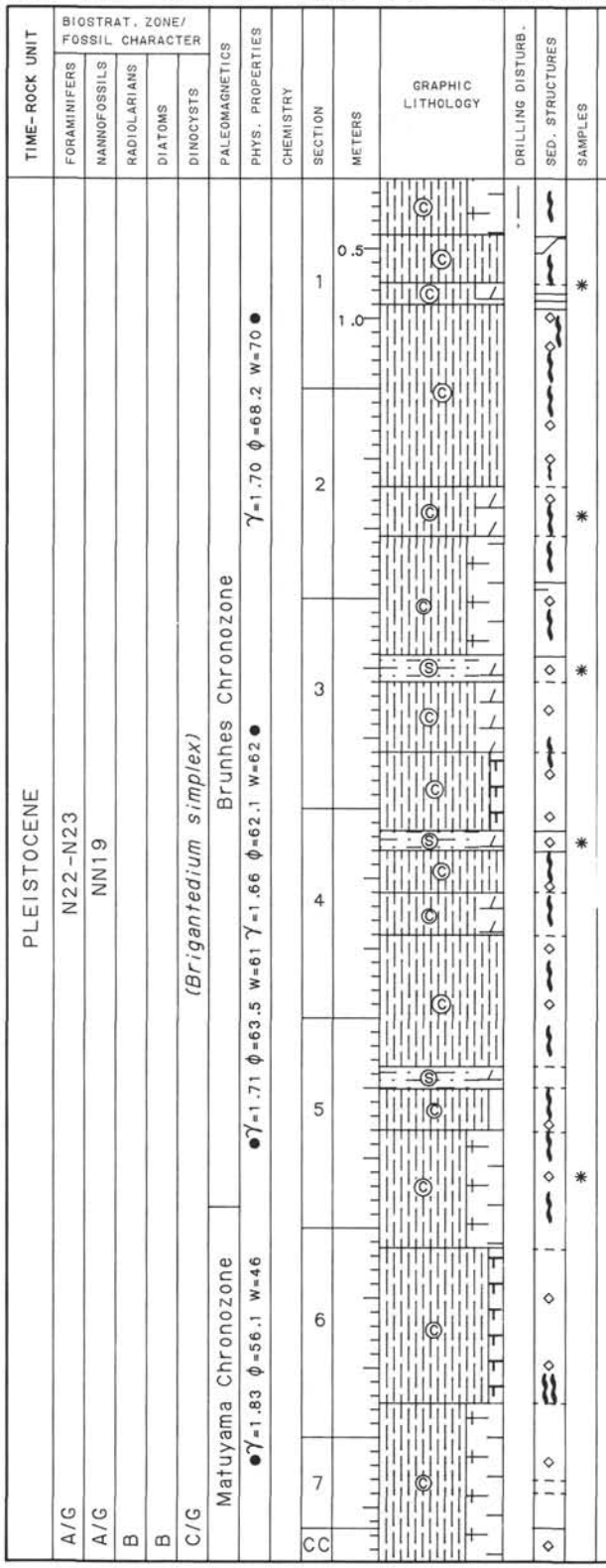

LITHOLOGIC DESCRIPTION

SILTY CLAY, FORAMINIFER–NANNOFOSSIL AND NANNOFOSSIL–FORAMINIFER SILTY CLAY

Silty clay, dark gray and gray (5Y 4/1, 5Y 5/1), with scattered granules, small pebbles, sand pockets, soft clay clasts. Slightly bioturbated and locally foraminifer-bearing. Local occurrences of detricarbonate grains. May have color mottling and banding in shades of gray.

Foraminifer–nannofossil and nannofossil–foraminiferal silty clay, gray to light gray (5Y 6/1) with very sparse local granules. Slightly burrowed.

Minor lithologies:
a. Section 1, 74–83 cm: relatively sharp-based, faintly laminated, dark reddish gray (5YR 4/2), detricarbonate silty clay — probable turbidites.
b. Section 3, 46–62 cm; Section 4, 14–26 cm; Section 5, 36–49 cm: detricarbonate silty mud, gray (10YR 5/1), with scattered granules and small pebbles — ice rafted.

SMEAR SLIDE SUMMARY (%):

	1, 81 M	2, 85 D	3, 57 D	4, 24 D	5, 129 D	6, 86
TEXTURE:						
Sand	1	20	20	15	22	15
Silt	60	30	45	60	20	10
Clay	39	50	35	25	58	75
COMPOSITION:						
Quartz	40	20	40	35	10	15
Feldspar	1	2	1	3	1	—
Mica	—	Tr	—	Tr	Tr	—
Clay	38	47	29	22	57	70
Calcite/dolomite	20	20	30	40	2	5
Accessory minerals	Tr	Tr	Tr	Tr	Tr	Tr
Foraminifers	Tr	10	—	—	20	10
Nannofossils	1	1	Tr	Tr	10	Tr

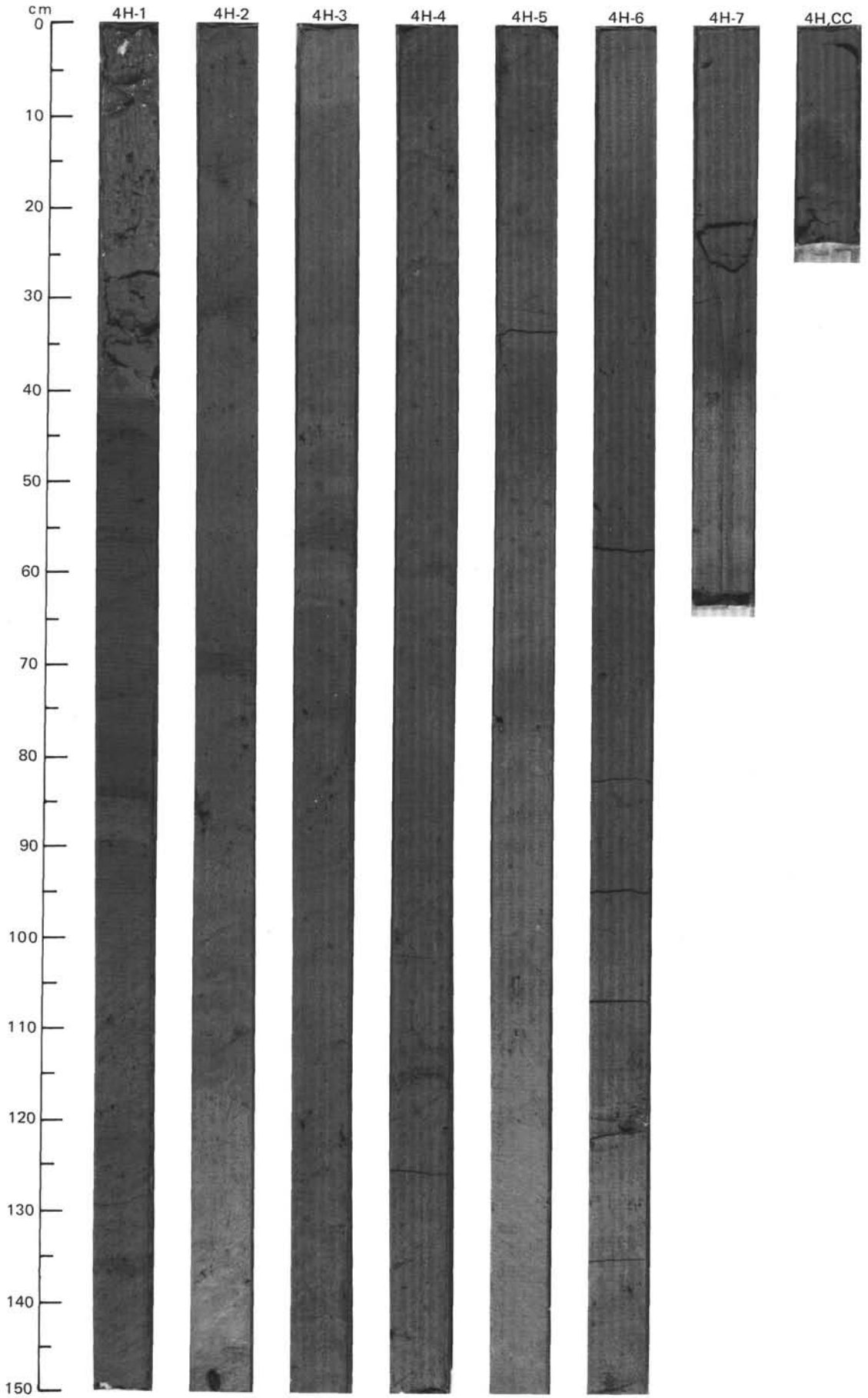
cm
0
10
20
30
40
50
60
70
80
90
100
110
120
130
140
150
4H-1
4H-2
4H-3
4H-4
4H-5
4H-6
4H-7
4H,CC

SITE 647 HOLE B CORE 5 H CORED INTERVAL 3896.0-3905.7 mbsl; 35.8-45.5 mbsf

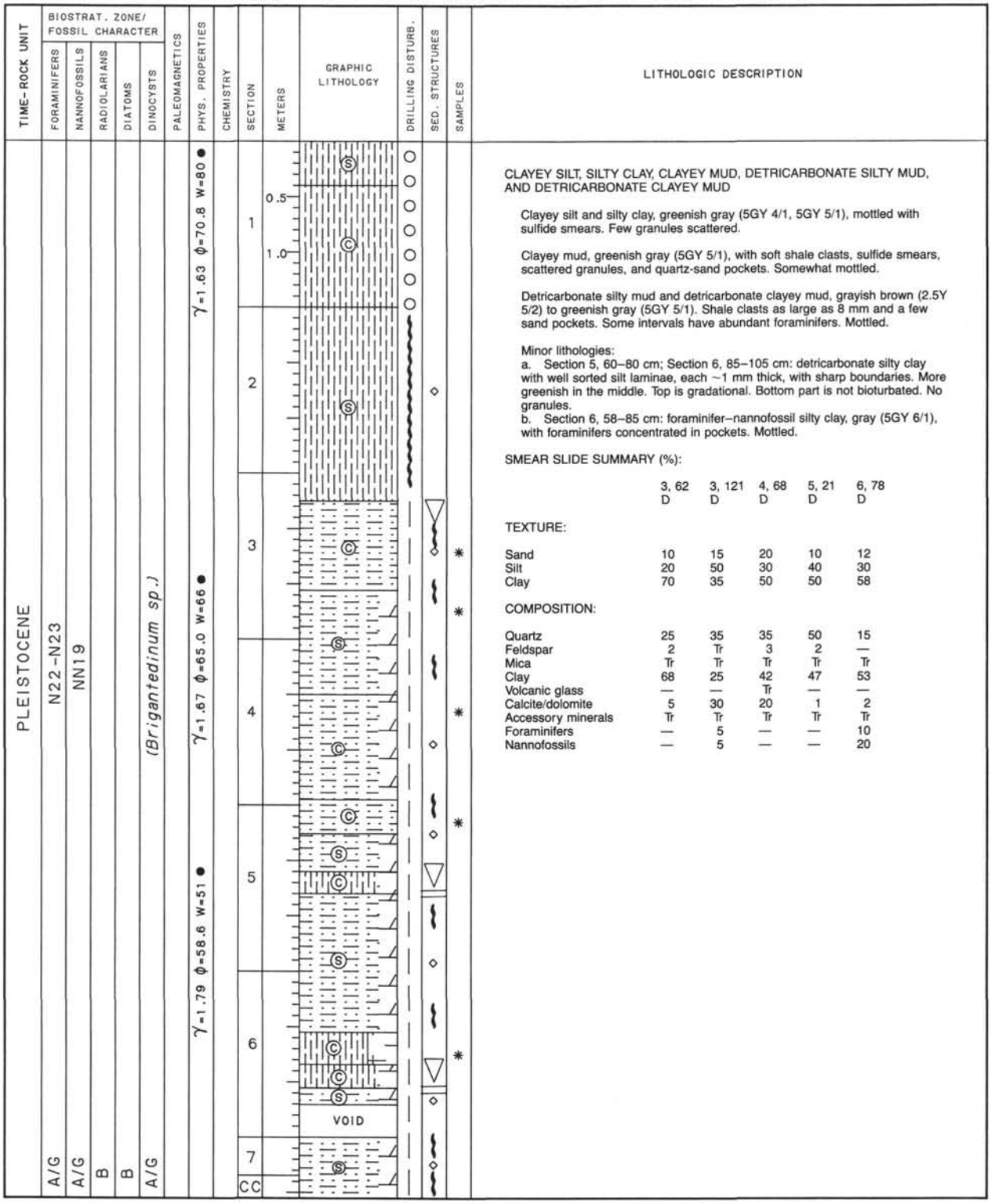

CLAYEY SILT, SILTY CLAY, CLAYEY MUD, DETRICARBONATE SILTY MUD, AND DETRICARBONATE CLAYEY MUD

Clayey silt and silty clay, greenish gray (5GY 4/1, 5GY 5/1), mottled with sulfide smears. Few granules scattered.

Clayey mud, greenish gray (5GY 5/1), with soft shale clasts, sulfide smears, scattered granules, and quartz-sand pockets. Somewhat mottled.

Detricarbonate silty mud and detricarbonate clayey mud, grayish brown (2.5Y 5/2) to greenish gray (5GY 5/1). Shale clasts as large as 8 mm and a few sand pockets. Some intervals have abundant foraminifers. Mottled.

Minor lithologies:
a. Section 5, 60–80 cm; Section 6, 85–105 cm: detricarbonate silty clay with well sorted silt laminae, each ~1 mm thick, with sharp boundaries. More greenish in the middle. Top is gradational. Bottom part is not bioturbated. No granules.
b. Section 6, 58–85 cm: foraminifer–nannofossil silty clay, gray (5GY 6/1), with foraminifers concentrated in pockets. Mottled.

SMEAR SLIDE SUMMARY (%):

	3, 62 D	3, 121 D	4, 68 D	5, 21 D	6, 78 D
TEXTURE:					
Sand	10	15	20	10	12
Silt	20	50	30	40	30
Clay	70	35	50	50	58
COMPOSITION:					
Quartz	25	35	35	50	15
Feldspar	2	Tr	3	2	—
Mica	Tr	Tr	Tr	Tr	Tr
Clay	68	25	42	47	53
Volcanic glass	—	—	Tr	—	—
Calcite/dolomite	5	30	20	1	2
Accessory minerals	Tr	Tr	Tr	Tr	Tr
Foraminifers	—	5	—	—	10
Nannofossils	—	5	—	—	20

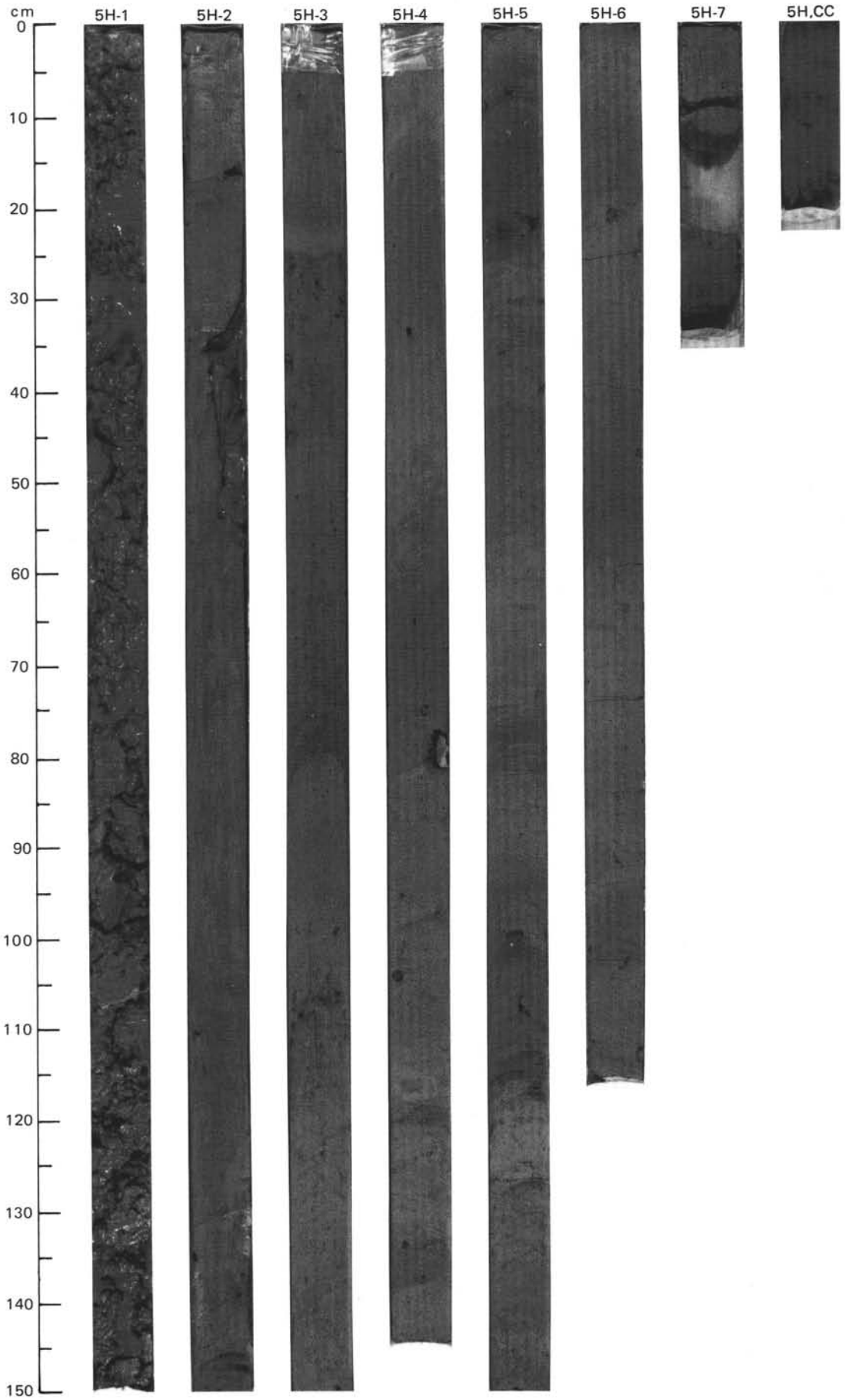
cm
0
10
20
30
40
50
60
70
80
90
100
110
120
130
140
150
5H-1
5H-2
5H-3
5H-4
5H-5
5H-6
5H-7
5H,CC

SITE 647 HOLE B CORE 6 H CORED INTERVAL 3905.7-3915.3 mbsl; 45.5-55.1 mbsf

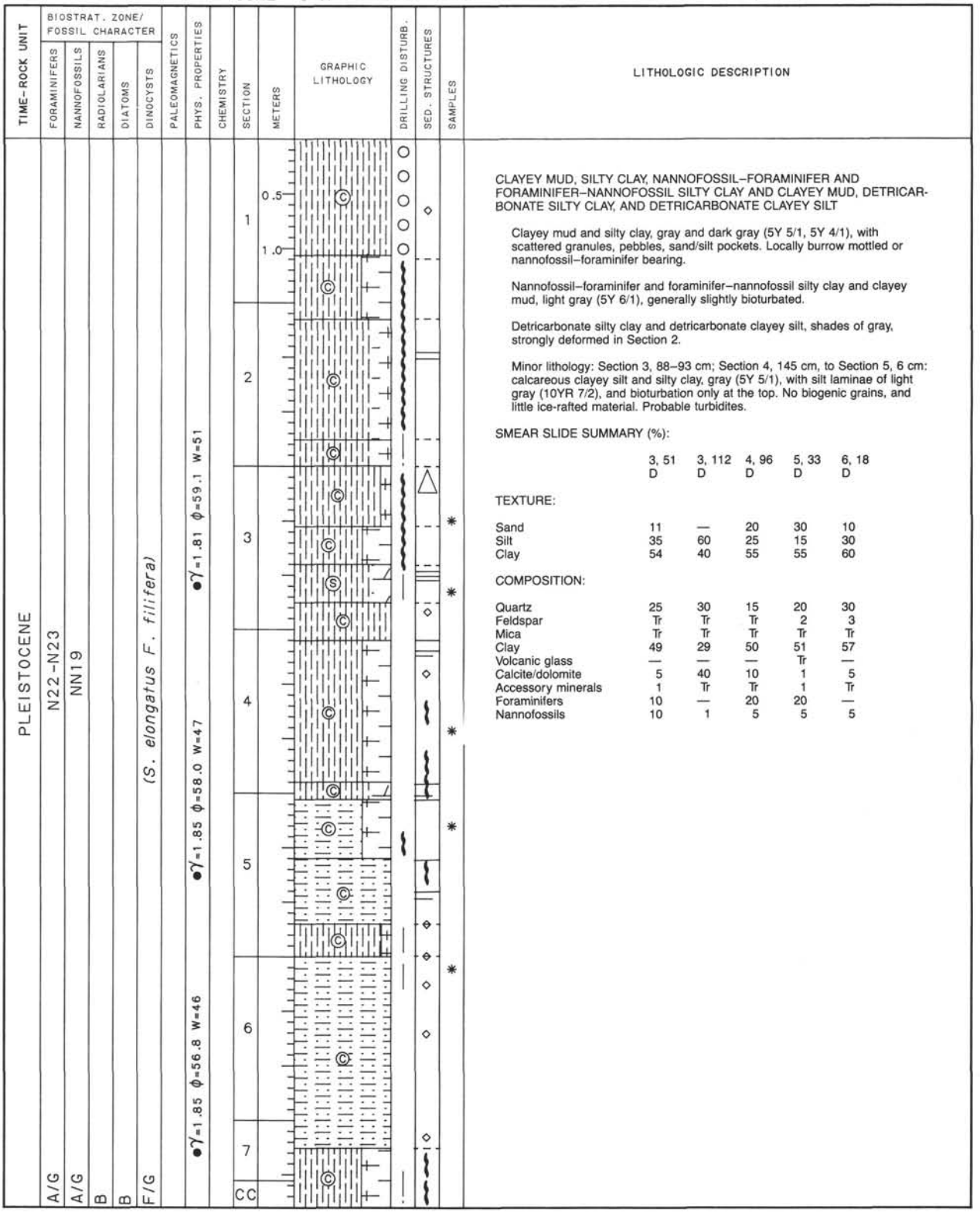

LITHOLOGIC DESCRIPTION

CLAYEY MUD, SILTY CLAY, NANNOFOSSIL–FORAMINIFER AND FORAMINIFER–NANNOFOSSIL SILTY CLAY AND CLAYEY MUD, DETRICARBONATE SILTY CLAY, AND DETRICARBONATE CLAYEY SILT

Clayey mud and silty clay, gray and dark gray (5Y 5/1, 5Y 4/1), with scattered granules, pebbles, sand/silt pockets. Locally burrow mottled or nannofossil–foraminifer bearing.

Nannofossil–foraminifer and foraminifer–nannofossil silty clay and clayey mud, light gray (5Y 6/1), generally slightly bioturbated.

Detricarbonate silty clay and detricarbonate clayey silt, shades of gray, strongly deformed in Section 2.

Minor lithology: Section 3, 88–93 cm; Section 4, 145 cm, to Section 5, 6 cm: calcareous clayey silt and silty clay, gray (5Y 5/1), with silt laminae of light gray (10YR 7/2), and bioturbation only at the top. No biogenic grains, and little ice-rafted material. Probable turbidites.

SMEAR SLIDE SUMMARY (%):

	3, 51 D	3, 112 D	4, 96 D	5, 33 D	6, 18 D
TEXTURE:					
Sand	11	—	20	30	10
Silt	35	60	25	15	30
Clay	54	40	55	55	60
COMPOSITION:					
Quartz	25	30	15	20	30
Feldspar	Tr	Tr	Tr	2	3
Mica	Tr	Tr	Tr	Tr	Tr
Clay	49	29	50	51	57
Volcanic glass	—	—	—	Tr	—
Calcite/dolomite	5	40	10	1	5
Accessory minerals	1	Tr	Tr	1	Tr
Foraminifers	10	—	20	20	—
Nannofossils	10	1	5	5	5

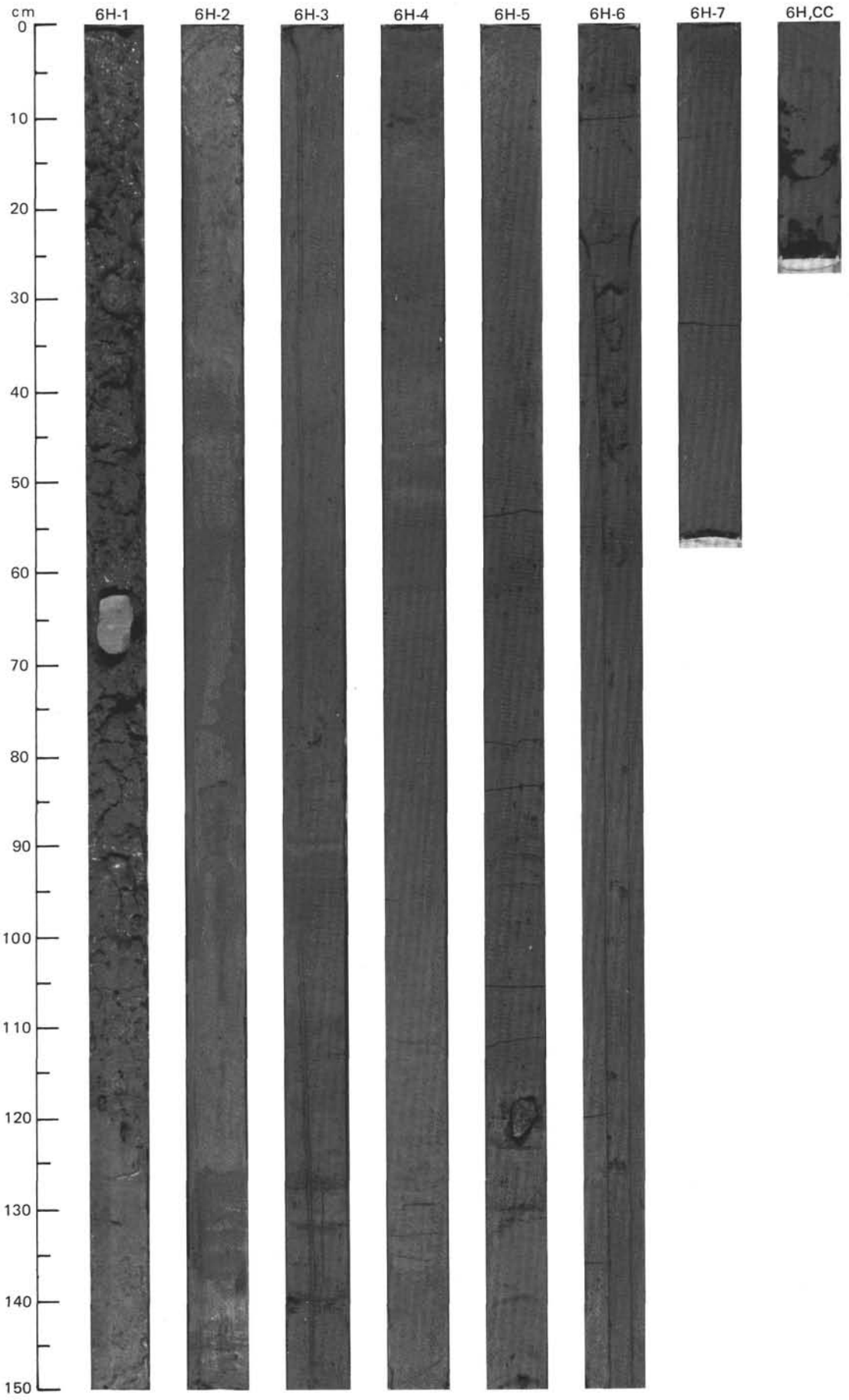
cm
0
10
20
30
40
50
60
70
80
90
100
110
120
130
140
150
6H-1
6H-2
6H-3
6H-4
6H-5
6H-6
6H-7
6H,CC

SITE 647 HOLE B CORE 7 H CORED INTERVAL 3915.3-3924.9 mbsl; 55.1-64.7 mbsf

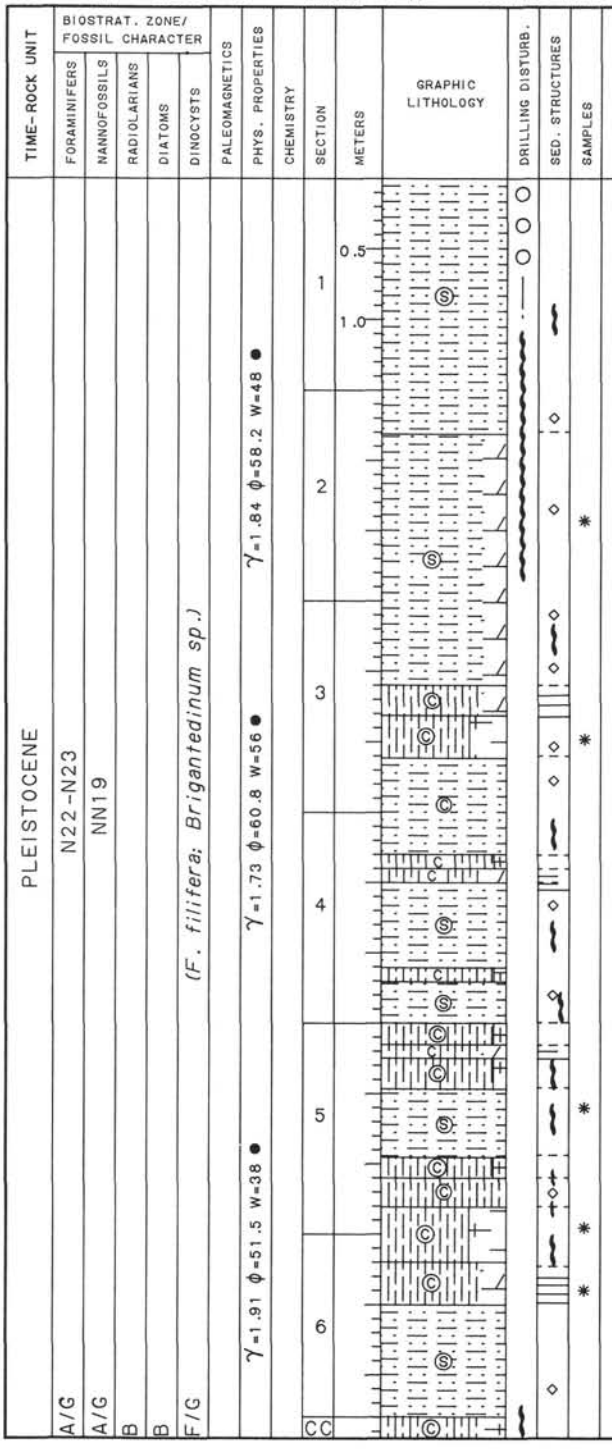

LITHOLOGIC DESCRIPTION

SILTY MUD, CLAYEY MUD, SILTY CLAY, NANNOFOSSIL–FORAMINIFER-BEARING SILTY CLAY, AND NANNOFOSSIL–FORAMINIFER SILTY CLAY

Silty mud, clayey mud, and silty clay, dark gray and gray (5Y 4/1, 5Y 5/1); slightly burrowed, with scattered granules, sand pockets, and pebbles to ~1 cm. Local black sulfide smears. Locally calcareous (e.g., Section 2, 33 cm, to Section 3, 57 cm).

Nannofossil–foraminifer-bearing silty clay, and nannofossil–foraminifer silty clay, gray to light gray (5Y 5/1, 5Y 6/1); slightly burrowed with very scattered granules. Lighter tones correspond to more biogenics.

Minor lithology: Section 3, 61–81 cm; Section 4, 37–50 cm; Section 5, 17–25 cm; Section 6, 21–52 cm: detricarbonate silty clay, light greenish gray (5GY 6/1), with few burrows, and basal parallel laminations in detricarbonate silt. The lamination is in the form of <1 cm, graded, laminated couplets — turbidites. These units have sharp bases and gradational tops.

The upper two sections of this core are highly disturbed. Cyclicity is striking between (a) biogenic carbonate-rich silty clays, (b) silty muds and silty clays/clayey silts with ice-rafted debris, and (c) detricarbonate, laminated, turbidite units.

SMEAR SLIDE SUMMARY (%):

	2, 92 D	3, 96 D	5, 62 M	5, 149 D	6, 147 M
TEXTURE:					
Sand	15	25	30	25	1
Silt	50	30	20	20	40
Clay	35	45	50	55	59
COMPOSITION:					
Quartz	40	30	55	10	15
Feldspar	5	—	2	—	Tr
Mica	Tr	Tr	Tr	Tr	Tr
Clay	34	38	41	54	54
Volcanic glass	—	—	Tr	—	—
Calcite/dolomite	20	2	—	1	30
Accessory minerals	1	Tr	2	Tr	—
Foraminifers	Tr	25	—	25	1
Nannofossils	—	5	Tr	10	Tr

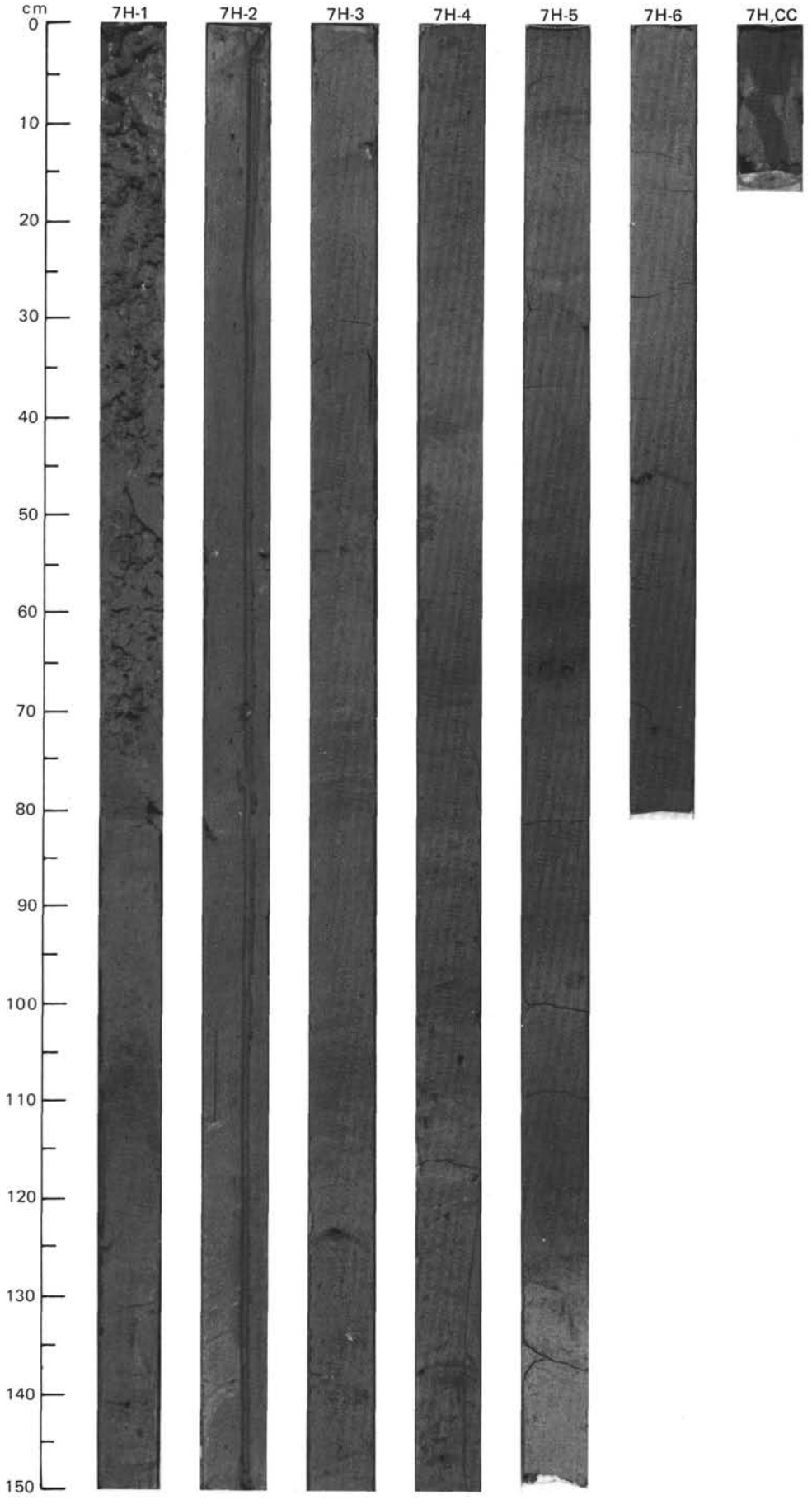
cm
0
10
20
30
40
50
60
70
80
90
100
110
120
130
140
150
7H-1
7H-2
7H-3
7H-4
7H-5
7H-6
7H,CC

SITE 647 HOLE B CORE 8 H CORED INTERVAL 3924.9-3934.5 mbsl; 64.7-74.3 mbsf

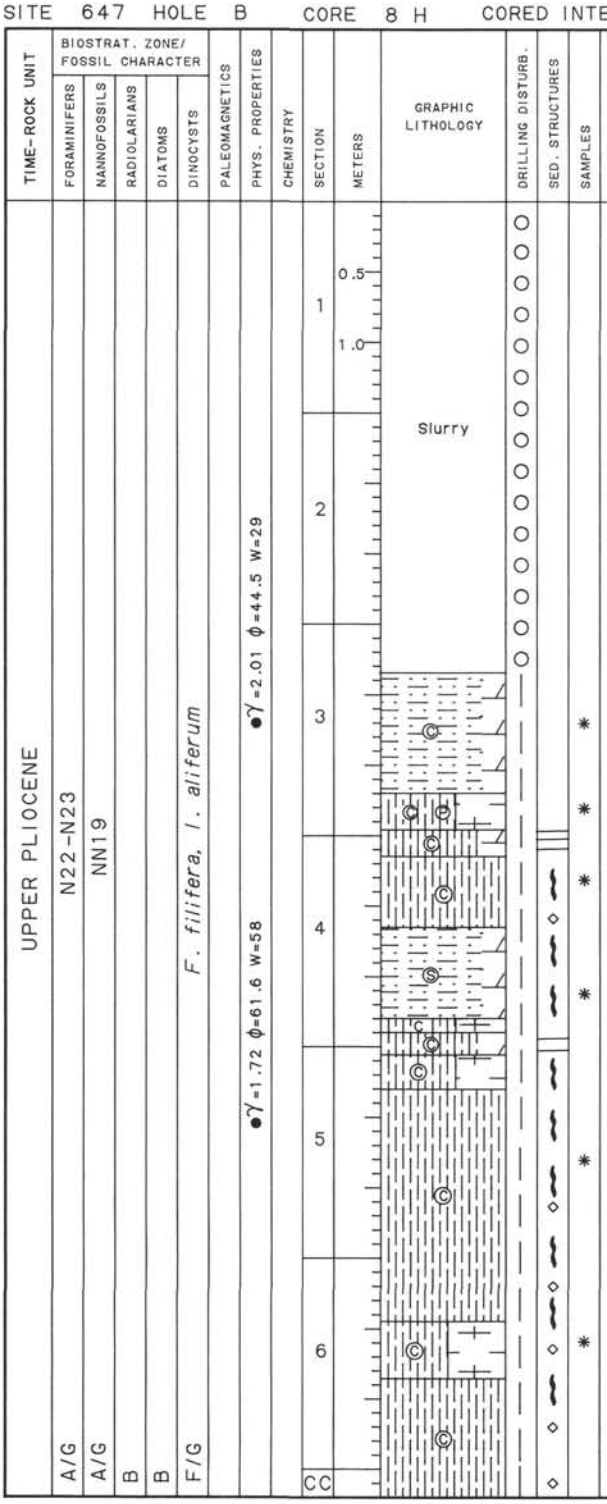

LITHOLOGIC DESCRIPTION

DETRICARBONATE CLAYEY MUD, DETRICARBONATE SILTY MUD, FORAMINIFER–NANNOFOSSIL SILTY CLAY, AND SILTY CLAY

Detricarbonate clayey mud and detricarbonate silty mud, greenish gray (5GY 5/1) and grayish brown (2.5YR 5/2), mottled, with pockets of sand, few black shale clasts to 6 mm, and scattered granules. Black Fe sulfide colors some burrows.

Foraminifer–nannofossil silty clay, greenish gray to gray (5GY 6/1, 5Y 6/1), with one pyrite-cemented burrow. Foraminifers are commonly concentrated in bands (burrows).

Silty clay, greenish gray (5GY 5/1), mottled and color banded, with black sulfide smears, soft greenish shale clasts, scattered sand pockets, and burrows. The burrows are darker than the surrounding sediment.

Minor lithology: Section 3, 141–150 cm; Section 4, 0–14 cm; Section 5, 0–6 cm: detricarbonate silty clay, pale green (10G 6/2) to gray (5Y 6/1), with yellowish gray silt laminae up to 1 mm thick. These silt laminae have sharp boundaries, and are well sorted. The detricarbonate beds have no granules, and are only burrowed in their upper part.

SMEAR SLIDE SUMMARY (%):

	3, 73 D	3, 131 D	4, 31 D	4, 112 D	5, 82 D	6, 60 D
TEXTURE:						
Sand	10	20	5	10	5	30
Silt	40	30	40	50	35	20
Clay	50	50	55	40	60	50
COMPOSITION:						
Quartz	35	10	45	20	30	10
Feldspar	2	Tr	3	3	2	Tr
Mica	Tr	Tr	Tr	1	Tr	Tr
Clay	42	48	51	34	57	44
Volcanic glass	Tr	—	—	—	Tr	—
Calcite/dolomite	20	2	1	40	10	1
Accessory minerals	1	Tr	Tr	2	Tr	Tr
Foraminifers	—	20	—	—	Tr	30
Nannofossils	Tr	20	—	—	1	15

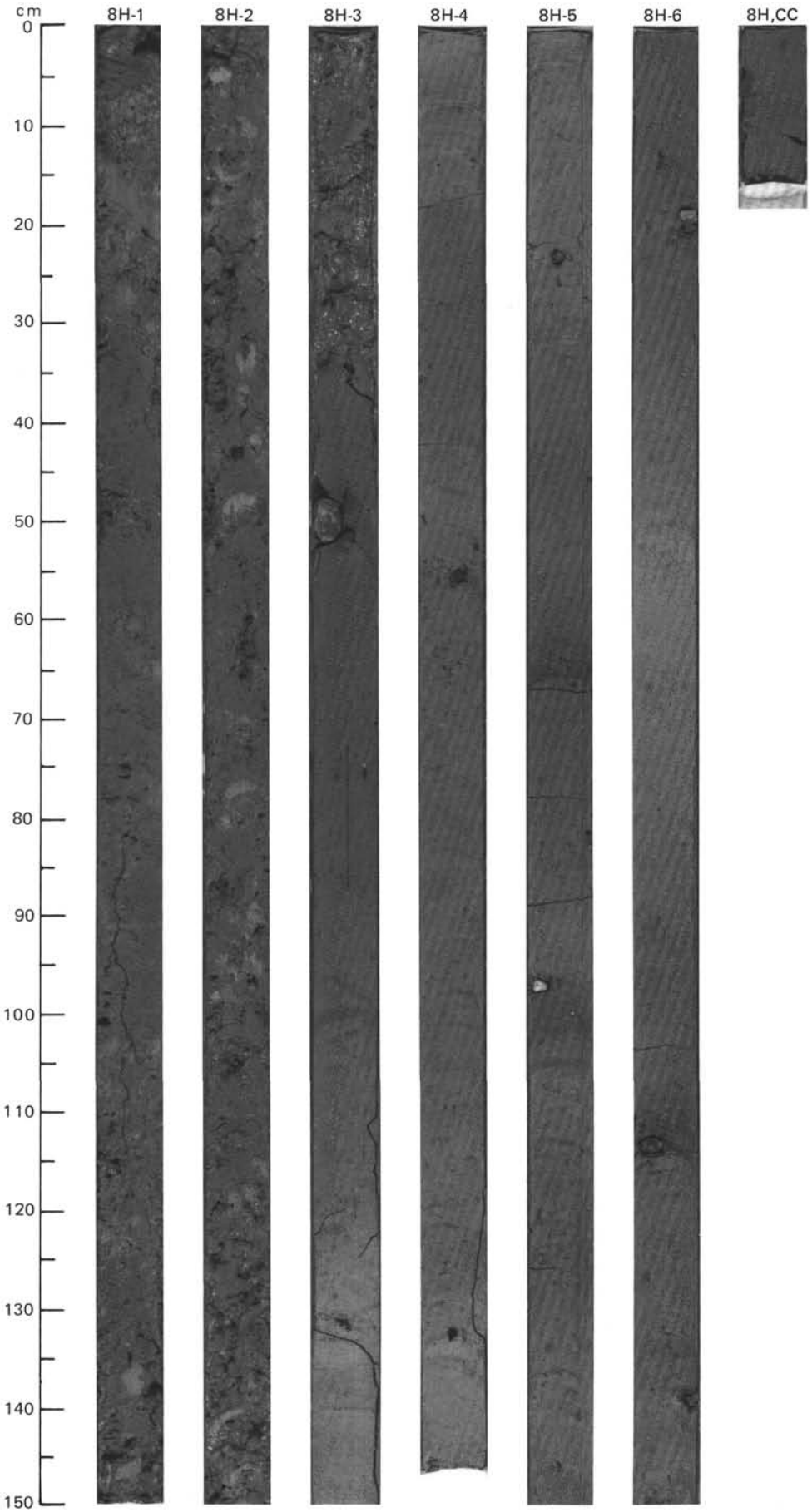
cm
0
10
20
30
40
50
60
70
80
90
100
110
120
130
140
150
8H-1
8H-2
8H-3
8H-4
8H-5
8H-6
8H,CC

SITE 647 HOLE B CORE 9 H CORED INTERVAL 3934.5-3944.1 mbsl; 74.3-83.9 mbsf

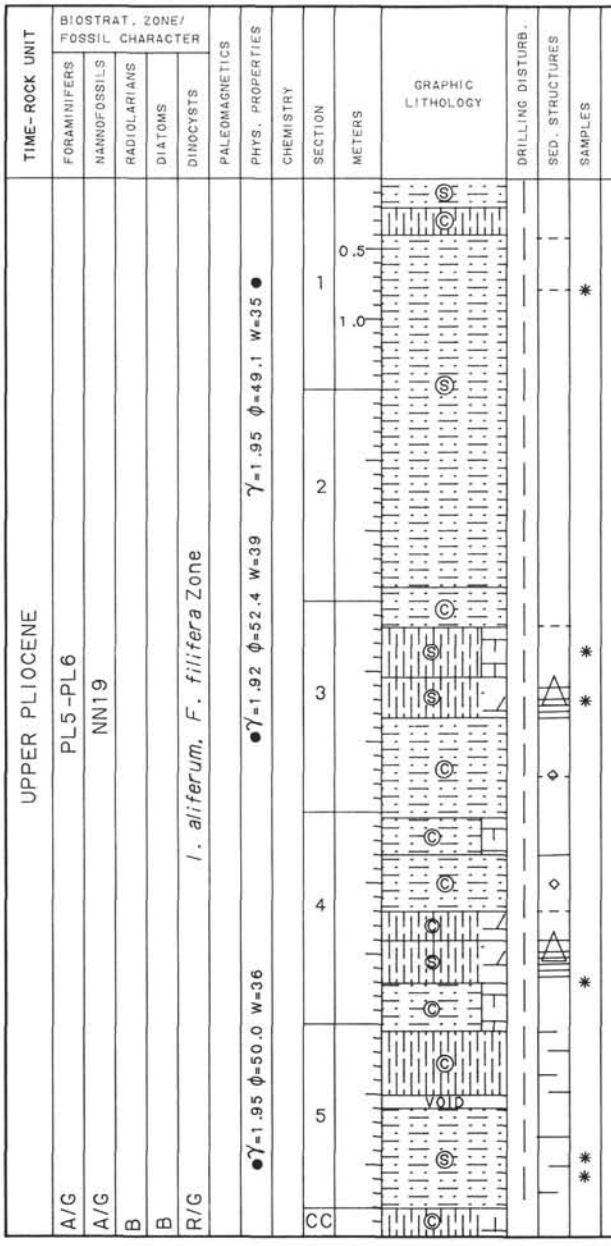

LITHOLOGIC DESCRIPTION

SILTY MUD, CLAYEY MUD, DETRICARBONATE CLAYEY SILT, AND DETRICARBONATE SILTY CLAY

Silty mud, gray and dark gray (5Y 4/1, 5Y 5/1), with scattered white sand/silt pockets and Fe sulfide specks.

Clayey mud, gray (5Y 4/1), and dark brownish gray (2.5Y 4/2), with a few silt pockets and mud clasts. There are two pebbles: granite and dolostone.

Detricarbonate clayey silt and detricarbonate silty clay, dark brownish gray (2.5Y 4/2). There are two graded beds, each containing ~12 detricarbonate silt laminae.

Minor lithologies:
a. Section 3, 17–56 cm: light gray nannofossil clayey silt.
b. Section 4, 6–34, 120–150 cm: light gray nannofossil–foraminifer-bearing clayey mud.
c. Section 5, 12–68 cm: color-banded silty clay.

SMEAR SLIDE SUMMARY (%):

	1, 82 D	3, 45 D	3, 72 D	4, 127 D	5, 95 D	5, 114 M
TEXTURE:						
Sand	30	5	—	35	15	70
Silt	40	70	65	30	45	30
Clay	30	25	35	35	40	—
COMPOSITION:						
Quartz	50	30	30	32	45	77
Feldspar	—	—	—	3	5	10
Rock fragments	—	—	—	—	—	5
Mica	—	—	—	2	2	3
Clay	30	23	31	35	40	—
Calcite/dolomite	12	25	30	3	3	—
Accessory minerals	5	—	5	3	5	5
Glauconite	Tr	—	—	—	—	—
Pyrite	2	—	2	—	—	—
Foraminifers	—	2	—	20	—	—
Nannofossils	1	20	2	2	—	—
Plant debris	Tr	—	—	—	—	—

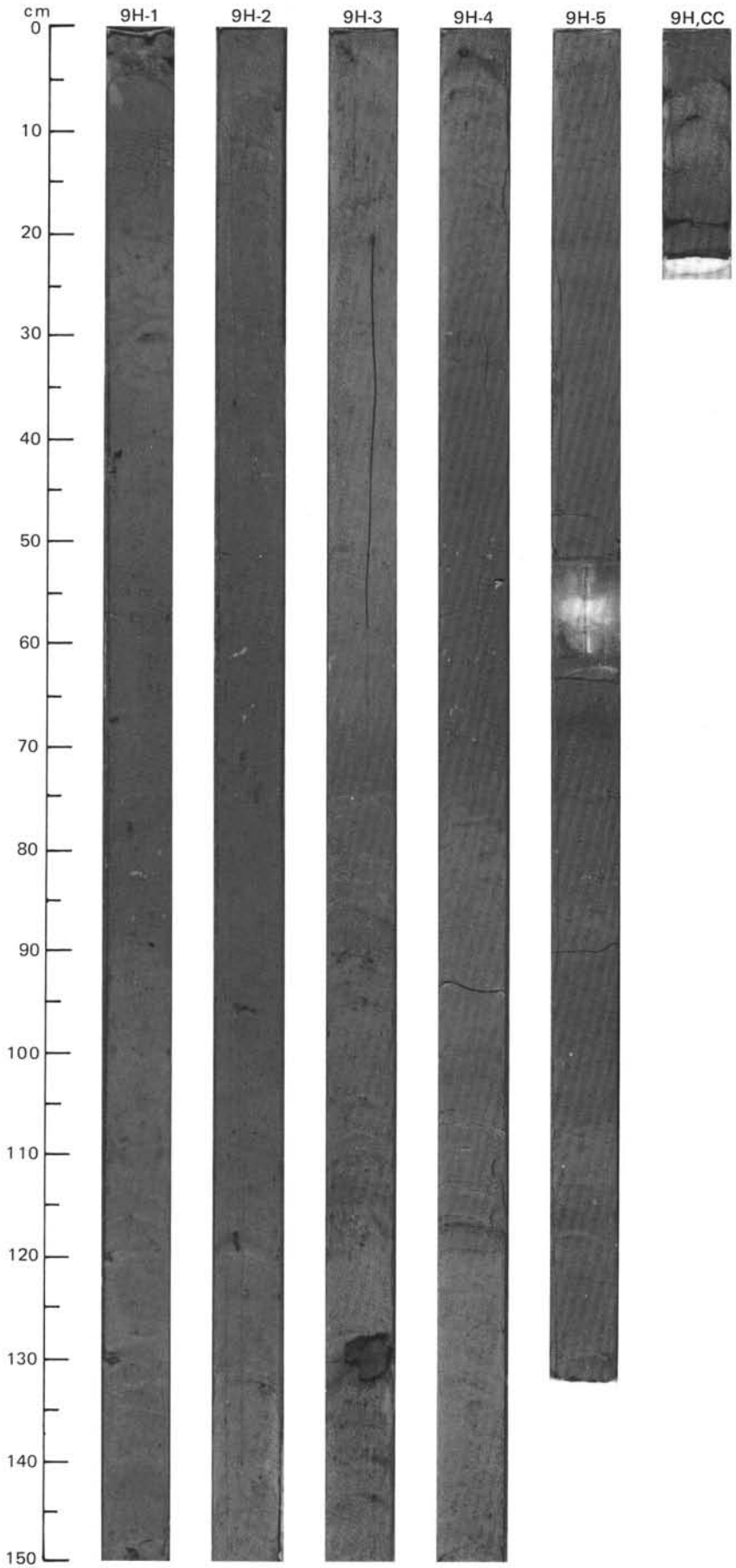
cm
0
10
20
30
40
50
60
70
80
90
100
110
120
130
140
150
9H-1
9H-2
9H-3
9H-4
9H-5
9H,CC

SITE 647 HOLE B CORE 10 H CORED INTERVAL 3944.1-3953.7 mbsl; 83.9-93.5 mbsf

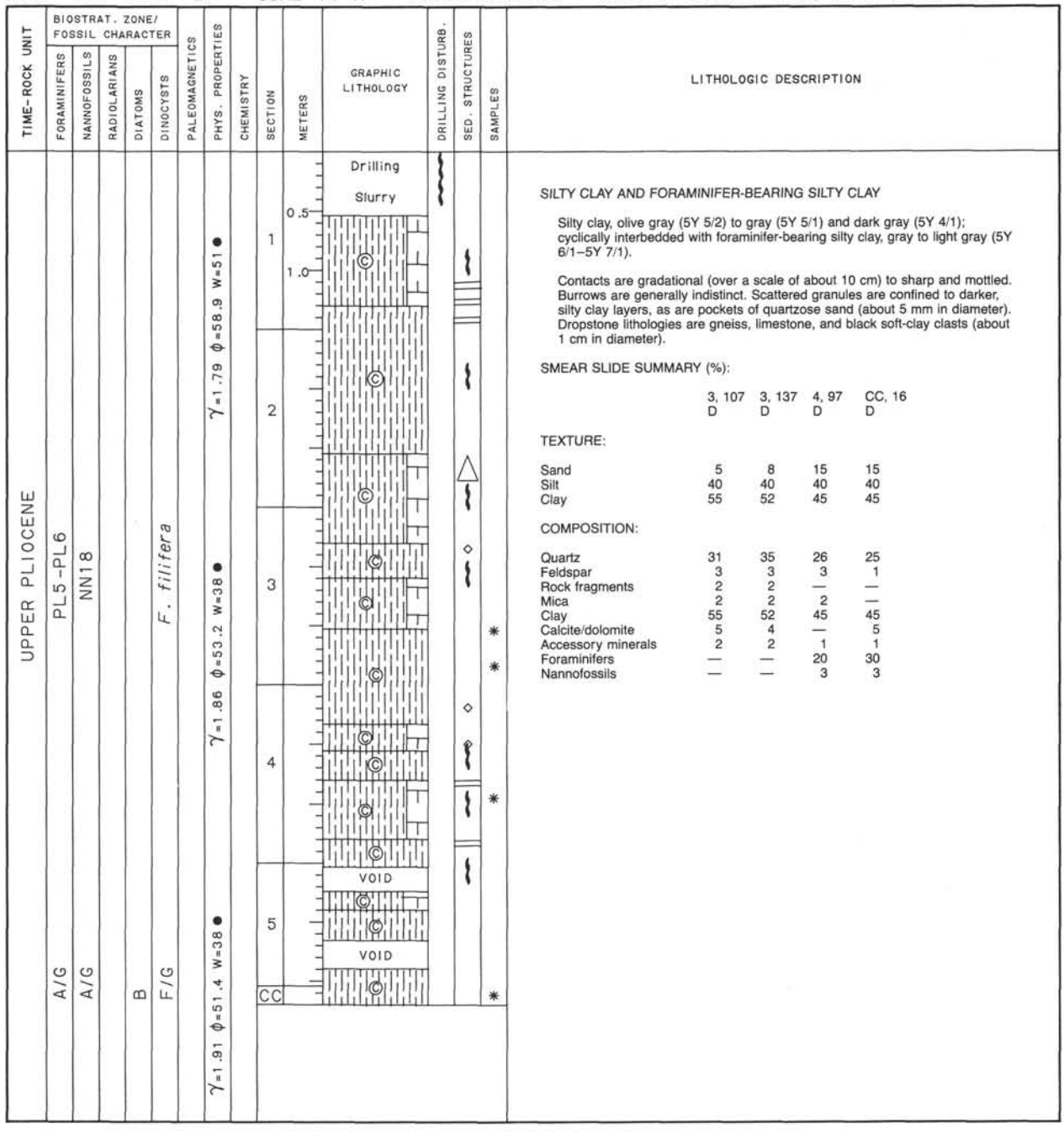

SILTY CLAY AND FORAMINIFER-BEARING SILTY CLAY

Silty clay, olive gray (5Y 5/2) to gray (5Y 5/1) and dark gray (5Y 4/1); cyclically interbedded with foraminifer-bearing silty clay, gray to light gray (5Y 6/1–5Y 7/1).

Contacts are gradational (over a scale of about 10 cm) to sharp and mottled. Burrows are generally indistinct. Scattered granules are confined to darker, silty clay layers, as are pockets of quartzose sand (about 5 mm in diameter). Dropstone lithologies are gneiss, limestone, and black soft-clay clasts (about 1 cm in diameter).

SMEAR SLIDE SUMMARY (%):

	3, 107 D	3, 137 D	4, 97 D	CC, 16 D
TEXTURE:				
Sand	5	8	15	15
Silt	40	40	40	40
Clay	55	52	45	45
COMPOSITION:				
Quartz	31	35	26	25
Feldspar	3	3	3	1
Rock fragments	2	2	—	—
Mica	2	2	2	—
Clay	55	52	45	45
Calcite/dolomite	5	4	—	5
Accessory minerals	2	2	1	1
Foraminifers	—	—	20	30
Nannofossils	—	—	3	3

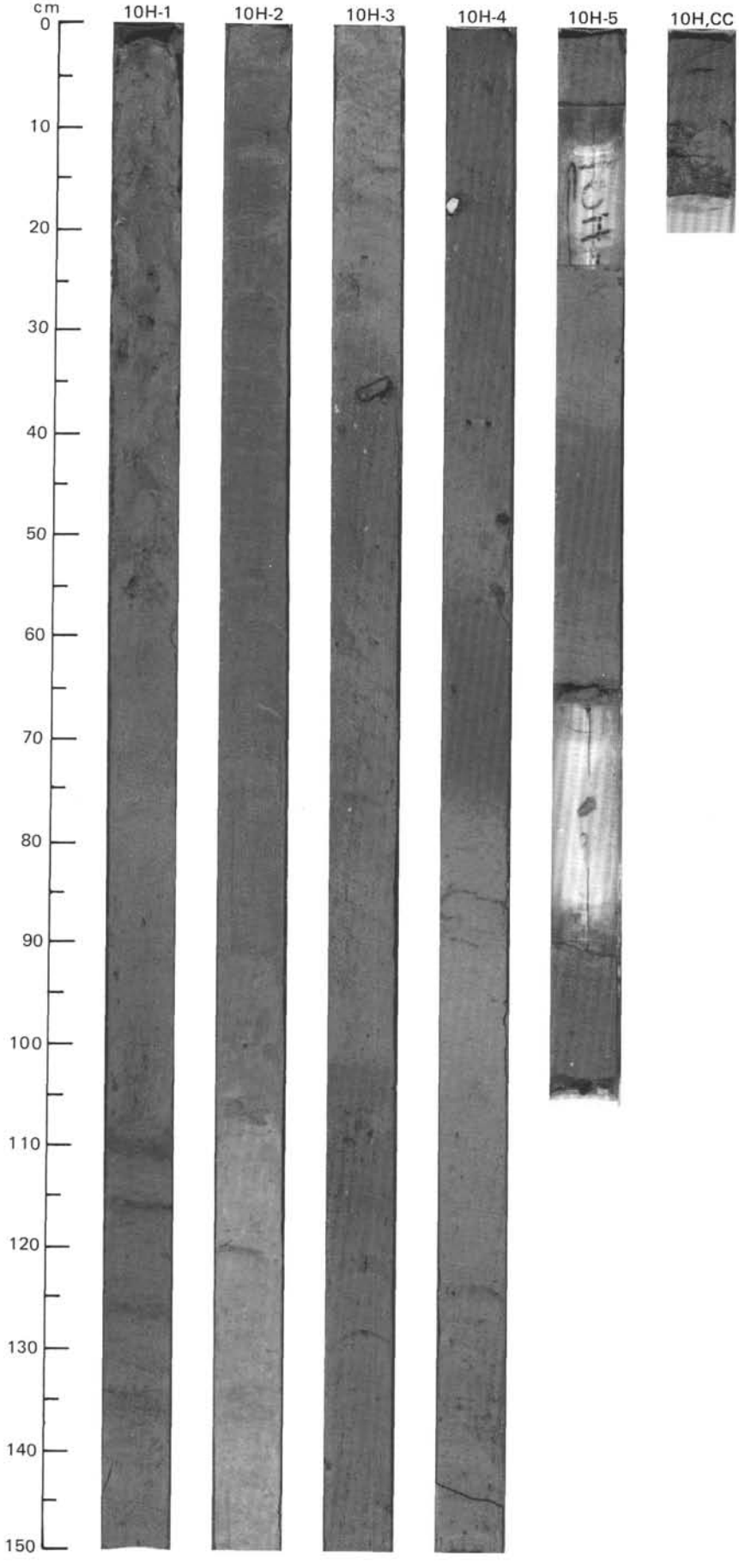
cm
0
10
20
30
40
50
60
70
80
90
100
110
120
130
140
150
10H-1
10H-2
10H-3
10H-4
10H-5
10H,CC

SITE 647 HOLE B CORE 11 H CORED INTERVAL 3953.7-3963.5 mbsl; 93.5-103.3 mbsf

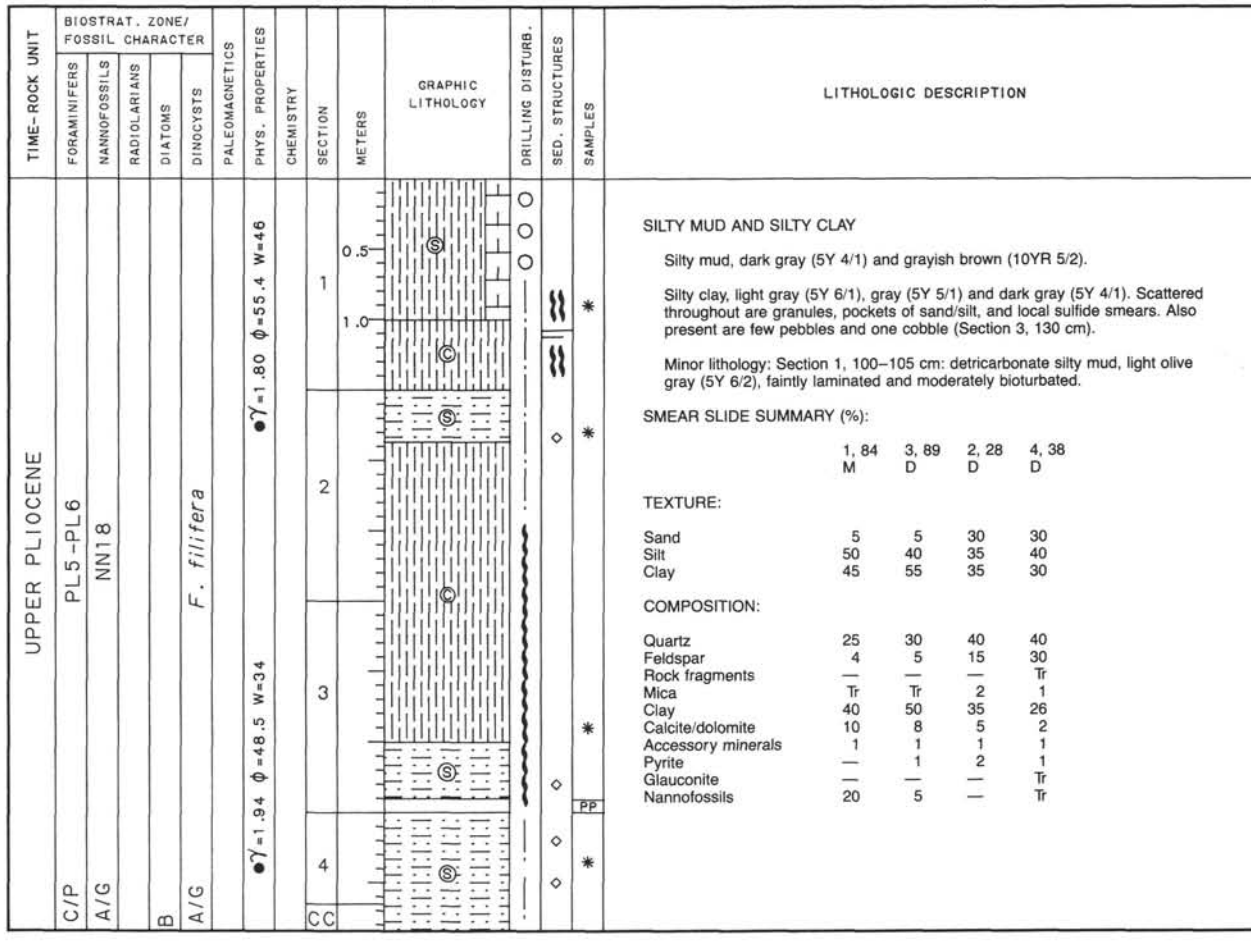

SILTY MUD AND SILTY CLAY

Silty mud, dark gray (5Y 4/1) and grayish brown (10YR 5/2).

Silty clay, light gray (5Y 6/1), gray (5Y 5/1) and dark gray (5Y 4/1). Scattered throughout are granules, pockets of sand/silt, and local sulfide smears. Also present are few pebbles and one cobble (Section 3, 130 cm).

Minor lithology: Section 1, 100–105 cm: detricarbonate silty mud, light olive gray (5Y 6/2), faintly laminated and moderately bioturbated.

SMEAR SLIDE SUMMARY (%):

	1, 84 M	3, 89 D	2, 28 D	4, 38 D
TEXTURE:				
Sand	5	5	30	30
Silt	50	40	35	40
Clay	45	55	35	30
COMPOSITION:				
Quartz	25	30	40	40
Feldspar	4	5	15	30
Rock fragments	—	—	—	Tr
Mica	Tr	Tr	2	1
Clay	40	50	35	26
Calcite/dolomite	10	8	5	2
Accessory minerals	1	1	1	1
Pyrite	—	1	2	1
Glauconite	—	—	—	Tr
Nannofossils	20	5	—	Tr

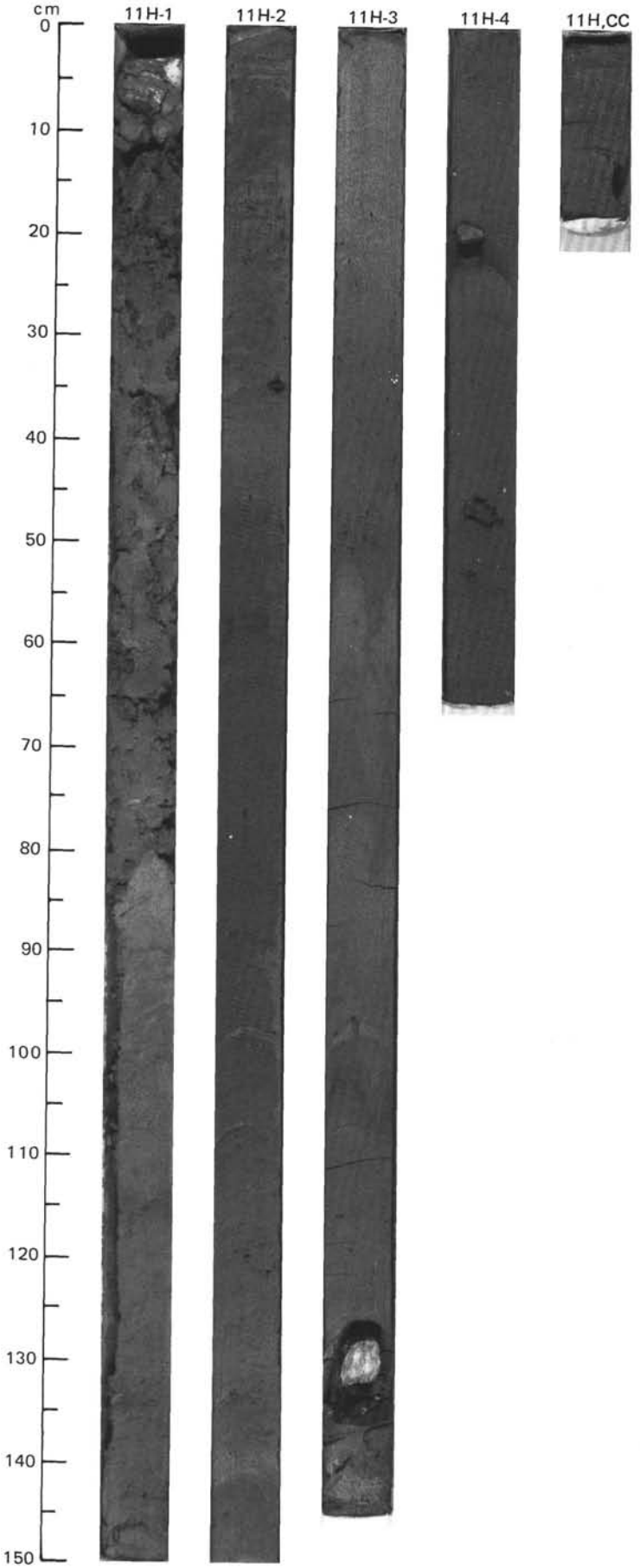
cm
0
10
20
30
40
50
60
70
80
90
100
110
120
130
140
150
11H-1
11H-2
11H-3
11H-4
11H,CC

GRAPE bulk-density profiles

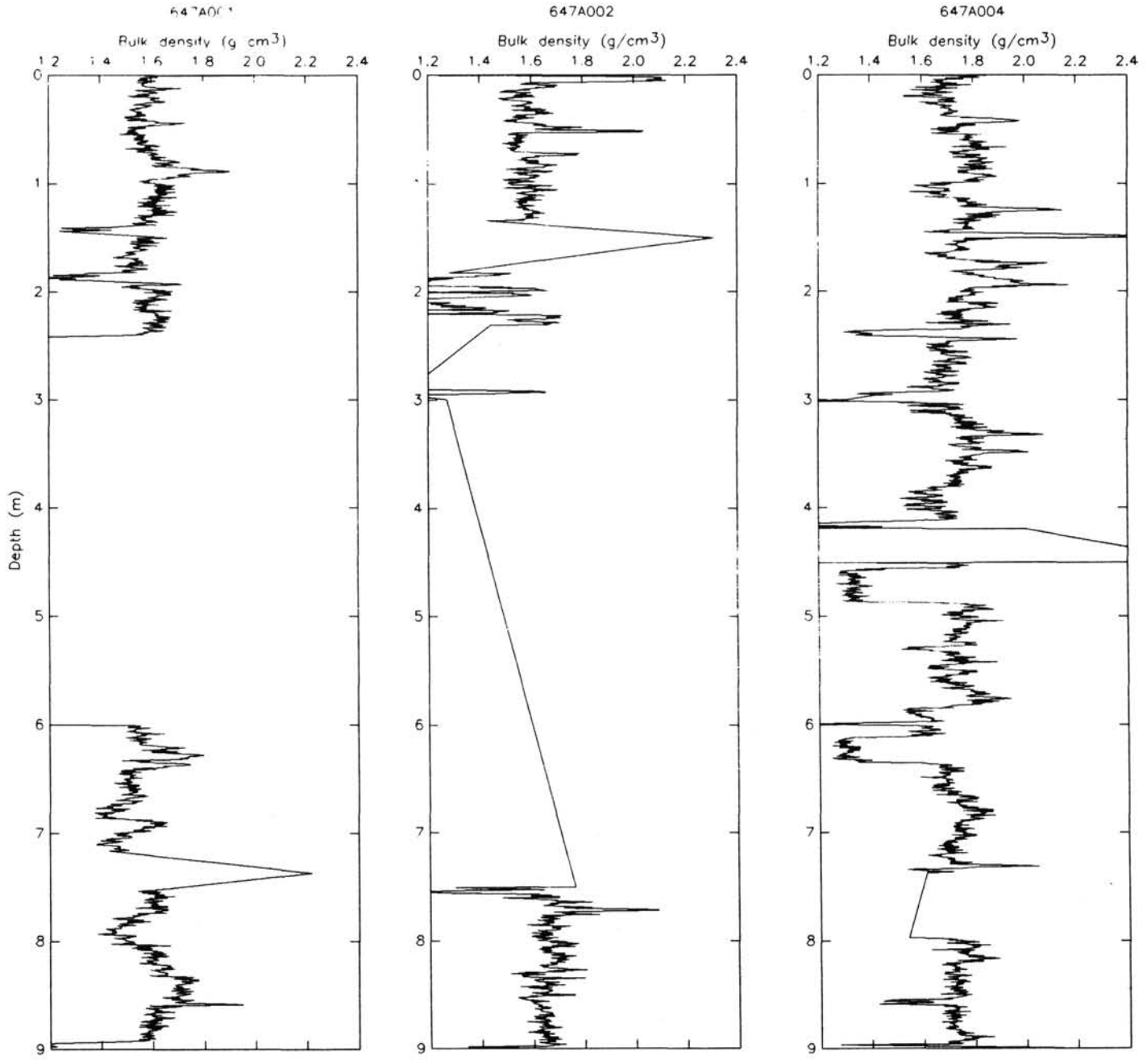

GRAPE bulk-density profiles

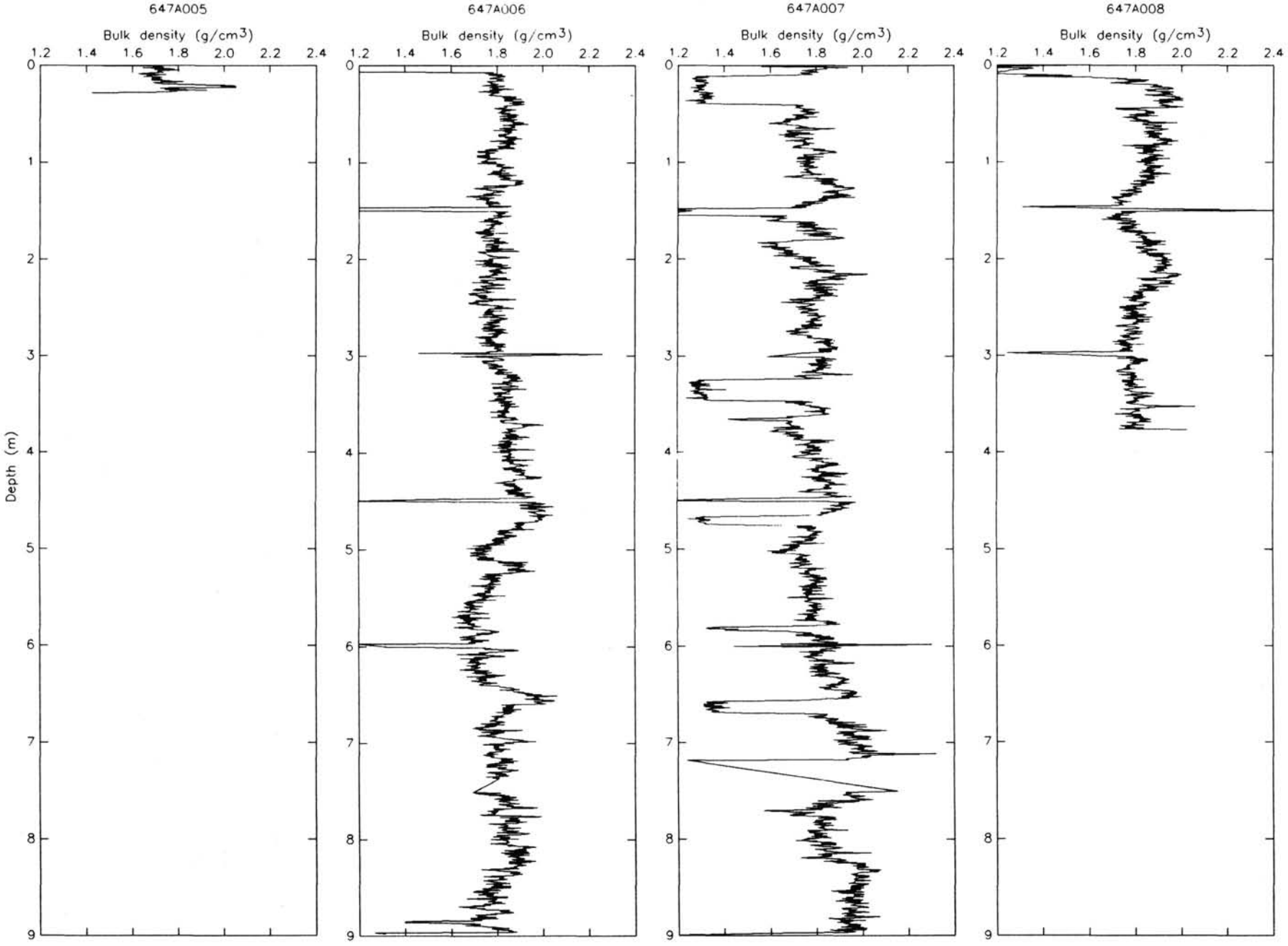

GRAPE bulk-density profiles

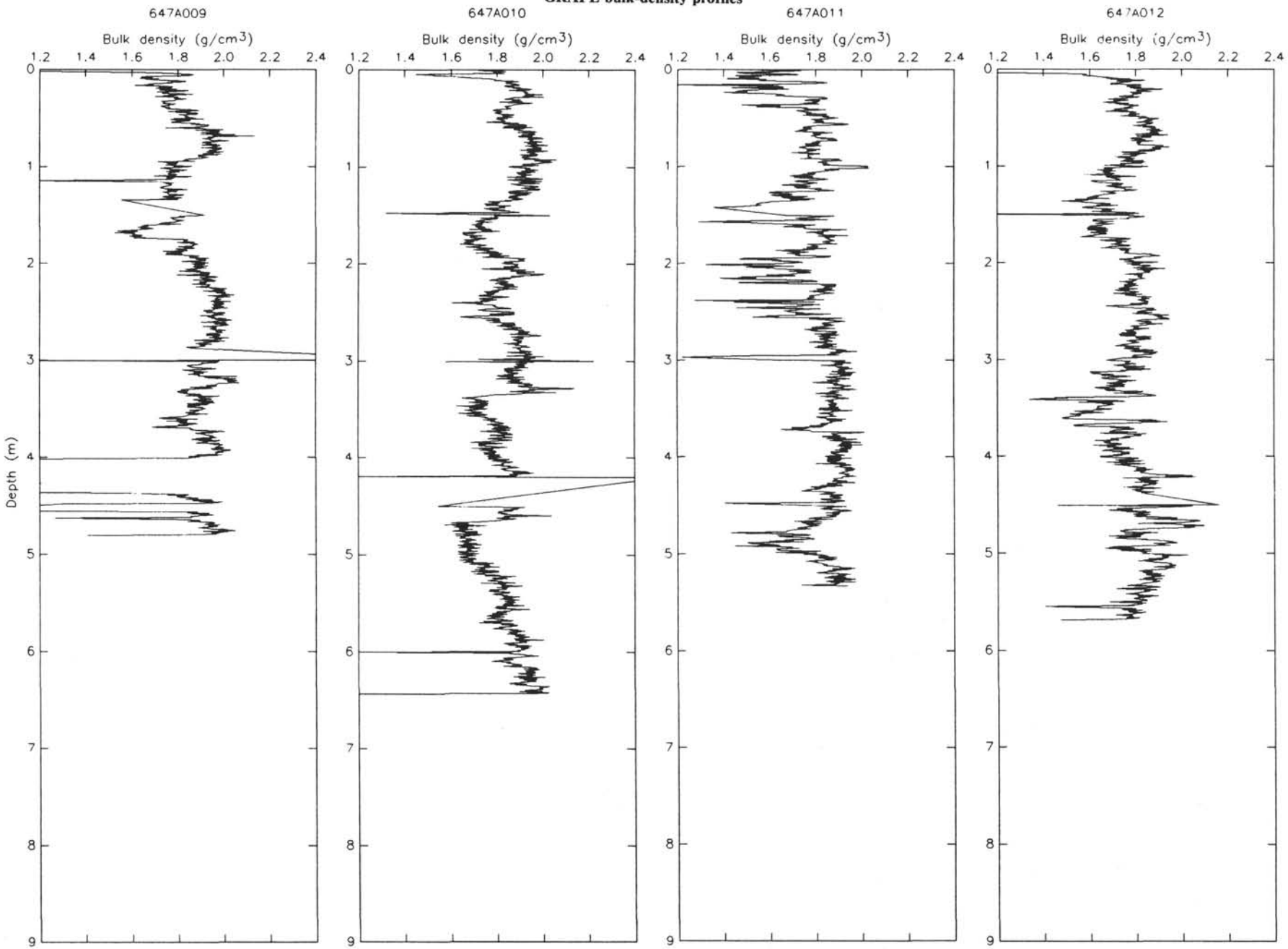

GRAPE bulk-density profiles

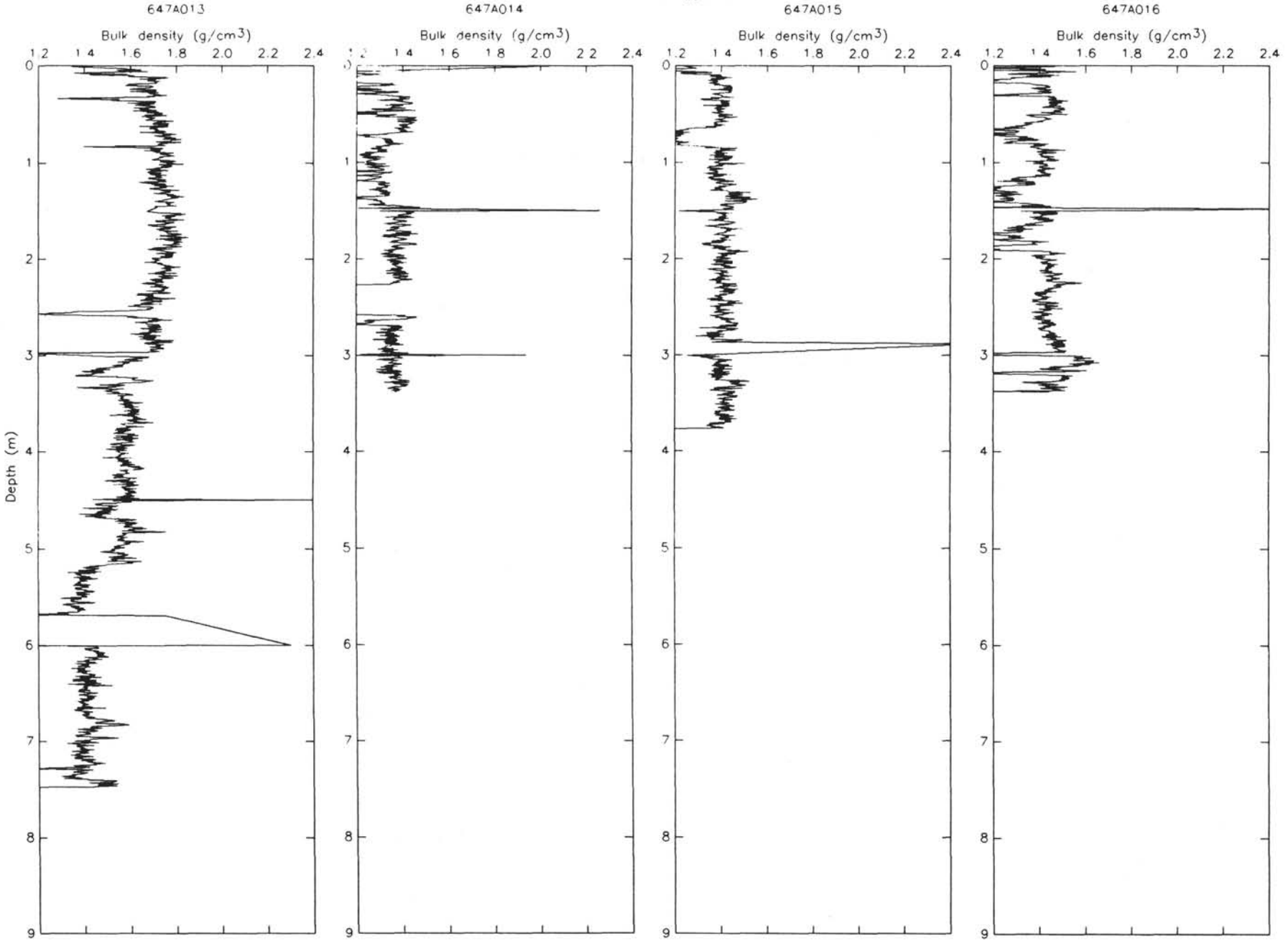

GRAPE bulk-density profiles

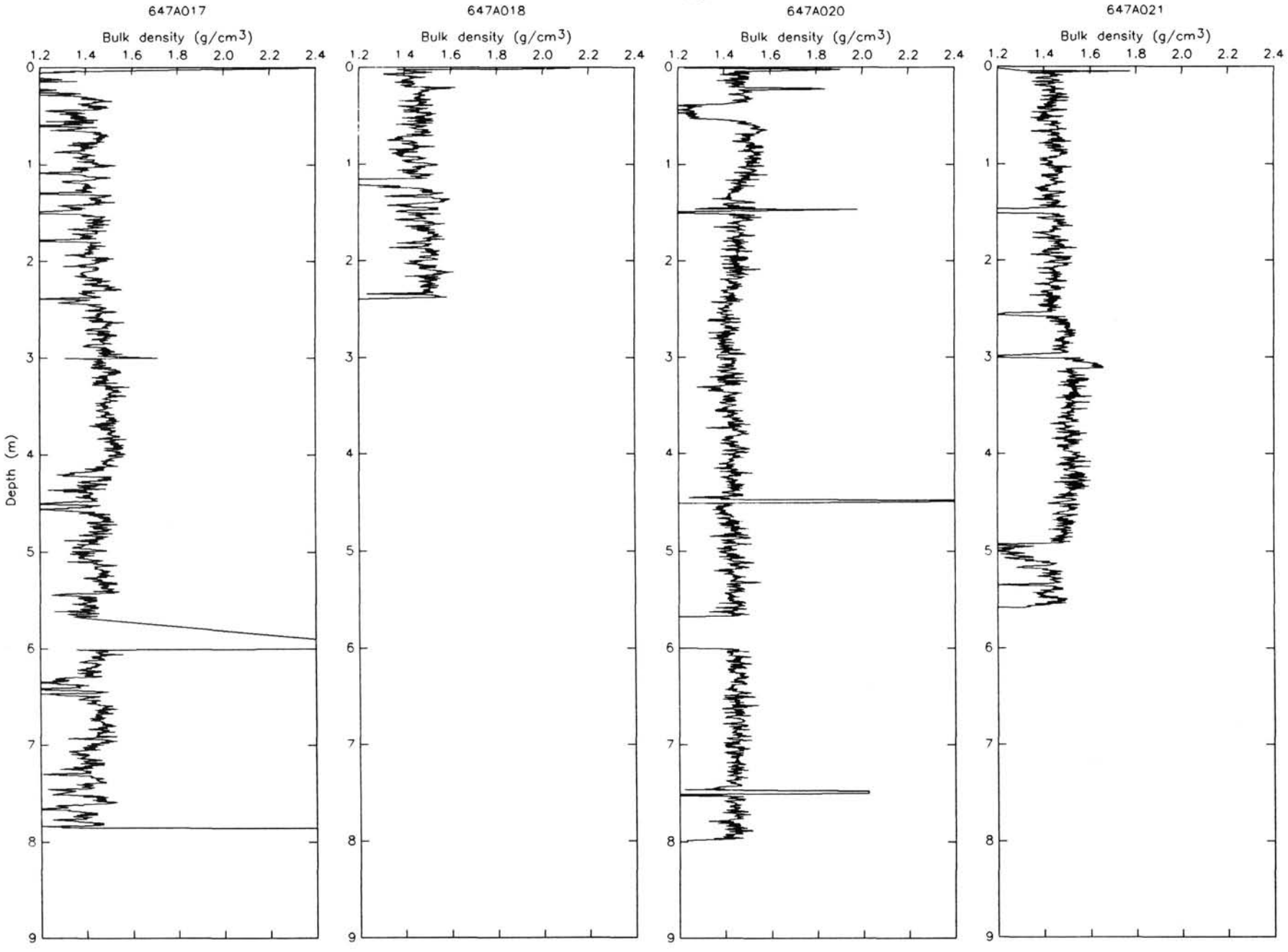

GRAPE bulk-density profiles

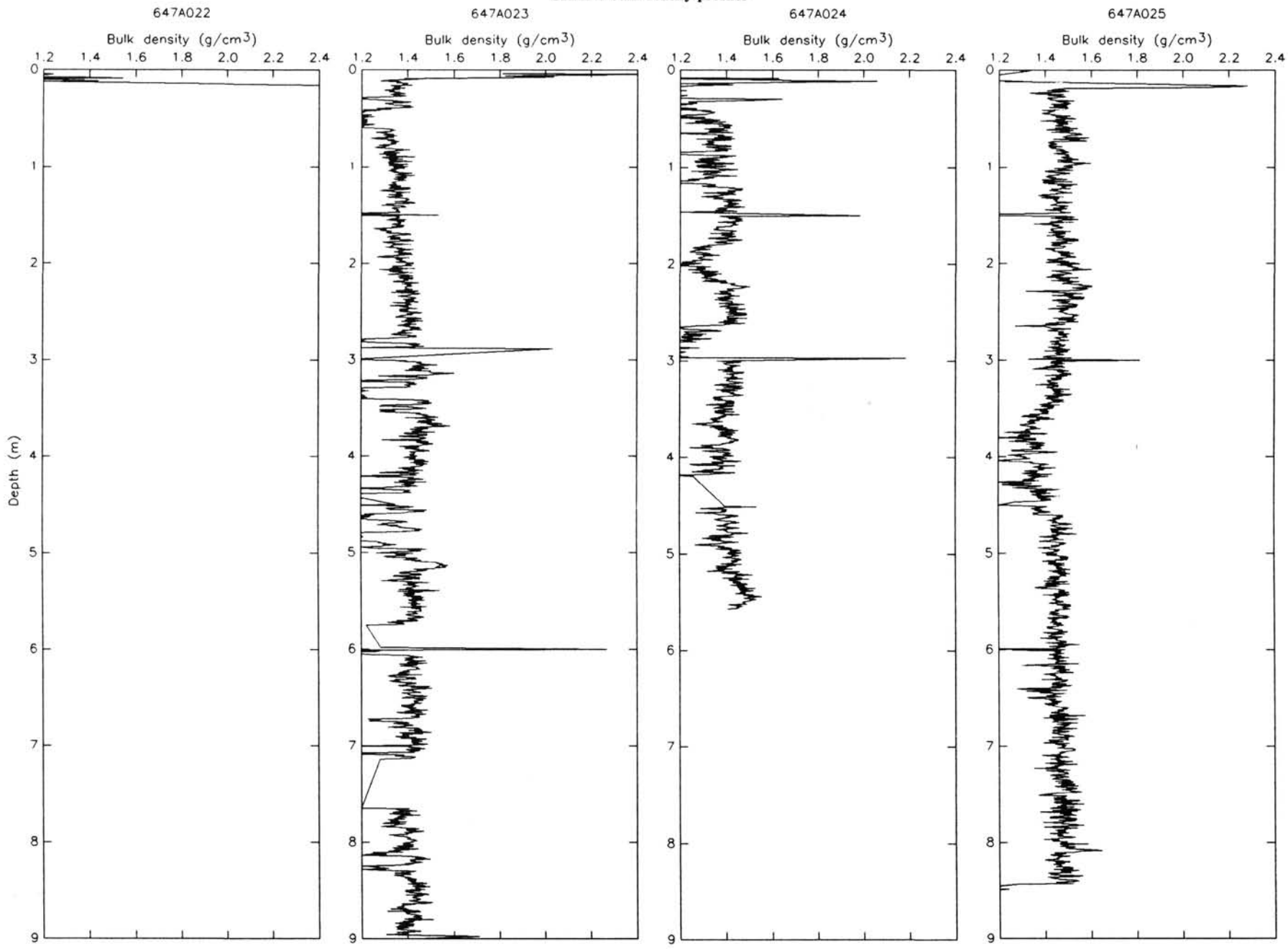

GRAPE bulk-density profiles

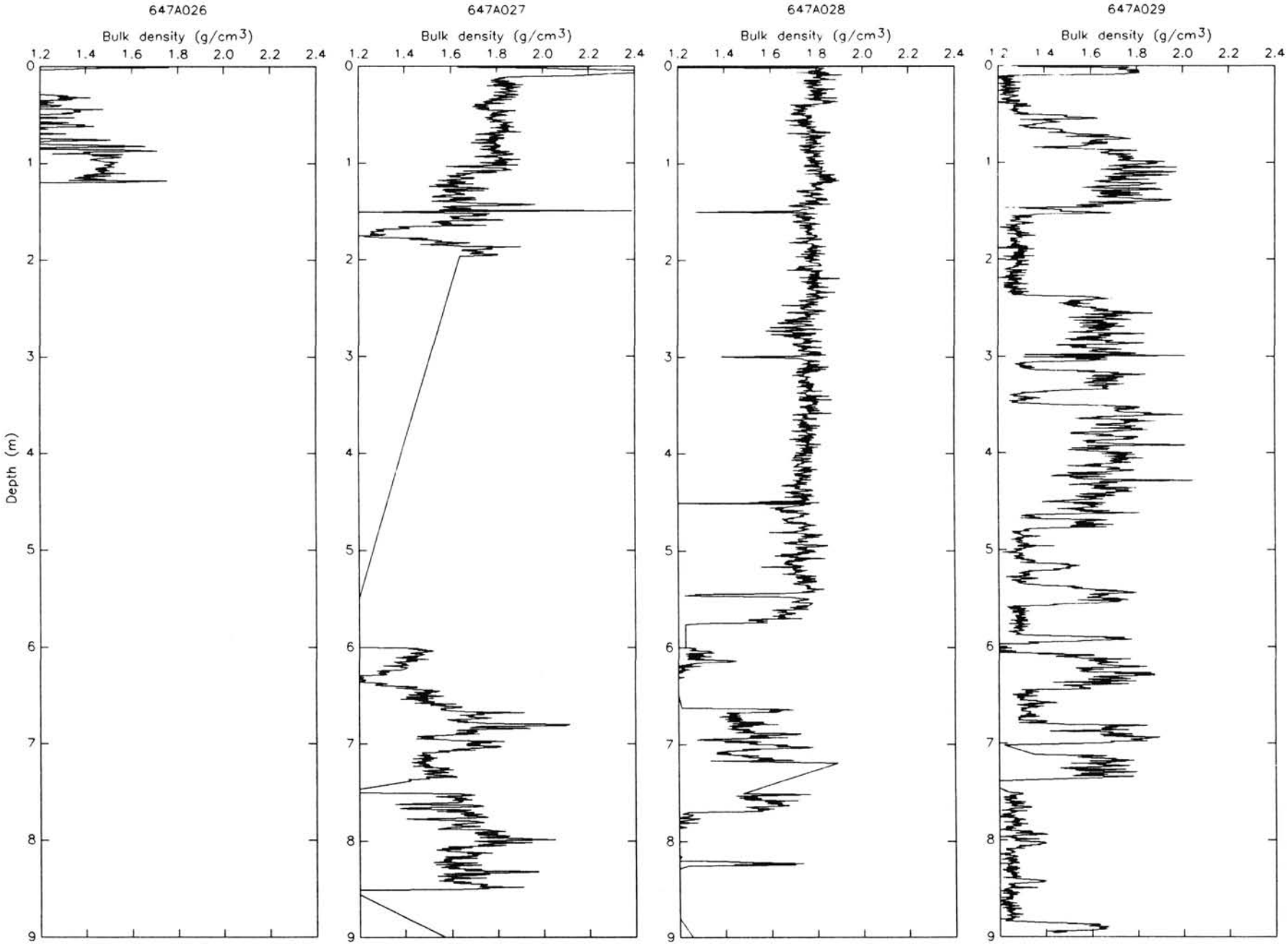

GRAPE bulk-density profiles

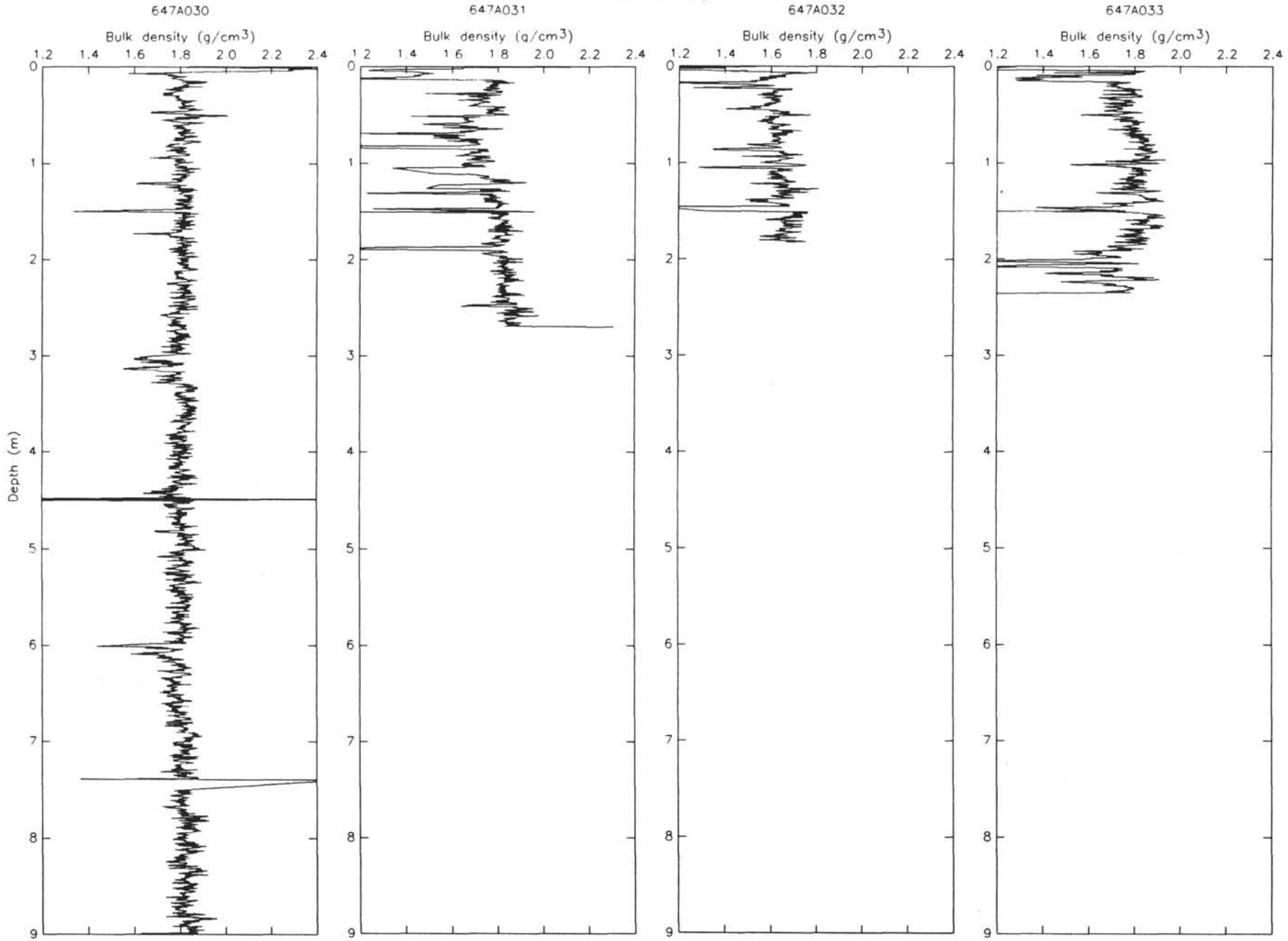

GRAPE bulk-density profiles

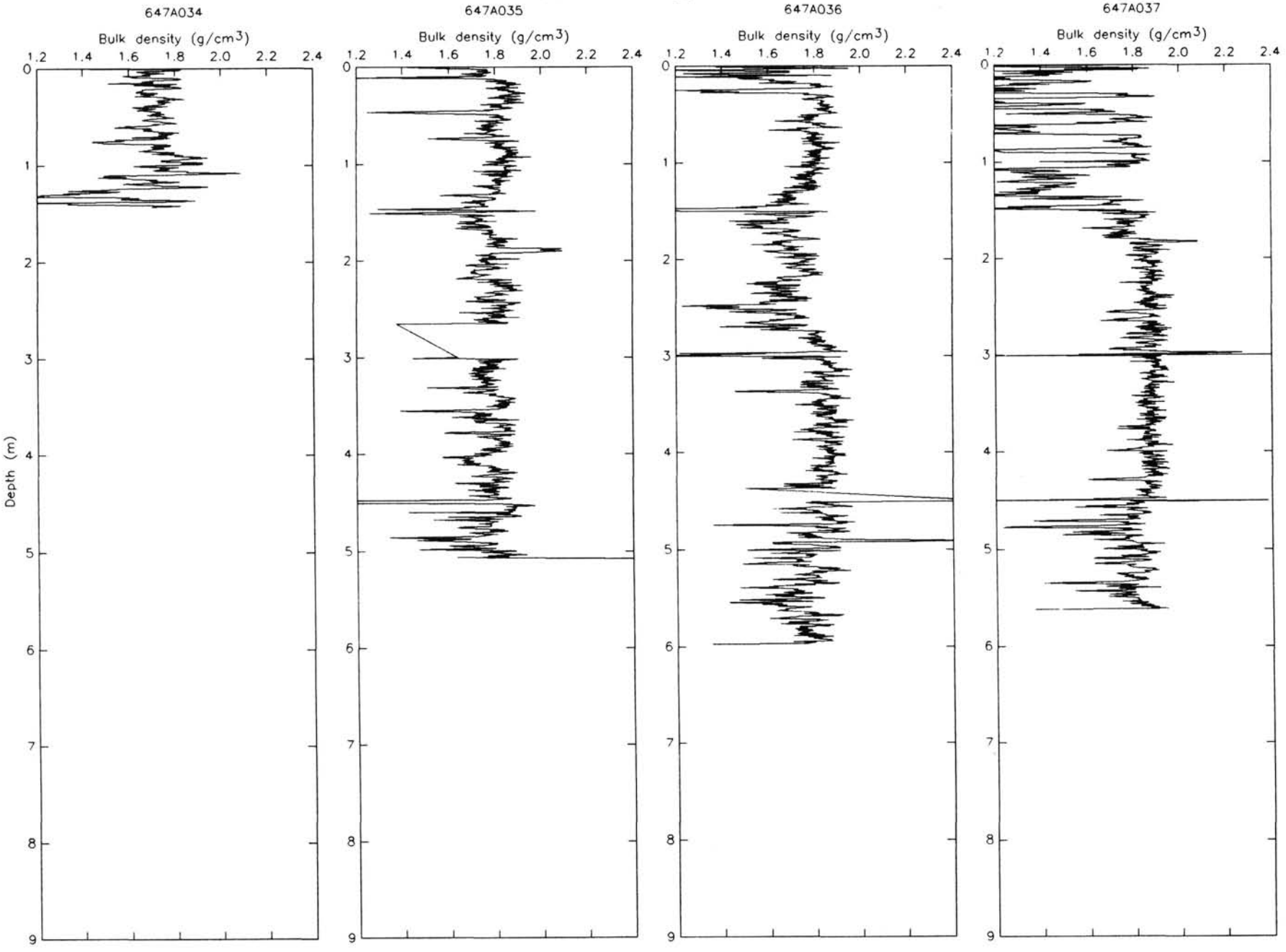

GRAPE bulk-density profiles

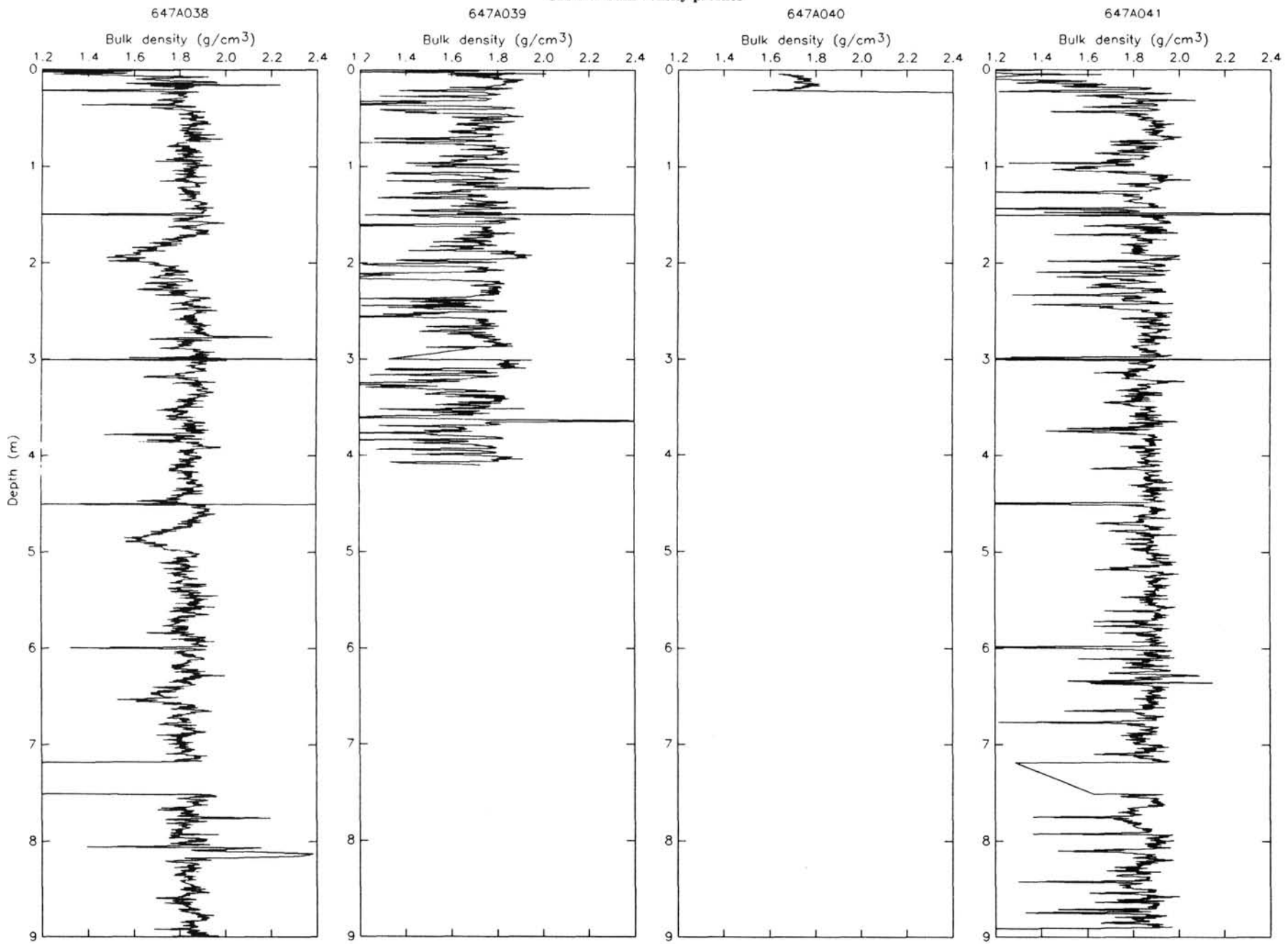

GRAPE bulk-density profiles

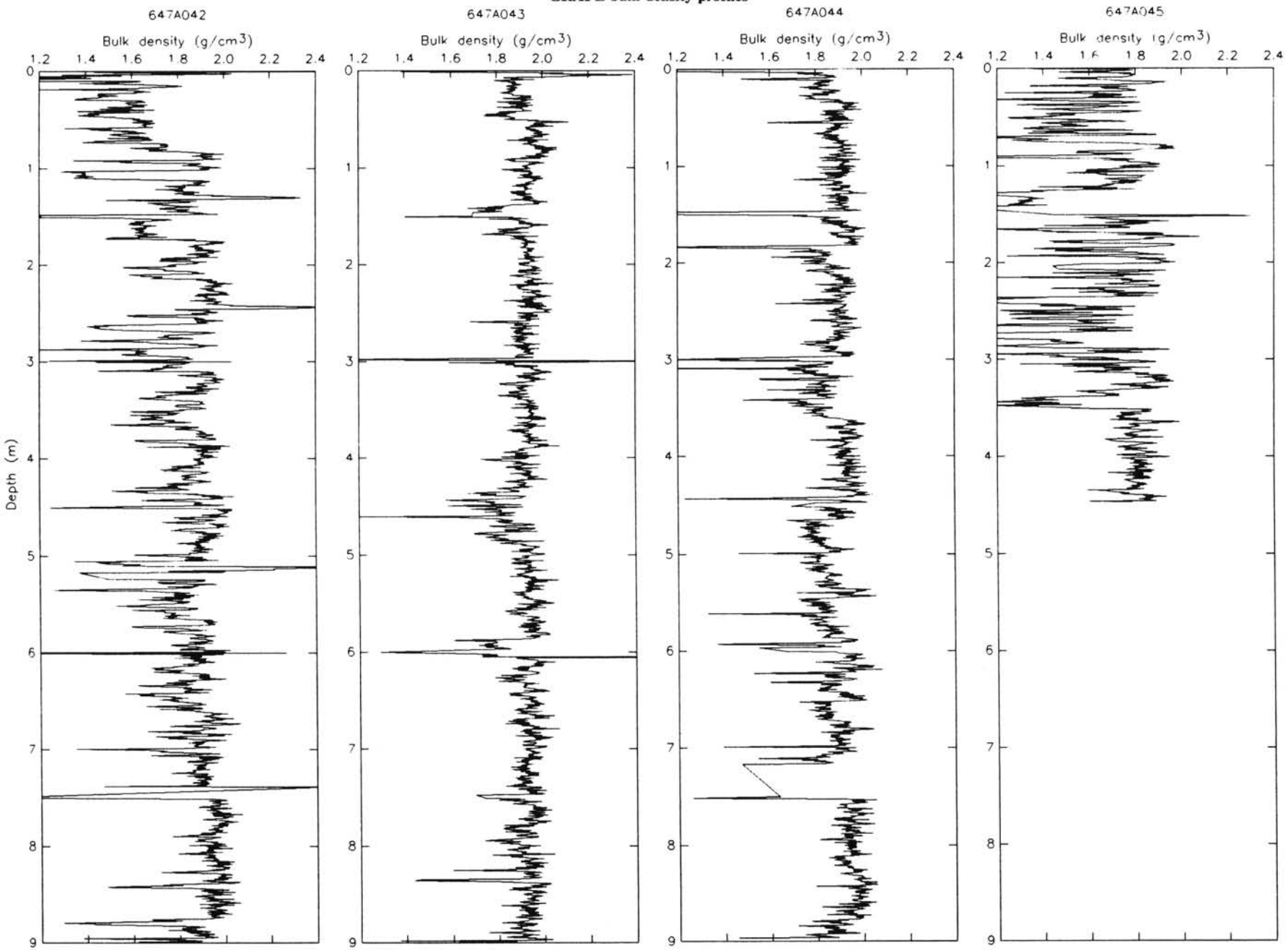

GRAPE bulk-density profiles

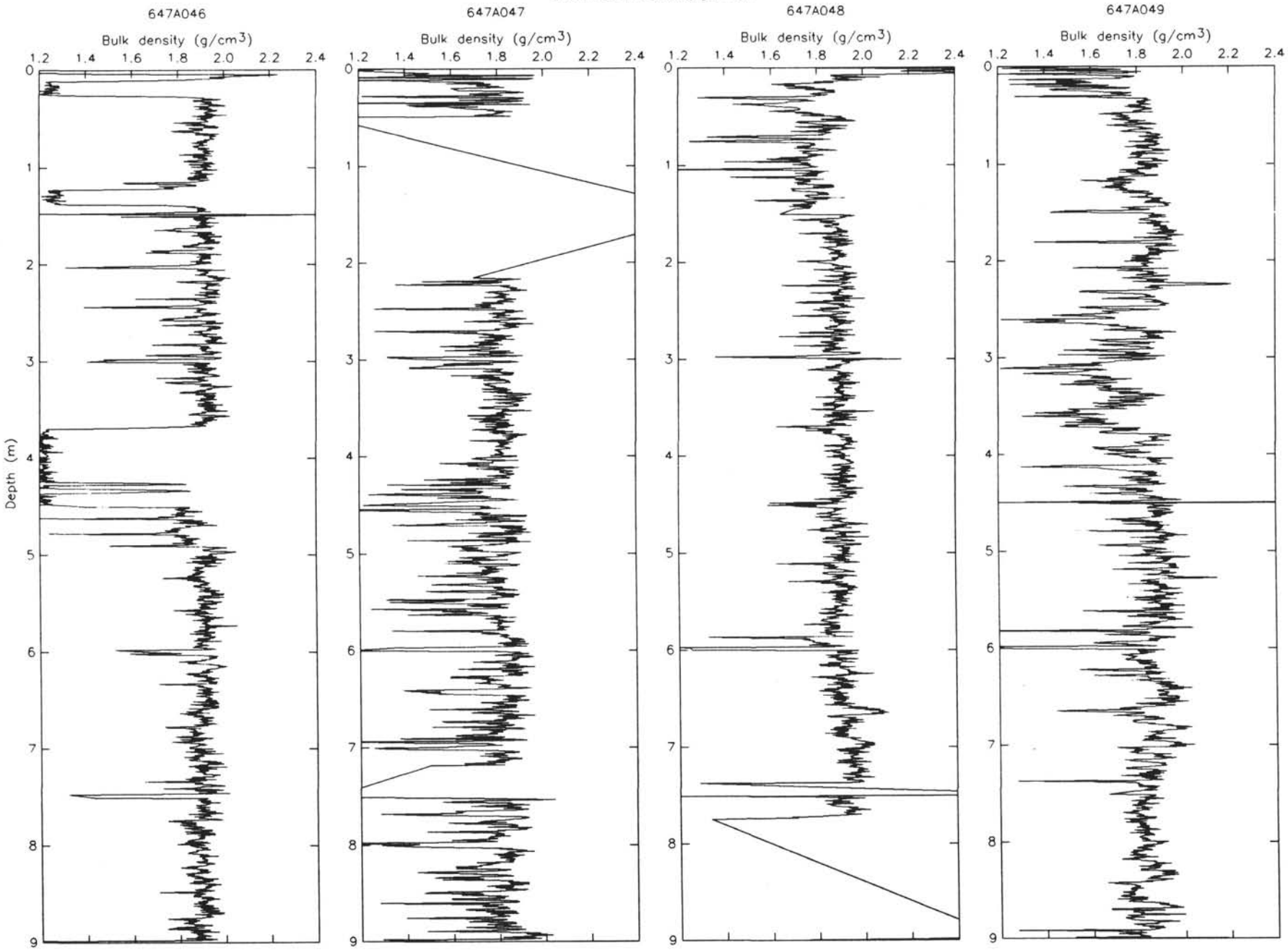

GRAPE bulk-density profiles

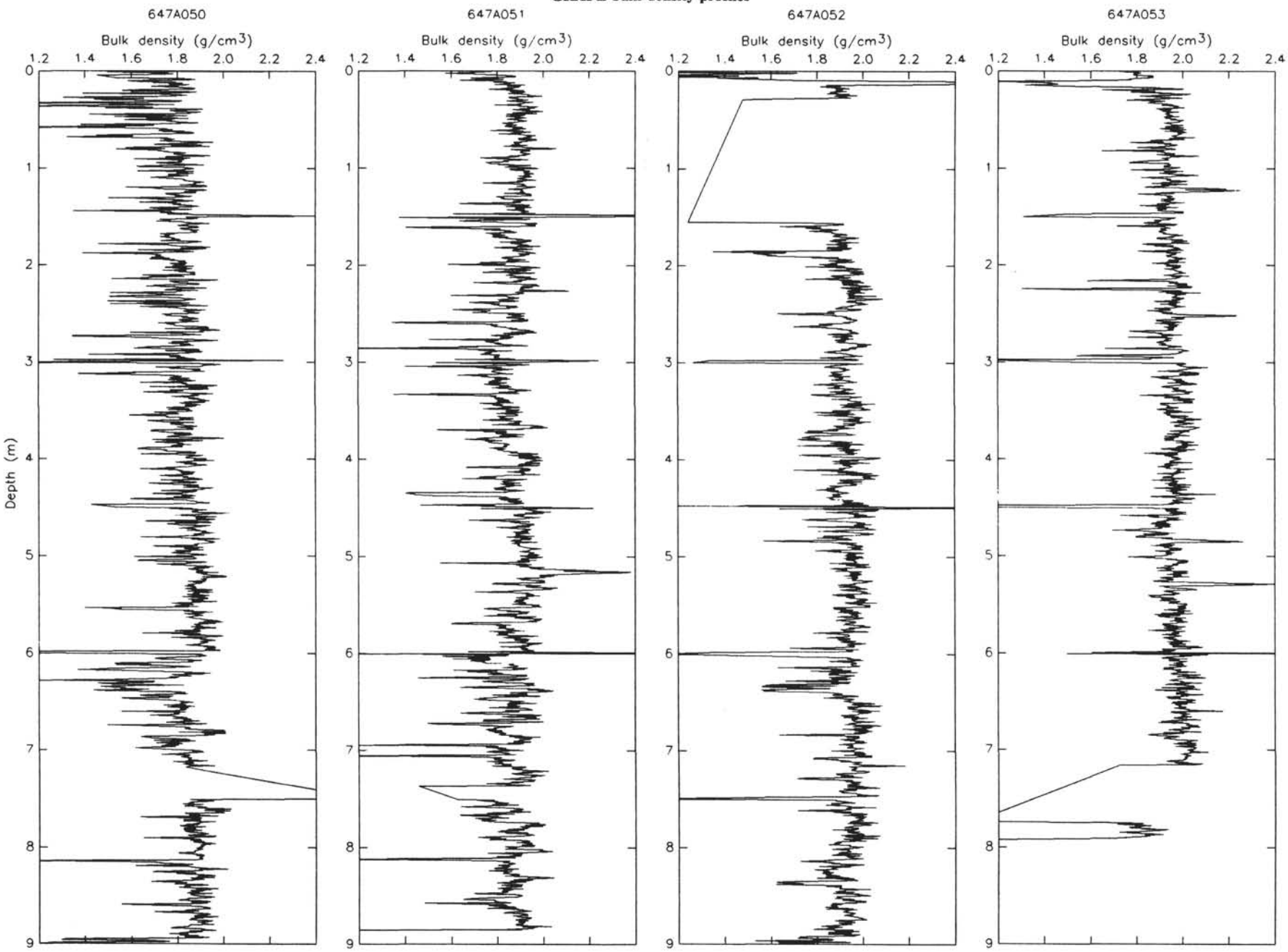

GRAPE bulk-density profiles

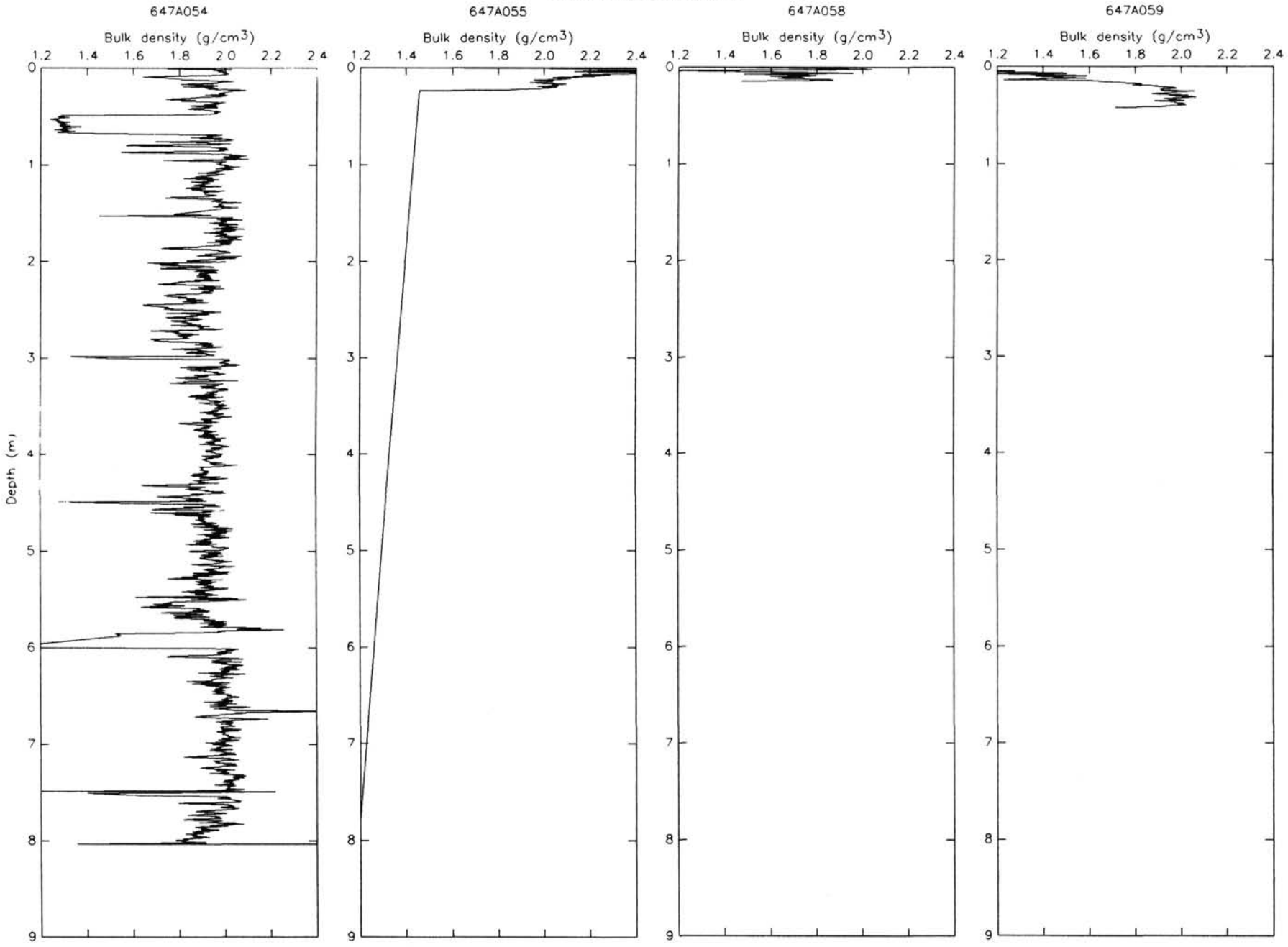

GRAPE bulk-density profiles

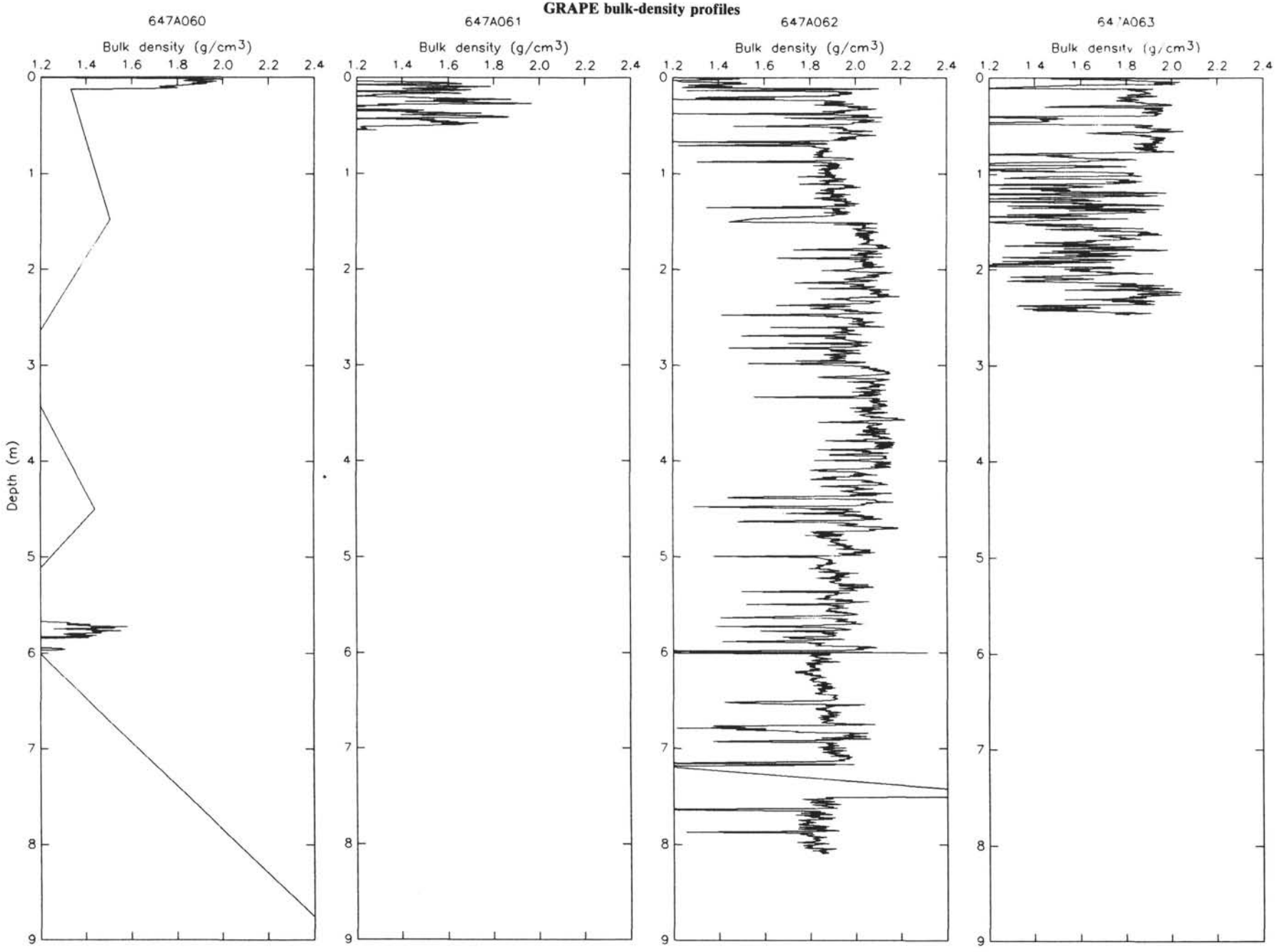

GRAPE bulk-density profiles

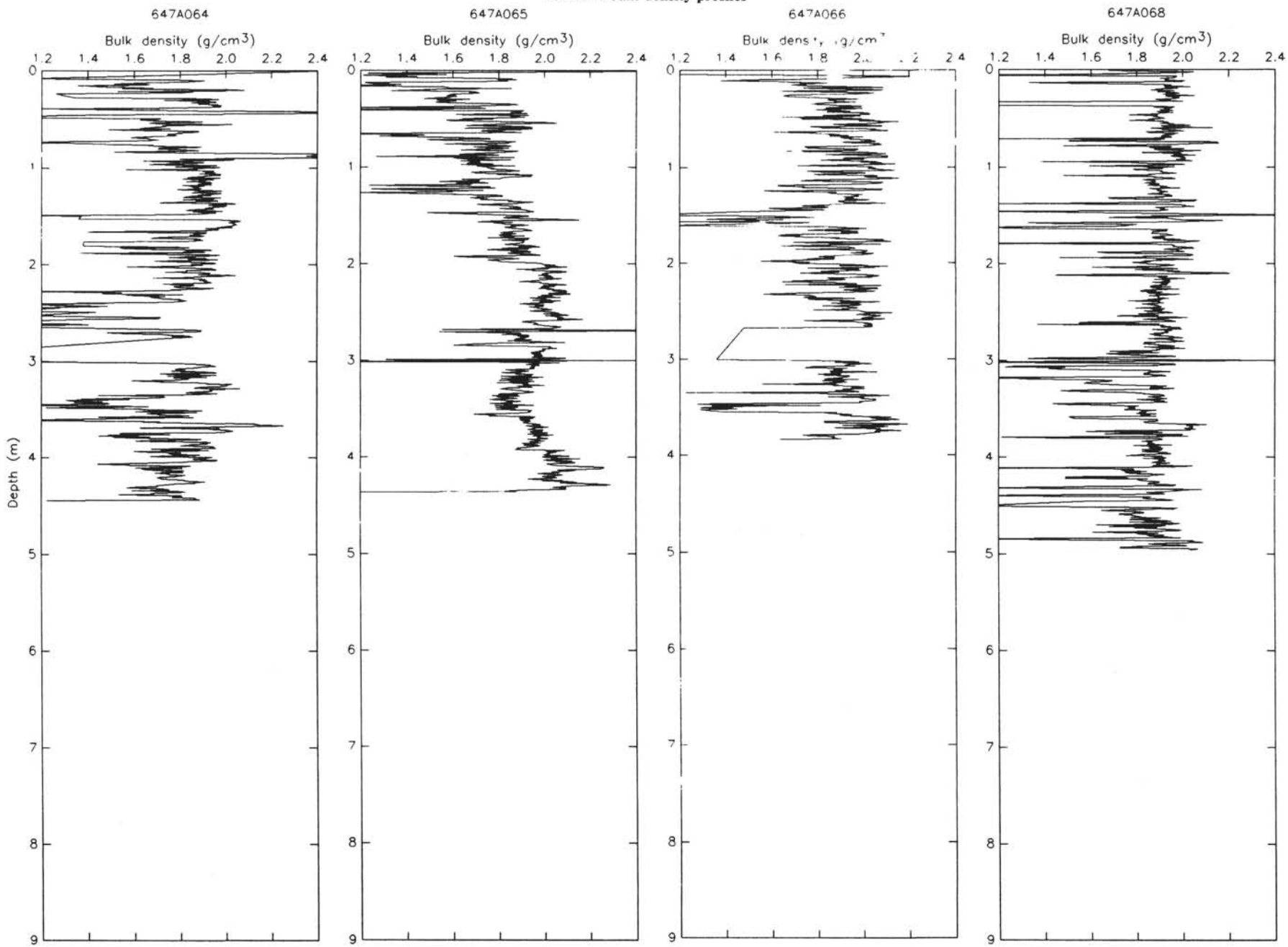

GRAPE bulk-density profiles

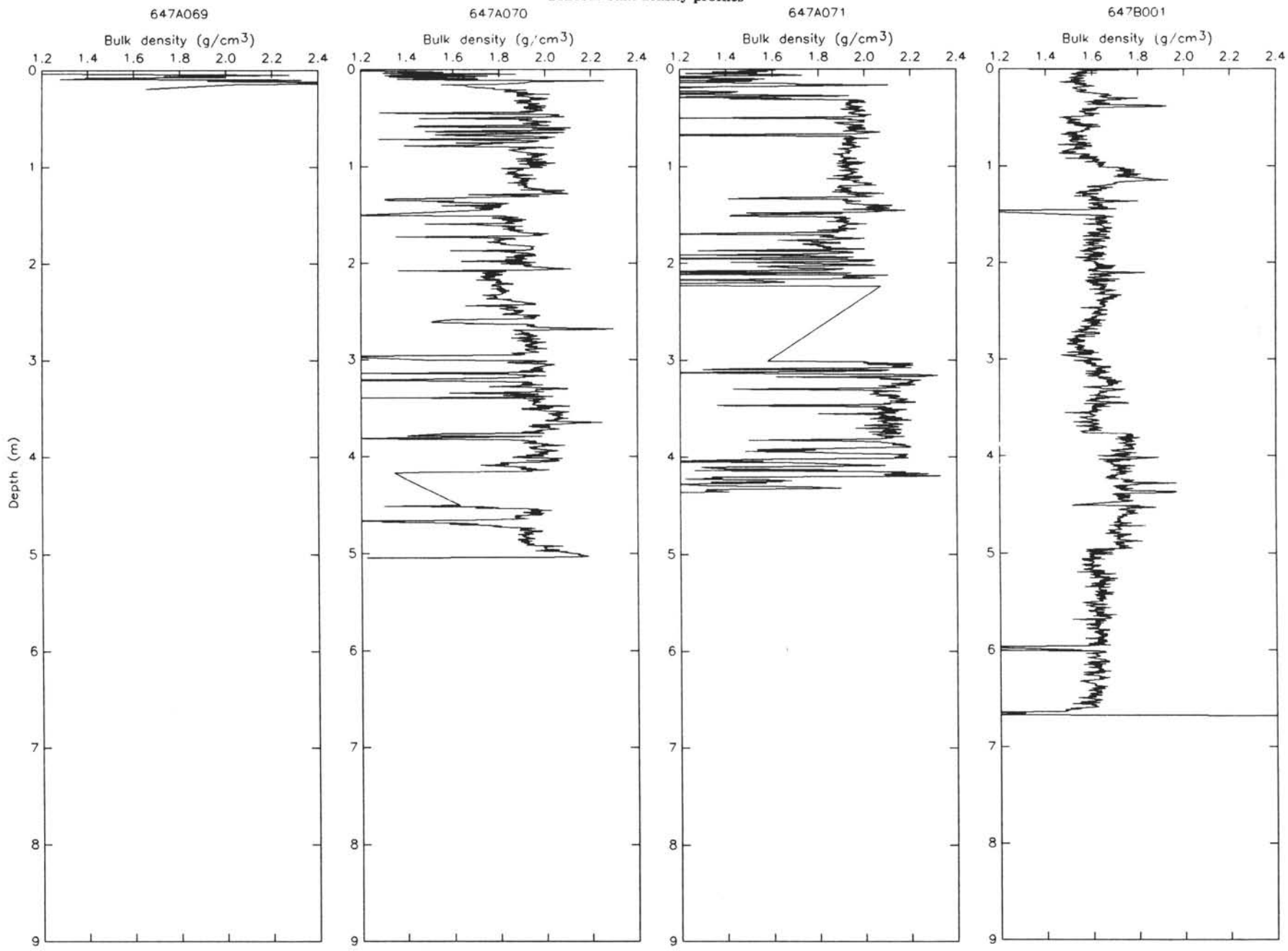

GRAPE bulk-density profiles

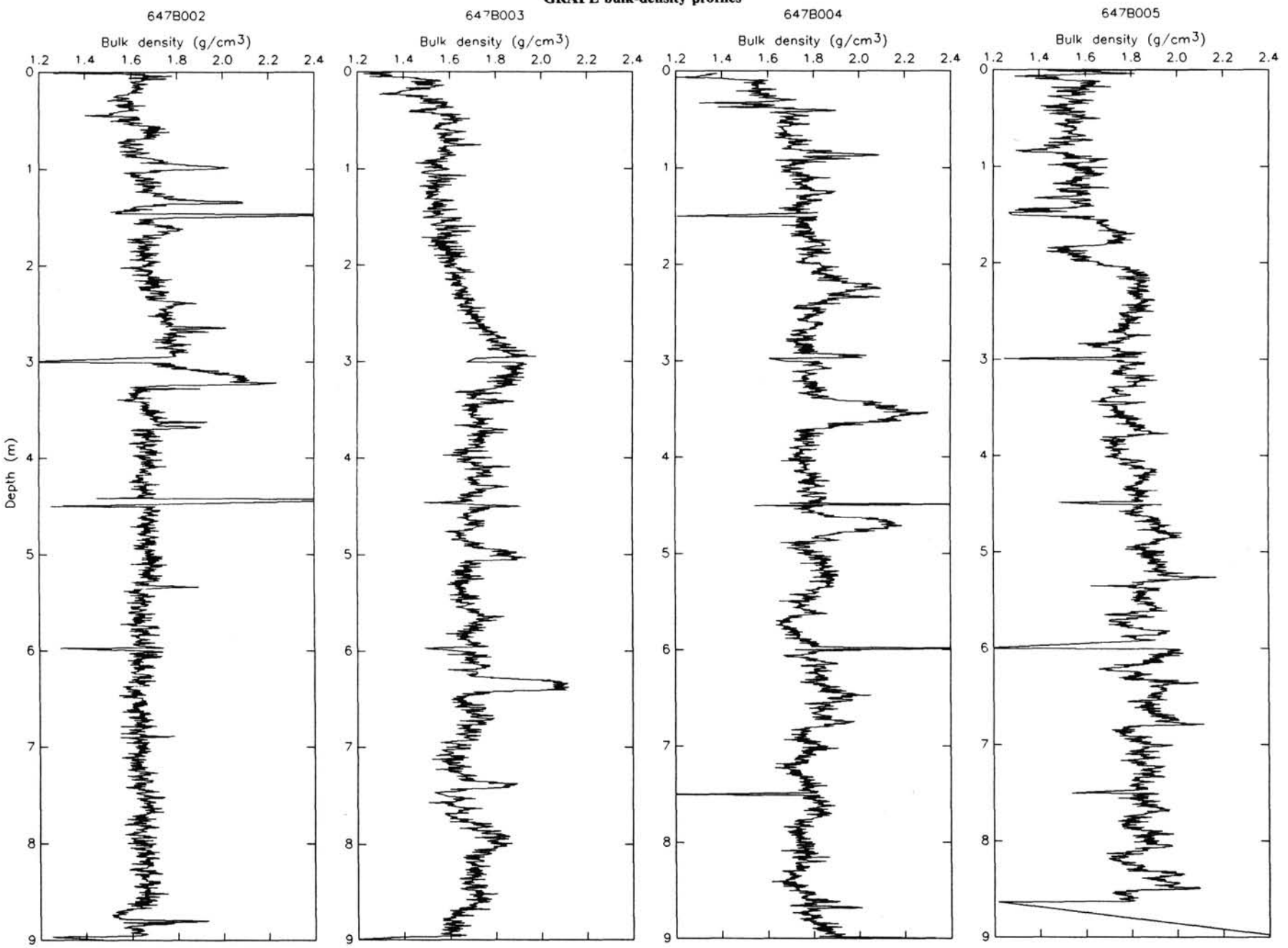

GRAPE bulk-density profiles

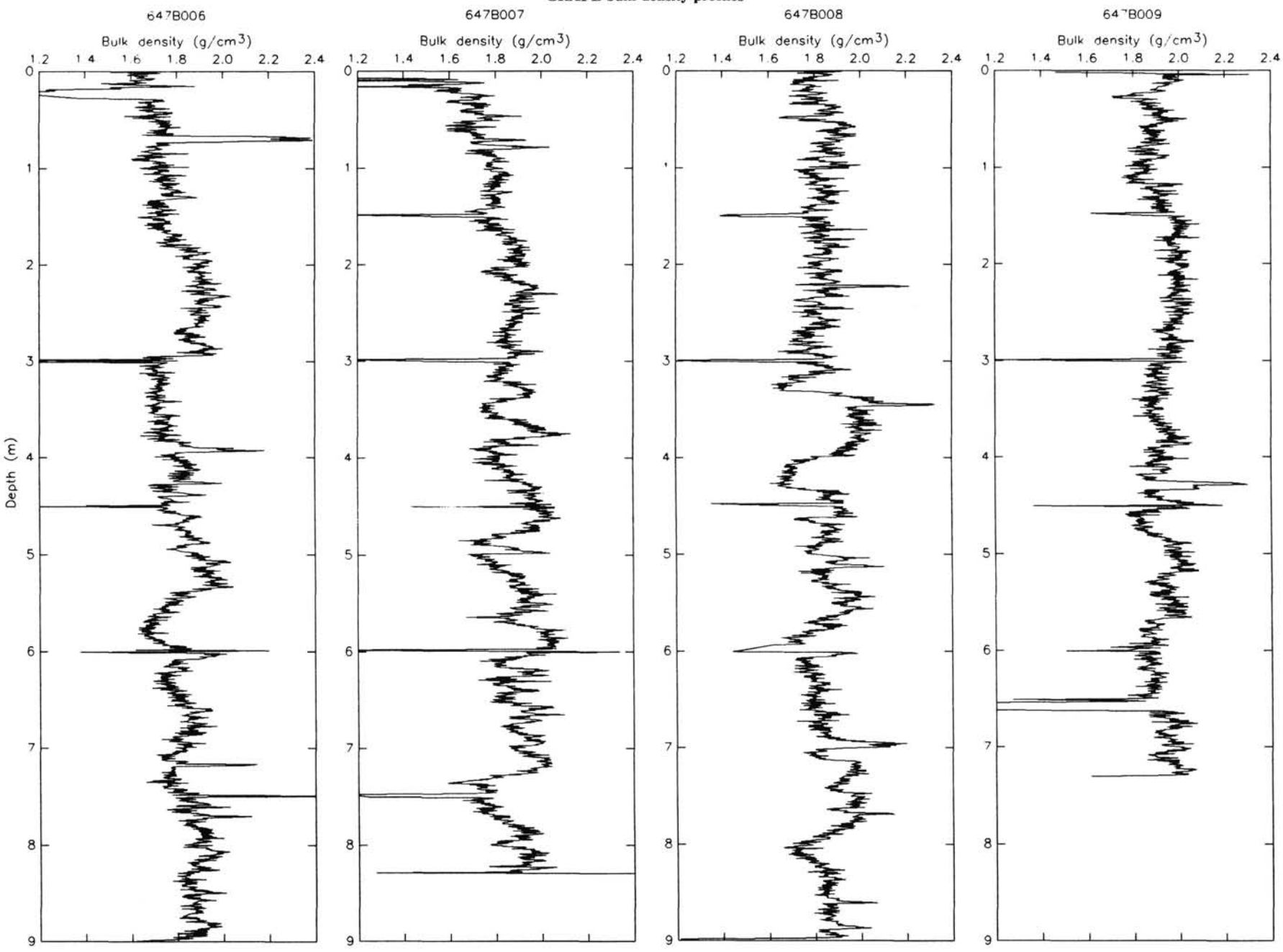

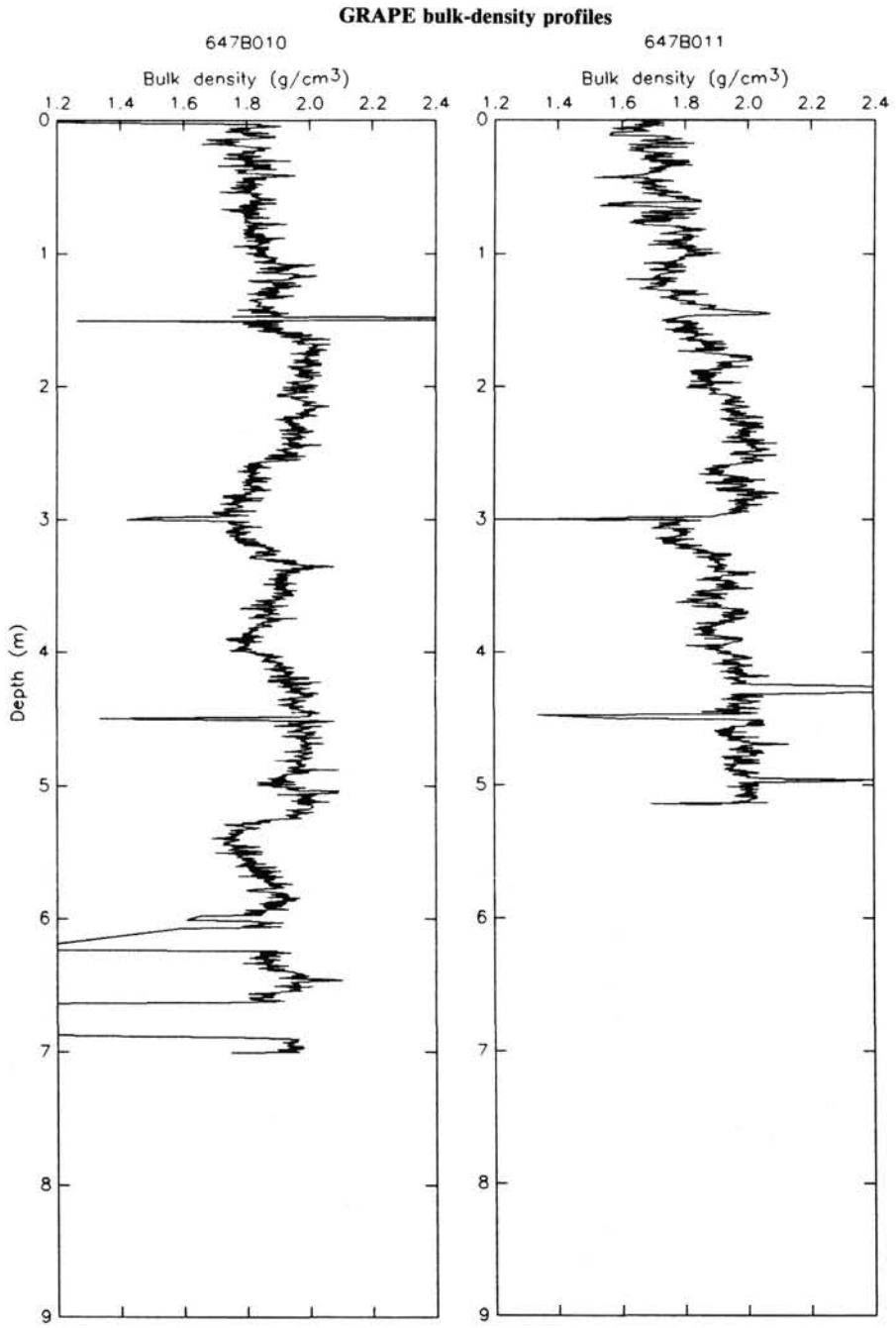
GRAPE bulk-density profiles
647B010
647B011
Bulk density (g/cm3)
Bulk density (g/cm3)
1.2
1.4
1.6
1.8
2.0
2.2
2.4
Depth (m)
0
1
2
3
4
5
6
7
8
9